ATOMIC WEAPONS ESTABLISHMENT

AWE REPORT NO. O 4/88

P-Wave Seismograms from Underground Explosions at the Shagan River Test Site Recorded at Four Arrays (UK UNCLASSIFIED)

R C Stewart

Recommended for issue by

Mr A Douglas, Superintendent

Approved by

Mr B L Elphick, Head of Division

CONTENTS

SUMMARY

This report presents the P-wave seismograms recorded at four medium-aperture arrays from 62 underground explosions fired at the test site at Shagan River, USSR. Four types of seismogram are illustrated for each explosion: the short-period (SP), the SP seismogram with additional attenuation equivalent to a t* (ratio of travel time to specific quality factor, Q) of 0.2 s, a broad-band (BB) seismogram and a BB seismogram corrected for anelastic attenuation using a t* of 0.15 s. The attenuation-corrected seismogram is used to investigate the nature of the P-pulse radiated from the source.

From each recording of an explosion, measurements are made of the body-wave magnitude, the P-pulse rise time, the P-pulse duration and the P-pulse area. From the pulse area an estimate is made of the long-term level of the reduced displacement potential, ψ_∞, which should be directly related to the yield of the explosion. The measurements made are used to obtain least-squares estimates of network values and station effects. Estimates are given of the time between the direct P arrival and the free-surface reflection pP, although identification of the latter is not always straightforward.

Rise times measured on the BB seismograms corrected for attenuation are estimates of the rise time of the source function. Using the estimates of ψ_∞ as a measure of yield, the rise times of Shagan River explosions are roughly proportional to the fourteenth root of the yield. The pulse durations show a similar scaling with yield, but also depend on in which of the two regions of the test site the explosion was fired (the test site being readily divided into two parts on variations in the observed waveforms). The measured pP-P times also seem to depend on the region of firing, suggesting a possible difference in depth or overburden wave-speed between explosions in the two parts of the test site.

The seismograms from one of the disturbances are unusual and can be explained as resulting from two explosions separated by about 5½ km and detonated simultaneously.

There is one earthquake recorded at teleseismic distances known to have occurred close to the test site. The array recordings of this, processed in the same manner as the explosions, are presented to provide a comparison with the explosion recordings.

1. INTRODUCTION

This report presents short-period (SP) and broad-band (BB) seismograms from 62 underground explosions at the Shagan River test site, USSR for four array stations: Eskdalemuir (EKA) Scotland, Yellowknife (YKA) Canada, Gauribidanur (GBA) India and Warramunga (WRA) Australia. The locations of the arrays are given in table 1 and are shown in figure 1 on an azimuthal great-circle map centred on the Shagan River test site.

The distances and azimuths of the stations from the test site are given in table 1. All the stations are within the 30 to 90° distance range which Thirlaway (1) calls the "source window" as it is the range where the effects of the transmission path on the signal are smallest and so it is possible to obtain the most information on the source function. Note also that the stations are roughly evenly distributed in azimuth about the test site.

The explosions used are those listed by Marshall et al (2). Their epicentres are given in table 2 and displayed on a map in figure 2. The epicentres were obtained by the method of Joint Epicentre Determination (3) using the P-wave arrival times published by the International Seismological Centre (ISC). The relocations are relative to the known location (from satellite data (4)) of the 15 January 1965 cratering explosion.

Various estimates of SP body-wave magnitude, m_b, are presented and the estimates are compared with each other and with the maximum-likelihood magnitude (m_b^{ML}) (Lilwall, unpublished results) estimated using the method of Marshall et al (5) from the observations given in the bulletin of the ISC. The m_b^{ML} estimates should be a more consistent measure of magnitude than the standard ISC m_b because station corrections are applied and allowance is made for the detection thresholds of the stations.

Also investigated is the effect on magnitude of the differences in attenuation in the upper mantle beneath the Shagan River test site and the Nevada test site (NTS). This is done by filtering the SP seismograms using the attenuation operator of Carpenter (6) with a t* of 0.2 s; t*, the ratio of travel time to specific quality factor, being assumed to be 0.2 s greater for paths out of NTS compared to those of E Kazakh (7).

The BB seismograms are not direct recordings but are derived by processing the recorded SP data. Two forms of BB seismogram are presented, one is an estimate of ground displacement at the station and the other is this estimate corrected for the effects of attenuation on the path between the test site and the array. The BB seismograms corrected for attenuation are referred to as the deconvolved seismograms. Following Lyman et al (8) the deconvolved seismograms are used to study the properties of the explosion source.

The main body of this report includes a description of the data used and the processing methods, and a discussion of the results. Appendix A contains the seismograms and appendix B contains tables of additional data from the seismograms not discussed in the main text. Appendix C shows the SP and BB seismograms of the 20 March 1976 earthquake which occurred near the test site. These seismograms allow a comparison to be made between the seismograms from the explosions and an earthquake located in the same region.

2. THE RECORDED SEISMOGRAMS

Most of the original data used in this report are SP array recordings. Figure 3 shows the layouts of the arrays, all have 19 or 20 vertical-component Willmore SP seismometers in two roughly perpendicular lines and their outputs are recorded on analogue or digital magnetic tape.

The sampling rate for both digitally recorded data and digitised analogue data is 20 samples per second. The frequency response of the SP recording system of one array is shown in figure 4. The actual responses of the arrays differ slightly at high frequencies from the response shown but such differences, and anyvariations in the system gain, are known and have been taken account of in the data processing. Full details of the array station are given in Mowat and Burch (9).

Table 3 shows what recorded data are available. For some of the explosions, array records are not available because the signal amplitude was so large the system overloaded. This is particularly true for YKA which has a lower noise level and thus is run at a higher sensitivity than the other stations. However, there is a velocity broad-band (VBB) instrument at YKA, operating at a lower gain than the SP array, and where possible the VBB is used when the SP channels are overloaded. The VBB seismograph has an amplitude response proportional to velocity in the range 0.1 to 5.0 Hz. There has also been, on occasion, a low-gain SP channel operating at the arrays. If available, this is used in place of the array recordings when these are overloaded even though the sensitivity of the low-gain SP channel is not known with enough confidence to allow amplitude measurements to be made. Absence of data can be due to a number of factors, such as: a lost or damaged magnetic tape, a failure in the time code, a failure in the recording system or erasure of the tape. One explosion, on 16 April 1974, was too small for its signal to be seen at EKA.

3. PROCESSING OF THE DATA

The seismograms are shown in appendix A, figures A1 to A176, each figure showing the SP and BB seismograms of one explosion recorded at one array. An index to these figures is provided in table 3. Seismogram (a) is the SP seismogram. Usually this is the array sum but if array recordings are not available, a directly recorded low-gain SP or a SP seismogram derived from a VBB channel (seismogram (e)) is used. Seismogram (b) is the same as (a) but filtered, using Carpenter's Q operator (6), for a t* of 0.2 s. Seismogram (c) is the BB version of seismogram (a). This is obtained by multiplying the spectrum of the signal by $|a(\omega)|/b(\omega)$ where $a(\omega)$ and $b(\omega)$ are the responses of the BB and SP instruments respectively at frequency ω. The amplitude response of the BB instrument is flat to displacement from 0.1 to 10 Hz. By using $|a(\omega)|$ rather than $a(\omega)$ all phase shifts due to the recording system are removed and so the system should have a minimal effect on pulse shapes (10). (In practice, the phase shifts only have a significant effect on pulse shape at the long periods - for short-duration explosion-generated pulses removing the BB phase shifts has a negligible effect.) In addition to the instrument conversion, each seismogram has been filtered using a single-channel Wiener filter (11) designed on the noise preceding the signal. A noise sample of 60 s duration is normally used although this sometimes has to be reduced when insufficient pre-signal noise is included in the edited file: the duration of the shortest noise sample used is about 25 s. The resulting BB seismogram gives, it is hoped, a reliable estimate of the true ground displacement at the recording station.

Seismogram (d) is the deconvolved seismogram derived in the same way as seismogram (c) except that an additional filter is included that corrects for, or "puts back", a path attenuation of $t^* = 0.15$ s. The value of 0.15 s is chosen to be consistent with estimates of the minimum attenuation for transmission paths from Central Asia to the four arrays (12).

4. ANALYSES AND RESULTS

In this section various observations made from the seismograms are described. The analyses carried out on these observations are also described†. It is assumed that the observations can be expressed, either directly or by taking logs, as the sum of a source effect, a station effect and an error. The effects are estimated in the presence of the error by least squares using the method of Douglas (13). The source terms are referred to as network effects and the station terms as station effects.

4.1 SP seismograms

For both the original and attenuated SP seismograms three different measurements of amplitude (A) are taken and two of period (T) (figure 5(a)). The amplitudes measured are A_{oa}, the height of the first peak; A_{ab}, first peak to first trough; and A_{bc}, the maximum peak-to-peak amplitude in the first few cycles - normally from the first trough to second peak. The periods measured are T_{ox}, the time from onset to the second crossing of the base-line, and T_{bc}, twice the time between the trough and peak used to define the A_{bc} amplitude. Log(A/T) (where A is the amplitude in nanometres corrected for the response of the instrument at period T) was calculated in three ways:-

$$\log(A/T)_{oa} = \log(A_{oa}/T_{ox})$$

$$\log(A/T)_{ab} = \log(\tfrac{1}{2}A_{ab}/T_{ox})$$

$$\log(A/T)_{pp} = \log(\tfrac{1}{2}A_{bc}/T_{bc})$$

If the b-c swing has an inflection (eg, see figure A87(a)) the period T_{ox} is used in place of T_{bc}. All the measurements of amplitude, period and log(A/T) are given in table B1.

A body-wave magnitude m_b at each array is given by,

$$m_b = \log(A/T)_{pp} + B(\Delta)$$

where $B(\Delta)$ (table 4(b)) is the Gutenberg-Richter (14) distance-correction factor. The magnitude estimates are given in table 4(a).

---

† The YKA recording of the 28 October 1979 Shagan River explosion was discovered and processed at a late stage during the preparation of this report. The measurements made from these seismograms (shown in figure A111.1) are not included in the least-squares analyses described here, although they are given in tables 4 to 8 and B2 to B9.

As only one seismogram has been lost due to signals being below station detection thresholds, there is no benefit in using the maximum-likelihood method to calculate magnitudes. Therefore, the network magnitude is calculated using the array magnitudes for those explosions recorded at two or more arrays. The station effects (table 4(b)) are then used to determine network magnitudes for the explosions recorded at only one station. The network magnitudes are listed in table 4(a). The "network bias" is the mean of the differences between the network magnitudes and the magnitudes published by Marshall et al (2). The value obtained (+ 0.12 magnitude units) can be used to calculate a station bias for each array, a term that can be subtracted from that station's magnitude for a Shagan River explosion to give an unbiased estimate of m_b. The station biases are given in table 4(b).

Magnitude estimates made using the other log (A/T) measurements and those made on the attenuated SP records are discussed in section 5(a).

4.2 BB seismograms

The rise time, duration and area of each initial P pulse, measured from the deconvolved seismograms, is given in tables 5 to 7. The manner in which such measurements are made is illustrated in figure 5.1.

The pulse rise time, τ, is a measure of the steepness of the leading edge of the pulse and is defined as the peak pulse amplitude divided by the maximum gradient on the leading edge (15). The network rise times and station effects are given in table 5.

Pulse duration, T_D, is initially taken as the time from the pulse onset to the time when the signal returns to the same amplitude level. On the rare occasions where the pulse does not return fully (eg, figure A35(d)), the time to its apparent end is taken. Sometimes, however, there appear to be two pulses arriving close together (eg, figure A19(d)). Why these double pulses are seen is not clear but if it is assumed that the first pulse represents the explosion P-wave that is to be measured, then the presence of the second pulse (possibly from tectonic release) would lead to an overestimate of the pulse duration and of the pulse area . For the double pulses a revised pulse duration is taken as the time from onset to the point where the interfering pulse apparently arrives (figure 5(c)). This value will be a slight underestimate of the actual duration of the first pulse. The network durations and station effects are given in table 6. If a revised pulse duration is used, it is flagged in table 6 and the initial estimate of pulse duration is given in table B2.

The area under the pulse is measured (see figure 5(b)) by integrating the pulse from its onset for its duration T_D. For double pulses this method should, it is hoped, produce a reasonable estimate of the area of the first pulse (see figure 5(c)). The pulse area after correction for the loss of amplitude due to geometrical spreading (16) and for amplification at the free surface at the recording station (assumed to be a factor of 2) provides an estimate of ψ_∞, the long-term level of the reduced displacement potential, in cubic metres. Table 7 gives log ψ_∞ with any revised values flagged (the original estimates of log ψ_∞ are given in table B3). Network values for log ψ_∞ and station effects are also given in table 7. The results in table 7 are repeated in table B4 where the estimates of ψ_∞, not their logarithms, are given.

The method used to obtain network values and station effects is designed for use with magnitudes where, since it is the logarithm of the amplitude that is being considered, the additive station effects represent factors which multiply the amplitude - caused by variations in both elastic (geometric spreading) and anelastic attenuation over the transmission path; that is departures from the average earth model implied by the distance correction factor, $B(\Delta)$. Pulse rise times and durations, however, are independent of absolute amplitude so the station effects reflect only the variations in path attenuation. Therefore, since for a source impulse both duration and rise time vary linearly with attenuation (15), the station effects are additive. The ψ_∞ estimates, on the other hand, should not be affected by variations in path attenuation (7): the only effect on pulse area of correcting for attenuation is to reduce the duration of the pulse sufficiently for the area to be measured uncontaminated by the effects of other arrivals. The station effects then reflect only variations in elastic attenuation and should be applied, as for magnitudes, to the logarithms of the estimates of ψ_∞.

It is interesting to compare the various station effects at a station. For EKA and YKA the effects are similar for ψ_∞, but for rise time and duration the observations at YKA are shorter than at EKA. The relatively large magnitudes measured at YKA are thus due to low attenuation on the Shagan River - YKA transmission path. For GBA, on the other hand, the effects are close to the mean for rise time and duration, but below average for ψ_∞. The small magnitudes measured at GBA are then probably not due to anelastic attenuation but to some property of the path that simply reduces the amplitude, such as focussing or defocussing of the wave front in the receiver region.

The results discussed above are measured on the deconvolved seismogram and so it is hoped should be estimates of source properties. The duration of the P pulse may however be affected by interference from the free-surface reflection pP. The pP-P time should be measurable on the seismograms but the identification of pP is not always straightforward and some of the estimated times may therefore be in error. The estimated delay times of the apparent pP are given in table 8; because of the doubts on the reliability of these, no attempt was to estimate network delay times, and hence the depths of the explosions. In many of the seismograms (eg, figure A43(d)) the apparent pP is seen, as expected, as a large negative pulse following immediately after P. The delay time is taken as the time between the peaks of the P and pP pulses since the pP onset is seldom clear. Sometimes, however, (eg, figure A20(d)), there appear to be two negative pulses following P which could be interpreted as the overshoot of P followed by pP (the delay times of the peaks of both pulses are included in table 8). In some examples the record seems to have no negative pulses after P (eg, figure A94(d)) or to have one which is most probably the overshoot of P (eg, figure A106(d)) and for some of the WRA records (eg, figure A83(d)) the second arrival is too late (> 1 s delay time) and of the wrong polarity to be pP.

5. DISCUSSION

5.1 Magnitudes

Figure 6 shows $\log(A/T)_{oa}$ and $\log(A/T)_{ab}$ plotted against $\log(A/T)_{pp}$ for all the measurements made on the original SP seismograms. Both plots show a clear linear relationship and least-squares lines through the data have slopes that are not significantly different at the 5% level from unity. The lines drawn in figure 6 are the least-squares fits with the slope constrained to unity and have intercepts at 0.41 and 0.15 for $\log(A/T)_{oa}$ and $\log(A/T)_{ab}$ respectively - these values are therefore the corrections that should be added to normalise the magnitudes to those measured using the peak-to-peak amplitude. Tables B5 and B6 contain estimates of m_b determined at each station using the oa and ab amplitudes and the network magnitudes and station effects. Notes that the scatter in figure 6 is less for the ab amplitudes than for the oa, which indicates that $\log(A/T)_{ab}$ may be the more stable measurement. However, the variances of the network-magnitude determinations are not significantly different at the 5% level from that obtained for the peak-to-peak amplitude data. A comparison of the three magnitudes with m_b^{ML} also shows no significant differences.

The peak-to-peak amplitudes on the attenuated SP seismograms are treated in the same manner as the original recordings. That is, magnitudes are determined for each station and estimates made of network and station effects (table B7). A similar procedure is carried out, after applying the corrections determined above, with the oa and ab amplitudes and the results are given in tables B8 and B9 respectively.

Figure 7 shows Δm_b, the difference between the estimates of network magnitude (peak-to-peak amplitude data) made from the original and attenuated seismograms for each explosion, as a function of the array-network m_b and so is a plot of the magnitude bias due to the attenuation. The mean value of this bias is 0.348 ± 0.041 (sample standard deviation). A least-squares line through the data (excluding the two explosions at low m_b and those explosions for which only one recording is available) shows a decrease in the bias with increasing m_b (figure 7). This relationship is,

$$\Delta m_b = - 0.034\ m_b \pm 0.544$$

and predicts a bias of 0.37 at m_b 5.0 and 0.32 at m_b 6.5.

Figure 8 shows Δm_b against m_b for the oa and ab amplitude data. The results are very similar to those in figure 7 and show that the magnitude bias does not depend on how the magnitude is measured.

The variation of the bias with magnitude seen in figures 7 and 8 arises because magnitude bias is frequency-dependent. The corner frequency of the P waves from small-magnitude explosions is higher than for larger explosions and thus the effects of attenuation are more pronounced (17). This makes comparison with other estimates of the NTS-Shagan River bias difficult. A bias of 0.3 units is an estimate which is often quoted (7) and the slightly higher estimate obtained here could well be due to the arrays' better high-frequency response compared to other SP seismographs such as the World Wide Standard Seismograph Network (WWSSN). Murphy and Tzeng (18) estimate the magnitude bias by comparing

signals recorded near NTS and Semipalatinsk from Aleutian Island's earthquakes. These earthquakes are of similar magnitude to the explosions considered here but were presumably of lower dominant frequency than observed for explosions. Murphy and Tzeng (18) estimate the magnitude bias as 0.24 ± 0.06 magnitude units and Δt^* to be 0.174 ± 0.042. Priestley et al (19) also compare the amplitudes of teleseismic signals recorded near the two test sites, but on seismographs with an extended high-frequency response and they estimate the bias to be 0.34 magnitude units.

5.2 Source size estimators

All the estimates made here that depend on source size, plus some estimates from other researchers are given in table 9. Three estimates of m_b from a global network (ISC data) are given: the mean reported by the ISC, the value calculated by Marshall et al (2) and m_b^{ML}. The network estimates of m_b calculated here are also listed.

The network estimates of pulse rise time, pulse duration and log ψ_∞ from the deconvolved BB records are given in table 9 together with estimates of seismic moment, M_o (20), calculated from ψ_∞ using

$$M_o = 4\pi\rho\alpha^2\psi_\infty$$

where ρ and α are respectively the density and the P-wave speed of the source material. Moment estimates for sources in granite (α = 5.0 km/s, ρ = 2.7 g/cc) and in a competent sediment (α = 4.2 km/, ρ = 2.4 g/cc) are given.

Table 9 includes two estimates of seismic moment for some of the explosions made by other researchers using surface-wave data, one from Sierra Geophysics (private communication) derived from the isotropic component of the source radiation in a constrained moment-tensor inversion and the other from Stevens (21) who calculates moments from the Rayleigh-wave spectra after an inversion for path effects.

A comparison of these estimates of source size should be made relative to the yields of the explosions but no yield data are available so following Lyman et al (8) m_b^{ML} is assumed to be a reliable estimate of log W, W being the yield in kilotons.

To allow the accuracy of the various estimates of source size to be compared, a measure of the scatter of the points about a best-fit line is needed. The standard deviation (σ) of the residuals about the line is used here but converted to the equivalent range in m_b^{ML}(σ_e).

Figure 9 shows the network m_b plotted against m_b^{ML}. The plot agrees well with the results presented in section 4.1 in which the network magnitudes are compared with those of Marshall et al (2): the array network is biased by, on average, + 0.12 magnitude units compared to the worldwide network. Examination of figure 9 indicates that the bias decreases slightly with increasing magnitude. A best least-squares line through the data (assuming no errors in m_b^{ML}) gives

$$m_b = 0.88\ (\pm\ 0.07)\ m_b^{ML} + 0.80\ (\pm\ 0.40),\ \sigma_e = 0.12$$

where the uncertainties are 95% confidence limits.

Figure 10 shows plots of the network rise time, τ, and duration, T_D, as functions of m_b^{ML} with the best least-squares lines of;

$$\tau = 0.037\ (\pm\ 0.011)\ m_b^{ML} - 0.010\ (\pm\ 0.066),\ \sigma_e = 0.68$$

and $$T_D = 0.12\ (\pm\ 0.039)\ m_b^{ML} - 0.10\ (\pm\ 0.23),\ \sigma_e = 0.61.$$

The scatter of these data is much larger than that of the body-wave magnitude and thus the rise times and durations do not appear to be useful for yield estimation.

Figure 11 shows the network log ψ_∞ plotted against m_b^{ML}. The best least-squares line through this data is

$$\log \psi_\infty = 1.08\ (\pm\ 0.08)\ m_b^{ML} - 2.52\ (\pm\ 0.47),\ \sigma_e = 0.12.$$

The errors in the fit are similar to those for the network magnitude and thus ψ_∞ as estimated here does seem to show promise as an indicator of yield. From theoretical considerations it is expected to be proportional to log W and it is assumed to be so for the discussion below.

In figure 12, the values of M_o calculated from the network ψ_∞ estimates are compared with the surface-wave M_o estimates; the source material is assumed to be granite. The body-wave moments are in remarkably good agreement with both the Sierra Geophysics and Stevens (21) moments, agreement being within a factor of 2 for almost all the explosions. Body-wave and surface-wave moments do not usually agree so well; for example the Lyman et al (8) estimates of ψ_∞ for NTS explosions give, on average, seismic moments a factor of 10 less than those of Stevens (21) (Douglas, private communication).

The duration and rise time of a seismic pulse should be inversely proportional to the corner frequency of the source. Thus the results should allow the scaling of the corner frequency of Shagan River explosions to be estimated. Figure 13 shows the network estimates of log τ and log T_D plotted against log ψ_∞ (= log W). Although there is a large scatter in the data, both τ and T_D do appear to increase with source size. Least-squares lines fitted to the data (assuming errors in both axes (22)) gives relationships of

$$\log \tau = 0.071\ (\pm\ 0.012)\ \log \psi_\infty - 0.963\ (\pm\ 0.077)$$

and $$\log T_D = 0.094\ (\pm\ 0.012)\ \log \psi_\infty - 0.581\ (\pm\ 0.075)$$

where the uncertainties represent one standard deviation, and the estimates of data error are taken from the least-squares analyses given earlier (tables 5 to 7). Thus the source corner frequency for Shagan River explosions scales, at the most, as $W^{-1/10}$. This is much less than the $W^{-1/3}$ scaling predicted by most source models (and seen by Lyman et al (8) in the rise times of NTS explosions) and the $W^{-1/5}$ scaling produced by a $W^{-1/3}$ source dependence combined with the effects of scaled depth of burial and assumed by Bache et al (23) in an analysis of the spectra of Shagan River explosions.

5.3 Division of the test site

Marshall et al (2) and Bache et al (23) demonstrate that the Shagan River test site can be divided into a north-east (NE) and south-west (SW) region as illustrated in figure 2 on the complexity of the SP waveforms recorded at the arrays. The variation in waveforms is discussed in the next section. The discussion below investigates whether the division can be seen in any of the measured parameters.

Network magnitudes and station effects estimated for each region of the test site shows no significant difference between the two sets of station effects. Similarly, no differences can be discerned in station effects for ψ_∞, pulse rise times or pulse durations. Therefore there appear to be no significant differences in the transmission paths from the two halves of the test site. When the source size estimates are examined relative to ψ_∞ there is no difference between the regions for magnitude or rise times. However, there is a significant difference in the pulse durations.

Figure 14 repeats the plot of figure 13(b), ie, log T_D against log ψ_∞, except that explosions in each region of the test site are identified. The two data sets do seem to separate and the best least-squares (no errors in log ψ_∞) lines through them are,

$$\text{NE:} \quad \log T_D = 0.118\ (\pm\ 0.038)\ \log \psi_\infty - 0.633\ (\pm\ 0.138)$$

$$\text{SW:} \quad \log T_D = 0.110\ (\pm\ 0.044)\ \log \psi_\infty - 0.666\ (\pm\ 0.170)$$

These lines are not significantly different (at the 5% level) in their slopes, but are significantly different (at the 1% level) in their intercepts. Thus the P pulses from explosions in the SW region of the test site are apparently of shorter duration than those from sources of the same size in the NE. It is significant that no such difference is evident in the pulse rise times. Both are measures of source duration and would be expected to vary together if the observed difference was due to the response of the source medium. Since they do not vary together, the results suggest that the apparent differences in pulse duration in the two parts of the test site is in fact due to differences in pP-P times, with the longer times in the NE presumably due to either a greater depth of burial or slower uphole P-wave speeds than in the SW.

The estimates of the pP delay time made from the deconvolved seismograms support the above hypothesis. Figure 15 shows, for each array, the estimates of delay time plotted as a function of m_b^{ML} (if two times are given in table 9, the later one is used - the earlier one is assumed to be for the overshoot of P). A separation can be seen similar to that seen for the pulse-durations in that the pP delay times seem to be larger for explosions in the NE than for those in the SW. There are some obvious exceptions to this, the longest pP delay times at YKA are from large SW explosions. Also the data from WRA shows no clear separation but this may be related to the difficulties in identifying pP discussed in section 4.2.

6. DISCUSSION OF SEISMOGRAMS

The seismograms shown in appendix A contain much of interest that will be used in the preparation of future publications. Two points are, however, discussed here, the waveform differences between the two regions of the test site and the anomalous waveforms observed from the seismic disturbance on 7 December 1976.

6.1 Division of the test site

Marshall et al's (2) division of the test site into two regions is illustrated in figure 16 which shows the SP waveforms at the four arrays from some NE and SW Shagan River explosions of various magnitudes. Examination of all the SP records (appendix A) confirms that these records are typical of their respective portions of the test site. In general, explosions in NE Shagan produce seismograms that are more complex than seen from those in SW Shagan at a particular station. Marshall et al (2) suggest that the differences in shape are due to a systematic difference in the corner frequencies of the explosions in the two parts of the test site. This is consistent with the pulse-duration results discussed in section 5.3, but not with those for pulse rise time. Thus the difference in shape is probably not a source corner-frequency effect but may be related to source depth. The deconvolved seismograms support this hypothesis.

Figure 17 shows the deconvolved BB versions of the SP seismograms shown in figure 16. There are two clear differences between the sets of waveforms that are common to all but one of the stations. First, the negative pulse (presumably pP) following immediately after the first positive pulse seems to be of larger amplitude, but shorter duration for the SW than the NE explosions: WRA is the exception. The second difference (Marshall et al's (2) complexity difference) is that at three of the stations, the signals from the NE explosions exhibit a coda of one or two cycles of energy with a longer period than the P pulse. This coda energy is much smaller, if present, in the signals from the SW explosions. WRA is again the exception: it does show more coda energy in the signals from the explosions in the NE but this is at periods very similar to that of the P pulse. However, the interpretation of the records at WRA is made difficult by the expected arrival of PcP a few seconds after P. Finally, it should be noted that the waveform differences between the stations for either NE or SW explosions are as large as the differences between the two areas at any one station.

6.2 The seismic disturbance of 7 December 1976

The GBA seismograms from the 7 December 1976 disturbance in SW Shagan do not show waveforms typical of explosions in that part of the test site. The EKA seismograms, however, do show typical waveforms. This is illustrated in figures 18 and 19 which show, respectively, the SP and deconvolved seismograms at GBA and EKA from the anomalous (7 December 1976) disturbance compared to those from a nearby explosion (29 June 1980) of comparable size. No records are available for YKA or WRA for the 7 December 1976 disturbance. The GBA SP seismogram from the anomalous disturbance has an unusual emergent P-wave onset (which is why this disturbance plots away from the main cluster of data points in figures 6(a) and 6(b)) and the deconvolved seismogram shows two positive pulses followed by a negative pulse, whereas that of the 29 June 1980

explosion shows a single positive pulse followed by a negative; the negative pulse for the 29 June 1980 explosion being of shorter duration that that of the anomalous disturbance. The form of the anomalous seismograms suggests that the 7 December 1976 disturbance was in fact a double explosion - the seismograms are very similar to those recorded from what Stewart and Marshall (24) interpret as a double explosion at Novaya Zemlya.

To investigate the possibility that the 7 December 1976 disturbance was a double explosion the deconvolved waveform at GBA from the 29 June 1980 explosion is used to try and simulate that from the anomalous disturbance. Figure 20 shows the waveform added to itself for a range of time shifts, the earlier arrival having an amplitude 0.3 times that of the later: the value of 0.3 is the measured relative amplitude of the two positive pulses in the deconvolved GBA record of the 7 December 1976 disturbance. At a relative time shift of 0.4 to 0.45 s there is a remarkable similarity between the model and the anomalous waveform, not only in the initial double pulse but also in the broadening and asymmetry of the following negative pulse. A double explosion would thus explain the anomalous GBA seismogram very well and the time between the arrivals measured from the record is 0.41 s. If there was a double explosion, their signals would have to arrive together at EKA to explain the similarity of the deconvolved P pulses from the two explosions there.

Assuming that the two explosions were fired simultaneously and that they were broadside-on relative to EKA (figure 21), the measured time difference of 0.41 s at GBA gives, for a phase velocity of 13.1 km s^{-1}, a separation of 5.4 km. The assumed phase velocity comes from the slowness of 8.4 s deg^{-1} predicted for a distance of 36.4° from GBA by the results of Corbishley (25). However, the rate of change in slowness is large at this distance, so the estimate of the separation may be significantly in error. Errors may also arise due to the assumptions on the geometry of the explosions or from errors in the estimated delay times. However, the observed seismograms are consistent with the 7 December 1976 disturbance being a double explosion, with the smaller of the two about 5½ km south-west of the larger.

7. CONCLUSIONS

The main purpose of the report is to present the SP and BB seismograms for 62 explosions at the Shagan River test site. Some analyses on the data have, however, also been carried out. The main conclusions arising from these analyses are as follows:-

(a) Estimates of the array-network magnitudes (m_b) determined from peak-to-peak SP amplitudes are 0.12 magnitude units greater than those of the world network.

(b) The bias between the NTS and Shagan River test sites due to differences in upper mantle attenuation (assumed to be equivalent to a t* difference of 0.2 s) is estimated to have a value of around 0.34 magnitude units but is frequency and hence magnitude dependent.

(c) The long-term level of the reduced displacement potential, ψ_∞, derived from the area of the BB pulse appears to be a reliable estimator of explosion size.

(d) The seismic moments calculated from ψ_∞ are in good agreement with published moments calculated from surface-wave data.

(e) From the variation of pulse rise time and duration with ψ_∞ it appears that the corner frequency of Shagan River explosions scales with yield much more slowly than would be predicted by theoretical considerations or from observations of NTS explosions in tuff. This may be due to the greater competence of the source material at Shagan River.

(f) The pulse durations of explosions in the NE portion of the test site are systematically longer than those of explosions in the SW. This is probably due to some difference in pP-P time between the two areas, eg, different scaled depths of burial, or uphole P-wave speed, or both.

(g) One of the disturbances generated waveforms unlike those normally seen. The deconvolved records show that this disturbance, on 7 December 1976, was probably a double explosion.

8. ACKNOWLEDGEMENTS

The recordings from the array stations were made available through the co-operation of the Eskdalemuir Array Station; the Earth Physics Branch, Department of Energy, Mines and Resources, Ottawa, Canada; the Bhabha Atomic Research Centre, Trombay, India; and the Australian National University (ANU), Canberra, Australia. The recordings from Australia were made available by the Natural Environmental Research Council (NERC) of the United Kingdom in co-operation with ANU. The conscientious work of the staff at all the arrays over the years has produced an unequalled collection of data, only a small part of which is presented in this report.

REFERENCES

1. H I S Thirlaway: "Seismology and Fundamental Geology". Discovery, 43-48 (May 1966)

2. P D Marshall, T C Bache and R C Lilwall: "Body Wave Magnitudes and Locations of Soviet Underground Explosions at the Semipalatinsk Test Site". AWRE Report No. O 16/84 (re-issue), HMSO (1985)

3. A Douglas: "Joint Epicentre Determination". Nature, 215, 47-48 (1967)

4. M J Shore: "Seismic Travel-Time Anomalies from Events in the Western Soviet Union". Bull Seism Soc Am, 72, 113-128 (1982)

5. P D Marshall, R C Lilwall and J Farthing: "Body Wave Magnitudes and Locations of Underground Nuclear Explosions at the Nevada Test Site 1971-1980". AWRE Report No. O 21/86, HMSO (1986)

6. E W Carpenter: "Absorption of Elastic Waves - An Operator for a Constant Q Mechanism". AWRE Report No. O 43/66, HMSO (1966)

7. A Douglas: "Differences in Upper Mantle Attenuation between the Nevada and Shagan River Test Sites: Can the Effects be seen in P-wave Seismograms?" Bull Seism Soc Am, 77, 270-276 (1987)

8. N S Lyman, A Douglas, P D Marshall and J B Young: "P Seismograms Recorded at Eskdalemuir, Scotland from Explosions in Nevada, USA". AWRE Report No. O 10/86, HMSO (1986)

9. W M H Mowat and R F Burch: "Handbook for the Stations which Provide Seismograms to the Blacknest Seismological Centre, United Kingdom". AWRE Blacknest Tech Report 44/47/29, Blacknest, Brimpton, Brimpton RG7 4RS (1977, revised 1985)

10. R C Stewart and A Douglas: "Seismograms from Phaseless Seismographs". Geophys J R Astr Soc, 72, 517-521 (1983)

11. A Douglas and J B Young: "The Estimation of Seismic Body Wave Signals in the Presence of Oceanic Microseims". AWRE Report No. O 14/81, HMSO (1981)

12. T C Bache, P D Marshall and L B Bache: "Q for Teleseismic P-Waves from Central Asia". J Geophys Res, 90, 3575-3587 (1985)

13. A Douglas: "A Special Purpose Least-Squares Programme". AWRE Report No. O 54/66, HMSO (1966)

14. B Gutenberg and C F Richter: "Magnitude and Energy of Earthquakes". Annali Geofis, 9, 1-15 (1956)

15. R C Stewart: "Q and the Rise and Fall of a Seismic Pulse". Geophys J R Astr Soc, 76, 793-805 (1984)

16. E W Carpenter: "A Quantitative Evaluation of Teleseismic Explosion Records". Proc Roy Soc, A, 290, 396-407 (1966)

17. P D Marshall, D L Springer and H C Rodean: "Magnitude Corrections for Attenuation in the Upper Mantle". Geophys J R Astr Soc, 57, 609-638 (1979)

18. J R Murphy and T K Tzeng: "Estimation of Magnitude/Yield Bias between the NTS and Semipalatinsk Nuclear Testing Areas". Systems, Science and Software, Report SSS-R-82-5603 (1982)

19. K F Priestley, D E Charez and J N Brune: "A Direct Estimate of m_b Bias between Eastern Kazakh and Nevada". Trans AGU EOS, 68, 362 (1987)

20. K Aki, M Bouchon and P Reasenberg: "Seismic Source Function for an Underground Nuclear Explosion". Bull Seism Soc Am, 64, 131-148 (1974)

21. J L Stevens: "Estimation of Scalar Moments from Explosion-Generated Surface Waves". Bull Seism Soc Am, 76, 123-151 (1986)

22. J H Williamson: "Least-Squares Fitting of a Straight Line". Can J Phys, 46, 1845-1847 (1968)

23. T C Bache, P D Marshall and J B Young: "Q and Its Effect on Short-Period P-Waves from Explosions in Central Asia". AWRE Report No. O 17/84, HMSO (1984)

24. R C Stewart and P D Marshall: "Seismic P-Waves from Novaya Zemlya Explosions: Seeing Double!" Geophysical Journal, 92, 335-338 (1988)

25. D J Corbishley: "Multiple Array Measurements of P-wave Travel-Time Derivative". Geophys J R Astr Soc, 19, 1-14 (1970)

26. C I Pooley, A Douglas and R G Pearce: "The Seismic Disturbance of 1976, March 20, East Kazakhstan: Earthquake or Explosions?" Geophys J R Astr Soc, 74, 621-631 (1983)

27. O Sandvin and D Tjostheim: "Multivariate Autoregressive Representation of Seismic P-wave Signals with Application to Short-Period Discrimination". Bull Seism Soc Am, 68, 735-756 (1978)

TABLE 1

Seismic Arrays Which Provide Data to MOD(PE), Blacknest

	Array Locations				Distances and Azimuths Relative to Shagan River Test Site		
	Array	Location	Geographic Co-ordinates of Crossover Point		Distance (Degrees)	Azimuth (Degrees Clockwise from North)	Back Bearing
			Latitude	Longitude			
1	EKA	Eskdalemuir, UK	55°19'59"N	3°09'32"W	47.1	310	60
2	YKA	Yellowknife, Canada	62°29'36"N	114°36'19"W	67.0	7	351
3	GBA	Gauribidanur, India	13°36'15"N	77°26'10"E	36.4	182	2
4	WRA	Warramunga, Australia	19°56'52"S	134°21'03"E	85.3	129	328

ARRAY OPERATORS

1. MOD(PE), Blacknest, UK
2. Department of Energy, Mines & Resources, Ottawa, Canada
3. Bhabha Atomic Research Centre, Trombay, India
4. Australian National University, Canberra, Australia.

TABLE 2

Shagan River Explosions: Epicentres and Least-Squares Estimates of Magnitude from Marshall et al (2)

no.	date	origin time (UTC)	latitude °N	longitude °E	m_b
01	15.01.65	05 59 58.40	49.940	79.010	5.85
02	19.06.68	05 05 57.31	49.982	79.003	5.35
03	30.11.69	03 32 57.07	49.913	78.961	6.00
04	30.06.71	03 56 57.37	49.949	78.986	5.29
05	10.02.72	05 02 57.52	50.014	78.878	5.37
06	02.11.72	01 26 57.62	49.923	78.815	6.14
07	10.12.72	04 27 07.31	50.001	78.973	6.00
08	23.07.73	01 22 57.64	49.962	78.812	6.18
09	14.12.73	07 46 57.15	50.044	78.987	5.82
10	16.04.74	05 52 57.40	50.041	78.943	4.44
11	31.05.74	03 26 57.47	49.950	78.852	5.83
12	16.10.74	06 32 57.58	49.979	78.898	5.47
13	27.12.74	05 46 56.87	49.943	79.011	5.50
14	27.04.75	05 36 57.25	49.949	78.926	5.56
15	30.06.75	03 26 57.58	50.004	78.957	4.63
16	29.10.75	04 46 57.33	49.946	78.878	5.74
17	25.12.75	05 16 57.16	50.044	78.814	5.70
18	21.04.76	05 02 57.19	49.890	78.827	5.28
19	09.06.76	03 02 57.23	49.989	79.022	5.12
20	04.07.76	02 56 57.46	49.909	78.911	5.81
21	28.08.76	02 56 57.48	49.969	78.930	5.82
22	23.11.76	05 02 57.28	50.008	78.963	5.87
23	07.12.76	04 56 57.38	49.922	78.846	5.90
24	29.05.77	02 56 57.58	49.937	78.770	5.77
25	29.06.77	03 06 57.76	50.006	78.869	5.22
26	05.09.77	03 02 57.34	50.035	78.921	5.74
27	29.10.77	03 07 02.47	50.069	78.975	5.54
28	30.11.77	04 06 57.36	49.958	78.885	5.92
29	11.06.78	02 56 57.57	49.898	78.797	5.86
30	05.07.78	02 46 57.47	49.887	78.871	5.83
31	29.08.78	02 37 06.25	50.000	78.978	5.95
32	15.09.78	02 36 57.42	49.916	78.879	5.99
33	04.11.78	05 05 57.32	50.034	78.943	5.56
34	29.11.78	04 33 02.49	49.949	78.798	6.07
35	01.02.79	04 12 57.64	50.090	78.870	5.38
36	23.06.79	02 56 57.52	49.903	78.855	6.22
37	07.07.79	03 46 57.33	50.026	78.991	5.83
38	04.08.79	03 56 57.09	49.894	78.904	6.16
39	18.08.79	02 51 57.13	49.943	78.938	6.12
40	28.10.79	03 16 56.94	49.973	78.997	5.96
41	02.12.79	04 36 57.45	49.891	78.796	6.01
42	23.12.79	04 56 57.44	49.916	78.755	6.18
43	25.04.80	03 56 57.53	49.973	78.755	5.50
44	12.06.80	03 26 57.62	49.980	79.001	5.59
45	29.06.80	02 32 57.69	49.939	78.815	5.74
46	14.09.80	02 42 39.13	49.921	78.802	6.21
47	12.10.80	03 34 14.10	49.961	79.028	5.90
48	14.12.80	03 47 06.40	49.899	78.938	5.95
49	27.12.80	04 09 08.08	50.057	78.981	5.88
50	29.03.81	04 03 50.03	50.007	78.982	5.61
51	22.04.81	01 17 11.34	49.885	78.810	6.05
52	27.05.81	03 58 12.34	49.985	78.980	5.46
53	13.09.81	02 17 18.25	49.910	78.915	6.18
54	18.10.81	03 57 02.64	49.923	78.859	6.11
55	29.11.81	03 35 08.60	49.887	78.860	5.73
56	27.12.81	03 43 14.13	49.923	78.795	6.31
57	25.04.82	03 23 05.37	49.903	78.913	6.1*
58	04.07.82	01 17 14.20	49.960	78.807	6.1*
59	31.08.82	01 31 00.70	49.924	78.761	5.4*
60	05.12.82	03 37 12.55	49.919	78.813	6.1*
61	26.12.82	03 35 14.20	50.071	78.988	5.7*

* m_b from NEIC PDE service

TABLE 3

Availability of Array Data for the Shagan River Explosions

no.	date	EKA	YKA	GBA	WRA
01	15.01.65	a (1)	n/a	n/a	n/a
02	19.06.68	a (2)	a (3)	a (4)	a (5)
03	30.11.69	a (6)	n/a	ov	a (7)
04	30.06.71	a (8)	a (9)	a (10)	a (11)
05	10.02.72	a (12)	n/a	n/a	a (13)
06	02.11.72	a (14)	sm (15)	n/a	ov
07	10.12.72	a (16)	sm (17)	n/a	ov
08	23.07.73	ov	sm (18)	ov	ov
09	14.12.73	a (19)	sm (20)	n/a	ov
10	16.04.74	ns	a (21)	n/a	n/a
11	31.05.74	a (22)	sm (23)	ov	n/a
12	16.10.74	a (24)	a (25)	a (26)	n/a
13	27.12.74	a (27)	a (28)	a (29)	n/a
14	27.04.75	a (30)	a (31)	a (32)	n/a
15	30.06.75	a (33)	a (34)	a (35)	n/a
16	29.10.75	a (36)	a (37)	a (38)	a (39)
17	25.12.75	a (40)	a (41)	a (42)	a (43)
18	21.04.76	a (44)	a (45)	a (46)	n/a
19	09.06.76	a (47)	a (48)	a (49)	n/a
20	04.07.76	a (50)	ov	n/a	n/a
21	28.08.76	a (51)	a (52)	a (53)	n/a
22	23.11.76	a (54)	ov	a (55)	n/a
23	07.12.76	a (56)	ov	a (57)	n/a
24	29.05.77	a (58)	ov	ov	n/a
25	29.06.77	a (59)	a (60)	a (61)	a (62)
26	05.09.77	a (63)	ov	a (64)	a (65)
27	29.10.77	a (66)	ov	a (67)	a (68)
28	30.11.77	a (69)	ov	sm (70)	a (71)
29	11.06.78	a (72)	vbb (73)	a (74)	a (75)
30	05.07.78	a (76)	vbb (77)	a (78)	a (79)
31	29.08.78	a (80)	vbb (81)	a (82)	a (83)
32	15.09.78	a (84)	vbb (85)	ov	a (86)
33	04.11.78	a (87)	vbb (88)	a (89)	a (90)
34	29.11.78	a (91)	vbb (92)	sm (93)	a (94)
35	01.02.79	a (95)	a (96)	a (97)	n/a
36	23.06.79	a (98)	vbb (99)	ov	a (100)
37	07.07.79	a (101)	vbb (102)	n/a	n/a
38	04.08.79	a (103)	vbb (104)	a (105)	a (106)
39	18.08.79	a (107)	vbb (108)	a (109)	a (110)
40	28.10.79	a (111)	vbb (111.1)	ov	a (112)
41	02.12.79	a (113)	ov	ov	a (114)
42	23.12.79	a (115)	ov	n/a	ov
43	25.04.80	n/a	a (116)	a (117)	a (118)
44	12.06.80	n/a	vbb (119)	a (120)	a (121)
45	29.06.80	a (122)	vbb (123)	a (124)	a (125)
46	14.09.80	ov	ov	a (126)	ov
47	12.10.80	a (127)	vbb (128)	a (129)	a (130)
48	14.12.80	a (131)	vbb (132)	a (133)	a (134)
49	27.12.80	a (135)	n/a	a (136)	a (137)
50	29.03.81	a (138)	vbb (139)	a (140)	n/a
51	22.04.81	a (141)	n/a	a (142)	a (143)
52	27.05.81	a (144)	vbb (145)	a (146)	a (147)
53	13.09.81	a (148)	vbb (149)	a (150)	a (151)
54	18.10.81	a (152)	vbb (153)	a (154)	a (155)
55	29.11.81	a (156)	vbb (157)	a (158)	a (159)
56	27.12.81	ov	vbb (160)	a (161)	ov
57	25.04.82	n/a	n/a	a (162)	a (163)
58	04.07.82	a (164)	ov	a (165)	ov
59	31.08.82	a (166)	a (167)	a (168)	a (169)
60	05.12.82	a (170)	vbb (171)	n/a	a (172)
61	26.12.82	a (173)	vbb (174)	a (175)	a (176)

Key

a	available
vbb	array overloaded, velocity broad band used (YKA only)
sm	array overloaded, strong motion channel used - gain unknown
ov	array overloaded
ns	not seen
n/a	not available

The number given in brackets is that of the figure in Appendix A which shows the data

TABLE 4

Shagan River Explosions: Magnitudes

a) Magnitude estimated at each station with network values and confidence limits (determined excluding the value marked x).

no.	date	EKA	YKA	GBA	WRA	network mean	95% c.l.
01	15.01.65	5.98				5.96	
02	19.06.68	5.70	5.86	5.06	5.77	5.60	0.16
03	30.11.69	6.30			6.02	6.14	0.22
04	30.06.71	5.34	5.70	5.12	5.01	5.29	0.16
05	10.02.72	5.58			5.62	5.58	0.22
06	02.11.72	6.41				6.39	
07	10.12.72	6.08				6.06	
08	23.07.73						
09	14.12.73	5.91				5.89	
10	16.04.74		4.99			4.75	
11	31.05.74	6.20				6.18	
12	16.10.74	5.44	5.62	5.11		5.40	0.18
13	27.12.74	5.24	5.67	5.02		5.32	0.18
14	27.04.75	5.80	5.89	5.55		5.76	0.18
15	30.06.75	4.75	4.92	4.41		4.71	0.18
16	29.10.75	5.90	5.98	5.52	5.18	5.72	0.17
17	25.12.75	6.02	5.97	5.68	5.62	5.82	0.16
18	21.04.76	5.35	5.71	5.06		5.38	0.18
19	09.06.76	5.04	5.70	5.10		5.29	0.18
20	04.07.76	6.17				6.15	
21	28.08.76	5.99	5.91	5.57		5.84	0.18
22	23.11.76	5.98		5.53		5.89	0.21
23	07.12.76	6.11		5.60		6.00	0.21
24	29.05.77	6.15				6.13	
25	29.06.77	5.49	5.70	5.19	5.09	5.37	0.16
26	05.09.77	6.08		5.71	5.95	6.00	0.18
27	29.10.77	5.87		5.40	5.99	5.83	0.18
28	30.11.77	6.24			5.86	6.02	0.22
29	11.06.78	6.18	6.44	5.70	6.23	6.14	0.16
30	05.07.78	6.12	6.20	5.84	6.12	6.07	0.16
31	29.08.78	6.11	6.42	5.69	6.24	6.12	0.16
32	15.09.78	6.21	6.32		6.17	6.14	0.18
33	04.11.78	5.78	6.13	5.41	5.84	5.79	0.16
34	29.11.78	6.37	6.53		6.20	6.27	0.18
35	01.02.79	5.60	5.92	5.48		5.68	0.18
36	23.06.79	6.01	6.54		6.39	6.22	0.18
37	07.07.79	5.50	6.39			5.82	0.22
38	04.08.79	6.06	6.40	6.13	6.32	6.23	0.16
39	18.08.79	6.02	6.34	6.17	6.16	6.17	0.16
40	28.10.79	5.66	6.46x		6.30	5.96	0.22
41	02.12.79	5.90			6.28	6.06	0.22
42	23.12.79	6.21				6.19	
43	25.04.80		5.89	5.35	5.87	5.71	0.18
44	12.06.80		5.99	5.41	5.91	5.78	0.18
45	29.06.80	6.02	6.22	5.69	6.07	6.00	0.16
46	14.09.80			6.15		6.44	
47	12.10.80	5.92	6.17	5.76	6.14	6.00	0.16
48	14.12.80	6.17	5.99	5.97	6.01	6.04	0.16
49	27.12.80	6.02		5.46	6.20	5.97	0.18
50	29.03.81	5.59	6.01	5.31		5.65	0.18
51	22.04.81	6.24		5.89	6.23	6.20	0.18
52	27.05.81	5.61	5.75	5.12	5.61	5.52	0.16
53	13.09.81	6.41	6.41	6.14	6.28	6.31	0.16
54	18.10.81	6.28	6.32	5.93	6.27	6.20	0.16
55	29.11.81	5.85	5.94	5.52	5.72	5.76	0.16
56	27.12.81		6.57	6.12		6.37	0.22
57	25.04.82			6.04	6.24	6.27	0.22
58	04.07.82	6.37		6.01		6.33	0.21
59	31.08.82	5.55	5.78	5.08	5.60	5.50	0.16
60	05.12.82	6.27	6.44		6.24	6.22	0.18
61	26.12.82	5.83	6.14	5.32	5.99	5.82	0.16

b) Array distance correction factors, station effects and station biases.

Array	B(Δ)	Station effect	95% c.l.	Station bias
EKA	3.90	0.02	0.04	0.14
YKA	4.00	0.24	0.05	0.36
GBA	3.56	-0.29	0.04	-0.17
WRA	3.97	0.03	0.05	0.15

TABLE 5

Shagan River Explosions: Pulse Rise Times (in seconds)

no.	date	EKA	YKA	GBA	WRA	network mean	95% c.l.
01	15.01.65	0.208				0.177	
02	19.06.68	0.198	0.135	0.192	0.140	0.166	0.031
03	30.11.69	0.232			0.175	0.195	0.043
04	30.06.71	0.205	0.168	0.132	0.134	0.160	0.031
05	10.02.72	0.235			0.205	0.212	0.043
06	02.11.72	0.277	0.148			0.209	0.043
07	10.12.72	0.274	0.179			0.223	0.043
08	23.07.73		0.249			0.273	
09	14.12.73	0.228	0.161			0.191	0.043
10	16.04.74		0.153			0.177	
11	31.05.74	0.245	0.195			0.217	0.043
12	16.10.74	0.205	0.218	0.190		0.199	0.035
13	27.12.74	0.198	0.160	0.200		0.181	0.035
14	27.04.75	0.222	0.235	0.202		0.215	0.035
15	30.06.75	0.165	0.185	0.185		0.174	0.035
16	29.10.75	0.225	0.203	0.222	0.202	0.213	0.031
17	25.12.75	0.220	0.280	0.182	0.188	0.214	0.031
18	21.04.76	0.135	0.152	0.208		0.160	0.035
19	09.06.76	0.165	0.232	0.170		0.185	0.035
20	04.07.76	0.242				0.211	
21	28.08.76	0.218	0.268	0.205		0.225	0.035
22	23.11.76	0.262		0.188		0.206	0.043
23	07.12.76	0.238		0.207		0.203	0.042
24	29.05.77	0.228				0.197	
25	29.06.77	0.185	0.245	0.190	0.165	0.195	0.031
26	05.09.77	0.282		0.245	0.208	0.237	0.035
27	29.10.77	0.211		0.160	0.171	0.173	0.035
28	30.11.77	0.235		0.191	0.244	0.215	0.035
29	11.06.78	0.245	0.168	0.216	0.168	0.199	0.031
30	05.07.78	0.225	0.121	0.228	0.180	0.189	0.031
31	29.08.78	0.250	0.165	0.185	0.192	0.198	0.031
32	15.09.78	0.225	0.165		0.212	0.203	0.035
33	04.11.78	0.225	0.170	0.192	0.175	0.191	0.031
34	29.11.78	0.282	0.153	0.257	0.177	0.217	0.031
35	01.02.79	0.245	0.170	0.198		0.200	0.035
36	23.06.79	0.270	0.154		0.174	0.202	0.035
37	07.07.79	0.252	0.162			0.204	0.043
38	04.08.79	0.245	0.175	0.245	0.185	0.212	0.031
39	18.08.79	0.218	0.163	0.221	0.235	0.209	0.031
40	28.10.79	0.258	0.135x		0.188	0.215	0.043
41	02.12.79	0.245			0.210	0.219	0.043
42	23.12.79	0.290				0.259	
43	25.04.80		0.192	0.230	0.170	0.208	0.035
44	12.06.80		0.171	0.210	0.158	0.190	0.035
45	29.06.80	0.240	0.140	0.224	0.175	0.195	0.031
46	14.09.80			0.250		0.242	
47	12.10.80	0.230	0.142	0.232	0.172	0.194	0.031
48	14.12.80	0.252	0.147	0.228	0.242	0.217	0.031
49	27.12.80	0.228		0.168	0.178	0.183	0.035
50	29.03.81	0.235	0.226	0.190		0.212	0.035
51	22.04.81	0.278		0.240	0.172	0.222	0.035
52	27.05.81	0.224	0.119	0.202	0.147	0.173	0.031
53	13.09.81	0.240	0.185	0.232	0.218	0.219	0.031
54	18.10.81	0.280	0.152	0.250	0.182	0.216	0.031
55	29.11.81	0.218	0.107	0.218	0.160	0.176	0.031
56	27.12.81		0.177	0.242		0.218	0.043
57	25.04.82			0.232	0.230	0.234	0.043
58	04.07.82	0.276		0.250		0.244	0.042
59	31.08.82	0.135	0.148	0.165	0.165	0.153	0.031
60	05.12.82	0.260	0.136		0.198	0.201	0.035
61	26.12.82	0.220	0.158	0.182	0.188	0.187	0.031
station effect		0.031	-0.024	0.008	-0.014		
95% c.l.		0.008	0.009	0.008	0.009		

Network values and station effects determined excluding the value marked x.

TABLE 6

Shagan River Explosions: Pulse Durations (in seconds)

no.	date	EKA	YKA	GBA	WRA	network mean	95% c.l.
01	15.01.65	0.65*				0.56	
02	19.06.68	0.59	0.41	0.68	0.43	0.53	0.09
03	30.11.69	0.66			0.61	0.61	0.12
04	30.06.71	0.52	0.46	0.44	0.34	0.44	0.09
05	10.02.72	0.50*			0.35*	0.40	0.12
06	02.11.72	0.80	0.54			0.66	0.12
07	10.12.72	1.05	0.52			0.77	0.12
08	23.07.73		0.65			0.71	
09	14.12.73	0.55*	0.47			0.50	0.12
10	16.04.74		0.36			0.42	
11	31.05.74	0.58	0.57			0.56	0.12
12	16.10.74	0.55*	0.67	0.59		0.59	0.10
13	27.12.74	0.60	0.40*	0.64		0.54	0.10
14	27.04.75	0.62	0.65	0.58		0.61	0.10
15	30.06.75	0.50*	0.52	0.55		0.51	0.10
16	29.10.75	0.60	0.62	0.54	0.71	0.62	0.09
17	25.12.75	0.67	0.71	0.45	0.52	0.59	0.09
18	21.04.76	0.48	0.48	0.52		0.48	0.10
19	09.06.76	0.58	0.60	0.50		0.55	0.10
20	04.07.76	0.68				0.59	
21	28.08.76	0.75	0.60*	0.64		0.65	0.10
22	23.11.76	0.75*		0.54		0.60	0.12
23	07.12.76	0.62		0.78		0.65	0.12
24	29.05.77	0.56				0.47	
25	29.06.77	0.50*	0.58	0.41	0.61	0.52	0.09
26	05.09.77	0.92		0.61	0.69	0.72	0.10
27	29.10.77	0.88		0.59	0.58	0.66	0.10
28	30.11.77	0.65		0.44	0.70	0.58	0.10
29	11.06.78	0.64	0.45	0.56	0.48	0.53	0.09
30	05.07.78	0.68	0.43	0.61	0.44	0.54	0.09
31	29.08.78	0.83	0.53	0.58	0.60	0.64	0.09
32	15.09.78	0.63	0.60		0.61	0.62	0.10
33	04.11.78	0.84	0.47	0.66	0.62	0.65	0.09
34	29.11.78	0.66	0.47	0.60	0.60	0.58	0.09
35	01.02.79	0.60	0.51	0.49		0.52	0.10
36	23.06.79	0.70	0.50		0.65	0.62	0.10
37	07.07.79	0.92	0.45			0.67	0.12
38	04.08.79	0.68	0.60	0.72	0.66	0.66	0.09
39	18.08.79	0.74	0.62	0.72	0.74	0.70	0.09
40	28.10.79	0.88	0.48x		0.57	0.70	0.12
41	02.12.79	0.65			0.55	0.57	0.12
42	23.12.79	0.61				0.52	
43	25.04.80		0.54	0.56	0.51	0.57	0.10
44	12.06.80		0.48	0.61	0.55	0.58	0.10
45	29.06.80	0.60	0.37	0.56	0.48	0.50	0.09
46	14.09.80			0.67		0.66	
47	12.10.80	0.87	0.54	0.69	0.59	0.67	0.09
48	14.12.80	0.79	0.57	0.65	0.68	0.67	0.09
49	27.12.80	0.65*		0.68	0.51	0.59	0.10
50	29.03.81	0.67	0.48	0.50		0.54	0.10
51	22.04.81	0.72		0.70	0.54	0.63	0.10
52	27.05.81	0.85	0.50	0.60	0.45	0.60	0.09
53	13.09.81	0.73	0.62	0.65	0.53	0.63	0.09
54	18.10.81	0.71	0.46	0.65	0.56	0.60	0.09
55	29.11.81	0.62	0.38	0.61	0.43	0.51	0.09
56	27.12.81		0.54	0.63		0.61	0.12
57	25.04.82			0.68	0.65	0.68	0.12
58	04.07.82	0.68		0.68		0.63	0.12
59	31.08.82	0.48	0.44	0.42	0.43	0.44	0.09
60	05.12.82	0.61	0.43		0.63	0.56	0.10
61	26.12.82	0.60*	0.43	0.64	0.51	0.54	0.09
station effect		0.09	-0.06	0.01	-0.03		
95% c.l.		0.02	0.02	0.02	0.03		

Network values and station effects determined excluding the value marked x. Data marked * are revised values.

TABLE 7

Shagan River Explosions: Estimates of Log ψ_∞

no.	date	EKA	YKA	GBA	WRA	network mean	95% c.l.
01	15.01.65	3.92*				3.87	
02	19.06.68	3.40	3.28	3.20	3.35	3.31	0.14
03	30.11.69	4.13			3.92	4.00	0.20
04	30.06.71	3.00	3.28	3.02	2.59	2.98	0.14
05	10.02.72	3.40*			3.08*	3.22	0.20
06	02.11.72	4.43				4.38	
07	10.12.72	4.43				4.38	
08	23.07.73						
09	14.12.73	3.89*				3.84	
10	16.04.74		2.30			2.25	
11	31.05.74	3.93				3.88	
12	16.10.74	3.17*	3.37	2.98		3.17	0.16
13	27.12.74	3.03	3.17*	3.03		3.07	0.16
14	27.04.75	3.64	3.65	3.36		3.55	0.16
15	30.06.75	2.36*	2.45	2.40		2.40	0.16
16	29.10.75	3.61	3.64	3.38	3.02	3.42	0.14
17	25.12.75	3.87	3.80	3.43	3.24	3.59	0.14
18	21.04.76	2.98	3.18	2.90		3.02	0.16
19	09.06.76	2.90	3.37	2.98		3.08	0.16
20	04.07.76	3.94				3.89	
21	28.08.76	3.74	3.71*	3.58		3.68	0.16
22	23.11.76	4.02*		3.57		3.81	0.20
23	07.12.76	3.95		3.62		3.80	0.20
24	29.05.77	3.85				3.80	
25	29.06.77	3.07*	3.19	2.96	2.93	3.04	0.14
26	05.09.77	4.11		3.70	3.92	3.93	0.16
27	29.10.77	3.83		3.59	3.78	3.75	0.16
28	30.11.77	4.05			3.83	3.92	0.20
29	11.06.78	3.97	3.91	3.71	3.89	3.87	0.14
30	05.07.78	3.97	3.72	3.76	3.83	3.82	0.14
31	29.08.78	4.08	4.06	3.77	4.00	3.98	0.14
32	15.09.78	4.01	4.00		3.96	3.96	0.16
33	04.11.78	3.75	3.68	3.54	3.68	3.66	0.14
34	29.11.78	4.21	4.03		4.09	4.08	0.16
35	01.02.79	3.37	3.38	3.15		3.30	0.16
36	23.06.79	3.92	4.13		4.30	4.08	0.16
37	07.07.79	3.62	3.93			3.73	0.20
38	04.08.79	3.92	4.12	4.22	4.25	4.13	0.14
39	18.08.79	3.94	4.16	4.23	4.20	4.13	0.14
40	28.10.79	3.76	4.04x		4.13	3.92	0.20
41	02.12.79	3.64			4.08	3.84	0.20
42	23.12.79	3.97				3.92	
43	25.04.80		3.52	3.39	3.43	3.46	0.16
44	12.06.80		3.56	3.46	3.58	3.55	0.16
45	29.06.80	3.77	3.67	3.69	3.71	3.71	0.14
46	14.09.80			4.28		4.36	
47	12.10.80	4.01	3.86	3.93	3.99	3.95	0.14
48	14.12.80	4.15	3.78	4.00	3.99	3.98	0.14
49	27.12.80	3.92*		3.78	3.92	3.89	0.16
50	29.03.81	3.37	3.49	3.28		3.38	0.16
51	22.04.81	4.14		4.00	4.03	4.07	0.16
52	27.05.81	3.50	3.33	3.21	3.26	3.32	0.14
53	13.09.81	4.31	4.14	4.17	4.11	4.18	0.14
54	18.10.81	4.21	3.91	4.02	4.06	4.05	0.14
55	29.11.81	3.69	3.37	3.53	3.52	3.53	0.14
56	27.12.81		4.15	4.19		4.19	0.20
57	25.04.82			4.10	4.13	4.16	0.20
58	04.07.82	4.29		4.15		4.24	0.20
59	31.08.82	2.96	3.14	2.93	3.10	3.03	0.14
60	05.12.82	4.05	3.95		4.10	4.01	0.16
61	26.12.82	3.64*	3.59	3.49	3.68	3.60	0.14
station effect		0.05	0.05	-0.08	-0.01		
95% c.l.		0.04	0.04	0.04	0.04		

Network values and station effects determined excluding the value marked x. Data marked * are revised values.

TABLE 8

Shagan River Explosions: pP Delay Times (in seconds)

no.	date	EKA	YKA	GBA	WRA
01	15.01.65	0.67			
02	19.06.68	0.73	0.25 0.79	(0.63)	0.25
03	30.11.69	0.63			0.54
04	30.06.71	0.63	0.42 0.79	0.59	(0.52)
05	10.02.72	0.63			0.42
06	02.11.72	0.69	0.38 0.86		
07	10.12.72	0.86	0.33 0.73		
08	23.07.73		0.46		
09	14.12.73	0.84	0.29 0.79		
10	16.04.74		0.27		
11	31.05.74	0.50	0.42		
12	16.10.74	0.63	0.40	0.40 0.61	
13	27.12.74	0.71	0.40 0.77	0.73	
14	27.04.75	0.54	0.44	0.33(0.63)	
15	30.06.75	0.46	0.44	*	
16	29.10.75	0.48	0.52	0.40	0.42
17	25.12.75	0.44	0.52	0.21(0.44)	0.42
18	21.04.76	0.42	0.42	0.42	
19	09.06.76	0.61	0.42	0.42	
20	04.07.76	0.61			
21	28.08.76	0.63	0.79	0.67	
22	23.11.76	0.73		0.88	
23	07.12.76	0.38		0.63	
24	29.05.77	0.25 0.67			
25	29.06.77	0.63	0.42	0.40	0.61
26	05.09.77	0.67		0.42 0.86	0.63
27	29.10.77	0.52 0.86		0.77	*
28	30.11.77	0.61		0.42 0.73	(0.40)
29	11.06.78	0.42	0.42	0.63	(0.31)
30	05.07.78	0.61	0.42	0.56	0.42 0.75
31	29.08.78	0.67	0.38 0.73	0.73	(0.40)
32	15.09.78	0.61	0.40 0.71		0.42 0.75
33	04.11.78	0.63	0.42(0.67)	0.42 0.84	(0.42)
34	29.11.78	0.42 0.75	0.42	0.67	*
35	01.02.79	0.79	0.42	0.40 0.63	
36	23.06.79	0.54	0.44 0.94		*
37	07.07.79	0.84	0.40 0.77		
38	04.08.79	0.46	0.42 0.86	0.54	(0.42)
39	18.08.79	0.48	0.42 0.84	0.48	0.59
40	28.10.79	0.63	0.44 0.73		0.42
41	02.12.79	0.42			(0.42)
42	23.12.79	0.40 0.61			
43	25.04.80		0.42	0.59	0.40
44	12.06.80		0.42 0.73	0.46 0.84	0.38
45	29.06.80	0.42 0.84	0.42 0.79	0.63	0.36 0.73
46	14.09.80			0.65	
47	12.10.80	0.63	0.46 0.71	0.61	0.46
48	14.12.80	0.63	0.73	0.50	0.42 0.73
49	27.12.80	0.61 0.73		0.77	(0.33)
50	29.03.81	0.73	0.42 0.84	0.46 0.71	
51	22.04.81	0.61 0.84		0.61	0.63
52	27.05.81	0.73	0.44 0.63	0.42 0.73	0.33
53	13.09.81	0.63	0.82	0.50	0.42 0.82
54	18.10.81	0.46 0.79	0.42 0.92	0.59	0.42(0.77)
55	29.11.81	0.56	0.38	0.59	0.38 0.77
56	27.12.81		0.42	0.54	
57	25.04.82			0.59	0.42 0.84
58	04.07.82	0.88		0.63	
59	31.08.82	0.42	0.42	0.42 0.63	0.40
60	05.12.82	0.42 0.75	0.42 0.86		0.40 0.67
61	26.12.82	0.46 0.84	0.38 0.73	0.63	0.36

key: ( ) very weak phase * no arrival or can't be measured

TABLE 9

Source Size Estimators for the Shaqan River Explosion

no.	date	ISC m_b	LSMF $m_b(2)$	m_b^{ML}	array m_b	T_D (s)	τ (s)	log Ψ_∞ ($logm^3$)	$logM_o$ granite (logNm)	$logM_o$ sediment (logNm)	$logM_o$ (Sierra) (logNm)	$logM_o$(LR) (21) (logNm)	loc.
01	15.01.65	5.8	5.85	5.95	5.96*	0.56*	0.177*	3.87*	15.80*	15.60*			NE
02	19.06.68	5.4	5.35	5.38	5.60	0.53	0.166	3.31	15.24	15.04			NE
03	30.11.69	6.0	6.00	6.09	6.14	0.61	0.195	4.00	15.93	15.73			NE
04	30.06.71	5.2	5.29	5.07	5.29	0.44	0.160	2.98	14.91	14.71			NE
05	10.02.72	5.4	5.37	5.38	5.58	0.40	0.212	3.22	15.15	14.95			NE
06	02.11.72	6.1	6.14	6.23	6.39*	0.66	0.209	4.38*	16.31*	16.11*			SW
07	10.12.72	6.0	6.00	6.02	6.06*	0.77	0.223	4.38*	16.31*	16.11*			NE
08	23.07.73	6.1	6.18	6.31		0.71*	0.273*						SW
09	14.12.73	5.8	5.82	5.88	5.89*	0.50	0.191	3.84*	15.77*	15.57*			NE
10	16.04.74	4.9	4.44	4.37	4.75*	0.42*	0.177*	2.25*	14.18*	13.98*			NE
11	31.05.74	5.9	5.83	5.88	6.18*	0.56	0.217	3.88*	15.81*	15.61*			SW
12	16.10.74	5.5	5.47	5.49	5.40	0.59	0.199	3.17	15.10	14.90			NE
13	27.12.74	5.6	5.50	5.57	5.32	0.54	0.181	3.07	15.00	14.80			NE
14	27.04.75	5.6	5.56	5.58	5.76	0.61	0.215	3.55	15.48	15.28			NE
15	30.06.75	5.0	4.63	4.54	4.71	0.51	0.174	2.40	14.33	14.13			NE
16	29.10.75	5.8	5.74	5.70	5.72	0.62	0.213	3.42	15.35	15.15			SW
17	25.12.75	5.7	5.70	5.76	5.82	0.59	0.214	3.59	15.52	15.32			NE
18	21.04.76	5.3	5.28	5.19	5.38	0.48	0.160	3.02	14.95	14.75			SW
19	09.06.76	5.3	5.12	5.16	5.29	0.55	0.185	3.08	15.01	14.81			NE
20	04.07.76	5.8	5.81	5.90	6.15*	0.59*	0.211*	3.89*	15.82*	15.62*		15.73	SW
21	28.08.76	5.8	5.82	5.81	5.84	0.65	0.225	3.68	15.61	15.41			NE
22	23.11.76	5.8	5.87	5.85	5.89	0.60	0.206	3.83	15.76	15.56			NE
23	07.12.76	5.9	5.90	5.89	6.00	0.65	0.203	3.80	15.73	15.53			SW
24	29.05.77	5.8	5.77	5.82	6.13*	0.47*	0.197*	3.80*	15.73*	15.53*			SW
25	29.06.77	5.3	5.22	5.29	5.37	0.52	0.195	3.04	14.97	14.77			NE
26	05.09.77	5.8	5.74	5.80	6.00	0.72	0.237	3.93	15.86	15.66			NE
27	29.10.77	5.6	5.54	5.64	5.83	0.66	0.173	3.75	15.68	15.48			NE
28	30.11.77	6.0	5.92	5.97	6.02	0.58	0.215	3.92	15.85	15.65			SW
29	11.06.78	5.9	5.86	5.92	6.14	0.53	0.199	3.87	15.80	15.60		15.94	SW
30	05.07.78	5.8	5.83	5.86	6.07	0.54	0.189	3.82	15.75	15.55			SW
31	29.08.78	5.9	5.95	6.00	6.12	0.64	0.198	3.98	15.91	15.71	15.76		NE
32	15.09.78	6.0	5.99	6.06	6.14	0.62	0.203	3.96	15.89	15.69	15.93	15.74	SW

TABLE 9 (Cont'd)

no.	date	ISC m_b	LSMF $m_b(2)$	m_b^{ML}	array m_b	T_D (s)	τ (s)	log Ψ_∞ (logm^3)	logM$_o$ granite (logNm)	logM$_o$ sediment (logNm)	logM$_o$ (Sierra) (logNm)	logM$_o$(LR) (21) (logNm)	loc.
33	04.11.78	5.6	5.56	5.64	5.79	0.65	0.191	3.66	15.59	15.39	15.74		NE
34	29.11.78	6.0	6.07	6.07	6.27	0.58	0.217	4.08	16.01	15.81	15.96	15.75	SW
35	01.02.79	5.4	5.38	5.37	5.68	0.52	0.200	3.30	15.23	15.03			NE
36	23.06.79	6.2	6.22	6.28	6.22	0.62	0.202	4.08	16.01	15.81	16.15	15.83	SW
37	07.07.79	5.8	5.83	5.87	5.82	0.67	0.204	3.73	15.66	15.46	15.83		NE
38	04.08.79	6.1	6.16	6.23	6.23	0.66	0.212	4.13	16.06	15.86	16.16	15.94	SW
39	18.08.79	6.1	6.12	6.24	6.17	0.70	0.209	4.13	16.06	15.86	15.87	15.69	NE
40	28.10.79	6.0	5.96	6.02	5.96	0.70	0.215	3.92	15.85	15.65	16.17	15.85	NE
41	02.12.79	6.0	6.01	6.09	6.06	0.57	0.219	3.84	15.77	15.57	16.04	15.96	SW
42	23.12.79	6.2	6.18	6.25	6.19*	0.52*	0.259*	3.92*	15.85*	15.65*	15.83	15.66	SW
43	25.04.80	5.5	5.50	5.52	5.71	0.57	0.208	3.46	15.39	15.19			SW
44	12.06.80	6.0	5.59	5.59	5.78	0.58	0.190	3.55	15.48	15.28	15.35		NE
45	29.06.80	5.7	5.74	5.78	6.00	0.50	0.195	3.71	15.64	15.44	15.49		SW
46	14.09.80	6.2	6.21	6.30	6.44*	0.66*	0.242*	4.36*	16.29*	16.09*	16.20	15.86	SW
47	12.10.80	5.9	5.90	5.95	6.00	0.67	0.194	3.95	15.88	15.68	16.06	15.94	NE
48	14.12.80	5.9	5.95	6.03	6.04	0.67	0.217	3.98	15.91	15.71	15.97		SW
49	27.12.80	5.9	5.88	5.87	5.97	0.59	0.183	3.89	15.82	15.62	15.35		NE
50	29.03.81	5.6	5.61	5.56	5.65	0.54	0.212	3.38	15.31	15.11	15.64		NE
51	22.04.81	6.0	6.05	6.02	6.20	0.63	0.222	4.07	16.00	15.80	16.00	15.92	SW
52	27.05.81	5.5	5.46	5.38	5.52	0.60	0.173	3.32	15.25	15.05			NE
53	13.09.81	6.1	6.18	6.17	6.31	0.63	0.219	4.18	16.11	15.91	16.13	15.87	SW
54	18.10.81	6.1	6.11	6.12	6.20	0.60	0.216	4.05	15.98	15.78		15.91	SW
55	29.11.81	5.7	5.73	5.70	5.76	0.51	0.176	3.53	15.46	15.26			SW
56	27.12.81	6.2	6.31	6.34	6.37	0.61	0.218	4.19	16.12	15.92		15.92	SW
57	25.04.82	6.1		6.14	6.27	0.68	0.234	4.16	16.09	15.89		15.85	SW
58	04.07.82	6.1		6.18	6.33	0.63	0.244	4.24	16.17	15.97			SW
59	31.08.82	5.3		5.27	5.50	0.44	0.153	3.03	14.96	14.76			SW
60	05.12.82	6.1		6.14	6.22	0.56	0.201	4.01	15.94	15.74		15.92	SW
61	26.12.82	5.7		5.65	5.82	0.54	0.187	3.60	15.53	15.33			NE

* values to which only one station of the four arrays contributes data

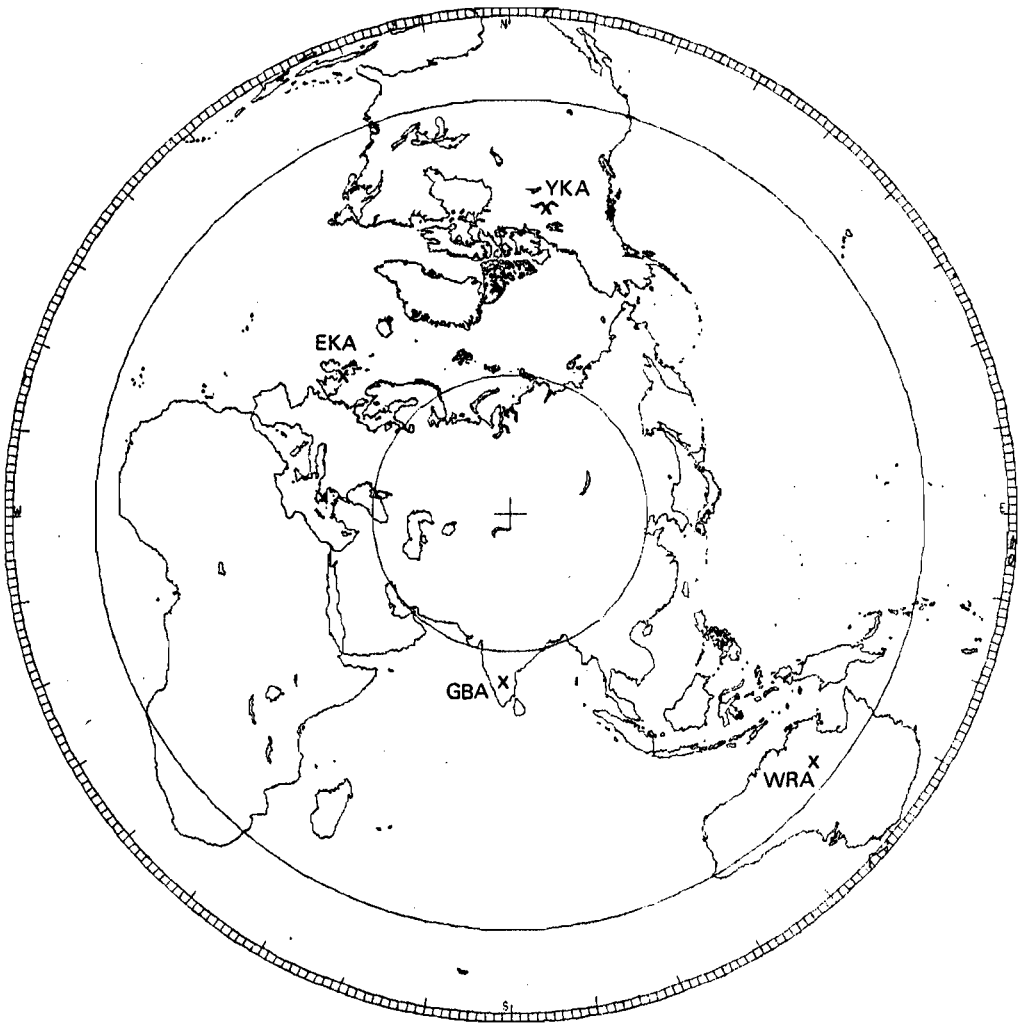

FIGURE 1. EPICENTRAL DISTANCE-AZIMUTH PROJECTION OF THE WORLD CENTRED ON THE SHAGAN RIVER TEST SITE (50°N 79°E) OUT TO 110°. THE LOCATIONS OF THE FOUR ARRAYS ARE SHOWN. THE TWO CIRCLES REPRESENT EPICENTRAL DISTANCES OF 30 AND 90° FROM THE TEST SITE

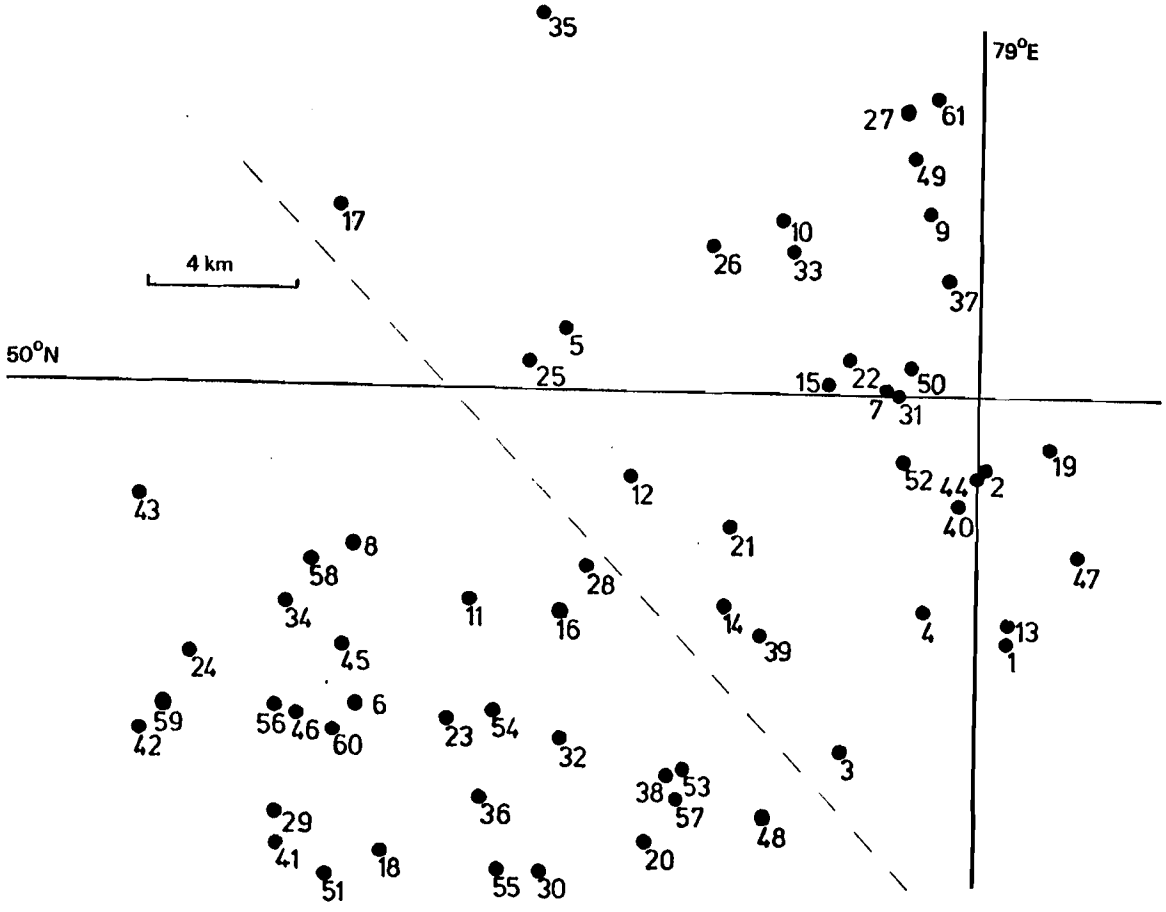

FIGURE 2. LOCATIONS OF THE SHAGAN RIVER EXPLOSIONS (AFTER MARSHALL ET AL (2)). THE DASHED LINE DIVIDES THE TEST SITE INTO ITS NORTH-EAST AND SOUTH-WEST REGIONS

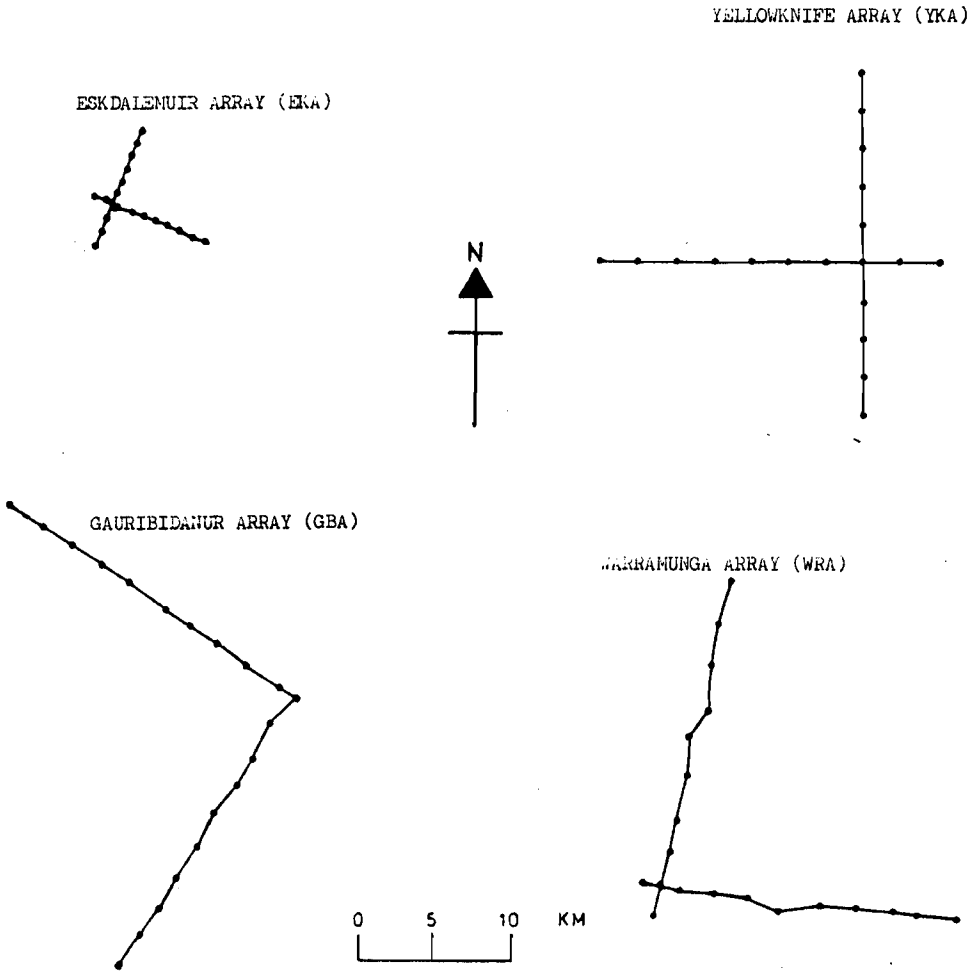

FIGURE 3. PLANS OF THE SHORT-PERIOD ARRAYS. EACH DOT REPRESENTS A SEISMOMETER IN THE ARRAY

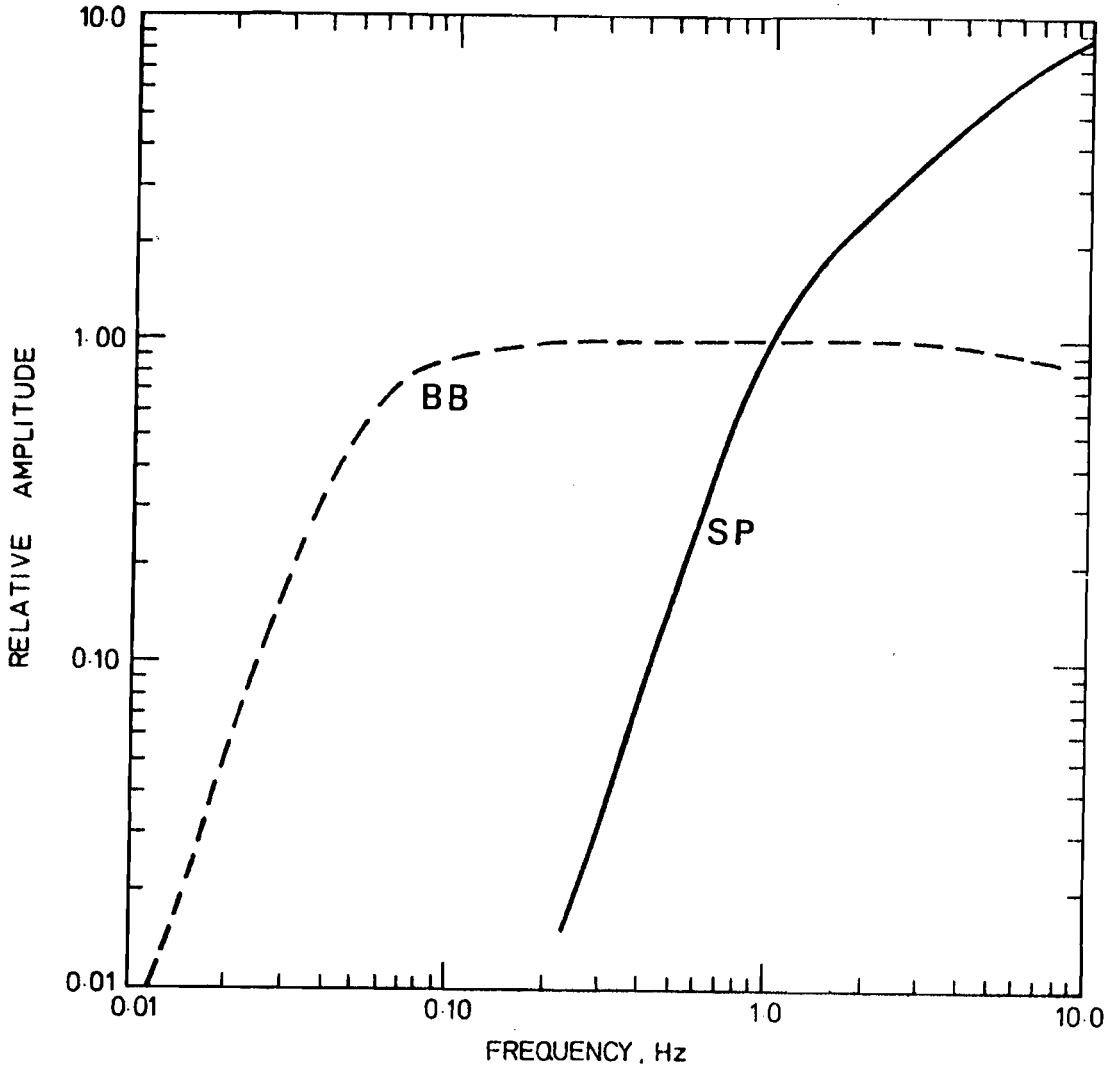

FIGURE 4. AMPLITUDE RESPONSE OF THE DISPLACEMENT BROAD-BAND (BB) AND ARRAY SHORT-PERIOD (SP) SEISMOGRAPHS. GAINS ARE NORMALISED TO UNITY AT 1 Hz

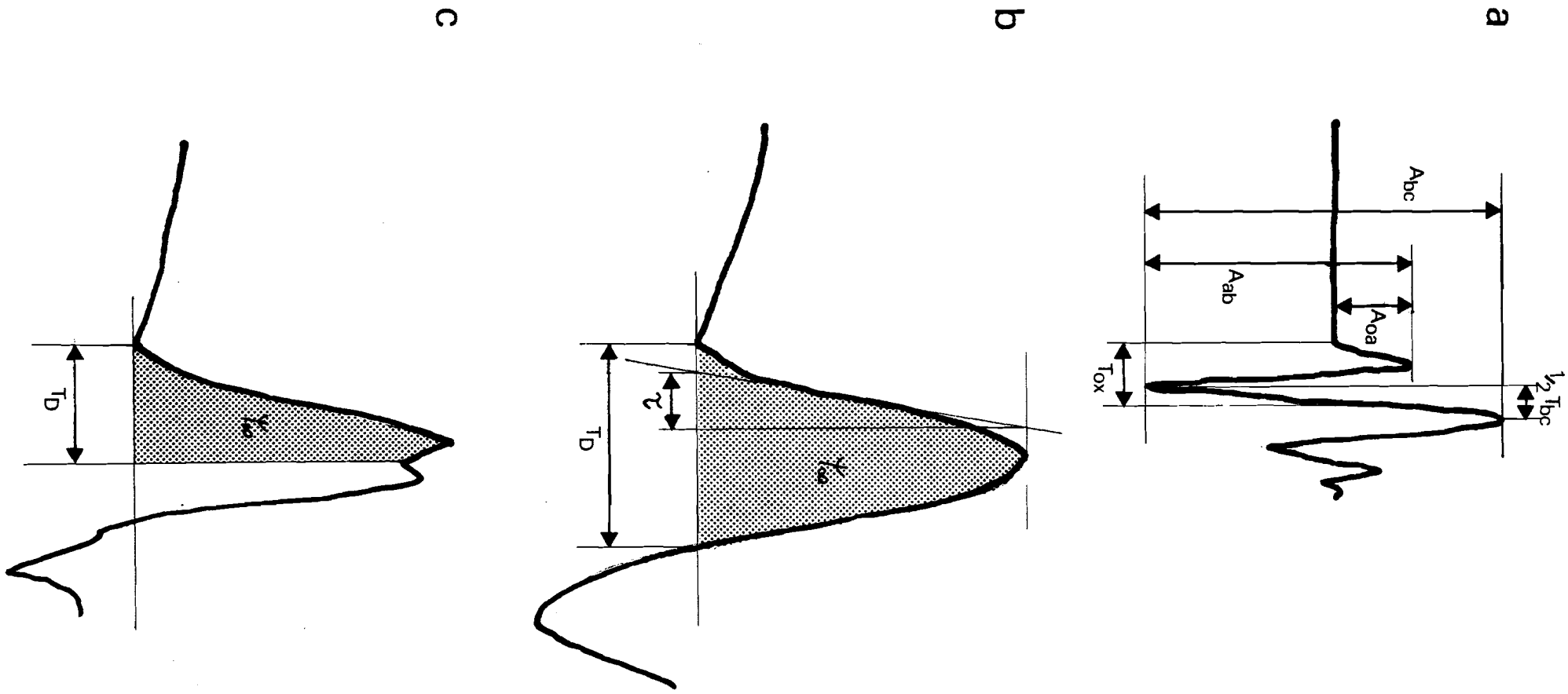

FIGURE 5. ILLUSTRATION OF MEASUREMENTS MADE ON SEISMOGRAMS

(a) The three measures of amplitude and two of period made on SP recordings.

(b) Rise time, duration and area measured on deconvolved BB pulses.

(c) Revised measures of duration and pulse area made on deconvolved BB signals interpreted as being double pulses.

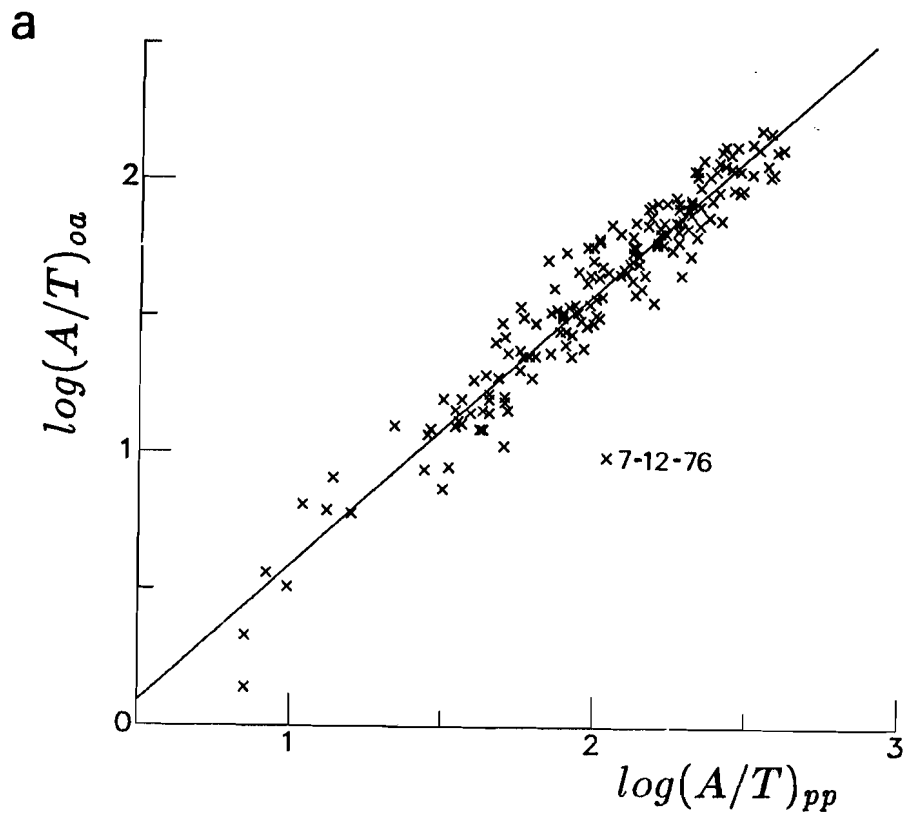

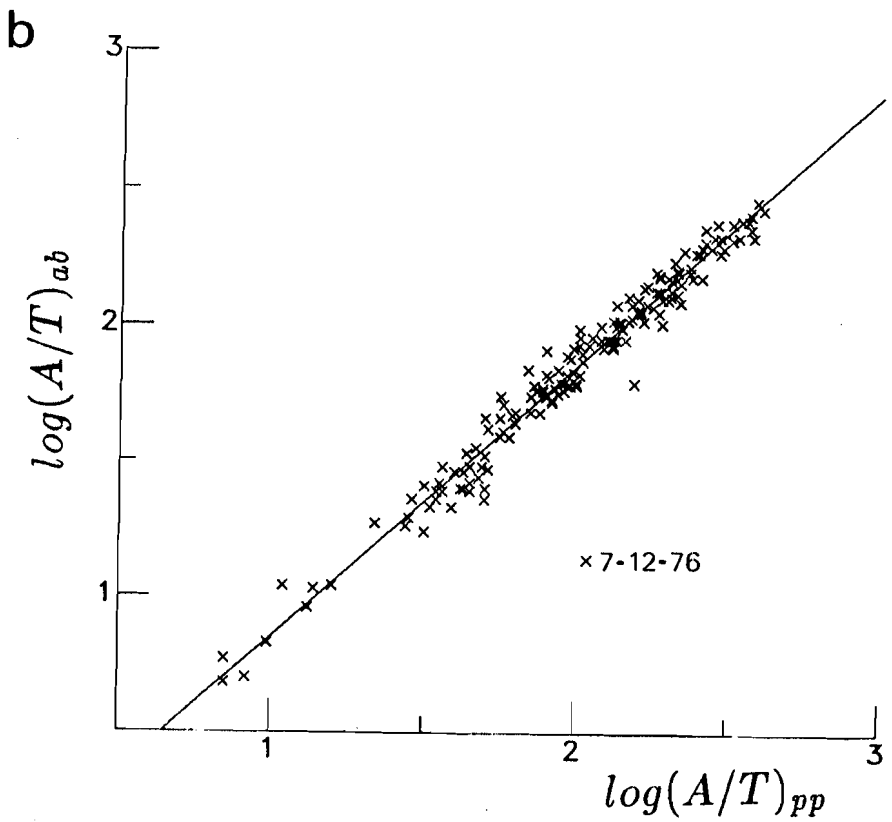

FIGURE 6. PLOTS OF THE ALTERNATIVE MEASUREMENTS OF LOG (A/T) AGAINST PEAK-TO-PEAK LOG (A/T). THE VALUES ESTIMATED FROM THE GBA RECORDING OF THE PRESUMED DOUBLE EXPLOSION ON 7 DECEMBER 1976 ARE ANNOTATED. LINES DRAWN THROUGH THE DATA ARE THE BEST LEAST-SQUARES STRAIGHT LINE WITH A SLOPE OF UNITY

(a) oa amplitudes

(b) ab amplitudes

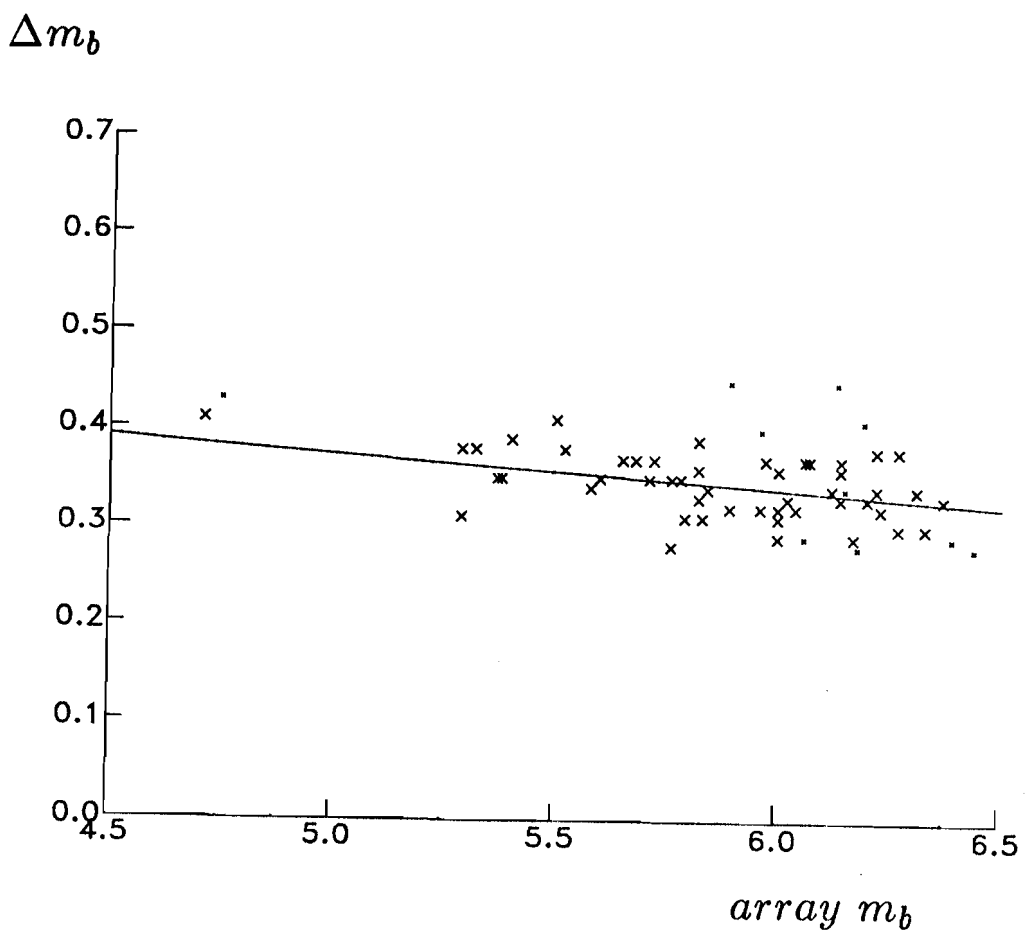

FIGURE 7. ATTENUATION BIAS. HERE THE DECREASE IN THE ARRAY-NETWORK MAGNITUDE (PEAK-TO-PEAK) DUE TO ATTENUATION OF t* = 0.2 s IS PLOTTED AGAINST THE ARRAY-NETWORK MAGNITUDE. THE LINE DRAWN THROUGH THE DATA IS THE BEST LEAST-SQUARES STRAIGHT LINE: CALCULATED EXCLUDING THE TWO POINTS BELOW m_b 5.0 AND THOSE FOR WHICH ONLY ONE STATION SUPPLIED DATA (PLOTTED AS THE SMALLER CROSSES)

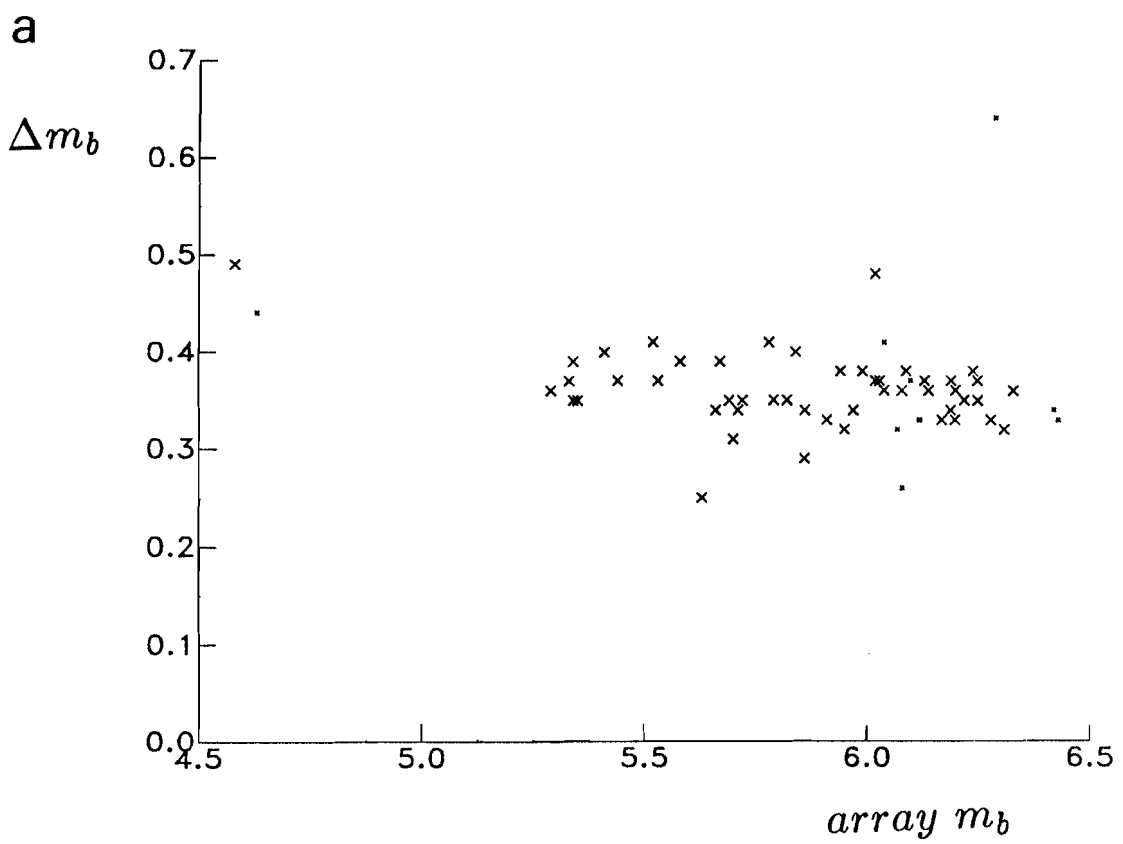

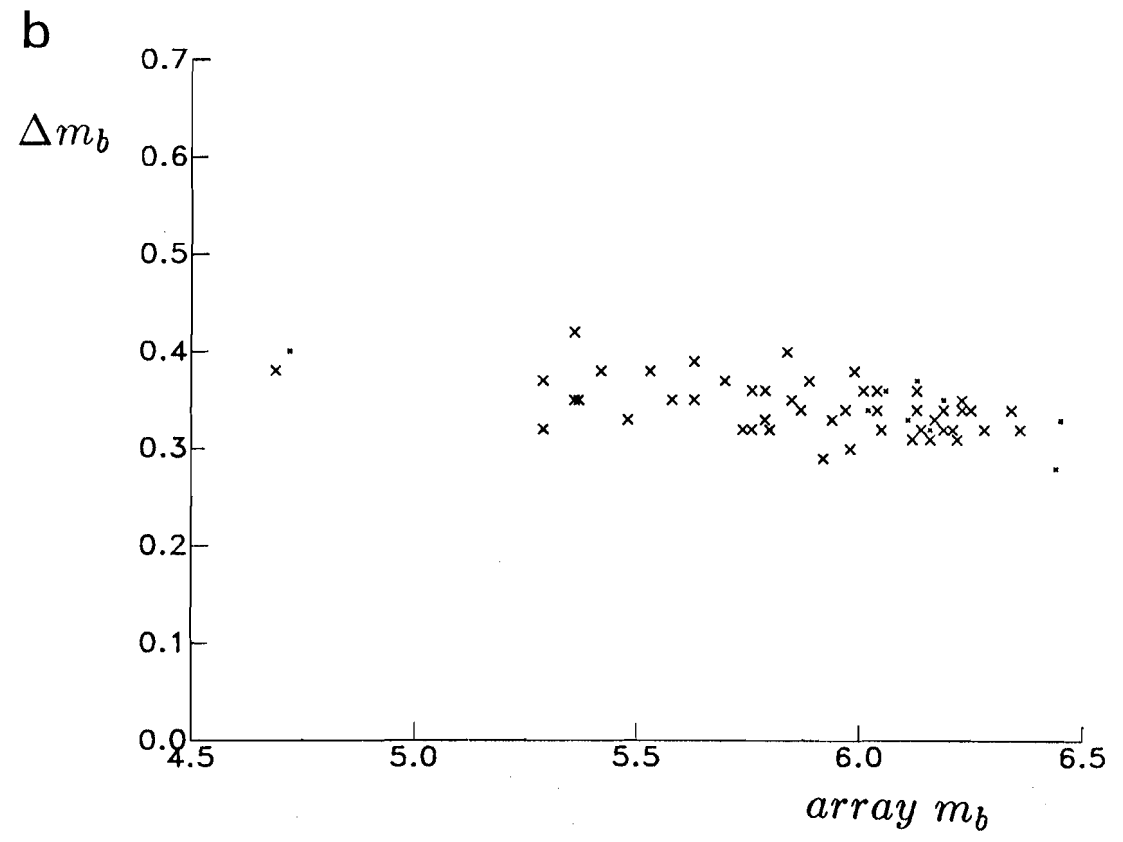

FIGURE 8. ATTENUATION BIAS. AS FOR FIGURE 8 USING (a) oa AMPLITUDE DATA AND (b) ab AMPLITUDE DATA

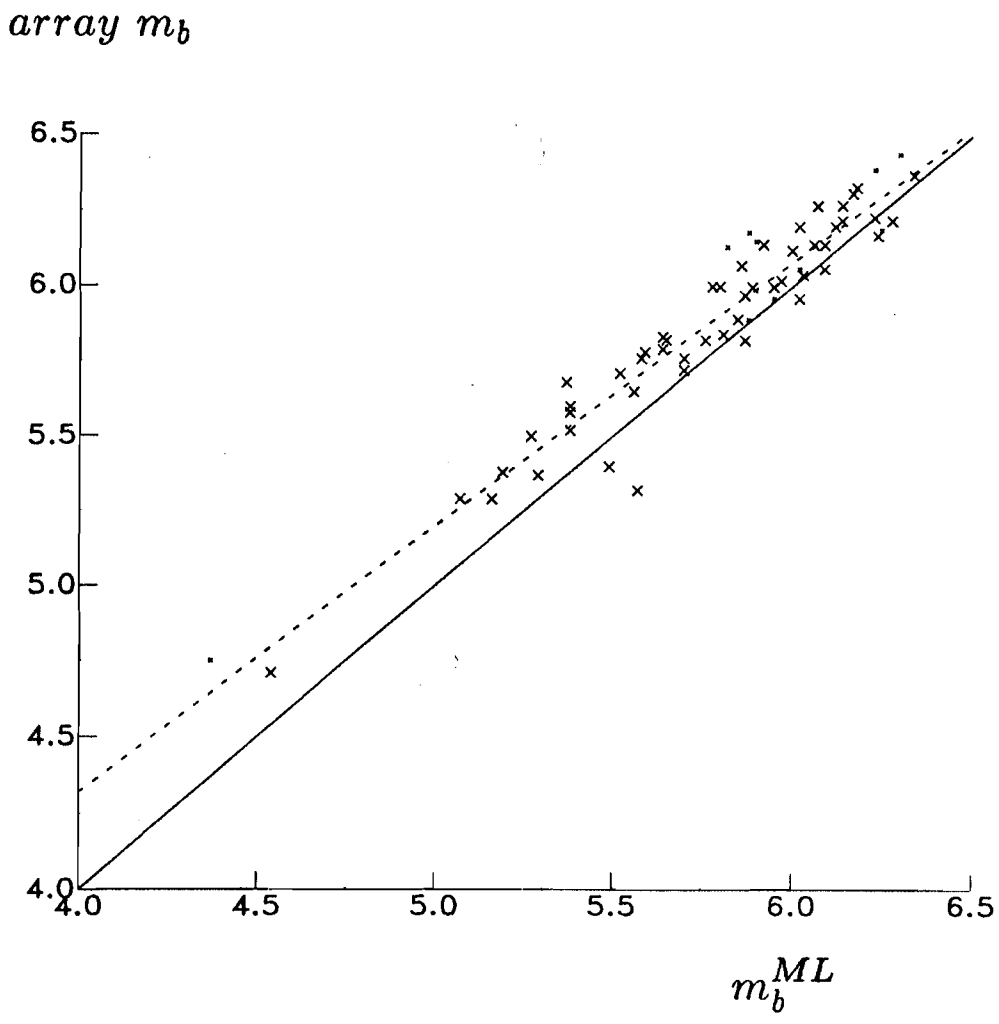

FIGURE 9. ARRAY-NETWORK m_b AGAINST MAXIMUM-LIKELIHOOD m_b (m_b^{ML}). THE LINE DRAWN THROUGH THE DATA REPRESENTS $m_b = m_b^{ML}$. POINTS FOR WHICH ONLY ONE STATION SUPPLIED DATA ARE PLOTTED AS THE SMALLER CROSSES. THE DASHED LINE REPRESENTS THE BEST LEAST-SQUARES STRAIGHT LINE

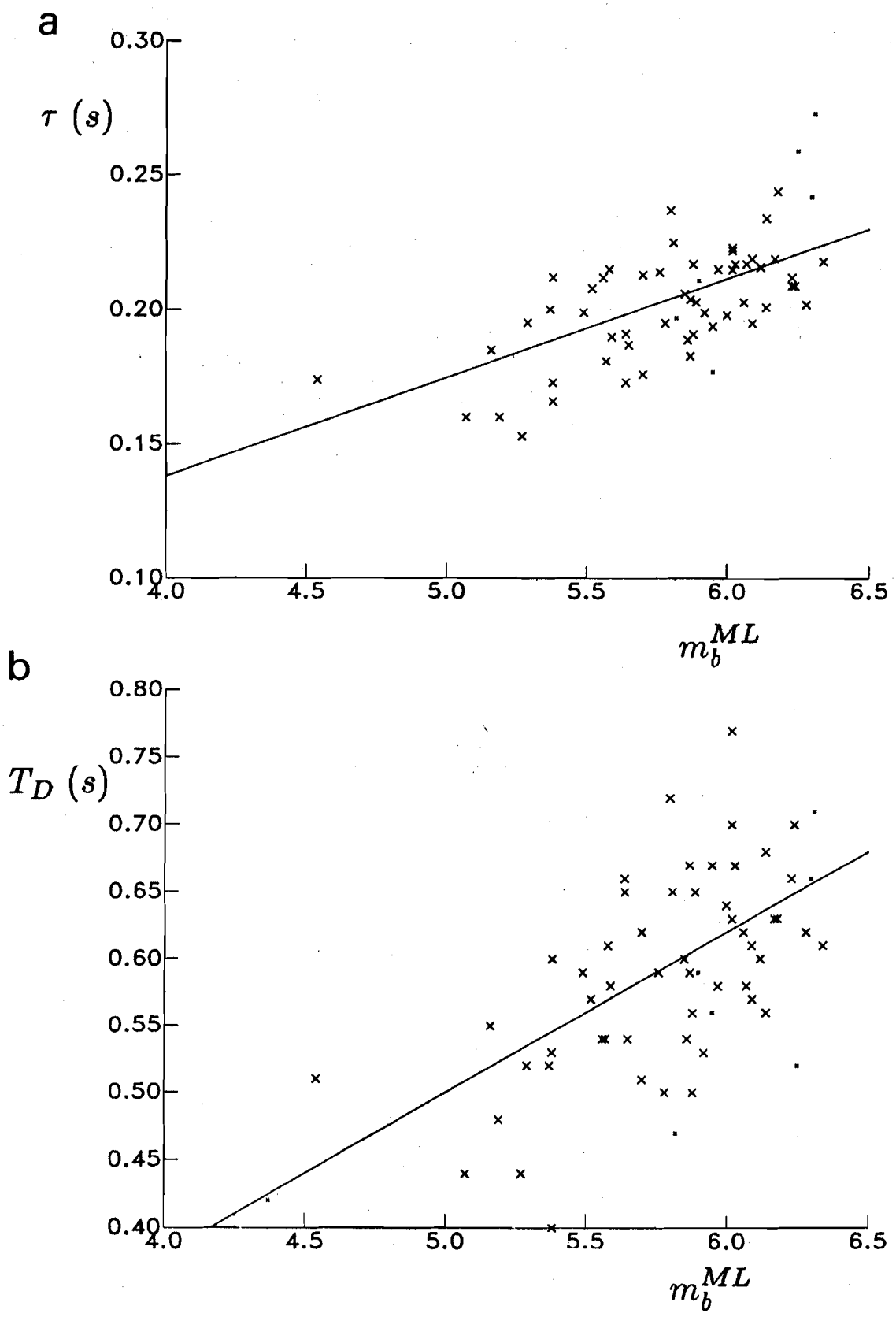

FIGURE 10. (a) ARRAY-NETWORK RISE TIME τ AGAINST m_b^{ML}

(b) ARRAY-NETWORK PULSE DURATION T_D AGAINST m_b^{ML}

Points for which only one station contributed data are plotted as the smaller crosses. The lines drawn through the data are the best least-squares straight lines

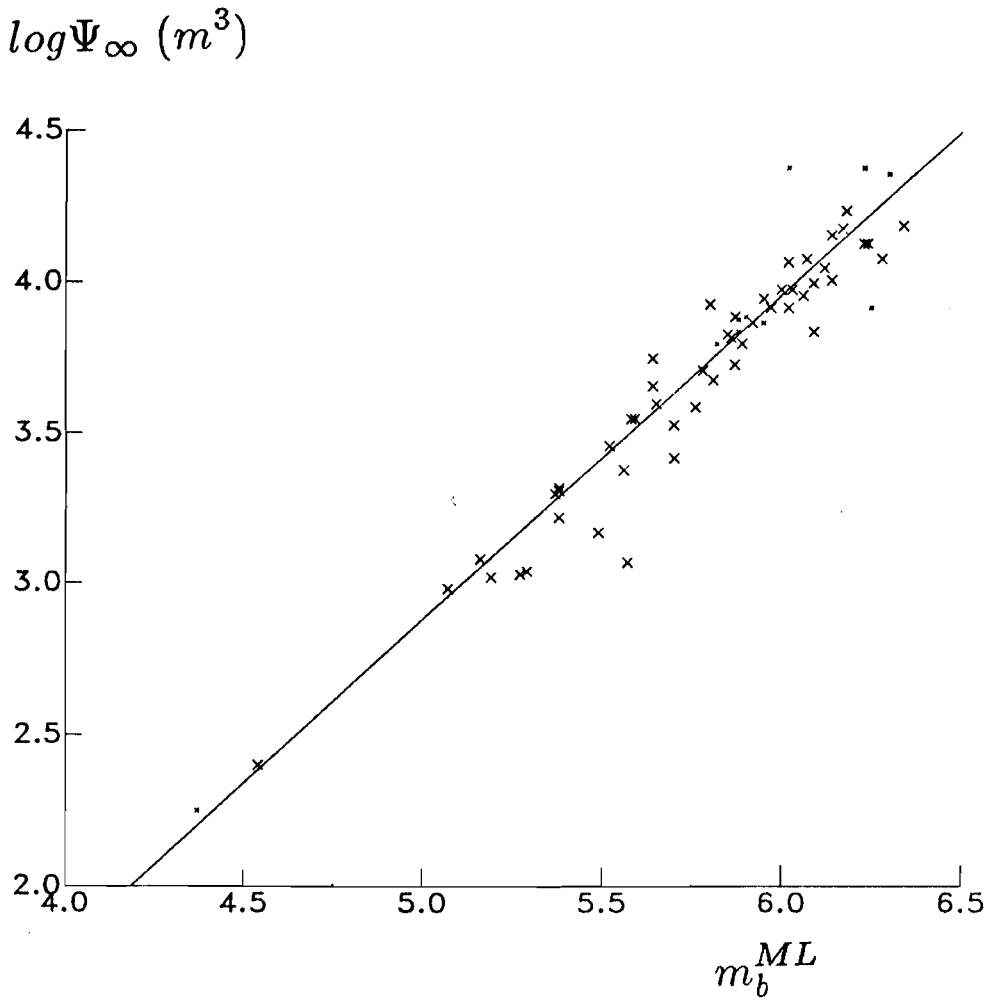

FIGURE 11. ARRAY-NETWORK LOG ψ_∞ PLOTTED AGAINST m_b^{ML}. THE LINE DRAWN THROUGH THE DATA IS THE BEST LEAST-SQUARES STRAIGHT LINE: CALCULATED EXCLUDING THE TWO DATA BELOW m_b^{ML} 5.0 AND THOSE VALUES FOR WHICH ONE ONE STATION PROVIDED DATA (PLOTTED AS THE SMALLER CROSSES)

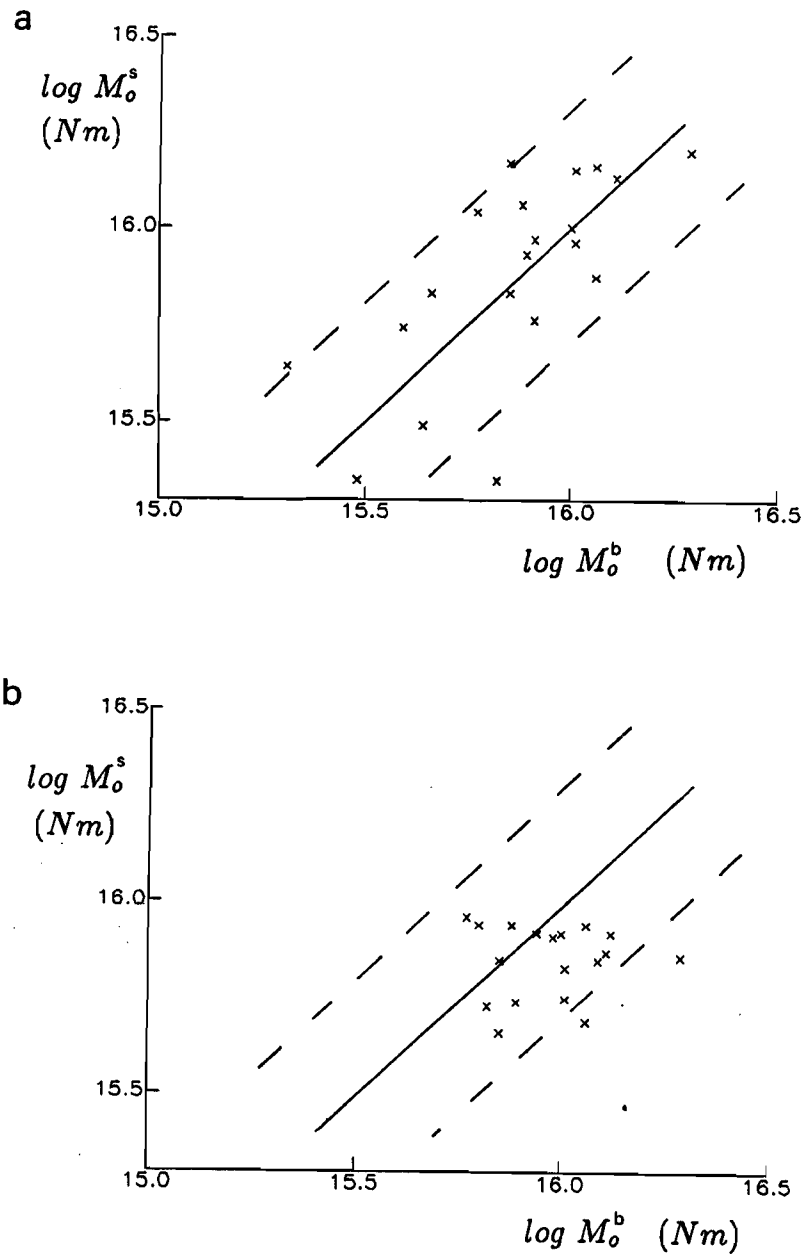

FIGURE 12. COMPARISON OF PUBLISHED SURFACE-WAVE ESTIMATES OF THE SEISMIC MOMENT (M_O^S) OF SHAGAN RIVER EXPLOSIONS WITH THE BODY-WAVE ESTIMATES MADE HERE ASSUMING A SOURCE IN GRANITE (M_O^b)

(a) (M_O^S) FROM SIERRA GEOPHYSICS (PRIVATE COMMUNICATION)

(b) (M_O^S) FROM STEVENS (21)

The solid line drawn in each graph represents $M_O^S = M_O^b$. The dashed lines represent log M_O^S = log $M_O^b \pm 0.3$; defining the area where the moment estimates agree within a factor of 2

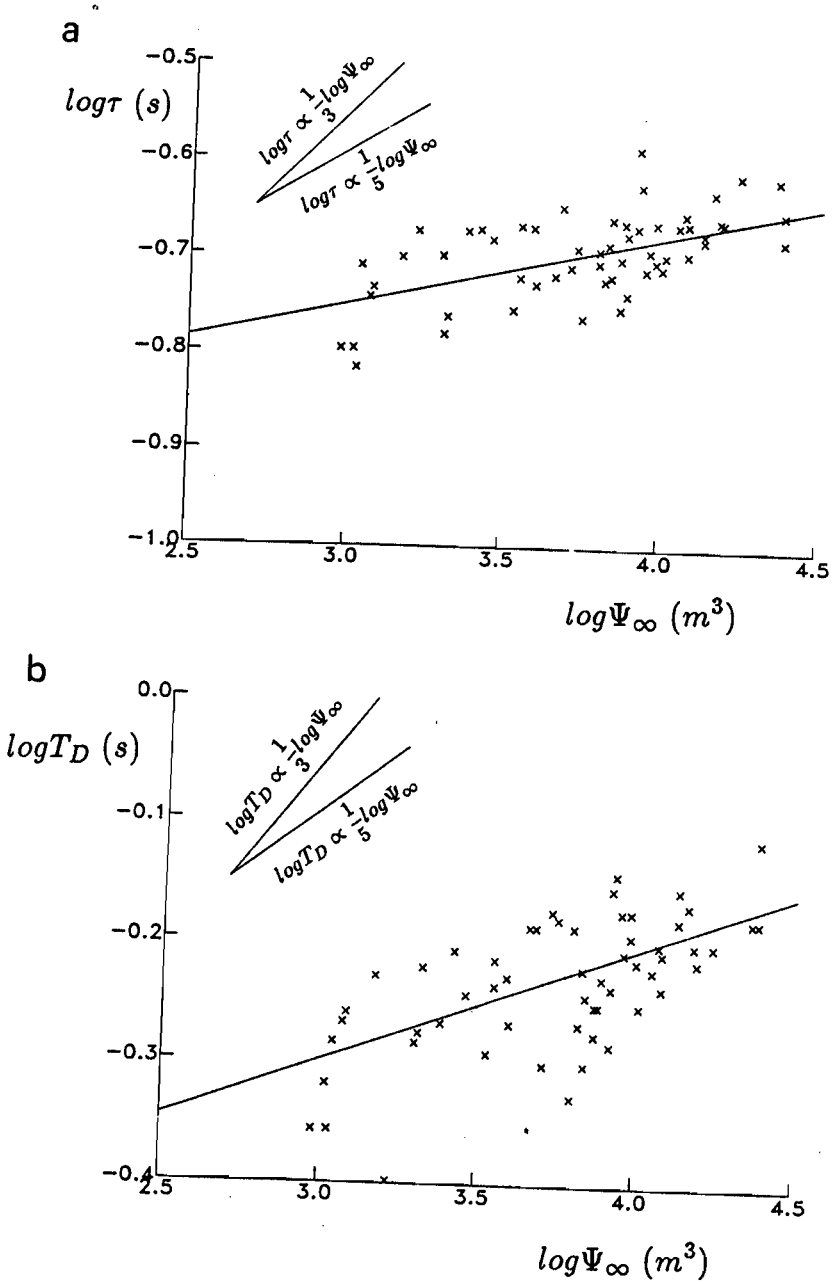

FIGURE 13. SOURCE SCALING OF SHAGAN RIVER EXPLOSIONS

(a) LOG-LOG PLOT OF RISE TIME τ AGAINST REDUCED DISPLACEMENT POTENTIAL ψ_∞ (= YIELD W)

(b) LOG-LOG PLOT OF DURATION T_D AGAINST ψ_∞

The lines drawn through the data are the best least-squares straight lines assuming errors in both axes. Lines corresponding to cube-root and fifth-root scaling with yield are also drawn

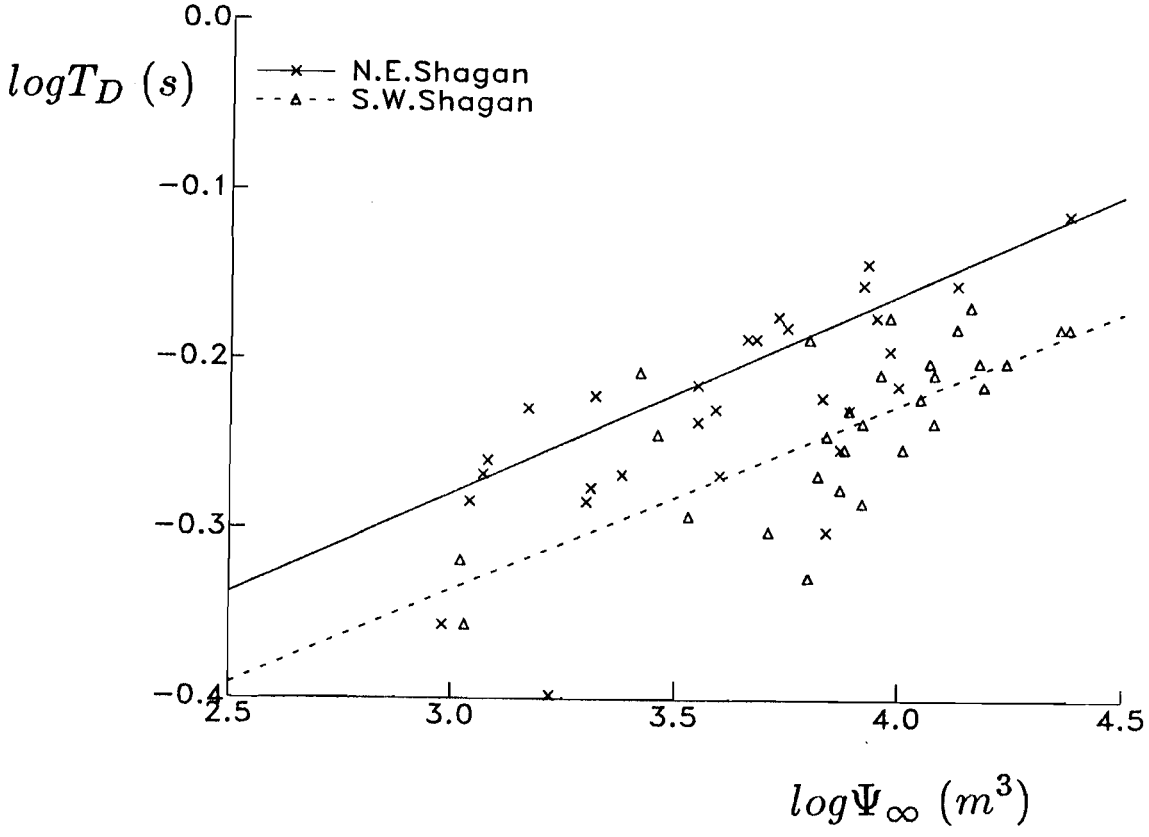

FIGURE 14. LOG-LOG PLOT OF DURATION T_D AGAINST REDUCED DISPLACEMENT POTENTIAL ψ_∞ FOR THE TWO HALVES OF THE TEST SITE. BEST LEAST-SQUARES STRAIGHT LINES ARE DRAWN FOR EACH DATA SET

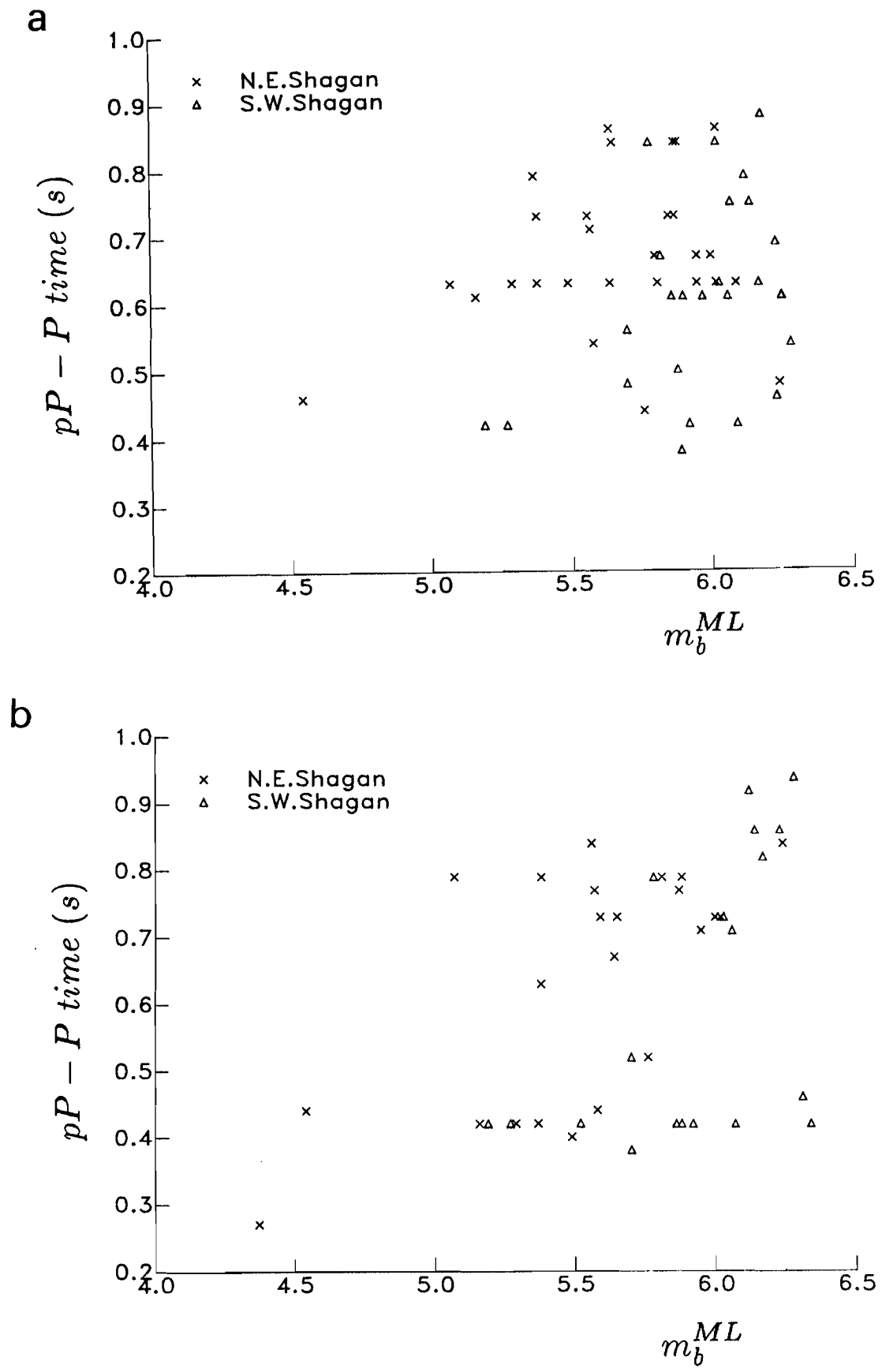

FIGURE 15. ESTIMATED pP DELAY TIMES PLOTTED AGAINST m_b^{ML} FOR THE TWO HALVES OF THE TEST SITE: (a) EKA, (b) YKA

c

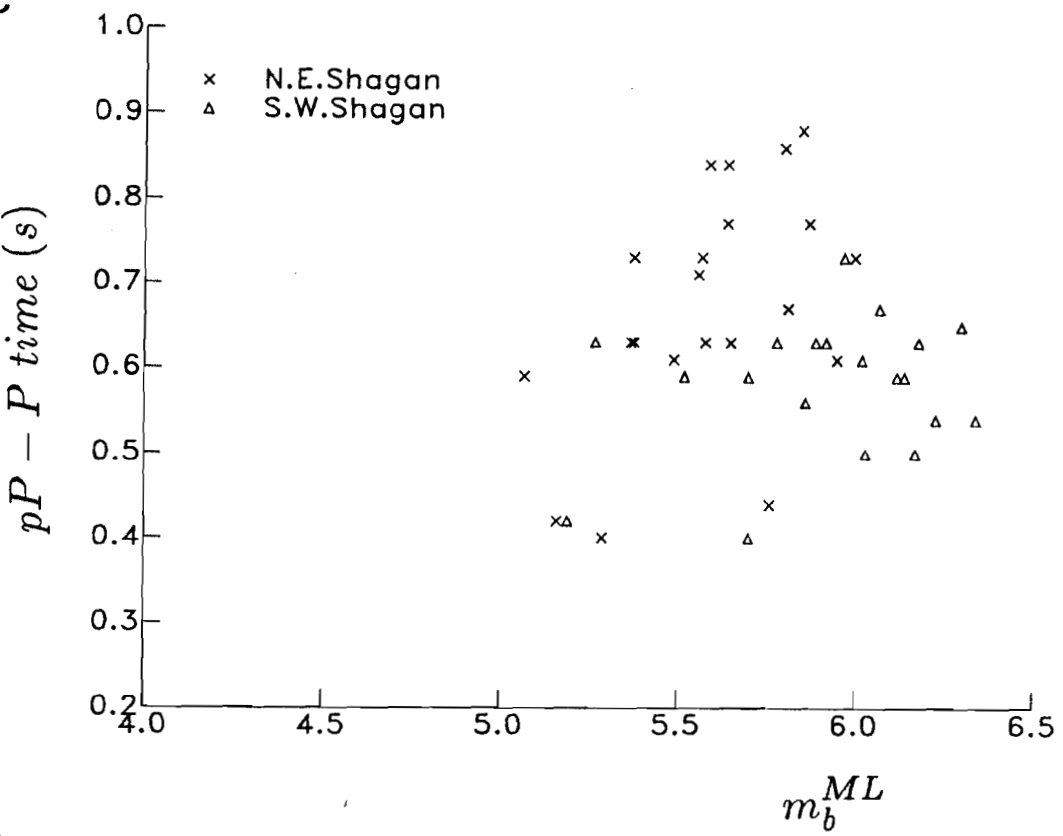

d

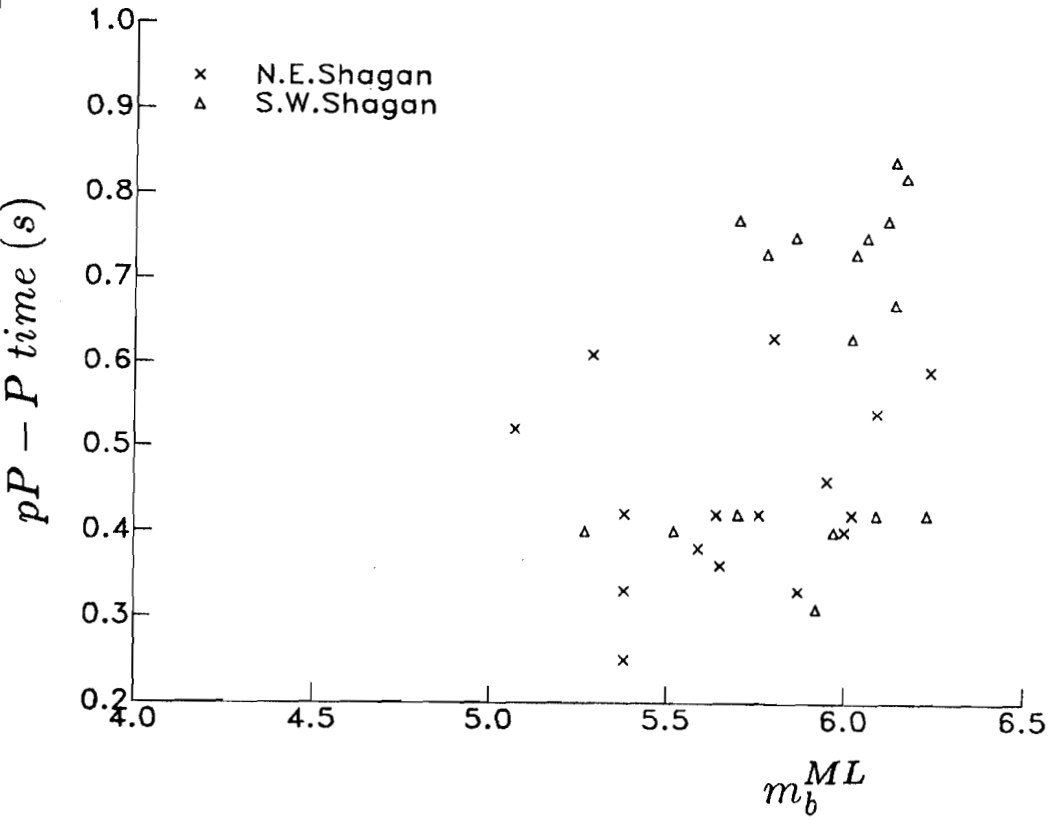

FIGURE 15. (Cont'd) (c) GBA, (d) WRA

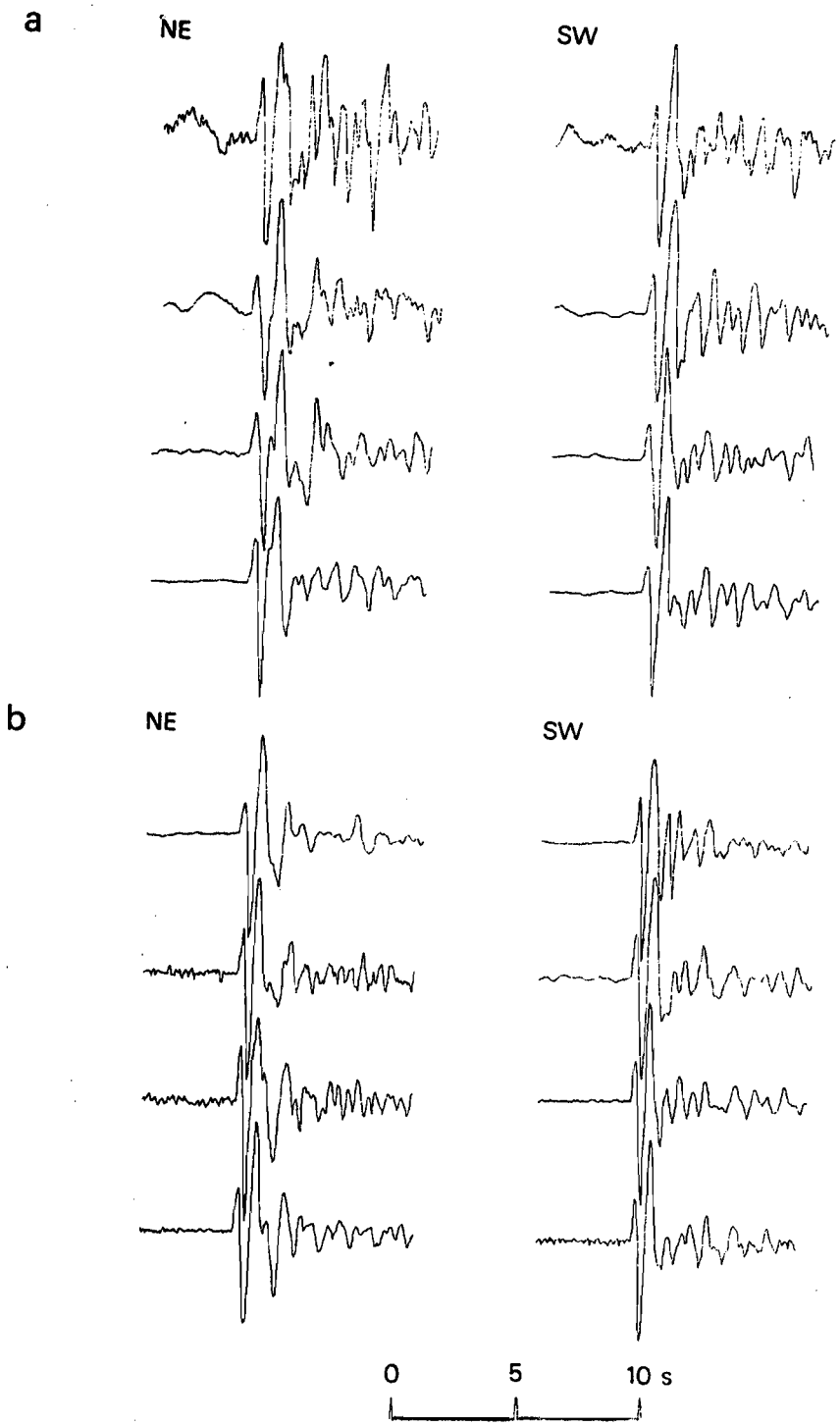

FIGURE 16. SOME TYPICAL SP WAVEFORMS AT THE FOUR ARRAYS FROM NE AND SW SHAGAN RIVER EXPLOSIONS (a) EKA; (b) YKA. FOUR SEISMOGRAMS ARE SHOWN FOR EACH AREA, COMING FROM EXPLOSIONS WITH m_b^{ML} OF AROUND (FROM THE TOP) 5.2 (NE: 9/6/76 (EXCEPT WRA: 29/6/77), SW: 21/4/76 (EXCEPT WRA: 31/8/82)), 5.7 (NE: 4/11/78 (EXCEPT GBA: 25/12/75), SW: 29/10/75), 6.0 (NE: 12/10/80) (EXCEPT EKA: 29/8/78), SW: 11/6/78) AND 6.2 (NE: 18/8/79, SW: 27/12/81 (EXCEPT EKA: 23/12/79 AND WRA: 23/6/79))

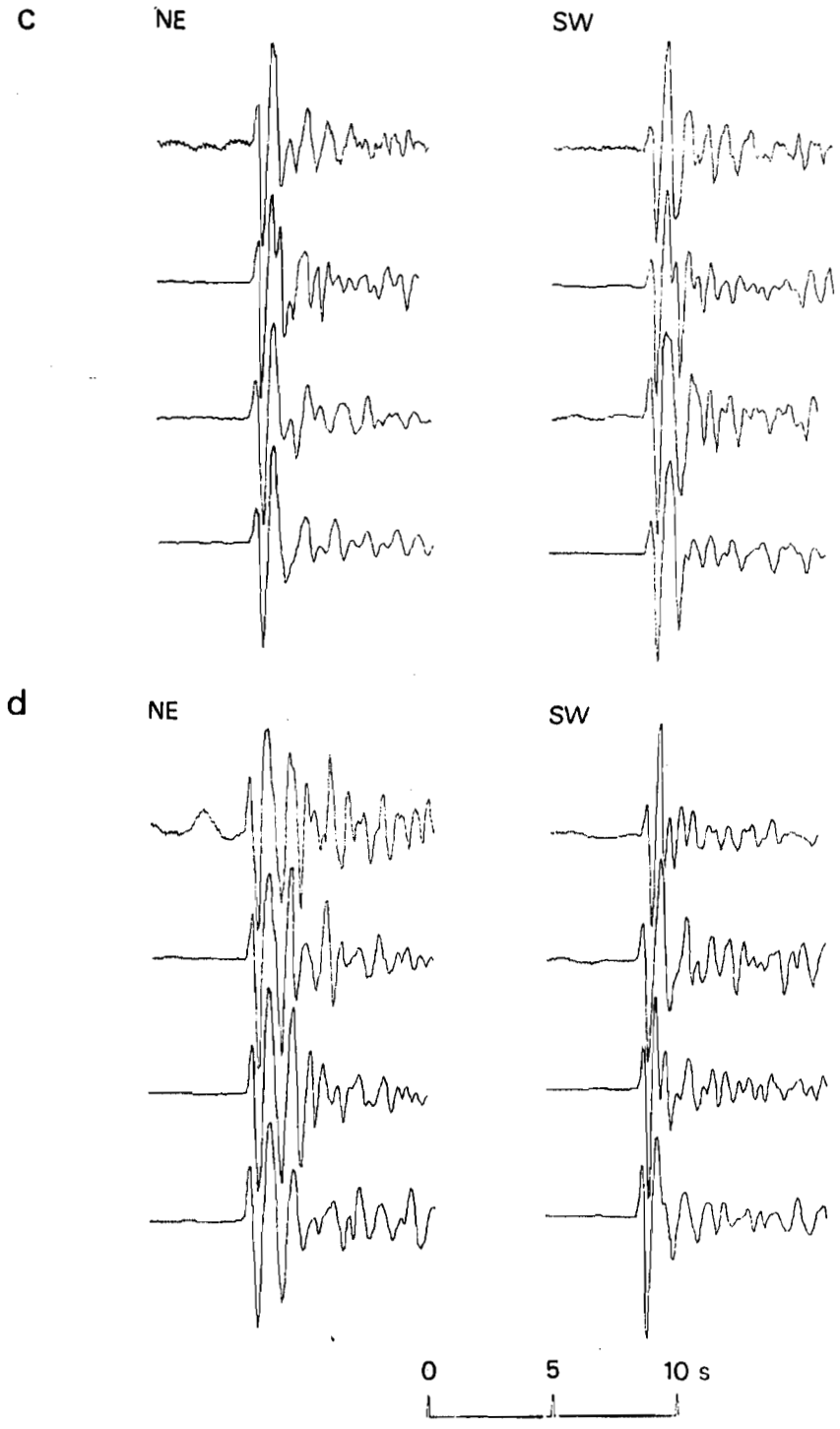

FIGURE 16. (Cont'd) (c) GBA, (d) WRA

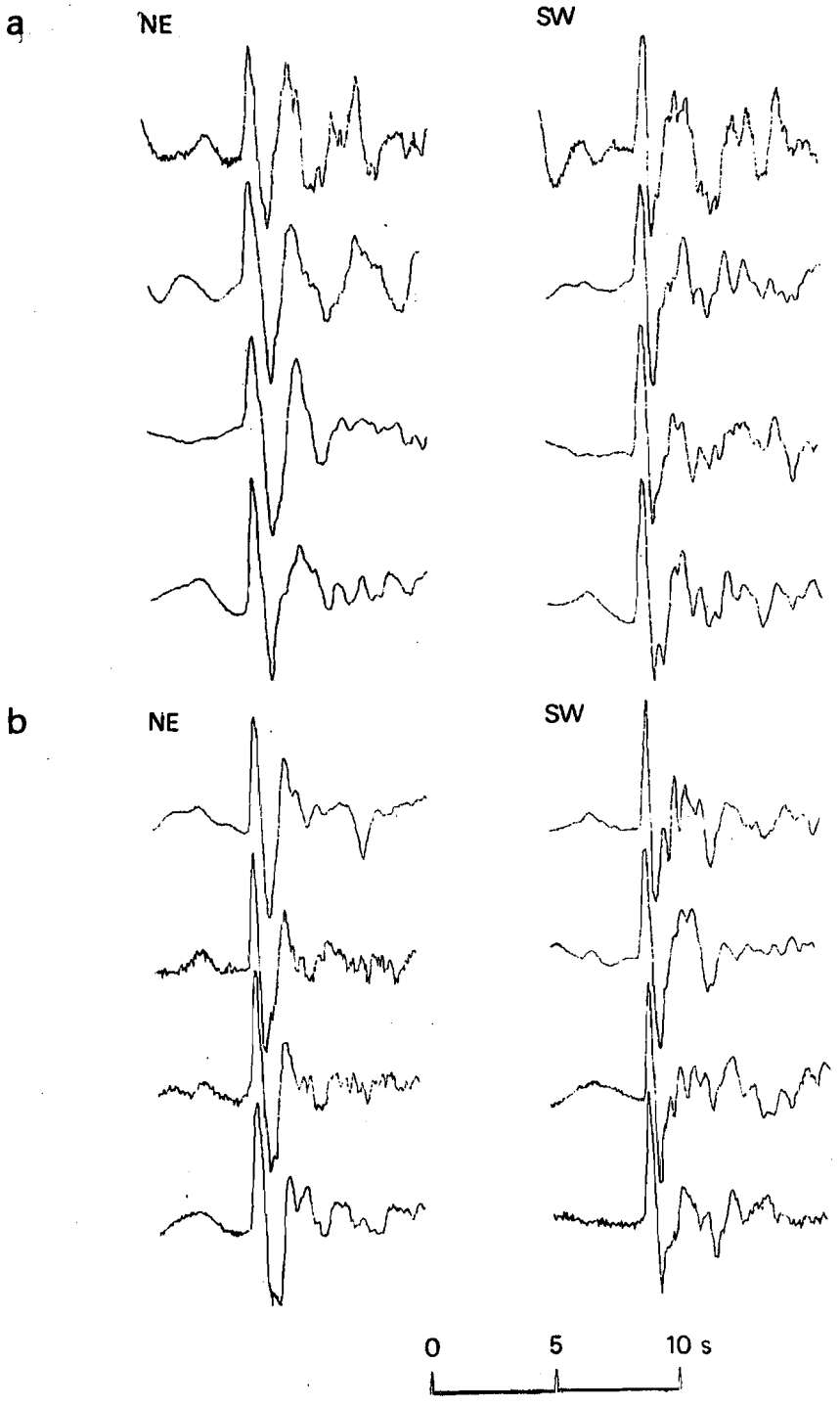

FIGURE 17. THE SEISMOGRAMS OF FIGURE 16 CONVERTED TO A PHASELESS-BROAD-BAND INSTRUMENT RESPONSE, WIENER FILTERED AND CORRECTED FOR ATTENUATION OF $t^* = 0.15$ s. (a) EKA, (b) YKA

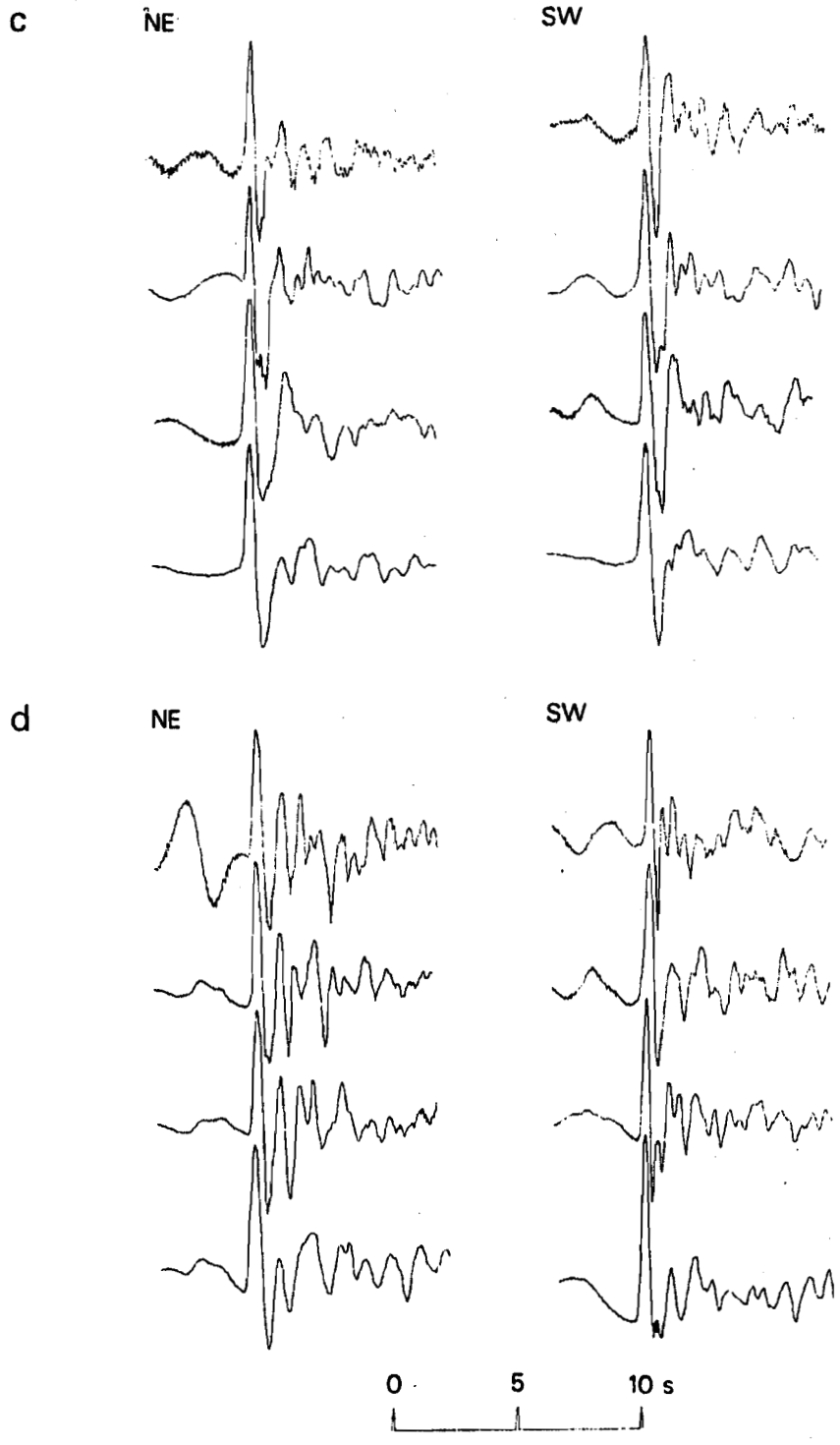

FIGURE 17. (Cont'd) (c) GBA, (d) WRA

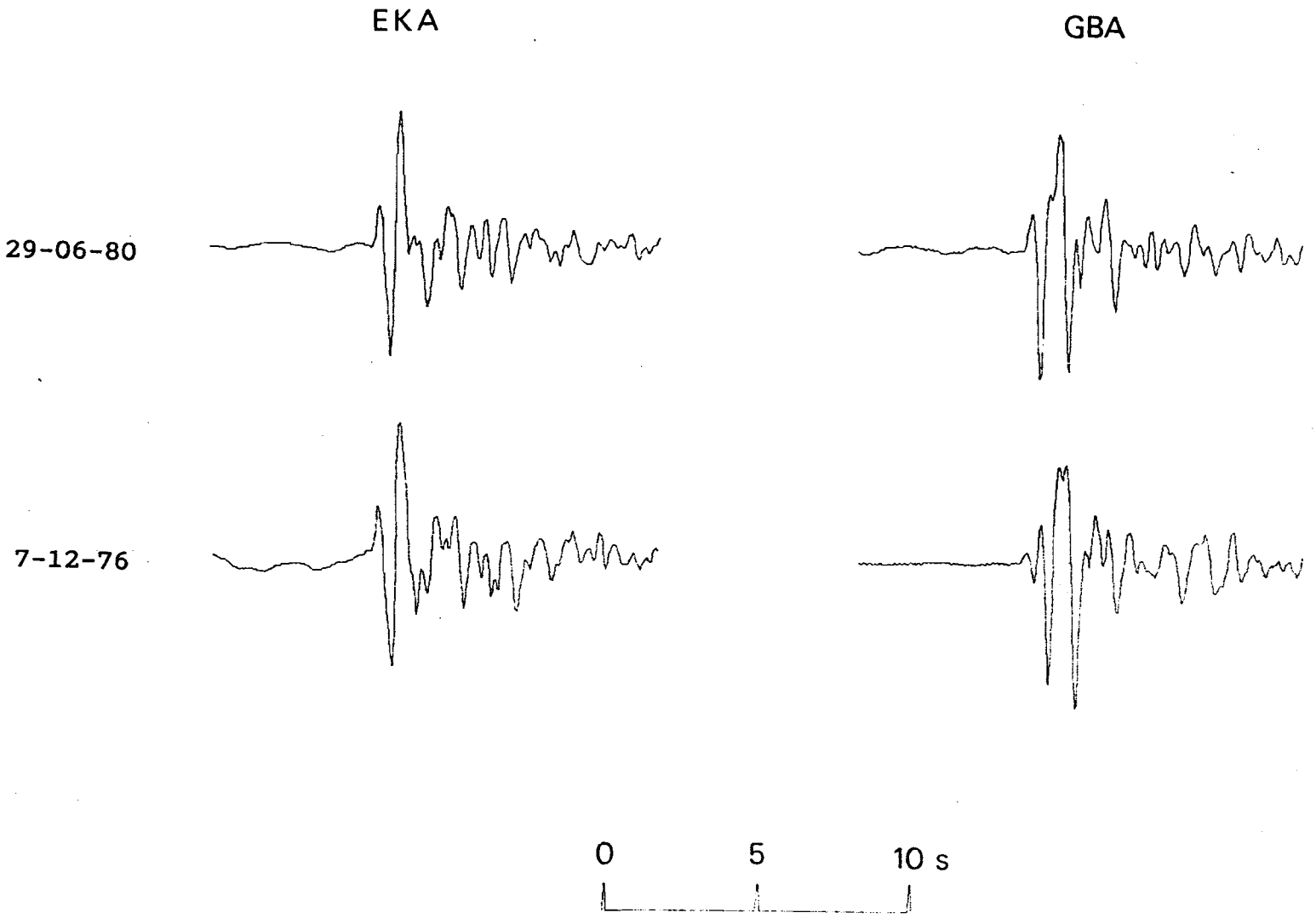

FIGURE 18. SP ARRAY-SUM SEISMOGRAMS RECORDED AT EKA AND GBA FROM THE "TYPICAL" 29 JUNE 1980 SW SHAGAN RIVER EXPLOSION AND THE ATYPICAL 7 DECEMBER 1976 DISTURBANCE NEARBY

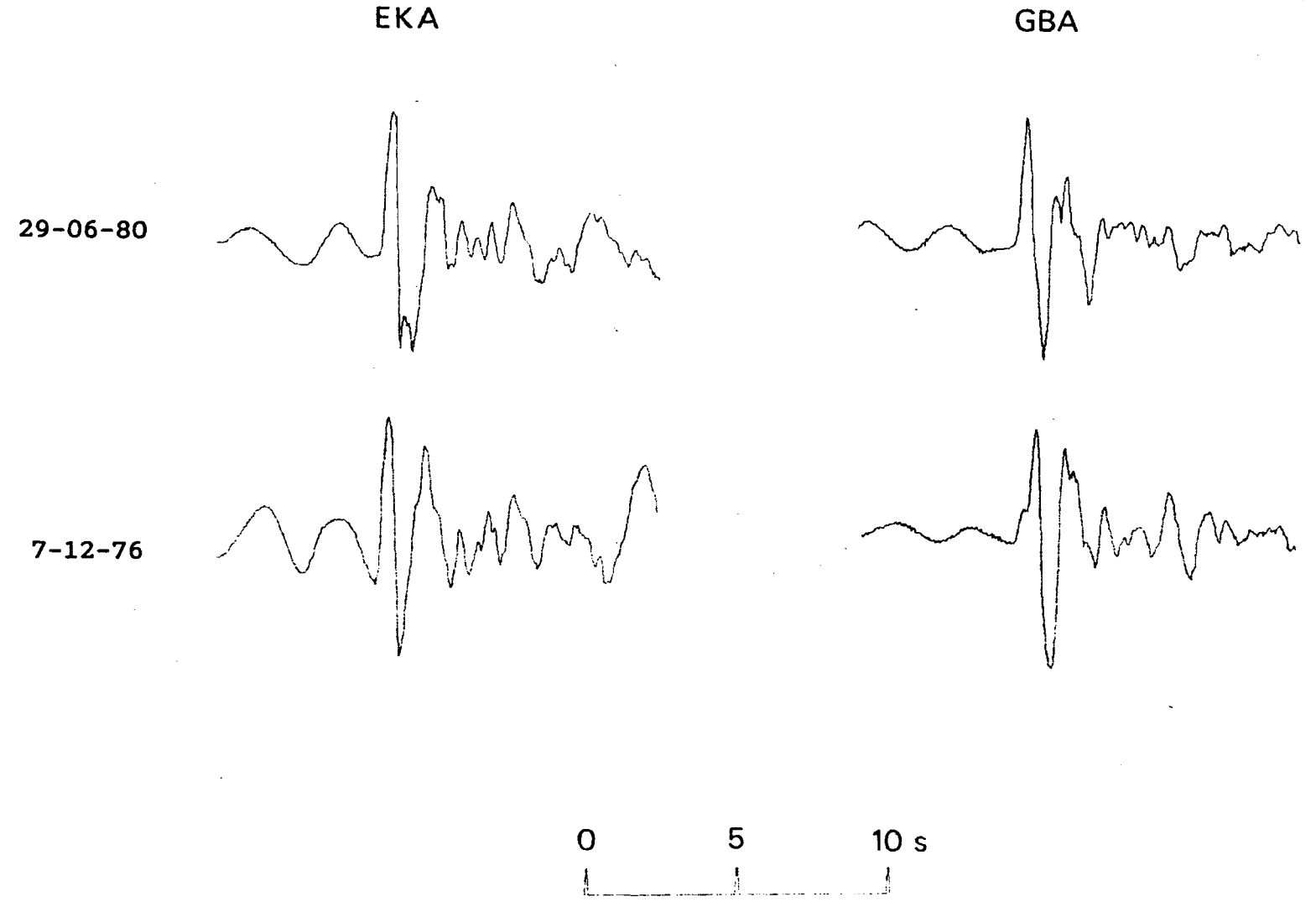

FIGURE 19. THE SEISMOGRAMS OF FIGURE 18 CONVERTED TO A PHASE-BROAD-BAND INSTRUMENT RESPONSE, WIENER FILTERED AND CORRECTED FOR ATTENUATION OF $t^* = 0.15$ s

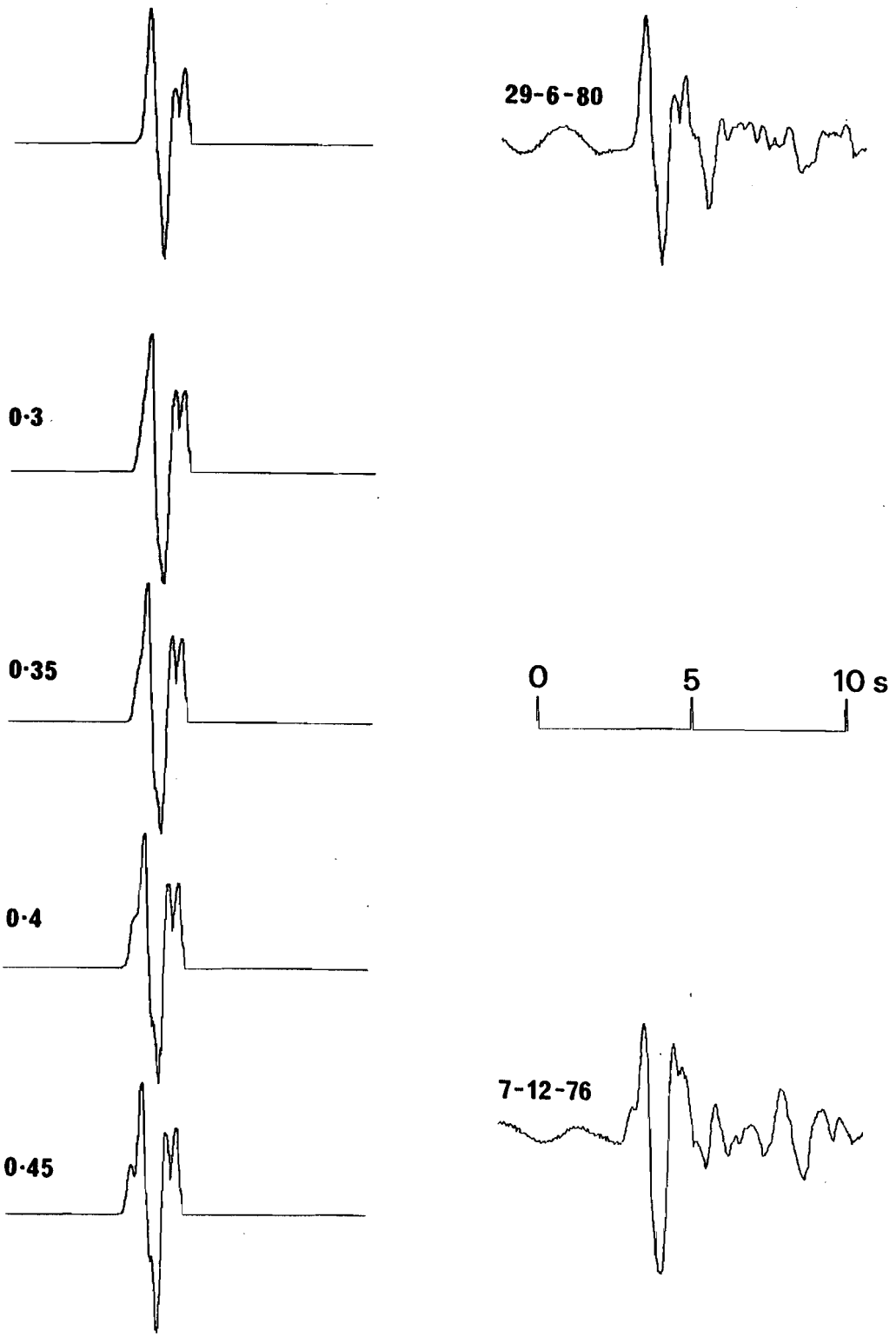

FIGURE 20. HERE THE DECONVOLVED BB WAVEFORM OF THE 29 JUNE 1980 EXPLOSION RECORDED AT GBA IS ADDED TO ITSELF AFTER RELATIVE TIME SHIFTS OF 0.3 TO 0.45 s - THE EARLIER ARRIVING SIGNAL HAS AN AMPLITUDE 0.3 TIMES THAT OF THE LATTER. THE DECONVOLVED BB WAVEFORM OF THE 7 DECEMBER 1976 EXPLOSION AT GBA IS SHOWN FOR COMPARISON

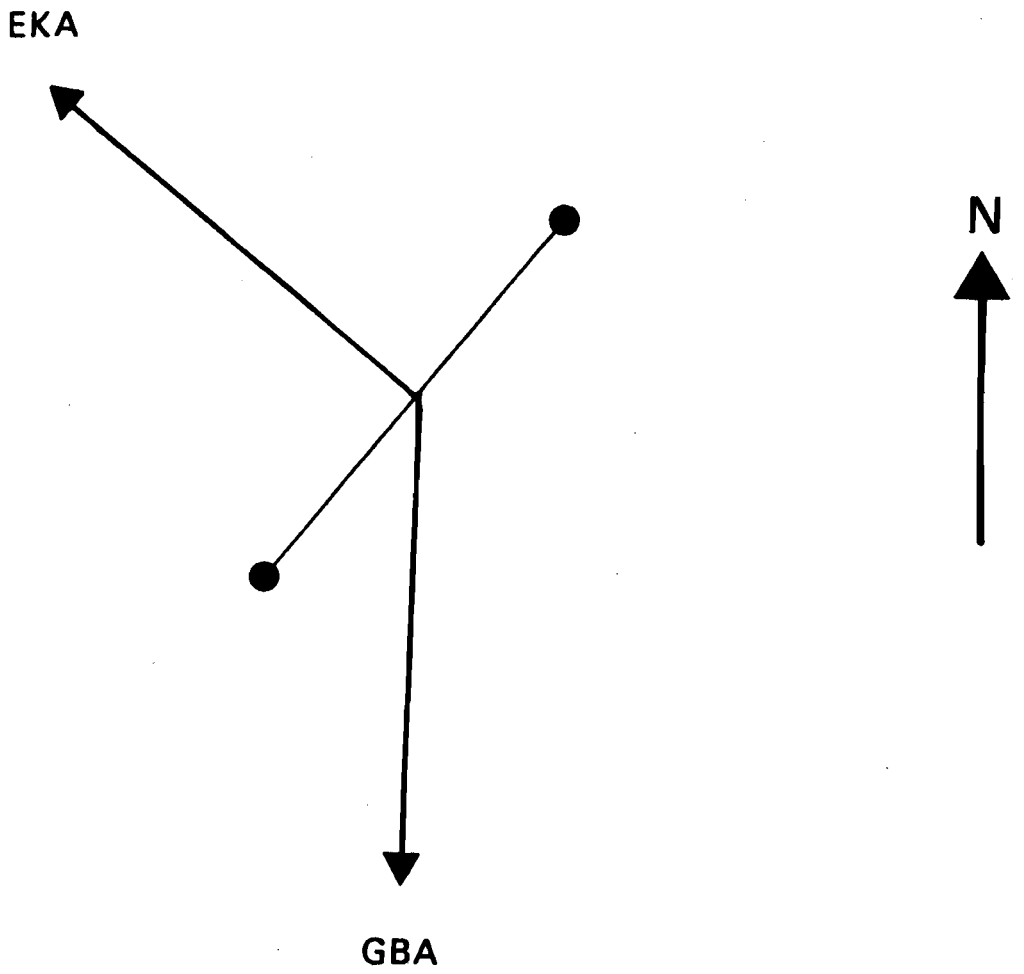

FIGURE 21. GEOMETRY OF THE PRESUMED DOUBLE EXPLOSION ON 7 DECEMBER 1976. THE AZIMUTHS TO EKA AND GBA ARE SHOWN

APPENDIX A

THE SEISMOGRAMS

This appendix contains figures showing all the seismograms available from the four medium-aperture arrays for the Shagan River explosions discussed in this report. These figures, A1 to A176, are indexed in table 3 - reproduced here as table A1.

Each figure is for one explosion recorded at one array and shows four or five seismograms. These are:-

(a) A short-period seismogram. This is normally the beam-formed array sum but, if the array is overloaded, a single-channel strong-motion record or one derived from the velocity-broad-band seismogram (YKA only) is substituted, when available.

(b) The short-period seismogram filtered to simulate an additional path attenuation of $t^* = 0.2$ s, illustrating what the recording would look like if the explosion were fired at the Nevada Test Site.

(c) The short-period seismogram converted to a phaseless-broad-band instrument response and filtered using a Wiener filter.

(d) As seismogram (c), except that an additional filter has been used, correcting for a path attenuation of $t^* = 0.15$ s. This record approximates the displacement pulses radiated from the source region.

(e) Velocity-broad-band seismogram (if used to produce (a)).

The gains of each channel have been scaled to normalise the peak amplitudes of the seismograms. Signals that appear smaller than normal are due to high-amplitude noise just outside the window included in the figure.

TABLE A1

Availability of Array Data for the Shagan River Explosions

no	date	EKA	YKA	GBA	WRA
01	15.01.65	a (1)	n/a	n/a	n/a
02	19.06.68	a (2)	a (3)	a (4)	a (5)
03	30.11.69	a (6)	n/a	ov	a (7)
04	30.06.71	a (8)	a (9)	a (10)	a (11)
05	10.02.72	a (12)	n/a	n/a	a (13)
06	02.11.72	a (14)	sm (15)	n/a	ov
07	10.12.72	a (16)	sm (17)	n/a	ov
08	23.07.73	ov	sm (18)	ov	ov
09	14.12.73	a (19)	sm (20)	n/a	ov
10	16.04.74	ns	a (21)	n/a	n/a
11	31.05.74	a (22)	sm (23)	ov	n/a
12	16.10.74	a (24)	a (25)	a (26)	n/a
13	27.12.74	a (27)	a (28)	a (29)	n/a
14	27.04.75	a (30)	a (31)	a (32)	n/a
15	30.06.75	a (33)	a (34)	a (35)	n/a
16	29.10.75	a (36)	a (37)	a (38)	a (39)
17	25.12.75	a (40)	a (41)	a (42)	a (43)
18	21.04.76	a (44)	a (45)	a (46)	n/a
19	09.06.76	a (47)	a (48)	a (49)	n/a
20	04.07.76	a (50)	ov	n/a	n/a
21	28.08.76	a (51)	a (52)	a (53)	n/a
22	23.11.76	a (54)	ov	a (55)	n/a
23	07.12.76	a (56)	ov	a (57)	n/a
24	29.05.77	a (58)	ov	ov	n/a
25	29.06.77	a (59)	a (60)	a (61)	a (62)
26	05.09.77	a (63)	ov	a (64)	a (65)
27	29.10.77	a (66)	ov	a (67)	a (68)
28	30.11.77	a (69)	ov	sm (70)	a (71)
29	11.06.78	a (72)	vbb (73)	a (74)	a (75)
30	05.07.78	a (76)	vbb (77)	a (78)	a (79)
31	29.08.78	a (80)	vbb (81)	a (82)	a (83)
32	15.09.78	a (84)	vbb (85)	ov	a (86)
33	04.11.78	a (87)	vbb (88)	a (89)	a (90)
34	29.11.78	a (91)	vbb (92)	sm (93)	a (94)
35	01.02.79	a (95)	a (96)	a (97)	n/a
36	23.06.79	a (98)	vbb (99)	ov	a (100)
37	07.07.79	a (101)	vbb (102)	n/a	n/a
38	04.08.79	a (103)	vbb (104)	a (105)	a (106)
39	18.08.79	a (107)	vbb (108)	a (109)	a (110)
40	28.10.79	a (111)	vbb (111.1)	ov	a (112)
41	02.12.79	a (113)	ov	ov	a (114)
42	23.12.79	a (115)	ov	n/a	ov
43	25.04.80	n/a	a (116)	a (117)	a (118)
44	12.06.80	n/a	vbb (119)	a (120)	a (121)
45	29.06.80	a (122)	vbb (123)	a (124)	a (125)
46	14.09.80	ov	ov	a (126)	ov
47	12.10.80	a (127)	vbb (128)	a (129)	a (130)
48	14.12.80	a (131)	vbb (132)	a (133)	a (134)
49	27.12.80	a (135)	n/a	a (136)	a (137)
50	29.03.81	a (138)	vbb (139)	a (140)	n/a
51	22.04.81	a (141)	n/a	a (142)	a (143)
52	27.05.81	a (144)	vbb (145)	a (146)	a (147)
53	13.09.81	a (148)	vbb (149)	a (150)	a (151)
54	18.10.81	a (152)	vbb (153)	a (154)	a (155)
55	29.11.81	a (156)	vbb (157)	a (158)	a (159)
56	27.12.81	ov	vbb (160)	a (161)	ov
57	25.04.82	n/a	n/a	a (162)	a (163)
58	04.07.82	a (164)	ov	a (165)	ov
59	31.08.82	a (166)	a (167)	a (168)	a (169)
60	05.12.82	a (170)	vbb (171)	n/a	a (172)
61	26.12.82	a (173)	vbb (174)	a (175)	a (176)

Key

a	available
vbb	array overloaded, velocity broad band used (YKA only)
sm	array overloaded, strong motion channel used - gain unknown
ov	array overloaded
ns	not seen
n/a	not available

The number given in brackets is that of the figure in Appendix A which shows the data

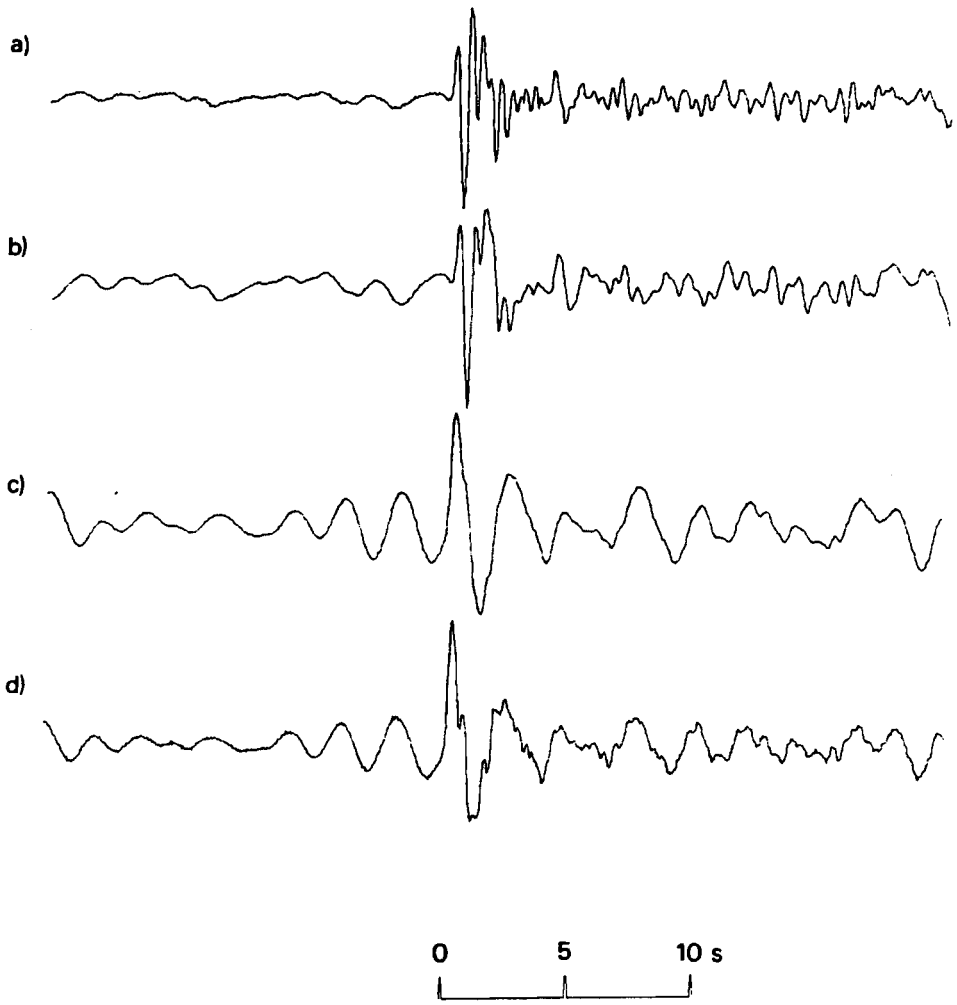

Figure A1 (a) Short-period array-sum seismogram recorded at EKA from the 15 January 1965 Shagan River explosion.
(b) Seismogram (a) filtered to simulate the effects of an additional t* of 0.2s.
(c) Seismogram (a) after Wiener filtering converted to a phaseless-broad-band instrument response.
(d) Same as seismogram (c) except that the effects of path attenuation of t* = 0.15s have been corrected for.

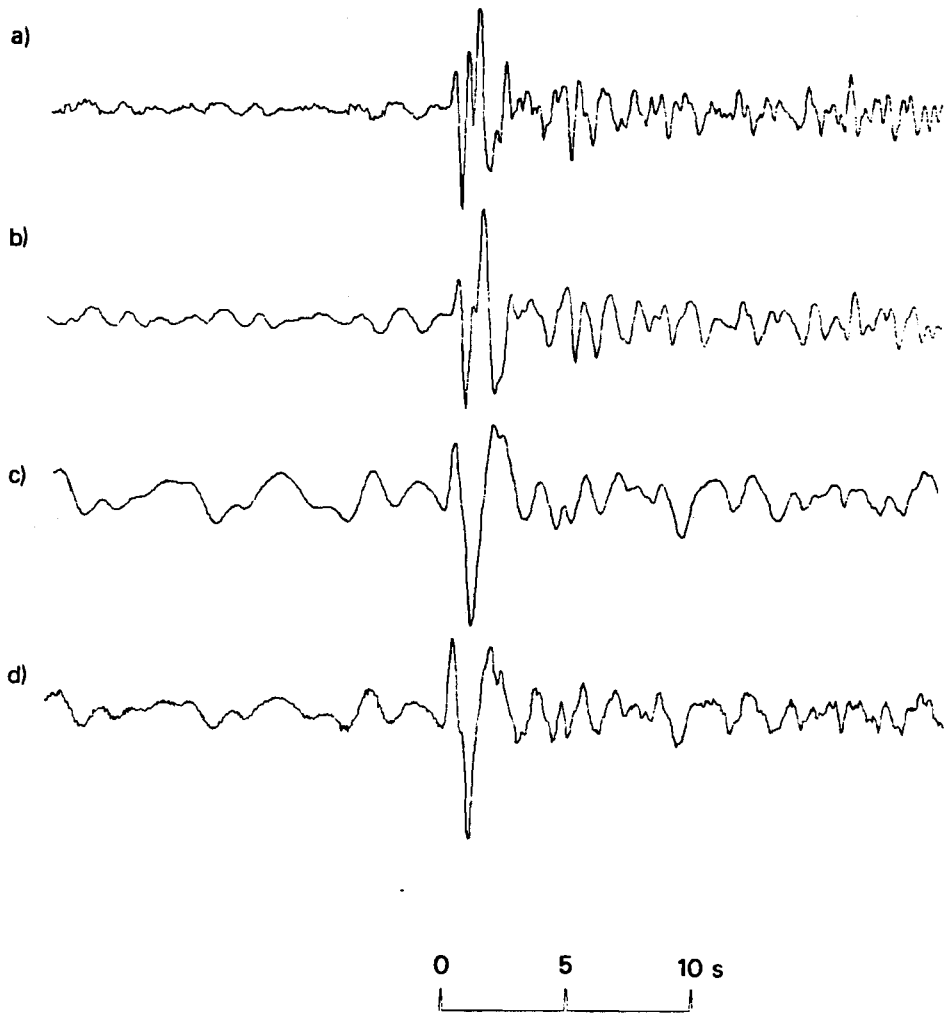

Figure A2 (a) Short-period array-sum seismogram recorded at EKA from the 19 June 1968 Shagan River explosion.
(b) Seismogram (a) filtered to simulate the effects of an additional t* of 0.2s.
(c) Seismogram (a) after Wiener filtering converted to a phaseless-broad-band instrument response.
(d) Same as seismogram (c) except that the effects of path attenuation of t* = 0.15s have been corrected for.

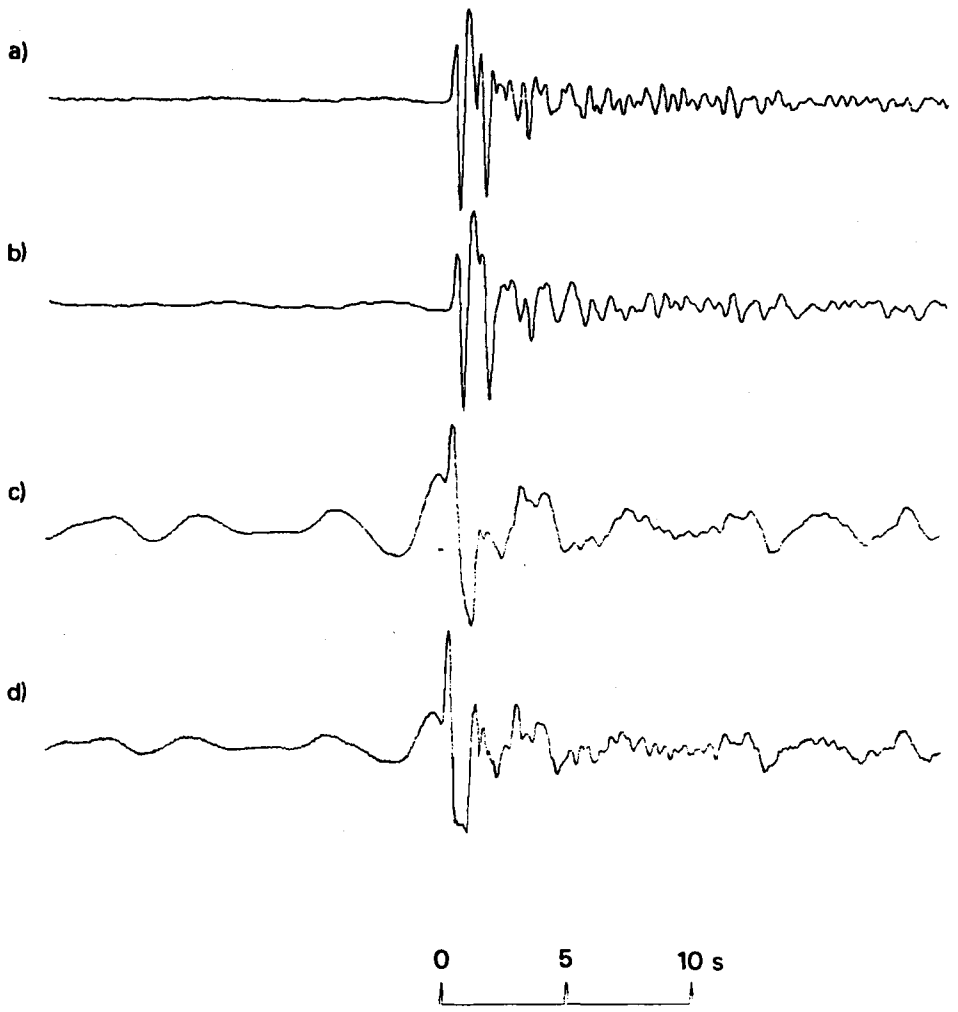

Figure A3 (a) Short-period array-sum seismogram recorded at YKA from the 19 June 1968 Shagan River explosion.
(b) Seismogram (a) filtered to simulate the effects of an additional t* of 0.2s.
(c) Seismogram (a) after Wiener filtering converted to a phaseless-broad-band instrument response.
(d) Same as seismogram (c) except that the effects of path attenuation of t* = 0.15s have been corrected for.

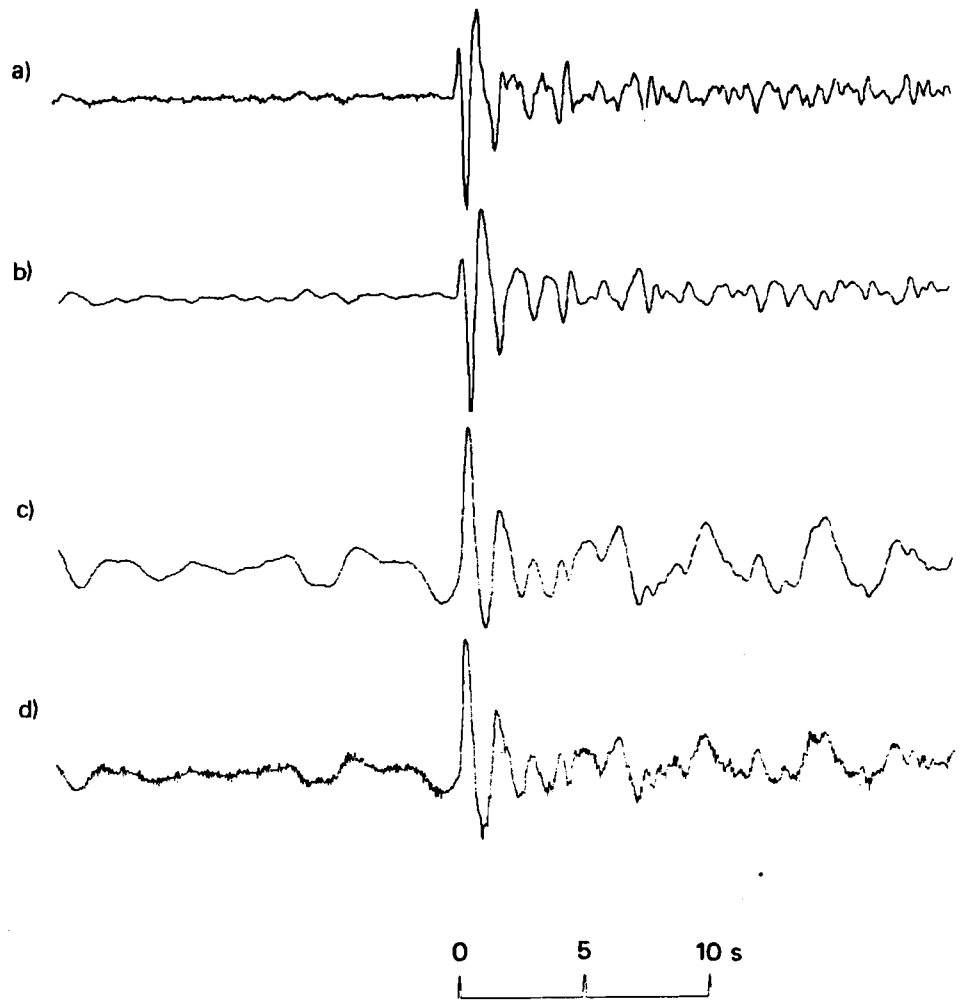

Figure A4 (a) Short-period array-sum seismogram recorded at GBA from the 19 June 1968 Shagan River explosion.
(b) Seismogram (a) filtered to simulate the effects of an additional t* of 0.2s.
(c) Seismogram (a) after Wiener filtering converted to a phaseless-broad-band instrument response.
(d) Same as seismogram (c) except that the effects of path attenuation of t* = 0.15s have been corrected for.

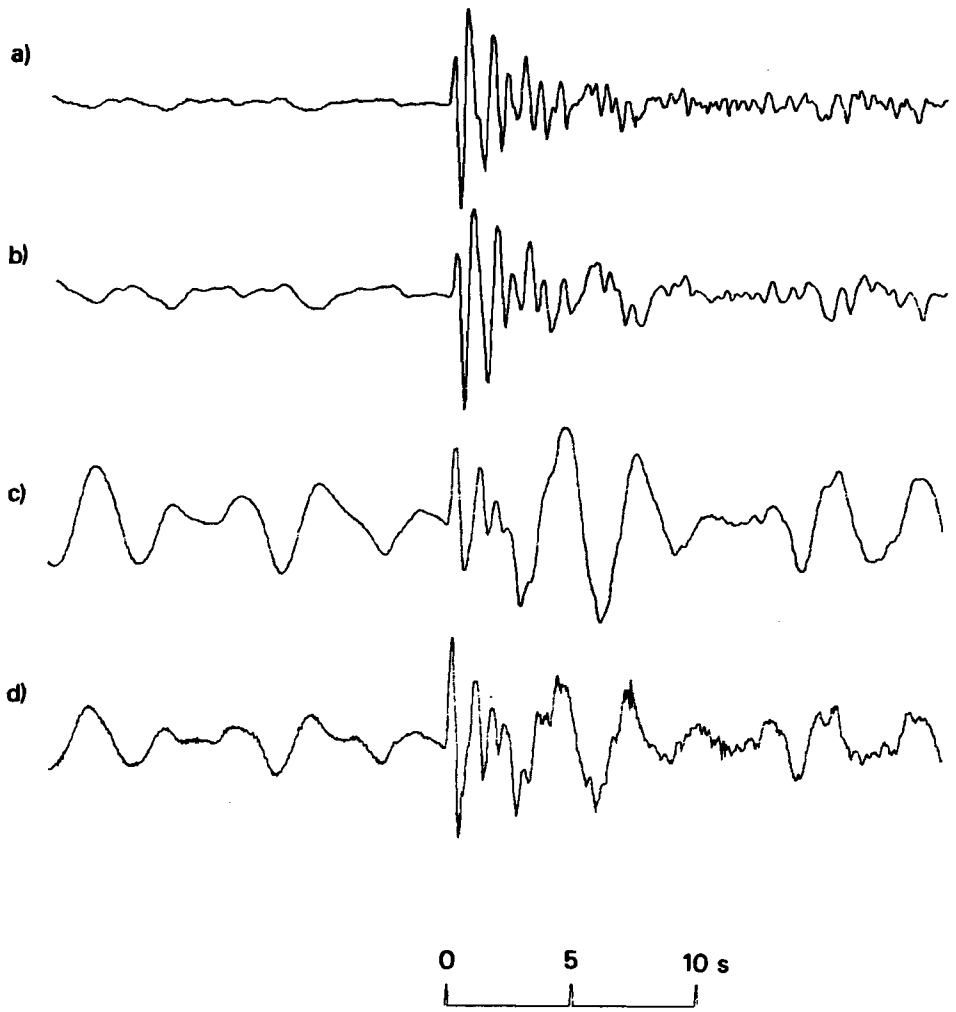

Figure A5 (a) Short-period array-sum seismogram recorded at WRA from the 19 June 1968 Shagan River explosion.
(b) Seismogram (a) filtered to simulate the effects of an additional t* of 0.2s.
(c) Seismogram (a) after Wiener filtering converted to a phaseless-broad-band instrument response.
(d) Same as seismogram (c) except that the effects of path attenuation of t* = 0.15s have been corrected for.
Note that PcP should arrive within a few seconds of P.

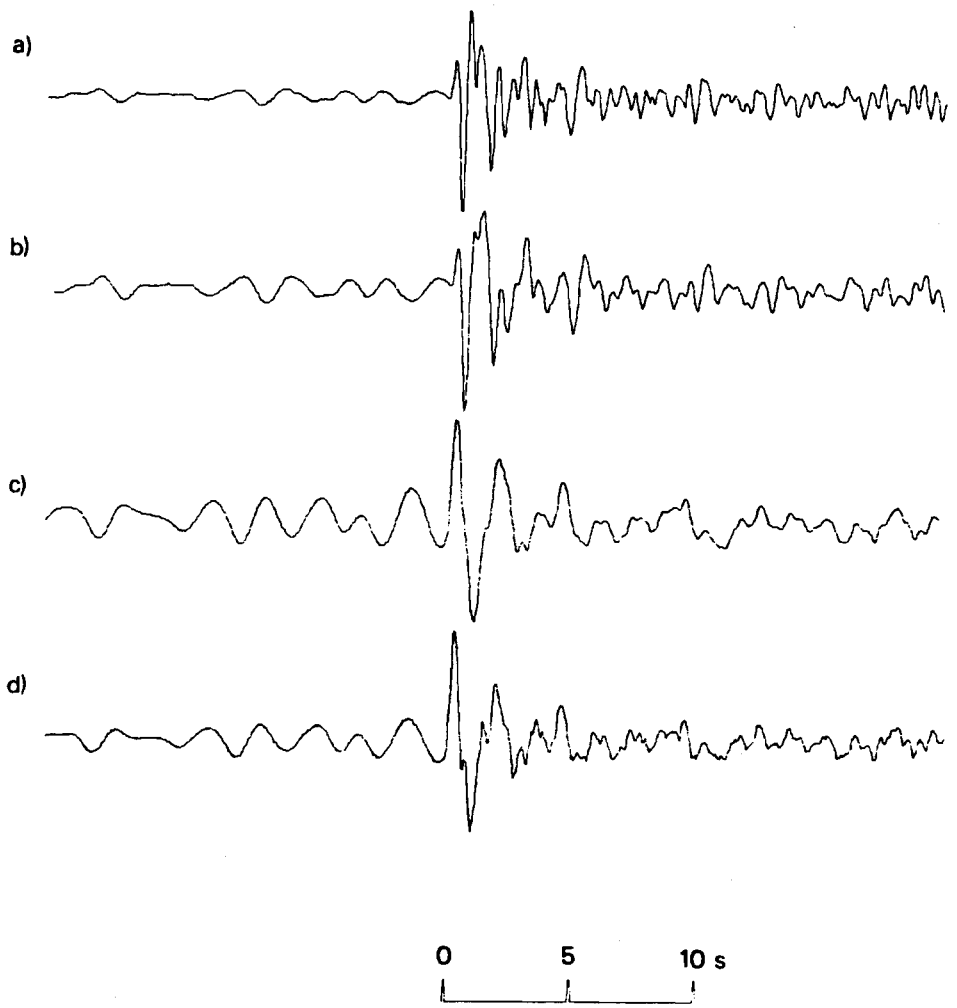

Figure A6 (a) Short-period array-sum seismogram recorded at EKA from the 30 November 1969 Shagan River explosion.
(b) Seismogram (a) filtered to simulate the effects of an additional t* of 0.2s.
(c) Seismogram (a) after Wiener filtering converted to a phaseless-broad-band instrument response.
(d) Same as seismogram (c) except that the effects of path attenuation of t* = 0.15s have been corrected for.

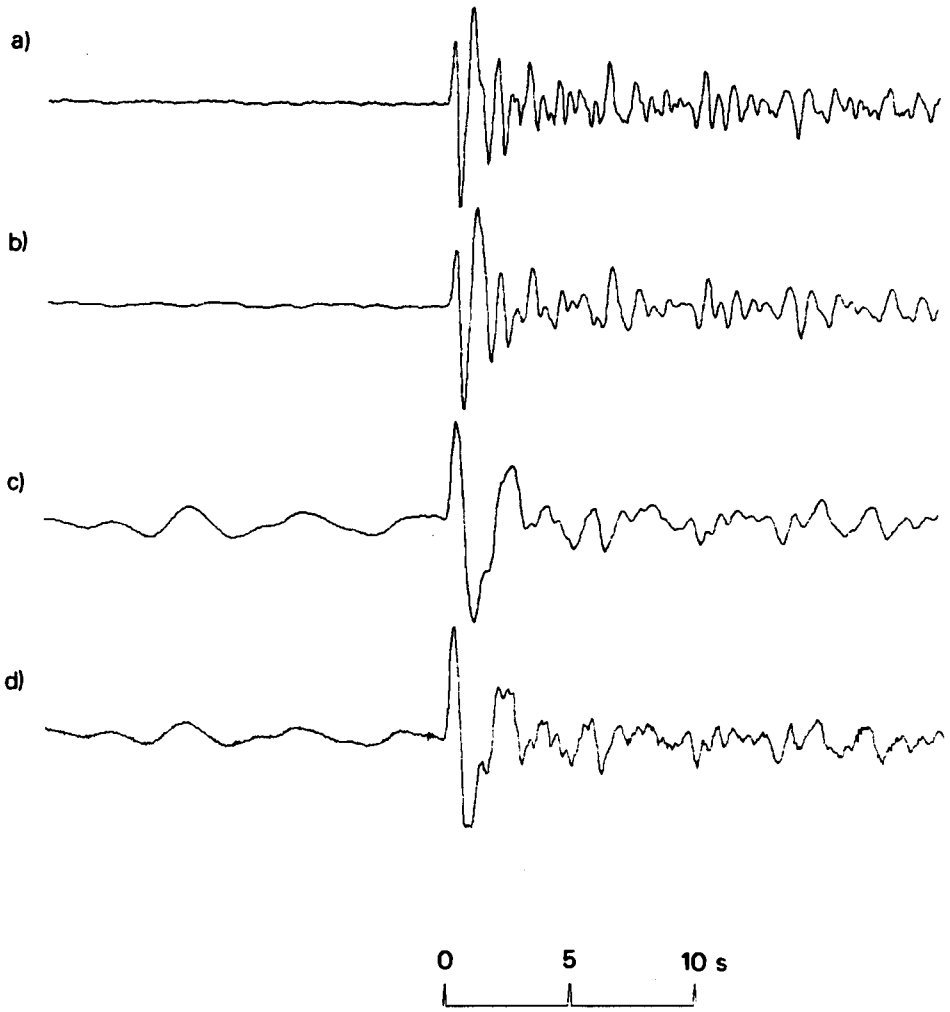

Figure A7 (a) Short-period array-sum seismogram recorded at WRA from the 30 November 1969 Shagan River explosion.
(b) Seismogram (a) filtered to simulate the effects of an additional t* of 0.2s.
(c) Seismogram (a) after Wiener filtering converted to a phaseless-broad-band instrument response.
(d) Same as seismogram (c) except that the effects of path attenuation of t* = 0.15s have been corrected for.
Note that PcP should arrive within a few seconds of P.

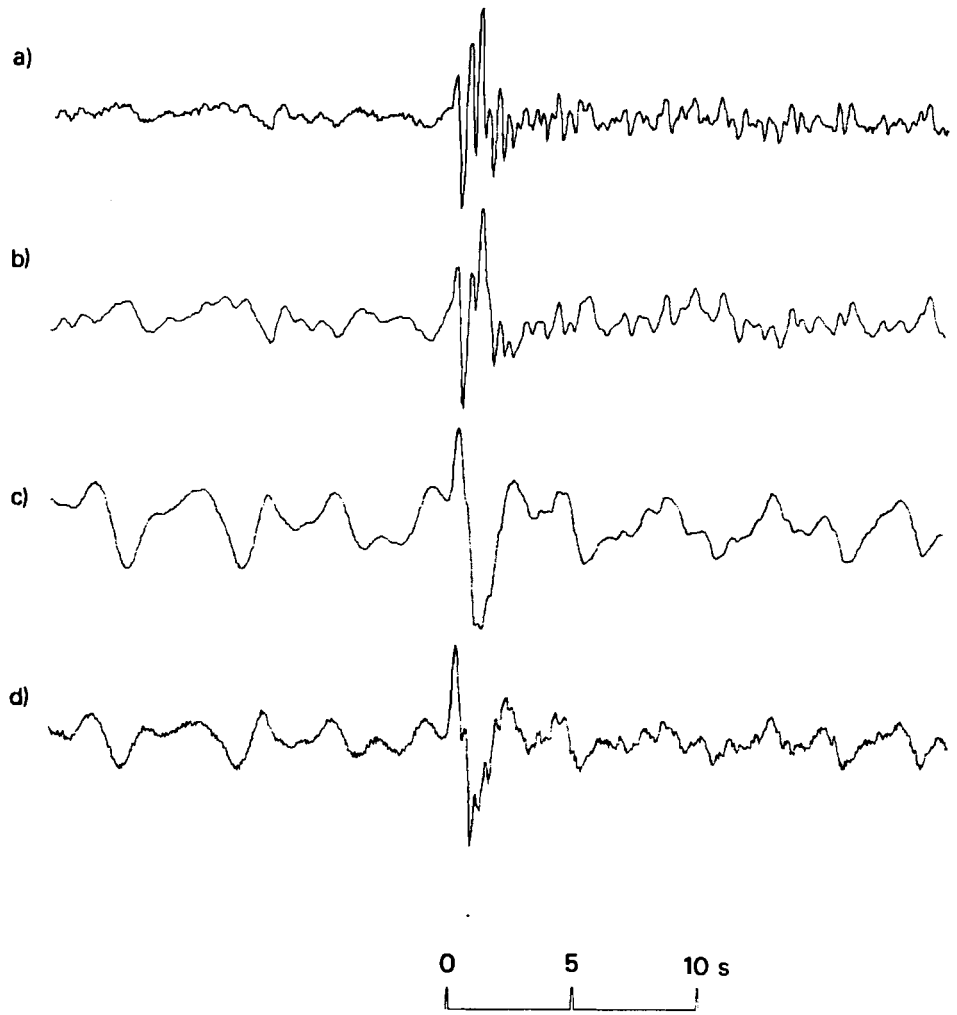

Figure A8 (a) Short-period array-sum seismogram recorded at EKA from the 30 June 1971 Shagan River explosion.
(b) Seismogram (a) filtered to simulate the effects of an additional t* of 0.2s.
(c) Seismogram (a) after Wiener filtering converted to a phaseless-broad-band instrument response.
(d) Same as seismogram (c) except that the effects of path attenuation of t* = 0.15s have been corrected for.

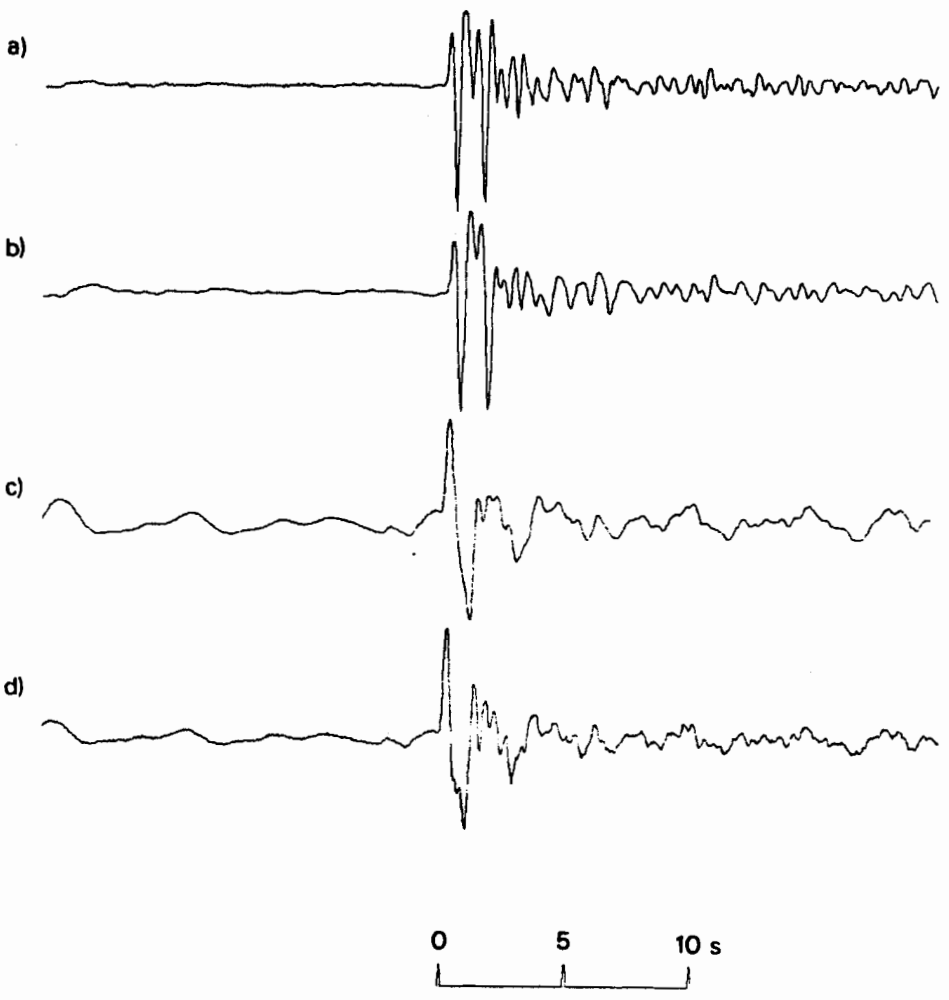

Figure A9 (a) Short-period array-sum seismogram recorded at YKA from the 30 June 1971 Shagan River explosion.
(b) Seismogram (a) filtered to simulate the effects of an additional t* of 0.2s.
(c) Seismogram (a) after Wiener filtering converted to a phaseless-broad-band instrument response.
(d) Same as seismogram (c) except that the effects of path attenuation of t* = 0.15s have been corrected for.

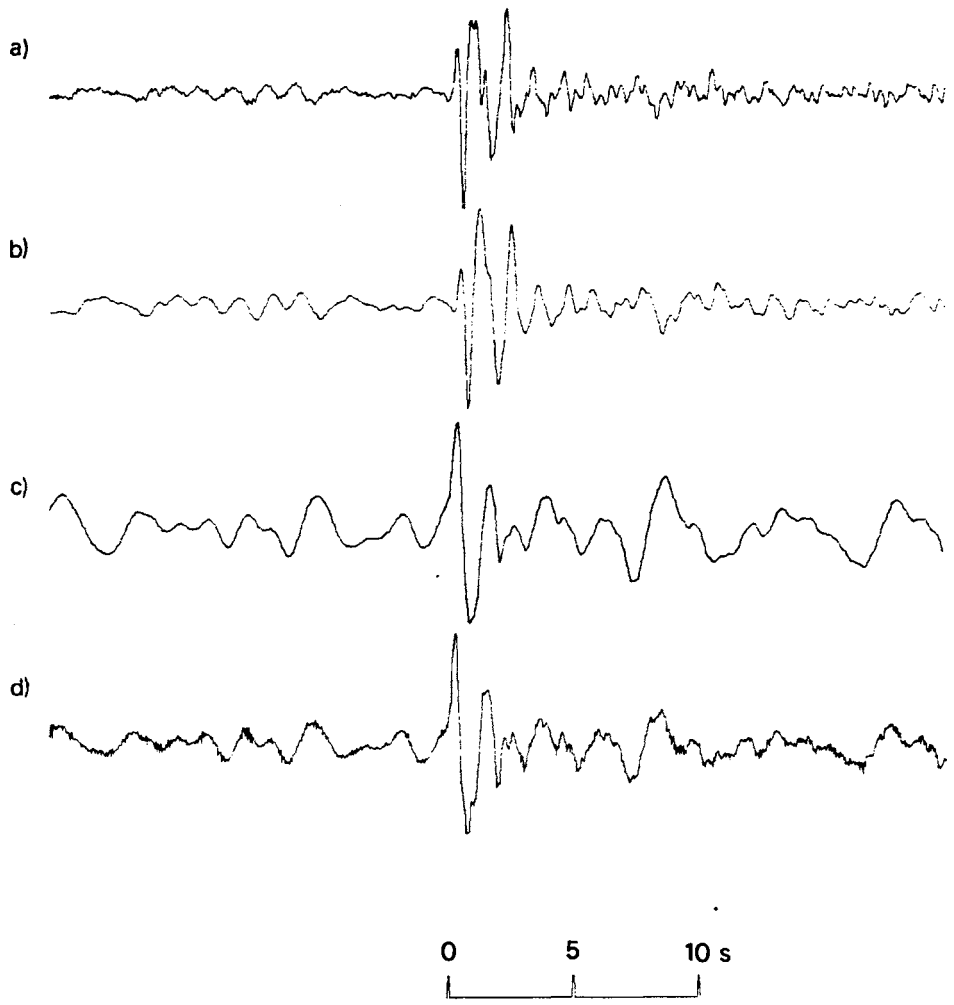

Figure A10 (a) Short-period array-sum seismogram recorded at GBA from the 30 June 1971 Shagan River explosion.
(b) Seismogram (a) filtered to simulate the effects of an additional t* of 0.2s.
(c) Seismogram (a) after Wiener filtering converted to a phaseless-broad-band instrument response.
(d) Same as seismogram (c) except that the effects of path attenuation of t* = 0.15s have been corrected for.

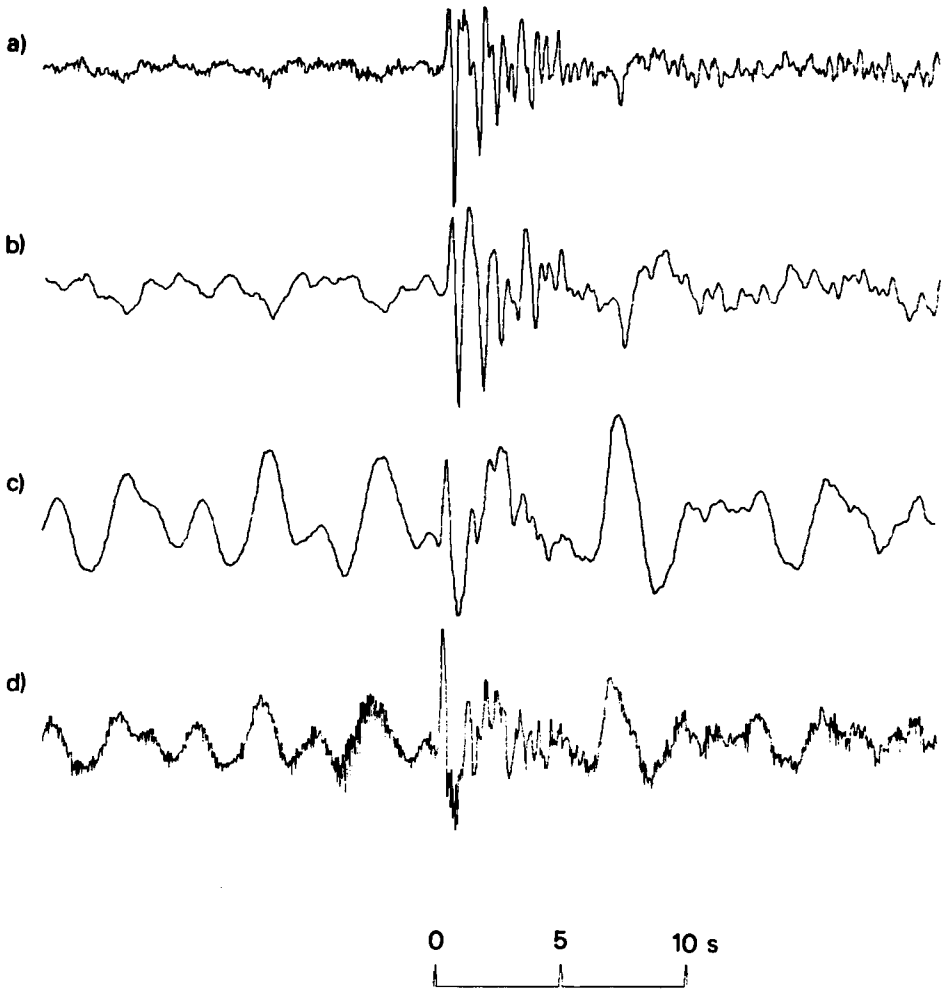

Figure A11 (a) Short-period array-sum seismogram recorded at WRA from the 30 June 1971 Shagan River explosion.
(b) Seismogram (a) filtered to simulate the effects of an additional t* of 0.2s.
(c) Seismogram (a) after Wiener filtering converted to a phaseless-broad-band instrument response.
(d) Same as seismogram (c) except that the effects of path attenuation of t* = 0.15s have been corrected for.
Note that PcP should arrive within a few seconds of P.

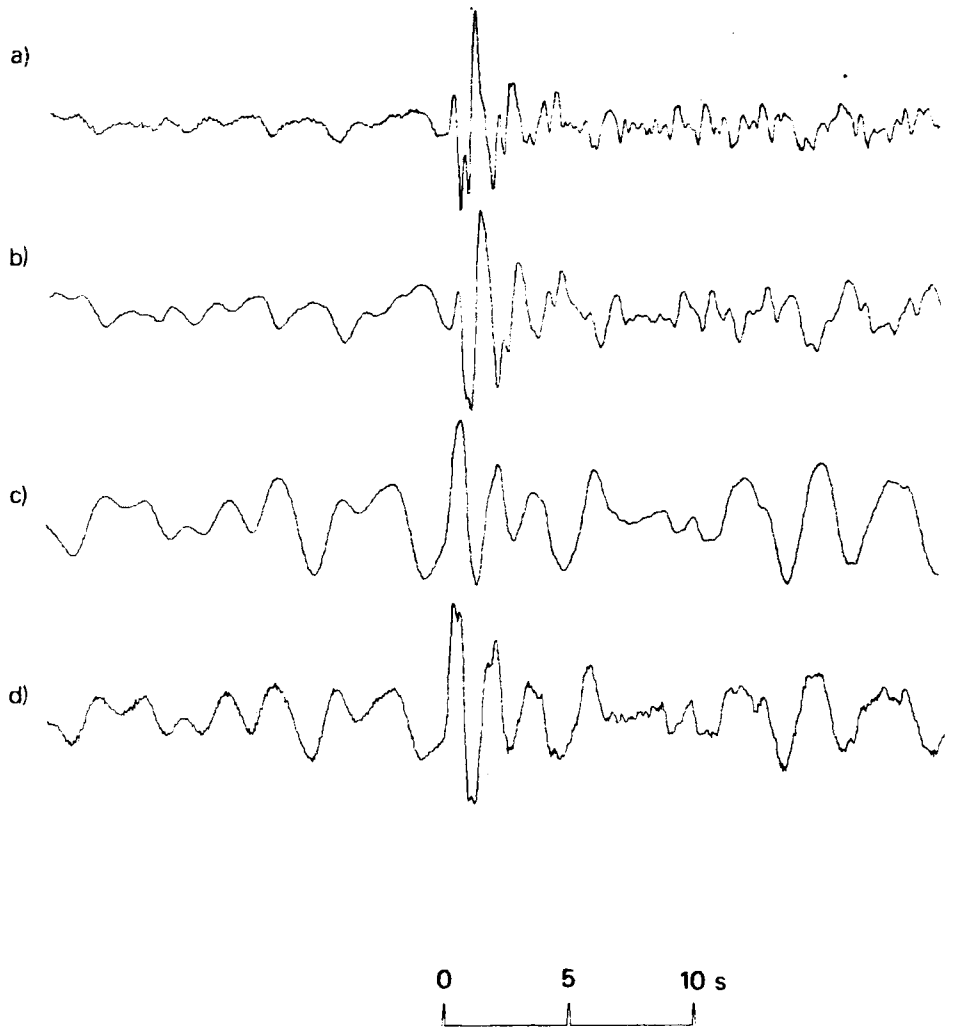

Figure A12 (a) Short-period array-sum seismogram recorded at EKA from the 10 February 1972 Shagan River explosion.
(b) Seismogram (a) filtered to simulate the effects of an additional t* of 0.2s.
(c) Seismogram (a) after Wiener filtering converted to a phaseless-broad-band instrument response.
(d) Same as seismogram (c) except that the effects of path attenuation of t* = 0.15s have been corrected for.

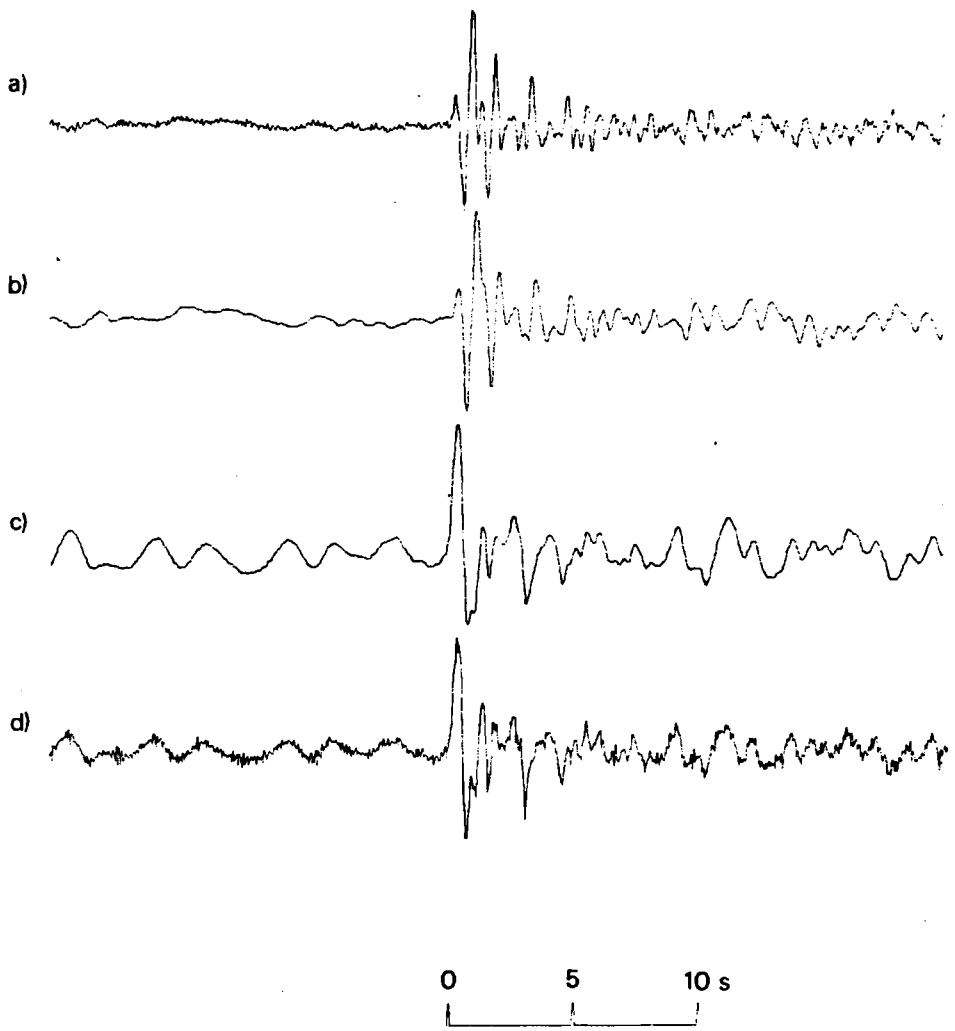

Figure A13 (a) Short-period array-sum seismogram recorded at WRA from the 10 February 1972 Shagan River explosion.
(b) Seismogram (a) filtered to simulate the effects of an additional t* of 0.2s.
(c) Seismogram (a) after Wiener filtering converted to a phaseless-broad-band instrument response.
(d) Same as seismogram (c) except that the effects of path attenuation of t* = 0.15s have been corrected for.
Note that PcP should arrive within a few seconds of P.

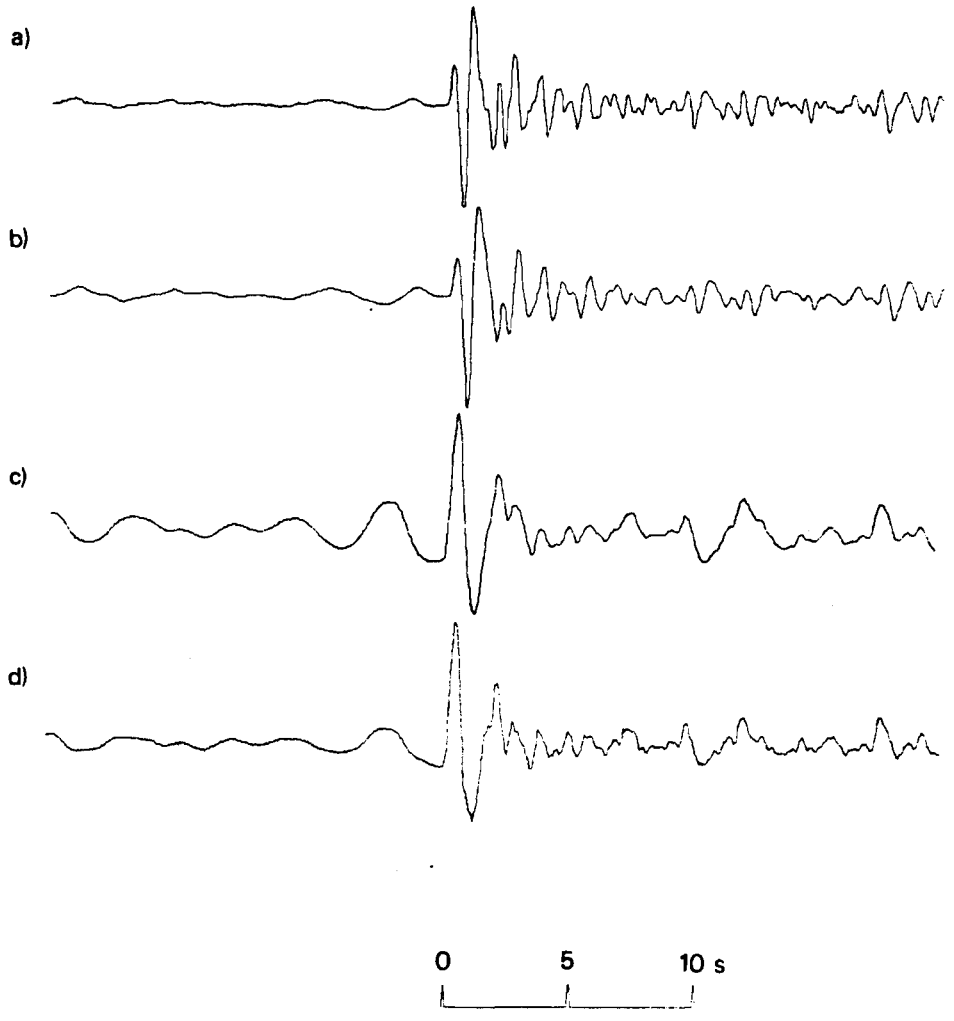

Figure A14 (a) Short-period array-sum seismogram recorded at EKA from the 2 November 1972 Shagan River explosion.
(b) Seismogram (a) filtered to simulate the effects of an additional t* of 0.2s.
(c) Seismogram (a) after Wiener filtering converted to a phaseless-broad-band instrument response.
(d) Same as seismogram (c) except that the effects of path attenuation of t* = 0.15s have been corrected for.

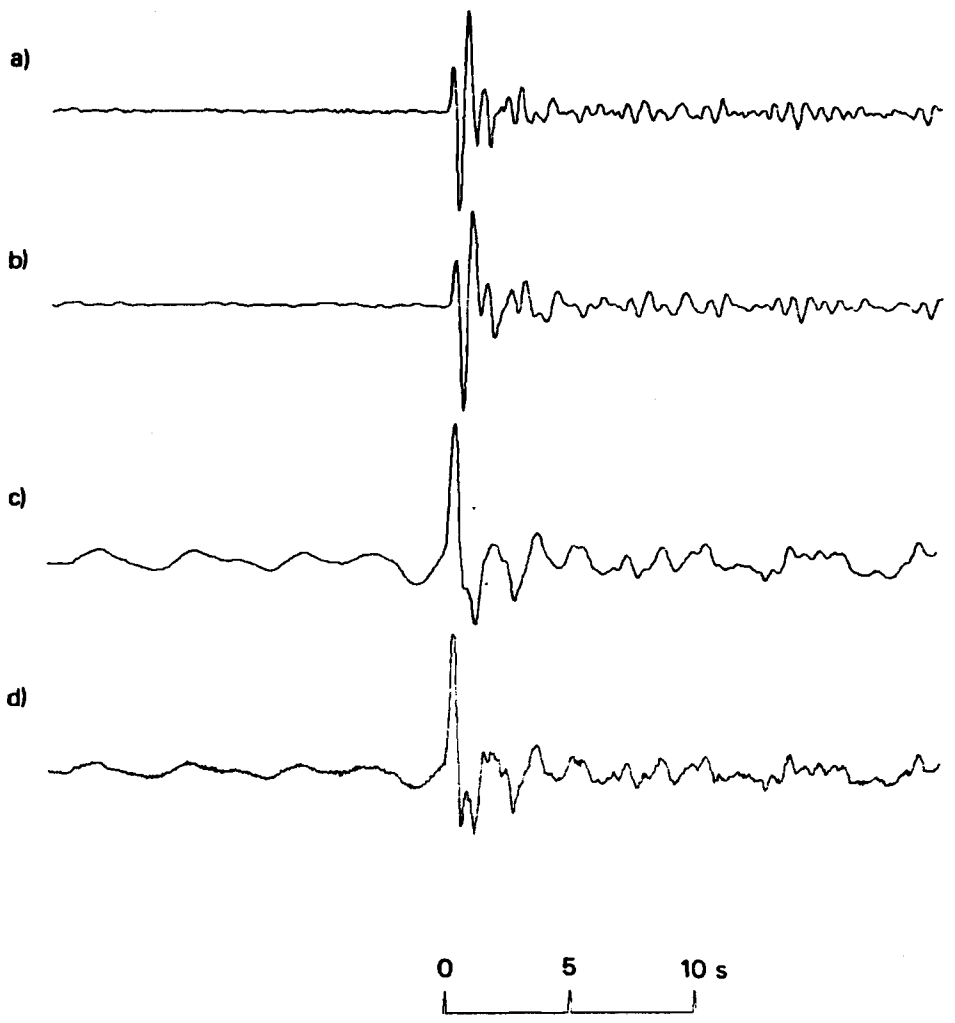

Figure A15 (a) Short-period strong-motion seismogram recorded at YKA from the 2 November 1972 Shagan River explosion.
(b) Seismogram (a) filtered to simulate the effects of an additional t* of 0.2s.
(c) Seismogram (a) after Wiener filtering converted to a phaseless-broad-band instrument response.
(d) Same as seismogram (c) except that the effects of path attenuation of t* = 0.15s have been corrected for.

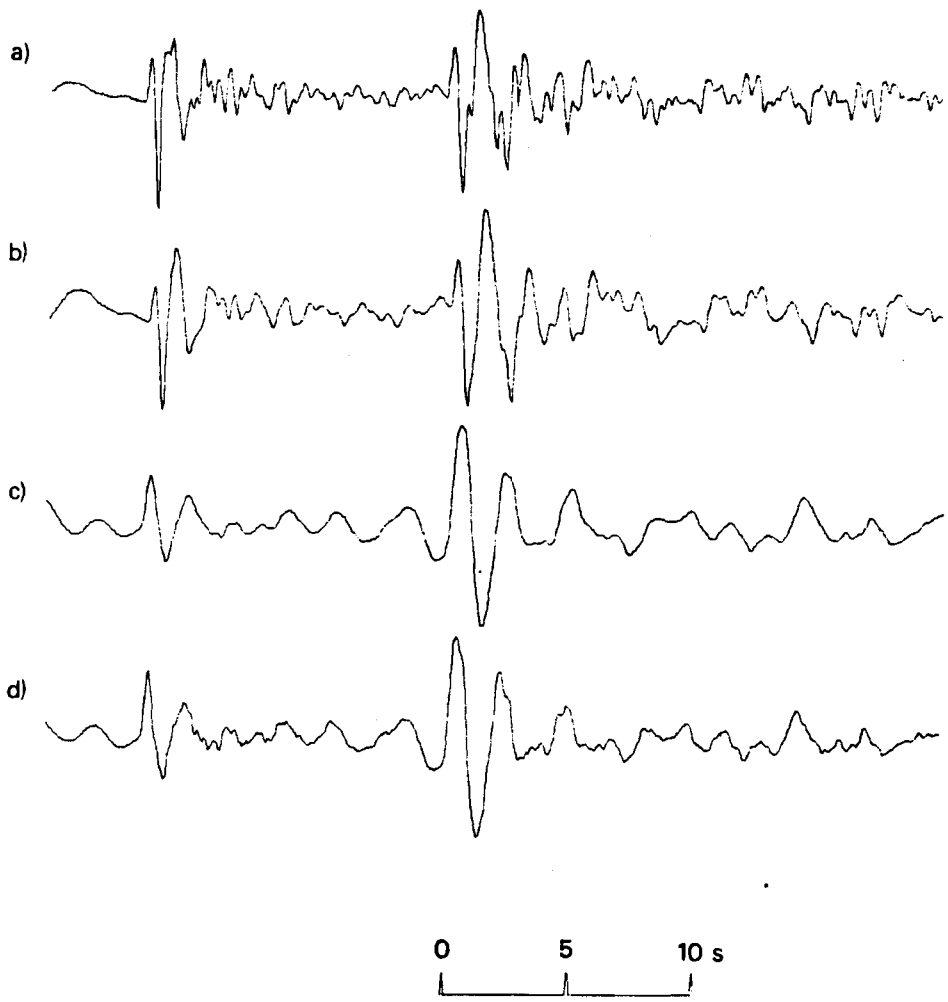

Figure A16 (a) Short-period array-sum seismogram recorded at EKA from the 10 December 1972 Shagan River explosion.
(b) Seismogram (a) filtered to simulate the effects of an additional t* of 0.2s.
(c) Seismogram (a) after Wiener filtering converted to a phaseless-broad-band instrument response.
(d) Same as seismogram (c) except that the effects of path attenuation of t* = 0.15s have been corrected for.
Note that the sample of noise used in designing the Wiener filter is taken ahead of the earlier arrival (from an explosion at Degelen Mountain).

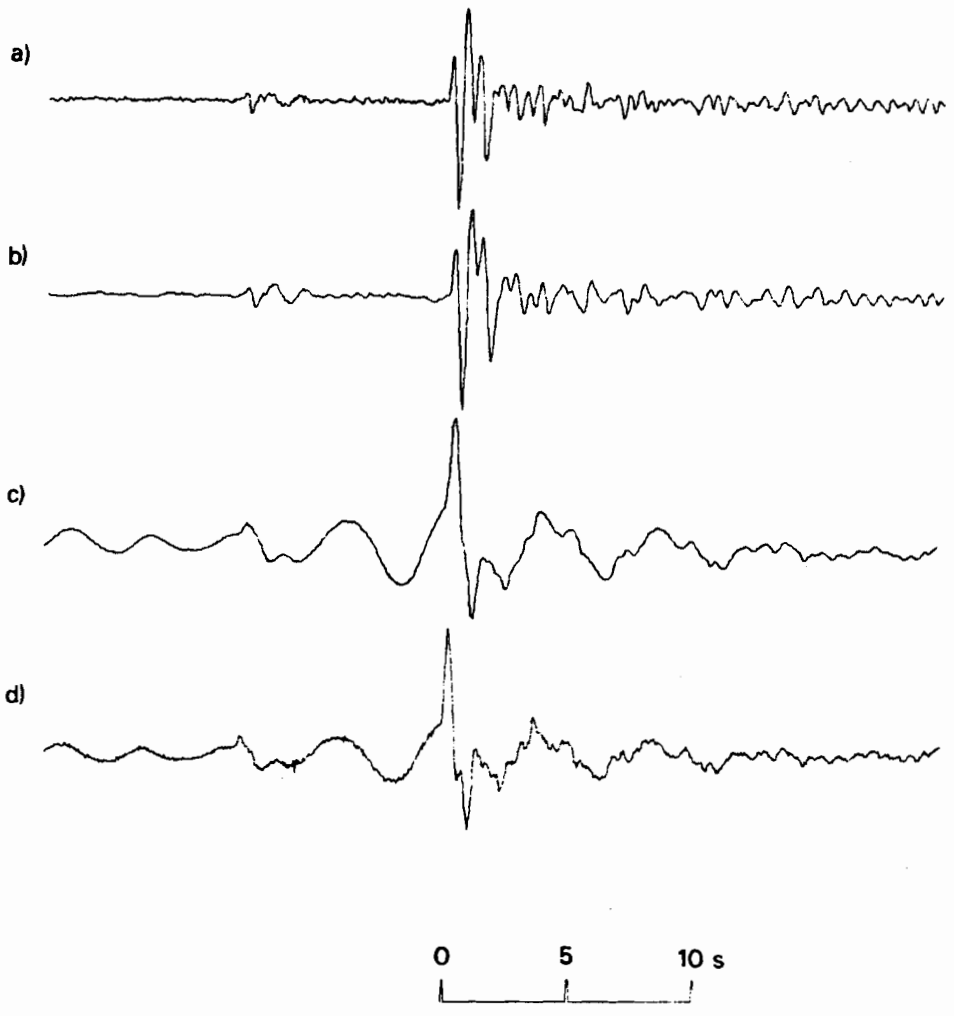

Figure A17 (a) Short-period strong-motion seismogram recorded at YKA from the 10 December 1972 Shagan River explosion.
(b) Seismogram (a) filtered to simulate the effects of an additional t* of 0.2s.
(c) Seismogram (a) after Wiener filtering converted to a phaseless-broad-band instrument response.
(d) Same as seismogram (c) except that the effects of path attenuation of t* = 0.15s have been corrected for.
Note that the sample of noise used in designing the Wiener filter is taken ahead of the earlier arrival (from an explosion at Degelen Mountain).

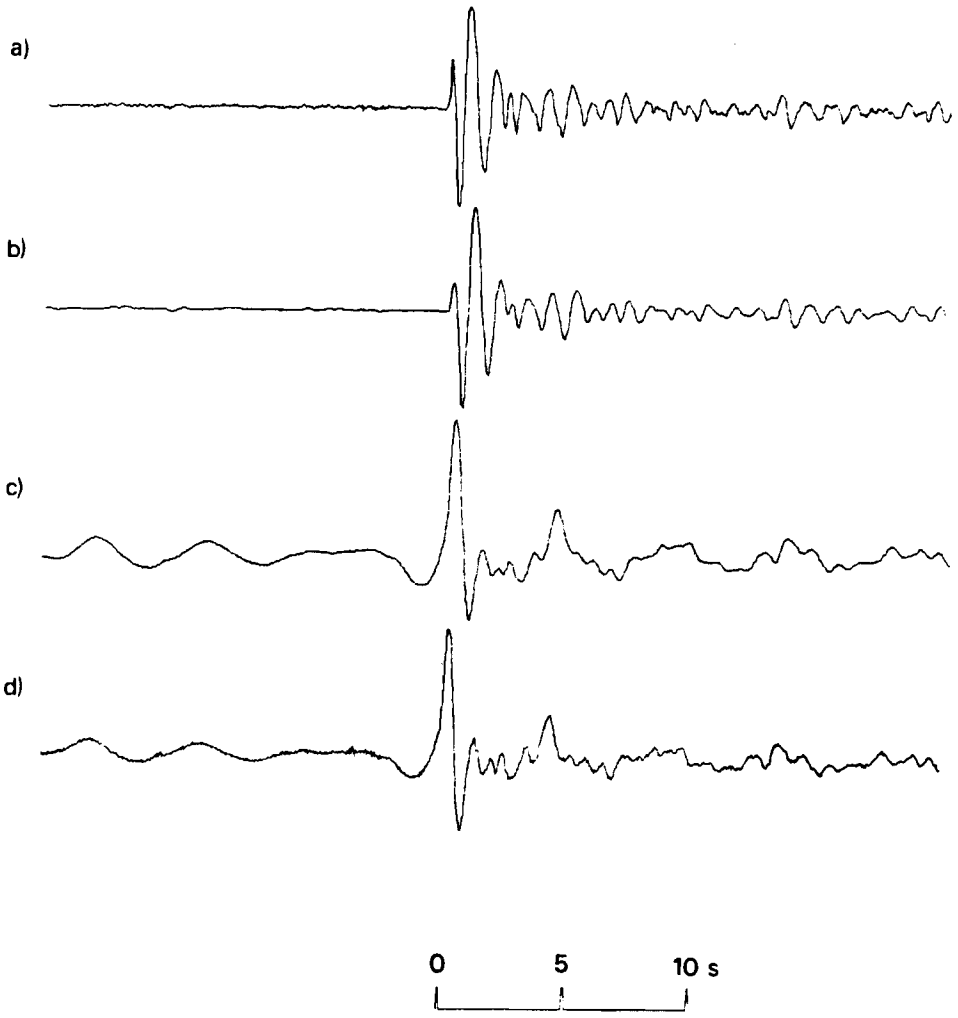

Figure A18 (a) Short-period strong-motion seismogram recorded at YKA from the 23 July 1973 Shagan River explosion.
(b) Seismogram (a) filtered to simulate the effects of an additional t* of 0.2s.
(c) Seismogram (a) after Wiener filtering converted to a phaseless-broad-band instrument response.
(d) Same as seismogram (c) except that the effects of path attenuation of t* = 0.15s have been corrected for.

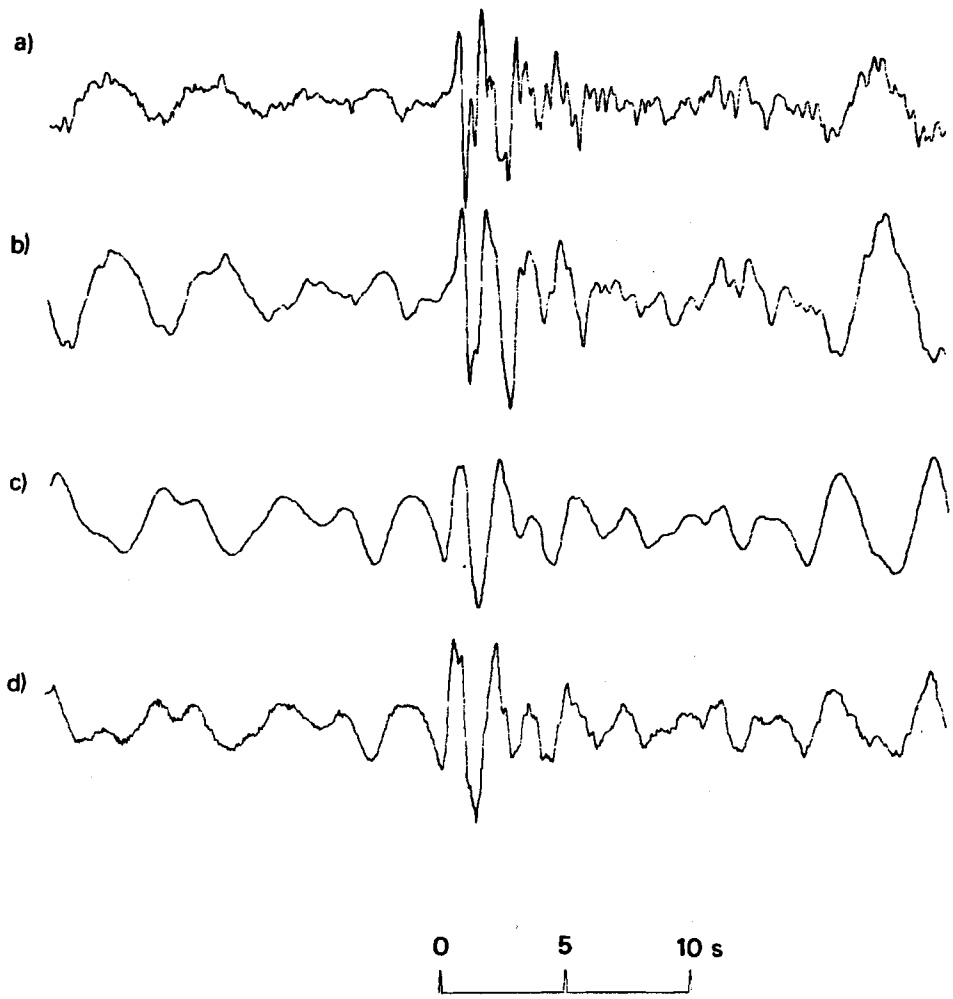

Figure A19 (a) Short-period array-sum seismogram recorded at EKA from the 14 December 1973 Shagan River explosion.
(b) Seismogram (a) filtered to simulate the effects of an additional t* of 0.2s.
(c) Seismogram (a) after Wiener filtering converted to a phaseless-broad-band instrument response.
(d) Same as seismogram (c) except that the effects of path attenuation of t* = 0.15s have been corrected for.

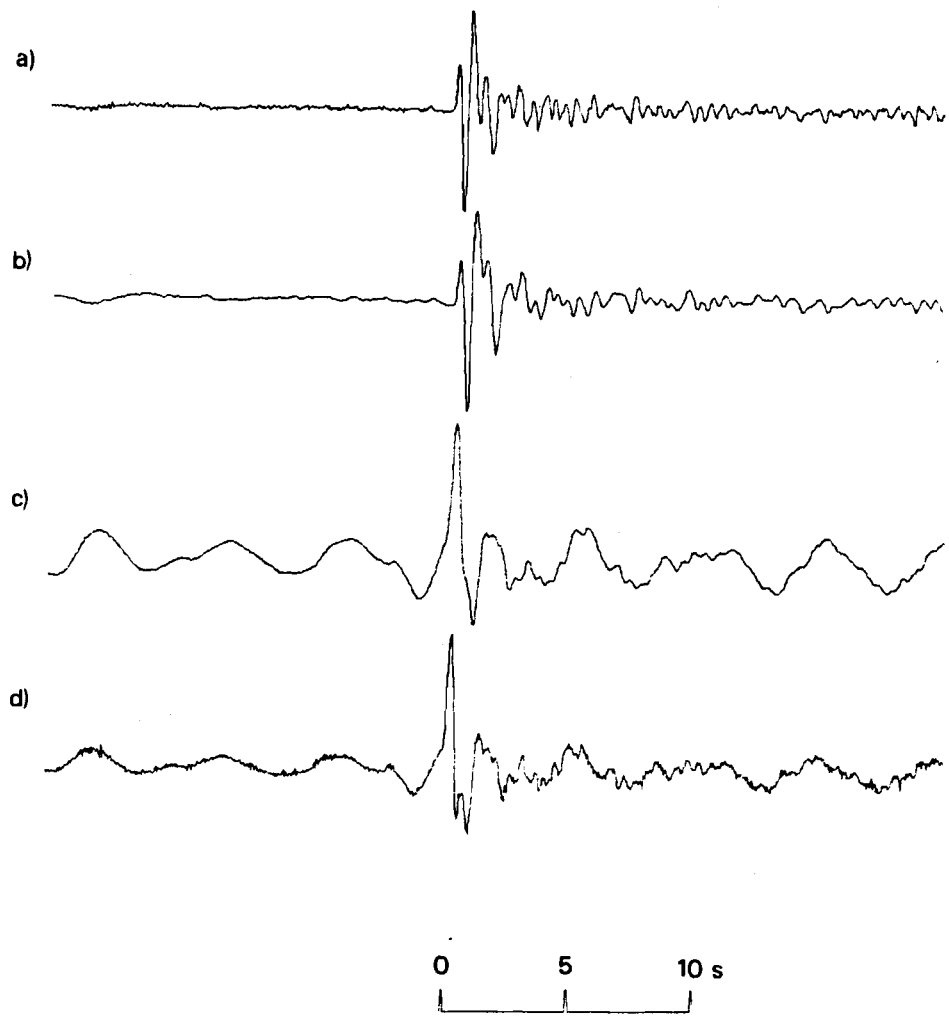

Figure A20 (a) Short-period strong-motion seismogram recorded at YKA from the 14 December 1973 Shagan River explosion.
(b) Seismogram (a) filtered to simulate the effects of an additional t* of 0.2s.
(c) Seismogram (a) after Wiener filtering converted to a phaseless-broad-band instrument response.
(d) Same as seismogram (c) except that the effects of path attenuation of t* = 0.15s have been corrected for.

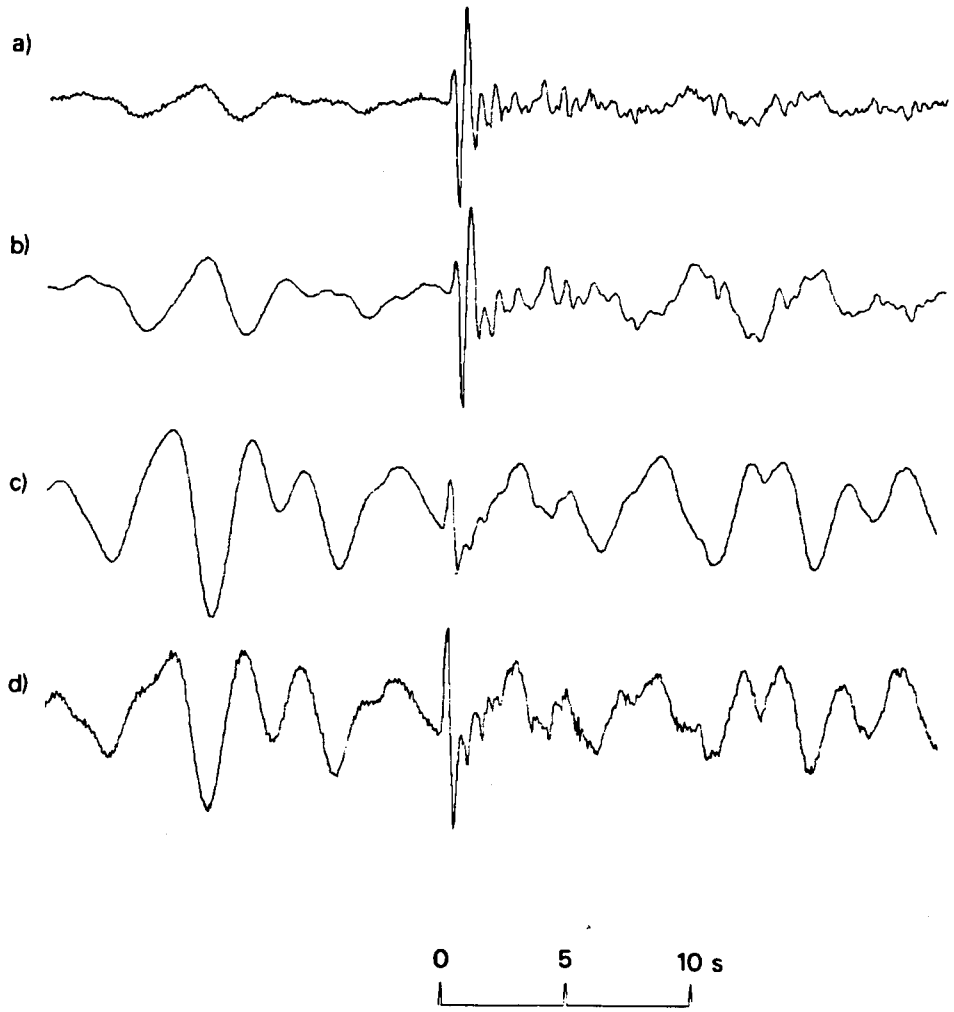

Figure A21 (a) Short-period array-sum seismogram recorded at YKA from the 16 April 1974 Shagan River explosion.
(b) Seismogram (a) filtered to simulate the effects of an additional t* of 0.2s.
(c) Seismogram (a) after Wiener filtering converted to a phaseless-broad-band instrument response.
(d) Same as seismogram (c) except that the effects of path attenuation of t* = 0.15s have been corrected for.

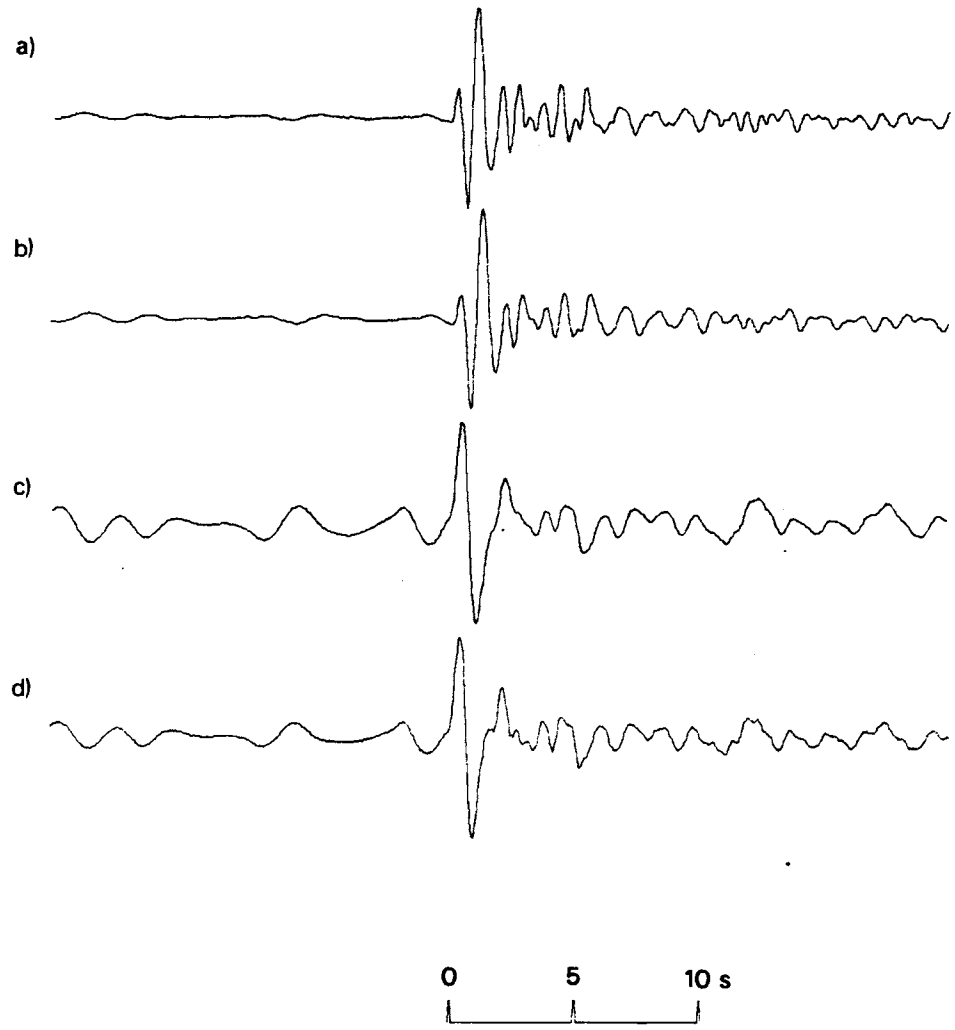

Figure A22 (a) Short-period array-sum seismogram recorded at EKA from the 31 May 1974 Shagan River explosion.
(b) Seismogram (a) filtered to simulate the effects of an additional t* of 0.2s.
(c) Seismogram (a) after Wiener filtering converted to a phaseless-broad-band instrument response.
(d) Same as seismogram (c) except that the effects of path attenuation of t* = 0.15s have been corrected for.

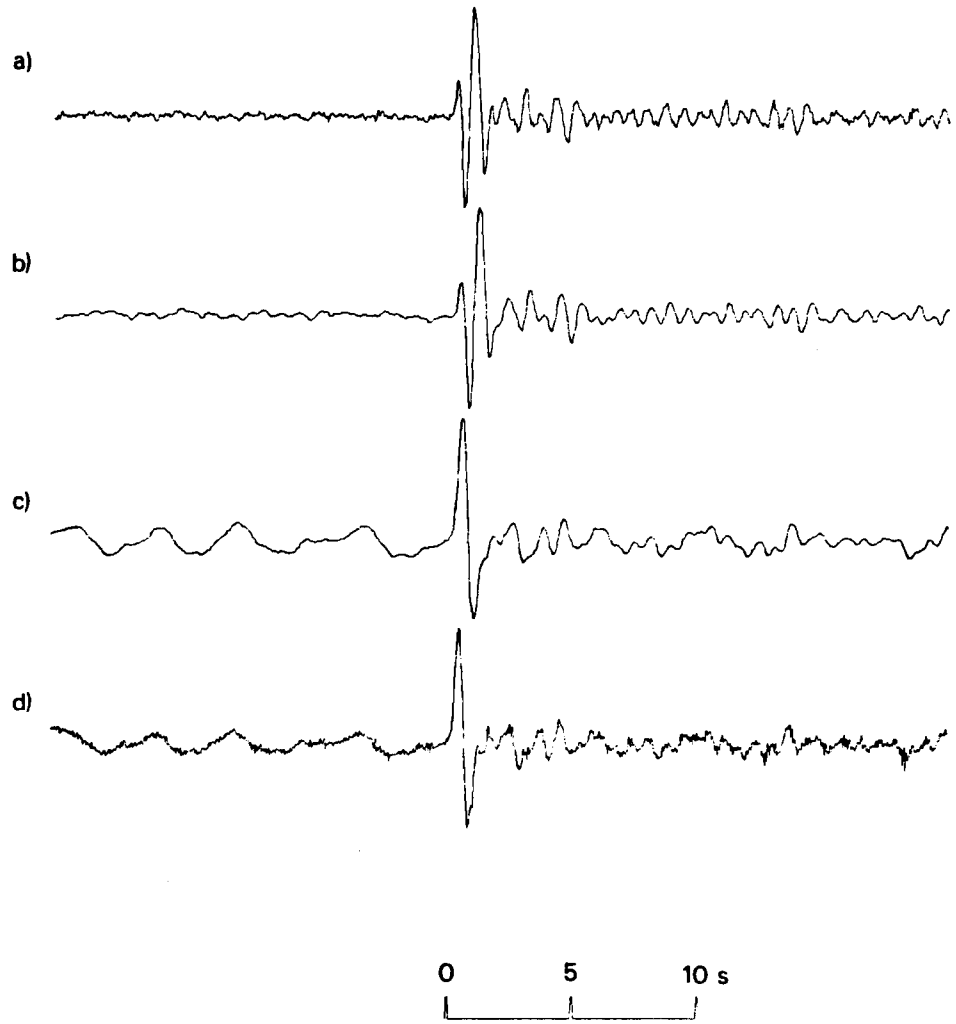

Figure A23 (a) Short-period strong-motion seismogram recorded at YKA from the 31 May 1974 Shagan River explosion.
(b) Seismogram (a) filtered to simulate the effects of an additional t* of 0.2s.
(c) Seismogram (a) after Wiener filtering converted to a phaseless-broad-band instrument response.
(d) Same as seismogram (c) except that the effects of path attenuation of t* = 0.15s have been corrected for.

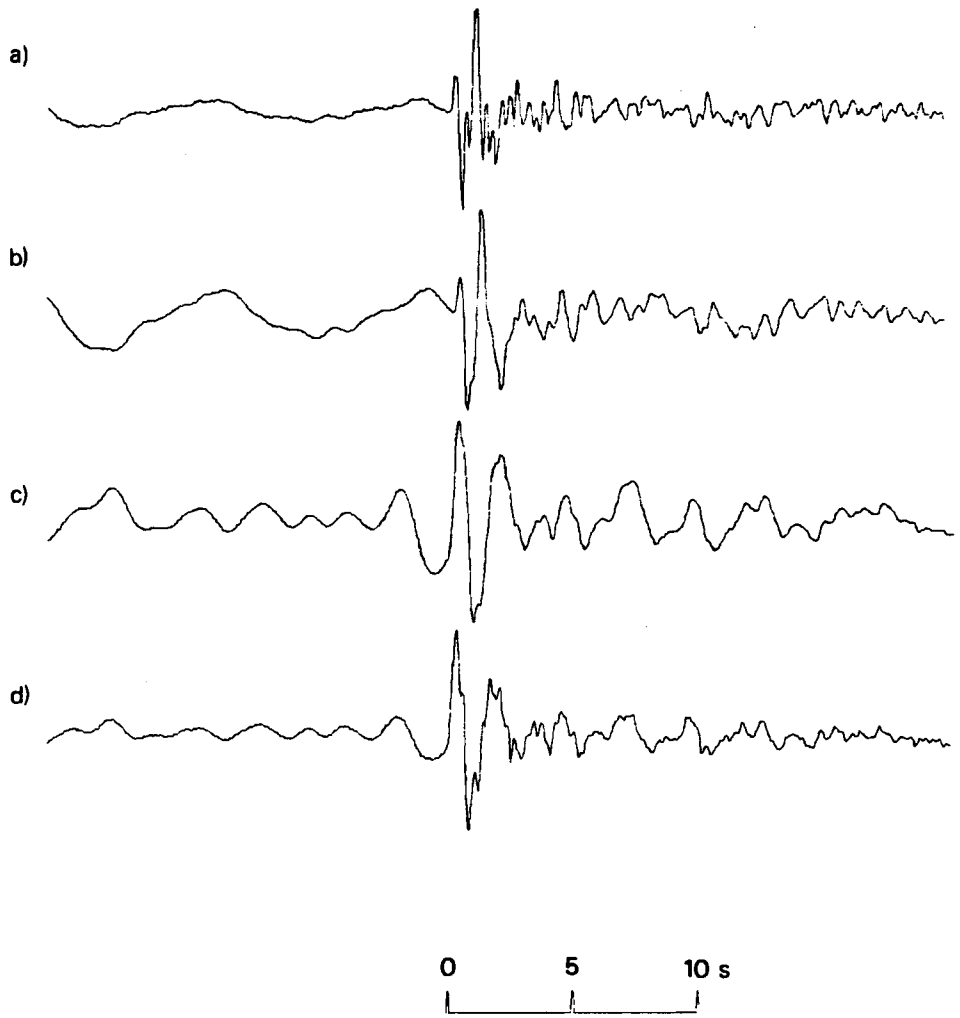

Figure A24 (a) Short-period array-sum seismogram recorded at EKA from the 16 October 1974 Shagan River explosion.
(b) Seismogram (a) filtered to simulate the effects of an additional t* of 0.2s.
(c) Seismogram (a) after Wiener filtering converted to a phaseless-broad-band instrument response.
(d) Same as seismogram (c) except that the effects of path attenuation of t* = 0.15s have been corrected for.

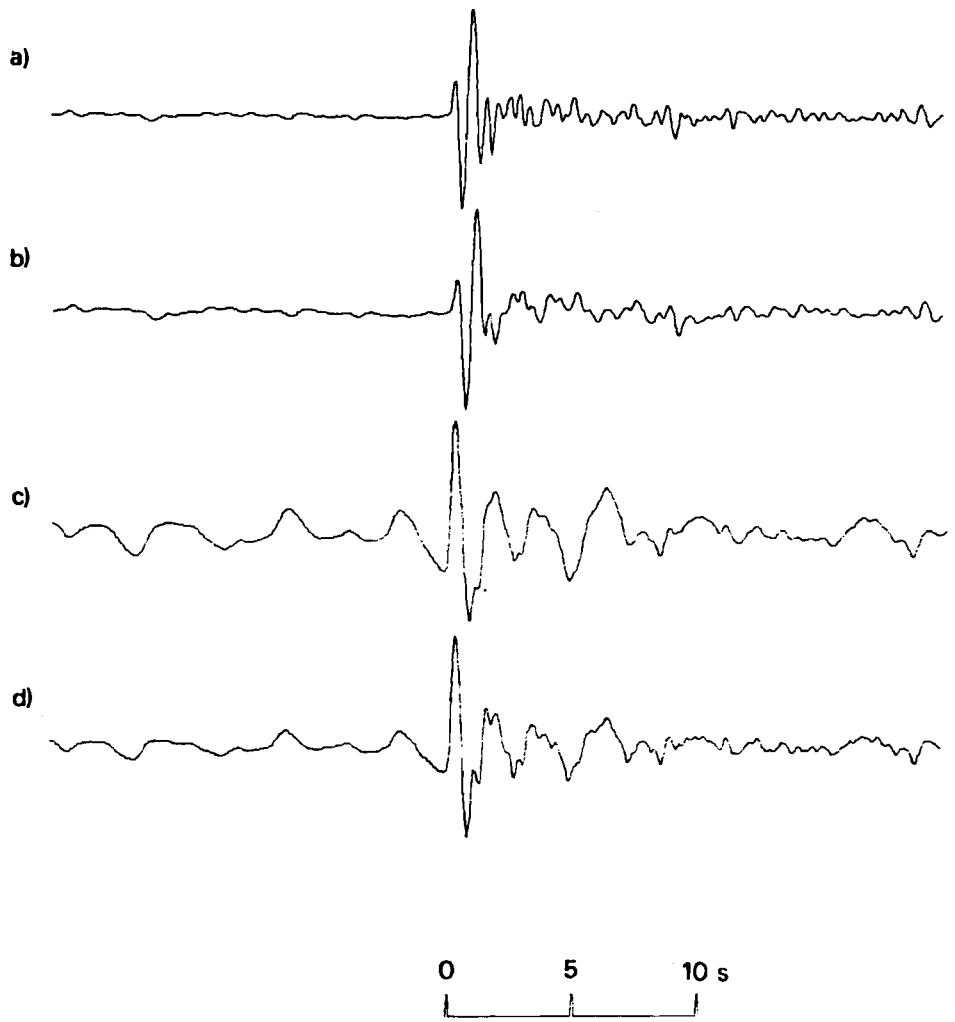

Figure A25 (a) Short-period array-sum seismogram recorded at YKA from the 16 October 1974 Shagan River explosion.
(b) Seismogram (a) filtered to simulate the effects of an additional t* of 0.2s.
(c) Seismogram (a) after Wiener filtering converted to a phaseless-broad-band instrument response.
(d) Same as seismogram (c) except that the effects of path attenuation of t* = 0.15s have been corrected for.

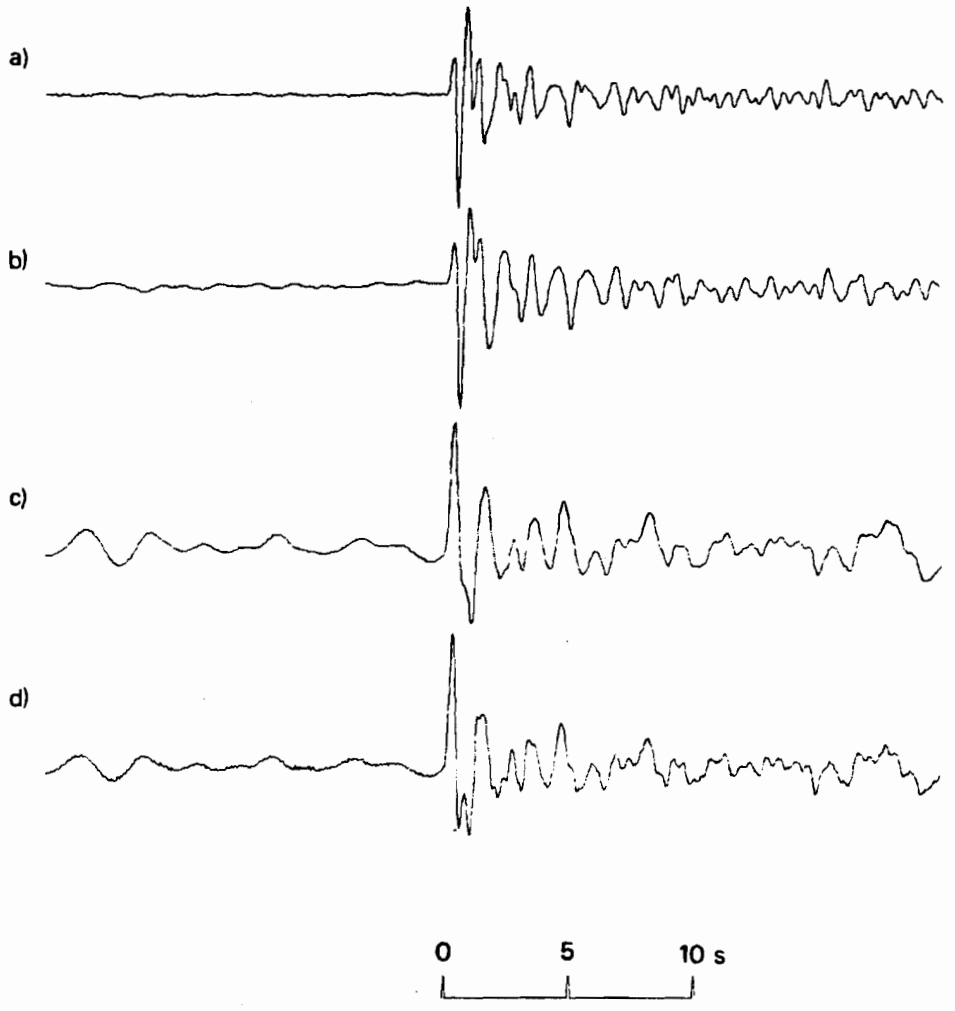

Figure A26 (a) Short-period array-sum seismogram recorded at GBA from the 16 October 1974 Shagan River explosion.
(b) Seismogram (a) filtered to simulate the effects of an additional t* of 0.2s.
(c) Seismogram (a) after Wiener filtering converted to a phaseless-broad-band instrument response.
(d) Same as seismogram (c) except that the effects of path attenuation of t* = 0.15s have been corrected for.

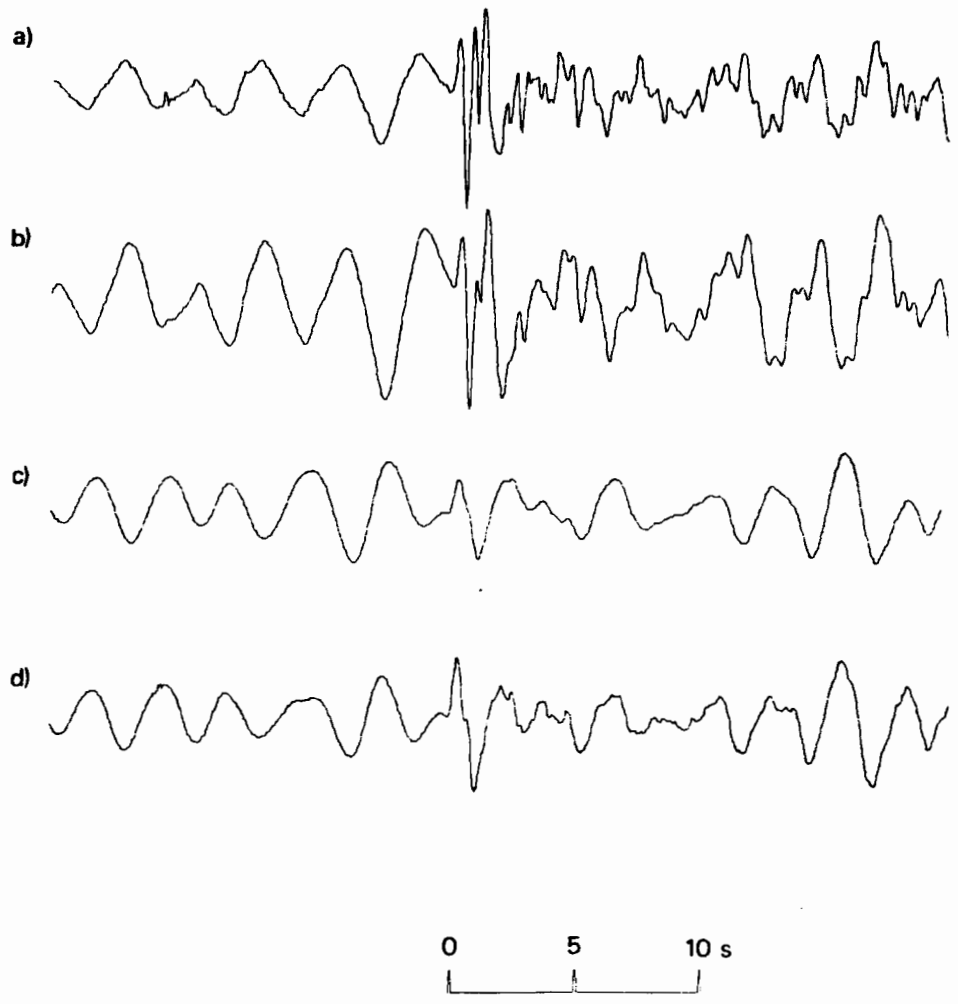

Figure A27 (a) Short-period array-sum seismogram recorded at EKA from the 27 December 1974 Shagan River explosion.
(b) Seismogram (a) filtered to simulate the effects of an additional t* of 0.2s.
(c) Seismogram (a) after Wiener filtering converted to a phaseless-broad-band instrument response.
(d) Same as seismogram (c) except that the effects of path attenuation of t* = 0.15s have been corrected for.

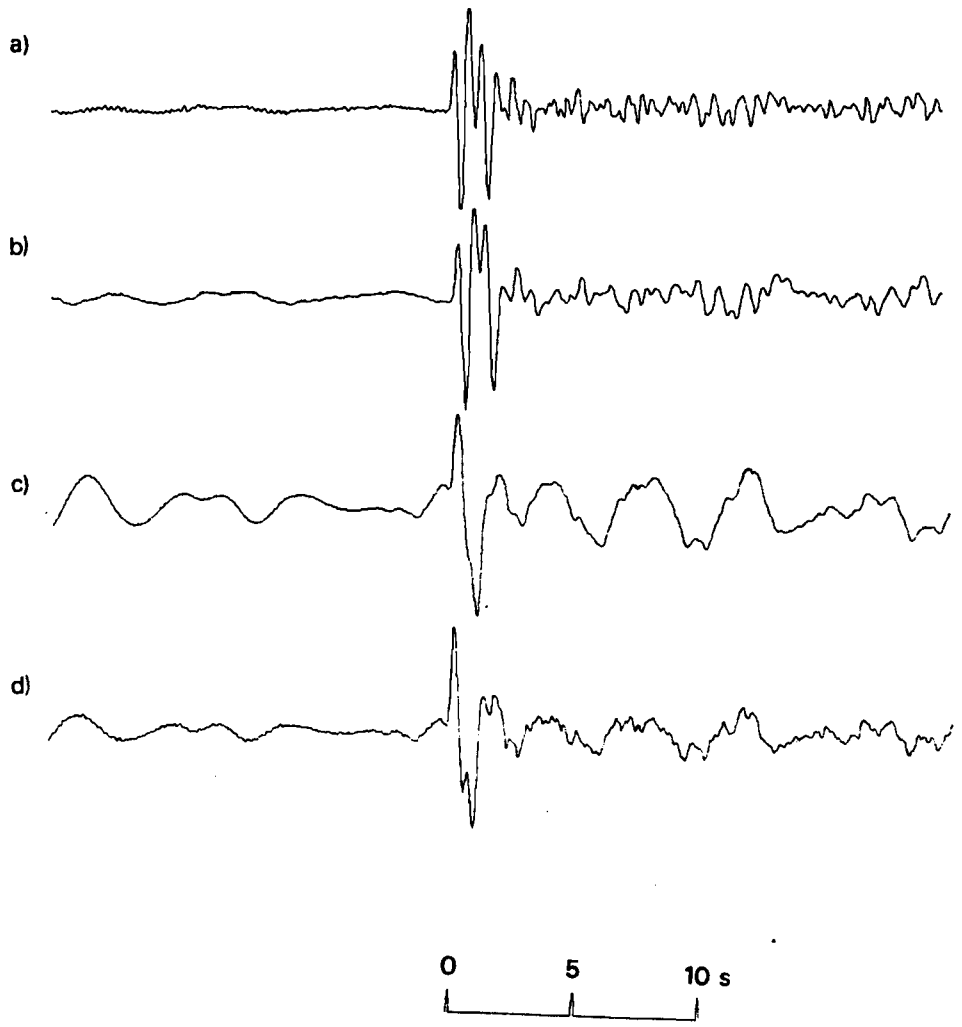

Figure A28 (a) Short-period array-sum seismogram recorded at YKA from the 27 December 1974 Shagan River explosion.
(b) Seismogram (a) filtered to simulate the effects of an additional t^* of 0.2s.
(c) Seismogram (a) after Wiener filtering converted to a phaseless-broad-band instrument response.
(d) Same as seismogram (c) except that the effects of path attenuation of $t^* = 0.15$s have been corrected for.

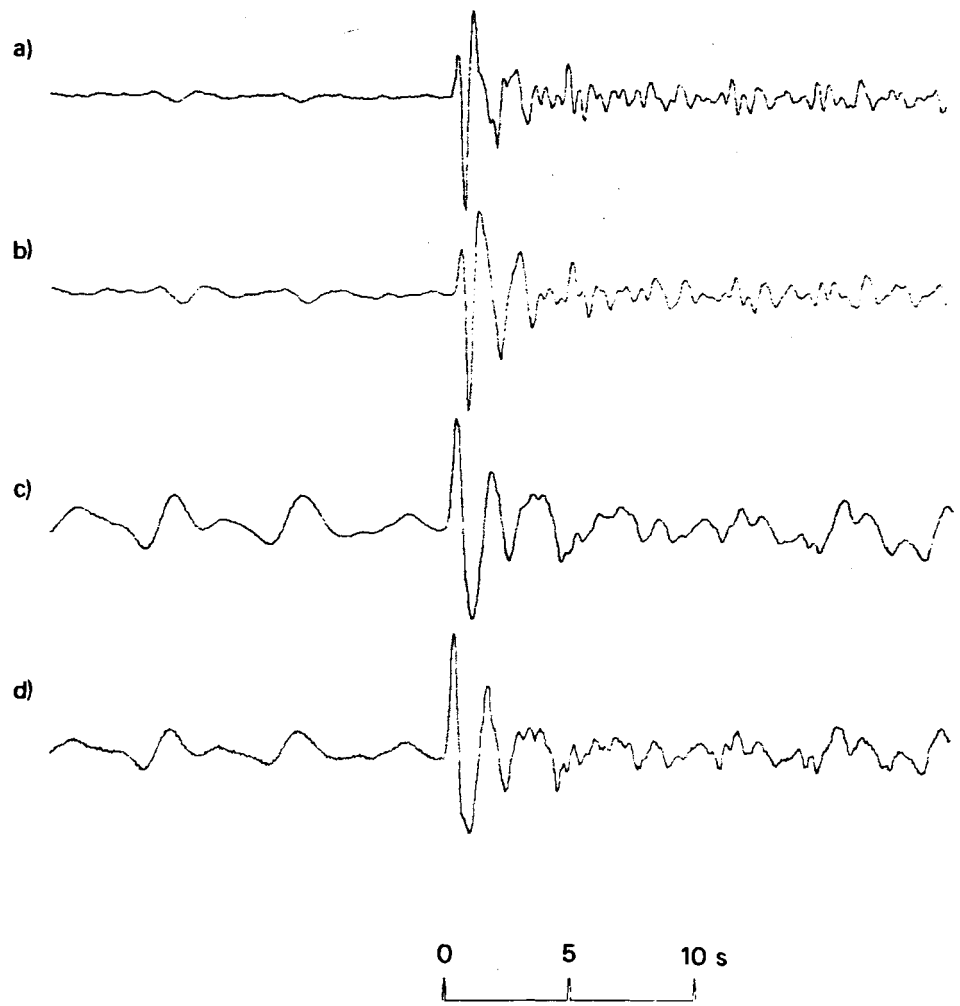

Figure A29 (a) Short-period array-sum seismogram recorded at GBA from the 27 December 1974 Shagan River explosion.
(b) Seismogram (a) filtered to simulate the effects of an additional t* of 0.2s.
(c) Seismogram (a) after Wiener filtering converted to a phaseless-broad-band instrument response.
(d) Same as seismogram (c) except that the effects of path attenuation of t* = 0.15s have been corrected for.

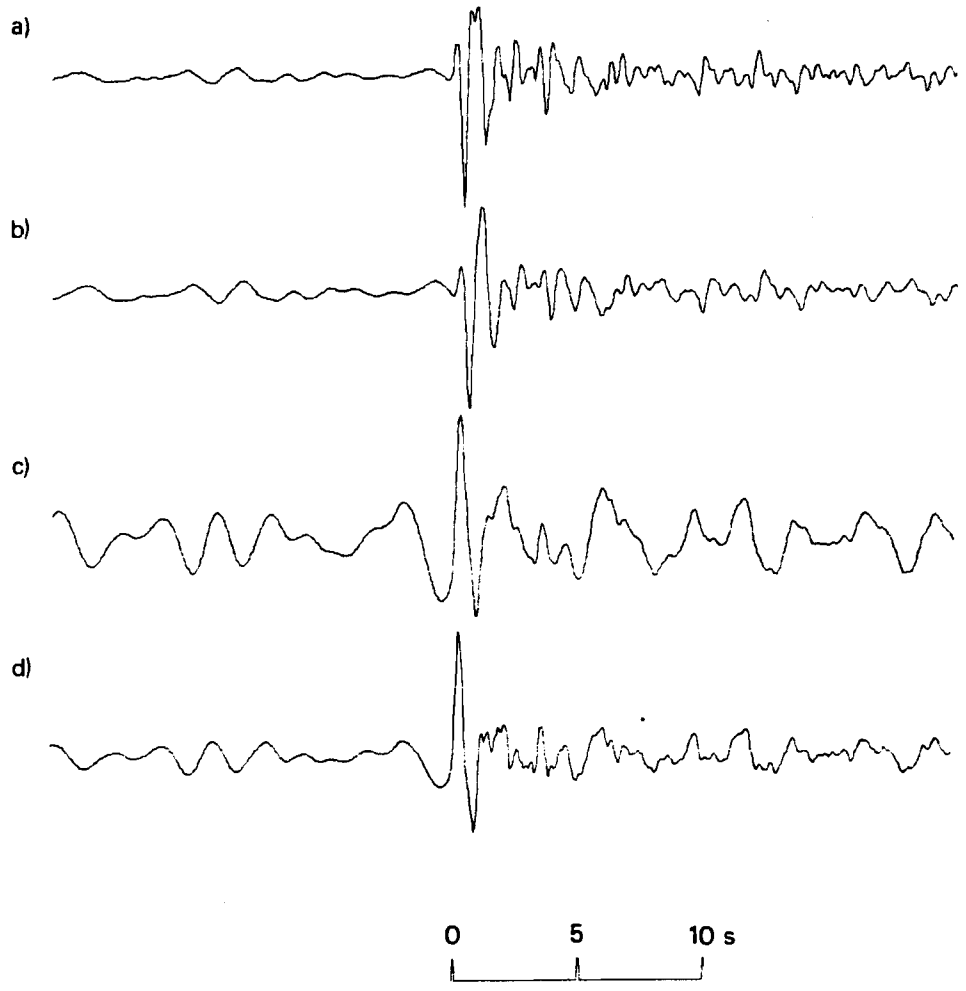

Figure A30 (a) Short-period array-sum seismogram recorded at EKA from the 27 April 1975 Shagan River explosion.
(b) Seismogram (a) filtered to simulate the effects of an additional t* of 0.2s.
(c) Seismogram (a) after Wiener filtering converted to a phaseless-broad-band instrument response.
(d) Same as seismogram (c) except that the effects of path attenuation of t* = 0.15s have been corrected for.

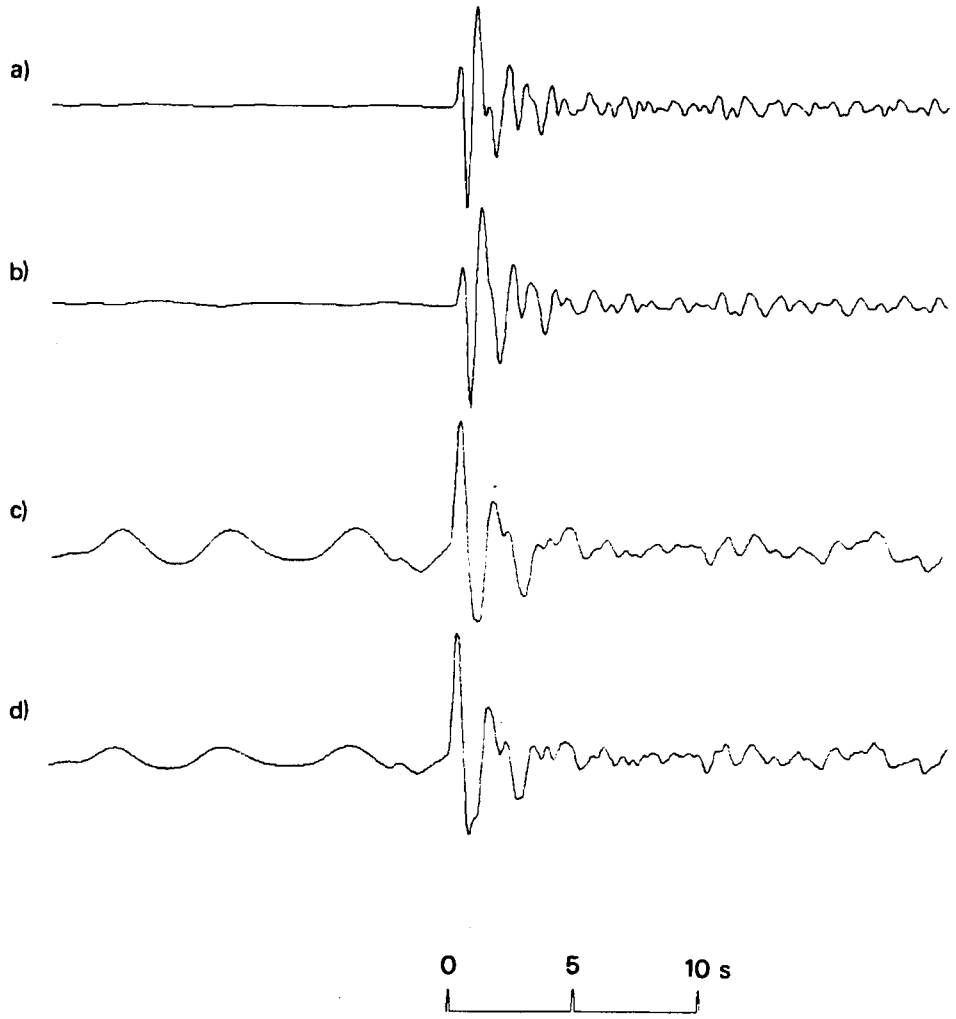

Figure A31 (a) Short-period array-sum seismogram recorded at YKA from the 27 April 1975 Shagan River explosion.
(b) Seismogram (a) filtered to simulate the effects of an additional t* of 0.2s.
(c) Seismogram (a) after Wiener filtering converted to a phaseless-broad-band instrument response.
(d) Same as seismogram (c) except that the effects of path attenuation of t* = 0.15s have been corrected for.

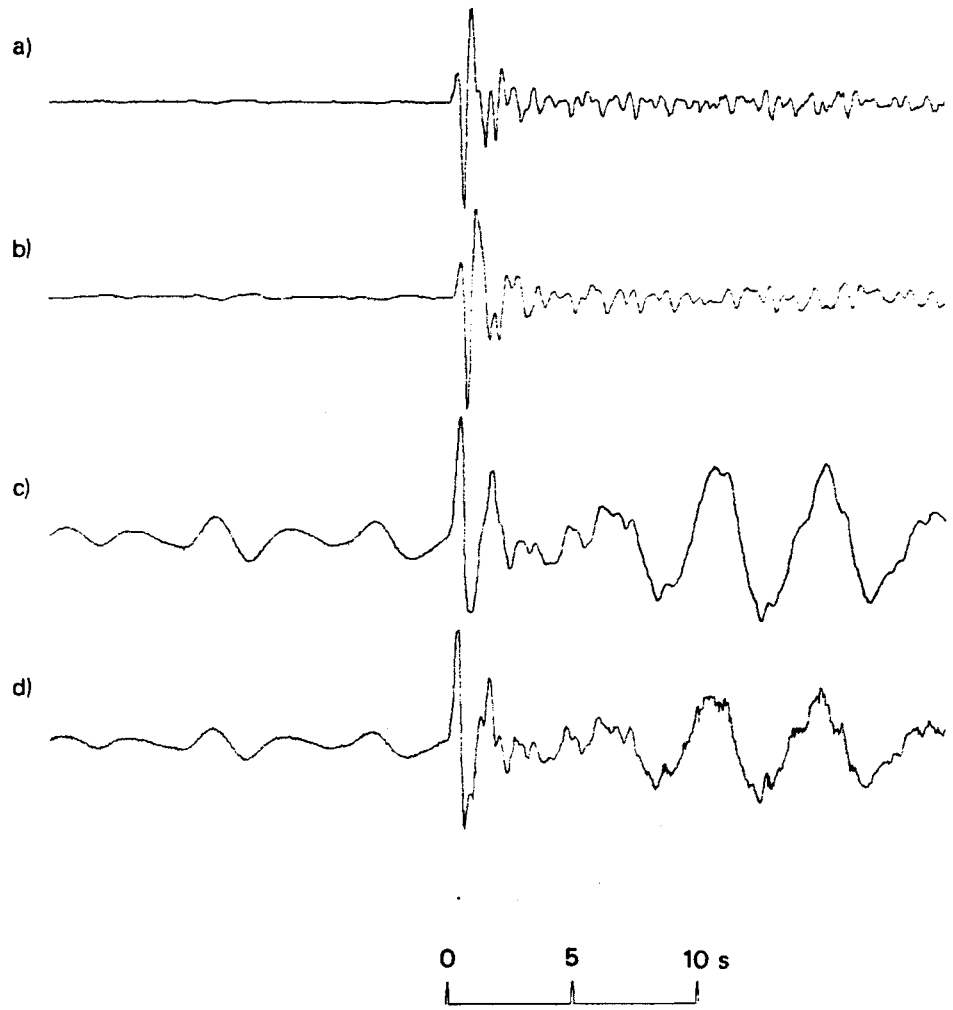

Figure A32 (a) Short-period array-sum seismogram recorded at GBA from the 27 April 1975 Shagan River explosion.
(b) Seismogram (a) filtered to simulate the effects of an additional t* of 0.2s.
(c) Seismogram (a) after Wiener filtering converted to a phaseless-broad-band instrument response.
(d) Same as seismogram (c) except that the effects of path attenuation of t* = 0.15s have been corrected for.

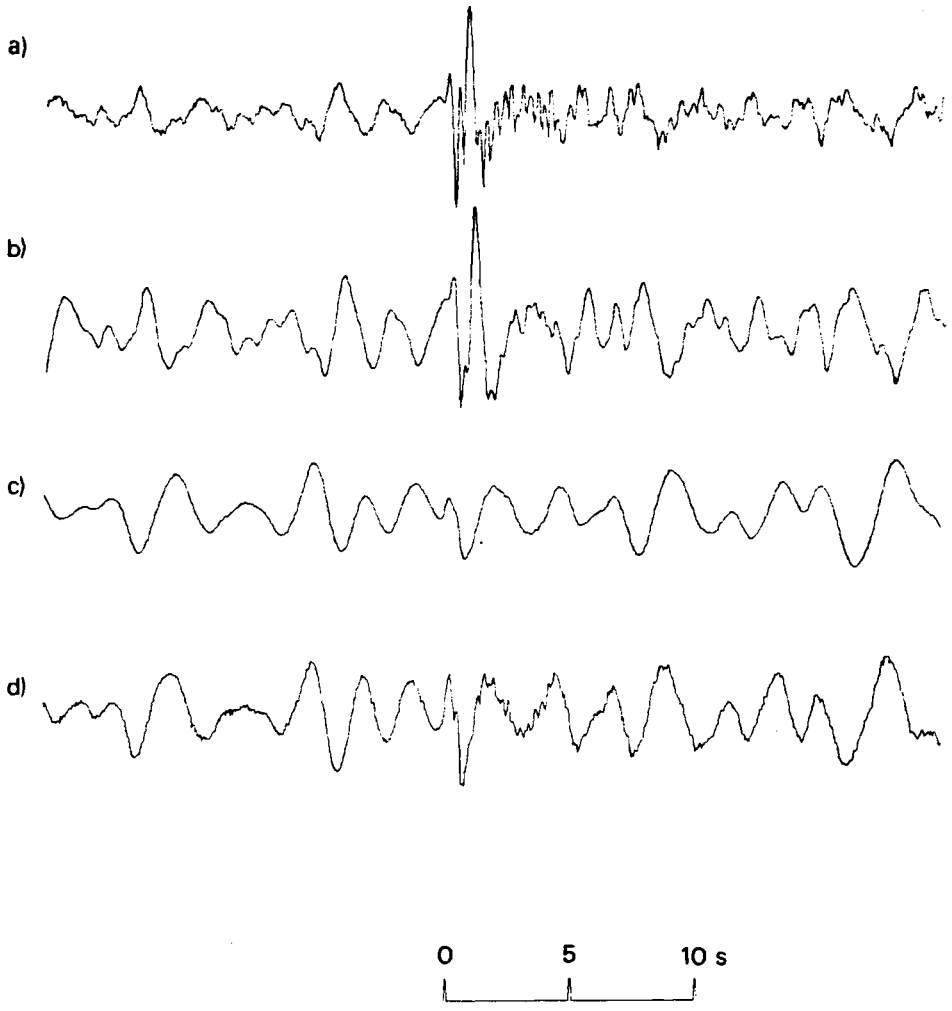

Figure A33 (a) Short-period array-sum seismogram recorded at EKA from the 30 June 1975 Shagan River explosion.
(b) Seismogram (a) filtered to simulate the effects of an additional t* of 0.2s.
(c) Seismogram (a) after Wiener filtering converted to a phaseless-broad-band instrument response.
(d) Same as seismogram (c) except that the effects of path attenuation of t* = 0.15s have been corrected for.

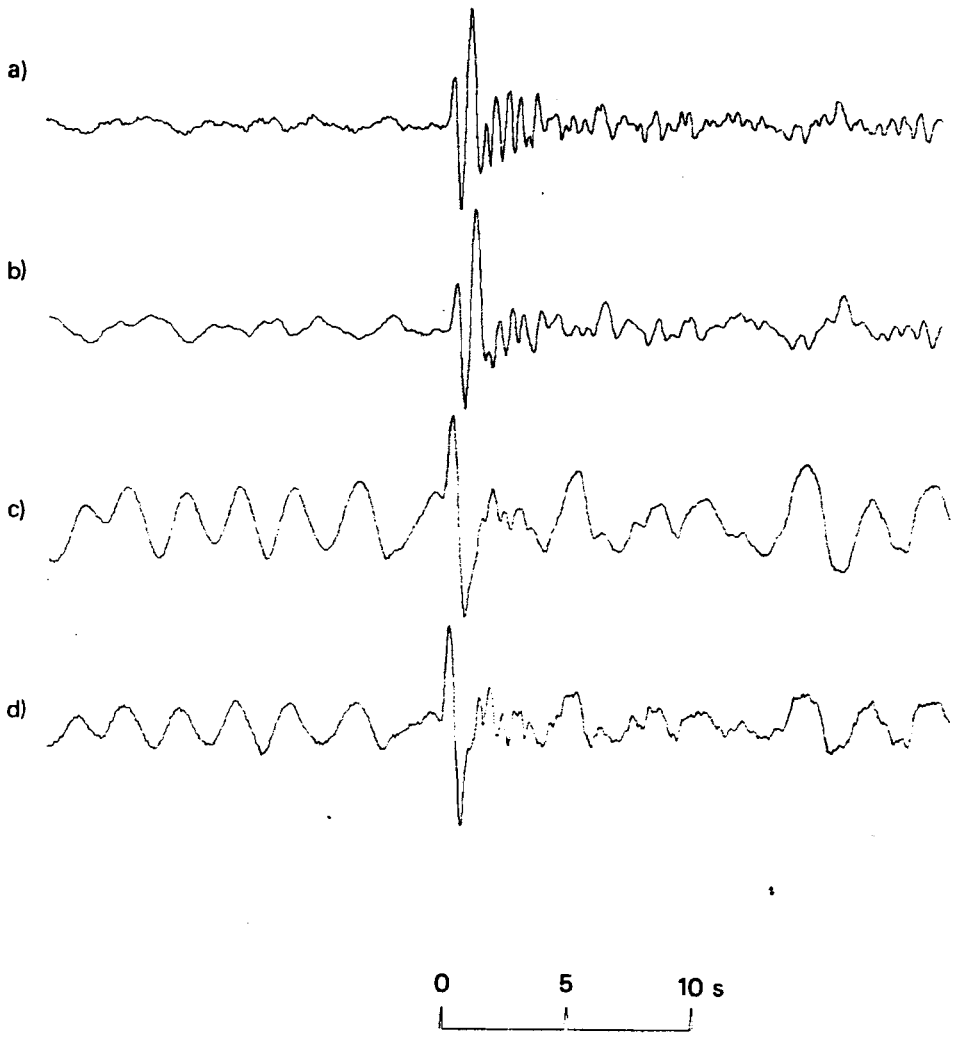

Figure A34 (a) Short-period array-sum seismogram recorded at YKA from the 30 June 1975 Shagan River explosion.
(b) Seismogram (a) filtered to simulate the effects of an additional t* of 0.2s.
(c) Seismogram (a) after Wiener filtering converted to a phaseless-broad-band instrument response.
(d) Same as seismogram (c) except that the effects of path attenuation of t* = 0.15s have been corrected for.

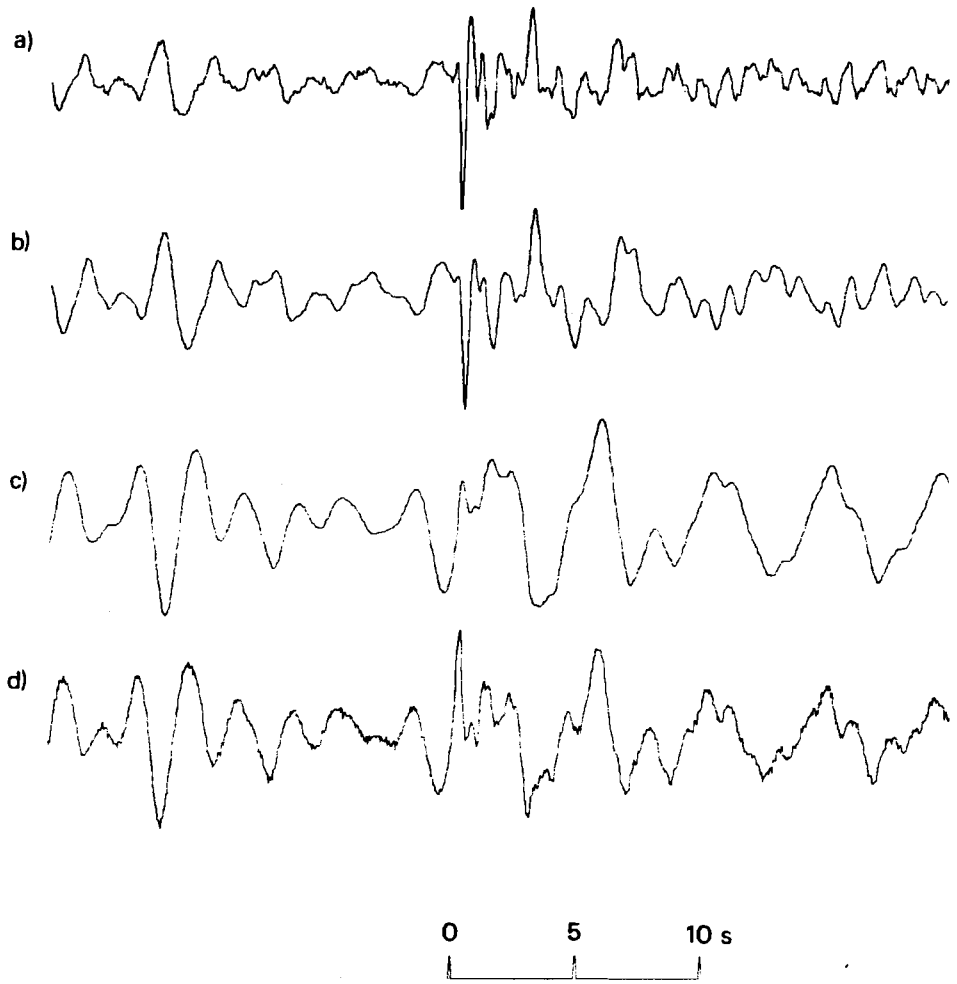

Figure A35 (a) Short-period array-sum seismogram recorded at GBA from the 30 June 1975 Shagan River explosion.
(b) Seismogram (a) filtered to simulate the effects of an additional t* of 0.2s.
(c) Seismogram (a) after Wiener filtering converted to a phaseless-broad-band instrument response.
(d) Same as seismogram (c) except that the effects of path attenuation of t* = 0.15s have been corrected for.

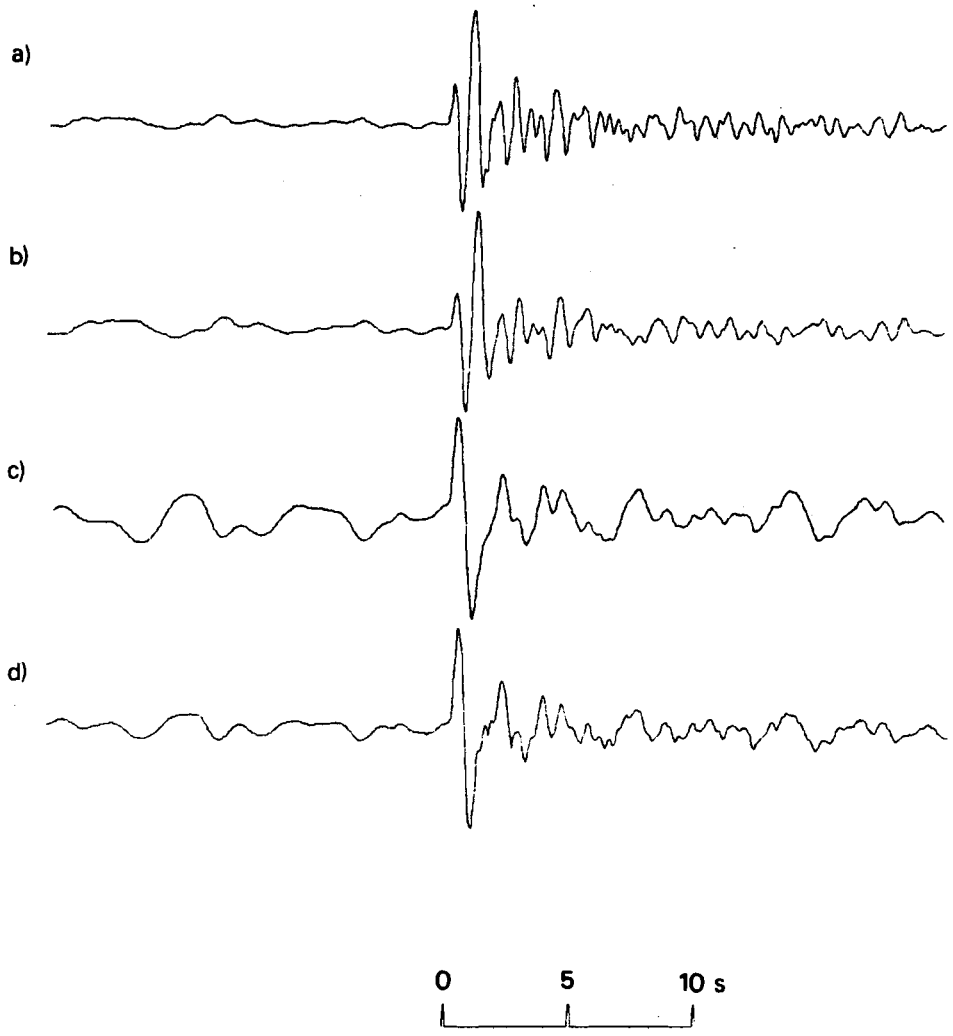

Figure A36 (a) Short-period array-sum seismogram recorded at EKA from the 29 October 1975 Shagan River explosion.
(b) Seismogram (a) filtered to simulate the effects of an additional t* of 0.2s.
(c) Seismogram (a) after Wiener filtering converted to a phaseless-broad-band instrument response.
(d) Same as seismogram (c) except that the effects of path attenuation of t* = 0.15s have been corrected for.

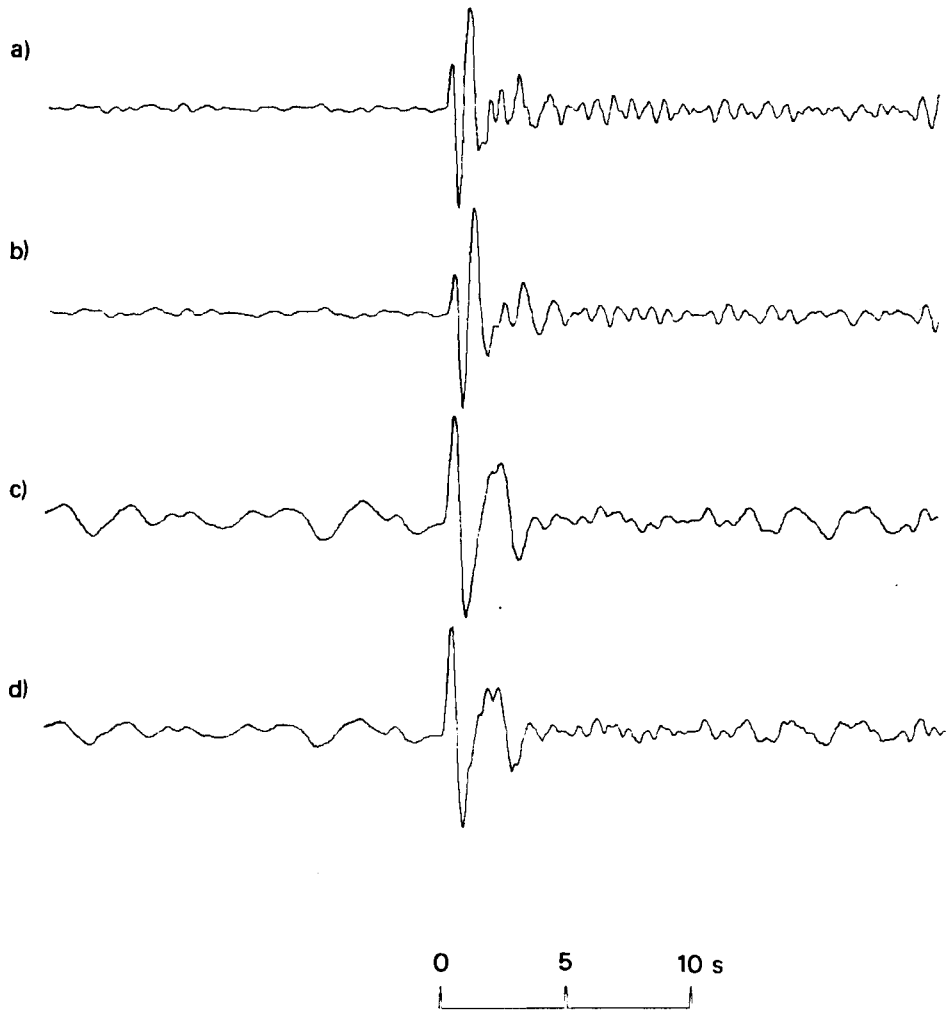

Figure A37 (a) Short-period array-sum seismogram recorded at YKA from the 29 October 1975 Shagan River explosion.
(b) Seismogram (a) filtered to simulate the effects of an additional t* of 0.2s.
(c) Seismogram (a) after Wiener filtering converted to a phaseless-broad-band instrument response.
(d) Same as seismogram (c) except that the effects of path attenuation of t* = 0.15s have been corrected for.

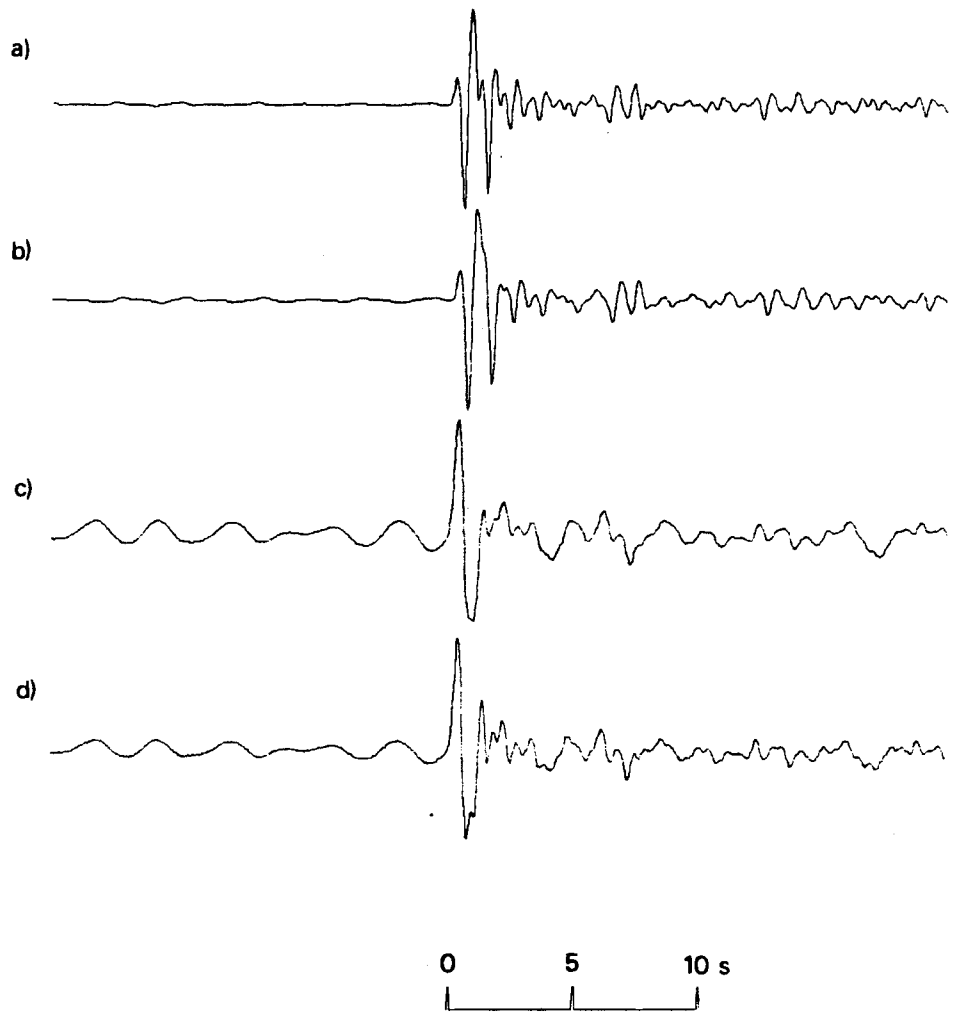

Figure A38 (a) Short-period array-sum seismogram recorded at GBA from the 29 October 1975 Shagan River explosion.
(b) Seismogram (a) filtered to simulate the effects of an additional t* of 0.2s.
(c) Seismogram (a) after Wiener filtering converted to a phaseless-broad-band instrument response.
(d) Same as seismogram (c) except that the effects of path attenuation of t* = 0.15s have been corrected for.

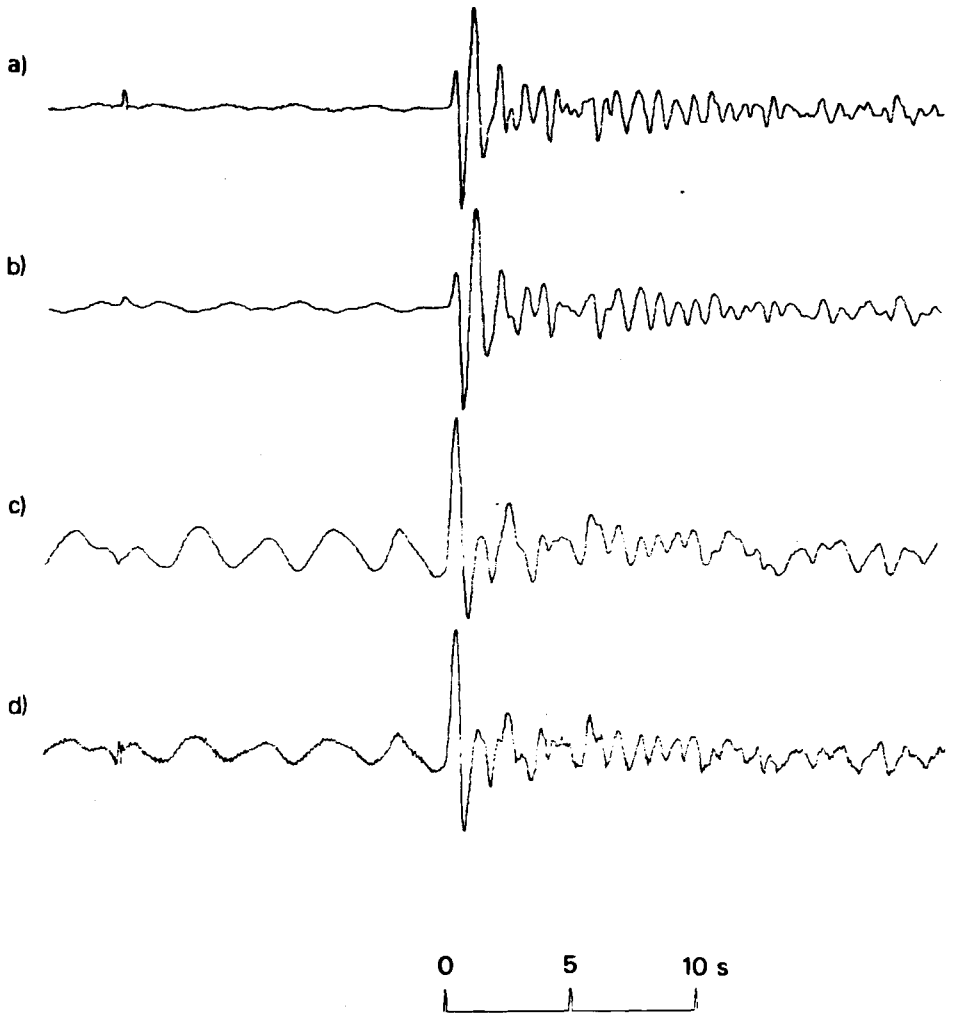

Figure A39 (a) Short-period array-sum seismogram recorded at WRA from the 29 October 1975 Shagan River explosion.
(b) Seismogram (a) filtered to simulate the effects of an additional t* of 0.2s.
(c) Seismogram (a) after Wiener filtering converted to a phaseless-broad-band instrument response.
(d) Same as seismogram (c) except that the effects of path attenuation of t* = 0.15s have been corrected for.
Note that PcP should arrive within a few seconds of P.

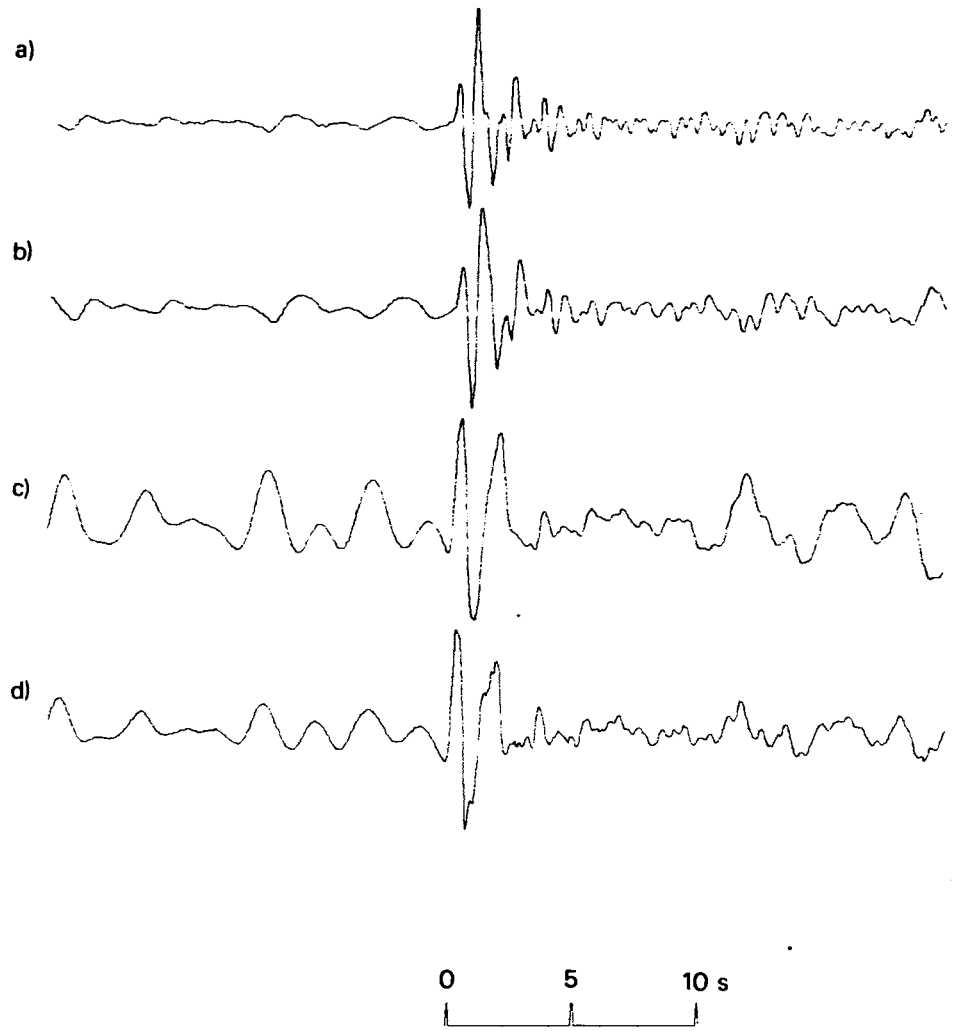

Figure A40 (a) Short-period array-sum seismogram recorded at EKA from the 25 December 1975 Shagan River explosion.
(b) Seismogram (a) filtered to simulate the effects of an additional t* of 0.2s.
(c) Seismogram (a) after Wiener filtering converted to a phaseless-broad-band instrument response.
(d) Same as seismogram (c) except that the effects of path attenuation of t* = 0.15s have been corrected for.

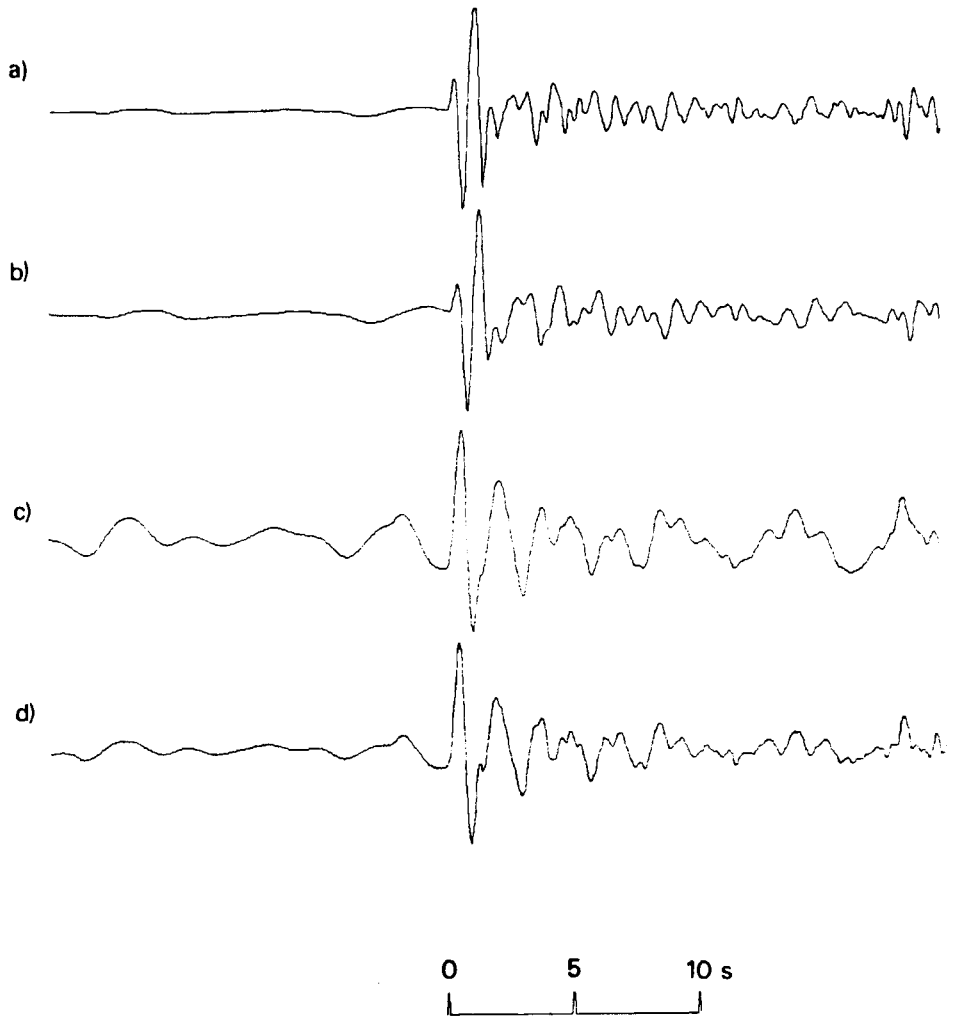

Figure A41 (a) Short-period array-sum seismogram recorded at YKA from the 25 December 1975 Shagan River explosion.
(b) Seismogram (a) filtered to simulate the effects of an additional t* of 0.2s.
(c) Seismogram (a) after Wiener filtering converted to a phaseless-broad-band instrument response.
(d) Same as seismogram (c) except that the effects of path attenuation of t* = 0.15s have been corrected for.

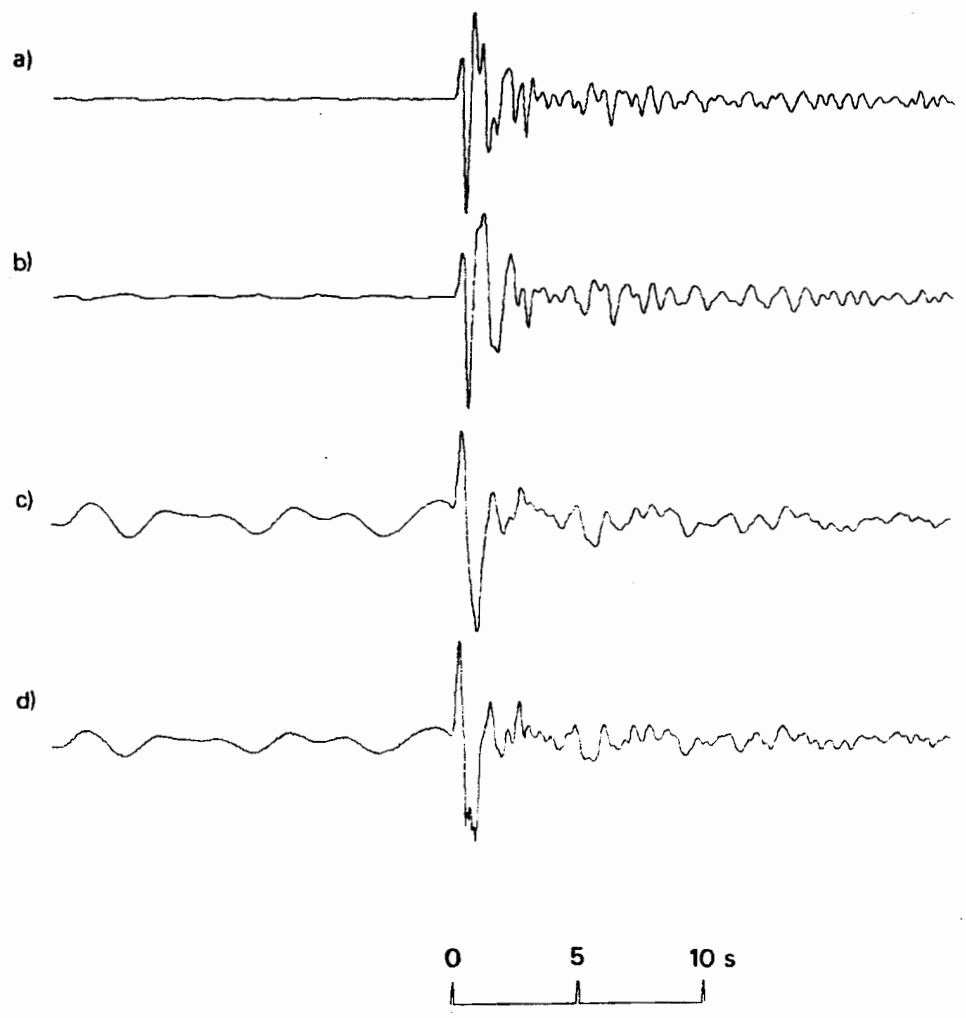

Figure A42 (a) Short-period array-sum seismogram recorded at GBA from the 25 December 1975 Shagan River explosion.
(b) Seismogram (a) filtered to simulate the effects of an additional t* of 0.2s.
(c) Seismogram (a) after Wiener filtering converted to a phaseless-broad-band instrument response.
(d) Same as seismogram (c) except that the effects of path attenuation of t* = 0.15s have been corrected for.

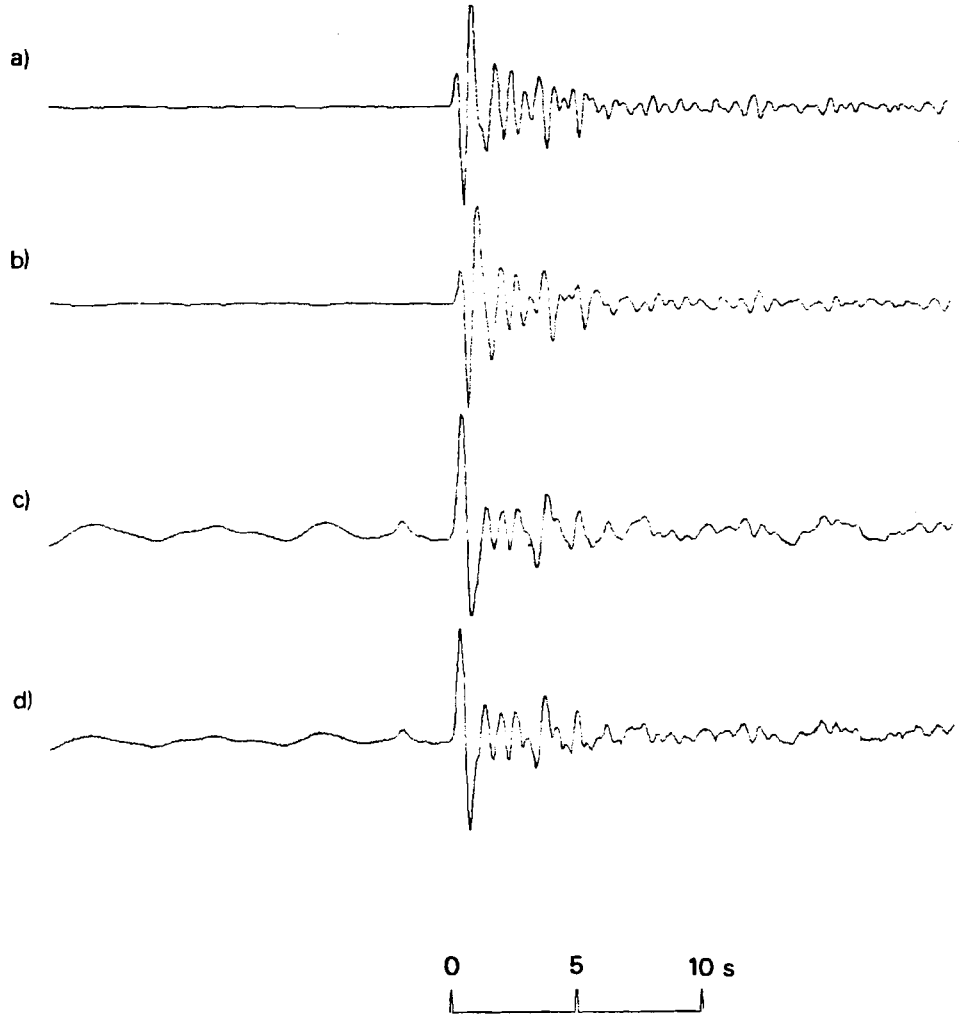

Figure A43 (a) Short-period array-sum seismogram recorded at WRA from the 25 December 1975 Shagan River explosion.
(b) Seismogram (a) filtered to simulate the effects of an additional t* of 0.2s.
(c) Seismogram (a) after Wiener filtering converted to a phaseless-broad-band instrument response.
(d) Same as seismogram (c) except that the effects of path attenuation of t* = 0.15s have been corrected for.
Note that PcP should arrive within a few seconds of P.

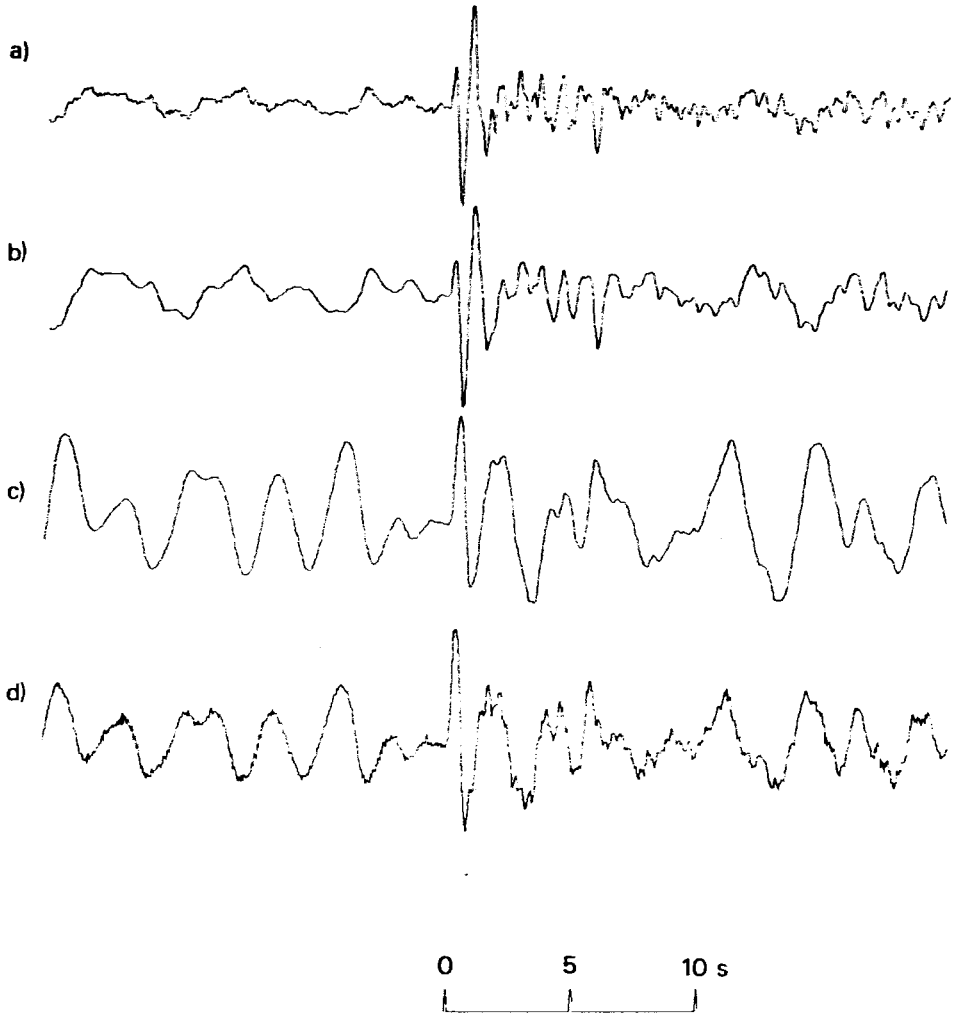

Figure A44 (a) Short-period array-sum seismogram recorded at EKA from the 21 April 1976 Shagan River explosion.
(b) Seismogram (a) filtered to simulate the effects of an additional t* of 0.2s.
(c) Seismogram (a) after Wiener filtering converted to a phaseless-broad-band instrument response.
(d) Same as seismogram (c) except that the effects of path attenuation of t* = 0.15s have been corrected for.
Note that Marshall et al (2) show the wrong EKA seismogram for this explosion: theirs is from an earlier explosion at Degelen Mountain.

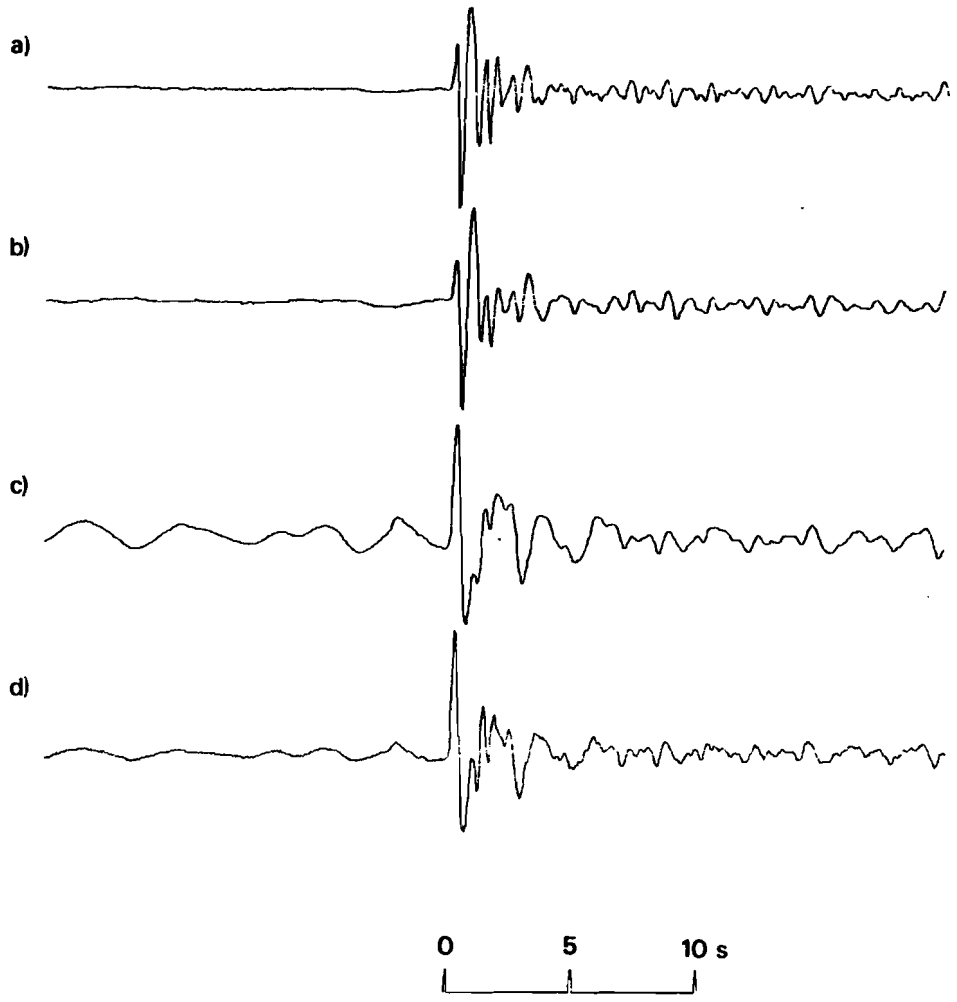

Figure A45 (a) Short-period array-sum seismogram recorded at YKA from the 21 April 1976 Shagan River explosion.
(b) Seismogram (a) filtered to simulate the effects of an additional t* of 0.2s.
(c) Seismogram (a) after Wiener filtering converted to a phaseless-broad-band instrument response.
(d) Same as seismogram (c) except that the effects of path attenuation of t* = 0.15s have been corrected for.

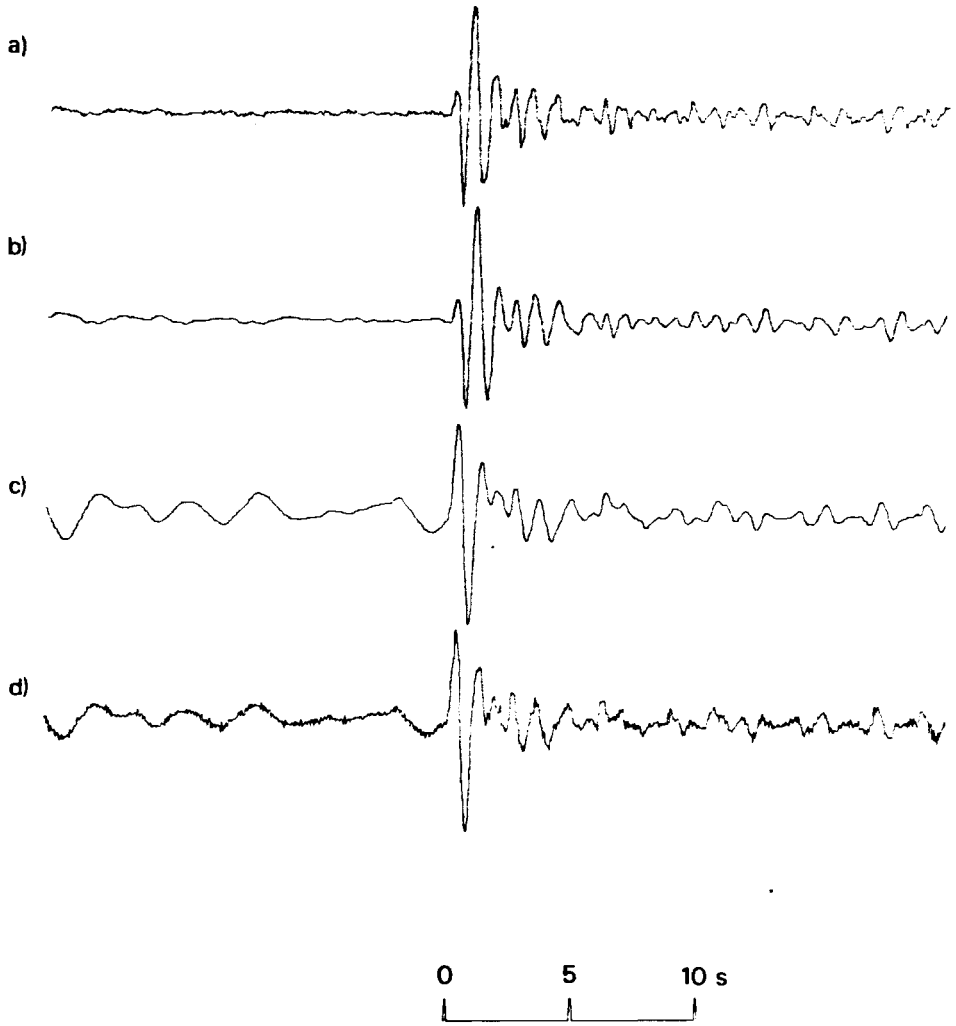

Figure A46 (a) Short-period array-sum seismogram recorded at GBA from the 21 April 1976 Shagan River explosion.
(b) Seismogram (a) filtered to simulate the effects of an additional t* of 0.2s.
(c) Seismogram (a) after Wiener filtering converted to a phaseless-broad-band instrument response.
(d) Same as seismogram (c) except that the effects of path attenuation of t* = 0.15s have been corrected for.

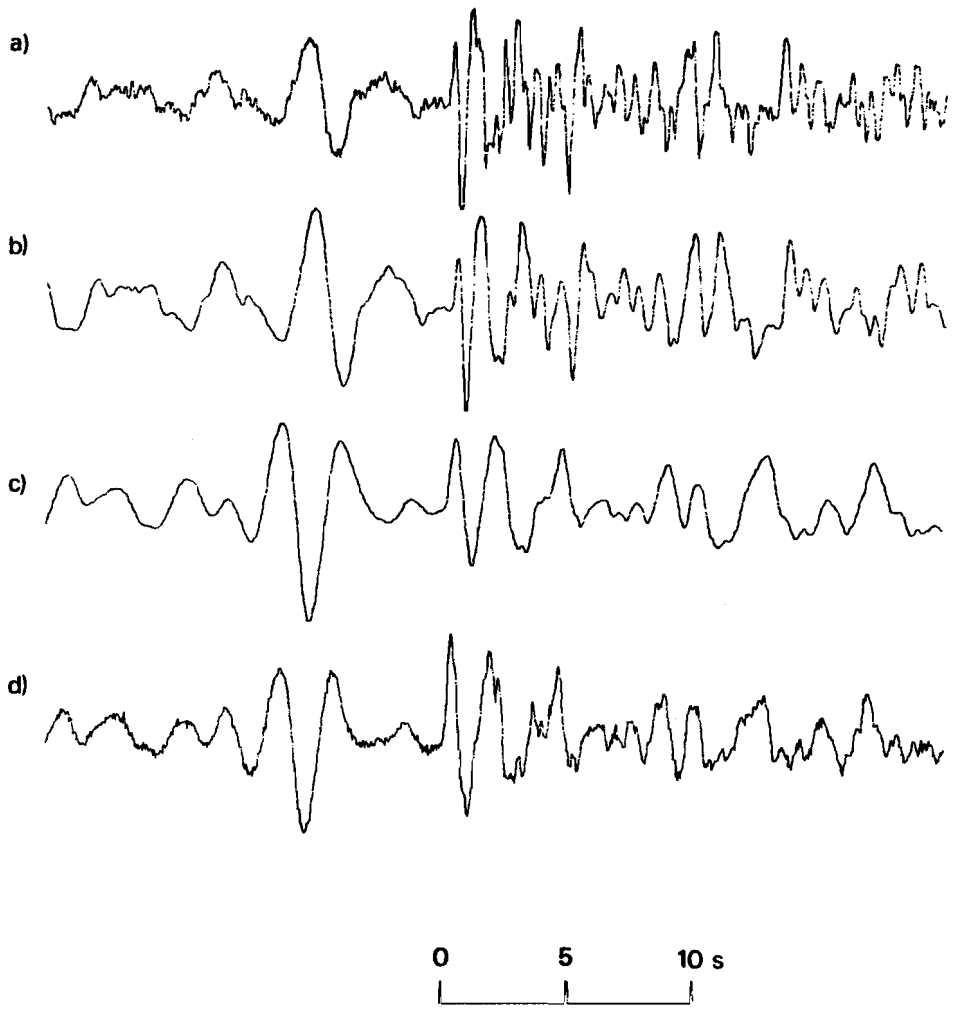

Figure A47 (a) Short-period array-sum seismogram recorded at EKA from the 9 June 1976 Shagan River explosion.
(b) Seismogram (a) filtered to simulate the effects of an additional t* of 0.2s.
(c) Seismogram (a) after Wiener filtering converted to a phaseless-broad-band instrument response.
(d) Same as seismogram (c) except that the effects of path attenuation of t* = 0.15s have been corrected for.

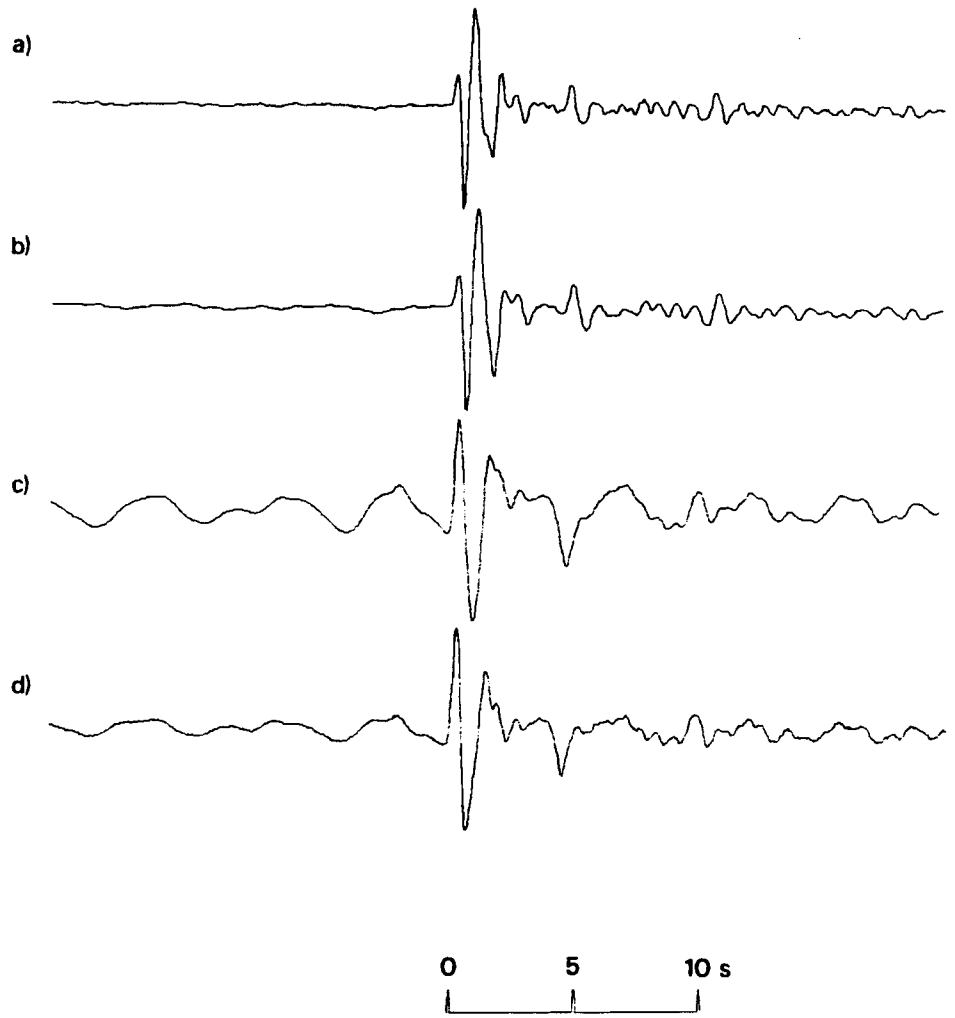

Figure A48 (a) Short-period array-sum seismogram recorded at YKA from the 9 June 1976 Shagan River explosion.
(b) Seismogram (a) filtered to simulate the effects of an additional t* of 0.2s.
(c) Seismogram (a) after Wiener filtering converted to a phaseless-broad-band instrument response.
(d) Same as seismogram (c) except that the effects of path attenuation of t* = 0.15s have been corrected for.

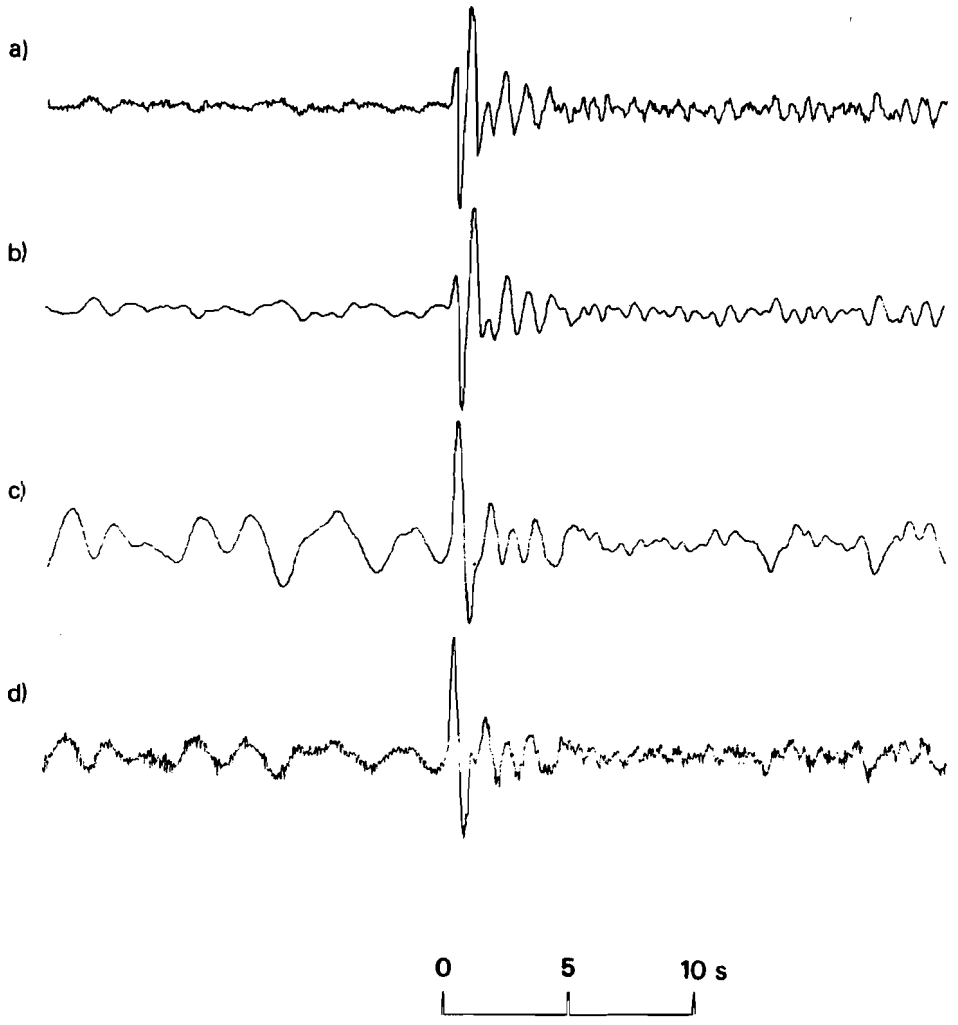

Figure A49 (a) Short-period array-sum seismogram recorded at GBA from the 9 June 1976 Shagan River explosion.
(b) Seismogram (a) filtered to simulate the effects of an additional t* of 0.2s.
(c) Seismogram (a) after Wiener filtering converted to a phaseless-broad-band instrument response.
(d) Same as seismogram (c) except that the effects of path attenuation of t* = 0.15s have been corrected for.

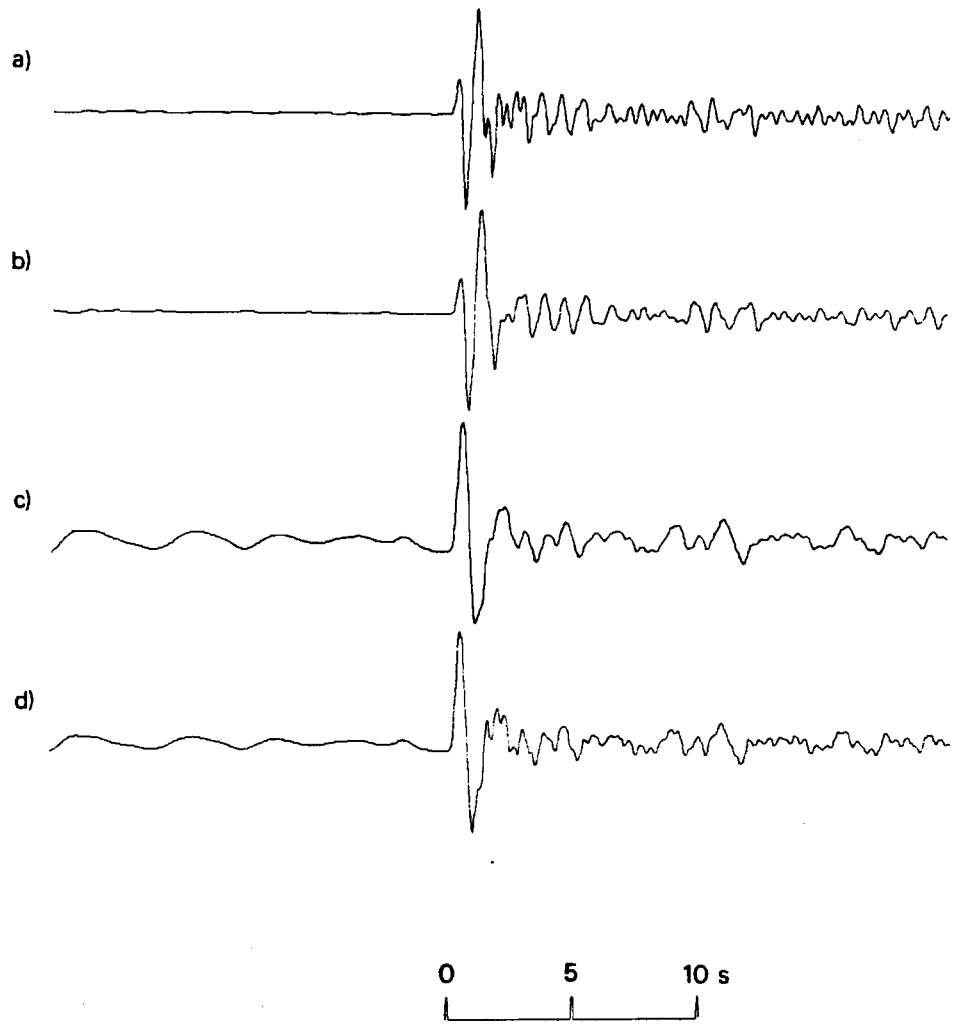

Figure A50 (a) Short-period array-sum seismogram recorded at EKA from the 4 July 1976 Shagan River explosion.
(b) Seismogram (a) filtered to simulate the effects of an additional t* of 0.2s.
(c) Seismogram (a) after Wiener filtering converted to a phaseless-broad-band instrument response.
(d) Same as seismogram (c) except that the effects of path attenuation of t* = 0.15s have been corrected for.

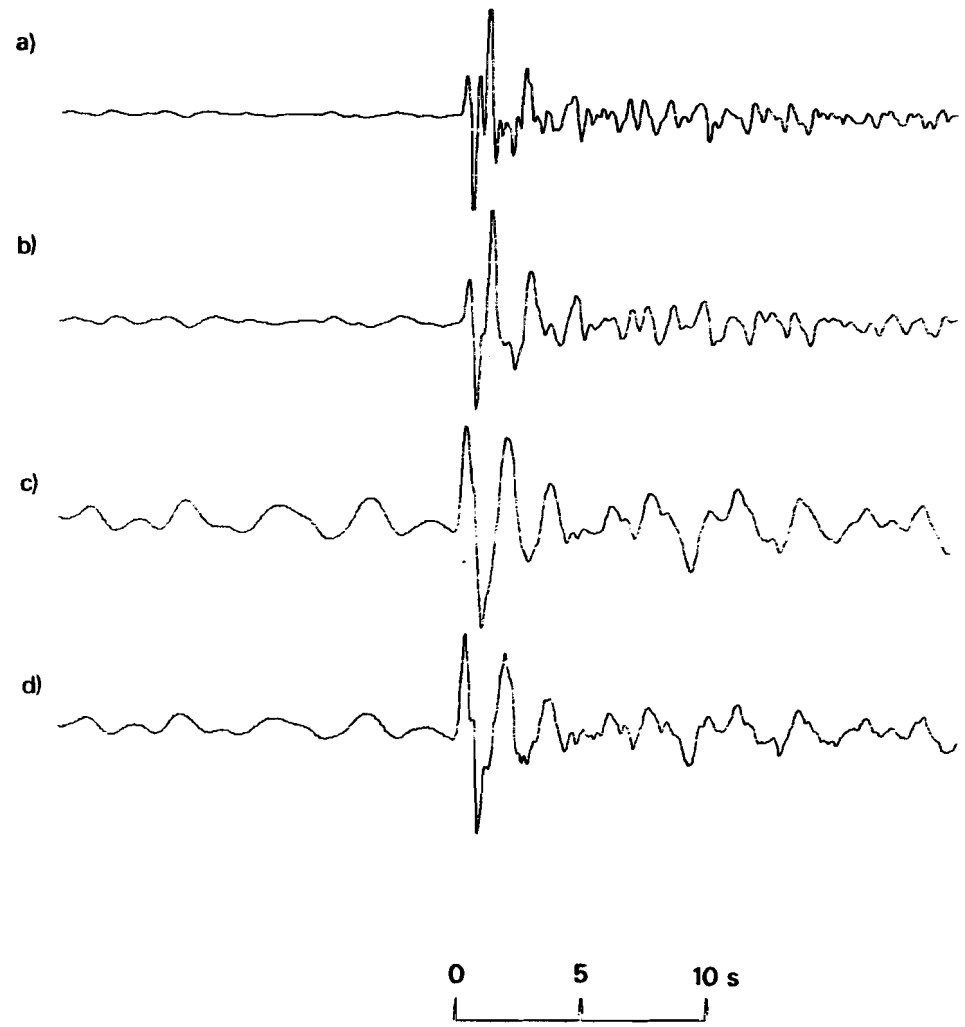

Figure A51 (a) Short-period array-sum seismogram recorded at EKA from the 28 August 1976 Shagan River explosion.
(b) Seismogram (a) filtered to simulate the effects of an additional t* of 0.2s.
(c) Seismogram (a) after Wiener filtering converted to a phaseless-broad-band instrument response.
(d) Same as seismogram (c) except that the effects of path attenuation of t* = 0.15s have been corrected for.

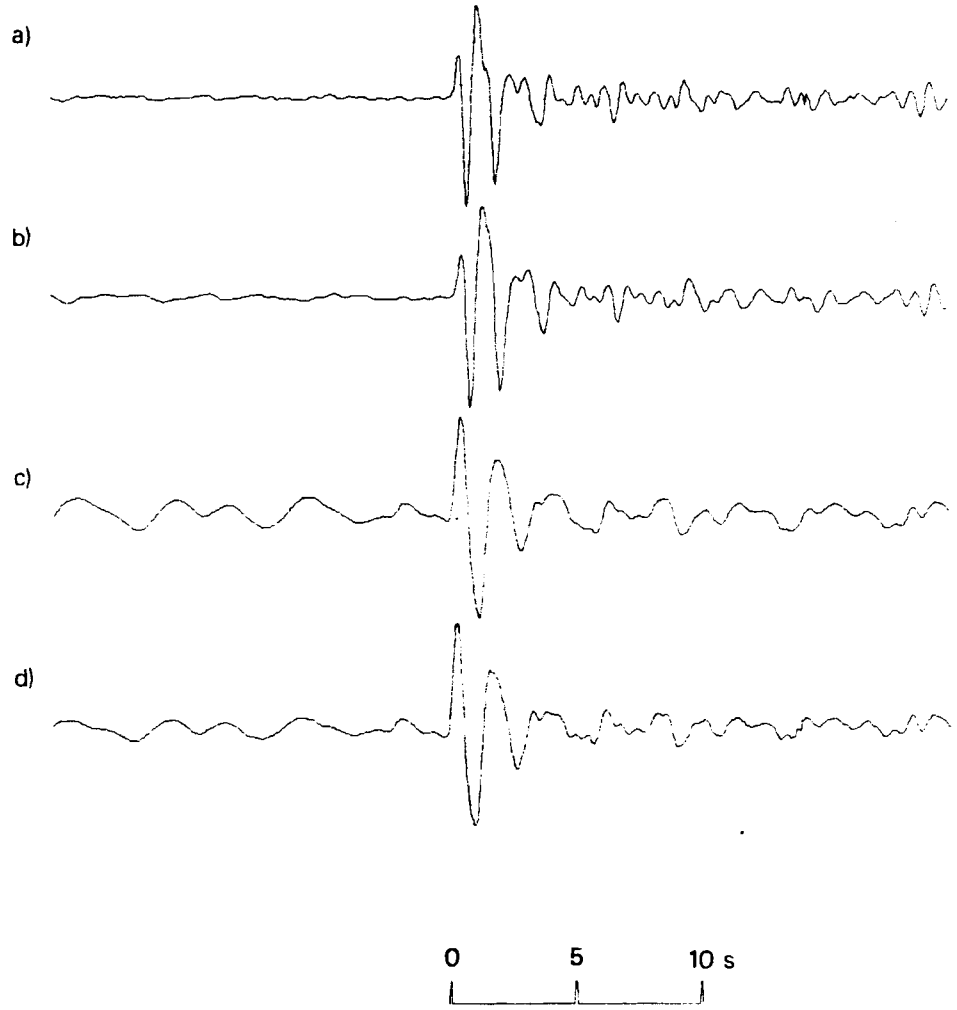

Figure A52 (a) Short-period array-sum seismogram recorded at YKA from the 28 August 1976 Shagan River explosion.
(b) Seismogram (a) filtered to simulate the effects of an additional t* of 0.2s.
(c) Seismogram (a) after Wiener filtering converted to a phaseless-broad-band instrument response.
(d) Same as seismogram (c) except that the effects of path attenuation of t* = 0.15s have been corrected for.

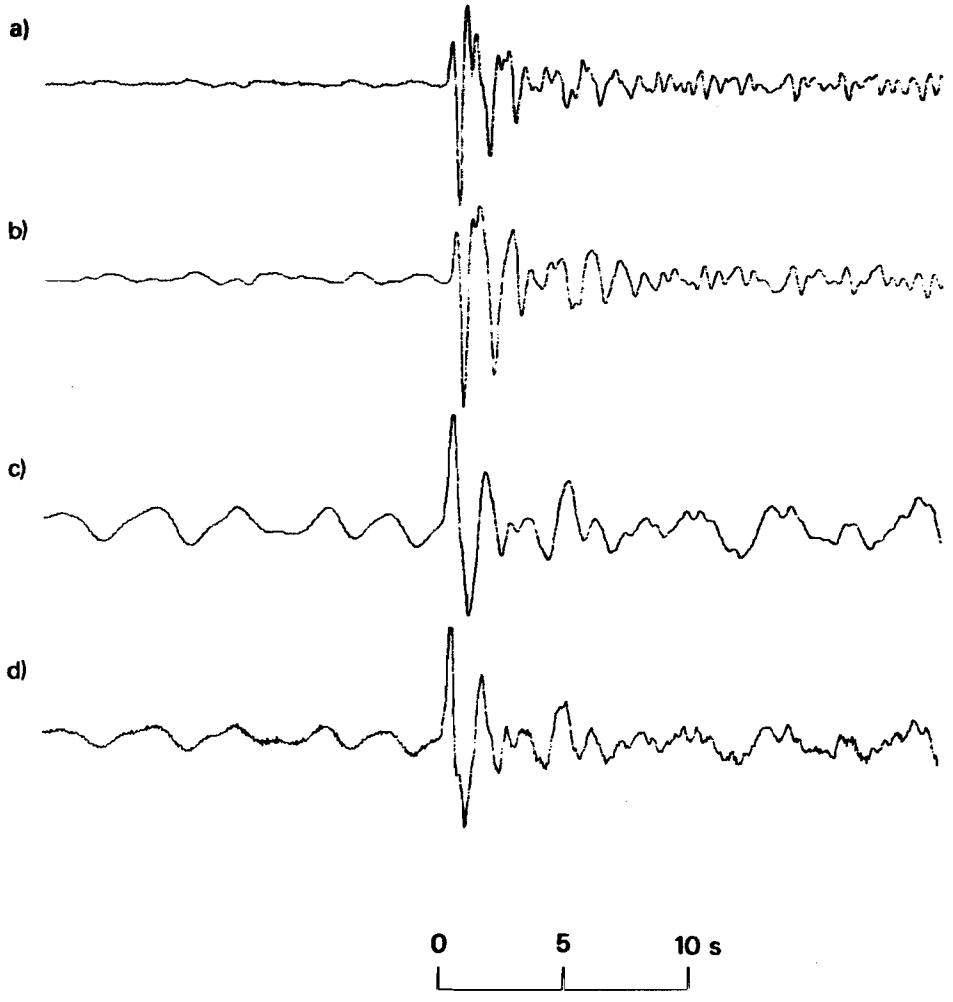

Figure A53 (a) Short-period array-sum seismogram recorded at GBA from the 28 August 1976 Shagan River explosion.
(b) Seismogram (a) filtered to simulate the effects of an additional t* of 0.2s.
(c) Seismogram (a) after Wiener filtering converted to a phaseless-broad-band instrument response.
(d) Same as seismogram (c) except that the effects of path attenuation of t* = 0.15s have been corrected for.

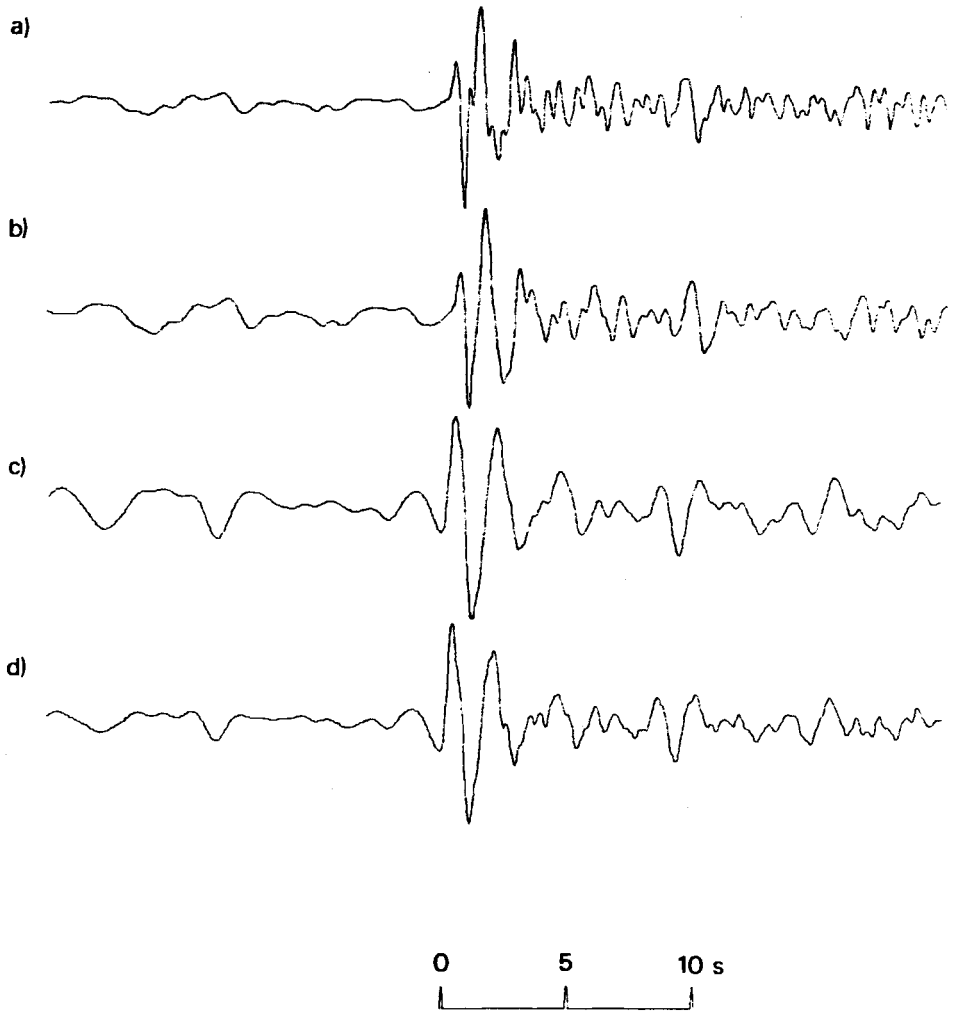

Figure A54 (a) Short-period array-sum seismogram recorded at EKA from the 23 November 1976 Shagan River explosion.
(b) Seismogram (a) filtered to simulate the effects of an additional t* of 0.2s.
(c) Seismogram (a) after Wiener filtering converted to a phaseless-broad-band instrument response.
(d) Same as seismogram (c) except that the effects of path attenuation of t* = 0.15s have been corrected for.

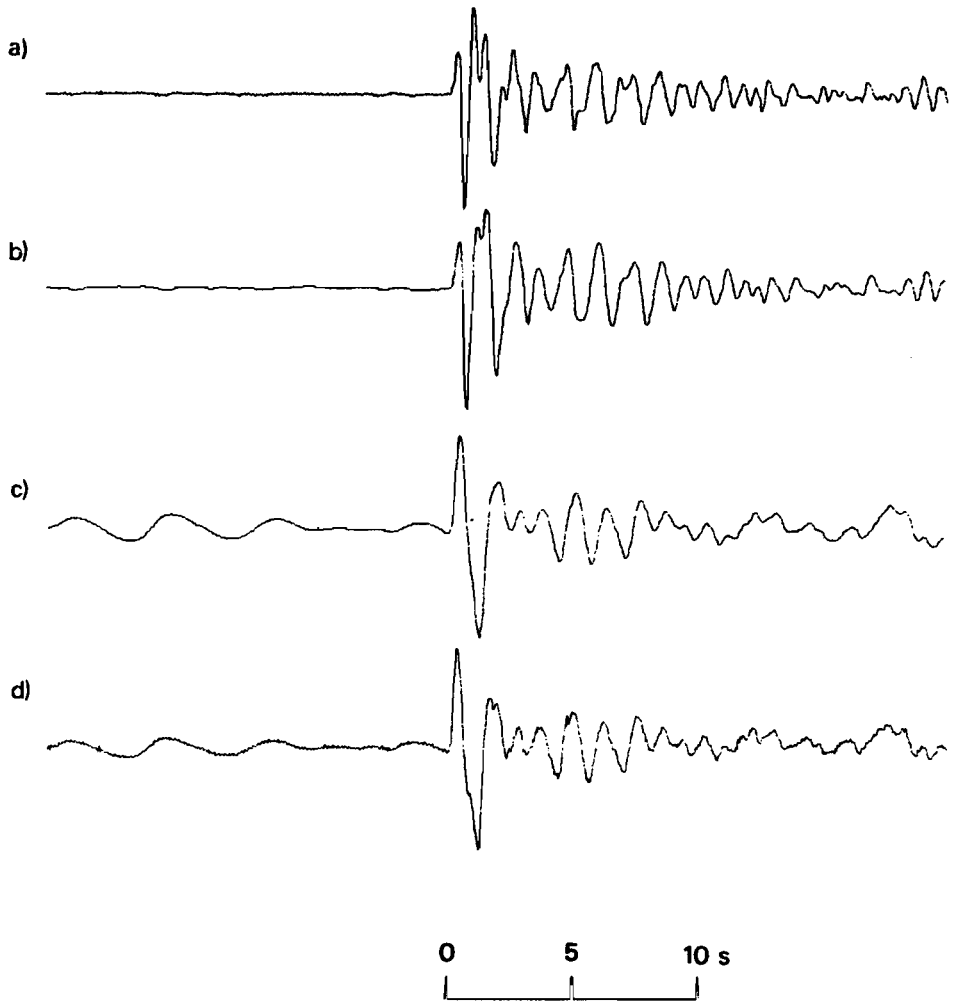

Figure A55 (a) Short-period array-sum seismogram recorded at GBA from the 23 November 1976 Shagan River explosion.
(b) Seismogram (a) filtered to simulate the effects of an additional t* of 0.2s.
(c) Seismogram (a) after Wiener filtering converted to a phaseless-broad-band instrument response.
(d) Same as seismogram (c) except that the effects of path attenuation of t* = 0.15s have been corrected for.

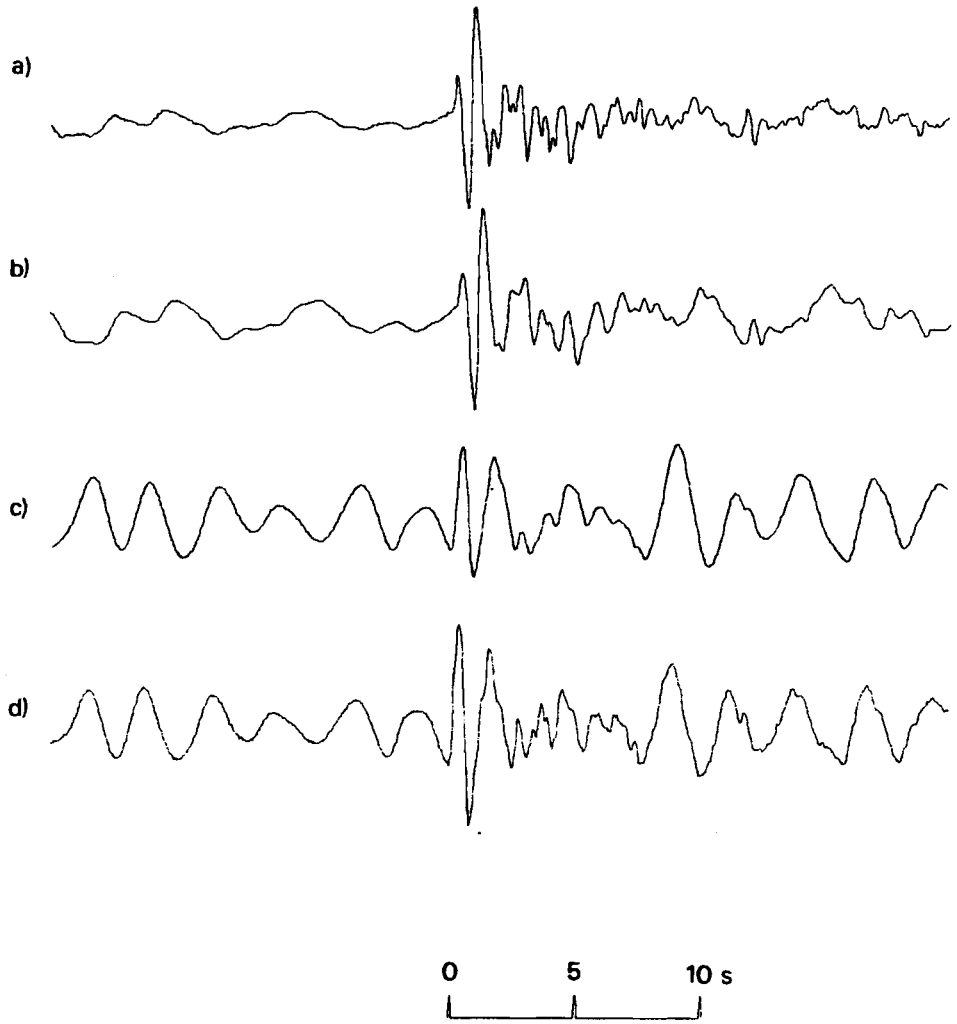

Figure A56 (a) Short-period array-sum seismogram recorded at EKA from the 7 December 1976 Shagan River explosion.
(b) Seismogram (a) filtered to simulate the effects of an additional t* of 0.2s.
(c) Seismogram (a) after Wiener filtering converted to a phaseless-broad-band instrument response.
(d) Same as seismogram (c) except that the effects of path attenuation of t* = 0.15s have been corrected for.

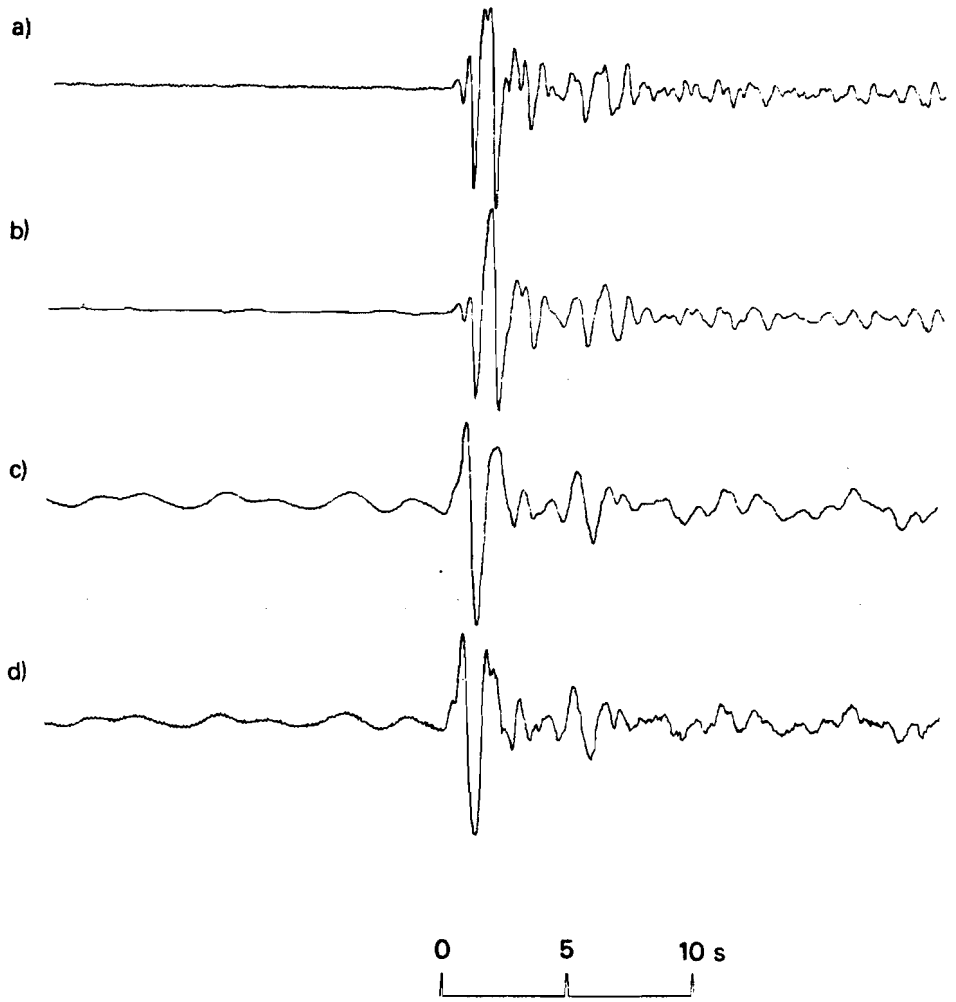

Figure A57 (a) Short-period array-sum seismogram recorded at GBA from the 7 December 1976 Shagan River explosion.
(b) Seismogram (a) filtered to simulate the effects of an additional t* of 0.2s.
(c) Seismogram (a) after Wiener filtering converted to a phaseless-broad-band instrument response.
(d) Same as seismogram (c) except that the effects of path attenuation of t* = 0.15s have been corrected for.

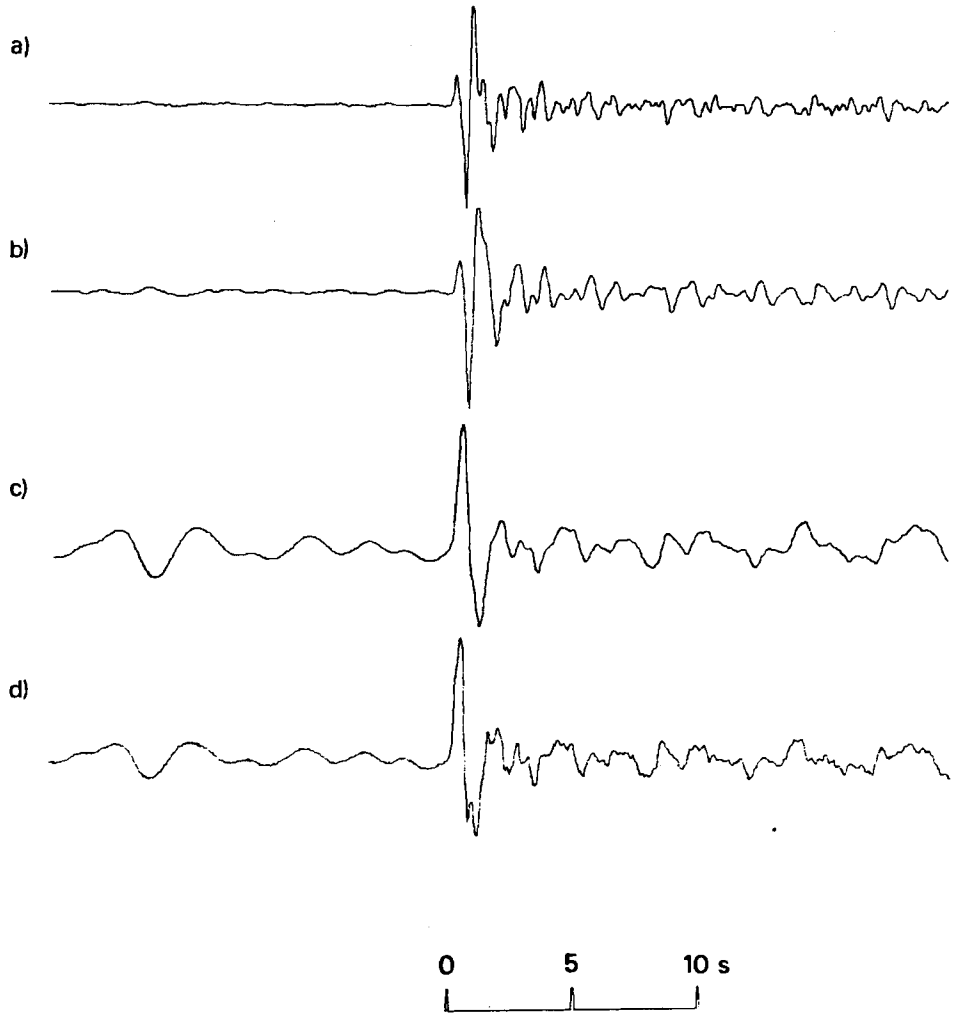

Figure A58 (a) Short-period array-sum seismogram recorded at EKA from the 29 May 1977 Shagan River explosion.
(b) Seismogram (a) filtered to simulate the effects of an additional t* of 0.2s.
(c) Seismogram (a) after Wiener filtering converted to a phaseless-broad-band instrument response.
(d) Same as seismogram (c) except that the effects of path attenuation of t* = 0.15s have been corrected for.

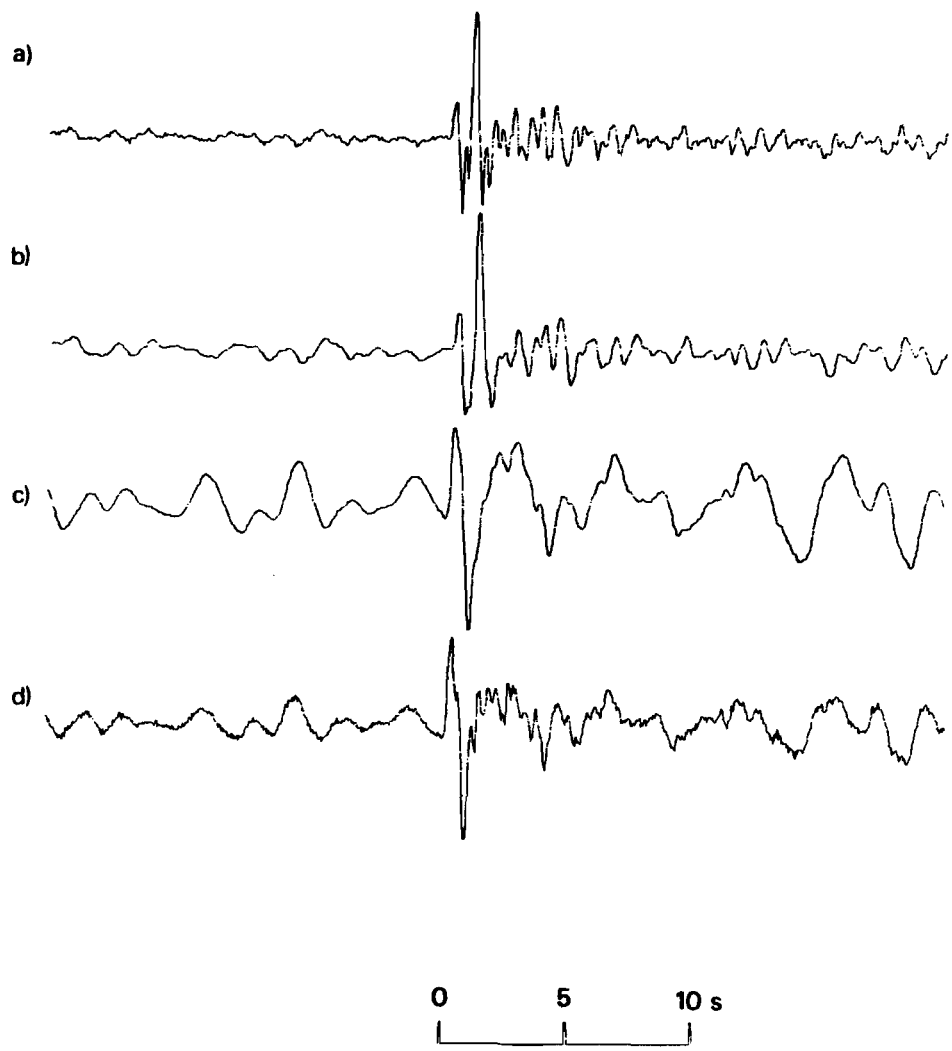

Figure A59 (a) Short-period array-sum seismogram recorded at EKA from the 29 June 1977 Shagan River explosion.
(b) Seismogram (a) filtered to simulate the effects of an additional t* of 0.2s.
(c) Seismogram (a) after Wiener filtering converted to a phaseless-broad-band instrument response.
(d) Same as seismogram (c) except that the effects of path attenuation of t* = 0.15s have been corrected for.

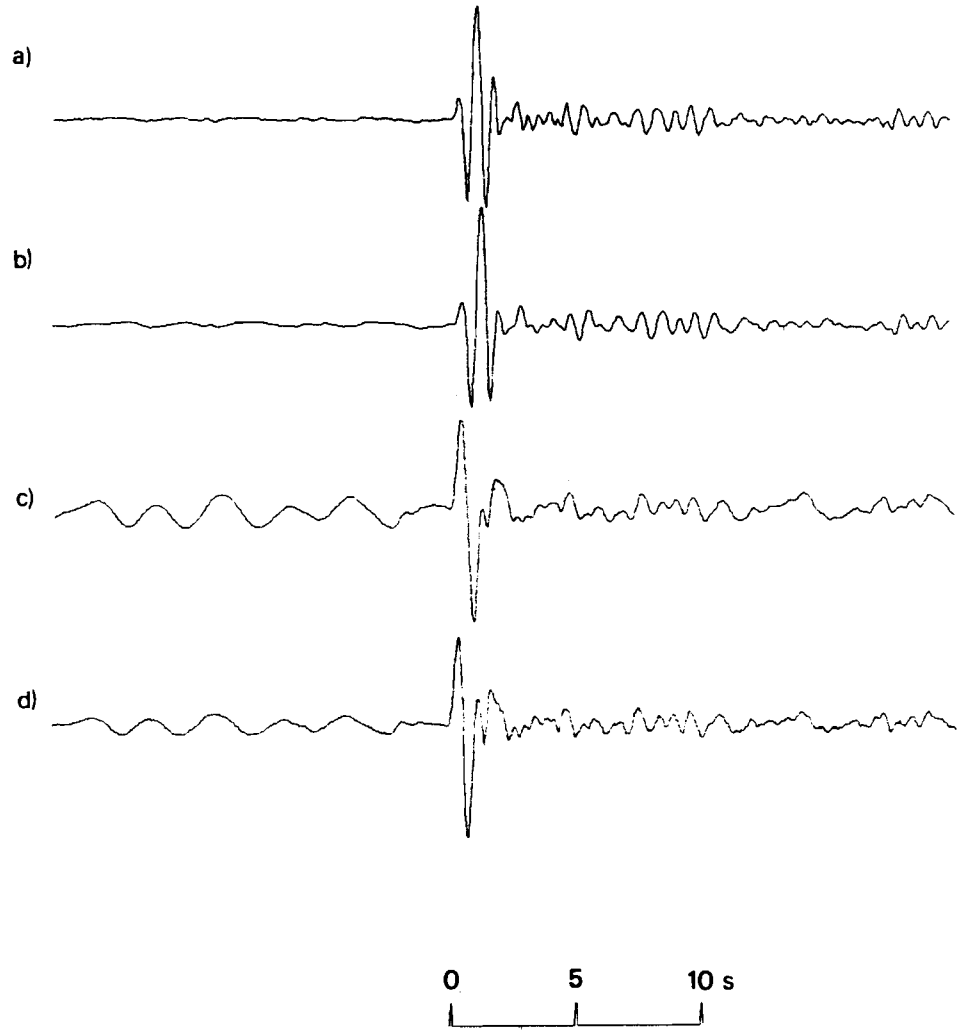

Figure A60 (a) Short-period array-sum seismogram recorded at YKA from the 29 June 1977 Shagan River explosion.
(b) Seismogram (a) filtered to simulate the effects of an additional t* of 0.2s.
(c) Seismogram (a) after Wiener filtering converted to a phaseless-broad-band instrument response.
(d) Same as seismogram (c) except that the effects of path attenuation of t* = 0.15s have been corrected for.

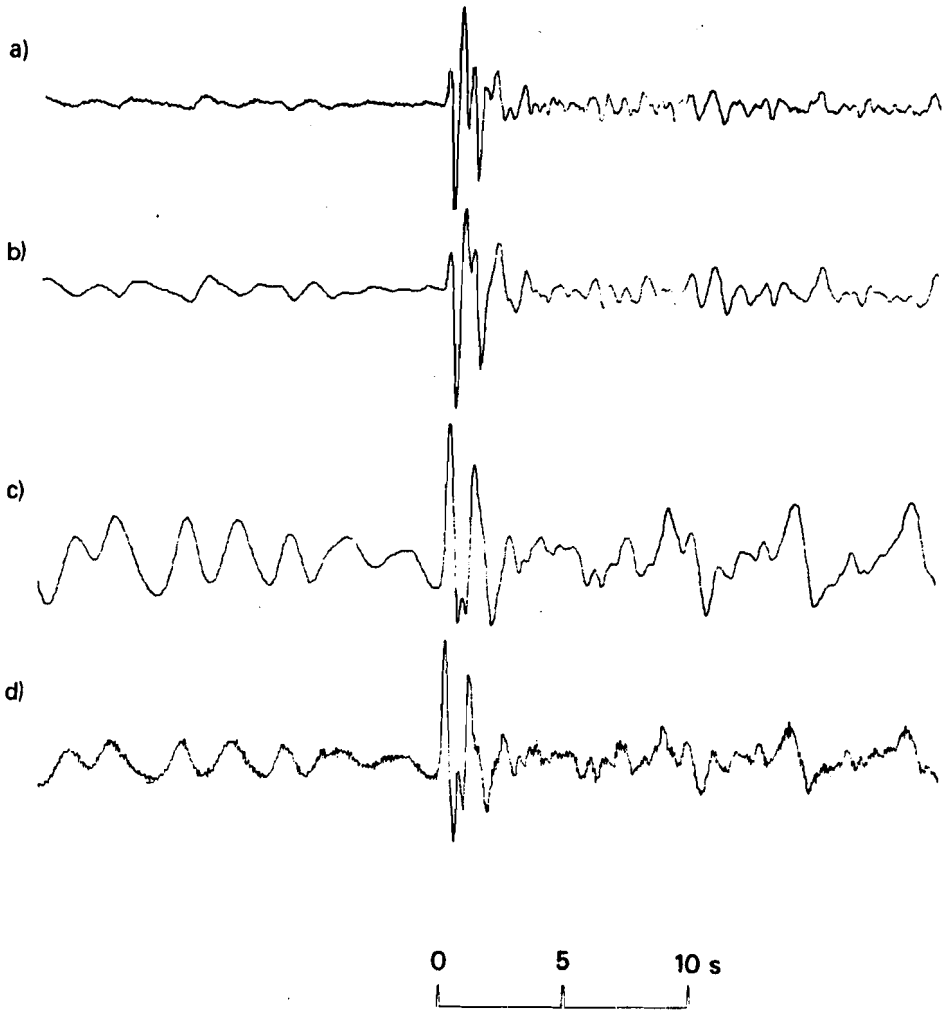

Figure A61 (a) Short-period array-sum seismogram recorded at GBA from the 29 June 1977 Shagan River explosion.
(b) Seismogram (a) filtered to simulate the effects of an additional t* of 0.2s.
(c) Seismogram (a) after Wiener filtering converted to a phaseless-broad-band instrument response.
(d) Same as seismogram (c) except that the effects of path attenuation of t* = 0.15s have been corrected for.

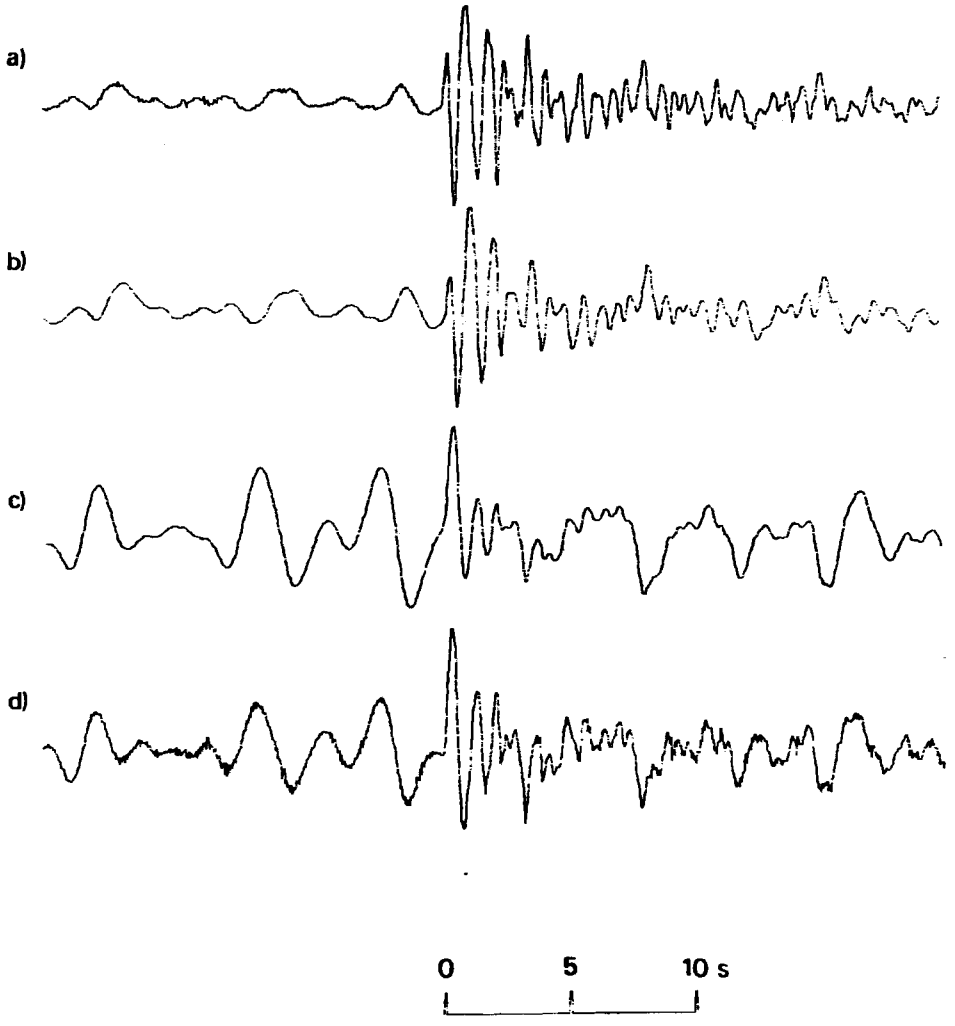

Figure A62 (a) Short-period array-sum seismogram recorded at WRA from the 29 June 1977 Shagan River explosion.
(b) Seismogram (a) filtered to simulate the effects of an additional t* of 0.2s.
(c) Seismogram (a) after Wiener filtering converted to a phaseless-broad-band instrument response.
(d) Same as seismogram (c) except that the effects of path attenuation of t* = 0.15s have been corrected for.
Note that PcP should arrive within a few seconds of P.

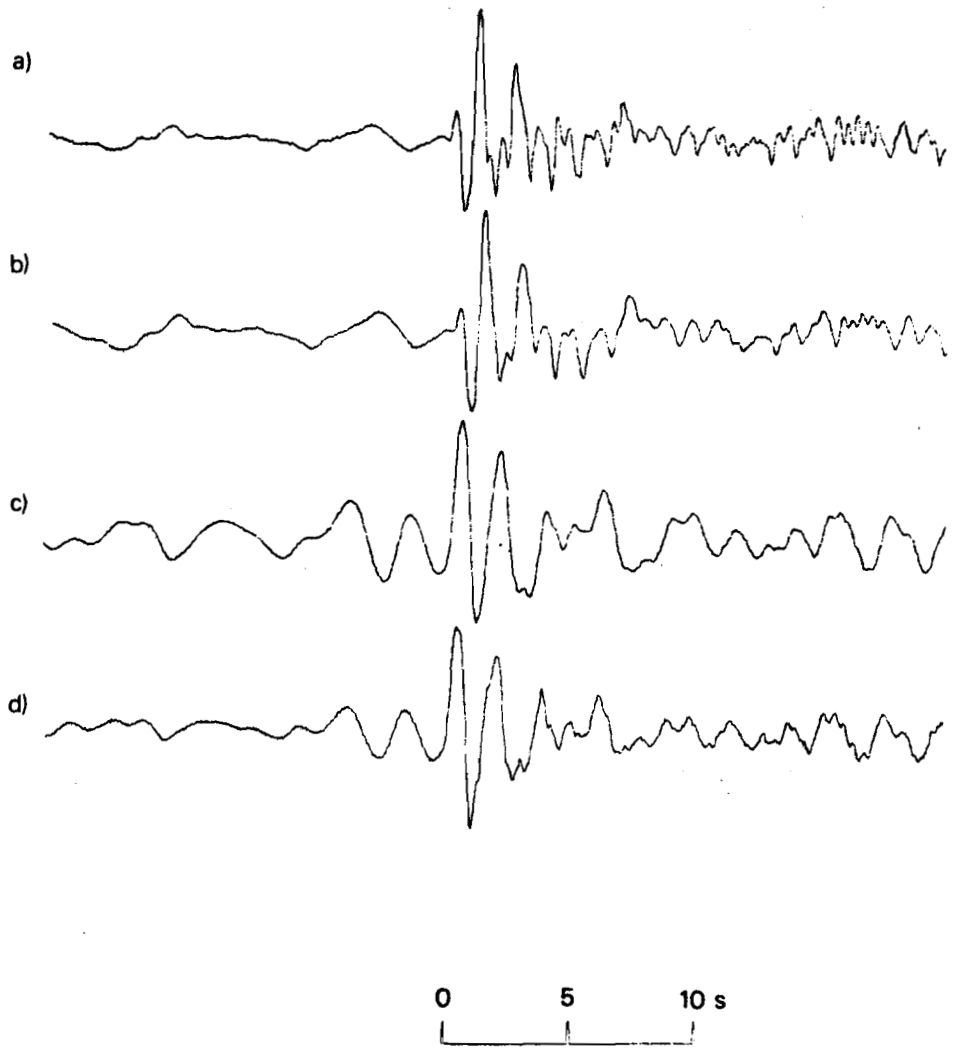

Figure A63 (a) Short-period array-sum seismogram recorded at EKA from the 5 September 1977 Shagan River explosion.
(b) Seismogram (a) filtered to simulate the effects of an additional t* of 0.2s.
(c) Seismogram (a) after Wiener filtering converted to a phaseless-broad-band instrument response.
(d) Same as seismogram (c) except that the effects of path attenuation of t* = 0.15s have been corrected for.

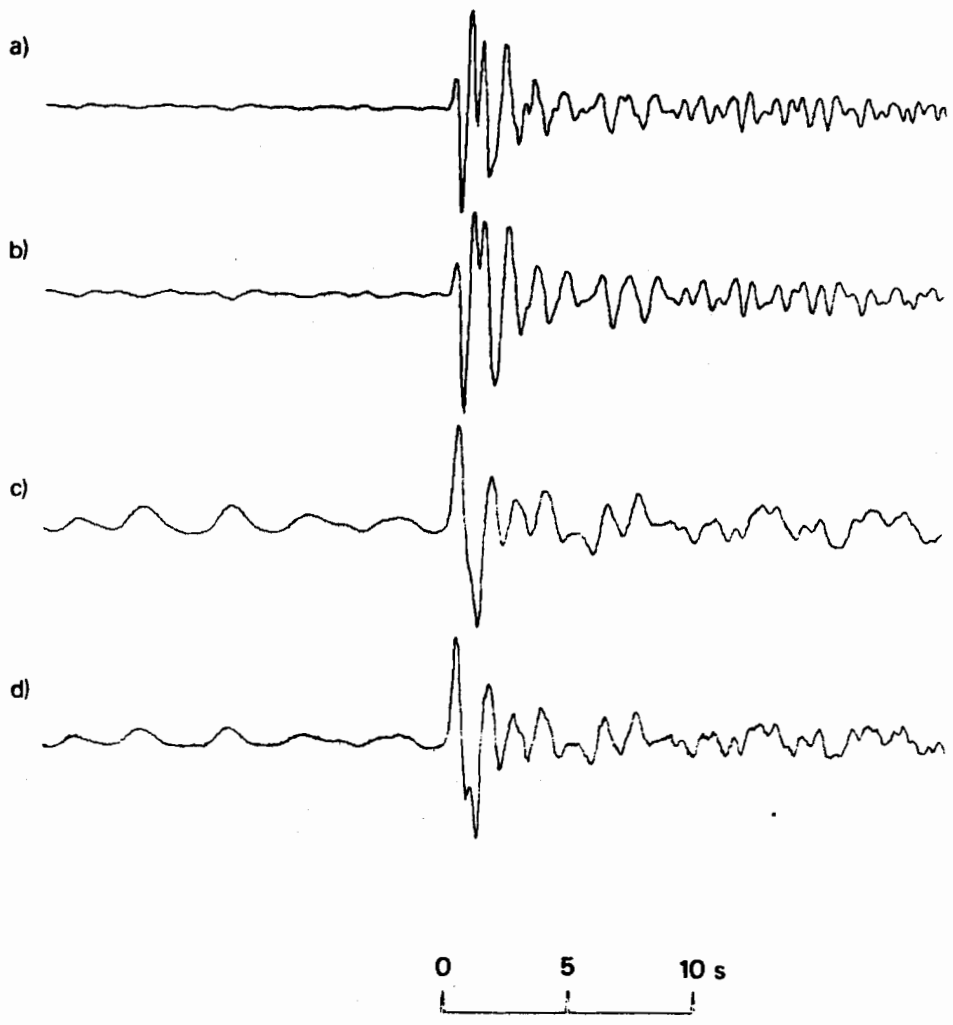

Figure A64 (a) Short-period array-sum seismogram recorded at GBA from the 5 September 1977 Shagan River explosion.
(b) Seismogram (a) filtered to simulate the effects of an additional t* of 0.2s.
(c) Seismogram (a) after Wiener filtering converted to a phaseless-broad-band instrument response.
(d) Same as seismogram (c) except that the effects of path attenuation of t* = 0.15s have been corrected for.

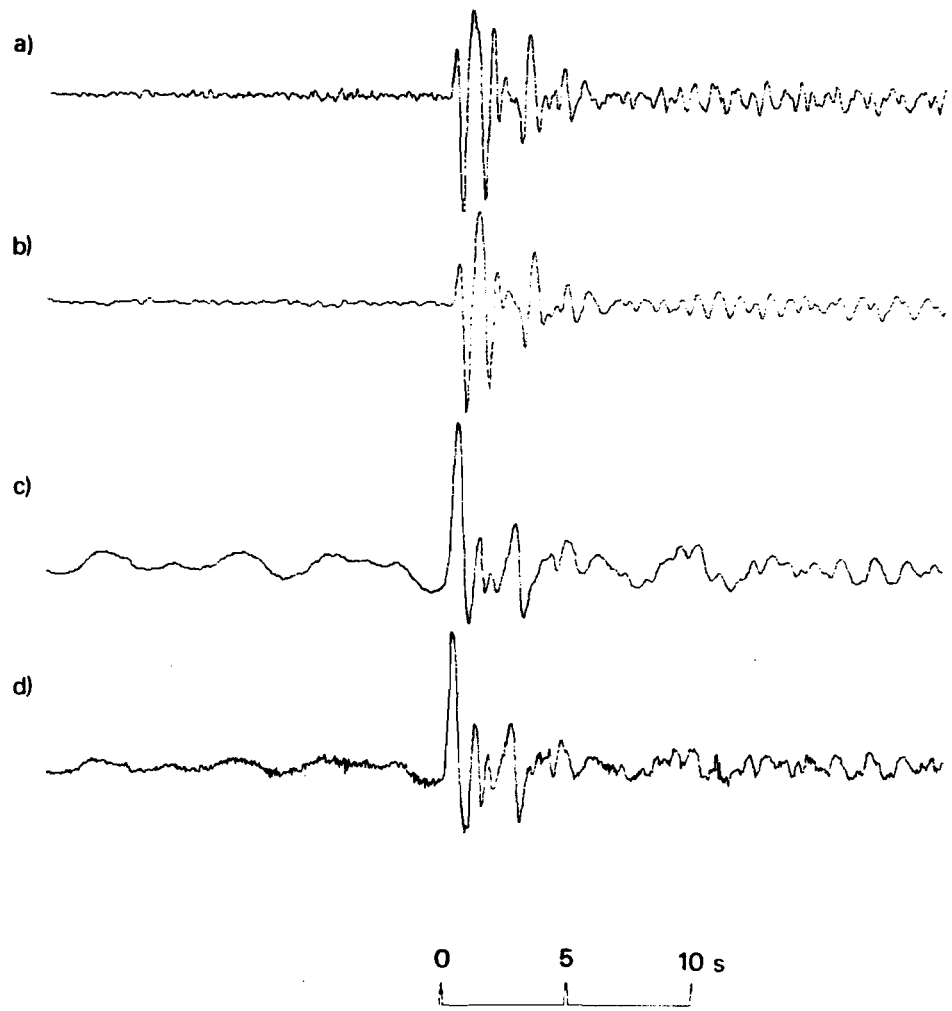

Figure A65 (a) Short-period array-sum seismogram recorded at WRA from the 5 September 1977 Shagan River explosion.
(b) Seismogram (a) filtered to simulate the effects of an additional t* of 0.2s.
(c) Seismogram (a) after Wiener filtering converted to a phaseless-broad-band instrument response.
(d) Same as seismogram (c) except that the effects of path attenuation of t* = 0.15s have been corrected for.
Note that PcP should arrive within a few seconds of P.

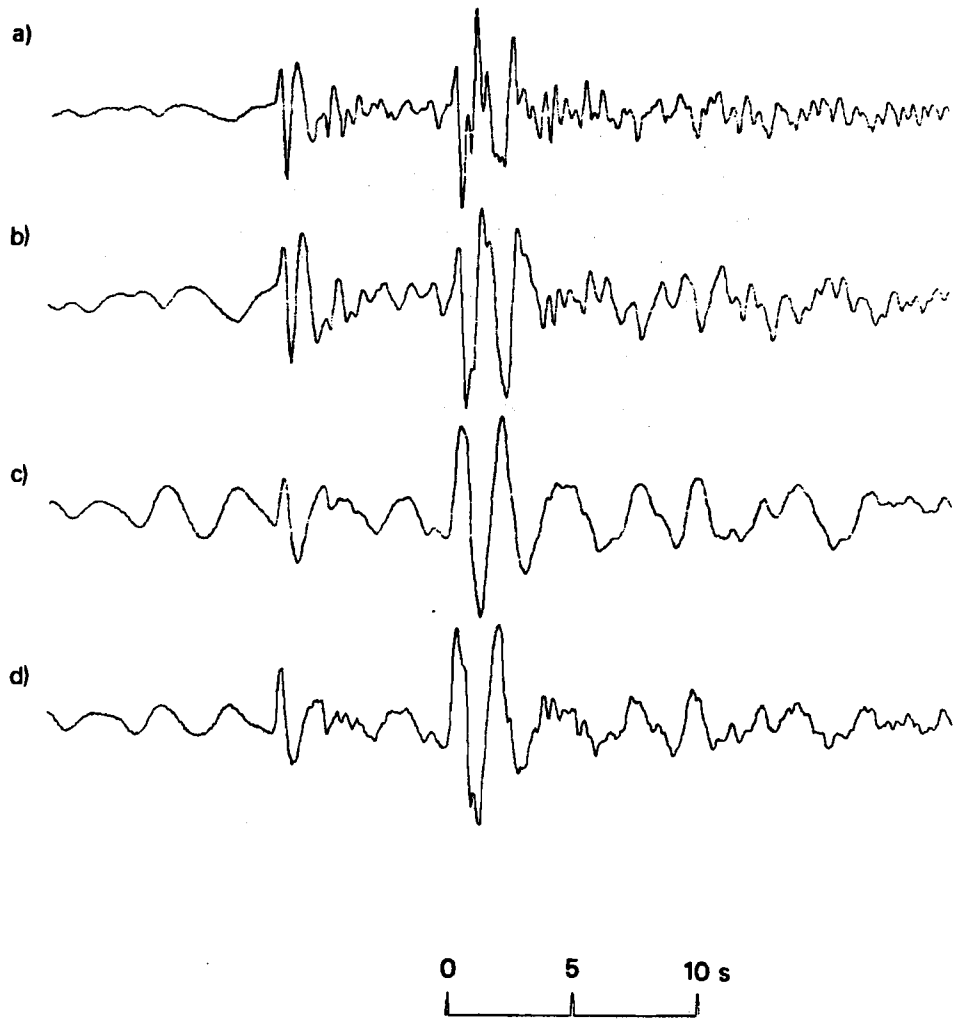

Figure A66 (a) Short-period array-sum seismogram recorded at EKA from the 29 October 1977 Shagan River explosion.
(b) Seismogram (a) filtered to simulate the effects of an additional t* of 0.2s.
(c) Seismogram (a) after Wiener filtering converted to a phaseless-broad-band instrument response.
(d) Same as seismogram (c) except that the effects of path attenuation of t* = 0.15s have been corrected for.
Note that the sample of noise used in designing the Wiener filter is taken ahead of the earlier arrival (from an explosion at Degelen Mountain).

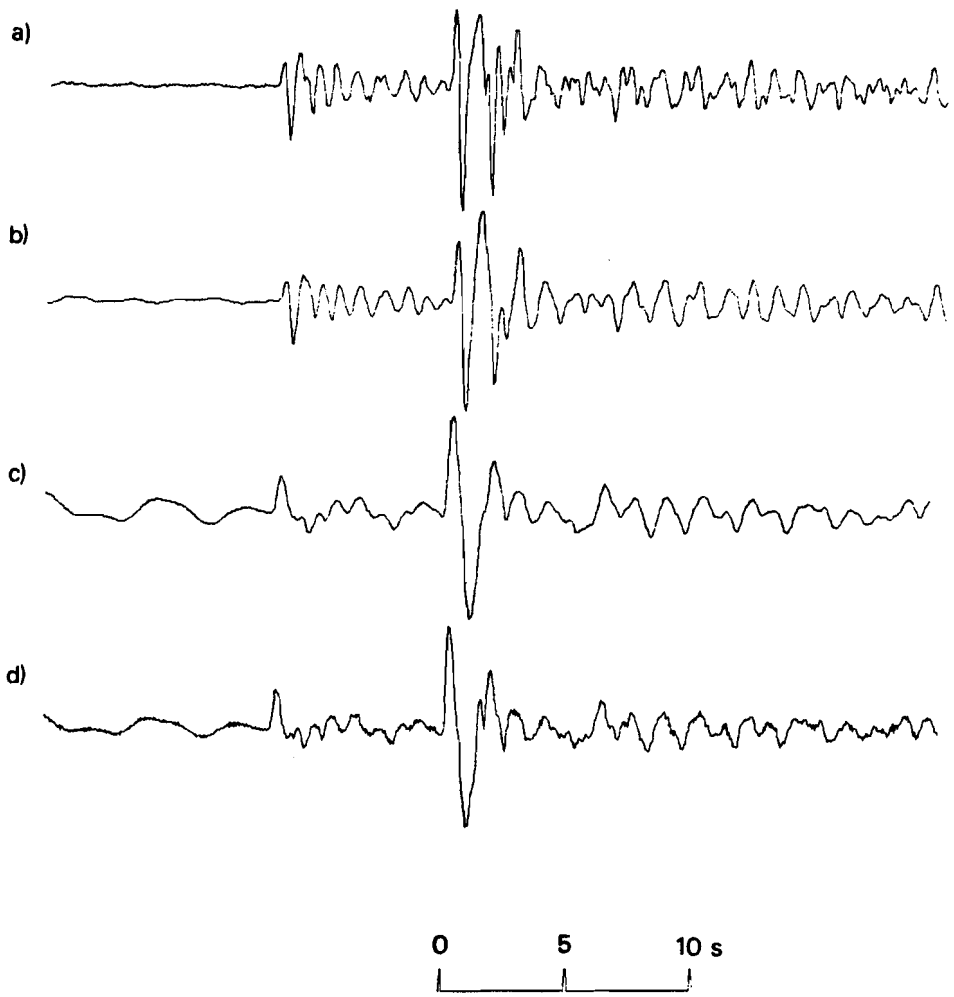

Figure A67 (a) Short-period array-sum seismogram recorded at GBA from the 29 October 1977 Shagan River explosion.
(b) Seismogram (a) filtered to simulate the effects of an additional t* of 0.2s.
(c) Seismogram (a) after Wiener filtering converted to a phaseless-broad-band instrument response.
(d) Same as seismogram (c) except that the effects of path attenuation of t* = 0.15s have been corrected for.
Note that the sample of noise used in designing the Wiener filter is taken ahead of the earlier arrival (from an explosion at Degelen Mountain).

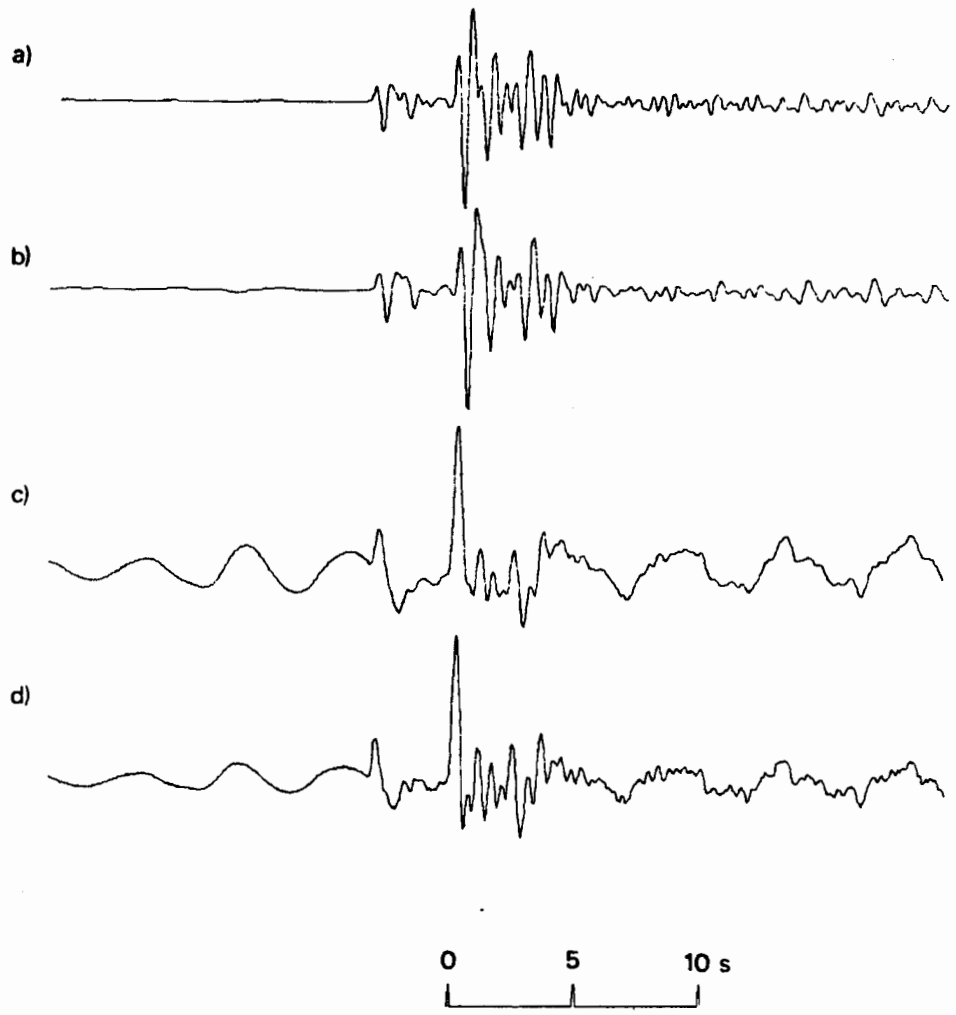

Figure A68 (a) Short-period array-sum seismogram recorded at WRA from the 29 October 1977 Shagan River explosion.
(b) Seismogram (a) filtered to simulate the effects of an additional t* of 0.2s.
(c) Seismogram (a) after Wiener filtering converted to a phaseless-broad-band instrument response.
(d) Same as seismogram (c) except that the effects of path attenuation of t* = 0.15s have been corrected for.
Note that the sample of noise used in designing the Wiener filter is taken ahead of the earlier arrival (from an explosion at Degelen Mountain).
Note also that PcP should arrive within a few seconds of P.

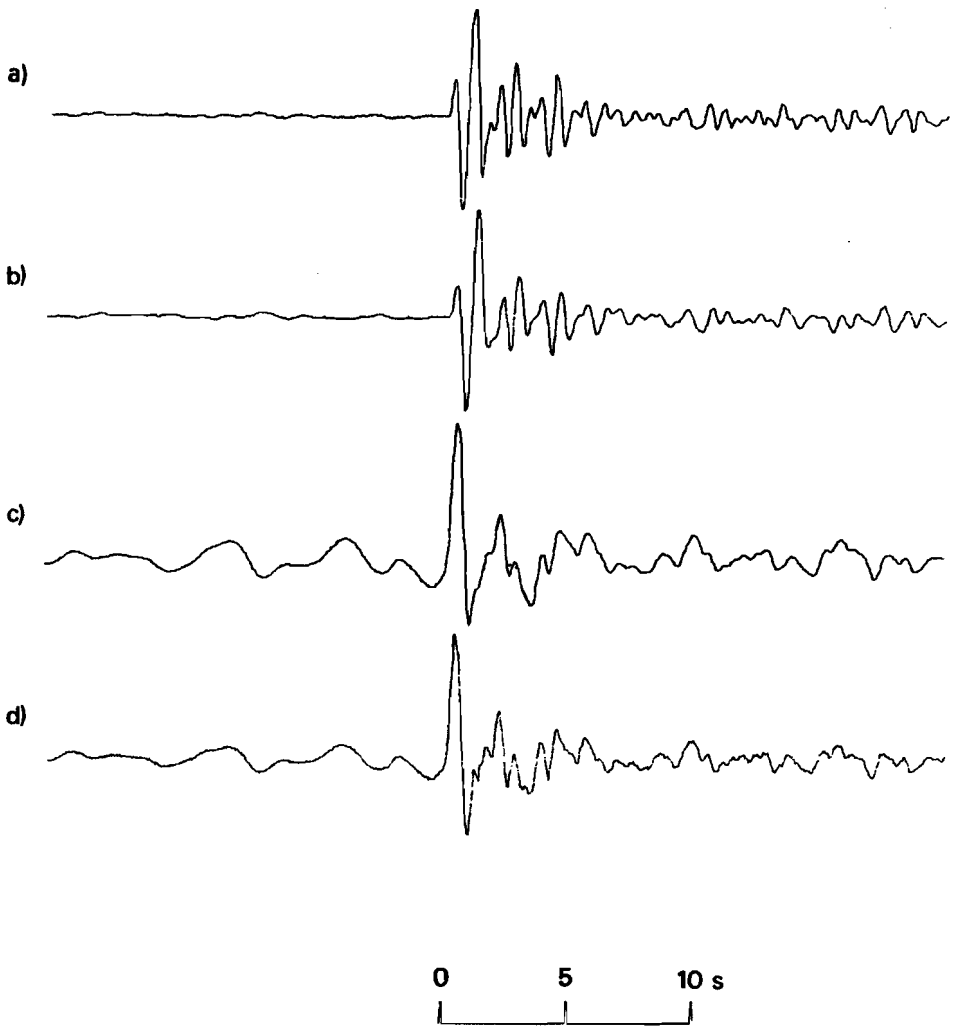

Figure A69 (a) Short-period array-sum seismogram recorded at EKA from the 30 November 1977 Shagan River explosion.
(b) Seismogram (a) filtered to simulate the effects of an additional t* of 0.2s.
(c) Seismogram (a) after Wiener filtering converted to a phaseless-broad-band instrument response.
(d) Same as seismogram (c) except that the effects of path attenuation of t* = 0.15s have been corrected for.

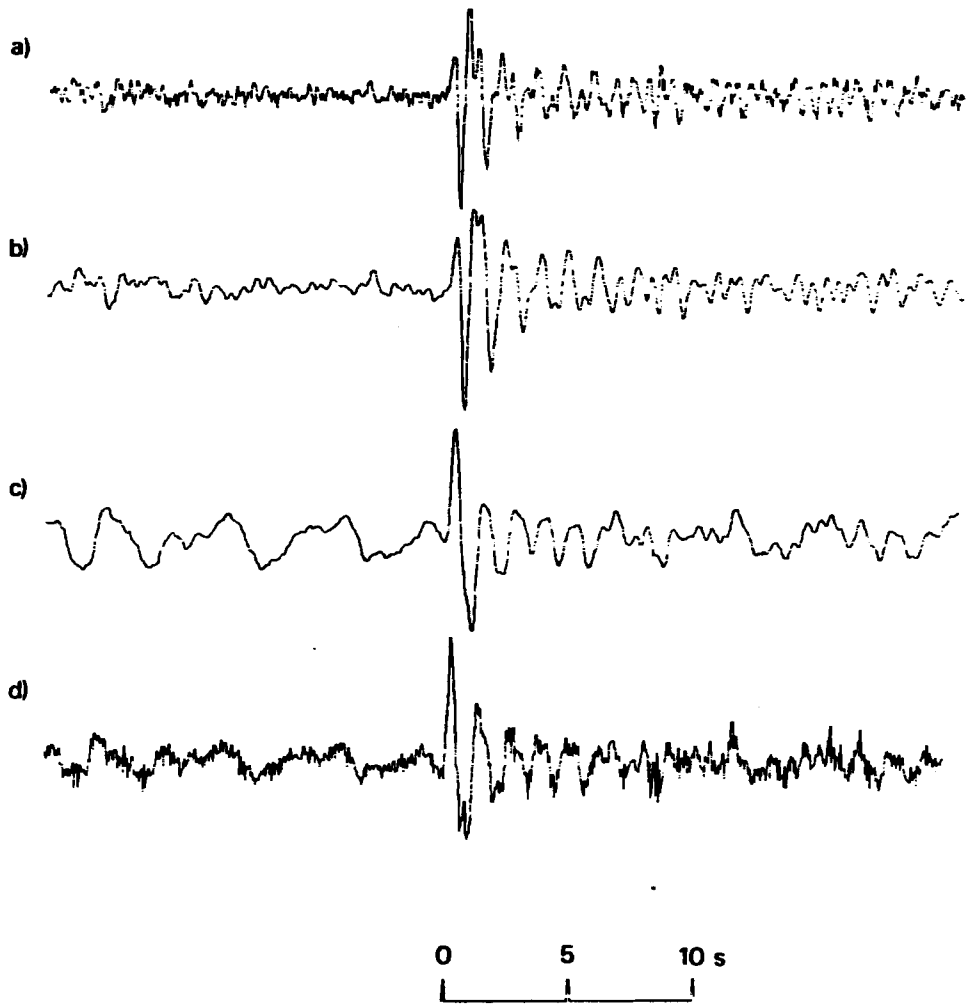

Figure A70 (a) Short-period strong-motion (gain not known) seismogram recorded at GBA from the 30 November 1977 Shagan River explosion.
(b) Seismogram (a) filtered to simulate the effects of an additional t* of 0.2s.
(c) Seismogram (a) after Wiener filtering converted to a phaseless-broad-band instrument response.
(d) Same as seismogram (c) except that the effects of path attenuation of t* = 0.15s have been corrected for.

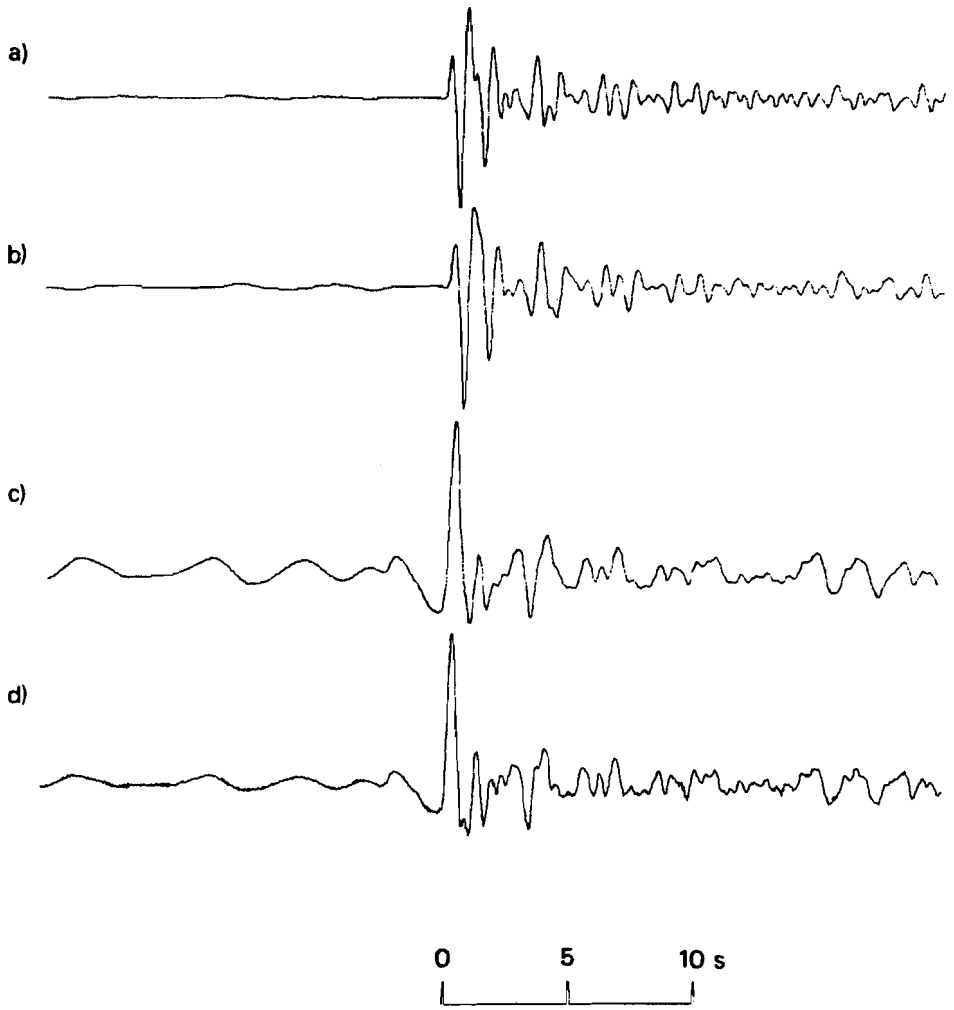

Figure A71 (a) Short-period array-sum seismogram recorded at WRA from the 30 November 1977 Shagan River explosion.
(b) Seismogram (a) filtered to simulate the effects of an additional t* of 0.2s.
(c) Seismogram (a) after Wiener filtering converted to a phaseless-broad-band instrument response.
(d) Same as seismogram (c) except that the effects of path attenuation of t* = 0.15s have been corrected for.
Note that PcP should arrive within a few seconds of P.

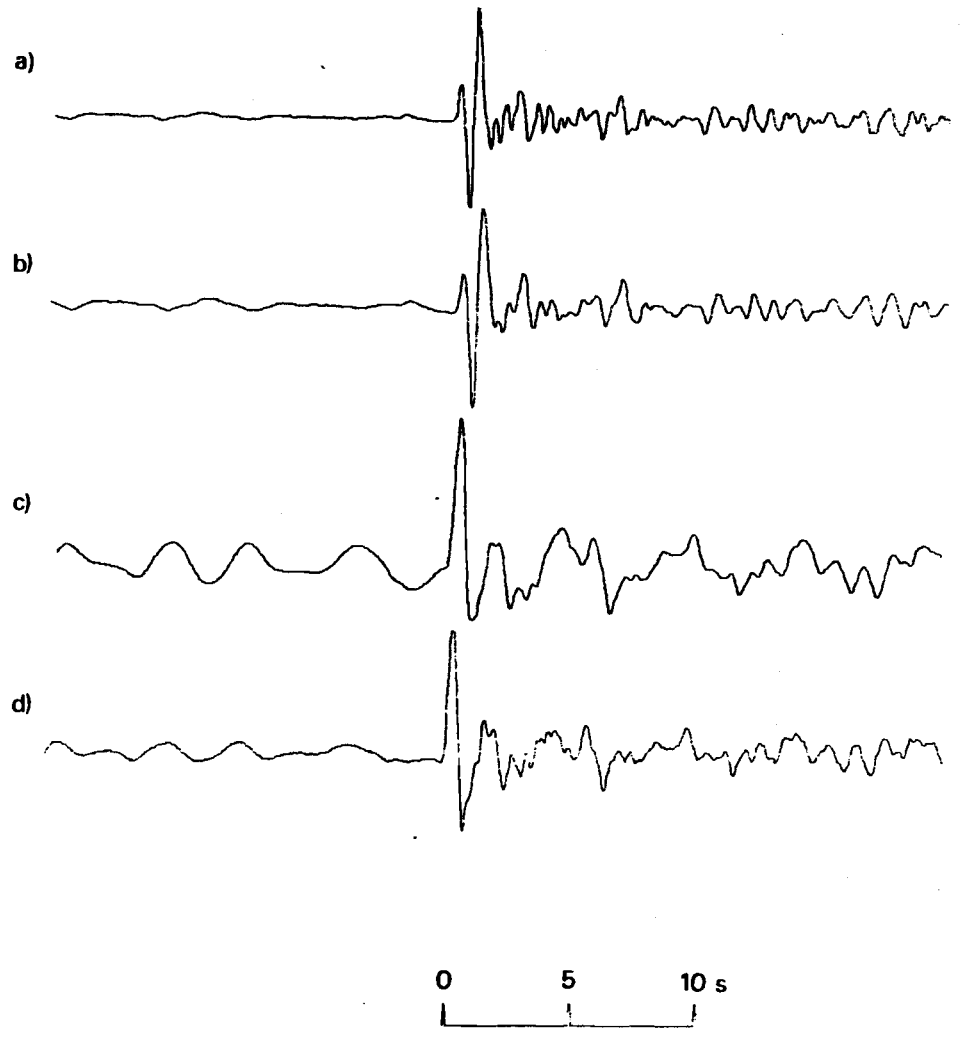

Figure A72 (a) Short-period array-sum seismogram recorded at EKA from the 11 June 1978 Shagan River explosion.
(b) Seismogram (a) filtered to simulate the effects of an additional t* of 0.2s.
(c) Seismogram (a) after Wiener filtering converted to a phaseless-broad-band instrument response.
(d) Same as seismogram (c) except that the effects of path attenuation of t* = 0.15s have been corrected for.

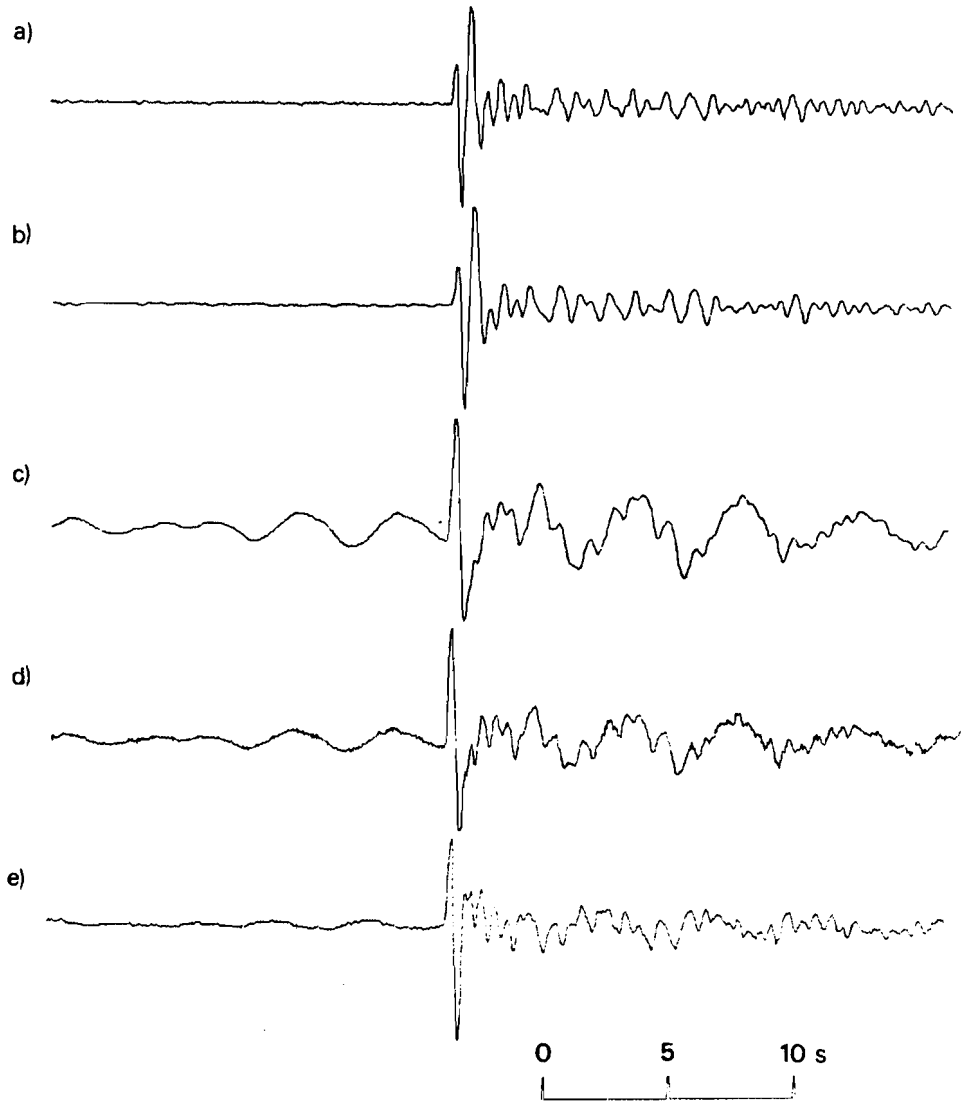

Figure A73 (a) Short-period seismogram that would be recorded at YKA from the 11 June 1978 Shagan River explosion: derived from the velocity-broad-band seismogram (e).
(b) Seismogram (a) filtered to simulate the effects of an additional t* of 0.2s.
(c) Seismogram (a) after Wiener filtering converted to a phaseless-broad-band instrument response.
(d) Same as seismogram (c) except that the effects of path attenuation of t* = 0.15s have been corrected for.
(e) Velocity-broad-band seismogram recorded at YKA.

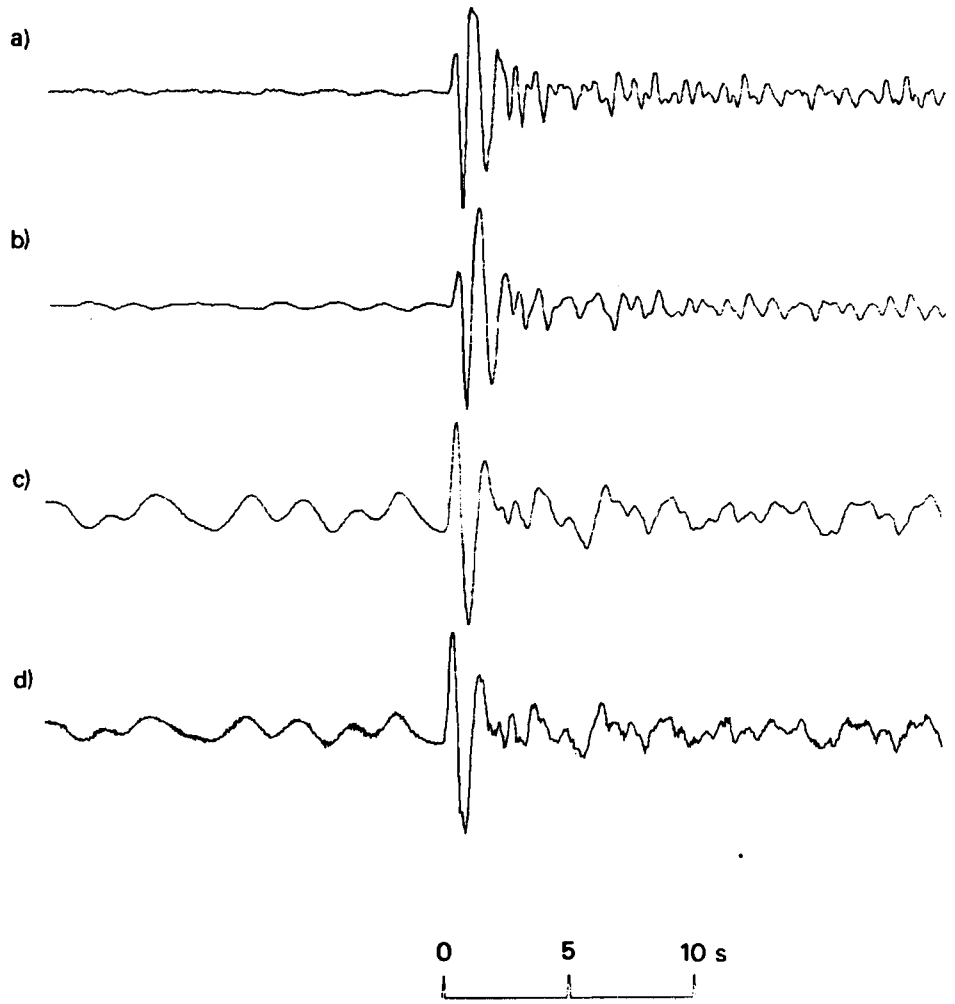

Figure A74 (a) Short-period array-sum seismogram recorded at GBA from the 11 June 1978 Shagan River explosion.
(b) Seismogram (a) filtered to simulate the effects of an additional t* of 0.2s.
(c) Seismogram (a) after Wiener filtering converted to a phaseless-broad-band instrument response.
(d) Same as seismogram (c) except that the effects of path attenuation of t* = 0.15s have been corrected for.

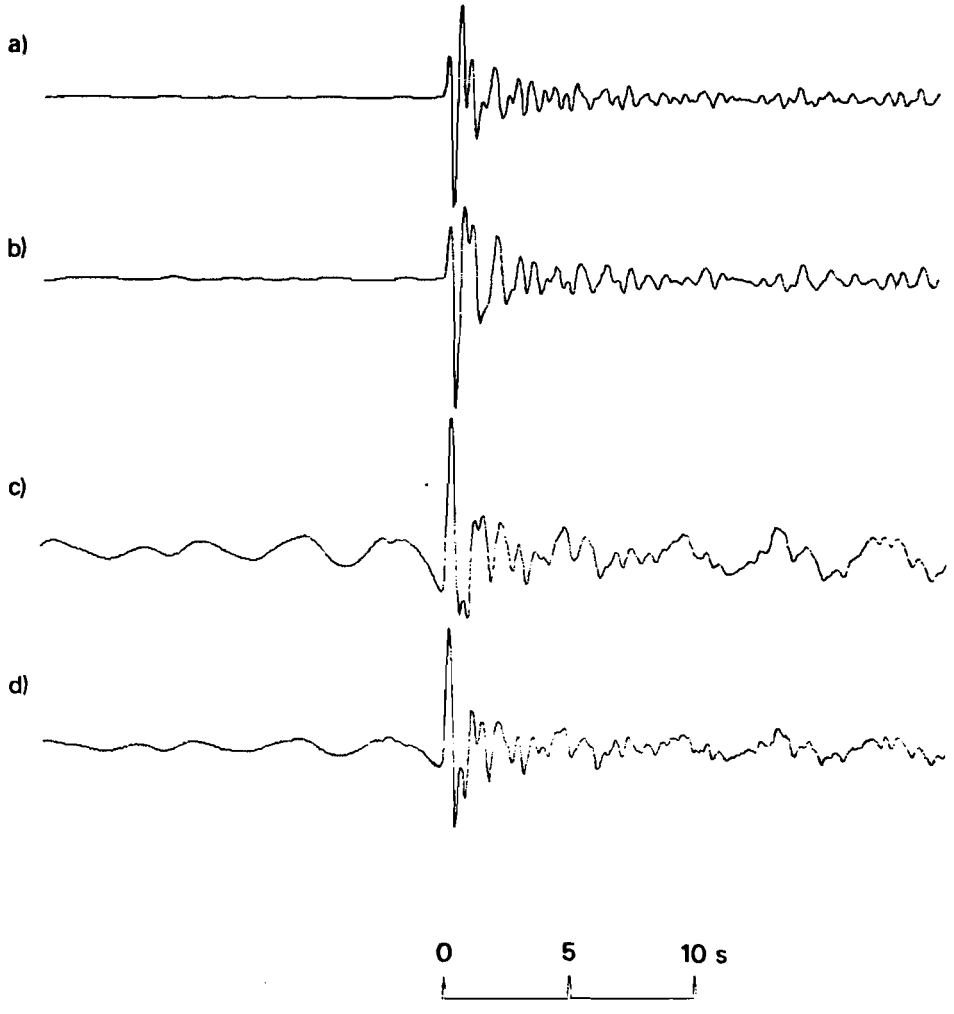

Figure A75 (a) Short-period array-sum seismogram recorded at WRA from the 11 June 1978 Shagan River explosion.
(b) Seismogram (a) filtered to simulate the effects of an additional t* of 0.2s.
(c) Seismogram (a) after Wiener filtering converted to a phaseless-broad-band instrument response.
(d) Same as seismogram (c) except that the effects of path attenuation of t* = 0.15s have been corrected for.
Note that PcP should arrive within a few seconds of P.

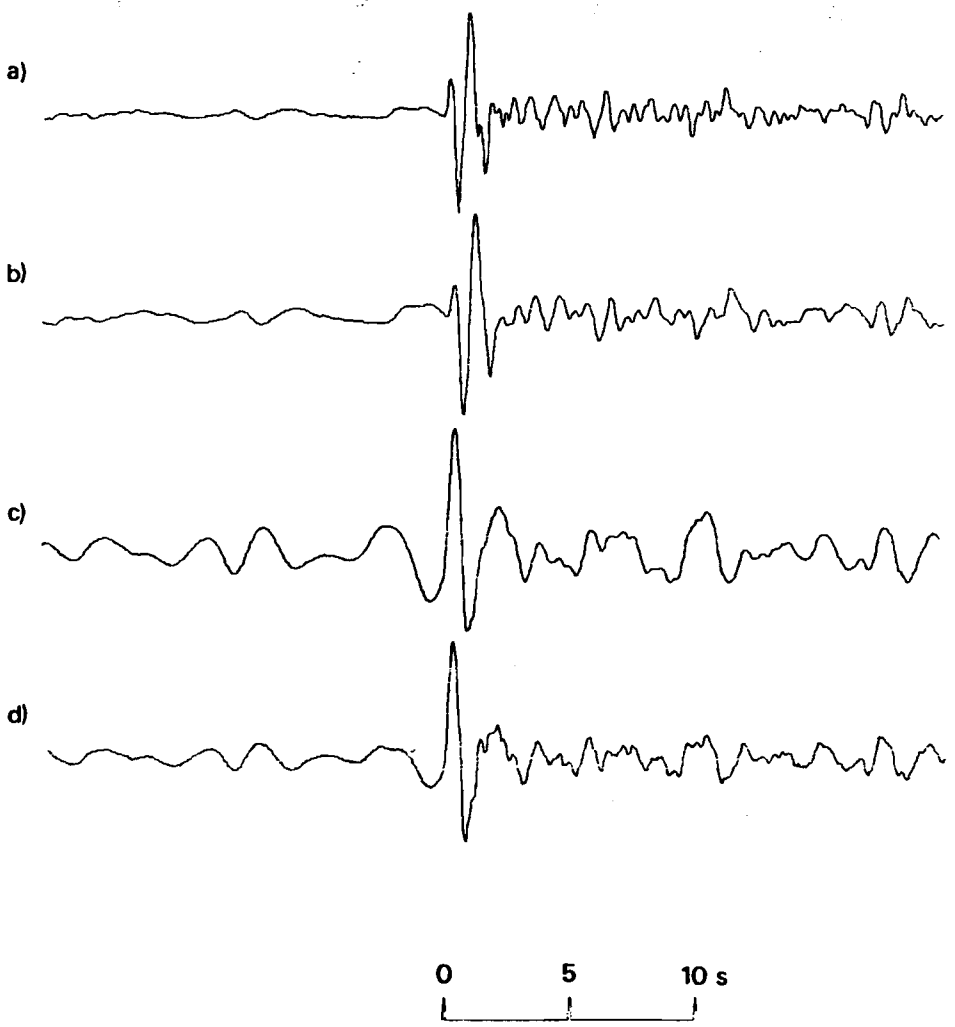

Figure A76 (a) Short-period array-sum seismogram recorded at EKA from the 5 July 1978 Shagan River explosion.
(b) Seismogram (a) filtered to simulate the effects of an additional t* of 0.2s.
(c) Seismogram (a) after Wiener filtering converted to a phaseless-broad-band instrument response.
(d) Same as seismogram (c) except that the effects of path attenuation of t* = 0.15s have been corrected for.

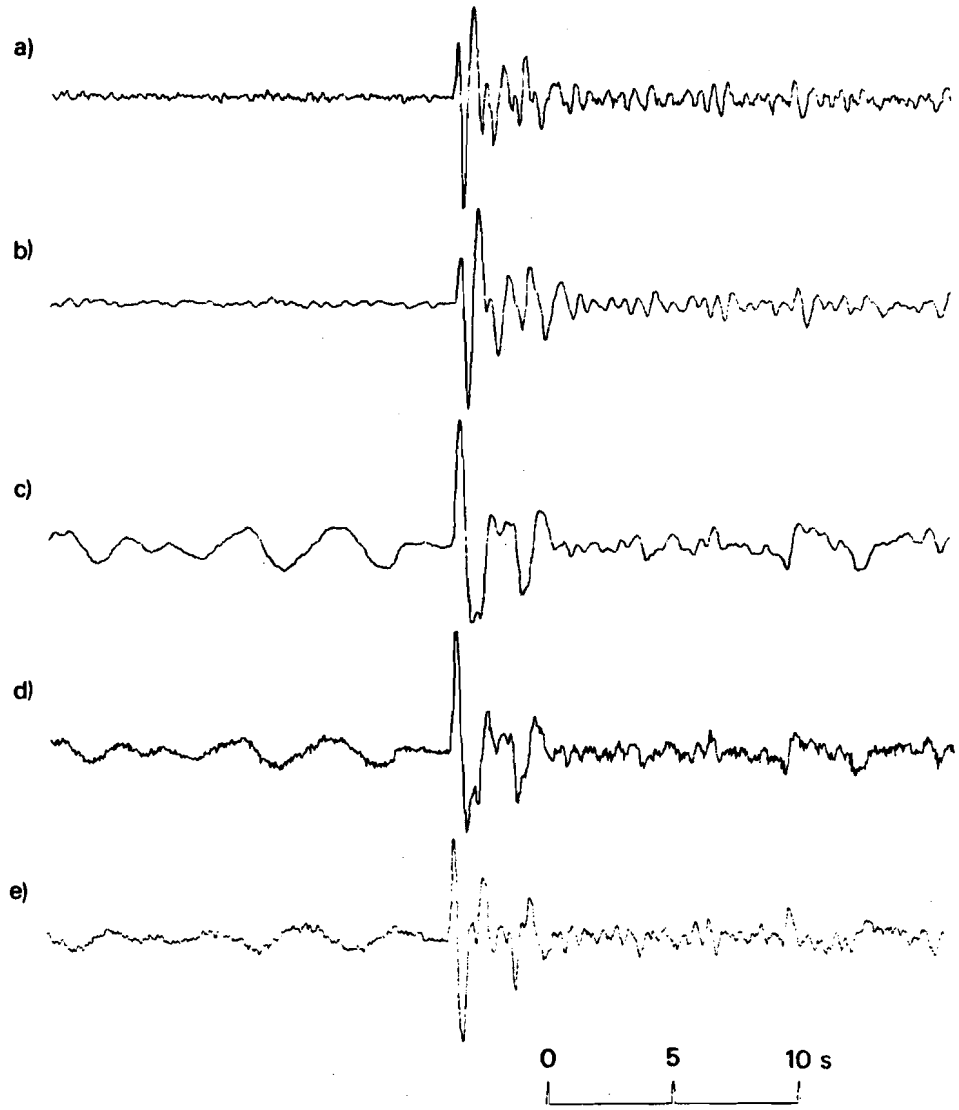

Figure A77 (a) Short-period seismogram that would be recorded at YKA from the 5 July 1978 Shagan River explosion: derived from the velocity-broad-band seismogram (e).
(b) Seismogram (a) filtered to simulate the effects of an additional t* of 0.2s.
(c) Seismogram (a) after Wiener filtering converted to a phaseless-broad-band instrument response.
(d) Same as seismogram (c) except that the effects of path attenuation of t* = 0.15s have been corrected for.
(e) Velocity-broad-band seismogram recorded at YKA.

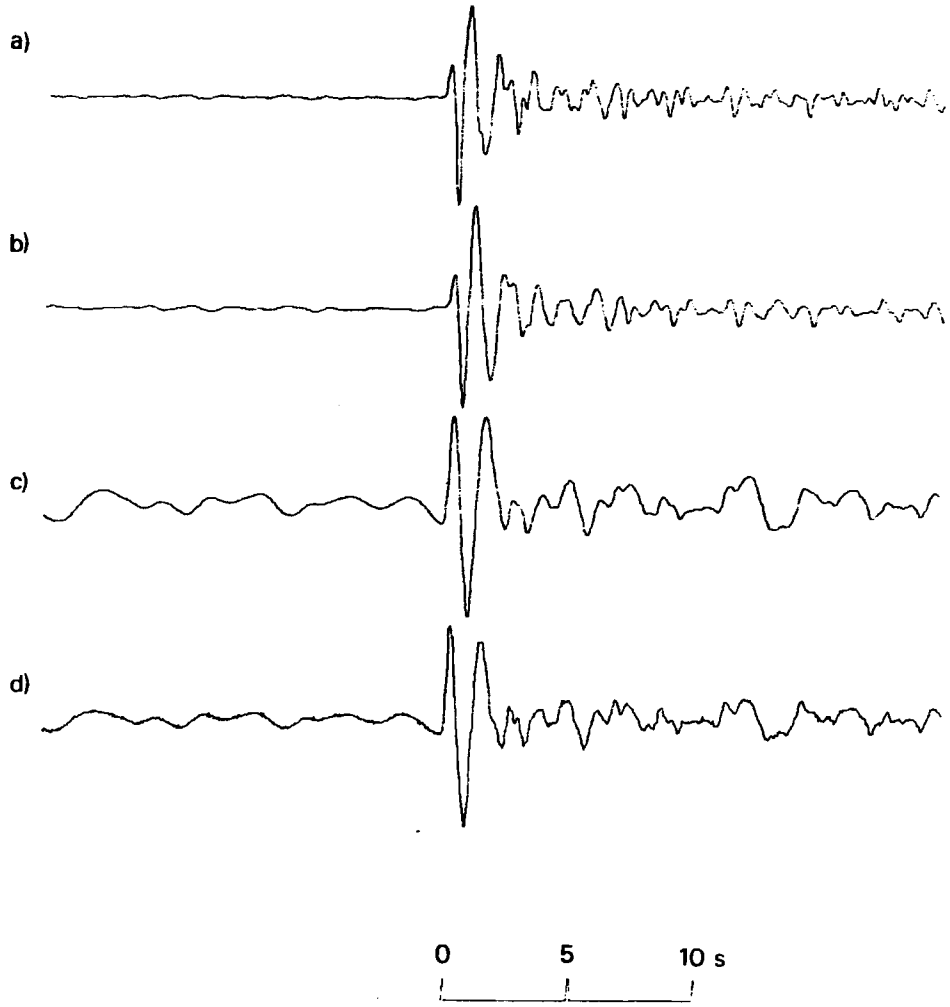

Figure A78 (a) Short-period array-sum seismogram recorded at GBA from the 5 July 1978 Shagan River explosion.
(b) Seismogram (a) filtered to simulate the effects of an additional t* of 0.2s.
(c) Seismogram (a) after Wiener filtering converted to a phaseless-broad-band instrument response.
(d) Same as seismogram (c) except that the effects of path attenuation of t* = 0.15s have been corrected for.

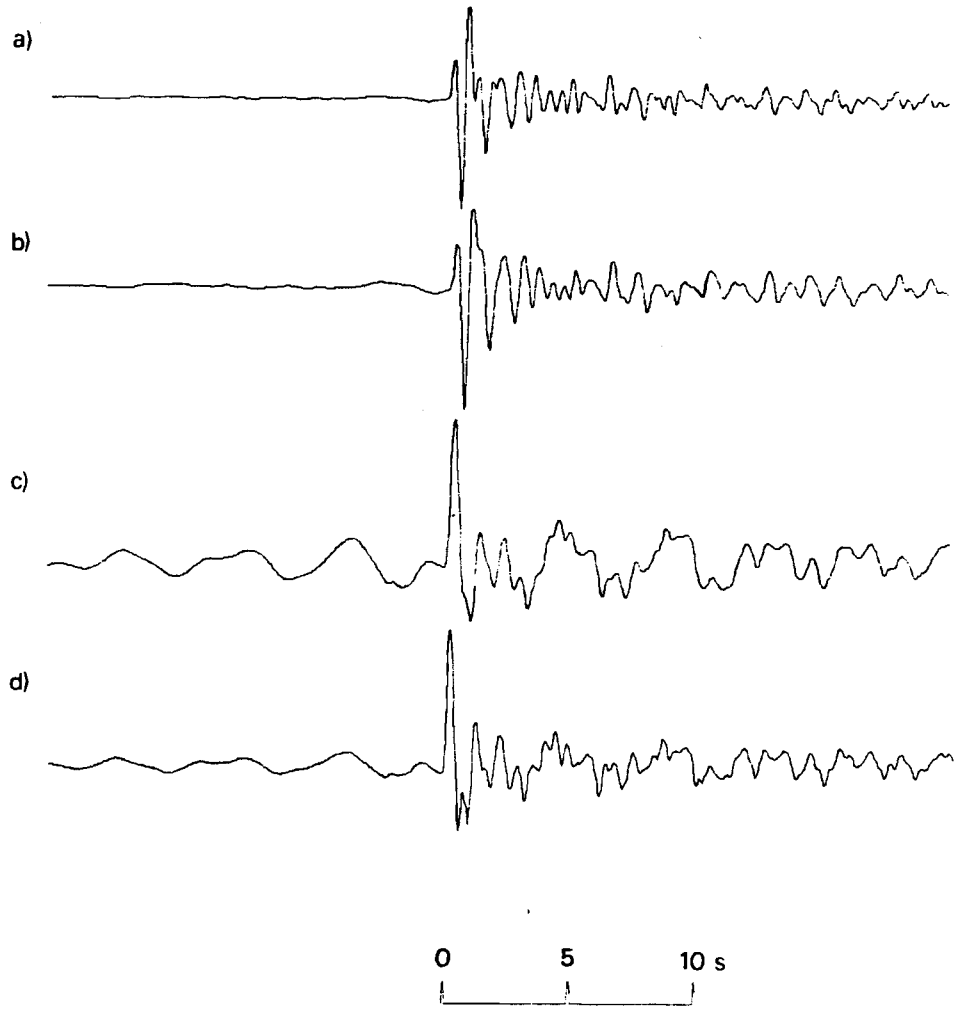

Figure A79 (a) Short-period array-sum seismogram recorded at WRA from the 5 July 1978 Shagan River explosion.
(b) Seismogram (a) filtered to simulate the effects of an additional t* of 0.2s.
(c) Seismogram (a) after Wiener filtering converted to a phaseless-broad-band instrument response.
(d) Same as seismogram (c) except that the effects of path attenuation of t* = 0.15s have been corrected for.
Note that PcP should arrive within a few seconds of P.

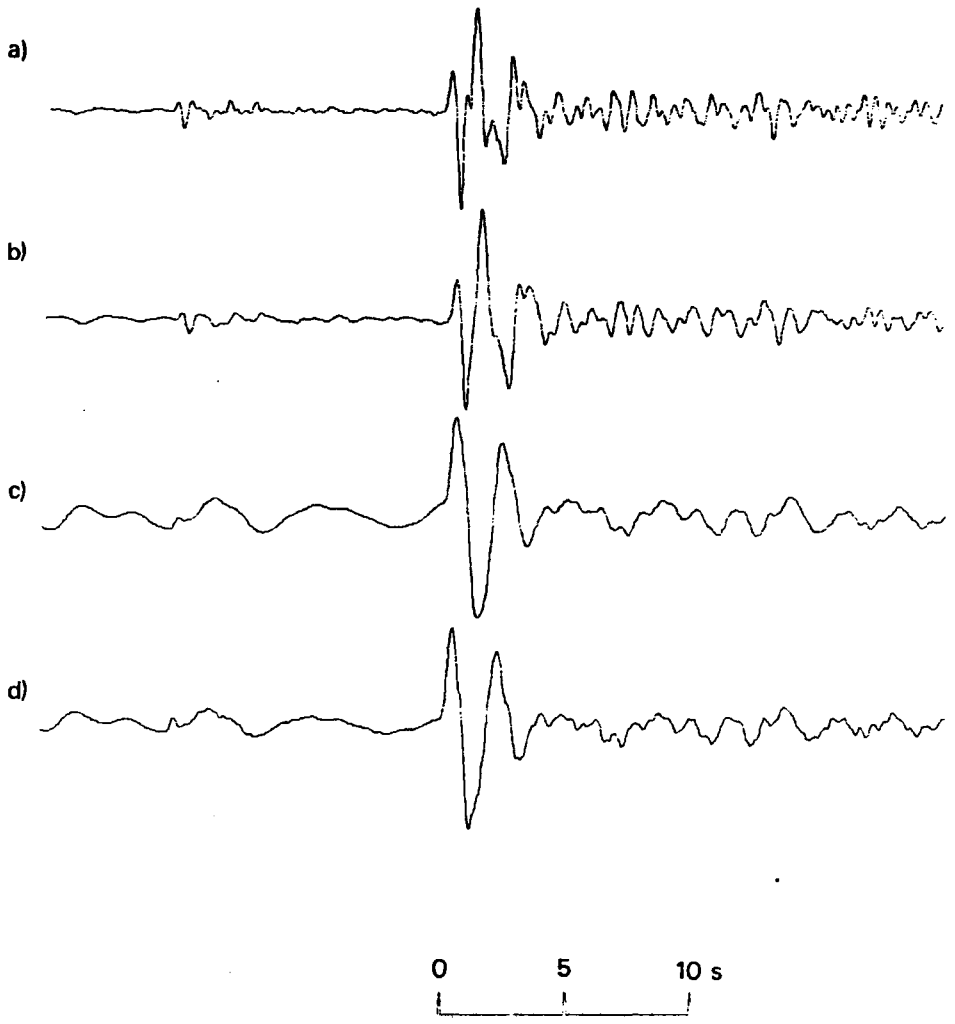

Figure A80 (a) Short-period array-sum seismogram recorded at EKA from the 29 August 1978 Shagan River explosion.
(b) Seismogram (a) filtered to simulate the effects of an additional t* of 0.2s.
(c) Seismogram (a) after Wiener filtering converted to a phaseless-broad-band instrument response.
(d) Same as seismogram (c) except that the effects of path attenuation of t* = 0.15s have been corrected for.
Note that the sample of noise used in designing the Wiener filter is taken ahead of the earlier arrival (from an explosion at Degelen Mountain).

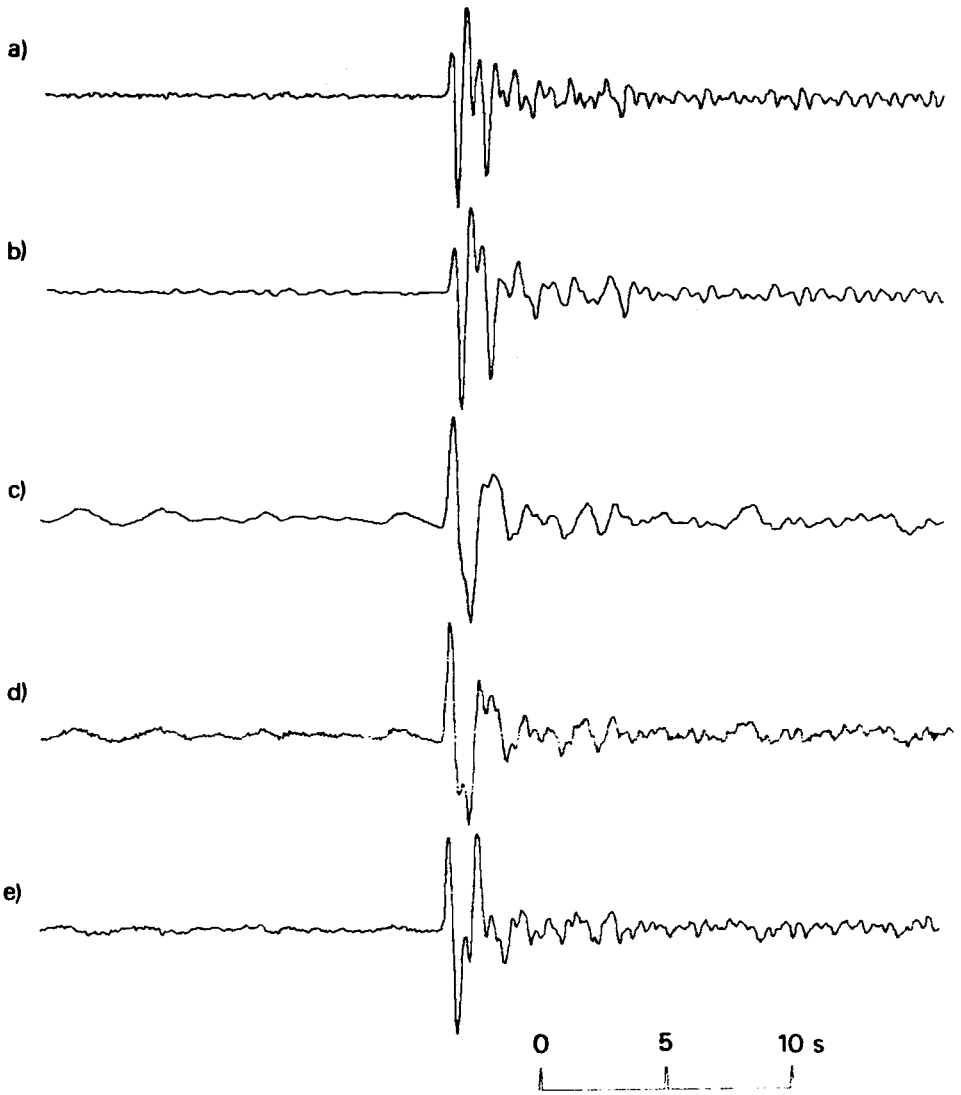

Figure A81 (a) Short-period seismogram that would be recorded at YKA from the 29 August 1978 Shagan River explosion: derived from the velocity-broad-band seismogram (e).
(b) Seismogram (a) filtered to simulate the effects of an additional t* of 0.2s.
(c) Seismogram (a) after Wiener filtering converted to a phaseless-broad-band instrument response.
(d) Same as seismogram (c) except that the effects of path attenuation of t* = 0.15s have been corrected for.
(e) Velocity-broad-band seismogram recorded at YKA.
Note that the sample of noise used in designing the Wiener filter is taken ahead of an earlier small arrival (from an explosion at Degelen Mountain).

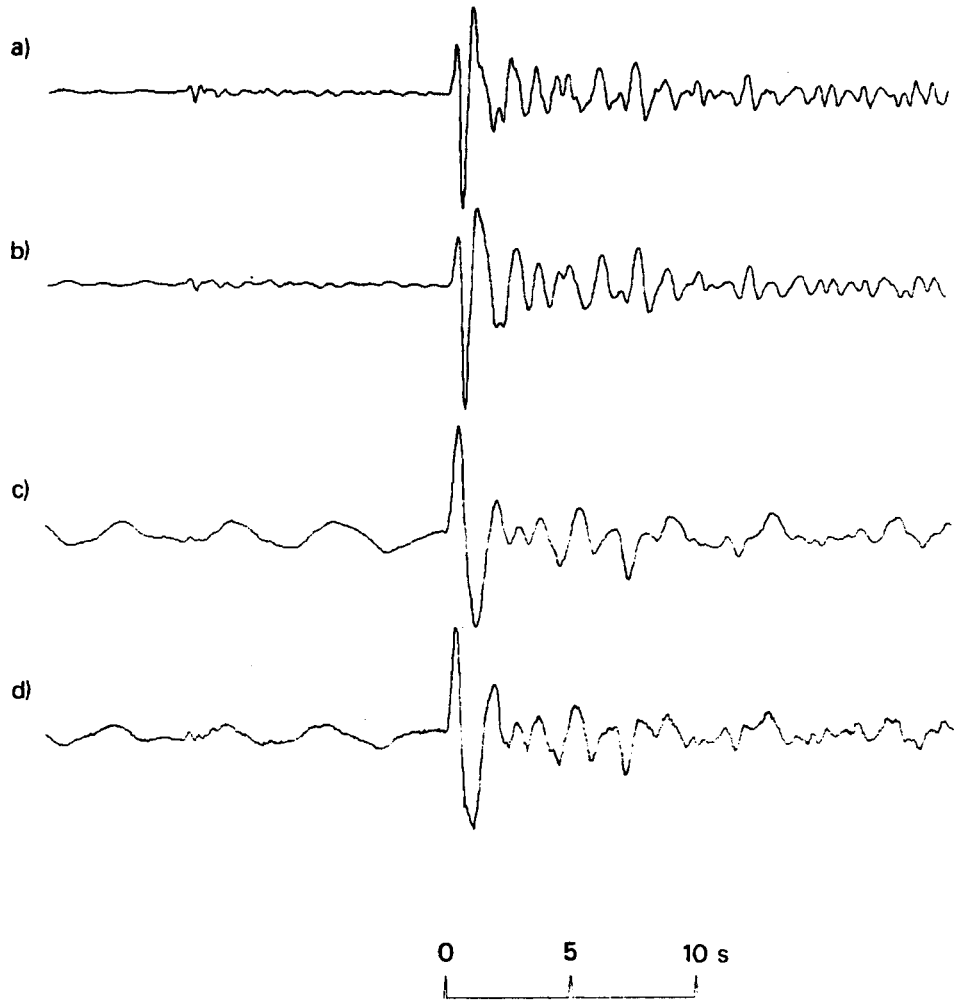

Figure A82 (a) Short-period array-sum seismogram recorded at GBA from the 29 August 1978 Shagan River explosion.
(b) Seismogram (a) filtered to simulate the effects of an additional t* of 0.2s.
(c) Seismogram (a) after Wiener filtering converted to a phaseless-broad-band instrument response.
(d) Same as seismogram (c) except that the effects of path attenuation of t* = 0.15s have been corrected for.
Note that the sample of noise used in designing the Wiener filter is taken ahead of the earlier arrival (from an explosion at Degelen Mountain).

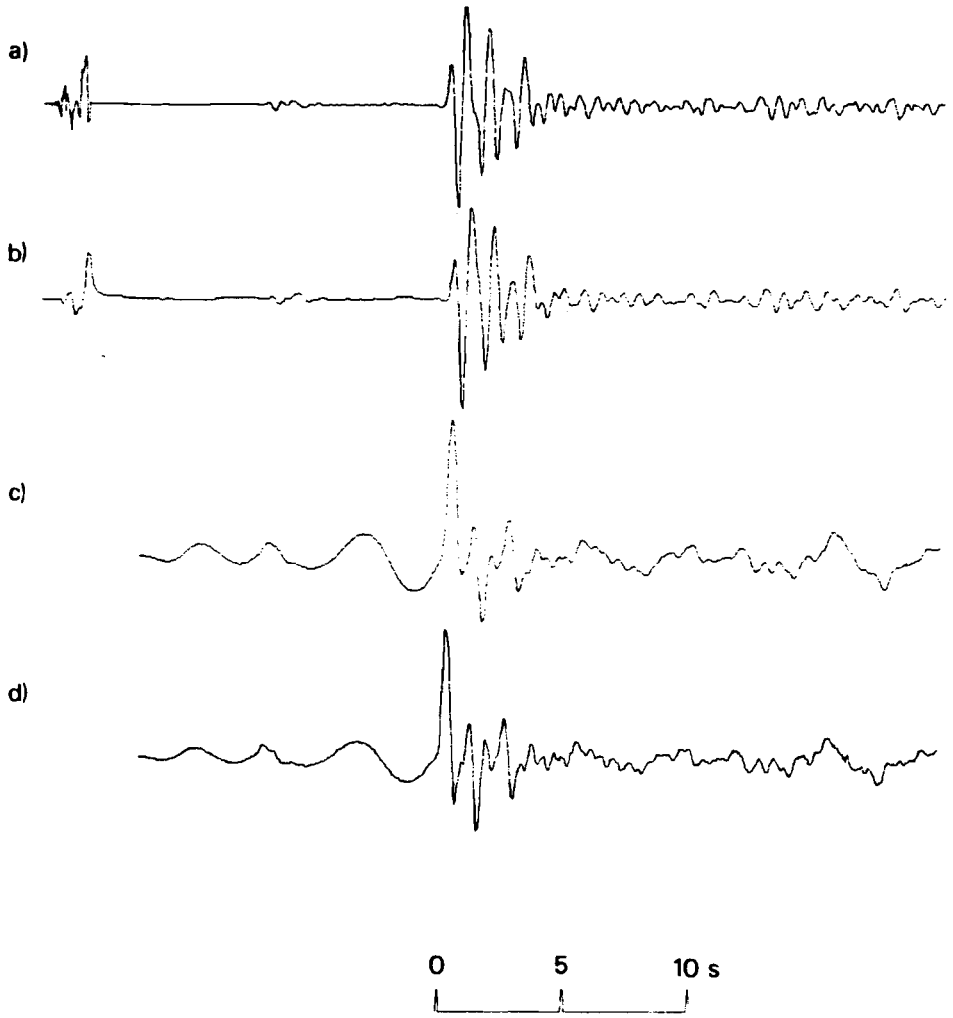

Figure A83 (a) Short-period array-sum seismogram recorded at WRA from the 29 August 1978 Shagan River explosion.
(b) Seismogram (a) filtered to simulate the effects of an additional t* of 0.2s.
(c) Seismogram (a) converted to a phaseless-broad-band instrument response.
(d) Same as seismogram (c) except that the effects of path attenuation of t* = 0.15s have been corrected for.
Note that no Wiener filter has been applied to (c) or (d): the noise burst and earlier arrival (from an explosion at Degelen Mountain) did not allow a sufficiently long noise sample to be taken.
Note also that PcP should arrive within a few seconds of P.

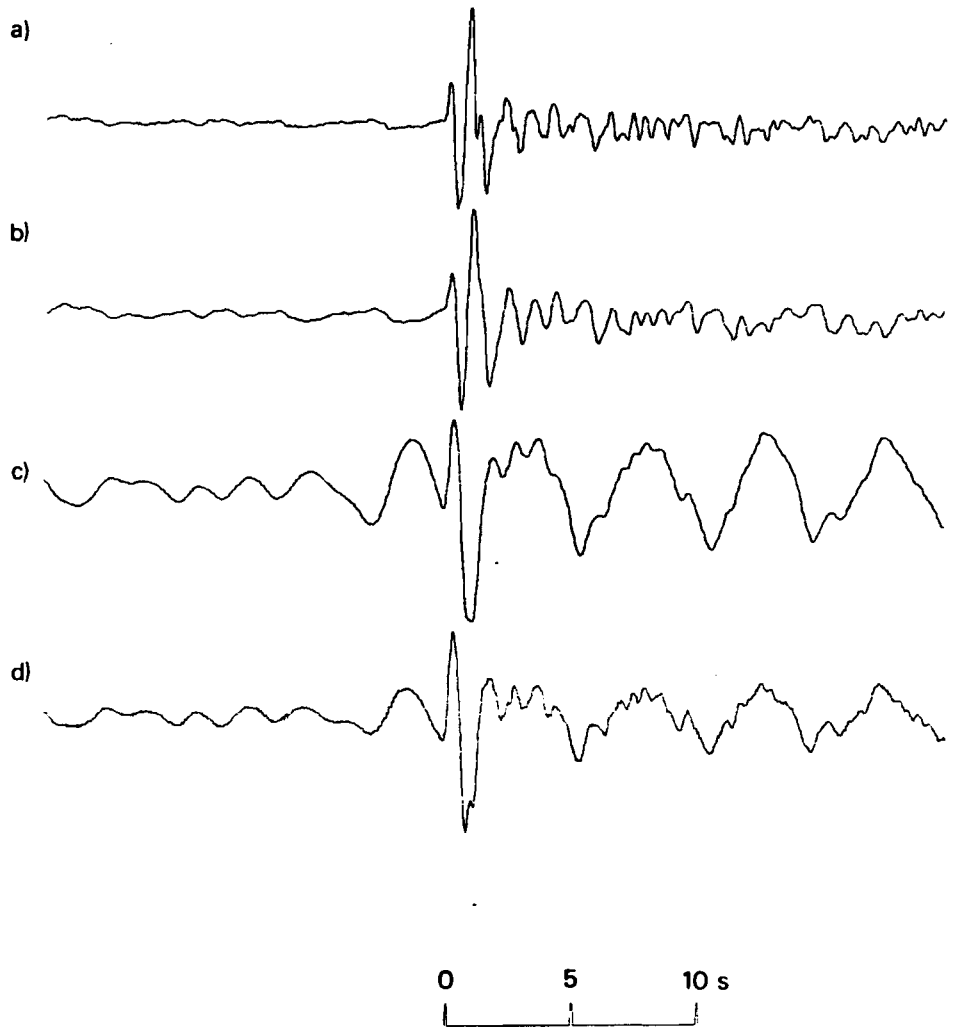

Figure A84 (a) Short-period array-sum seismogram recorded at EKA from the 15 September 1978 Shagan River explosion.
(b) Seismogram (a) filtered to simulate the effects of an additional t* of 0.2s.
(c) Seismogram (a) after Wiener filtering converted to a phaseless-broad-band instrument response.
(d) Same as seismogram (c) except that the effects of path attenuation of t* = 0.15s have been corrected for.

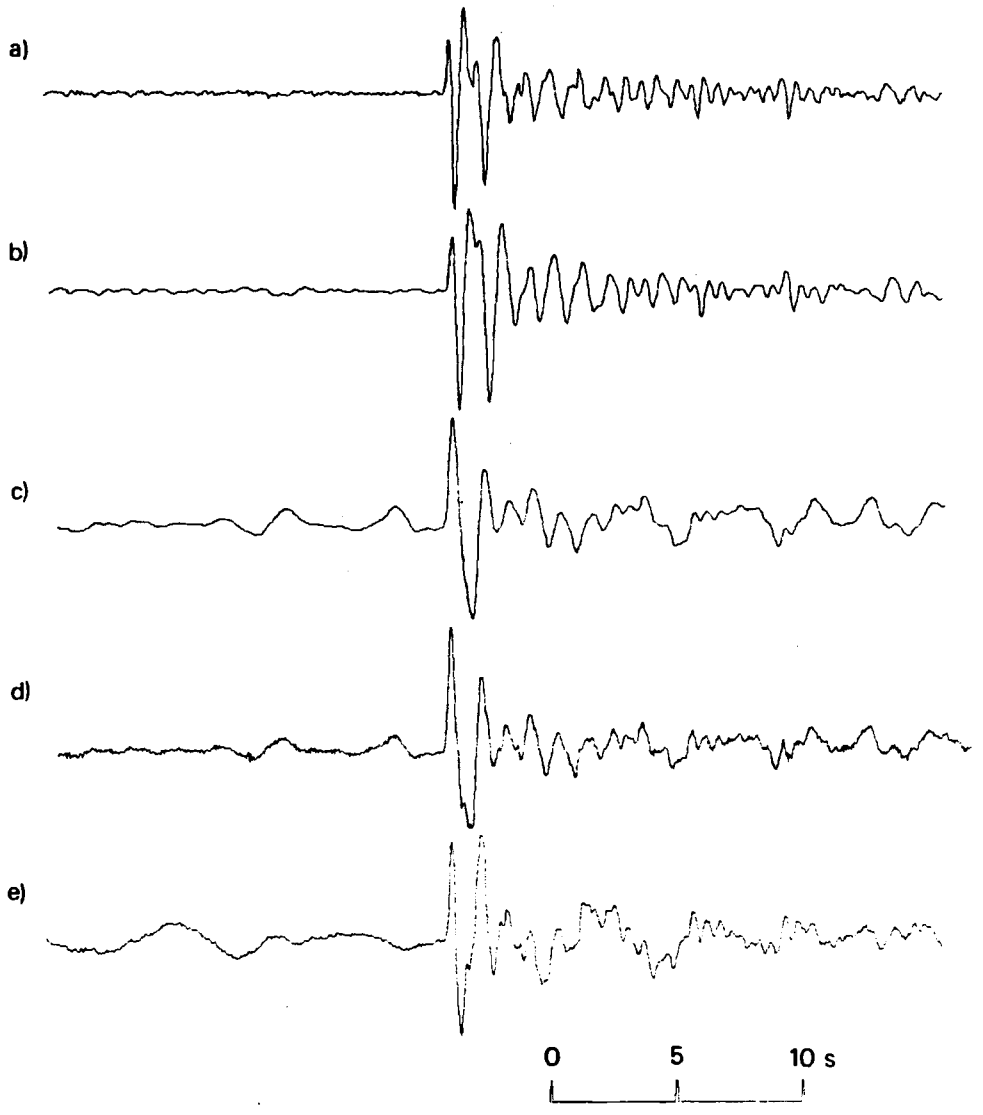

Figure A85 (a) Short-period seismogram that would be recorded at YKA from the 15 September 1978 Shagan River explosion: derived from the velocity-broad-band seismogram (e).
(b) Seismogram (a) filtered to simulate the effects of an additional t* of 0.2s.
(c) Seismogram (a) after Wiener filtering converted to a phaseless-broad-band instrument response.
(d) Same as seismogram (c) except that the effects of path attenuation of t* = 0.15s have been corrected for.
(e) Velocity-broad-band seismogram recorded at YKA.

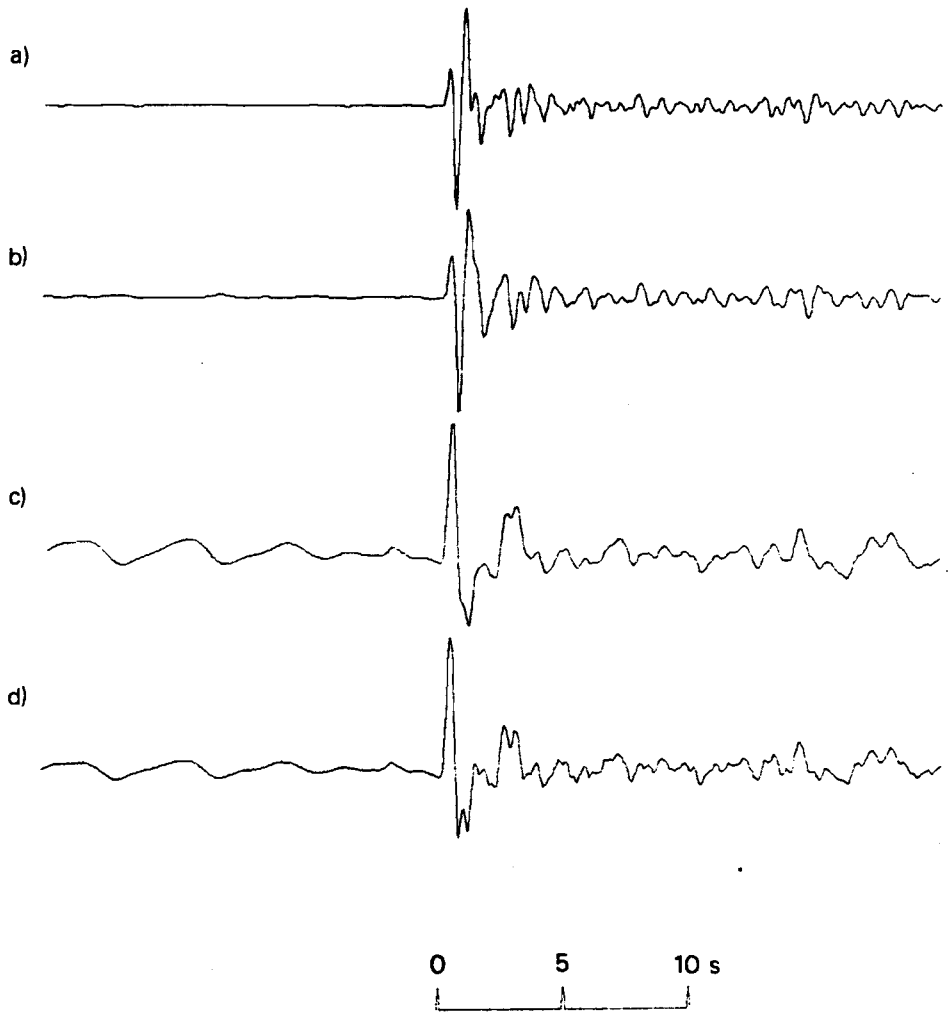

Figure A86 (a) Short-period array-sum seismogram recorded at WRA from the 15 September 1978 Shagan River explosion.
(b) Seismogram (a) filtered to simulate the effects of an additional t* of 0.2s.
(c) Seismogram (a) after Wiener filtering converted to a phaseless-broad-band instrument response.
(d) Same as seismogram (c) except that the effects of path attenuation of t* = 0.15s have been corrected for.
Note that PcP should arrive within a few seconds of P.

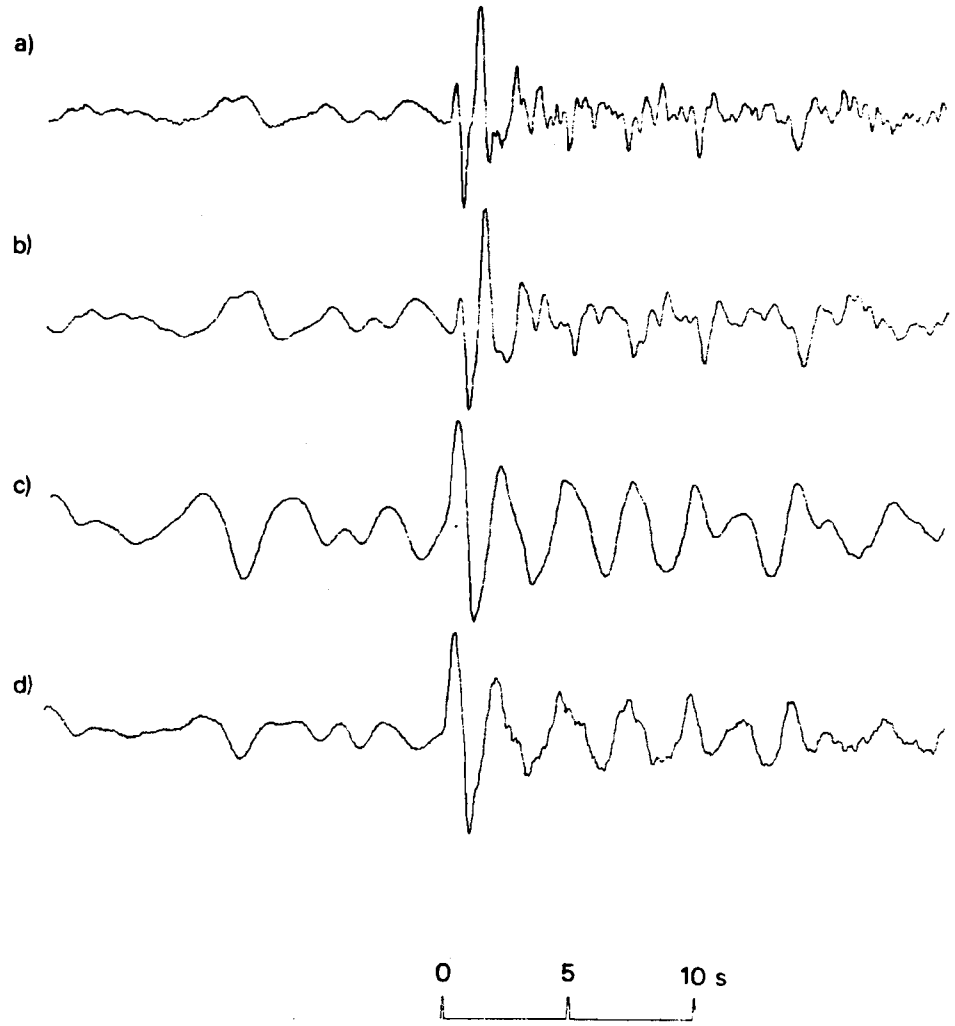

Figure A87 (a) Short-period array-sum seismogram recorded at EKA from the 4 November 1978 Shagan River explosion.
(b) Seismogram (a) filtered to simulate the effects of an additional t* of 0.2s.
(c) Seismogram (a) after Wiener filtering converted to a phaseless-broad-band instrument response.
(d) Same as seismogram (c) except that the effects of path attenuation of t* = 0.15s have been corrected for.

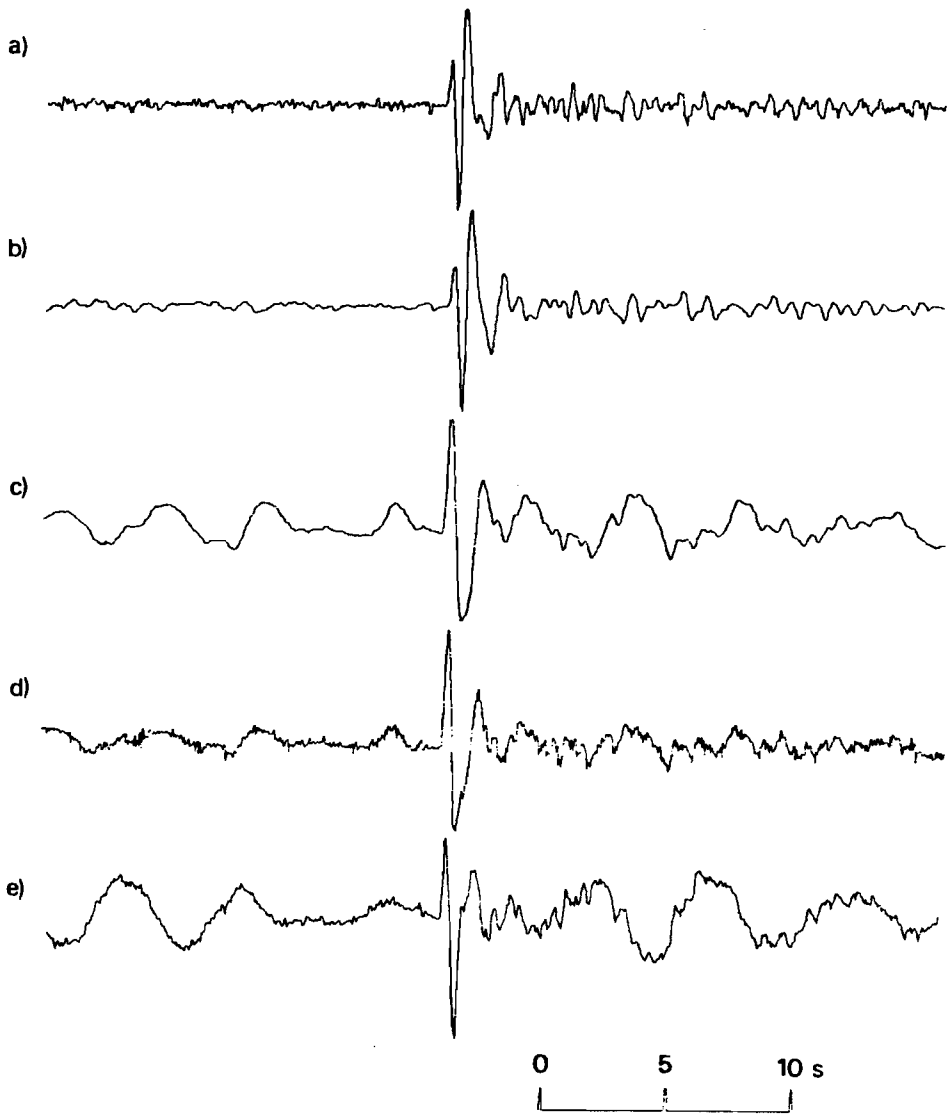

Figure A88 (a) Short-period seismogram that would be recorded at YKA from the 4 November 1978 Shagan River explosion: derived from the velocity-broad-band seismogram (e).
(b) Seismogram (a) filtered to simulate the effects of an additional t* of 0.2s.
(c) Seismogram (a) after Wiener filtering converted to a phaseless-broad-band instrument response.
(d) Same as seismogram (c) except that the effects of path attenuation of t* = 0.15s have been corrected for.
(e) Velocity-broad-band seismogram recorded at YKA.

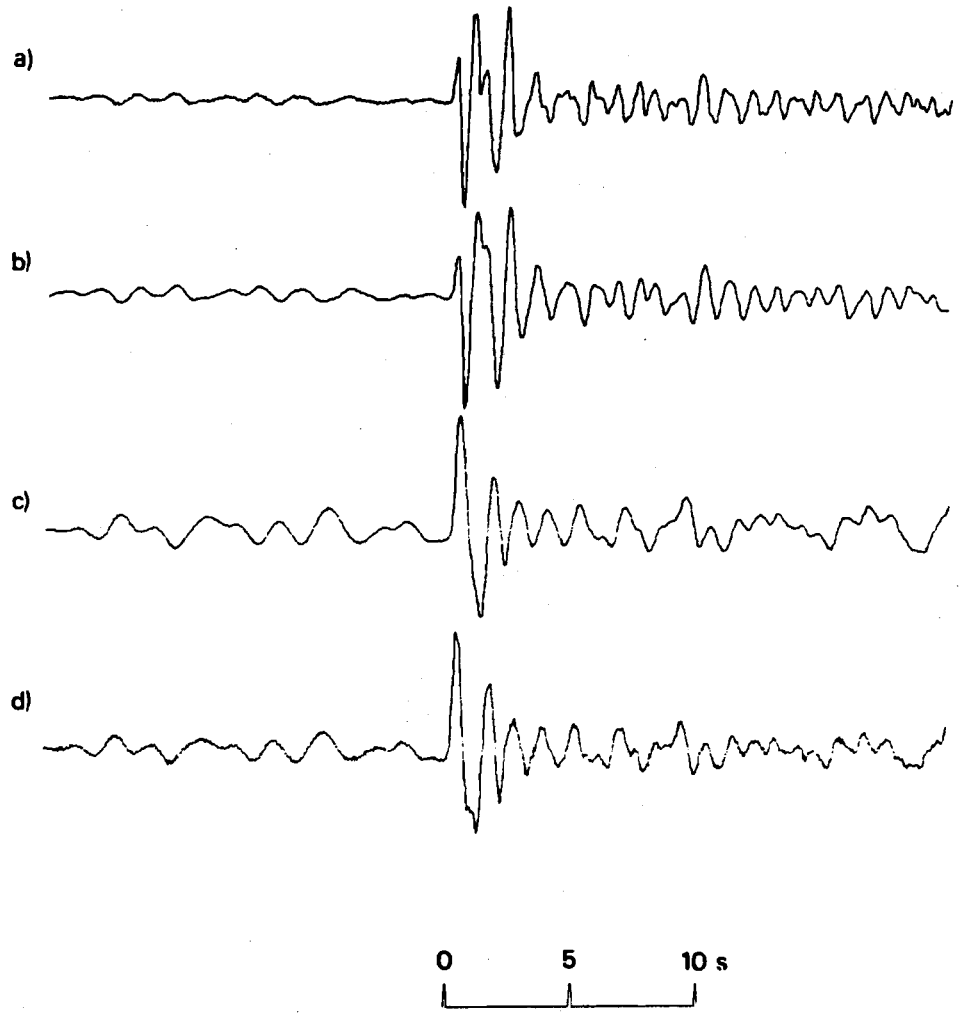

Figure A89 (a) Short-period array-sum seismogram recorded at GBA from the 4 November 1978 Shagan River explosion.
(b) Seismogram (a) filtered to simulate the effects of an additional t* of 0.2s.
(c) Seismogram (a) after Wiener filtering converted to a phaseless-broad-band instrument response.
(d) Same as seismogram (c) except that the effects of path attenuation of t* = 0.15s have been corrected for.

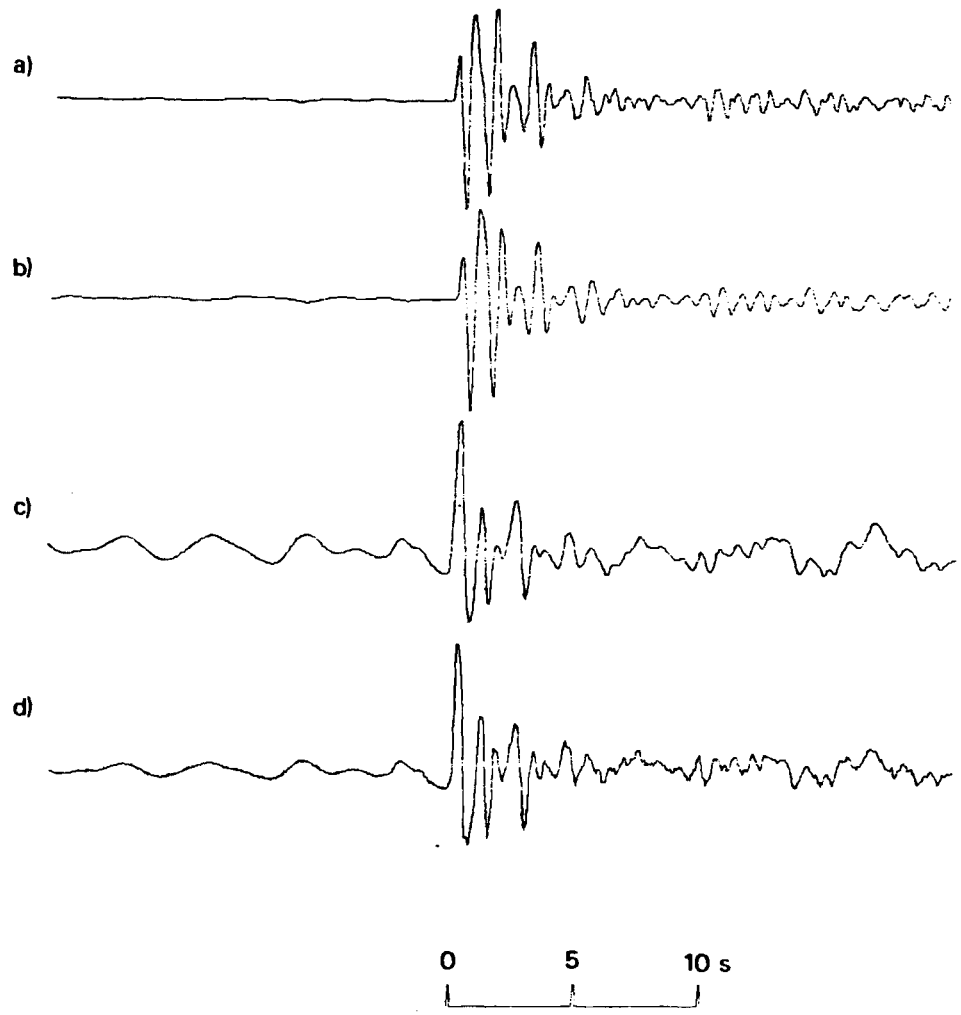

Figure A90 (a) Short-period array-sum seismogram recorded at WRA from the 4 November 1978 Shagan River explosion.
(b) Seismogram (a) filtered to simulate the effects of an additional t* of 0.2s.
(c) Seismogram (a) after Wiener filtering converted to a phaseless-broad-band instrument response.
(d) Same as seismogram (c) except that the effects of path attenuation of t* = 0.15s have been corrected for.
Note that PcP should arrive within a few seconds of P.

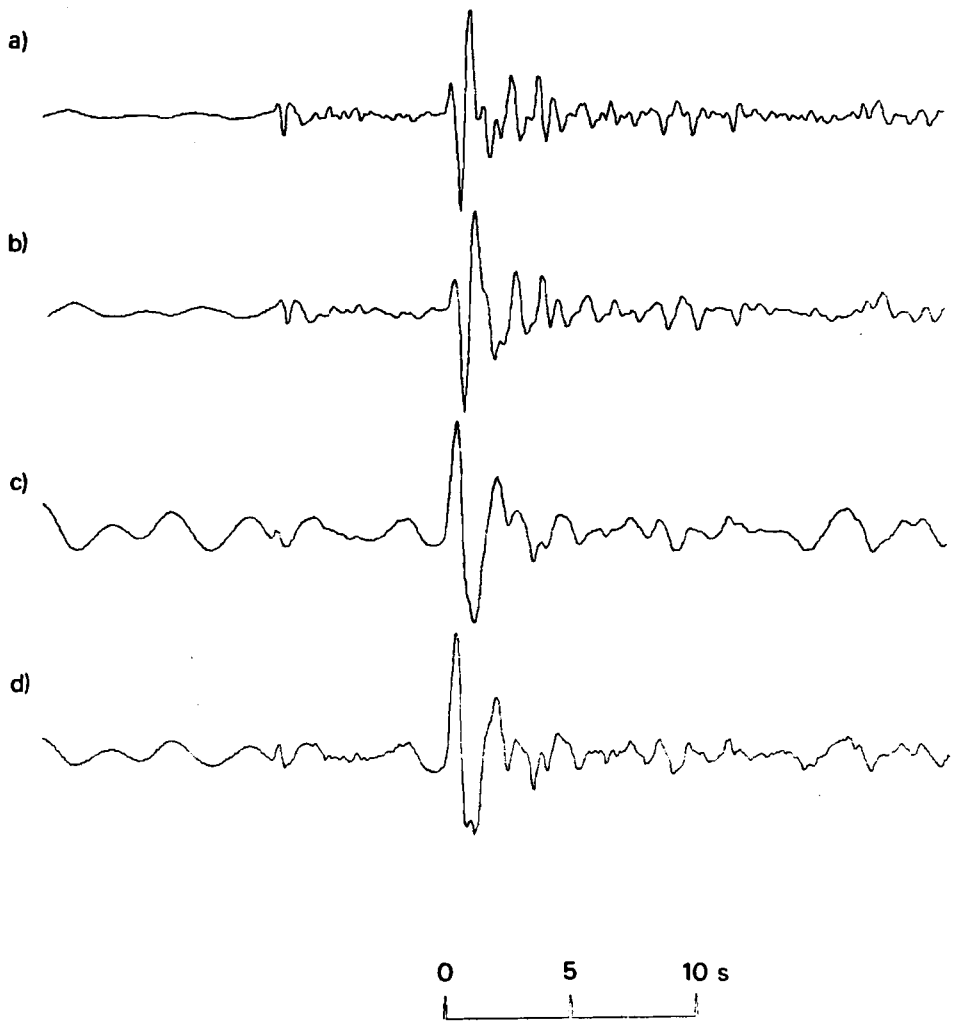

Figure A91 (a) Short-period array-sum seismogram recorded at EKA from the 29 November 1978 Shagan River explosion.
(b) Seismogram (a) filtered to simulate the effects of an additional t* of 0.2s.
(c) Seismogram (a) after Wiener filtering converted to a phaseless-broad-band instrument response.
(d) Same as seismogram (c) except that the effects of path attenuation of t* = 0.15s have been corrected for.
Note that the sample of noise used in designing the Wiener filter is taken ahead of the earlier arrival (from an explosion at Degelen Mountain).

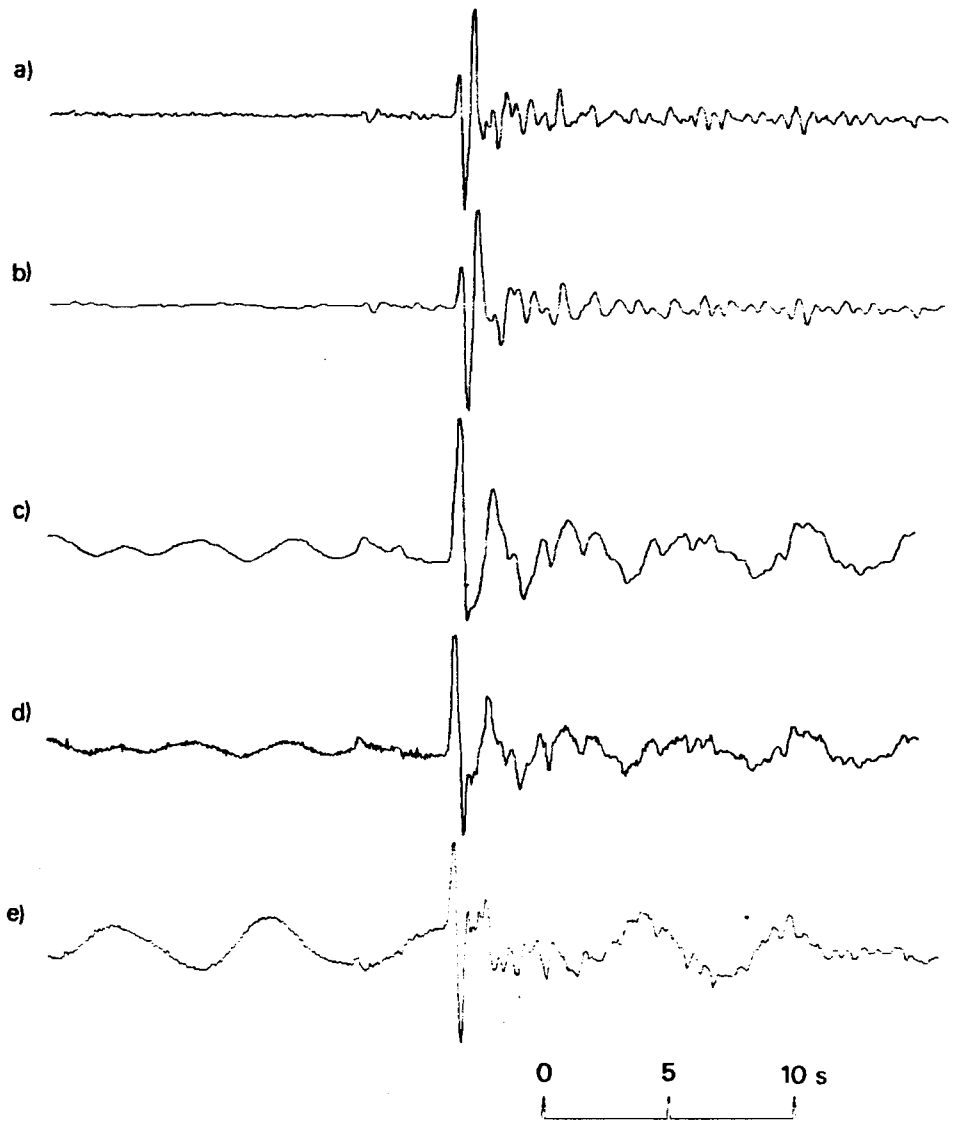

Figure A92 (a) Short-period seismogram that would be recorded at YKA from the 29 November 1978 Shagan River explosion: derived from the velocity-broad-band seismogram (e).
(b) Seismogram (a) filtered to simulate the effects of an additional t* of 0.2s.
(c) Seismogram (a) after Wiener filtering converted to a phaseless-broad-band instrument response.
(d) Same as seismogram (c) except that the effects of path attenuation of t* = 0.15s have been corrected for.
(e) Velocity-broad-band seismogram recorded at YKA.
Note that the sample of noise used in designing the Wiener filter is taken ahead of the earlier arrival (from an explosion at Degelen Mountain).

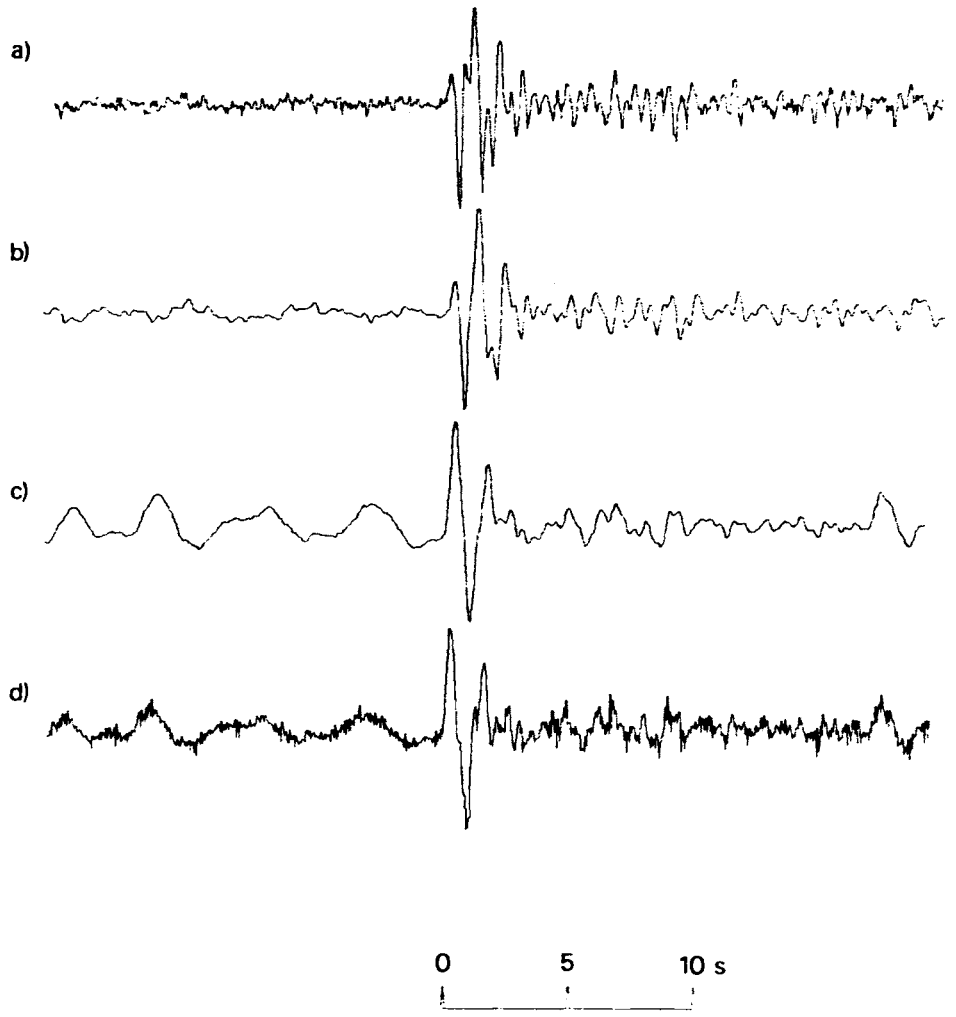

Figure A93 (a) Short-period strong-motion (gain not known) seismogram recorded at GBA from the 29 November 1978 Shagan River explosion.
(b) Seismogram (a) filtered to simulate the effects of an additional t* of 0.2s.
(c) Seismogram (a) after Wiener filtering converted to a phaseless-broad-band instrument response.
(d) Same as seismogram (c) except that the effects of path attenuation of t* = 0.15s have been corrected for.
Note that the sample of noise used in designing the Wiener filter is taken ahead of an earlier small arrival (from an explosion at Degelen Mountain).

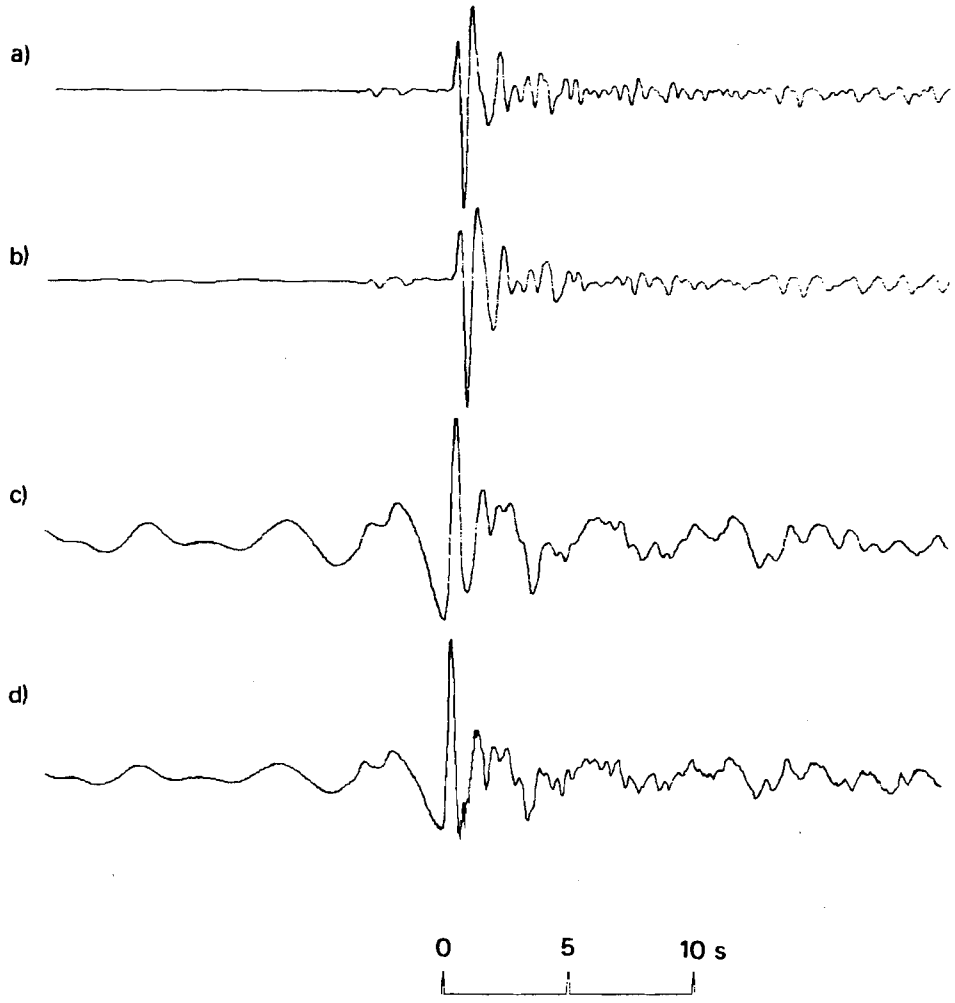

Figure A94 (a) Short-period array-sum seismogram recorded at WRA from the 29 November 1978 Shagan River explosion.
(b) Seismogram (a) filtered to simulate the effects of an additional t* of 0.2s.
(c) Seismogram (a) after Wiener filtering converted to a phaseless-broad-band instrument response.
(d) Same as seismogram (c) except that the effects of path attenuation of t* = 0.15s have been corrected for.
Note that the sample of noise used in designing the Wiener filter is taken ahead of the earlier arrival (from an explosion at Degelen Mountain).
Note also that PcP should arrive within a few seconds of P.

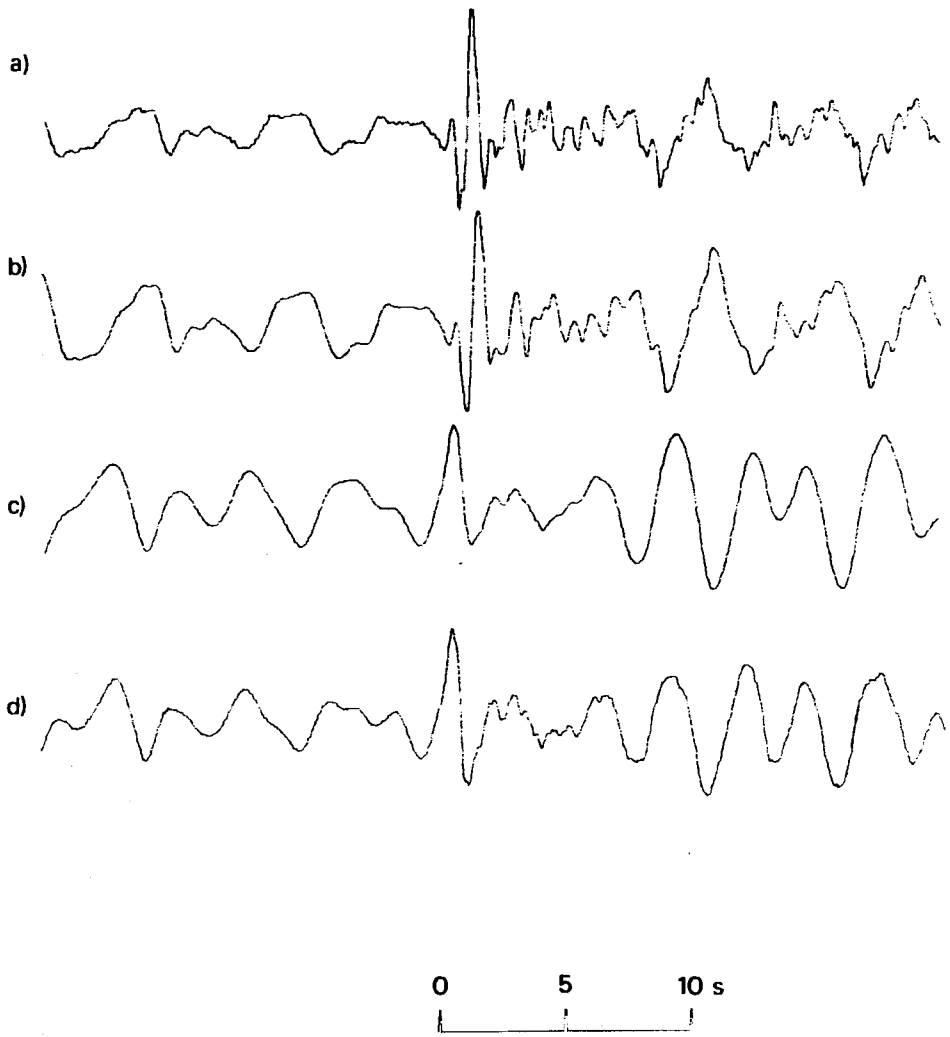

Figure A95 (a) Short-period array-sum seismogram recorded at EKA from the 1 February 1979 Shagan River explosion.
(b) Seismogram (a) filtered to simulate the effects of an additional t* of 0.2s.
(c) Seismogram (a) after Wiener filtering converted to a phaseless-broad-band instrument response.
(d) Same as seismogram (c) except that the effects of path attenuation of t* = 0.15s have been corrected for.

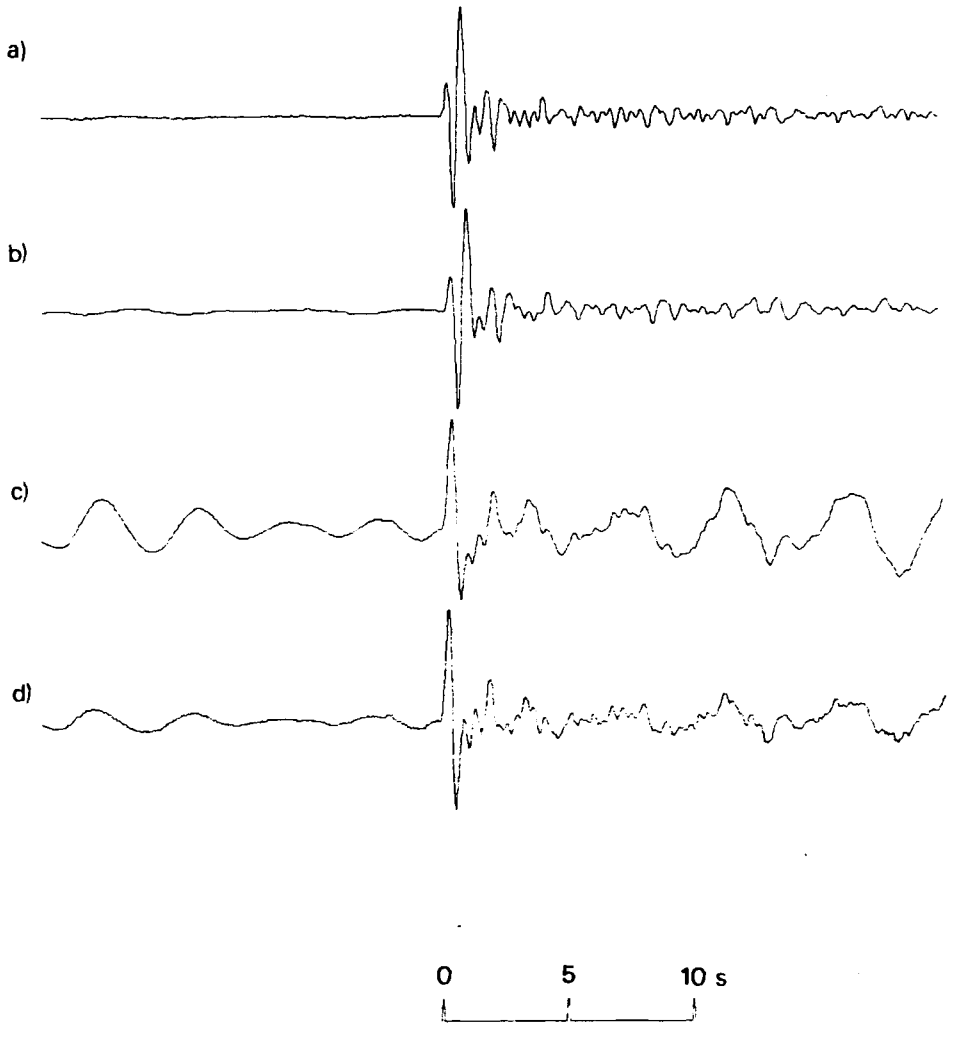

Figure A96 (a) Short-period array-sum seismogram recorded at YKA from the 1 February 1979 Shagan River explosion.
(b) Seismogram (a) filtered to simulate the effects of an additional t* of 0.2s.
(c) Seismogram (a) after Wiener filtering converted to a phaseless-broad-band instrument response.
(d) Same as seismogram (c) except that the effects of path attenuation of t* = 0.15s have been corrected for.

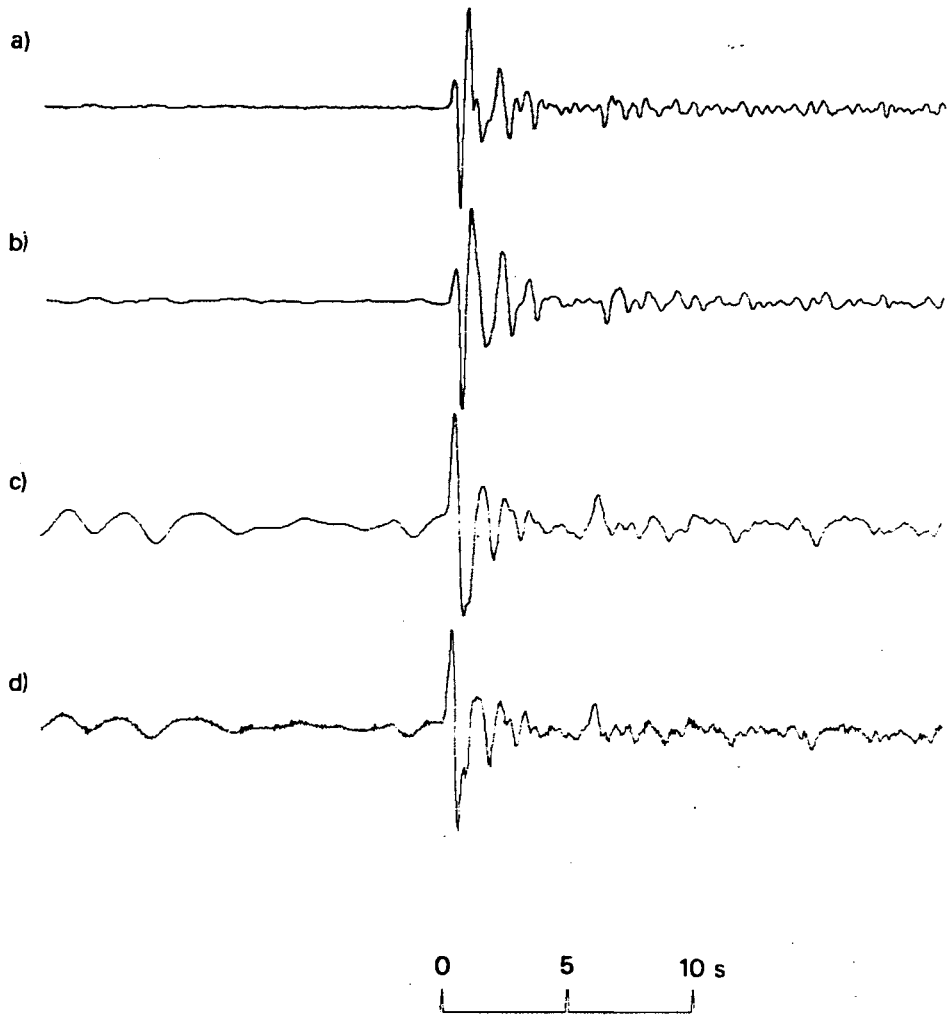

Figure A97 (a) Short-period array-sum seismogram recorded at GBA from the 1 February 1979 Shagan River explosion.
(b) Seismogram (a) filtered to simulate the effects of an additional t* of 0.2s.
(c) Seismogram (a) after Wiener filtering converted to a phaseless-broad-band instrument response.
(d) Same as seismogram (c) except that the effects of path attenuation of t* = 0.15s have been corrected for.

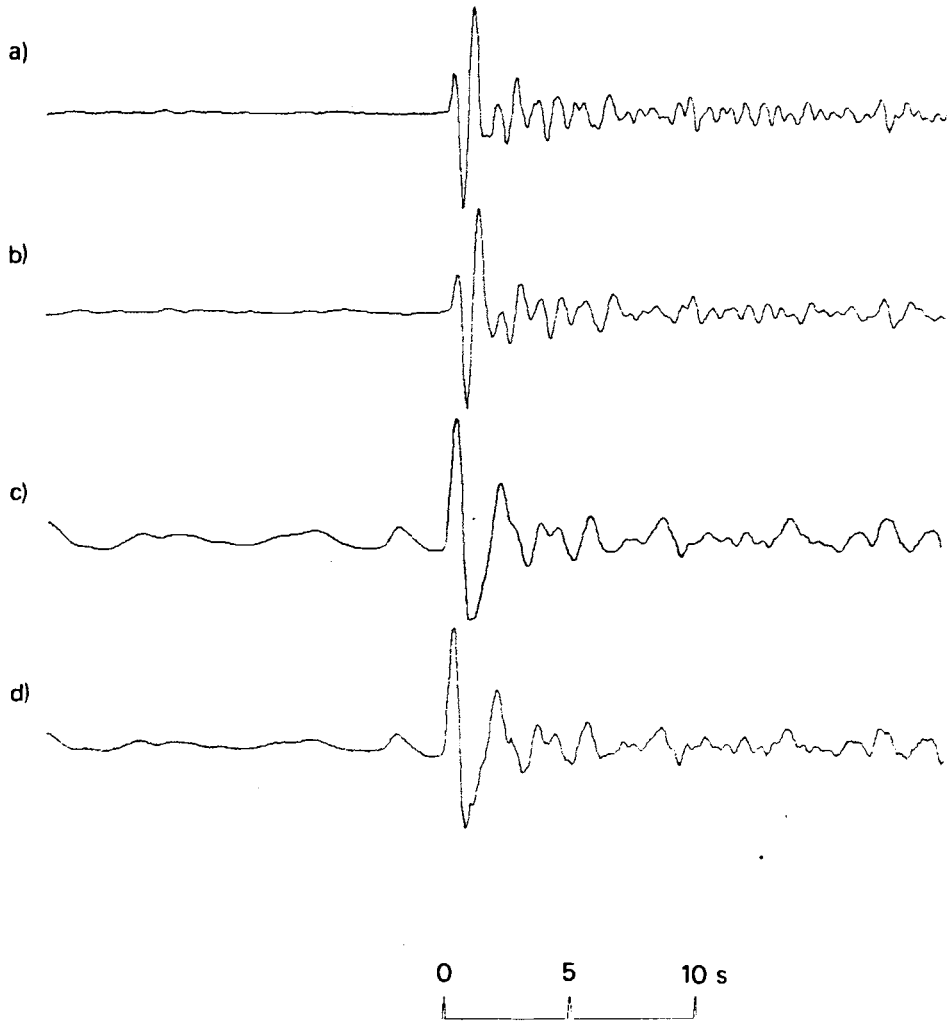

Figure A98 (a) Short-period array-sum seismogram recorded at EKA from the 23 June 1979 Shagan River explosion.
(b) Seismogram (a) filtered to simulate the effects of an additional t* of 0.2s.
(c) Seismogram (a) after Wiener filtering converted to a phaseless-broad-band instrument response.
(d) Same as seismogram (c) except that the effects of path attenuation of t* = 0.15s have been corrected for.

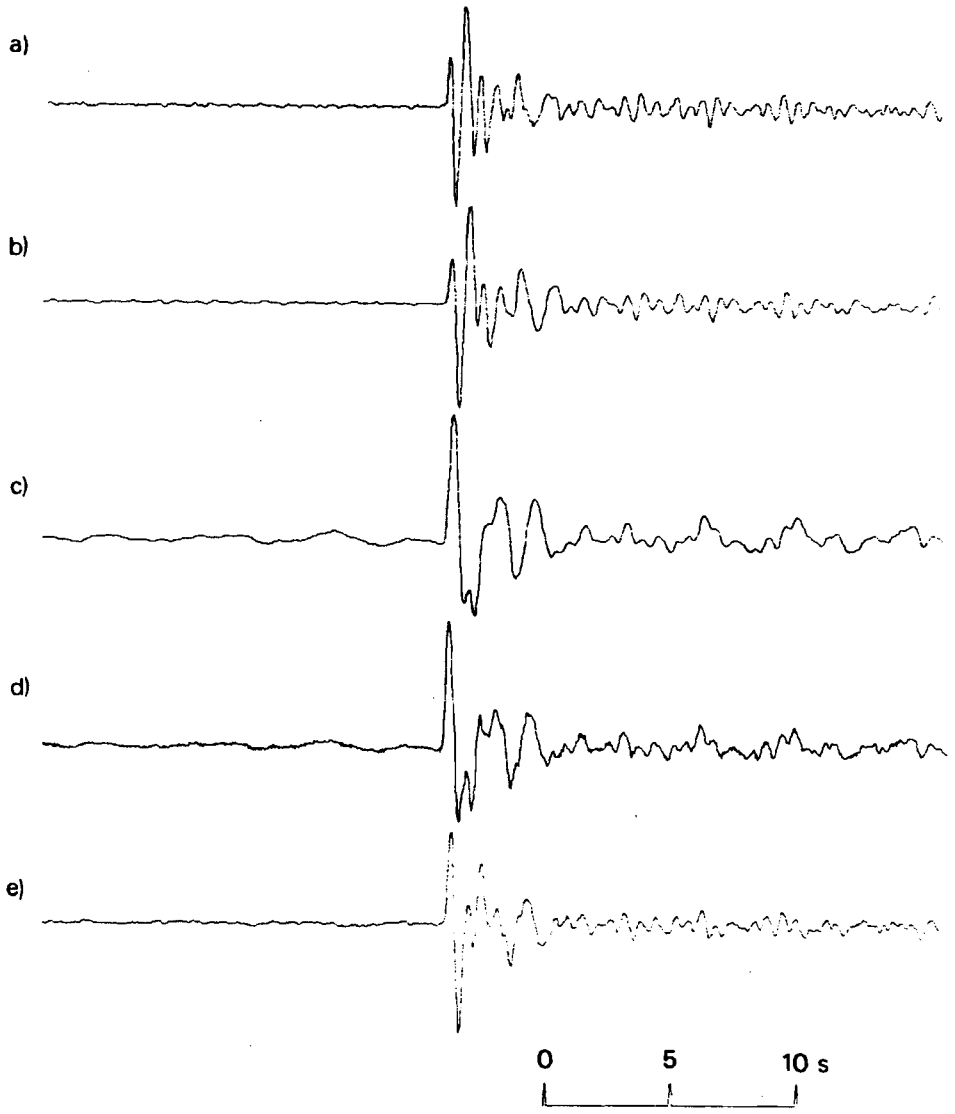

Figure A99 (a) Short-period seismogram that would be recorded at YKA from the 23 June 1979 Shagan River explosion: derived from the velocity-broad-band seismogram (e).
(b) Seismogram (a) filtered to simulate the effects of an additional t* of 0.2s.
(c) Seismogram (a) after Wiener filtering converted to a phaseless-broad-band instrument response.
(d) Same as seismogram (c) except that the effects of path attenuation of t* = 0.15s have been corrected for.
(e) Velocity-broad-band seismogram recorded at YKA.

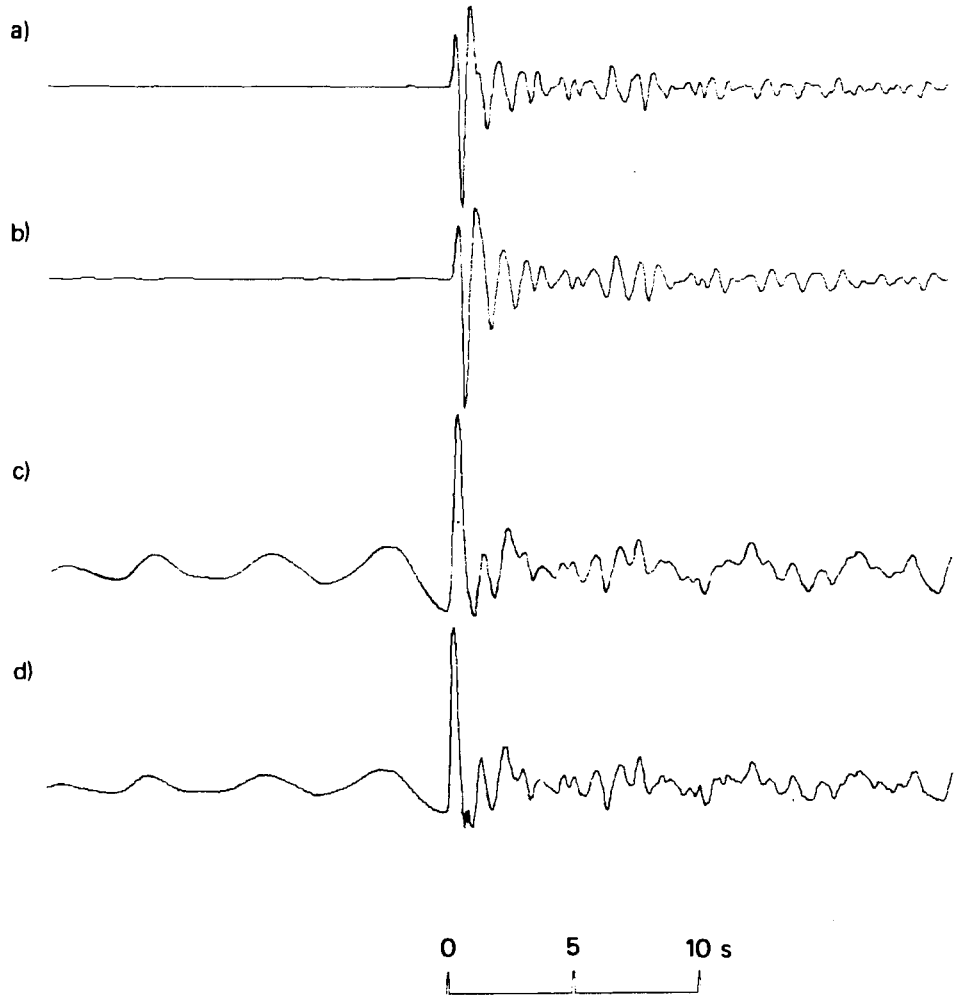

Figure A100 (a) Short-period array-sum seismogram recorded at WRA from the 23 June 1979 Shagan River explosion.
(b) Seismogram (a) filtered to simulate the effects of an additional t* of 0.2s.
(c) Seismogram (a) after Wiener filtering converted to a phaseless-broad-band instrument response.
(d) Same as seismogram (c) except that the effects of path attenuation of t* = 0.15s have been corrected for.
Note that PcP should arrive within a few seconds of P.

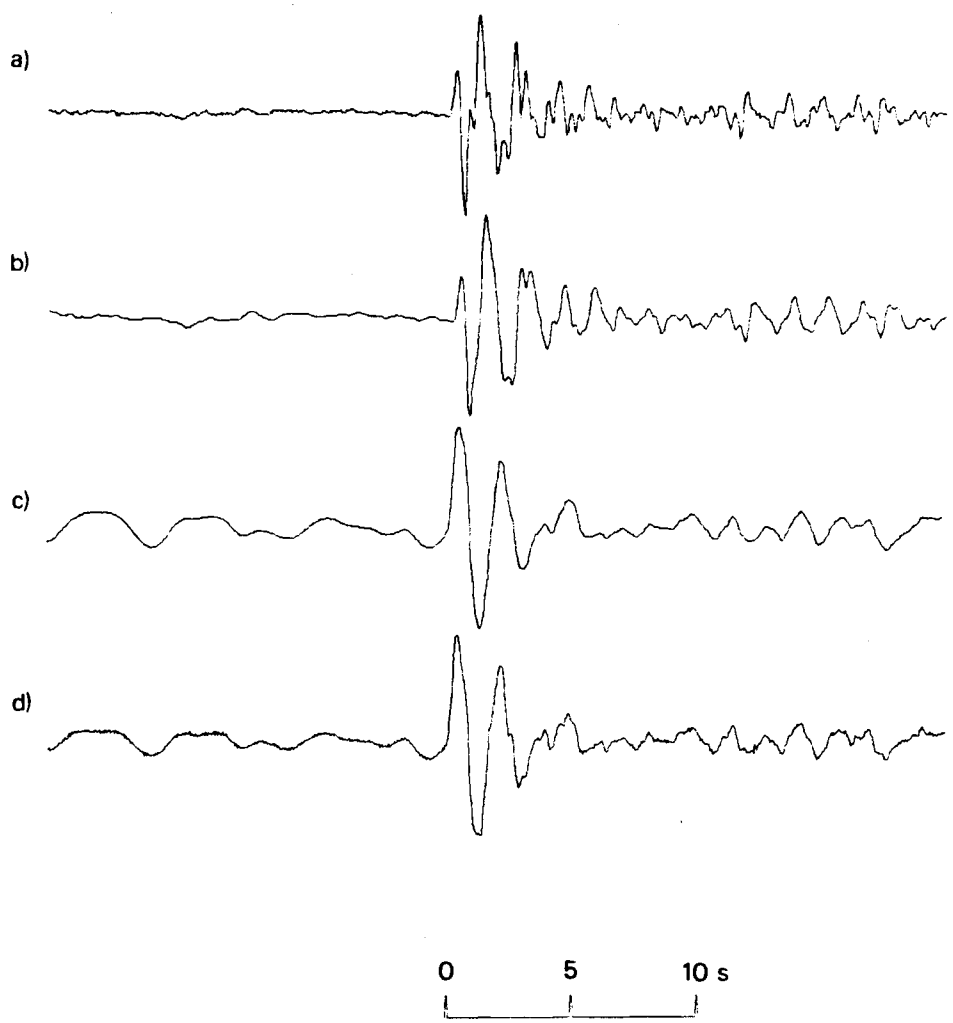

Figure A101 (a) Short-period array-sum seismogram recorded at EKA from the 7 July 1979 Shagan River explosion.
(b) Seismogram (a) filtered to simulate the effects of an additional t* of 0.2s.
(c) Seismogram (a) after Wiener filtering converted to a phaseless-broad-band instrument response.
(d) Same as seismogram (c) except that the effects of path attenuation of t* = 0.15s have been corrected for.

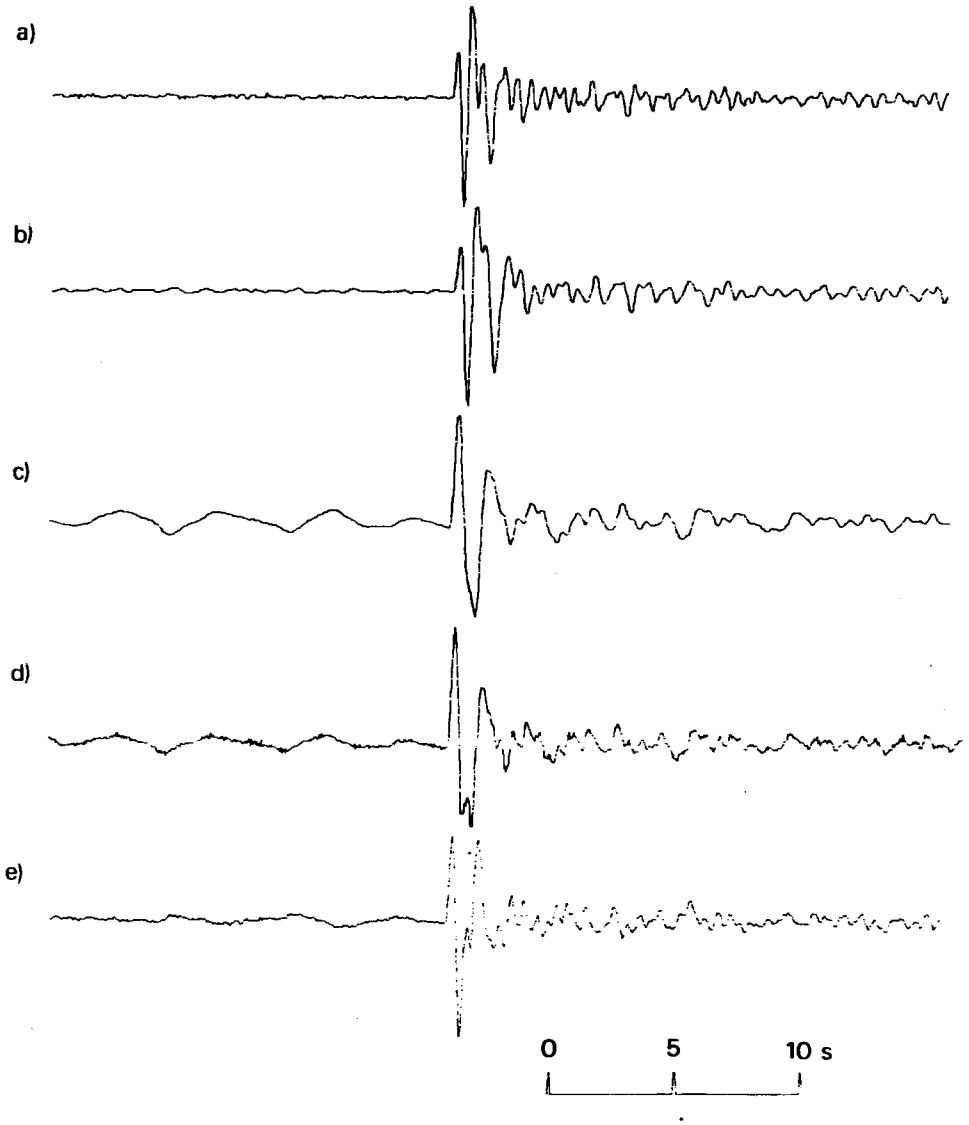

Figure A102 (a) Short-period seismogram that would be recorded at YKA from the 7 July 1979 Shagan River explosion: derived from the velocity-broad-band seismogram (e).
(b) Seismogram (a) filtered to simulate the effects of an additional t* of 0.2s.
(c) Seismogram (a) after Wiener filtering converted to a phaseless-broad-band instrument response.
(d) Same as seismogram (c) except that the effects of path attenuation of t* = 0.15s have been corrected for.
(e) Velocity-broad-band seismogram recorded at YKA.

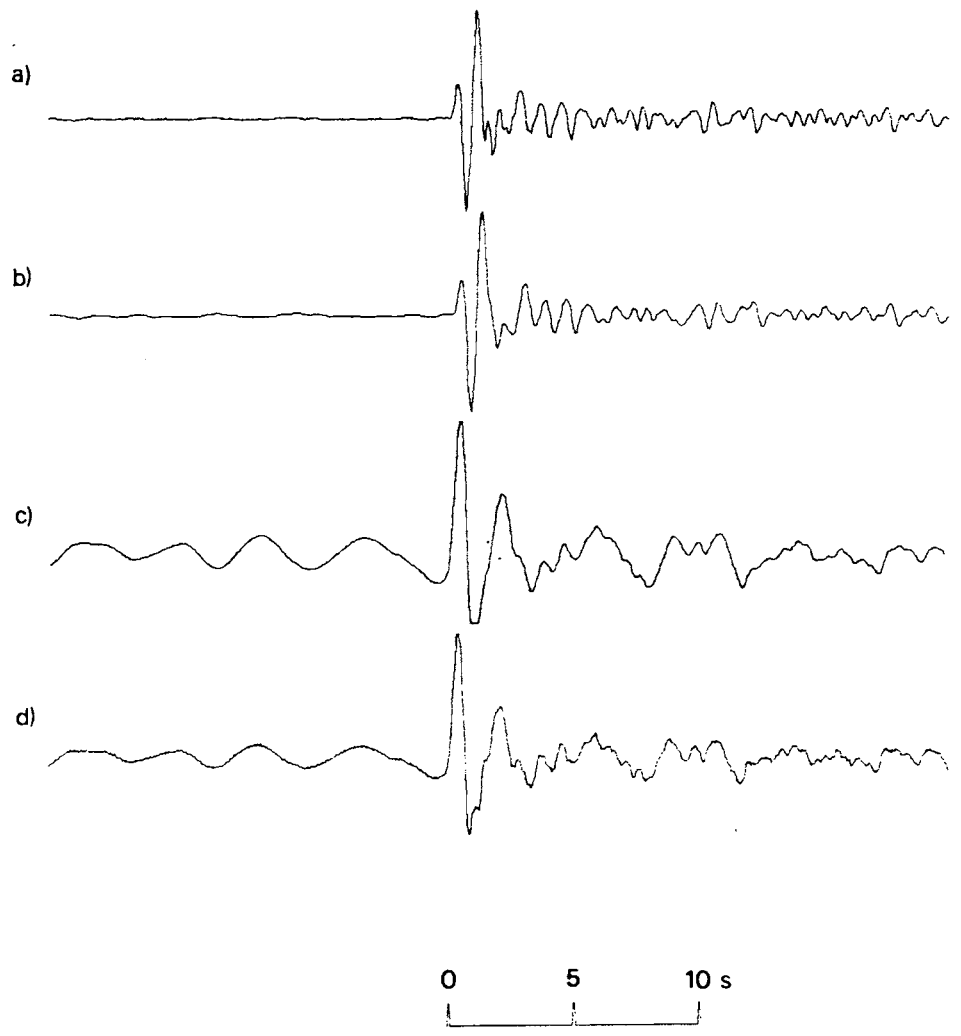

Figure A103 (a) Short-period array-sum seismogram recorded at EKA from the 4 August 1979 Shagan River explosion.
(b) Seismogram (a) filtered to simulate the effects of an additional t* of 0.2s.
(c) Seismogram (a) after Wiener filtering converted to a phaseless-broad-band instrument response.
(d) Same as seismogram (c) except that the effects of path attenuation of t* = 0.15s have been corrected for.

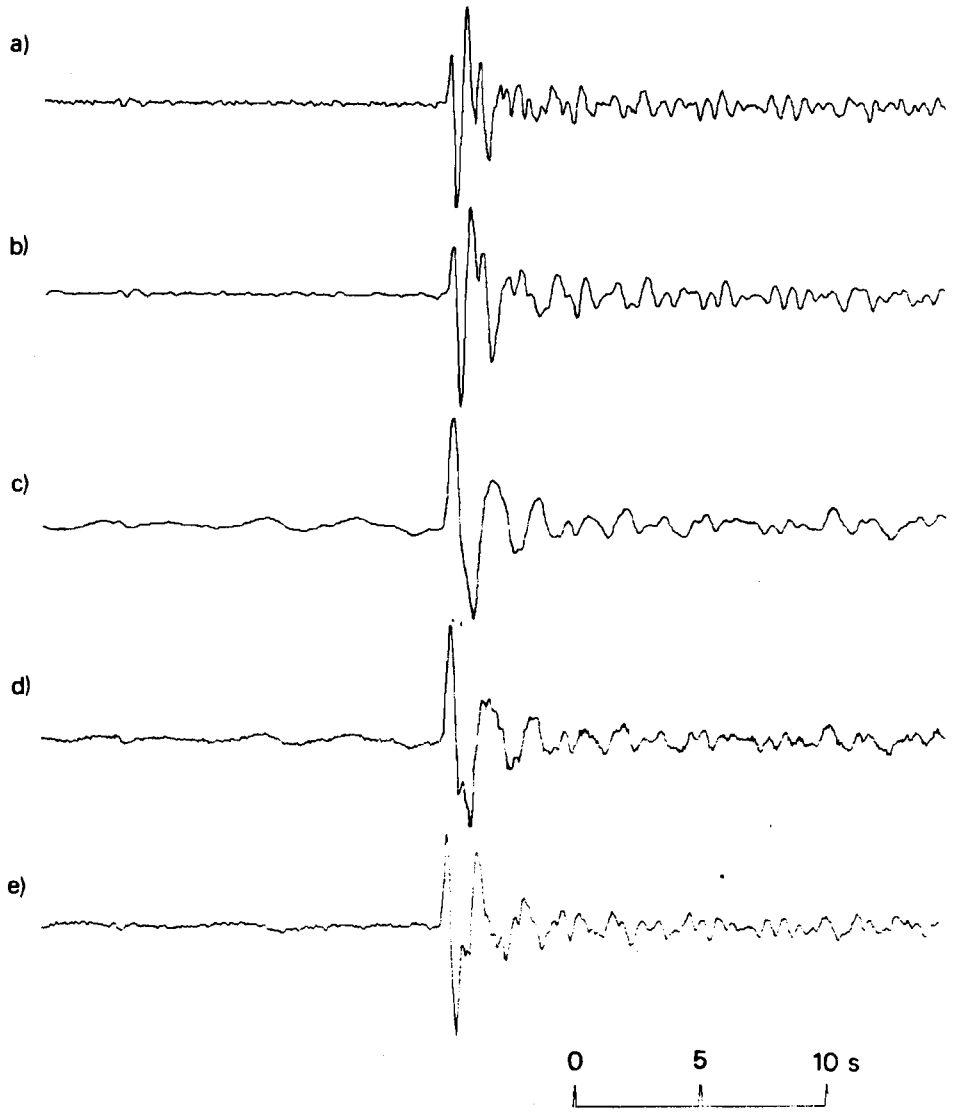

Figure A104 (a) Short-period seismogram that would be recorded at YKA from the 4 August 1979 Shagan River explosion: derived from the velocity-broad-band seismogram (e).
(b) Seismogram (a) filtered to simulate the effects of an additional t* of 0.2s.
(c) Seismogram (a) after Wiener filtering converted to a phaseless-broad-band instrument response.
(d) Same as seismogram (c) except that the effects of path attenuation of t* = 0.15s have been corrected for.
(e) Velocity-broad-band seismogram recorded at YKA.

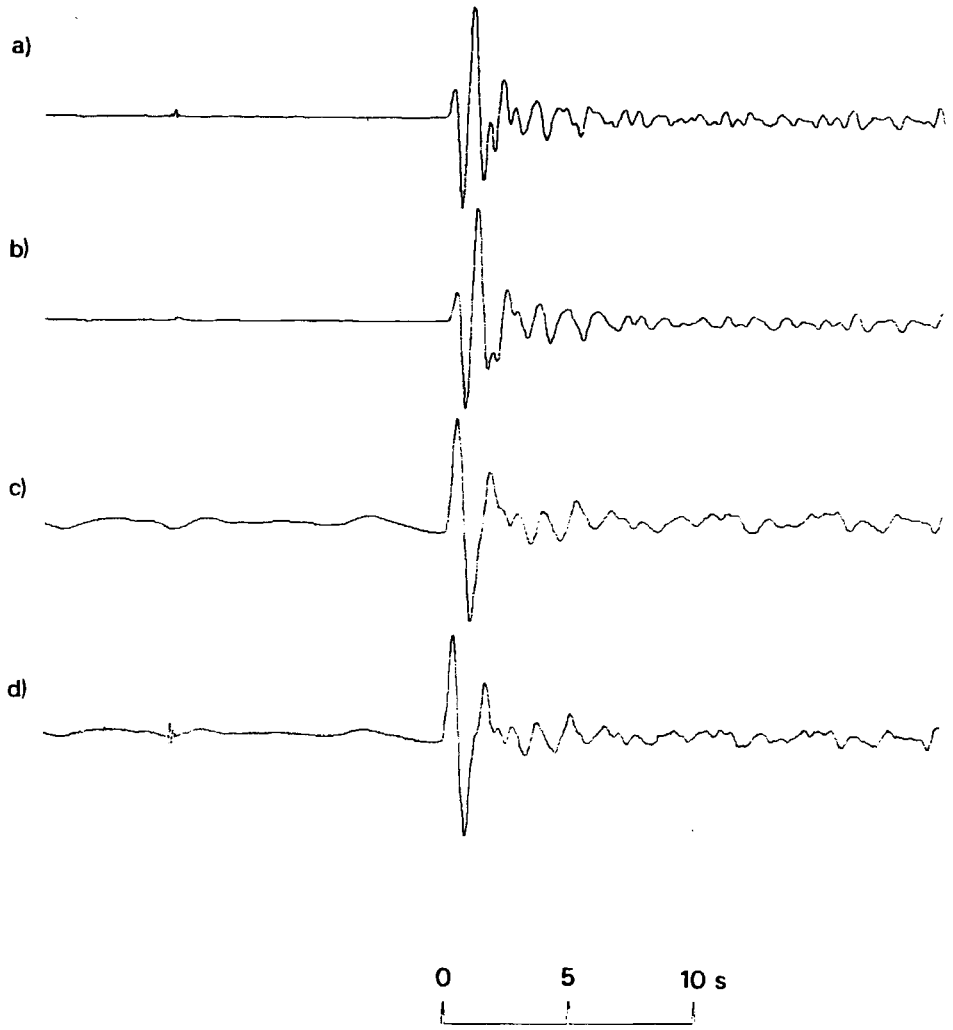

Figure A105 (a) Short-period array-sum seismogram recorded at GBA from the 4 August 1979 Shagan River explosion.
(b) Seismogram (a) filtered to simulate the effects of an additional t* of 0.2s.
(c) Seismogram (a) after Wiener filtering converted to a phaseless-broad-band instrument response.
(d) Same as seismogram (c) except that the effects of path attenuation of t* = 0.15s have been corrected for.

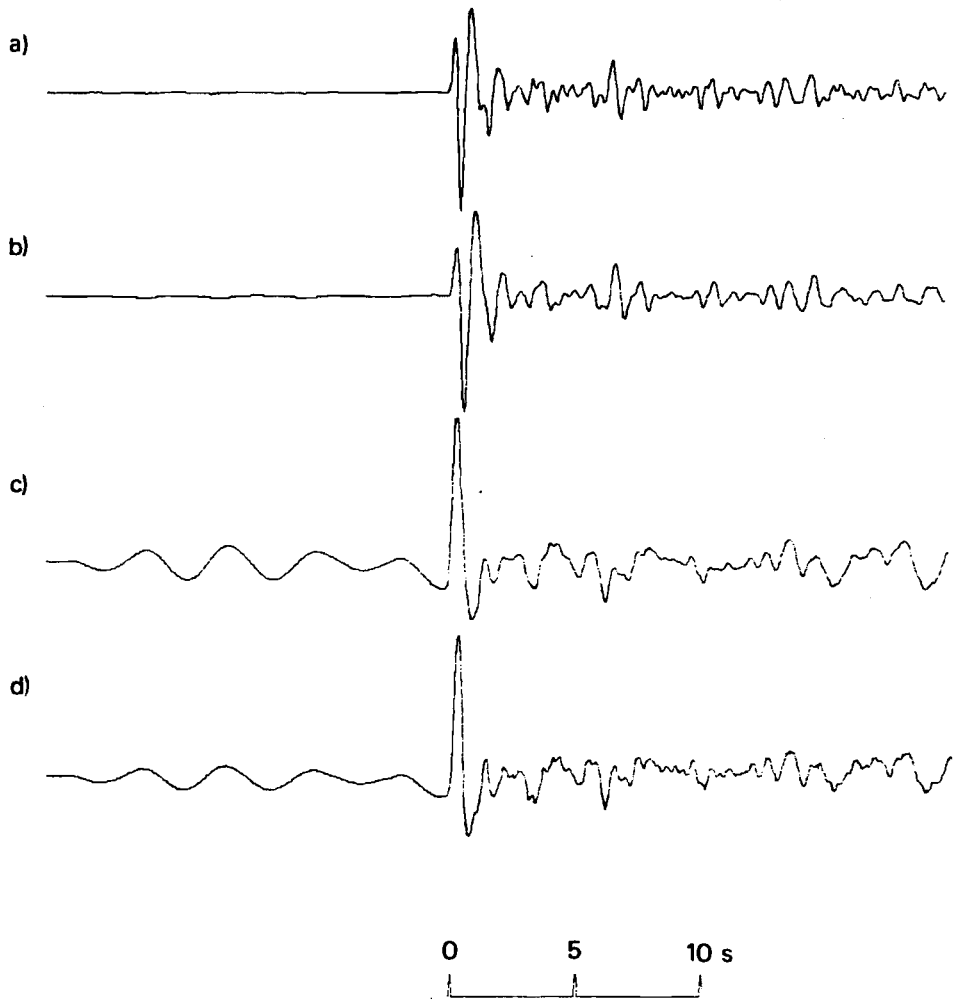

Figure A106 (a) Short-period array-sum seismogram recorded at WRA from the 4 August 1979 Shagan River explosion.
(b) Seismogram (a) filtered to simulate the effects of an additional t* of 0.2s.
(c) Seismogram (a) after Wiener filtering converted to a phaseless-broad-band instrument response.
(d) Same as seismogram (c) except that the effects of path attenuation of t* = 0.15s have been corrected for.
Note that PcP should arrive within a few seconds of P.

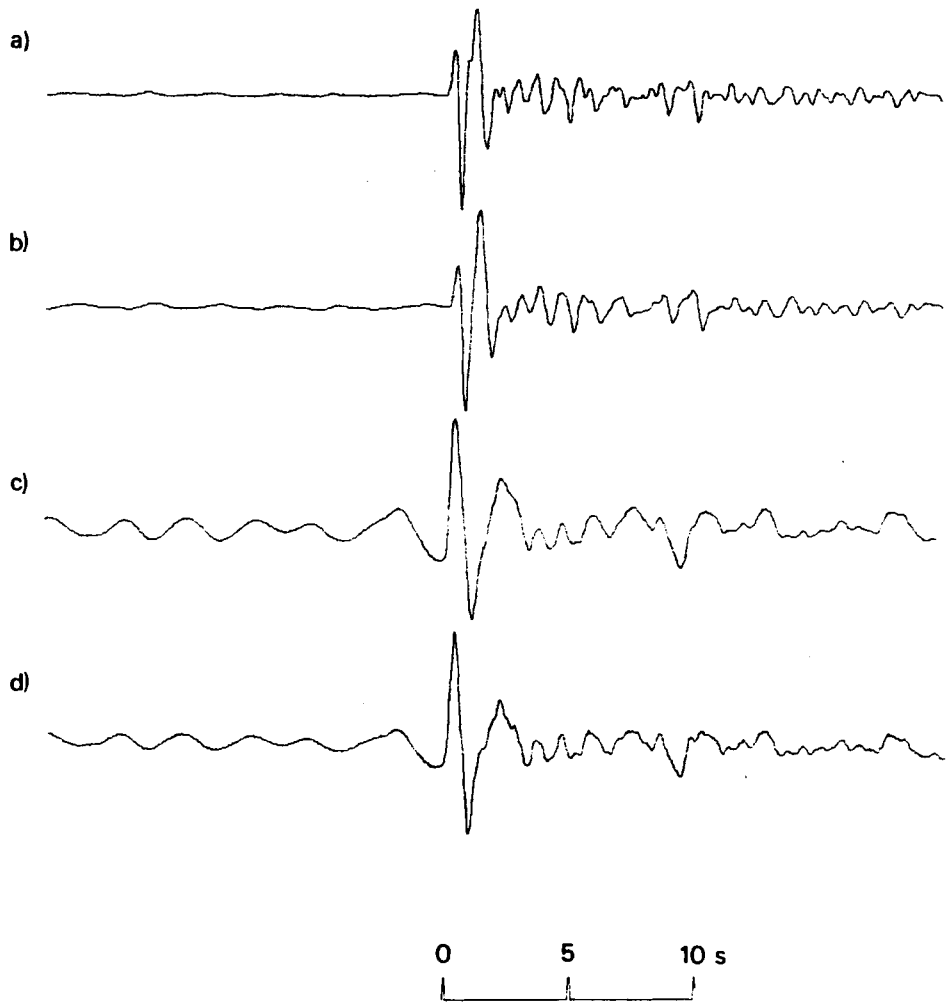

Figure A107 (a) Short-period array-sum seismogram recorded at EKA from the 18 August 1979 Shagan River explosion.
(b) Seismogram (a) filtered to simulate the effects of an additional t* of 0.2s.
(c) Seismogram (a) after Wiener filtering converted to a phaseless-broad-band instrument response.
(d) Same as seismogram (c) except that the effects of path attenuation of t* = 0.15s have been corrected for.

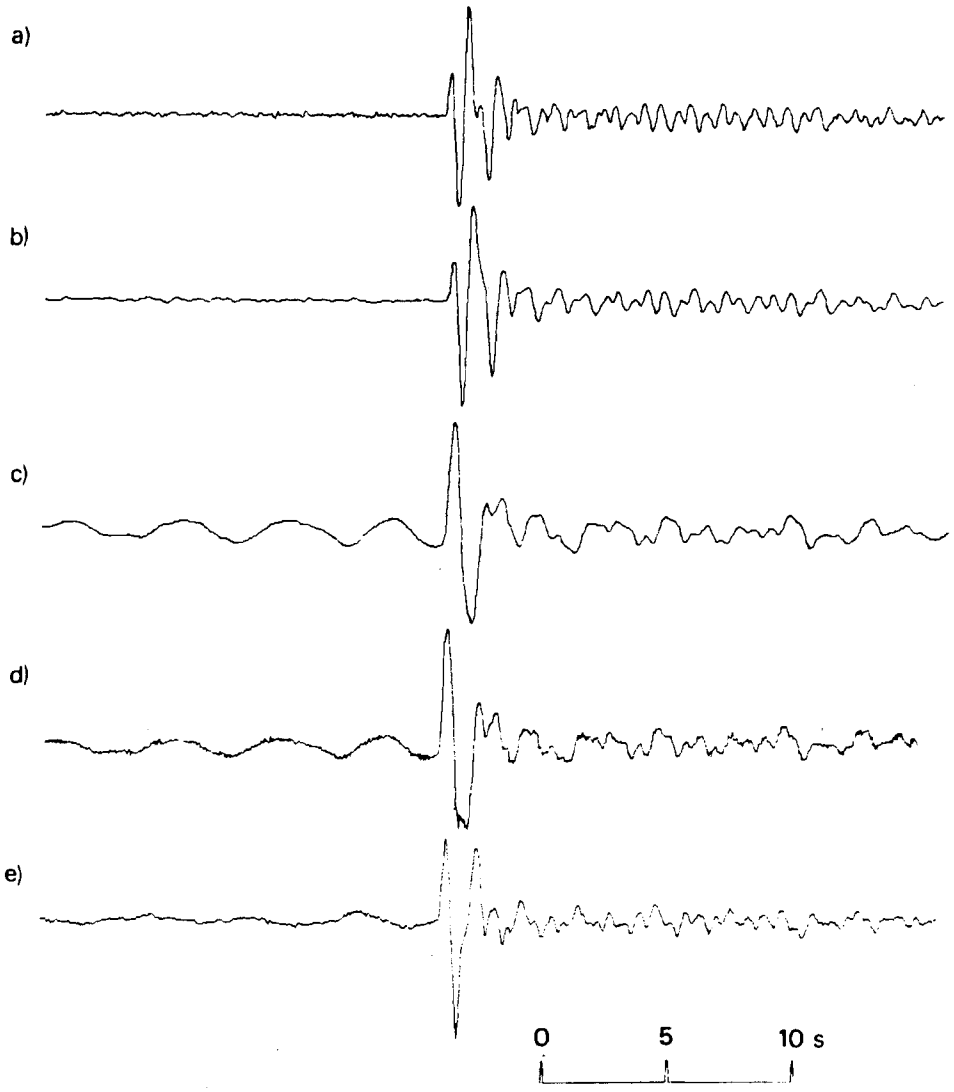

Figure A108 (a) Short-period seismogram that would be recorded at YKA from the 18 August 1979 Shagan River explosion: derived from the velocity-broad-band seismogram (e).
(b) Seismogram (a) filtered to simulate the effects of an additional t* of 0.2s.
(c) Seismogram (a) after Wiener filtering converted to a phaseless-broad-band instrument response.
(d) Same as seismogram (c) except that the effects of path attenuation of t* = 0.15s have been corrected for.
(e) Velocity-broad-band seismogram recorded at YKA.

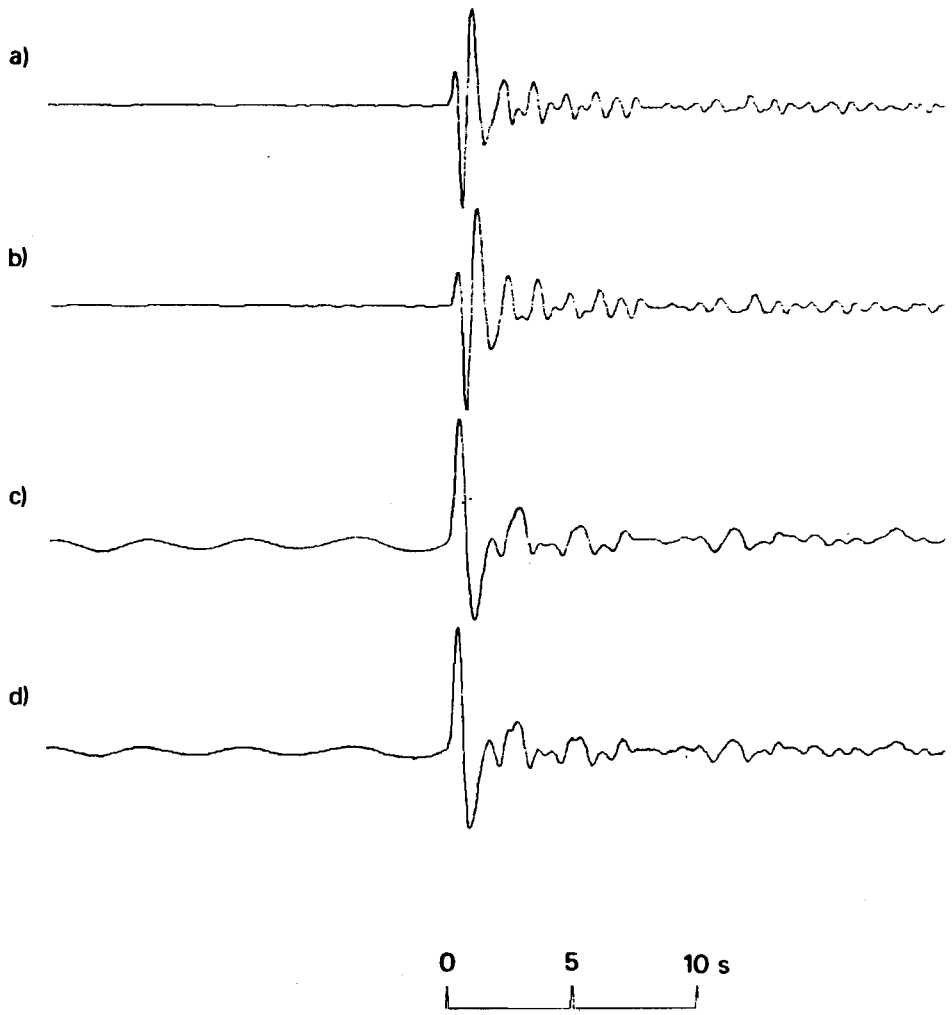

Figure A109 (a) Short-period array-sum seismogram recorded at GBA from the 18 August 1979 Shagan River explosion.
(b) Seismogram (a) filtered to simulate the effects of an additional t* of 0.2s.
(c) Seismogram (a) after Wiener filtering converted to a phaseless-broad-band instrument response.
(d) Same as seismogram (c) except that the effects of path attenuation of t* = 0.15s have been corrected for.

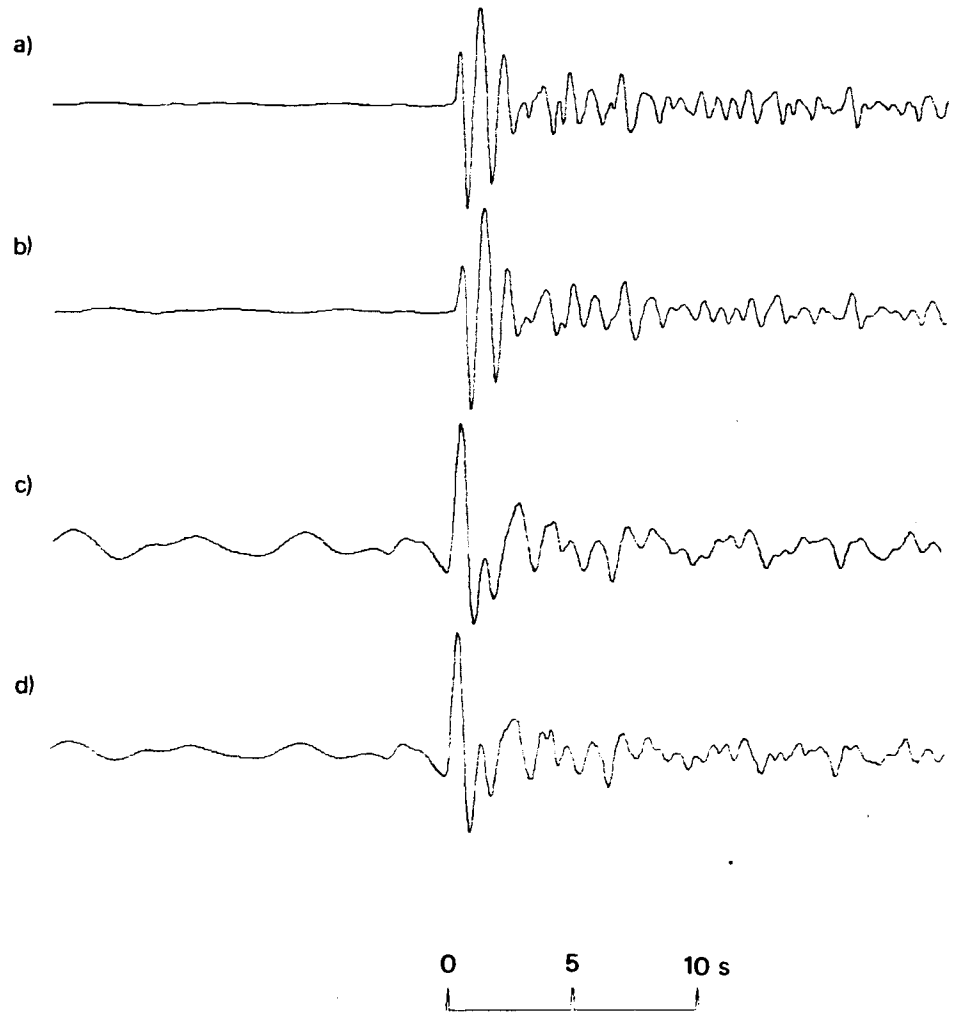

Figure A110 (a) Short-period array-sum seismogram recorded at WRA from the 18 August 1979 Shagan River explosion.
(b) Seismogram (a) filtered to simulate the effects of an additional t* of 0.2s.
(c) Seismogram (a) after Wiener filtering converted to a phaseless-broad-band instrument response.
(d) Same as seismogram (c) except that the effects of path attenuation of t* = 0.15s have been corrected for.
Note that PcP should arrive within a few seconds of P.

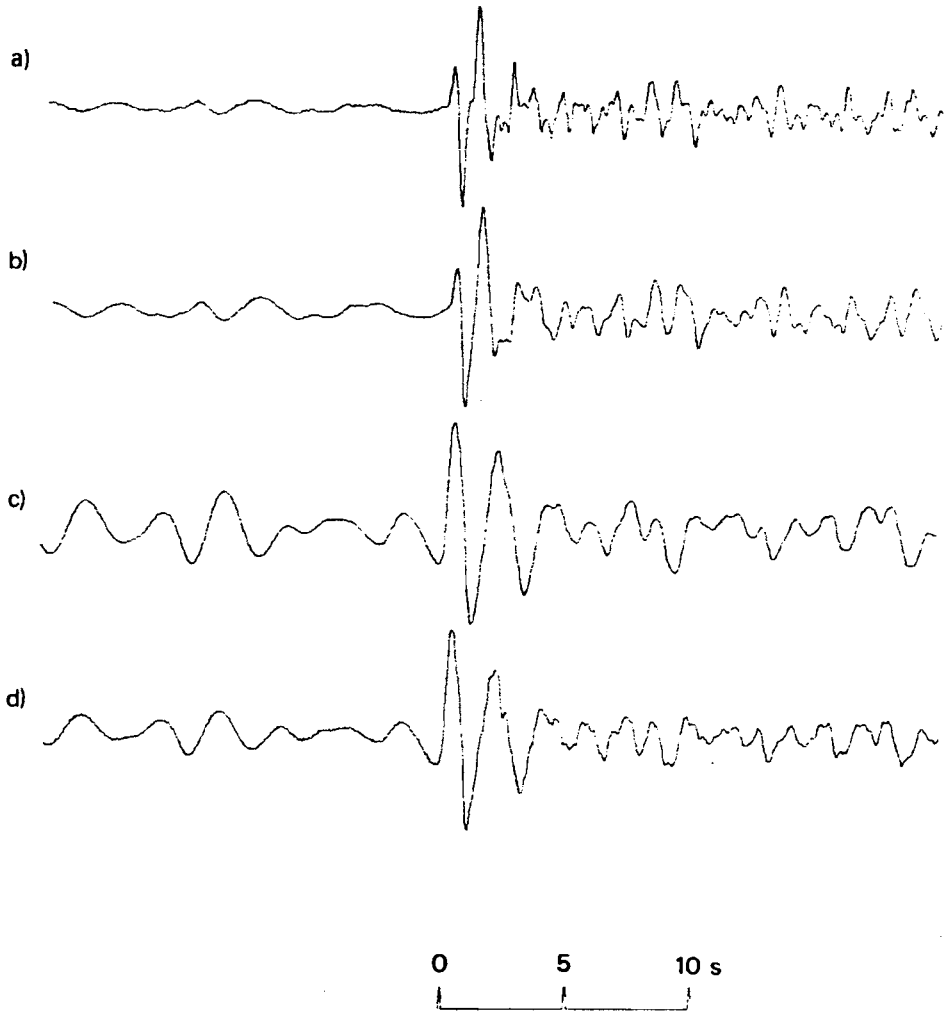

Figure A111 (a) Short-period array-sum seismogram recorded at EKA from the 28 October 1979 Shagan River explosion.
(b) Seismogram (a) filtered to simulate the effects of an additional t* of 0.2s.
(c) Seismogram (a) after Wiener filtering converted to a phaseless-broad-band instrument response.
(d) Same as seismogram (c) except that the effects of path attenuation of t* = 0.15s have been corrected for.

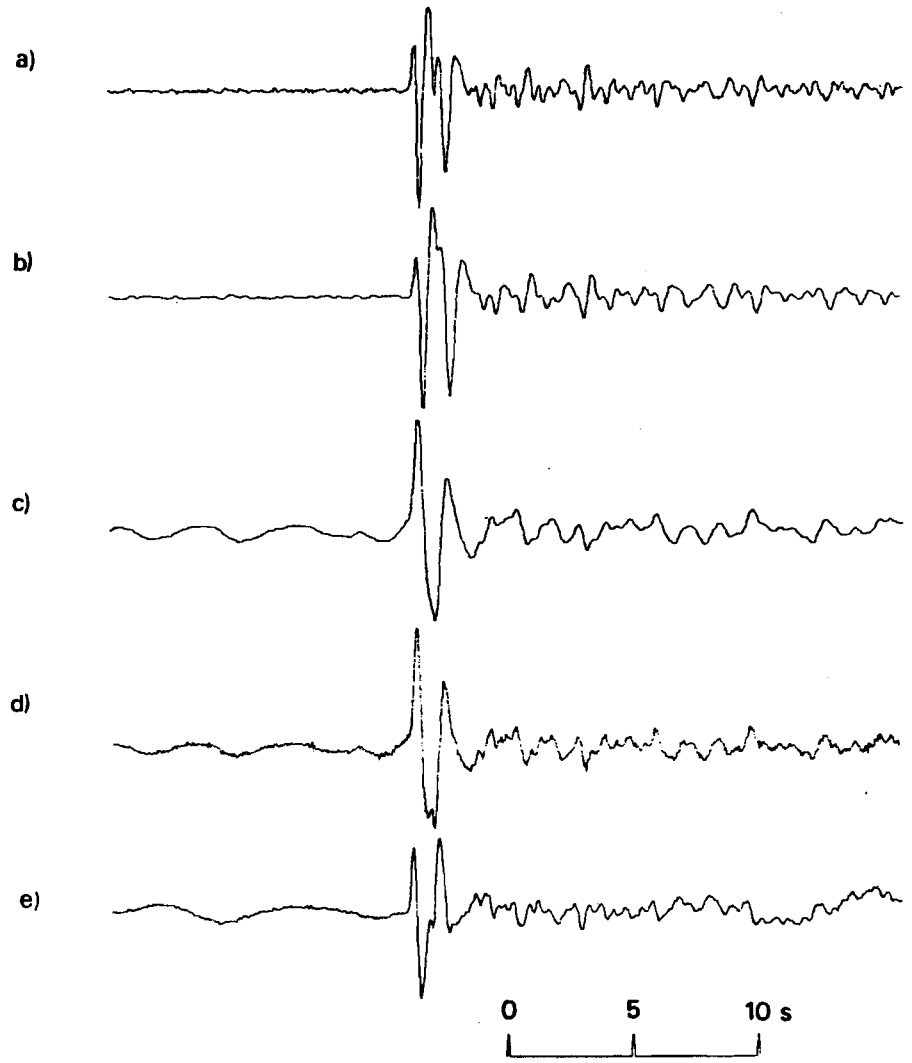

Figure A111.1(a) Short-period seismogram that would be recorded at YKA from the 28 October 1979 Shagan River explosion: derived from the velocity-broad-band seismogram (e).
(b) Seismogram (a) filtered to simulate the effects of an additional t* of 0.2s.
(c) Seismogram (a) after Wiener filtering converted to a phaseless-broad-band instrument response.
(d) Same as seismogram (c) except that the effects of path attenuation of t* = 0.15s have been corrected for.
(e) Velocity-broad-band seismogram recorded at YKA.

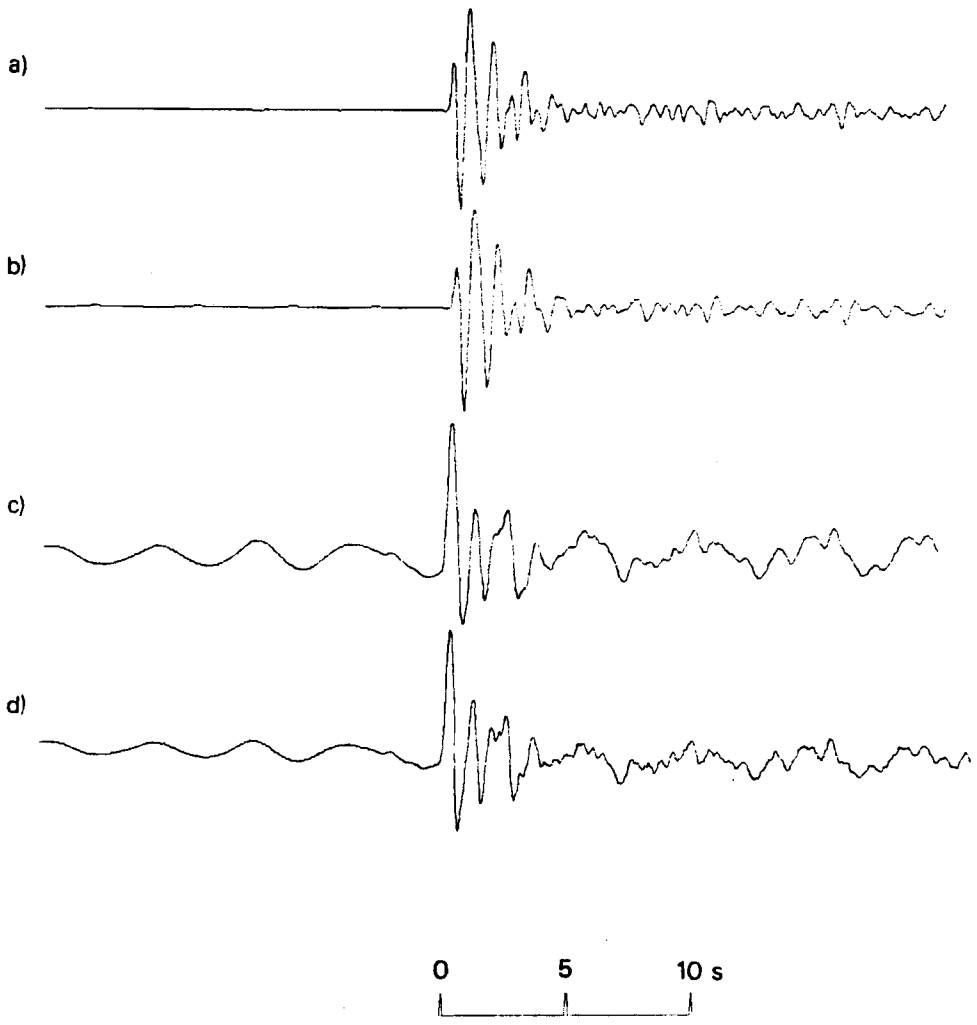

Figure A112 (a) Short-period array-sum seismogram recorded at WRA from the 28 October 1979 Shagan River explosion.
(b) Seismogram (a) filtered to simulate the effects of an additional t* of 0.2s.
(c) Seismogram (a) after Wiener filtering converted to a phaseless-broad-band instrument response.
(d) Same as seismogram (c) except that the effects of path attenuation of t* = 0.15s have been corrected for.
Note that PcP should arrive within a few seconds of P.

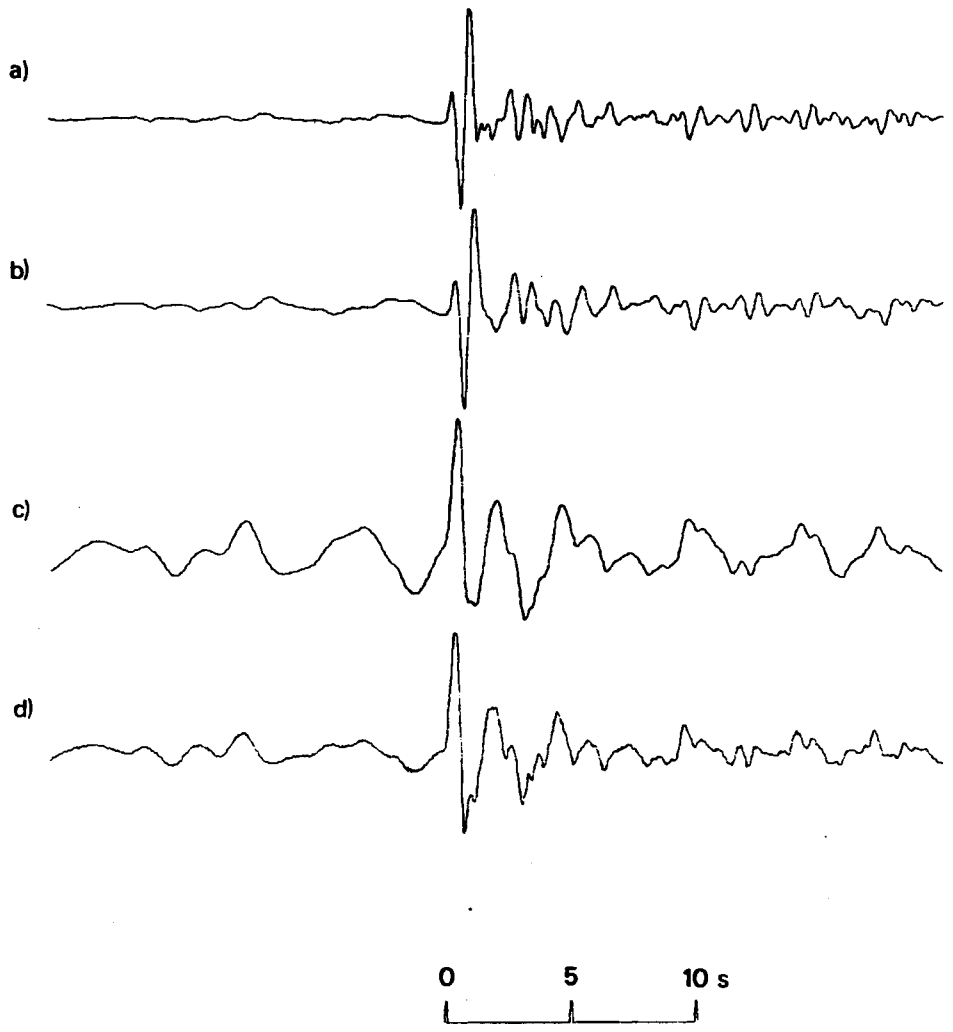

Figure A113 (a) Short-period array-sum seismogram recorded at EKA from the 2 December 1979 Shagan River explosion.
(b) Seismogram (a) filtered to simulate the effects of an additional t* of 0.2s.
(c) Seismogram (a) after Wiener filtering converted to a phaseless-broad-band instrument response.
(d) Same as seismogram (c) except that the effects of path attenuation of t* = 0.15s have been corrected for.

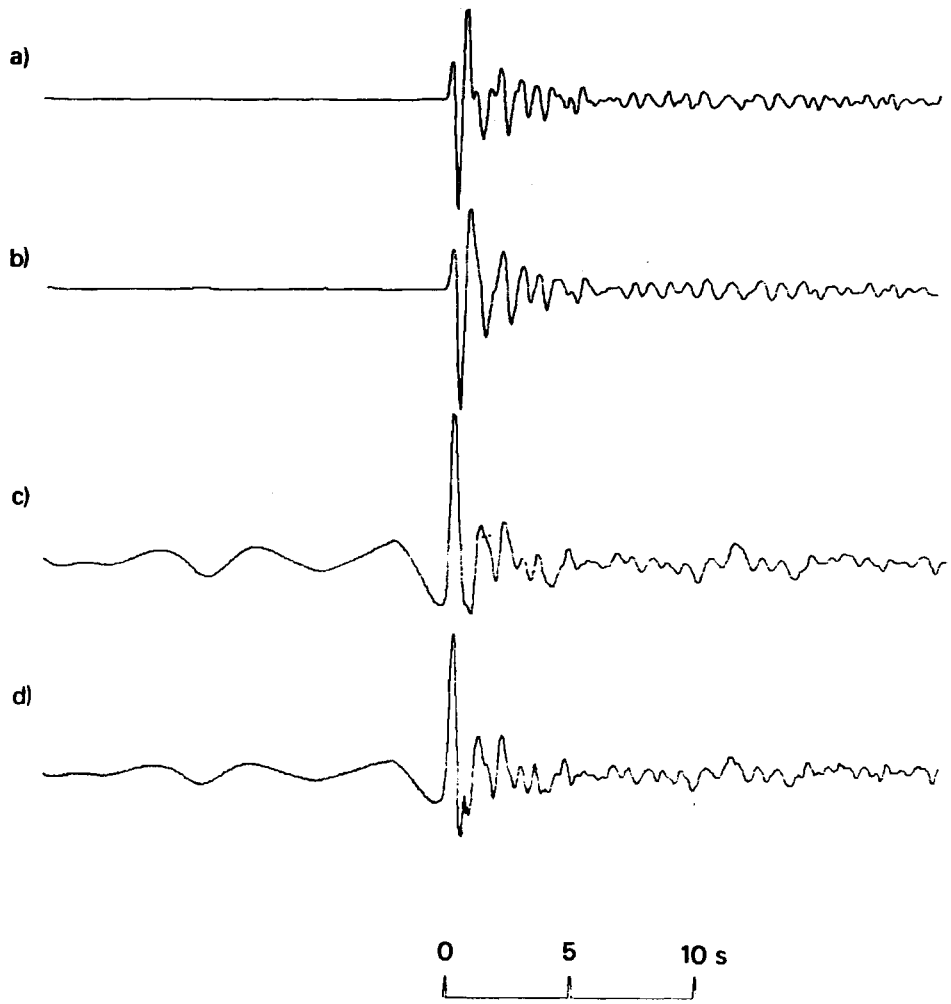

Figure A114 (a) Short-period array-sum seismogram recorded at WRA from the 2 December 1979 Shagan River explosion.
(b) Seismogram (a) filtered to simulate the effects of an additional t* of 0.2s.
(c) Seismogram (a) after Wiener filtering converted to a phaseless-broad-band instrument response.
(d) Same as seismogram (c) except that the effects of path attenuation of t* = 0.15s have been corrected for.
Note that PcP should arrive within a few seconds of P.

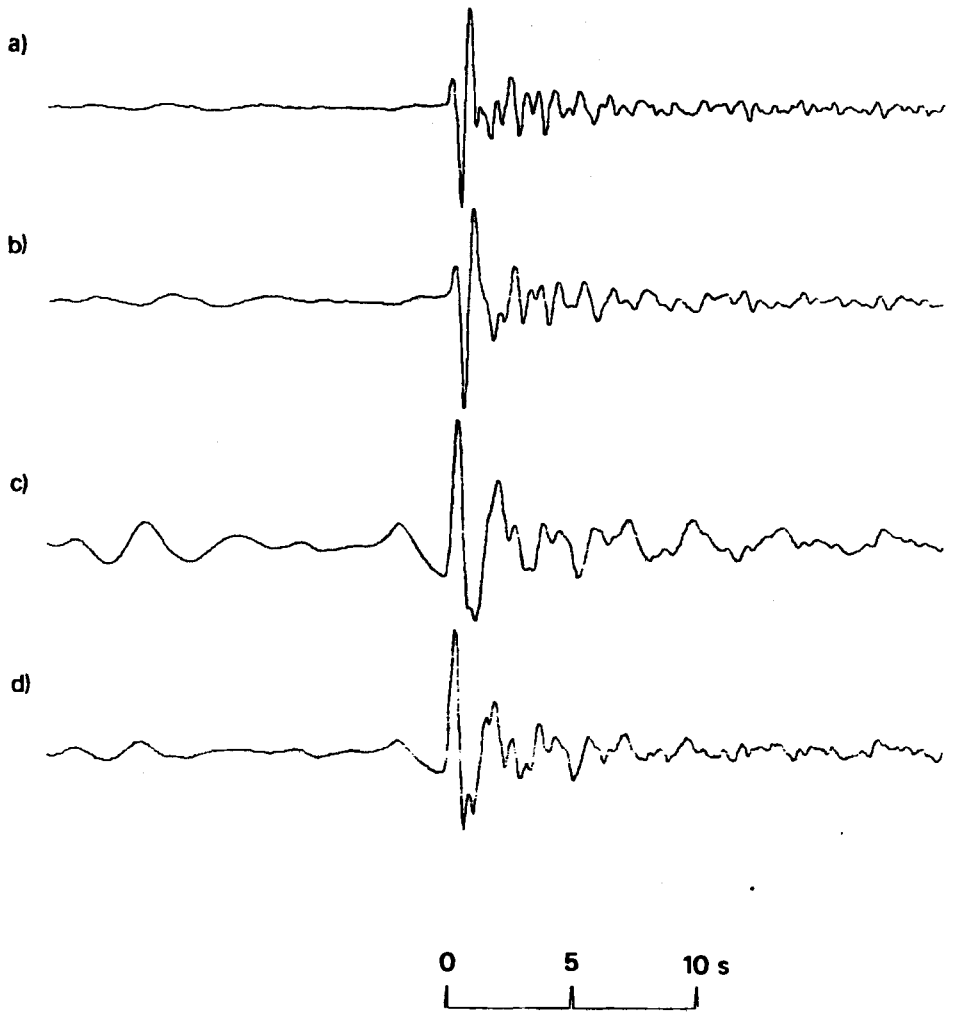

Figure A115 (a) Short-period array-sum seismogram recorded at EKA from the 23 December 1979 Shagan River explosion.
(b) Seismogram (a) filtered to simulate the effects of an additional t* of 0.2s.
(c) Seismogram (a) after Wiener filtering converted to a phaseless-broad-band instrument response.
(d) Same as seismogram (c) except that the effects of path attenuation of t* = 0.15s have been corrected for.

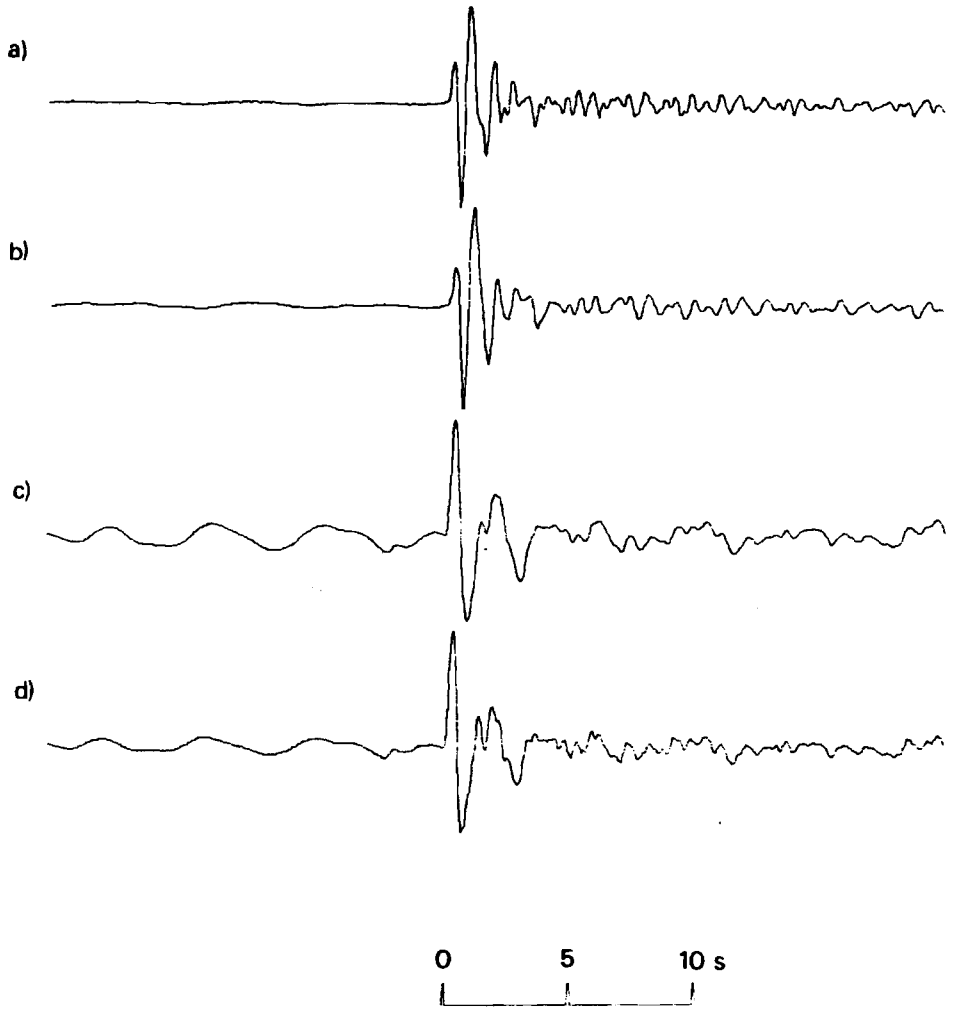

Figure A116 (a) Short-period array-sum seismogram recorded at YKA from the 25 April 1980 Shagan River explosion.
(b) Seismogram (a) filtered to simulate the effects of an additional t* of 0.2s.
(c) Seismogram (a) after Wiener filtering converted to a phaseless-broad-band instrument response.
(d) Same as seismogram (c) except that the effects of path attenuation of t* = 0.15s have been corrected for.

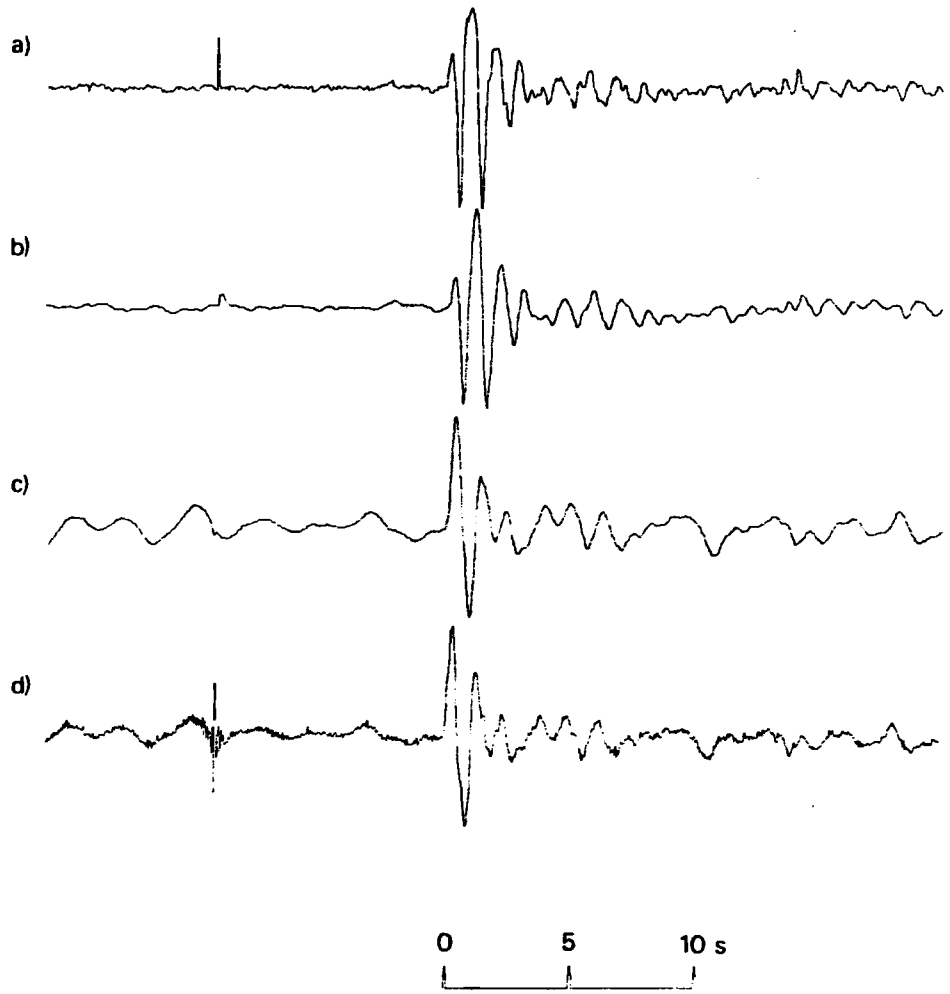

Figure A117 (a) Short-period array-sum seismogram recorded at GBA from the 25 April 1980 Shagan River explosion.
(b) Seismogram (a) filtered to simulate the effects of an additional t* of 0.2s.
(c) Seismogram (a) after Wiener filtering converted to a phaseless-broad-band instrument response.
(d) Same as seismogram (c) except that the effects of path attenuation of t* = 0.15s have been corrected for.
Note that the sample of noise used in designing the Wiener filter is taken ahead of the large spike in the seismogram.

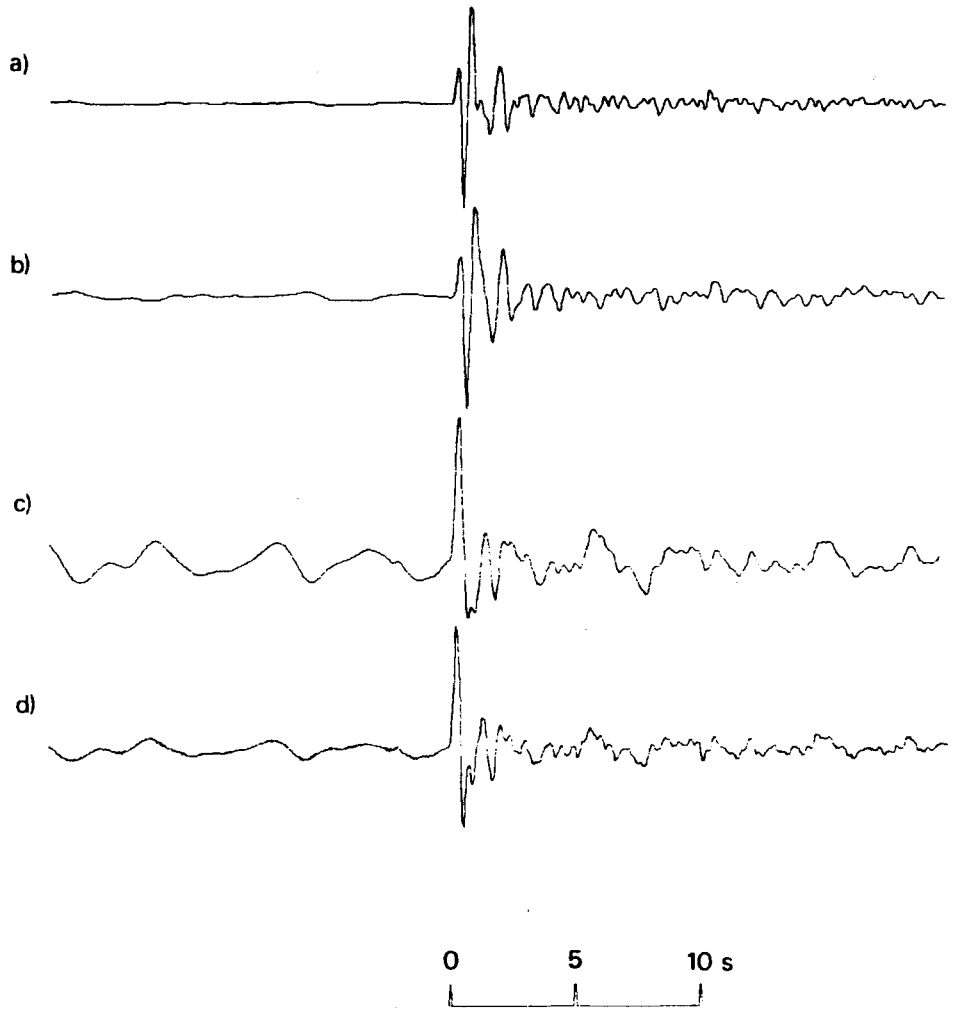

Figure A118 (a) Short-period array-sum seismogram recorded at WRA from the 25 April 1980 Shagan River explosion.
(b) Seismogram (a) filtered to simulate the effects of an additional t* of 0.2s.
(c) Seismogram (a) after Wiener filtering converted to a phaseless-broad-band instrument response.
(d) Same as seismogram (c) except that the effects of path attenuation of t* = 0.15s have been corrected for.
Note that PcP should arrive within a few seconds of P.

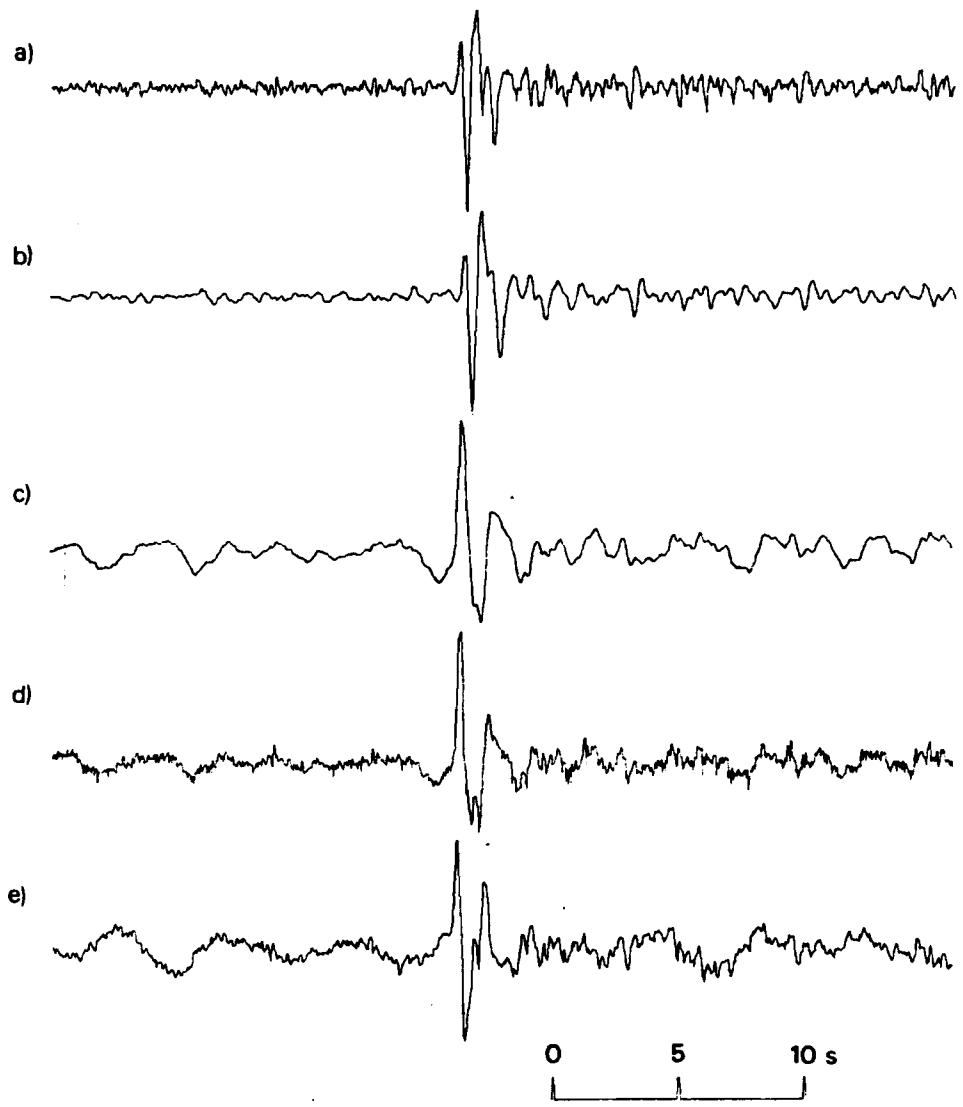

Figure A119 (a) Short-period seismogram that would be recorded at YKA from the 12 June 1980 Shagan River explosion: derived from the velocity-broad-band seismogram (e).
(b) Seismogram (a) filtered to simulate the effects of an additional t* of 0.2s.
(c) Seismogram (a) after Wiener filtering converted to a phaseless-broad-band instrument response.
(d) Same as seismogram (c) except that the effects of path attenuation of t* = 0.15s have been corrected for.
(e) Velocity-broad-band seismogram recorded at YKA.

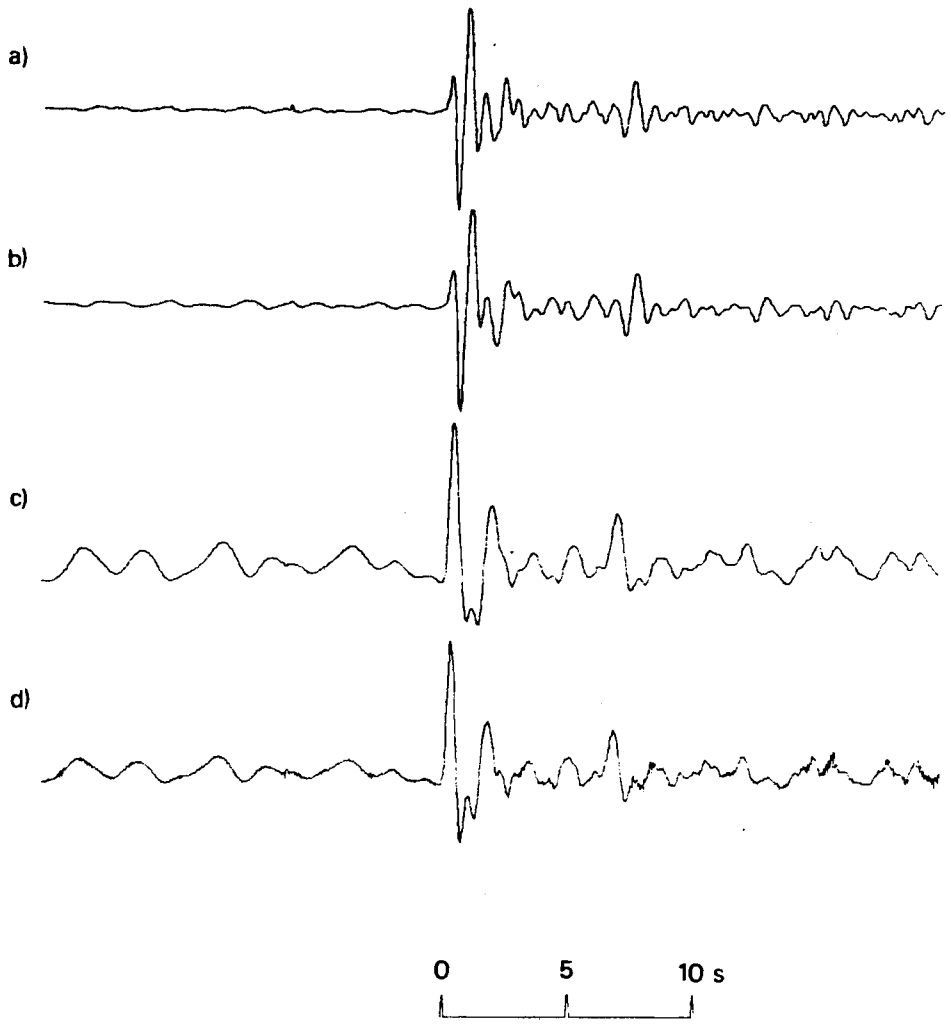

Figure A120 (a) Short-period array-sum seismogram recorded at GBA from the 12 June 1980 Shagan River explosion.
(b) Seismogram (a) filtered to simulate the effects of an additional t* of 0.2s.
(c) Seismogram (a) after Wiener filtering converted to a phaseless-broad-band instrument response.
(d) Same as seismogram (c) except that the effects of path attenuation of t* = 0.15s have been corrected for.

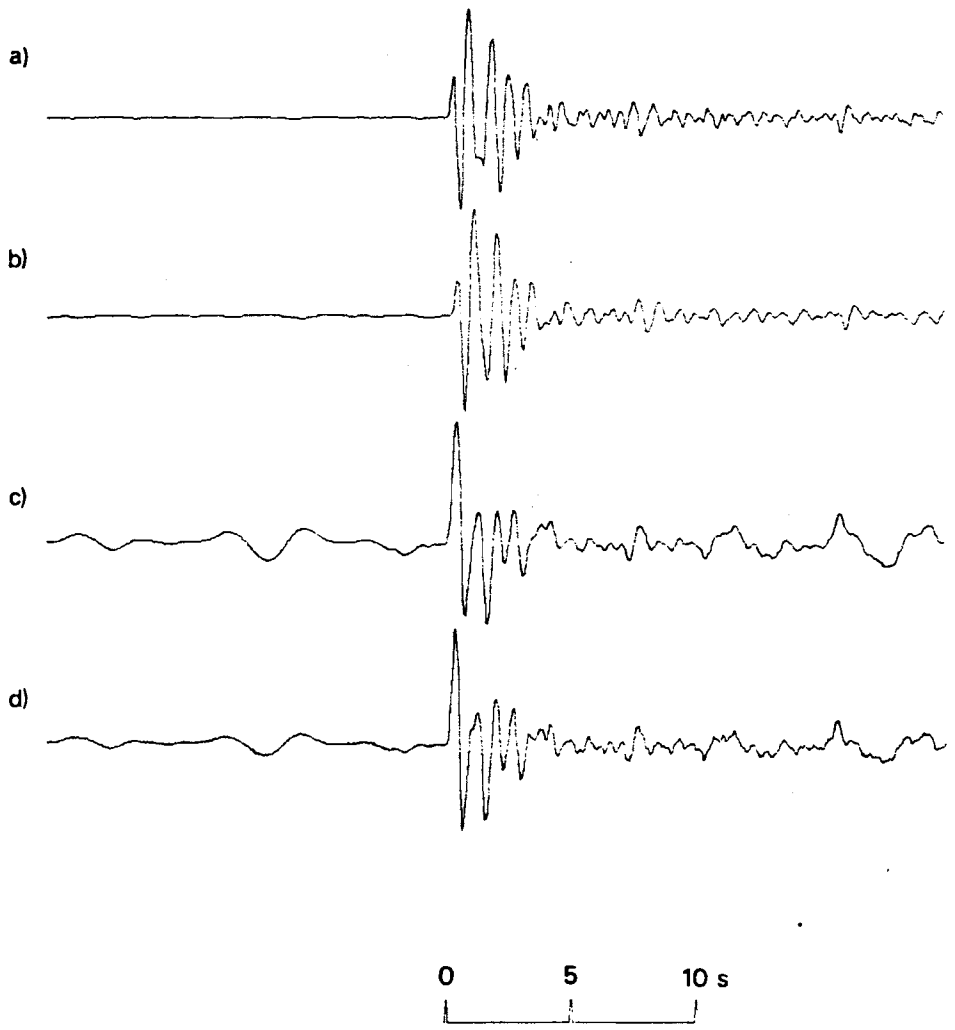

Figure A121 (a) Short-period array-sum seismogram recorded at WRA from the 12 June 1980 Shagan River explosion.
(b) Seismogram (a) filtered to simulate the effects of an additional t* of 0.2s.
(c) Seismogram (a) after Wiener filtering converted to a phaseless-broad-band instrument response.
(d) Same as seismogram (c) except that the effects of path attenuation of t* = 0.15s have been corrected for.
Note that PcP should arrive within a few seconds of P.

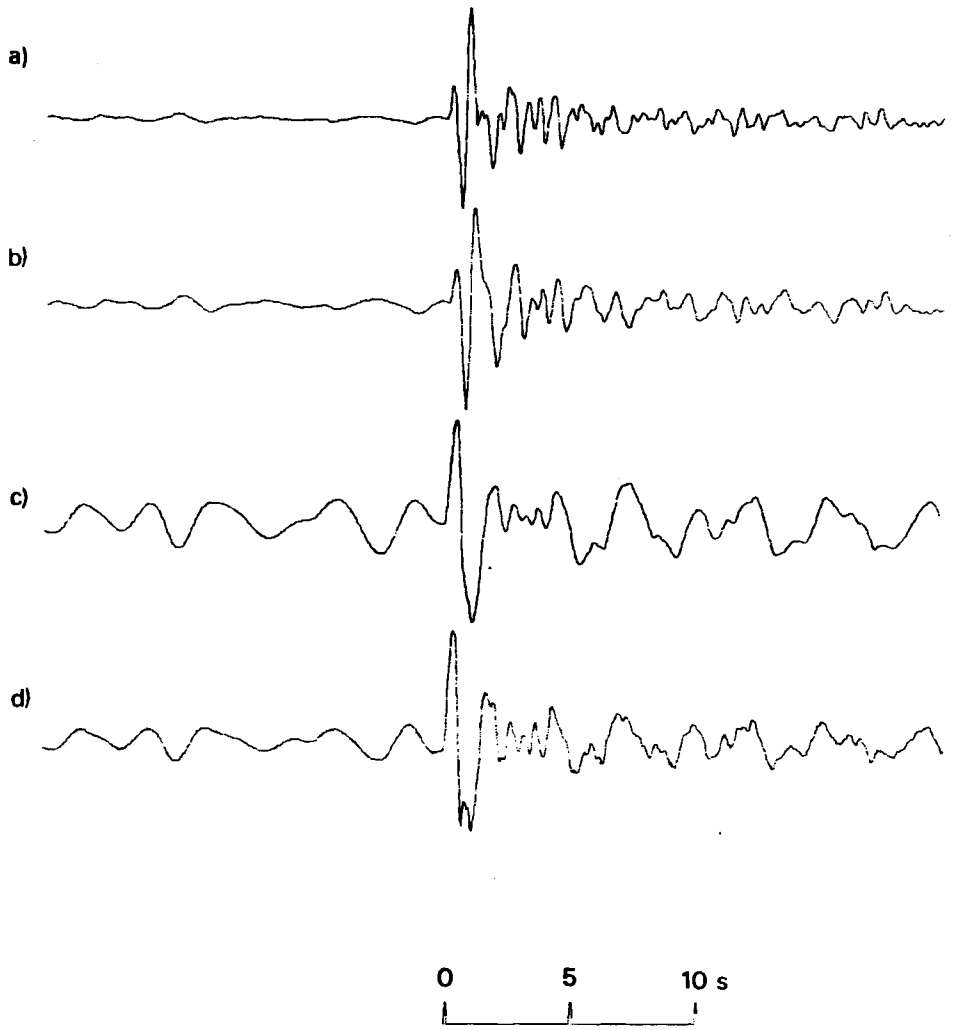

Figure A122 (a) Short-period array-sum seismogram recorded at EKA from the 29 June 1980 Shagan River explosion.
(b) Seismogram (a) filtered to simulate the effects of an additional t* of 0.2s.
(c) Seismogram (a) after Wiener filtering converted to a phaseless-broad-band instrument response.
(d) Same as seismogram (c) except that the effects of path attenuation of t* = 0.15s have been corrected for.

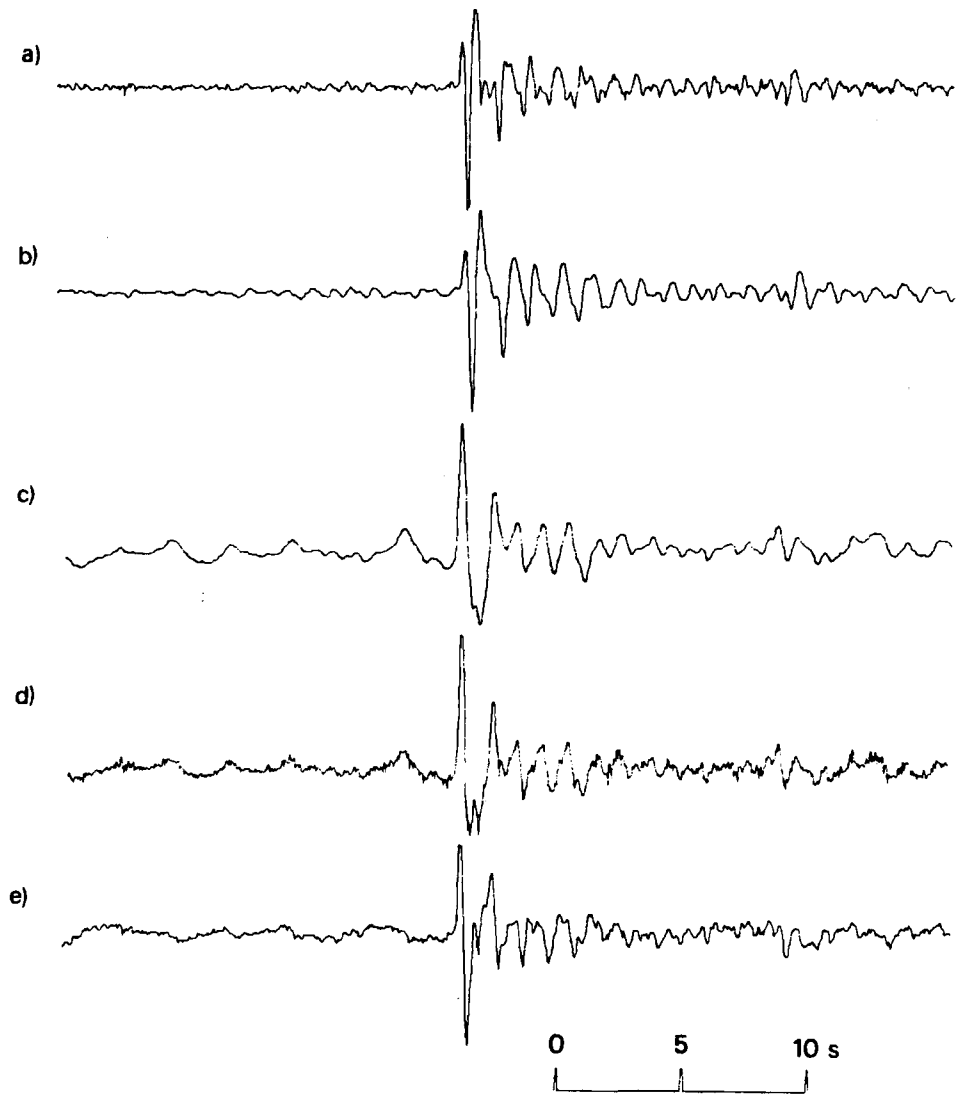

Figure A123 (a) Short-period seismogram that would be recorded at YKA from the 29 June 1980 Shagan River explosion: derived from the velocity-broad-band seismogram (e).
(b) Seismogram (a) filtered to simulate the effects of an additional t* of 0.2s.
(c) Seismogram (a) after Wiener filtering converted to a phaseless-broad-band instrument response.
(d) Same as seismogram (c) except that the effects of path attenuation of t* = 0.15s have been corrected for.
(e) Velocity-broad-band seismogram recorded at YKA.

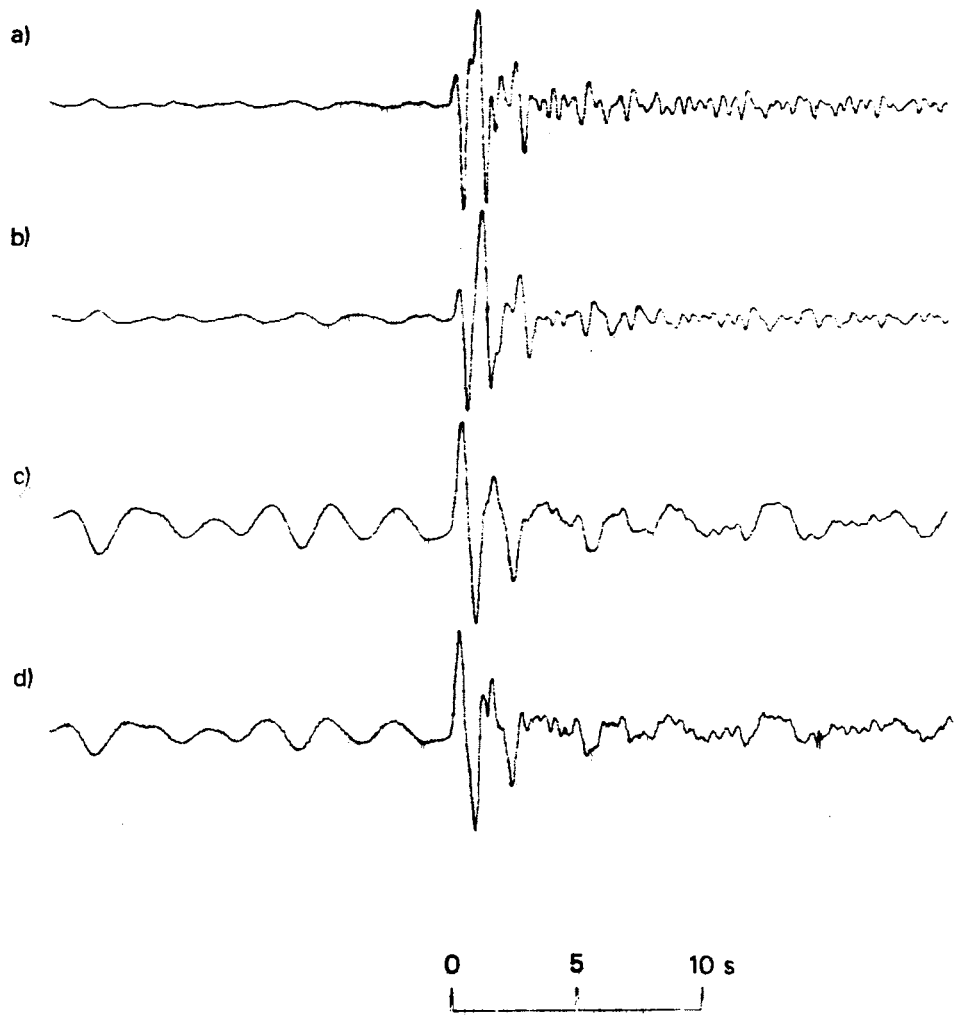

Figure A124 (a) Short-period array-sum seismogram recorded at GBA from the 29 June 1980 Shagan River explosion.
(b) Seismogram (a) filtered to simulate the effects of an additional t^* of 0.2s.
(c) Seismogram (a) after Wiener filtering converted to a phaseless-broad-band instrument response.
(d) Same as seismogram (c) except that the effects of path attenuation of $t^* = 0.15$s have been corrected for.

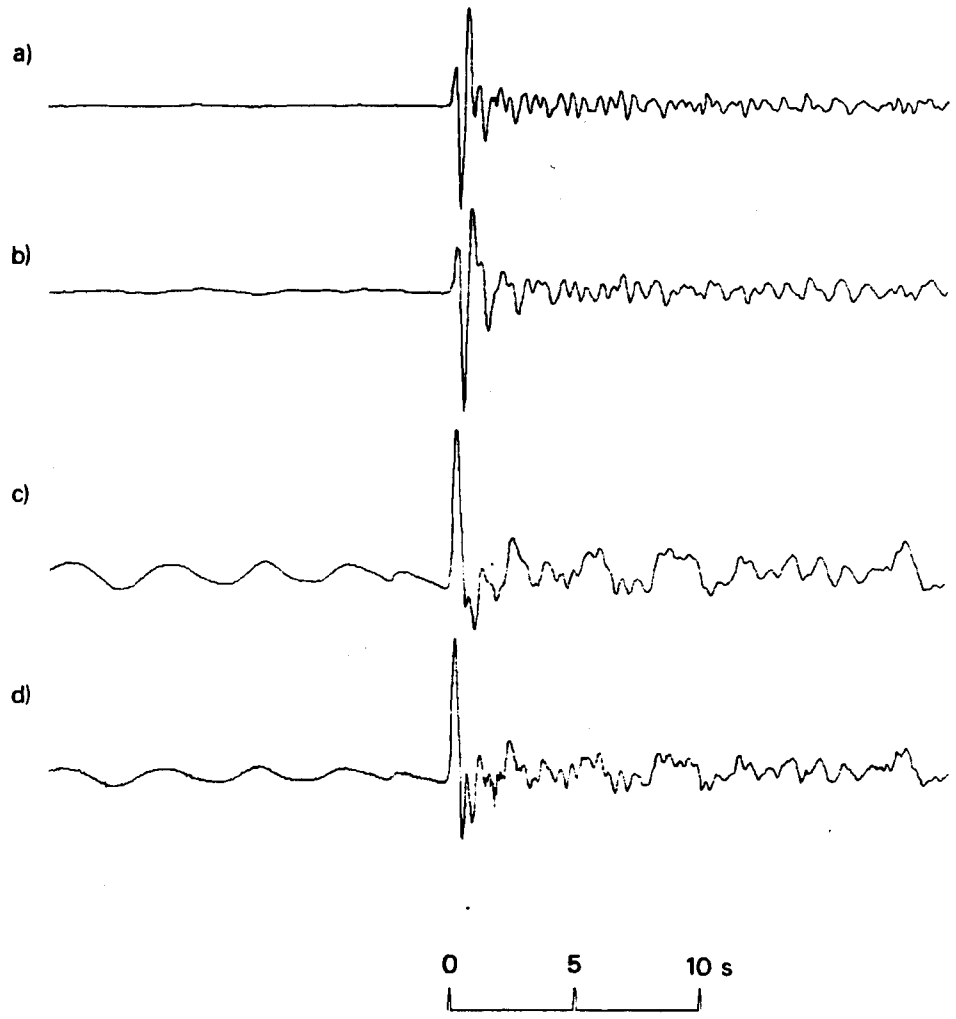

Figure A125 (a) Short-period array-sum seismogram recorded at WRA from the 29 June 1980 Shagan River explosion.
(b) Seismogram (a) filtered to simulate the effects of an additional t* of 0.2s.
(c) Seismogram (a) after Wiener filtering converted to a phaseless-broad-band instrument response.
(d) Same as seismogram (c) except that the effects of path attenuation of t* = 0.15s have been corrected for.
Note that PcP should arrive within a few seconds of P.

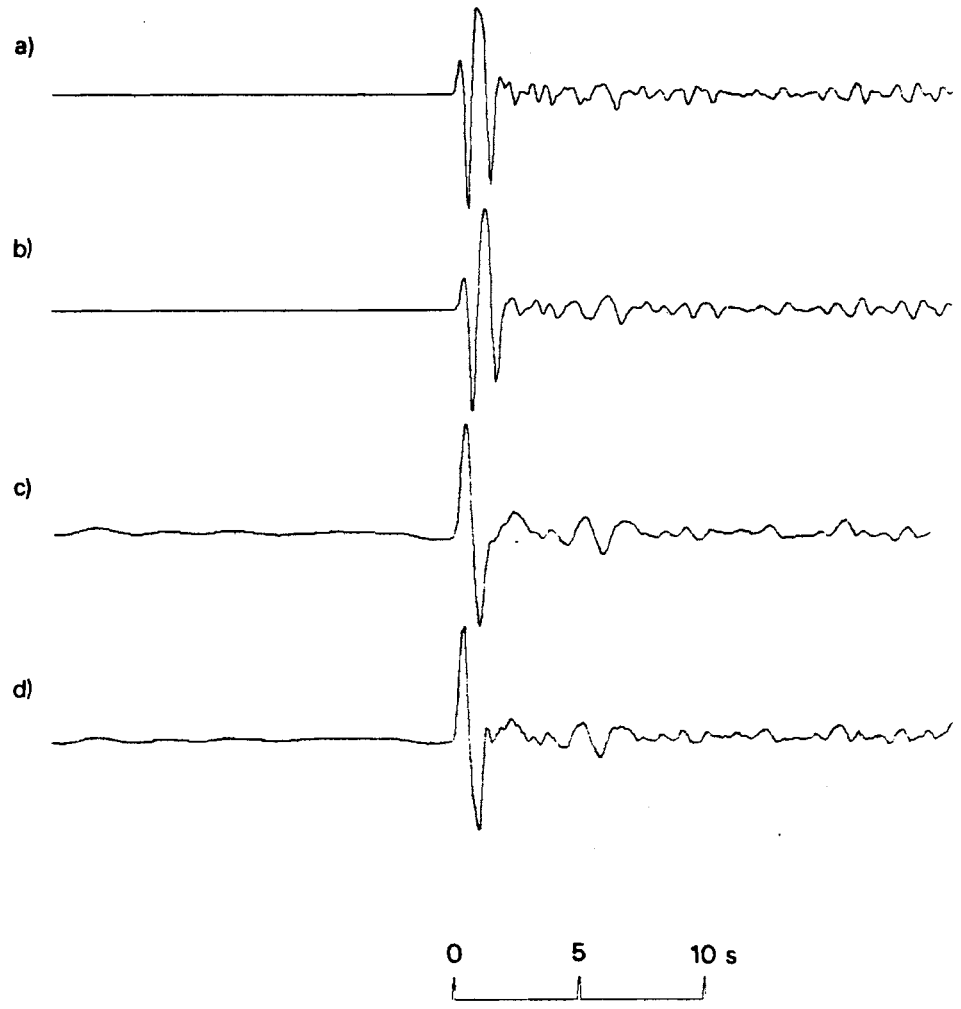

Figure A126 (a) Short-period array-sum seismogram recorded at GBA from the 14 September 1980 Shagan River explosion.
(b) Seismogram (a) filtered to simulate the effects of an additional t^* of 0.2s.
(c) Seismogram (a) after Wiener filtering converted to a phaseless-broad-band instrument response.
(d) Same as seismogram (c) except that the effects of path attenuation of $t^* = 0.15$s have been corrected for.

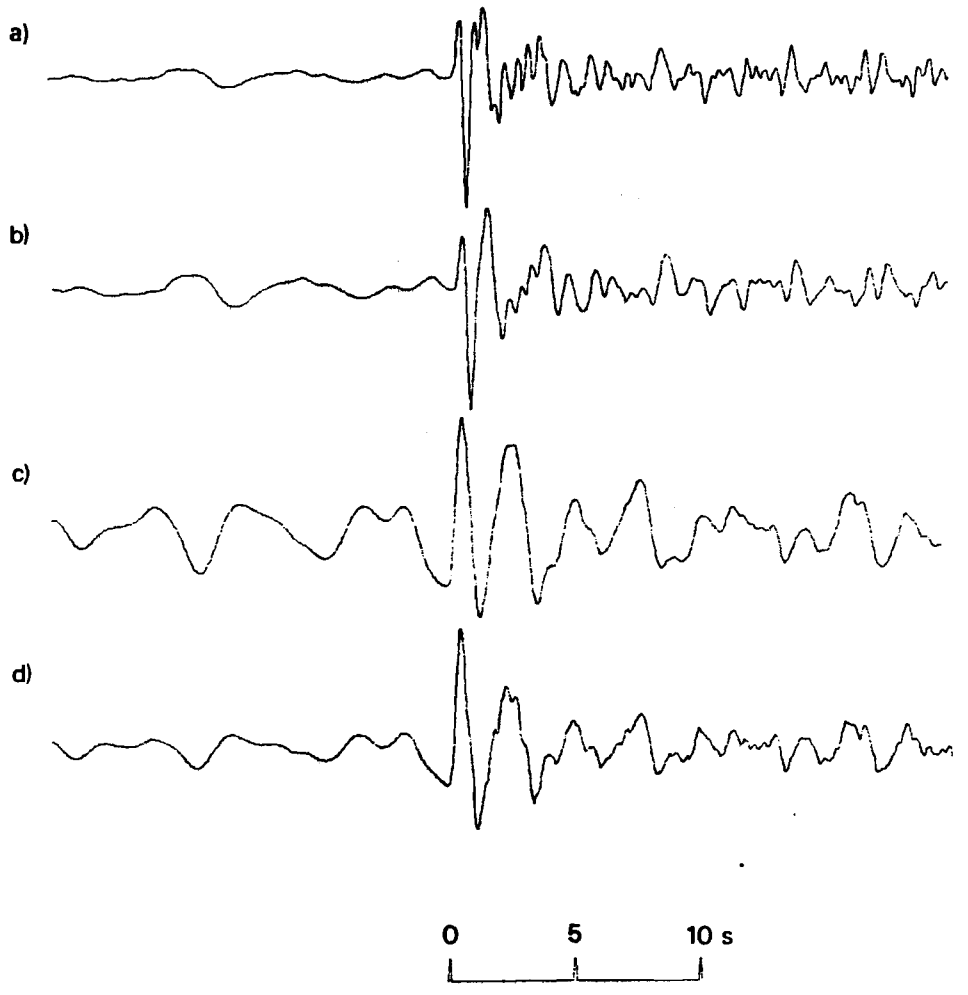

Figure A127 (a) Short-period array-sum seismogram recorded at EKA from the 12 October 1980 Shagan River explosion.
(b) Seismogram (a) filtered to simulate the effects of an additional t* of 0.2s.
(c) Seismogram (a) after Wiener filtering converted to a phaseless-broad-band instrument response.
(d) Same as seismogram (c) except that the effects of path attenuation of t* = 0.15s have been corrected for.

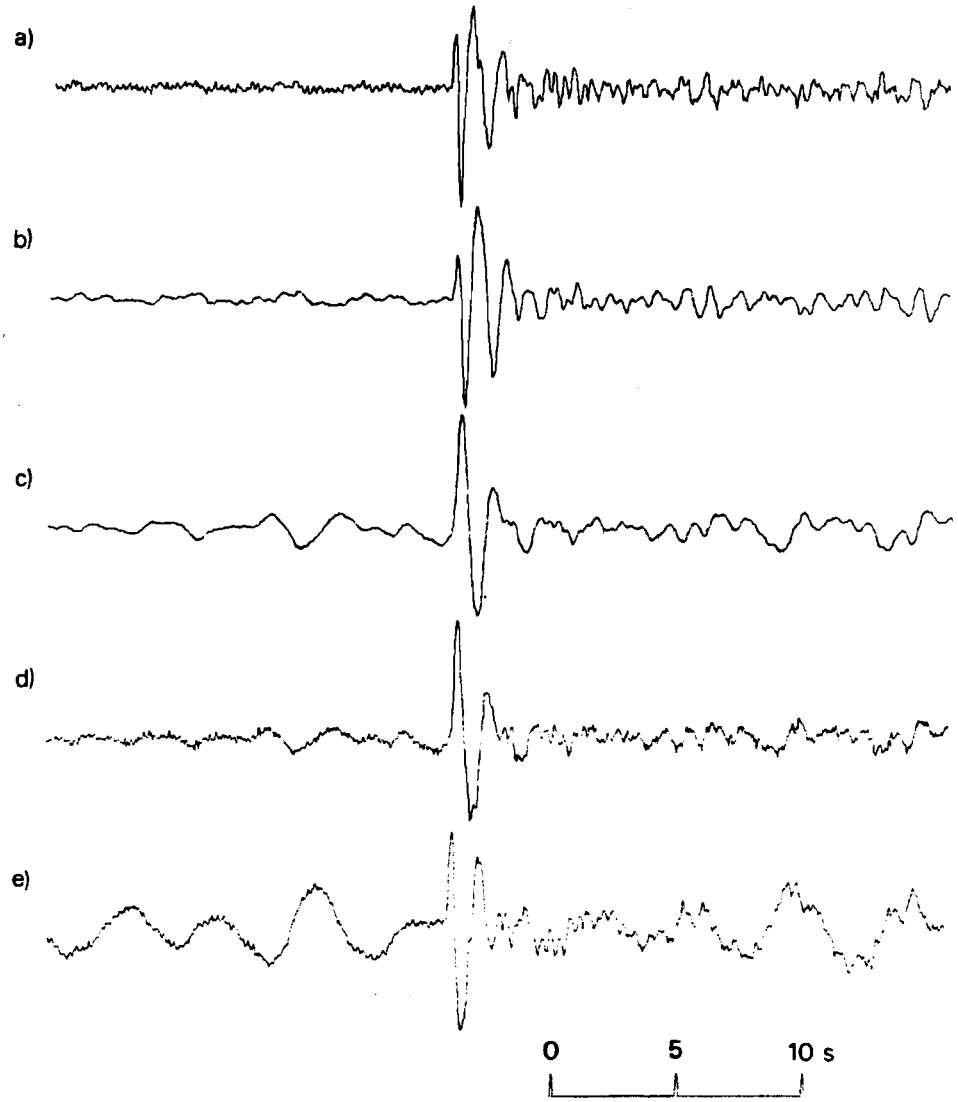

Figure A128 (a) Short-period seismogram that would be recorded at YKA from the 12 October 1980 Shagan River explosion: derived from the velocity-broad-band seismogram (e).
(b) Seismogram (a) filtered to simulate the effects of an additional t* of 0.2s.
(c) Seismogram (a) after Wiener filtering converted to a phaseless-broad-band instrument response.
(d) Same as seismogram (c) except that the effects of path attenuation of t* = 0.15s have been corrected for.
(e) Velocity-broad-band seismogram recorded at YKA.

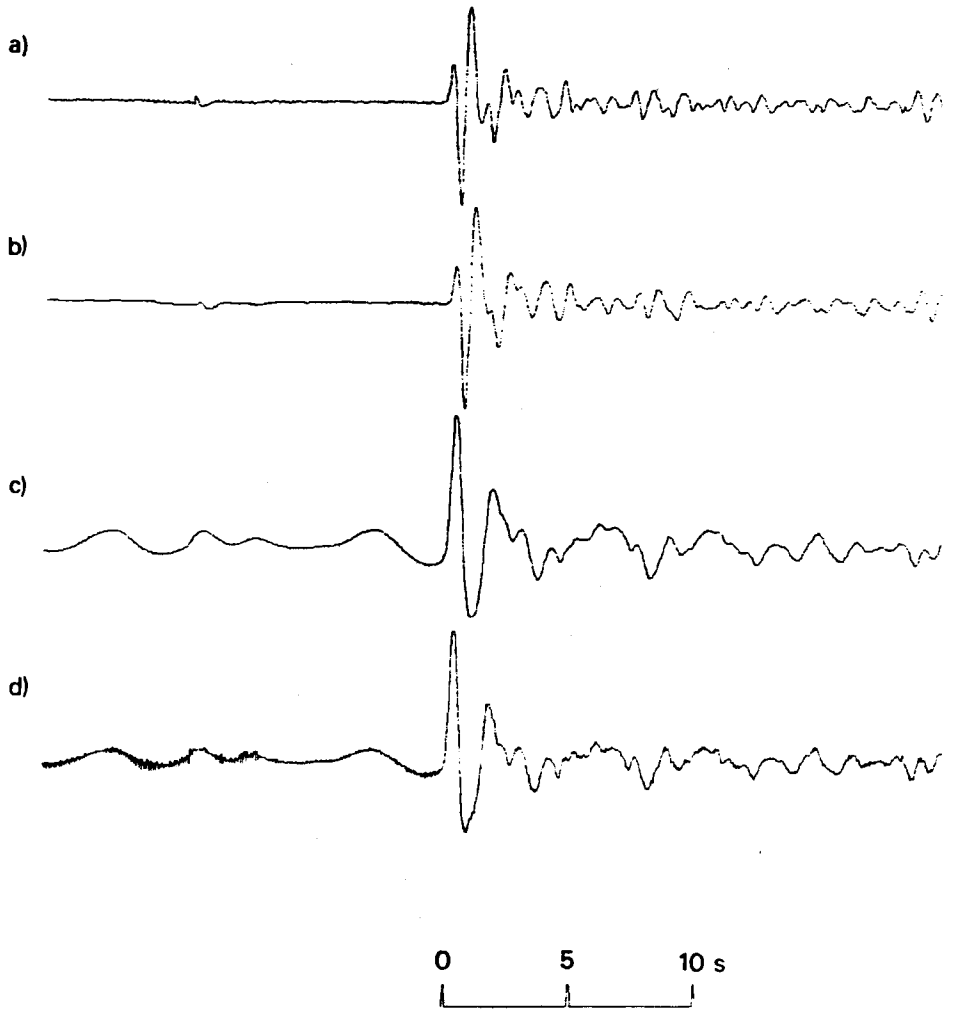

Figure A129 (a) Short-period array-sum seismogram recorded at GBA from the 12 October 1980 Shagan River explosion.
(b) Seismogram (a) filtered to simulate the effects of an additional t* of 0.2s.
(c) Seismogram (a) after Wiener filtering converted to a phaseless-broad-band instrument response.
(d) Same as seismogram (c) except that the effects of path attenuation of t* = 0.15s have been corrected for.

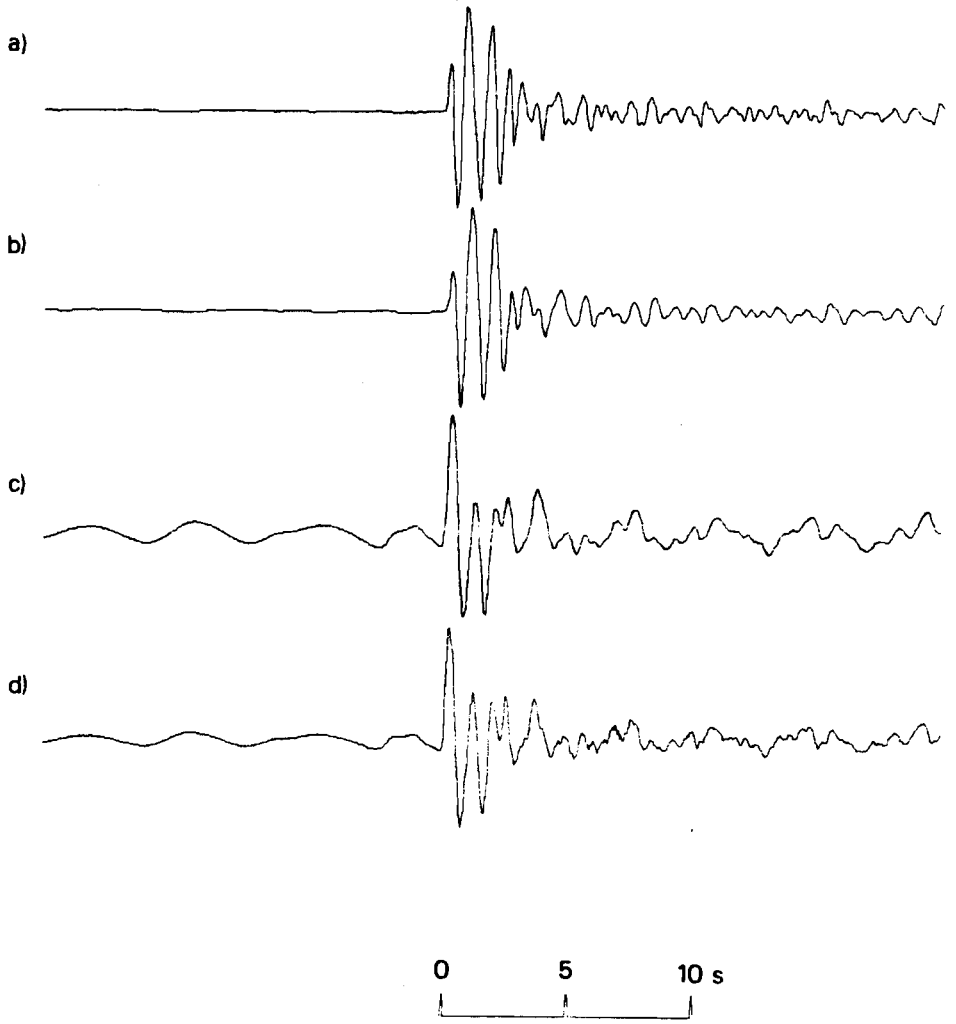

Figure A130 (a) Short-period array-sum seismogram recorded at WRA from the 12 October 1980 Shagan River explosion.
(b) Seismogram (a) filtered to simulate the effects of an additional t* of 0.2s.
(c) Seismogram (a) after Wiener filtering converted to a phaseless-broad-band instrument response.
(d) Same as seismogram (c) except that the effects of path attenuation of t* = 0.15s have been corrected for.
Note that PcP should arrive within a few seconds of P.

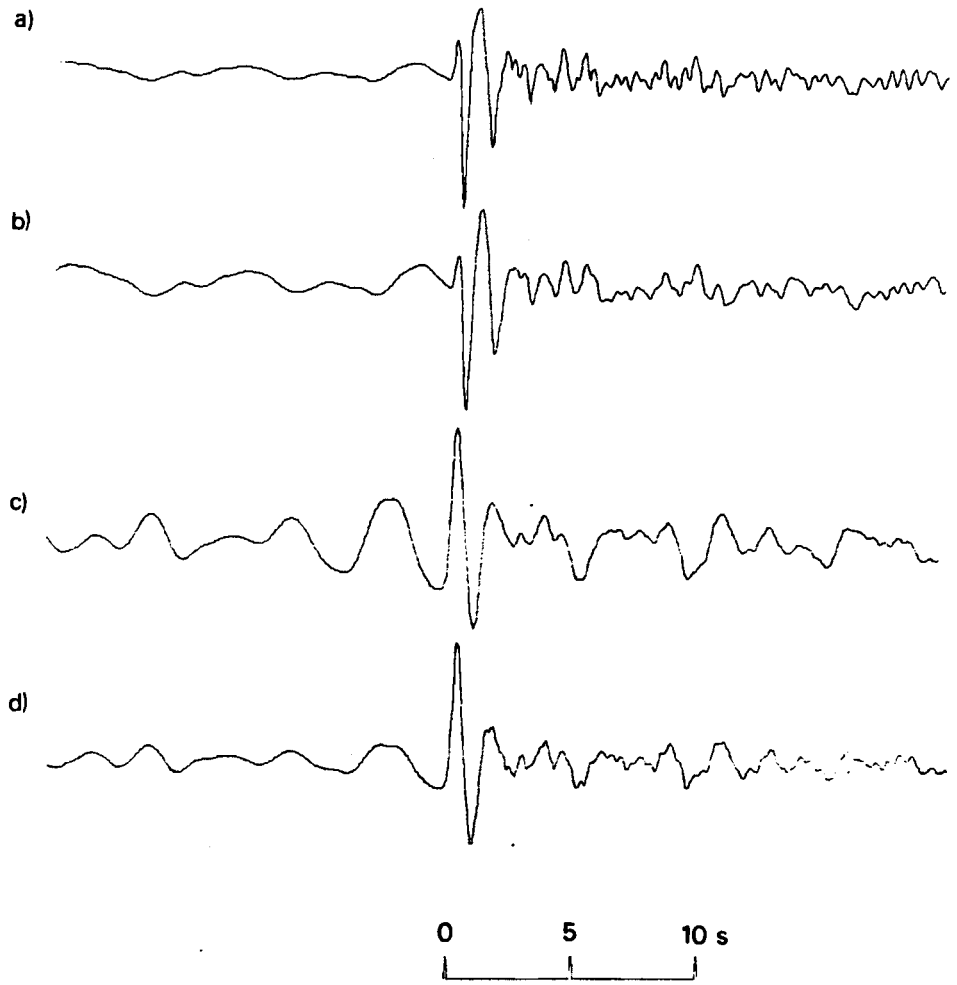

Figure A131 (a) Short-period array-sum seismogram recorded at EKA from the 14 December 1980 Shagan River explosion.
(b) Seismogram (a) filtered to simulate the effects of an additional t* of 0.2s.
(c) Seismogram (a) after Wiener filtering converted to a phaseless-broad-band instrument response.
(d) Same as seismogram (c) except that the effects of path attenuation of t* = 0.15s have been corrected for.

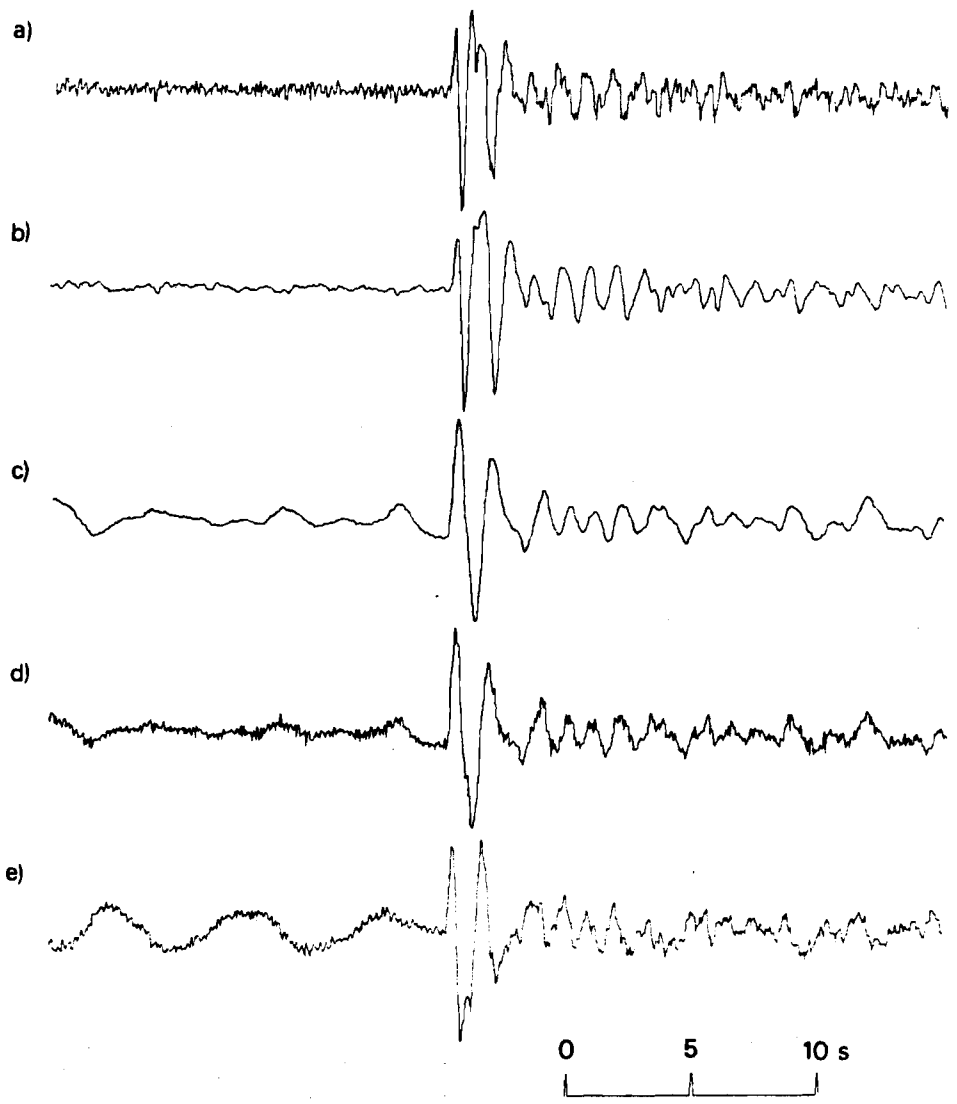

Figure A132 (a) Short-period seismogram that would be recorded at YKA from the 14 December 1980 Shagan River explosion: derived from the velocity-broad-band seismogram (e).
(b) Seismogram (a) filtered to simulate the effects of an additional t* of 0.2s.
(c) Seismogram (a) after Wiener filtering converted to a phaseless-broad-band instrument response.
(d) Same as seismogram (c) except that the effects of path attenuation of t* = 0.15s have been corrected for.
(e) Velocity-broad-band seismogram recorded at YKA.

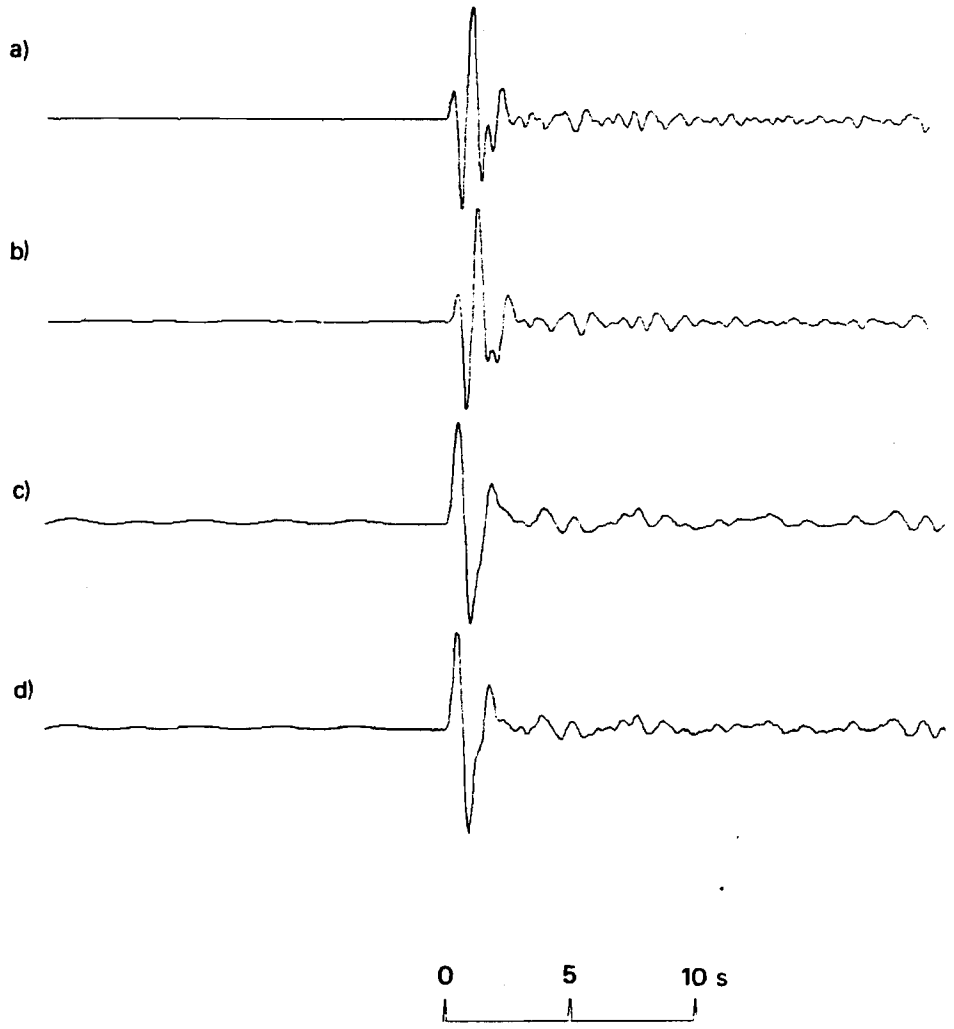

Figure A133 (a) Short-period array-sum seismogram recorded at GBA from the 14 December 1980 Shagan River explosion.
(b) Seismogram (a) filtered to simulate the effects of an additional t* of 0.2s.
(c) Seismogram (a) after Wiener filtering converted to a phaseless-broad-band instrument response.
(d) Same as seismogram (c) except that the effects of path attenuation of t* = 0.15s have been corrected for.

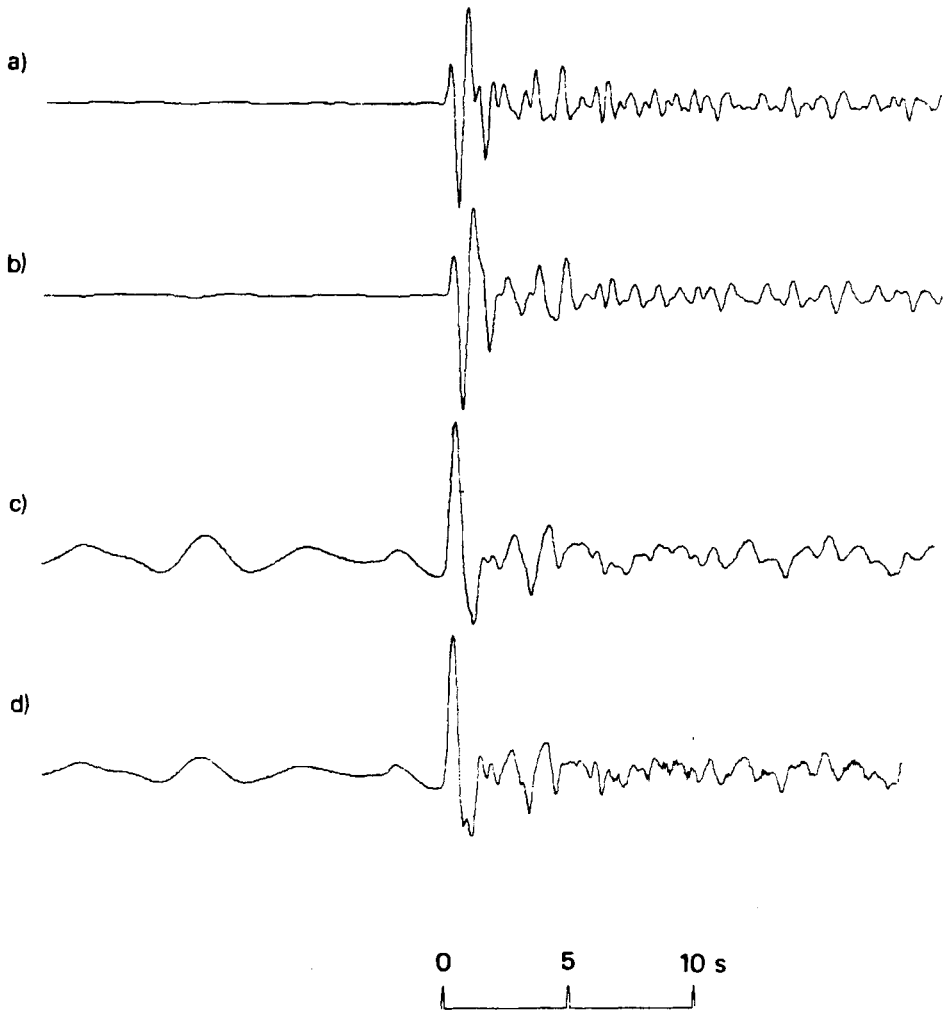

Figure A134 (a) Short-period array-sum seismogram recorded at WRA from the 14 December 1980 Shagan River explosion.
(b) Seismogram (a) filtered to simulate the effects of an additional t* of 0.2s.
(c) Seismogram (a) after Wiener filtering converted to a phaseless-broad-band instrument response.
(d) Same as seismogram (c) except that the effects of path attenuation of t* = 0.15s have been corrected for.
Note that PcP should arrive within a few seconds of P.

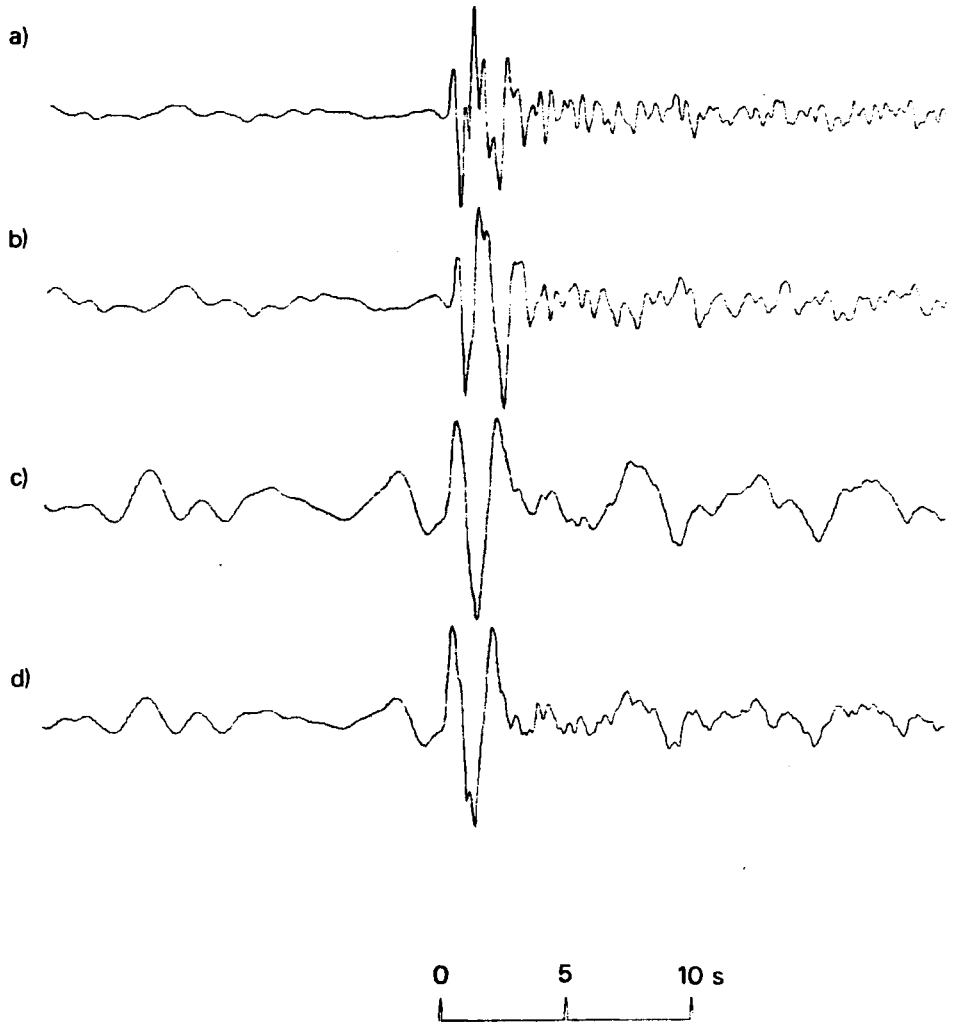

Figure A135 (a) Short-period array-sum seismogram recorded at EKA from the 27 December 1980 Shagan River explosion.
(b) Seismogram (a) filtered to simulate the effects of an additional t* of 0.2s.
(c) Seismogram (a) after Wiener filtering converted to a phaseless-broad-band instrument response.
(d) Same as seismogram (c) except that the effects of path attenuation of t* = 0.15s have been corrected for.

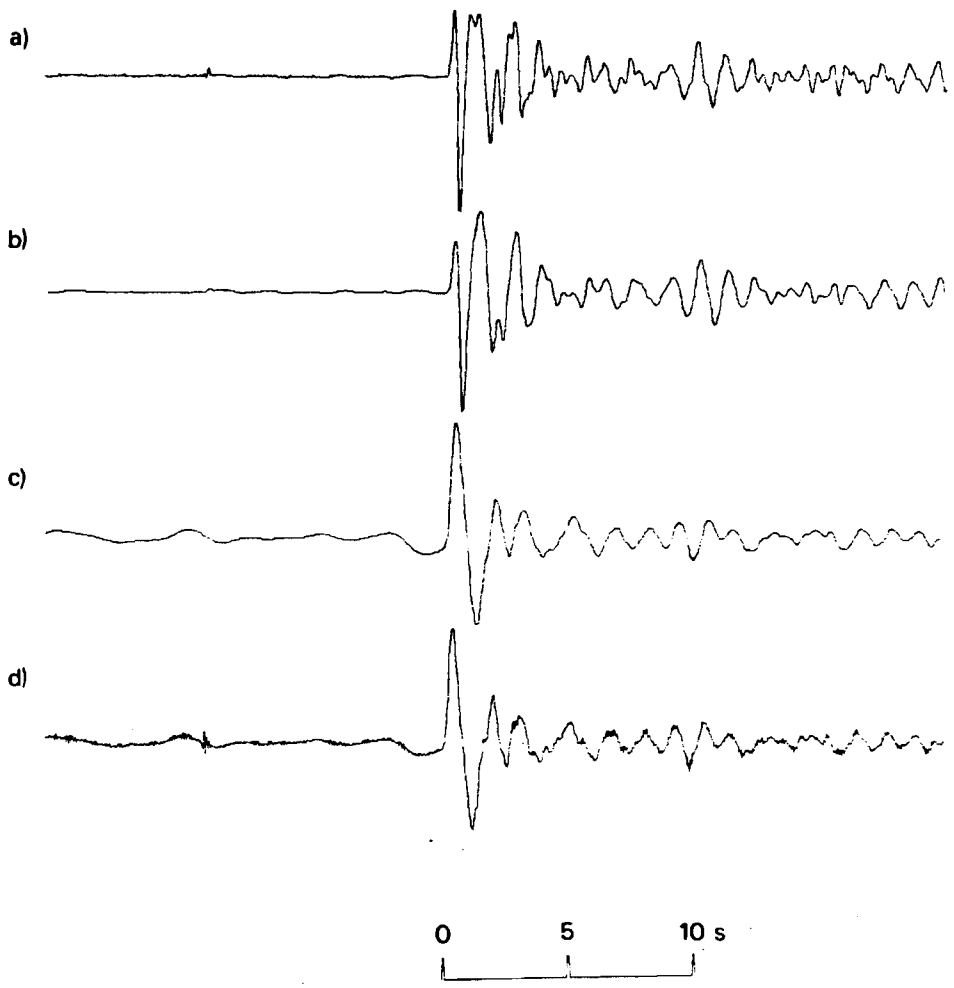

Figure A136 (a) Short-period array-sum seismogram recorded at GBA from the 27 December 1980 Shagan River explosion.
(b) Seismogram (a) filtered to simulate the effects of an additional t* of 0.2s.
(c) Seismogram (a) after Wiener filtering converted to a phaseless-broad-band instrument response.
(d) Same as seismogram (c) except that the effects of path attenuation of t* = 0.15s have been corrected for.

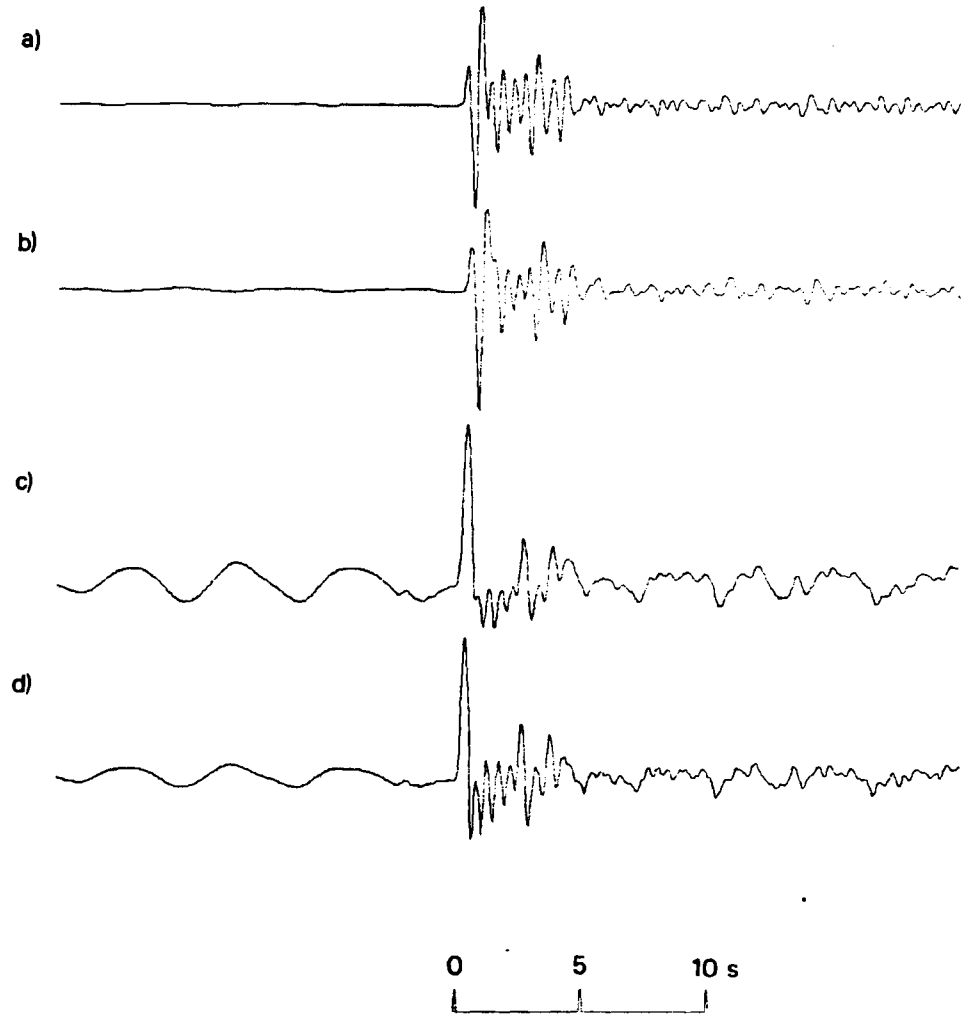

Figure A137 (a) Short-period array-sum seismogram recorded at WRA from the 27 December 1980 Shagan River explosion.
(b) Seismogram (a) filtered to simulate the effects of an additional t* of 0.2s.
(c) Seismogram (a) after Wiener filtering converted to a phaseless-broad-band instrument response.
(d) Same as seismogram (c) except that the effects of path attenuation of t* = 0.15s have been corrected for.
Note that PcP should arrive within a few seconds of P.

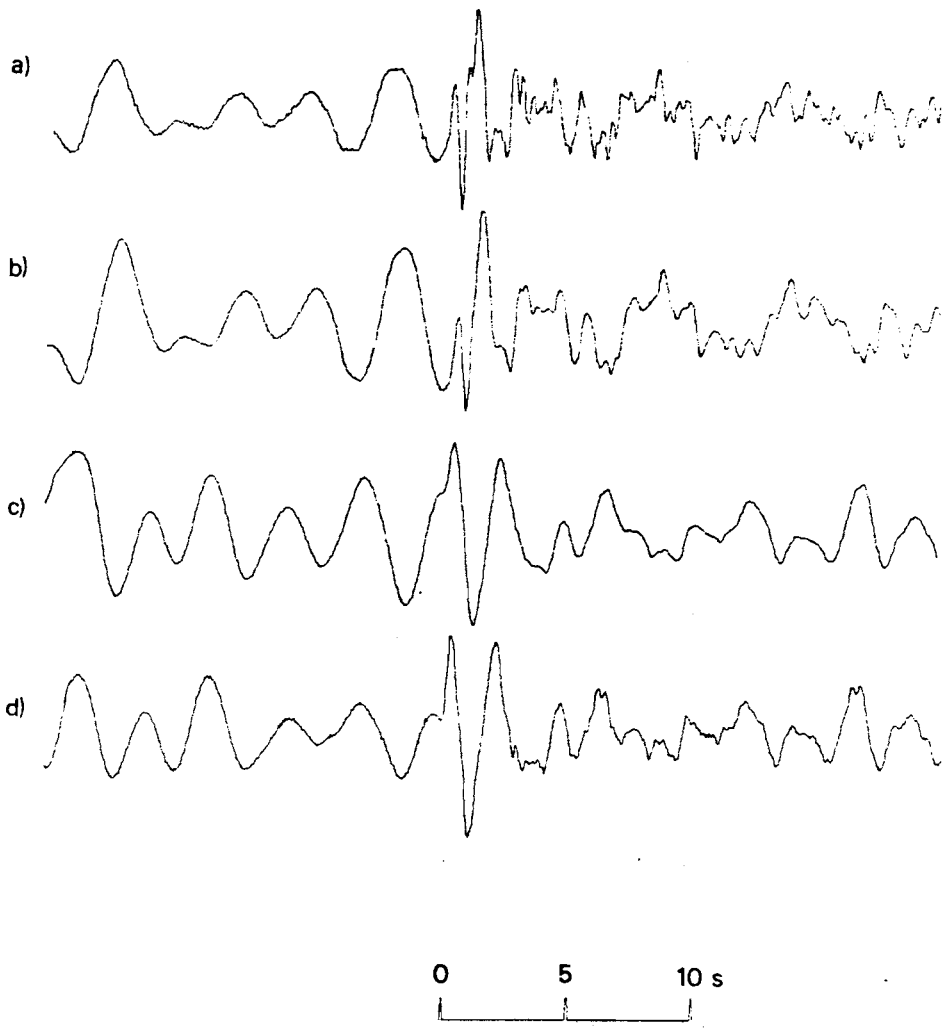

Figure A138 (a) Short-period array-sum seismogram recorded at EKA from the 29 March 1981 Shagan River explosion.
(b) Seismogram (a) filtered to simulate the effects of an additional t* of 0.2s.
(c) Seismogram (a) after Wiener filtering converted to a phaseless-broad-band instrument response.
(d) Same as seismogram (c) except that the effects of path attenuation of t* = 0.15s have been corrected for.

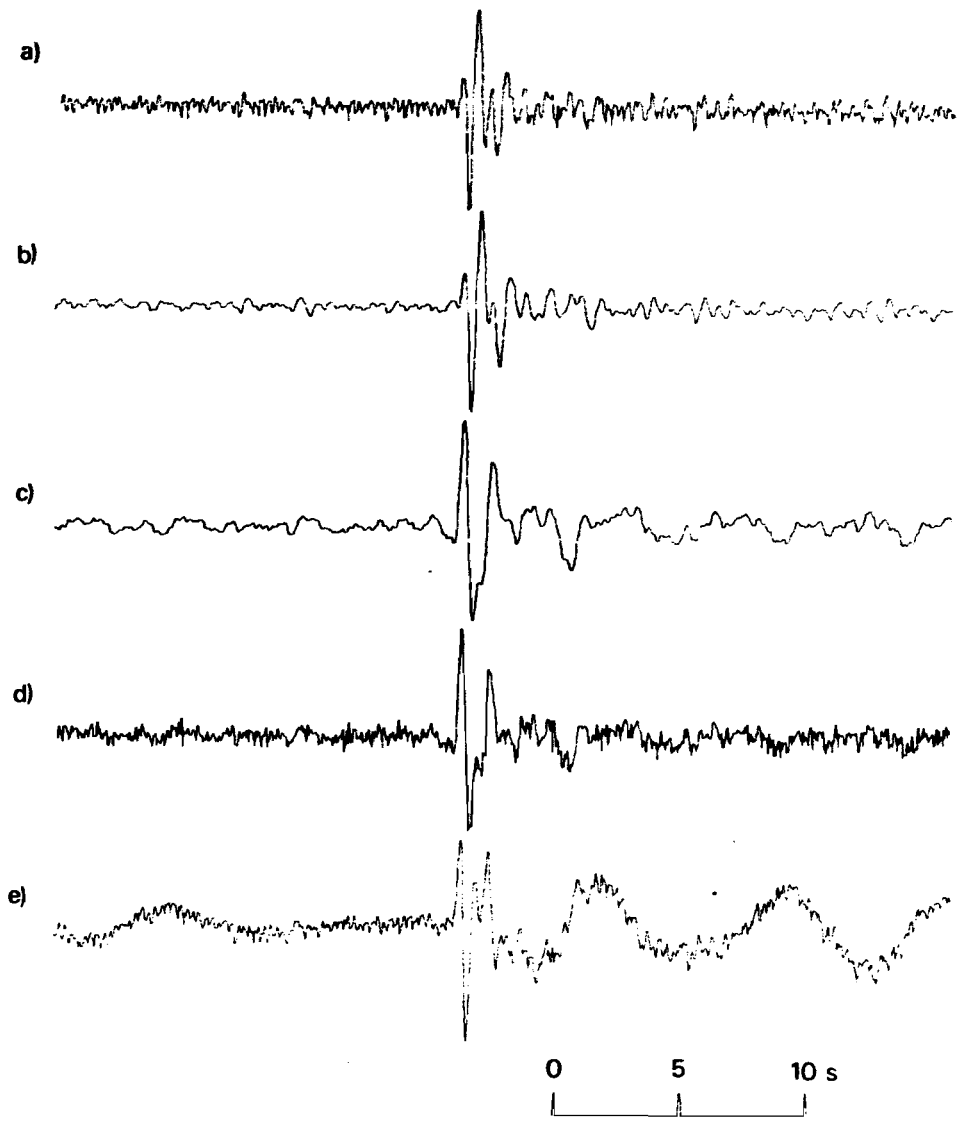

Figure A139 (a) Short-period seismogram that would be recorded at YKA from the 29 March 1981 Shagan River explosion: derived from the velocity-broad-band seismogram (e).
(b) Seismogram (a) filtered to simulate the effects of an additional t* of 0.2s.
(c) Seismogram (a) after Wiener filtering converted to a phaseless-broad-band instrument response.
(d) Same as seismogram (c) except that the effects of path attenuation of t* = 0.15s have been corrected for.
(e) Velocity-broad-band seismogram recorded at YKA.

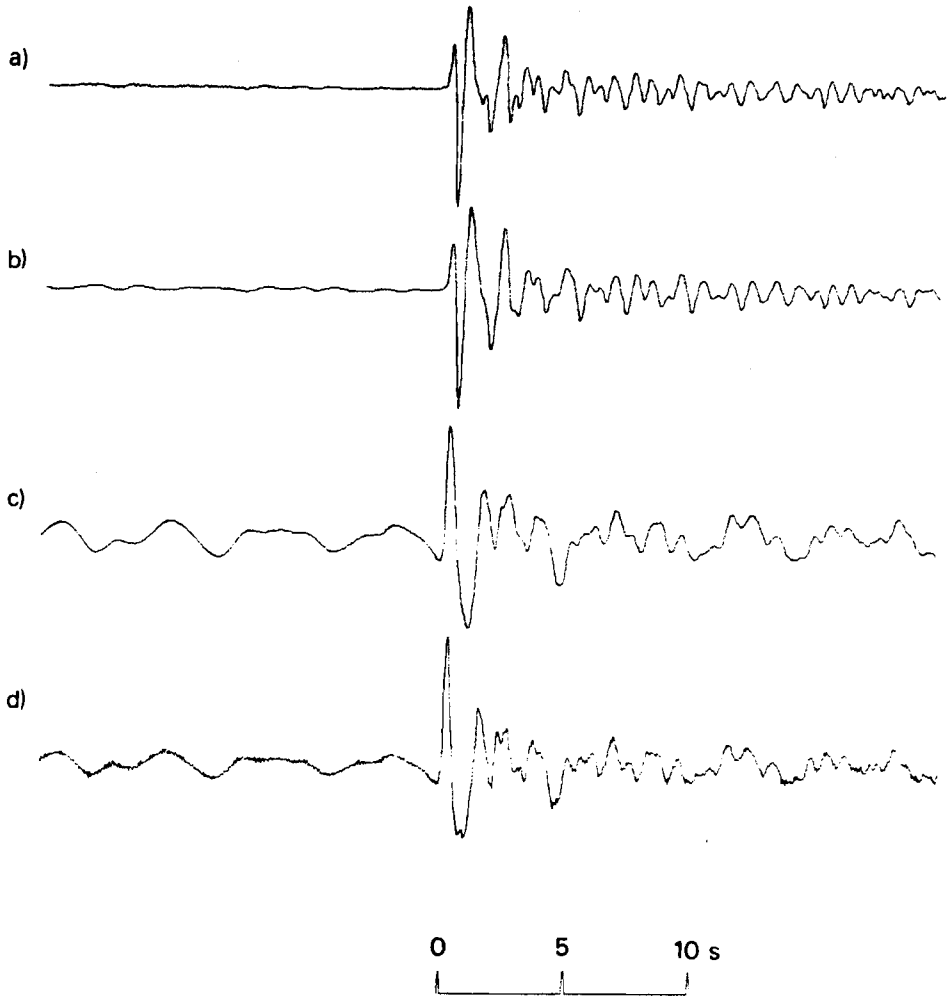

Figure A140 (a) Short-period array-sum seismogram recorded at GBA from the 29 March 1981 Shagan River explosion.
(b) Seismogram (a) filtered to simulate the effects of an additional t* of 0.2s.
(c) Seismogram (a) after Wiener filtering converted to a phaseless-broad-band instrument response.
(d) Same as seismogram (c) except that the effects of path attenuation of t* = 0.15s have been corrected for.

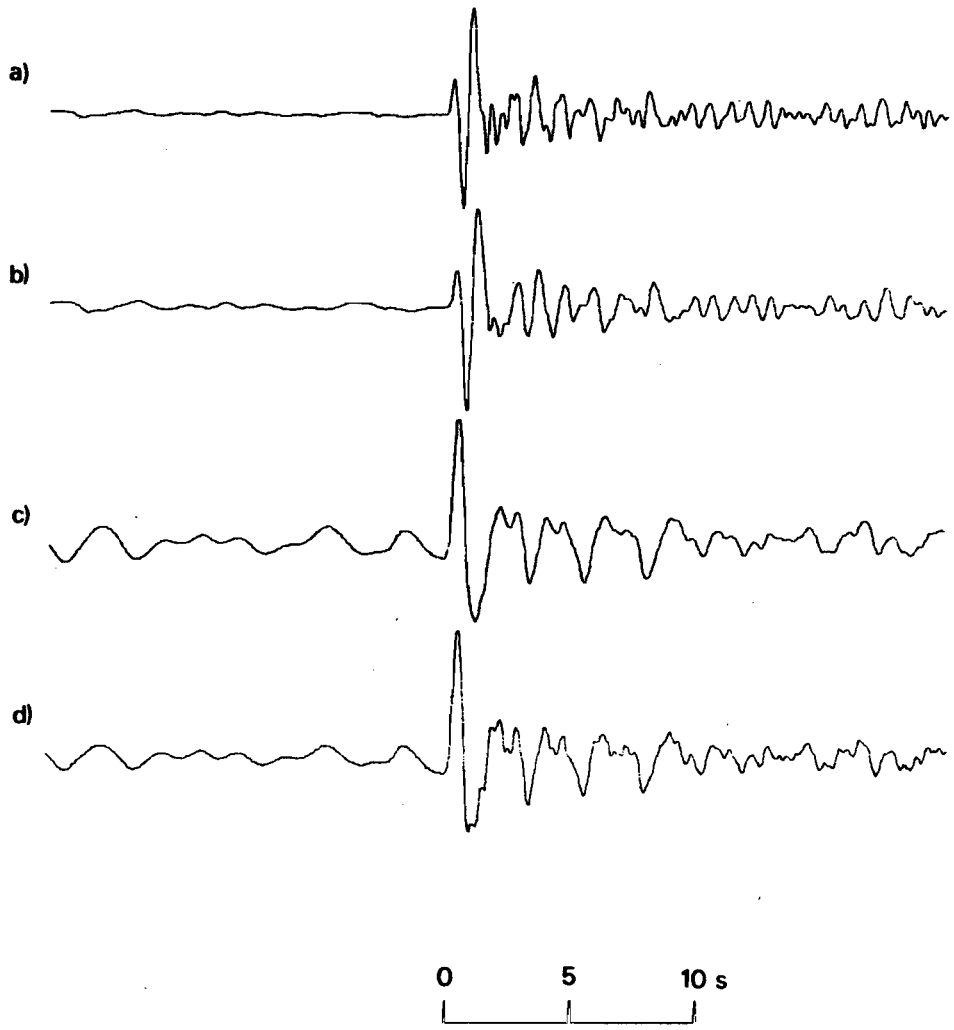

Figure A141 (a) Short-period array-sum seismogram recorded at EKA from the 22 April 1981 Shagan River explosion.
(b) Seismogram (a) filtered to simulate the effects of an additional t* of 0.2s.
(c) Seismogram (a) after Wiener filtering converted to a phaseless-broad-band instrument response.
(d) Same as seismogram (c) except that the effects of path attenuation of t* = 0.15s have been corrected for.

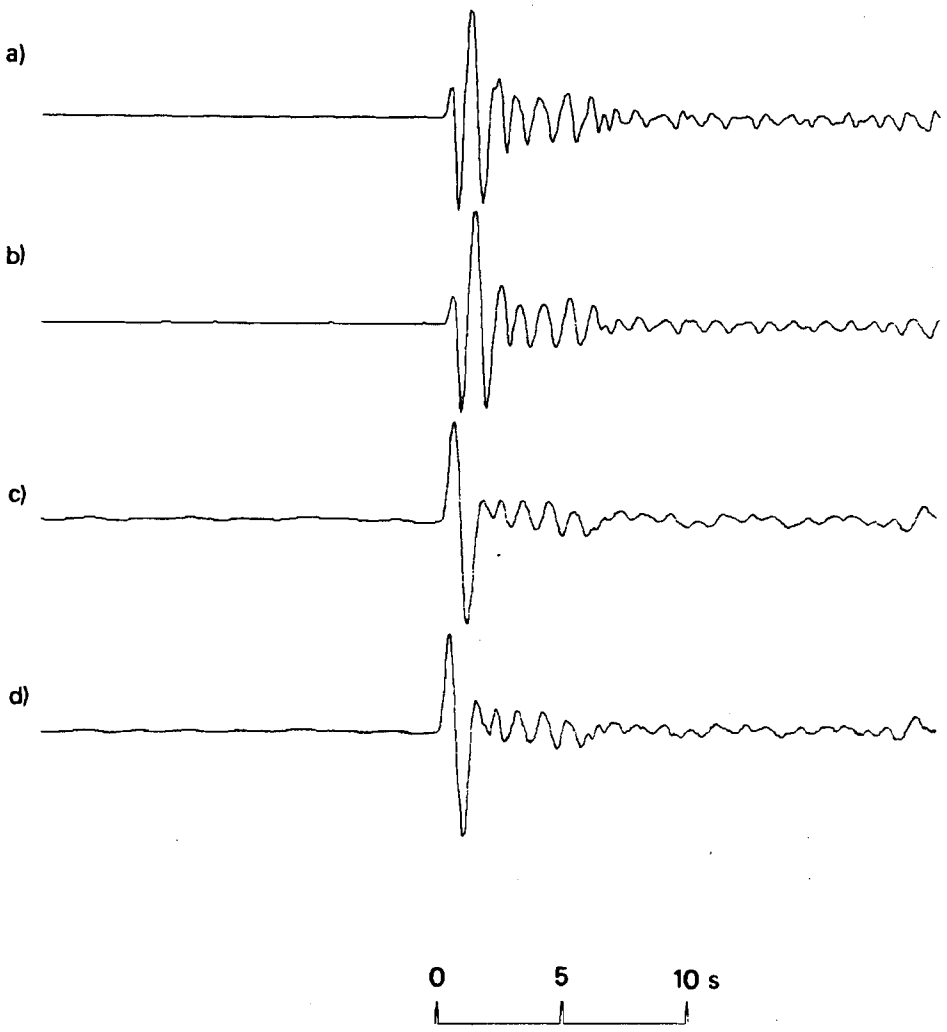

Figure A142 (a) Short-period array-sum seismogram recorded at GBA from the 22 April 1981 Shagan River explosion.
(b) Seismogram (a) filtered to simulate the effects of an additional t* of 0.2s.
(c) Seismogram (a) after Wiener filtering converted to a phaseless-broad-band instrument response.
(d) Same as seismogram (c) except that the effects of path attenuation of t* = 0.15s have been corrected for.

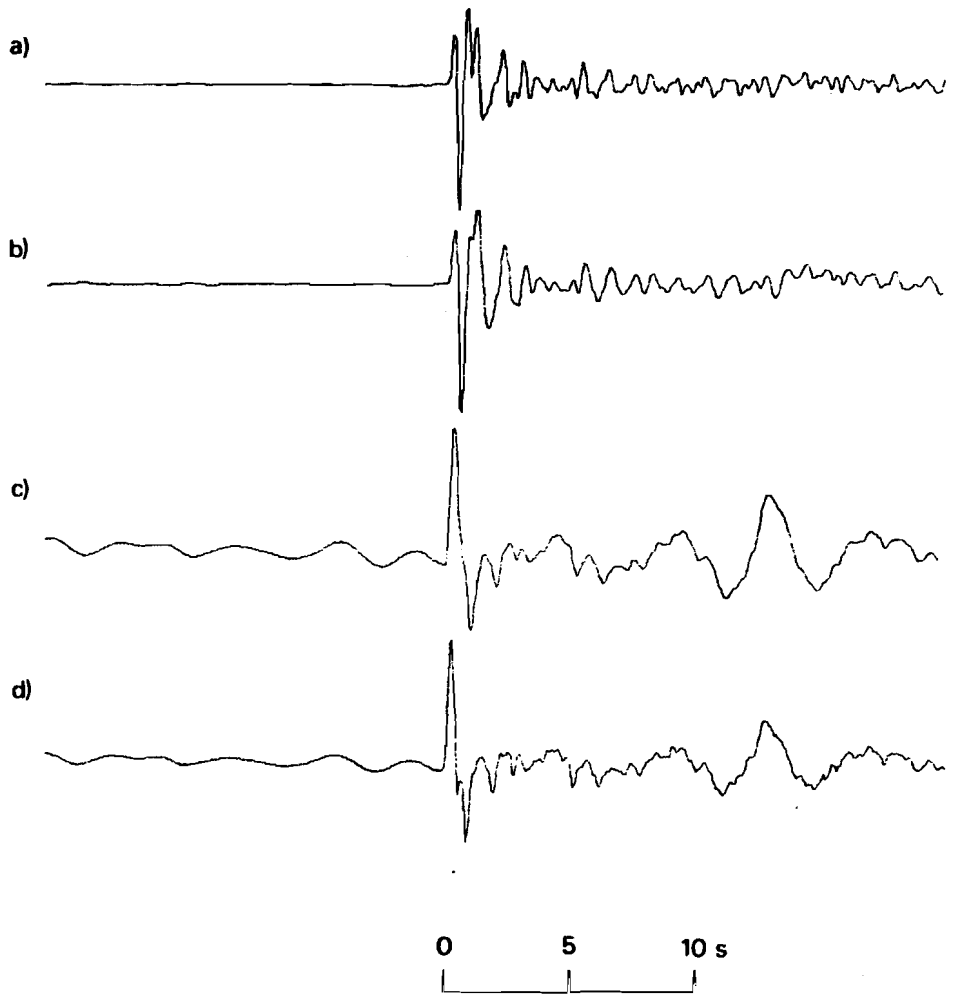

Figure A143 (a) Short-period array-sum seismogram recorded at WRA from the 22 April 1981 Shagan River explosion.
(b) Seismogram (a) filtered to simulate the effects of an additional t* of 0.2s.
(c) Seismogram (a) after Wiener filtering converted to a phaseless-broad-band instrument response.
(d) Same as seismogram (c) except that the effects of path attenuation of t* = 0.15s have been corrected for.
Note that PcP should arrive within a few seconds of P.

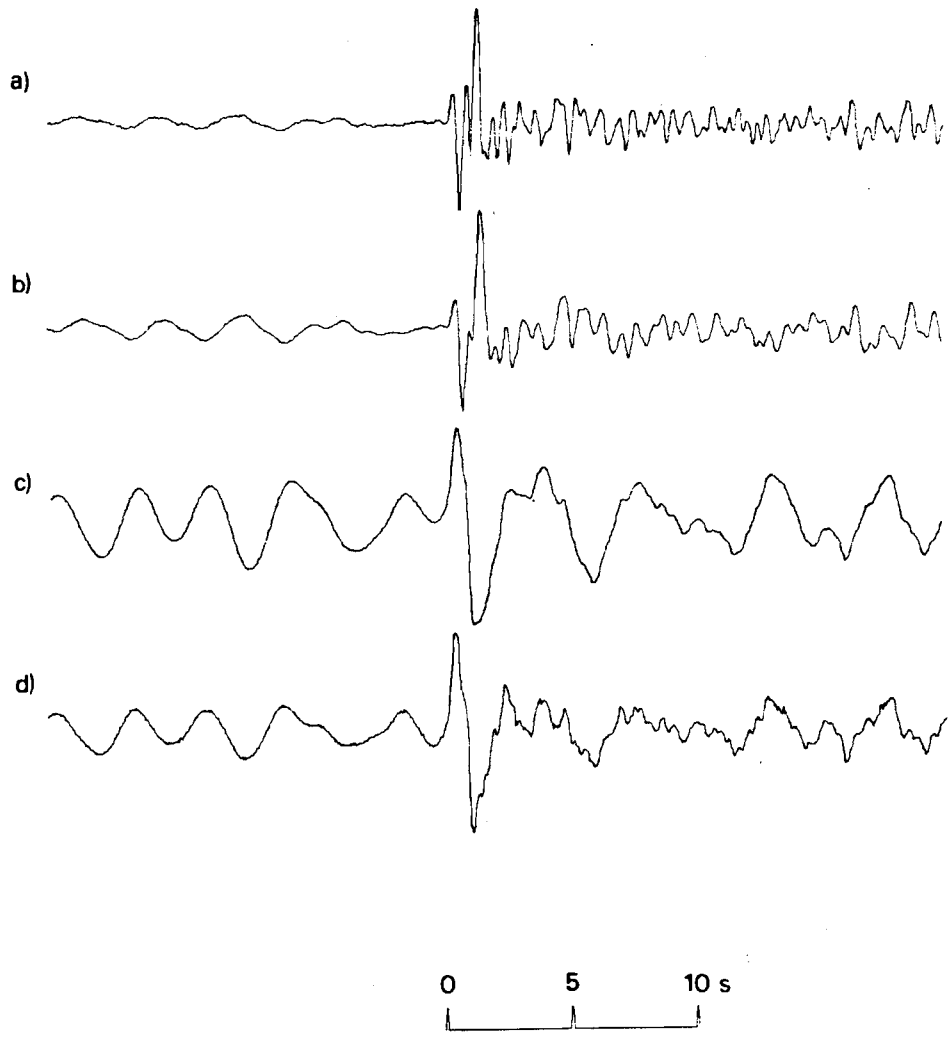

Figure A144 (a) Short-period array-sum seismogram recorded at EKA from the 27 May 1981 Shagan River explosion.
(b) Seismogram (a) filtered to simulate the effects of an additional t* of 0.2s.
(c) Seismogram (a) after Wiener filtering converted to a phaseless-broad-band instrument response.
(d) Same as seismogram (c) except that the effects of path attenuation of t* = 0.15s have been corrected for.

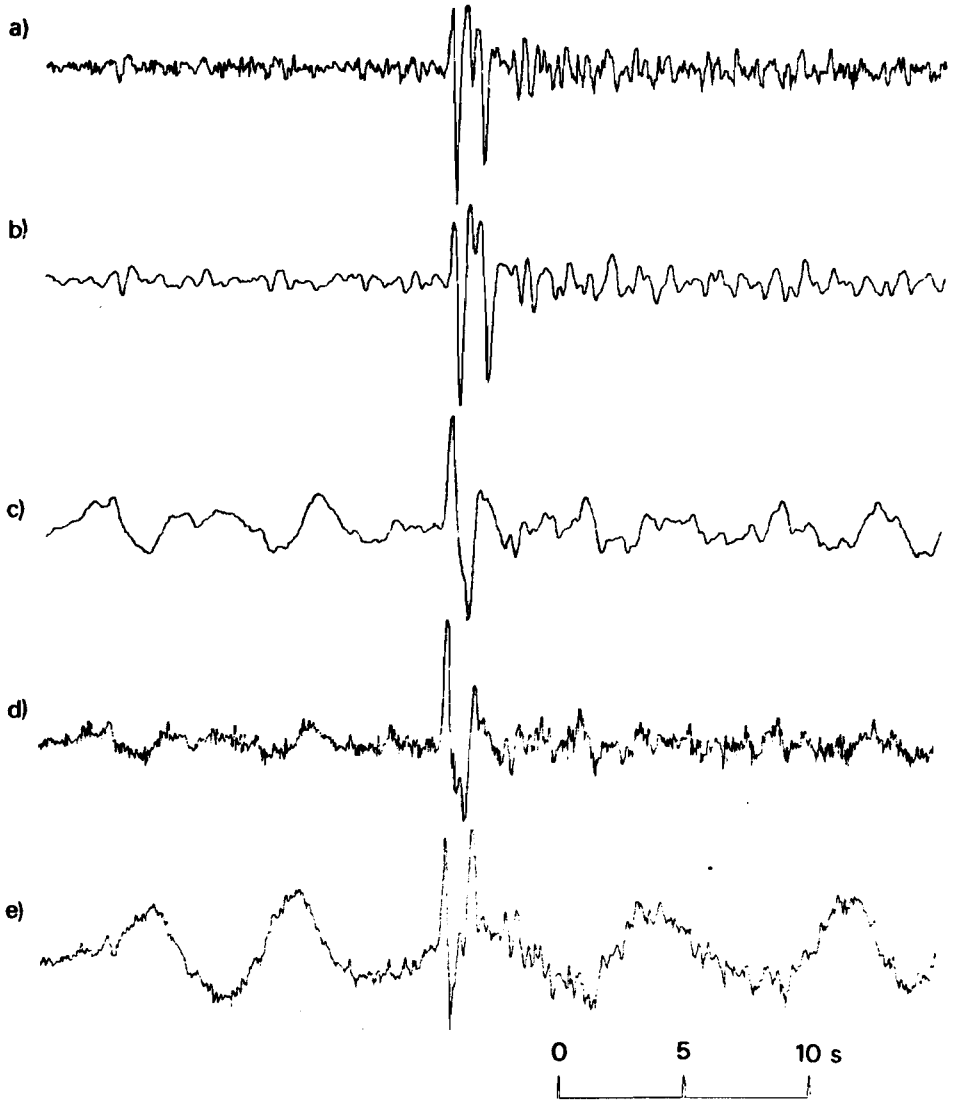

Figure A145 (a) Short-period seismogram that would be recorded at YKA from the 27 May 1981 Shagan River explosion: derived from the velocity-broad-band seismogram (e).
(b) Seismogram (a) filtered to simulate the effects of an additional t* of 0.2s.
(c) Seismogram (a) after Wiener filtering converted to a phaseless-broad-band instrument response.
(d) Same as seismogram (c) except that the effects of path attenuation of t* = 0.15s have been corrected for.
(e) Velocity-broad-band seismogram recorded at YKA.

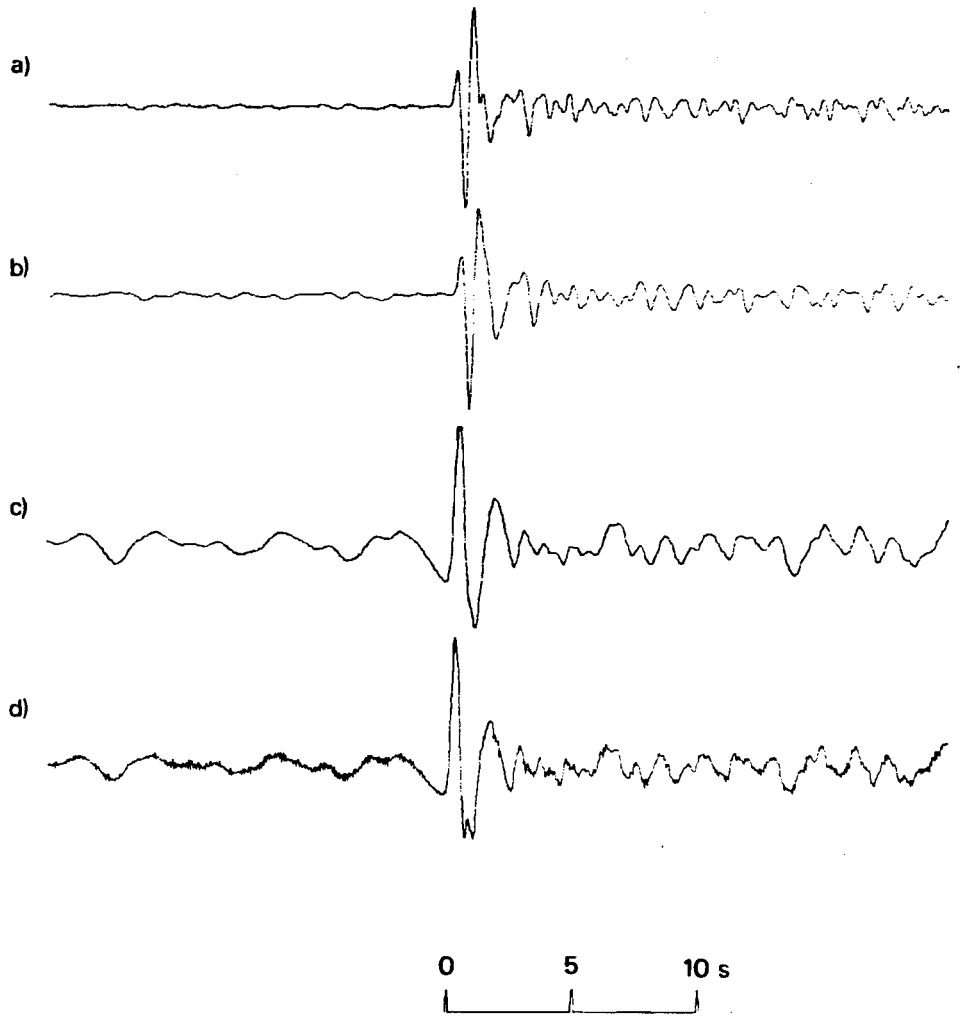

Figure A146 (a) Short-period array-sum seismogram recorded at GBA from the 27 May 1981 Shagan River explosion.
(b) Seismogram (a) filtered to simulate the effects of an additional t* of 0.2s.
(c) Seismogram (a) after Wiener filtering converted to a phaseless-broad-band instrument response.
(d) Same as seismogram (c) except that the effects of path attenuation of t* = 0.15s have been corrected for.

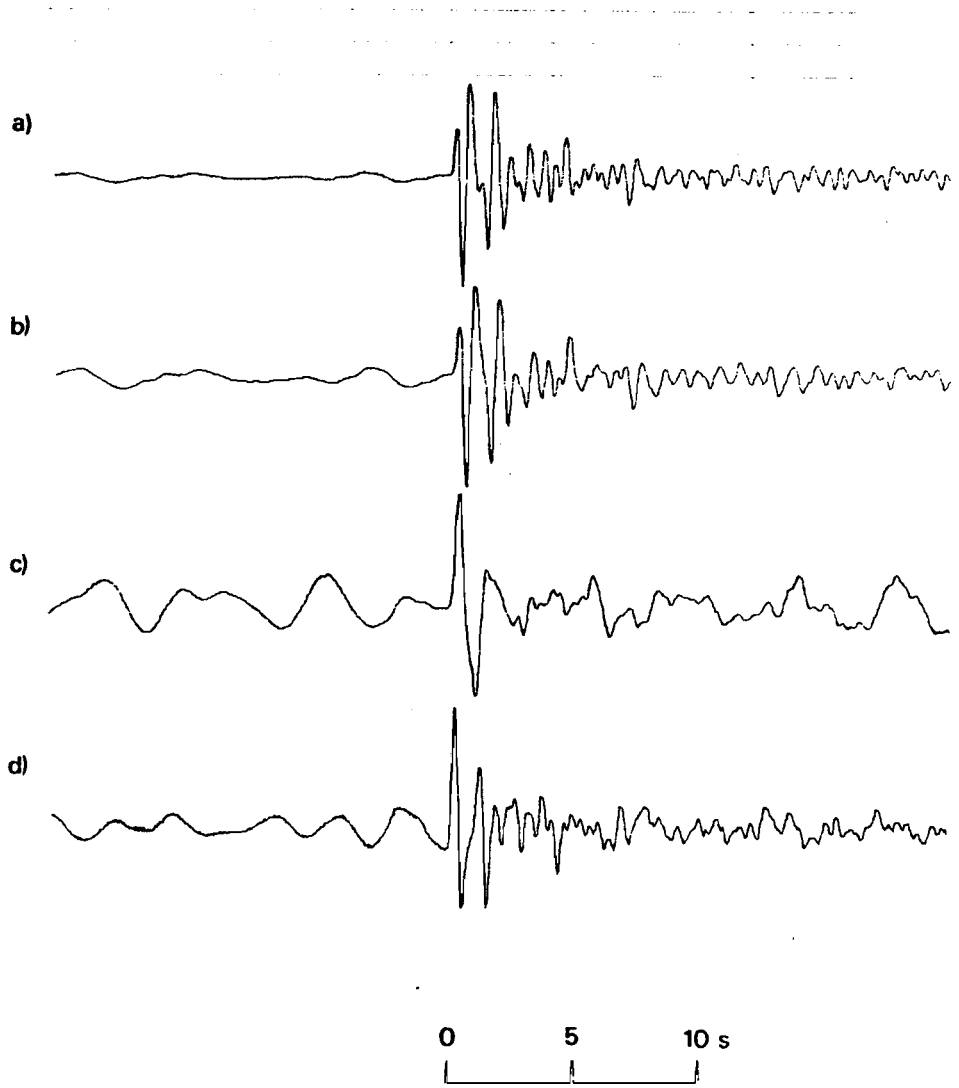

Figure A147 (a) Short-period array-sum seismogram recorded at WRA from the 27 May 1981 Shagan River explosion.
(b) Seismogram (a) filtered to simulate the effects of an additional t* of 0.2s.
(c) Seismogram (a) after Wiener filtering converted to a phaseless-broad-band instrument response.
(d) Same as seismogram (c) except that the effects of path attenuation of t* = 0.15s have been corrected for.
Note that PcP should arrive within a few seconds of P.

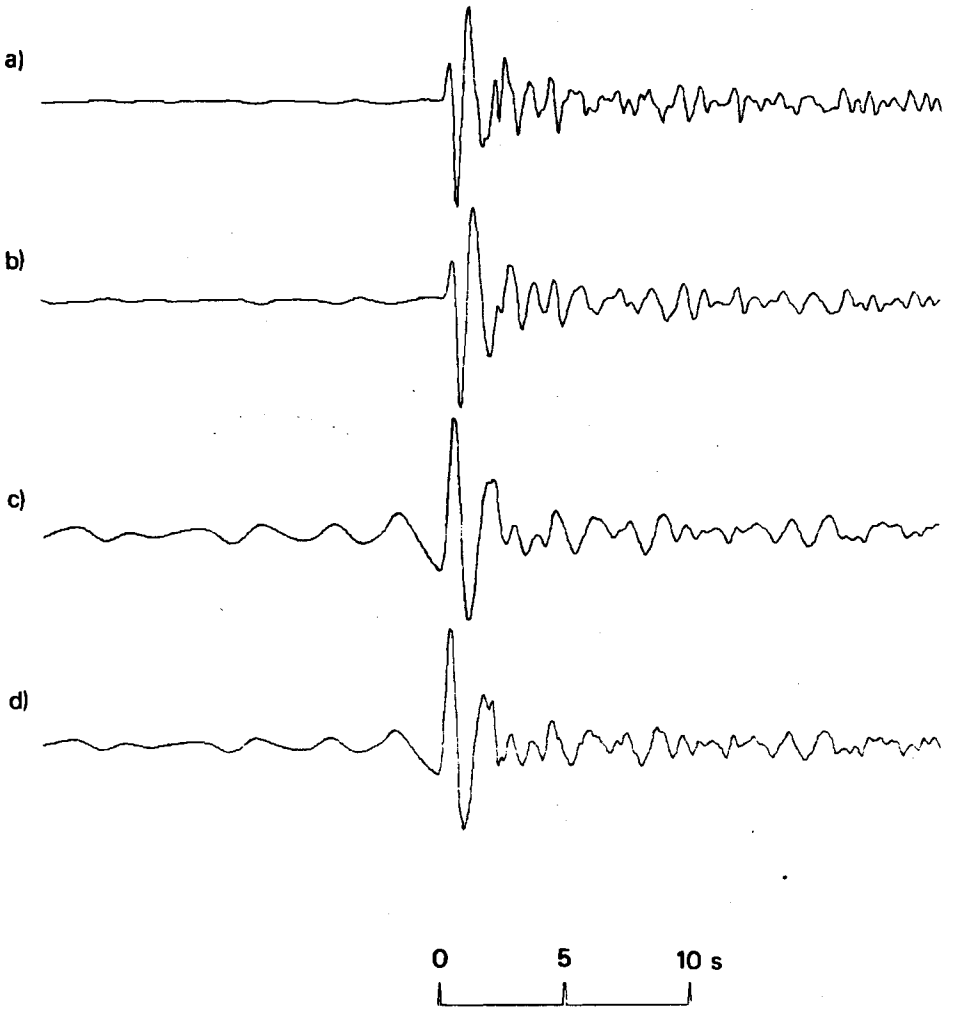

Figure A148 (a) Short-period array-sum seismogram recorded at EKA from the 13 September 1981 Shagan River explosion.
(b) Seismogram (a) filtered to simulate the effects of an additional t* of 0.2s.
(c) Seismogram (a) after Wiener filtering converted to a phaseless-broad-band instrument response.
(d) Same as seismogram (c) except that the effects of path attenuation of t* = 0.15s have been corrected for.

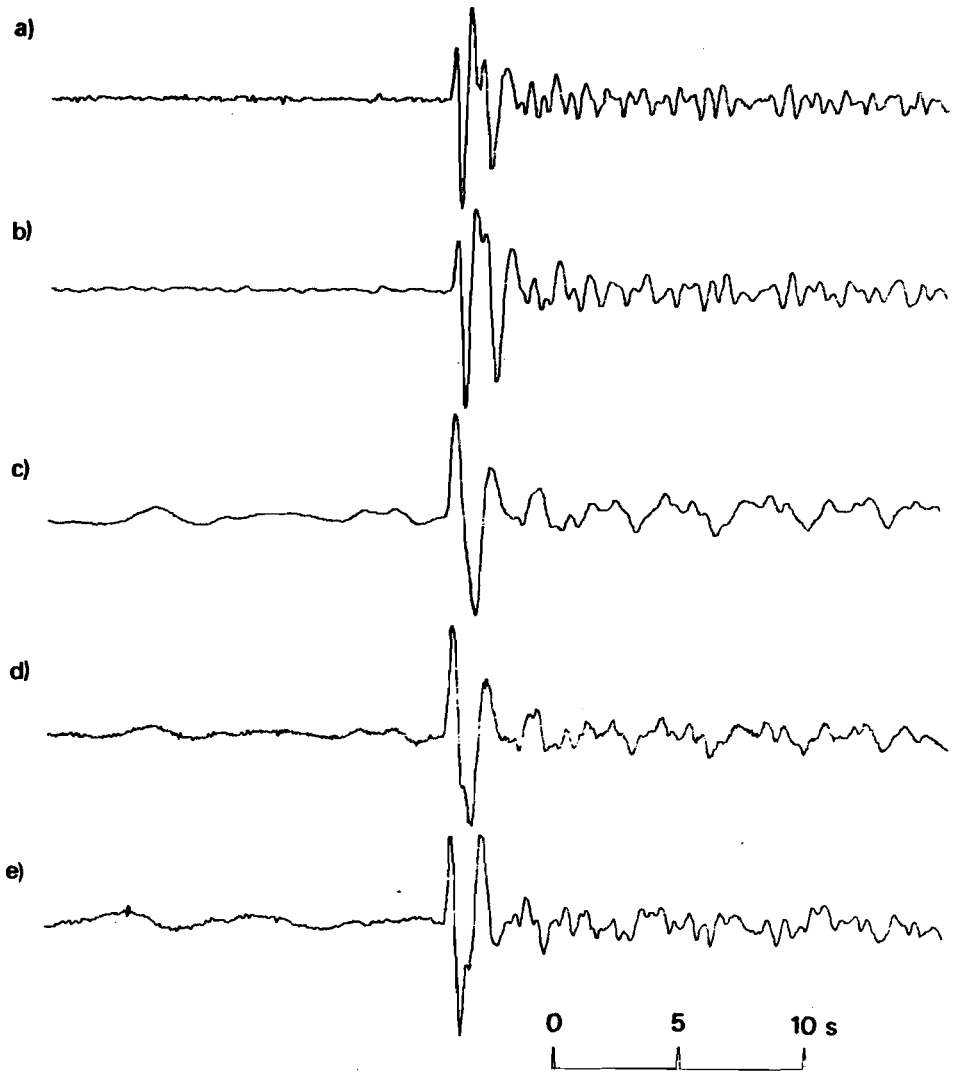

Figure A149 (a) Short-period seismogram that would be recorded at YKA from the 13 September 1981 Shagan River explosion: derived from the velocity-broad-band seismogram (e).
(b) Seismogram (a) filtered to simulate the effects of an additional t* of 0.2s.
(c) Seismogram (a) after Wiener filtering converted to a phaseless-broad-band instrument response.
(d) Same as seismogram (c) except that the effects of path attenuation of t* = 0.15s have been corrected for.
(e) Velocity-broad-band seismogram recorded at YKA.

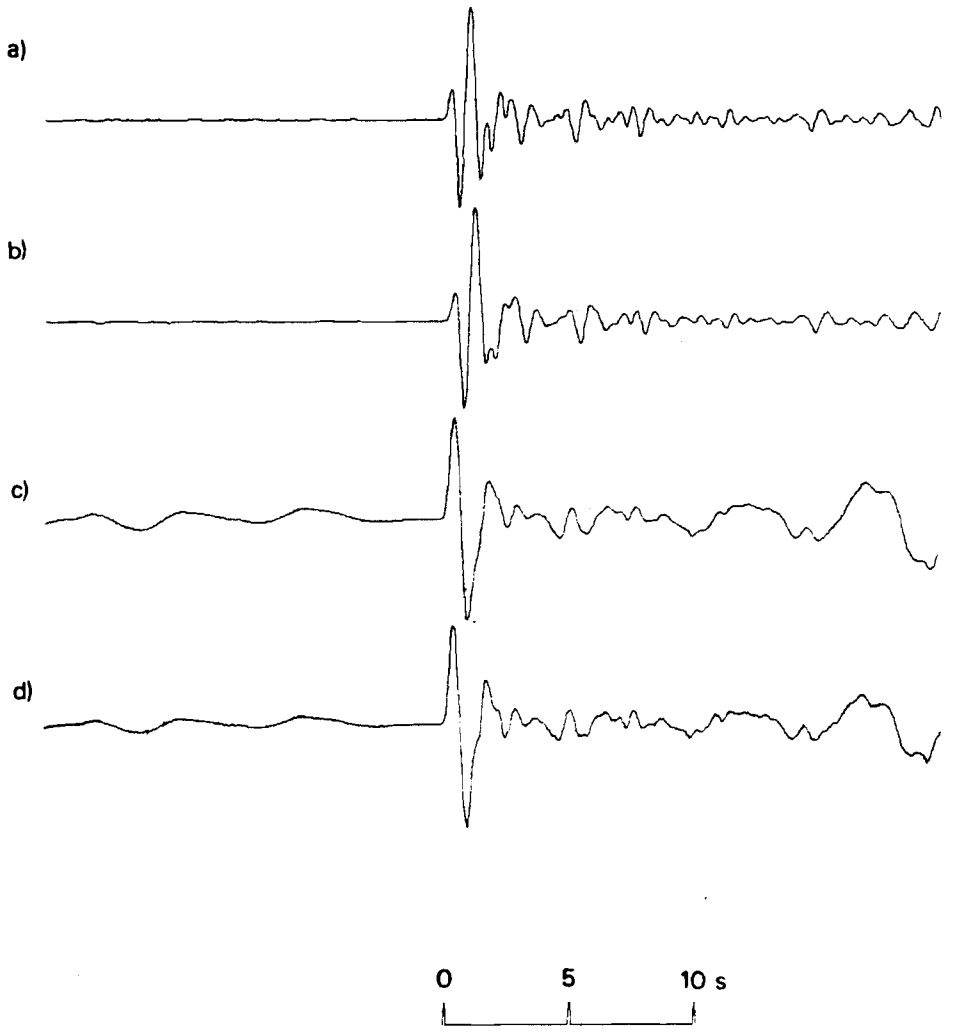

Figure A150 (a) Short-period array-sum seismogram recorded at GBA from the 13 September 1981 Shagan River explosion.
(b) Seismogram (a) filtered to simulate the effects of an additional t* of 0.2s.
(c) Seismogram (a) after Wiener filtering converted to a phaseless-broad-band instrument response.
(d) Same as seismogram (c) except that the effects of path attenuation of t* = 0.15s have been corrected for.

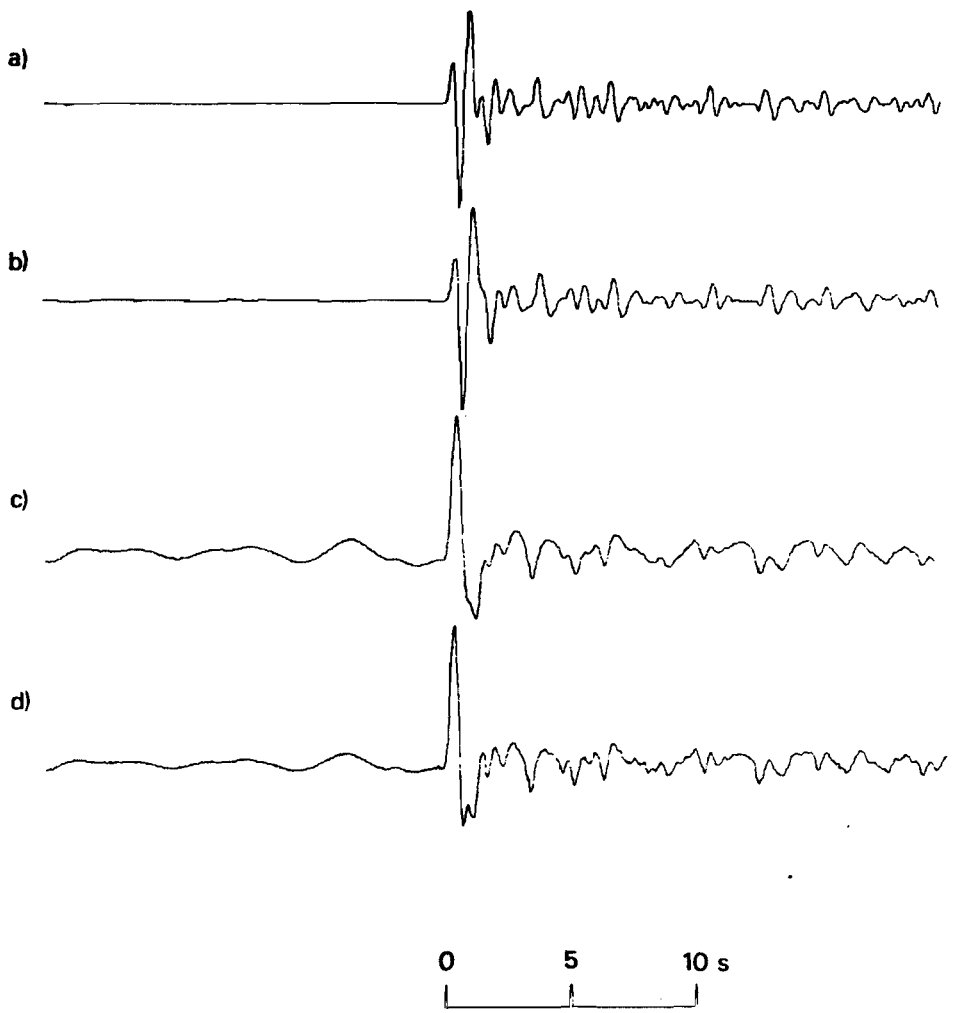

Figure A151 (a) Short-period array-sum seismogram recorded at WRA from the 13 September 1981 Shagan River explosion.
(b) Seismogram (a) filtered to simulate the effects of an additional t* of 0.2s.
(c) Seismogram (a) after Wiener filtering converted to a phaseless-broad-band instrument response.
(d) Same as seismogram (c) except that the effects of path attenuation of t* = 0.15s have been corrected for.
Note that PcP should arrive within a few seconds of P.

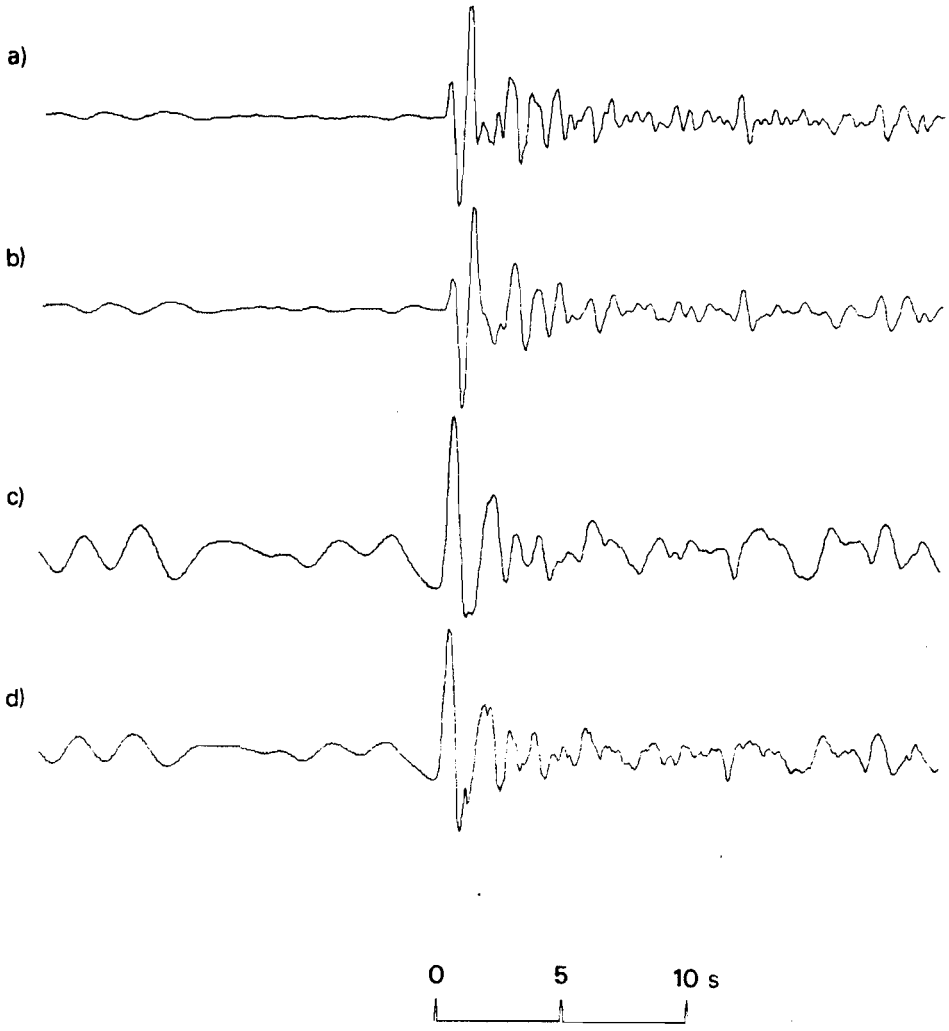

Figure A152 (a) Short-period array-sum seismogram recorded at EKA from the 18 October 1981 Shagan River explosion.
(b) Seismogram (a) filtered to simulate the effects of an additional t* of 0.2s.
(c) Seismogram (a) after Wiener filtering converted to a phaseless-broad-band instrument response.
(d) Same as seismogram (c) except that the effects of path attenuation of t* = 0.15s have been corrected for.

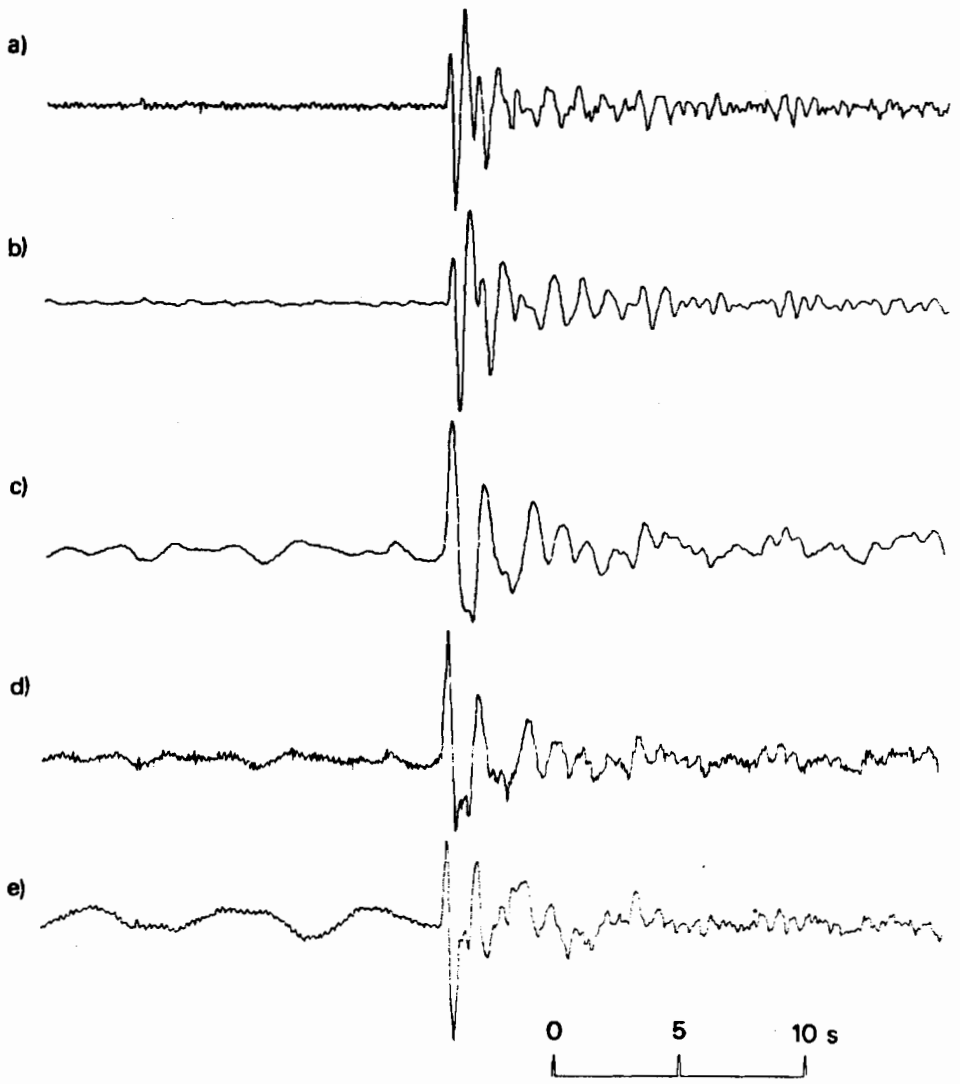

Figure A153 (a) Short-period seismogram that would be recorded at YKA from the 18 October 1981 Shagan River explosion: derived from the velocity-broad-band seismogram (e).
(b) Seismogram (a) filtered to simulate the effects of an additional t* of 0.2s.
(c) Seismogram (a) after Wiener filtering converted to a phaseless-broad-band instrument response.
(d) Same as seismogram (c) except that the effects of path attenuation of t* = 0.15s have been corrected for.
(e) Velocity-broad-band seismogram recorded at YKA.

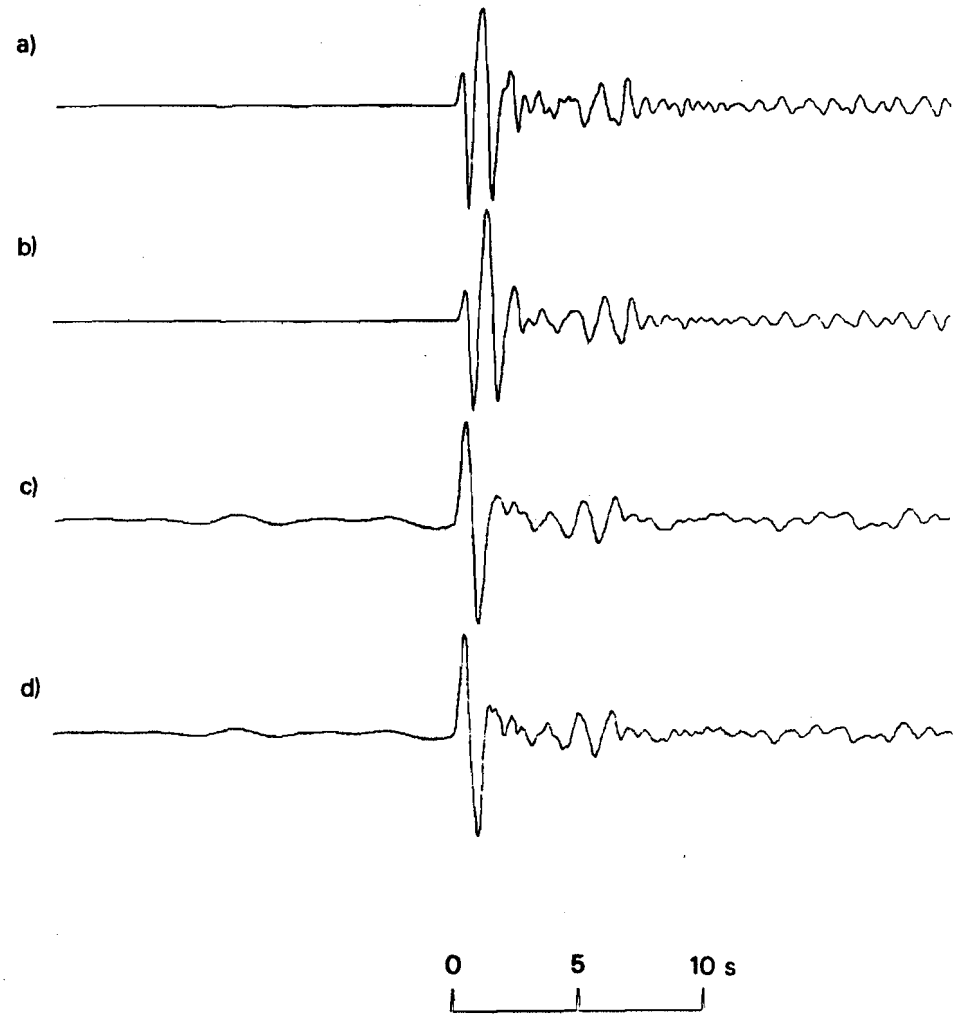

Figure A154 (a) Short-period array-sum seismogram recorded at GBA from the 18 October 1981 Shagan River explosion.
(b) Seismogram (a) filtered to simulate the effects of an additional t^* of 0.2s.
(c) Seismogram (a) after Wiener filtering converted to a phaseless-broad-band instrument response.
(d) Same as seismogram (c) except that the effects of path attenuation of $t^* = 0.15$s have been corrected for.

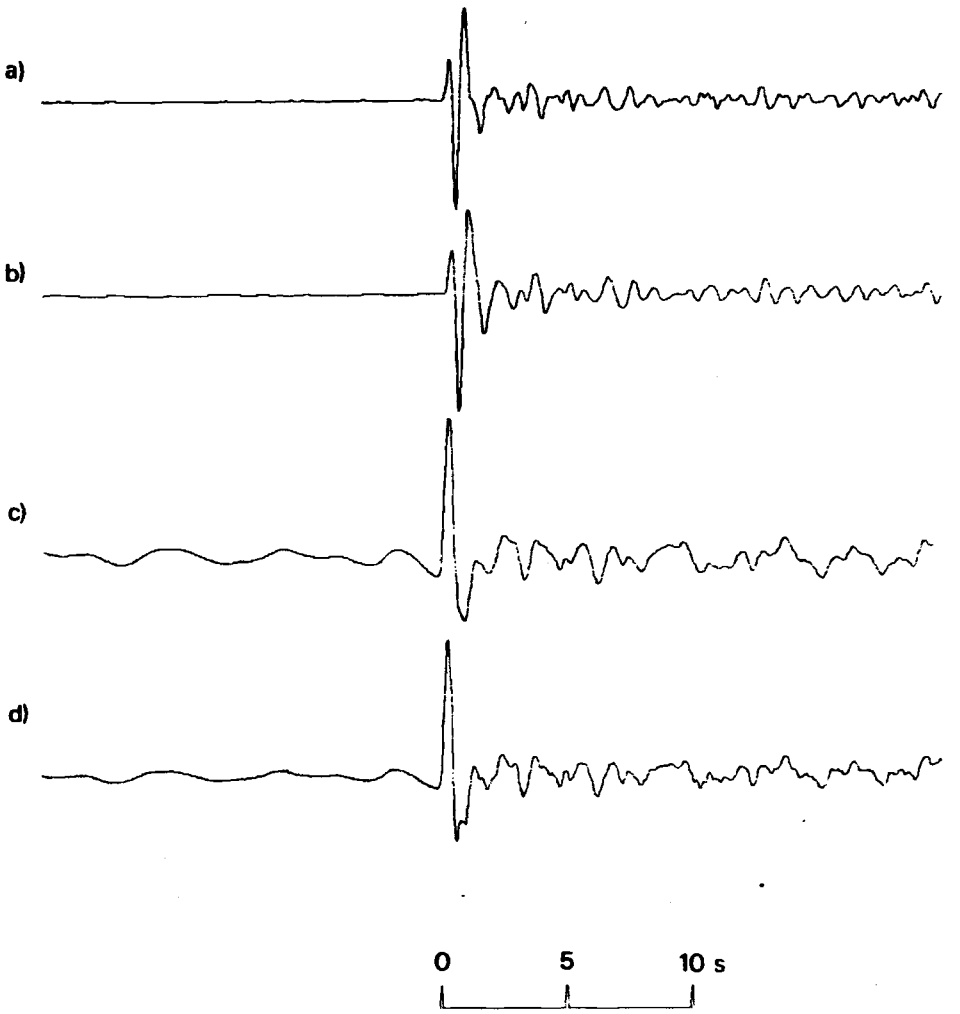

Figure A155 (a) Short-period array-sum seismogram recorded at WRA from the 18 October 1981 Shagan River explosion.
(b) Seismogram (a) filtered to simulate the effects of an additional t^* of 0.2s.
(c) Seismogram (a) after Wiener filtering converted to a phaseless-broad-band instrument response.
(d) Same as seismogram (c) except that the effects of path attenuation of $t^* = 0.15$s have been corrected for.
Note that PcP should arrive within a few seconds of P.

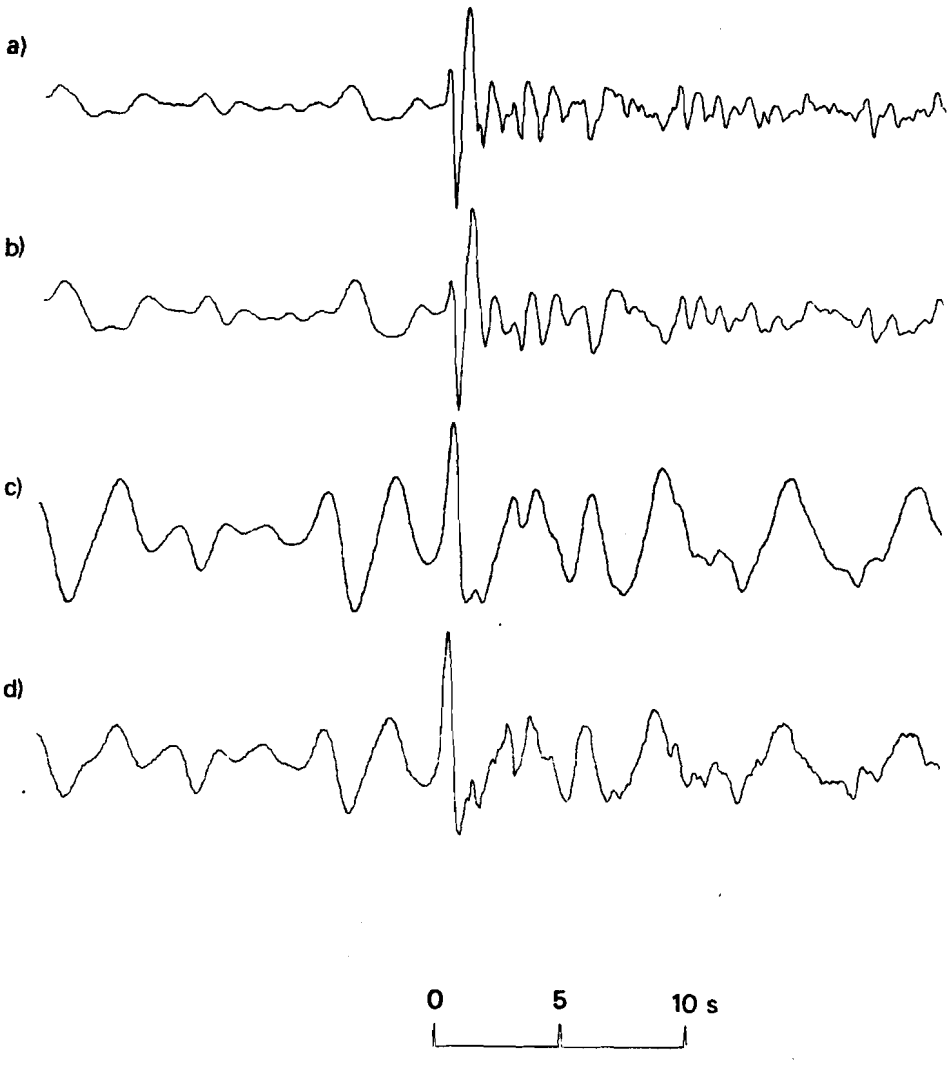

Figure A156 (a) Short-period array-sum seismogram recorded at EKA from the 29 November 1981 Shagan River explosion.
(b) Seismogram (a) filtered to simulate the effects of an additional t* of 0.2s.
(c) Seismogram (a) after Wiener filtering converted to a phaseless-broad-band instrument response.
(d) Same as seismogram (c) except that the effects of path attenuation of t* = 0.15s have been corrected for.

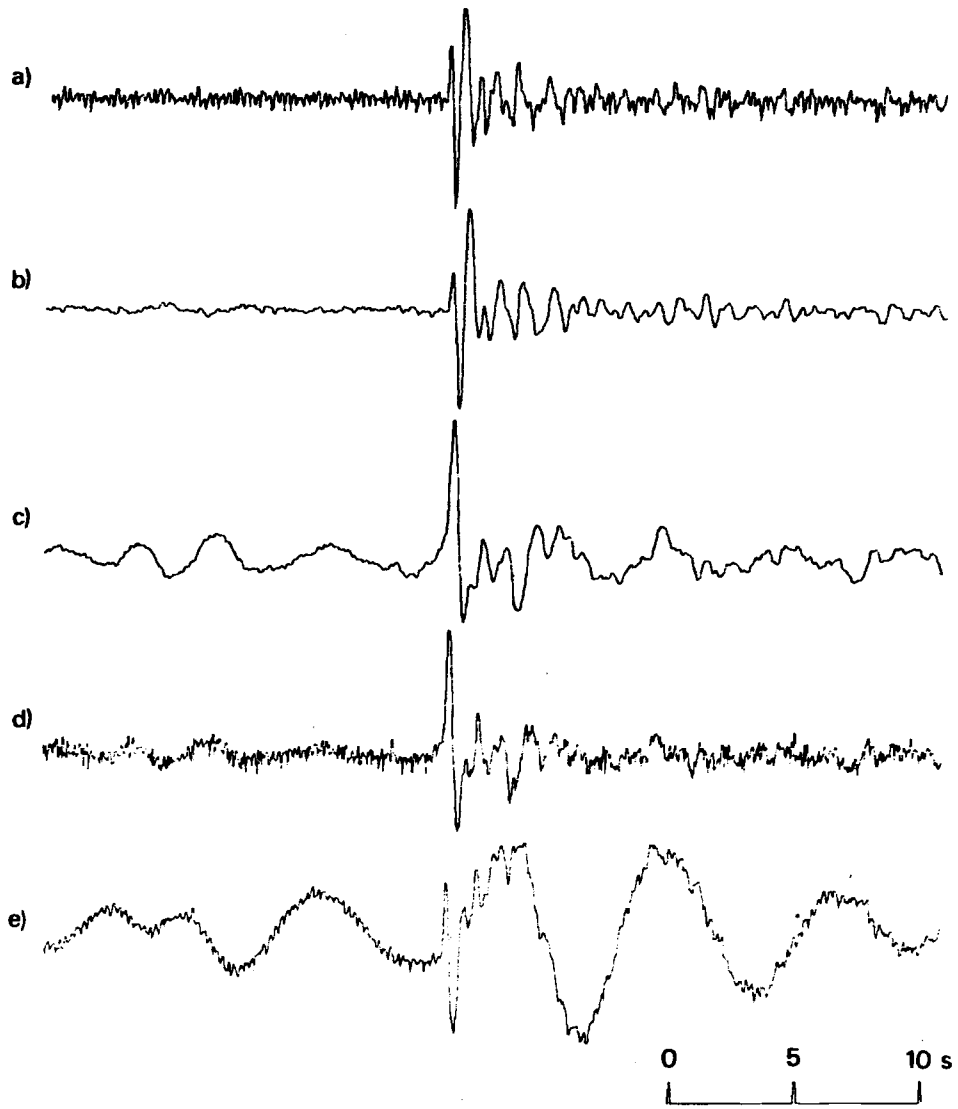

Figure A157 (a) Short-period seismogram that would be recorded at YKA from the 29 November 1981 Shagan River explosion: derived from the velocity-broad-band seismogram (e).
(b) Seismogram (a) filtered to simulate the effects of an additional t* of 0.2s.
(c) Seismogram (a) after Wiener filtering converted to a phaseless-broad-band instrument response.
(d) Same as seismogram (c) except that the effects of path attenuation of t* = 0.15s have been corrected for.
(e) Velocity-broad-band seismogram recorded at YKA.

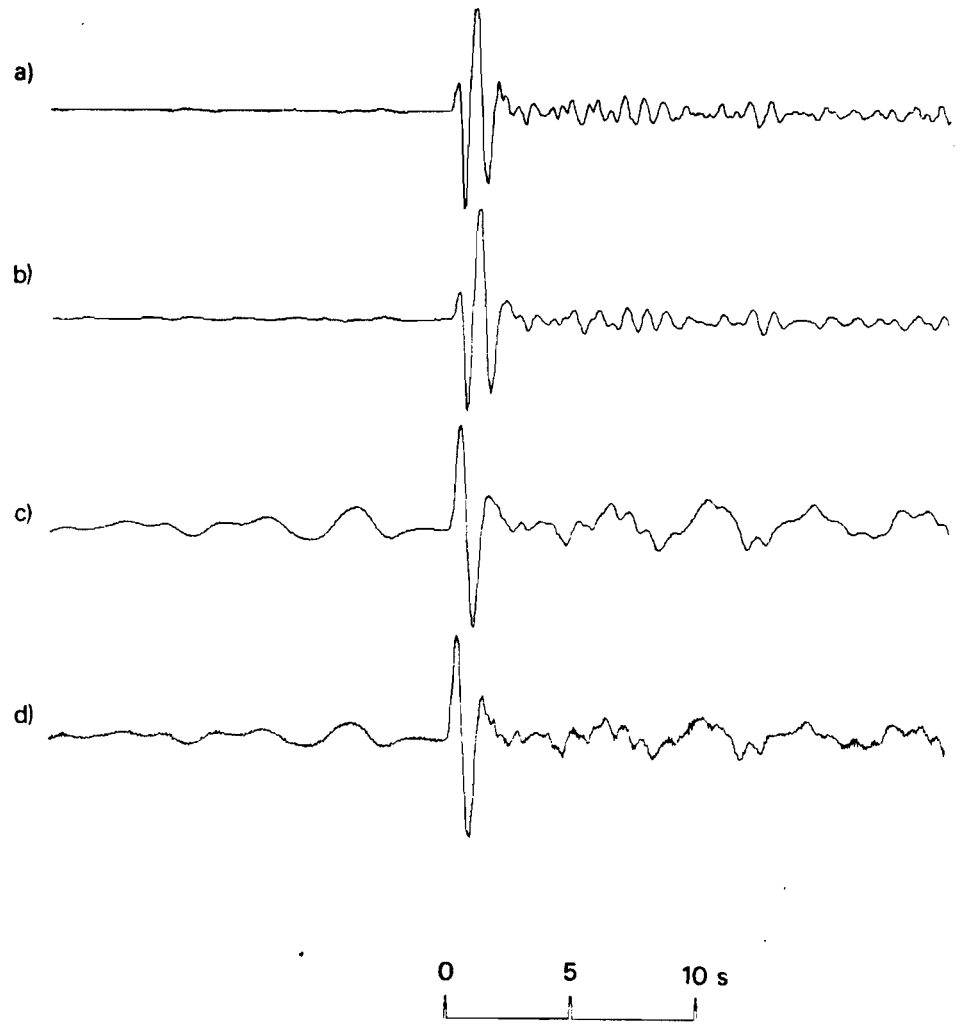

Figure A158 (a) Short-period array-sum seismogram recorded at GBA from the 29 November 1981 Shagan River explosion.
(b) Seismogram (a) filtered to simulate the effects of an additional t* of 0.2s.
(c) Seismogram (a) after Wiener filtering converted to a phaseless-broad-band instrument response.
(d) Same as seismogram (c) except that the effects of path attenuation of t* = 0.15s have been corrected for.

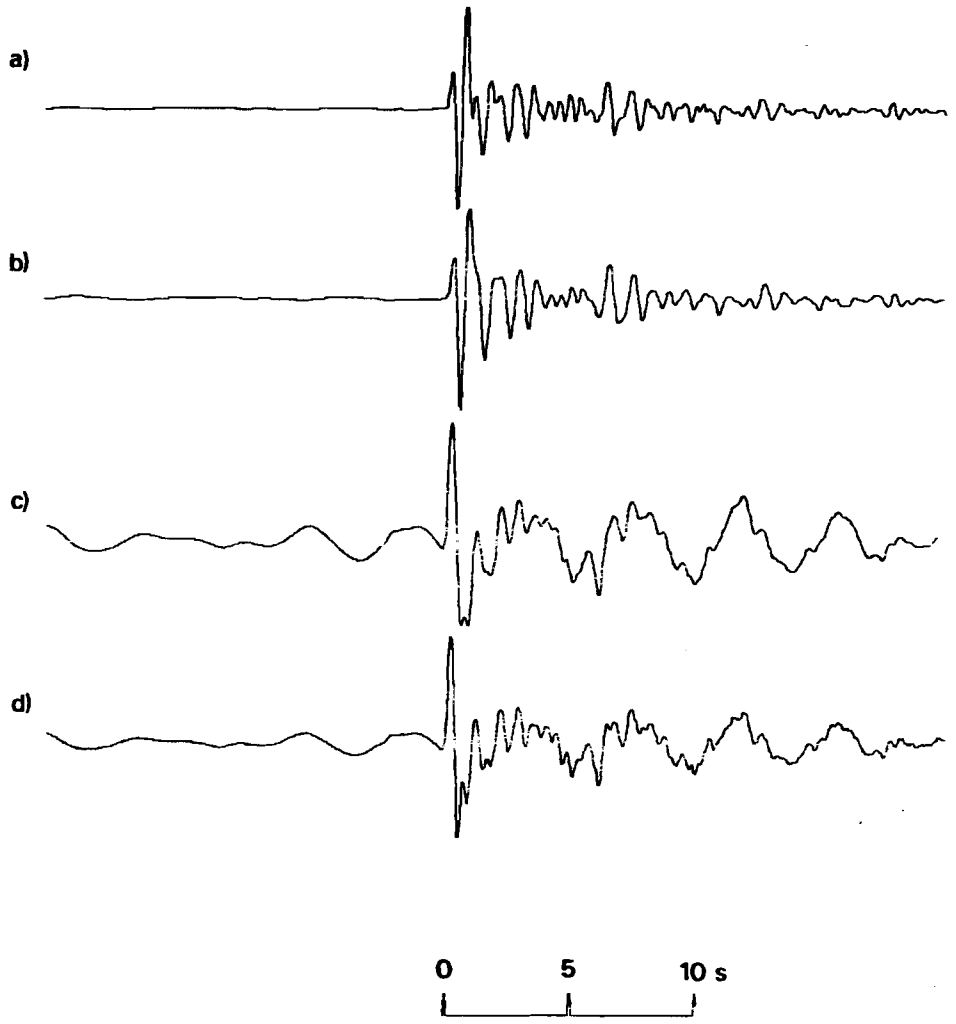

Figure A159 (a) Short-period array-sum seismogram recorded at WRA from the 29 November 1981 Shagan River explosion.
(b) Seismogram (a) filtered to simulate the effects of an additional t* of 0.2s.
(c) Seismogram (a) after Wiener filtering converted to a phaseless-broad-band instrument response.
(d) Same as seismogram (c) except that the effects of path attenuation of t* = 0.15s have been corrected for.
Note that PcP should arrive within a few seconds of P.

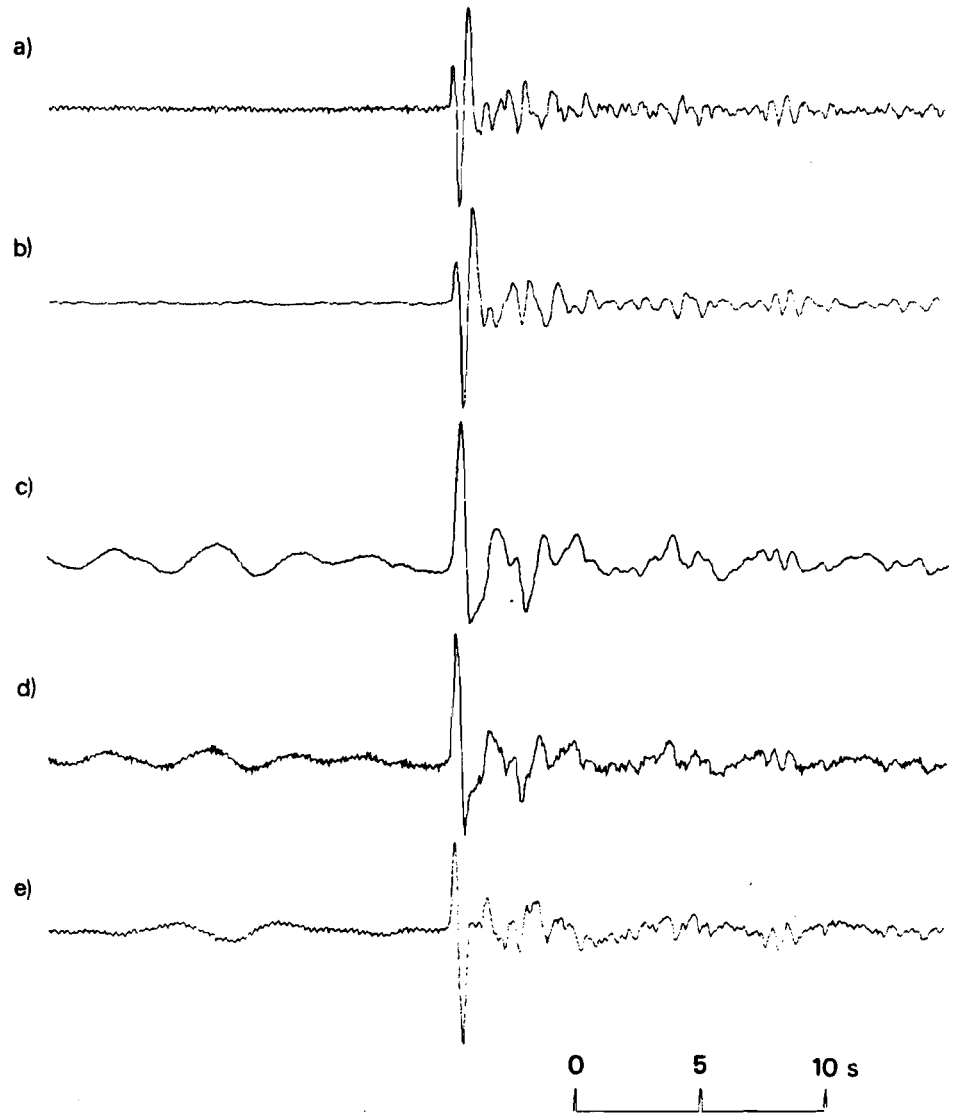

Figure A160 (a) Short-period seismogram that would be recorded at YKA from the 27 December 1981 Shagan River explosion: derived from the velocity-broad-band seismogram (e).
(b) Seismogram (a) filtered to simulate the effects of an additional t* of 0.2s.
(c) Seismogram (a) after Wiener filtering converted to a phaseless-broad-band instrument response.
(d) Same as seismogram (c) except that the effects of path attenuation of t* = 0.15s have been corrected for.
(e) Velocity-broad-band seismogram recorded at YKA.

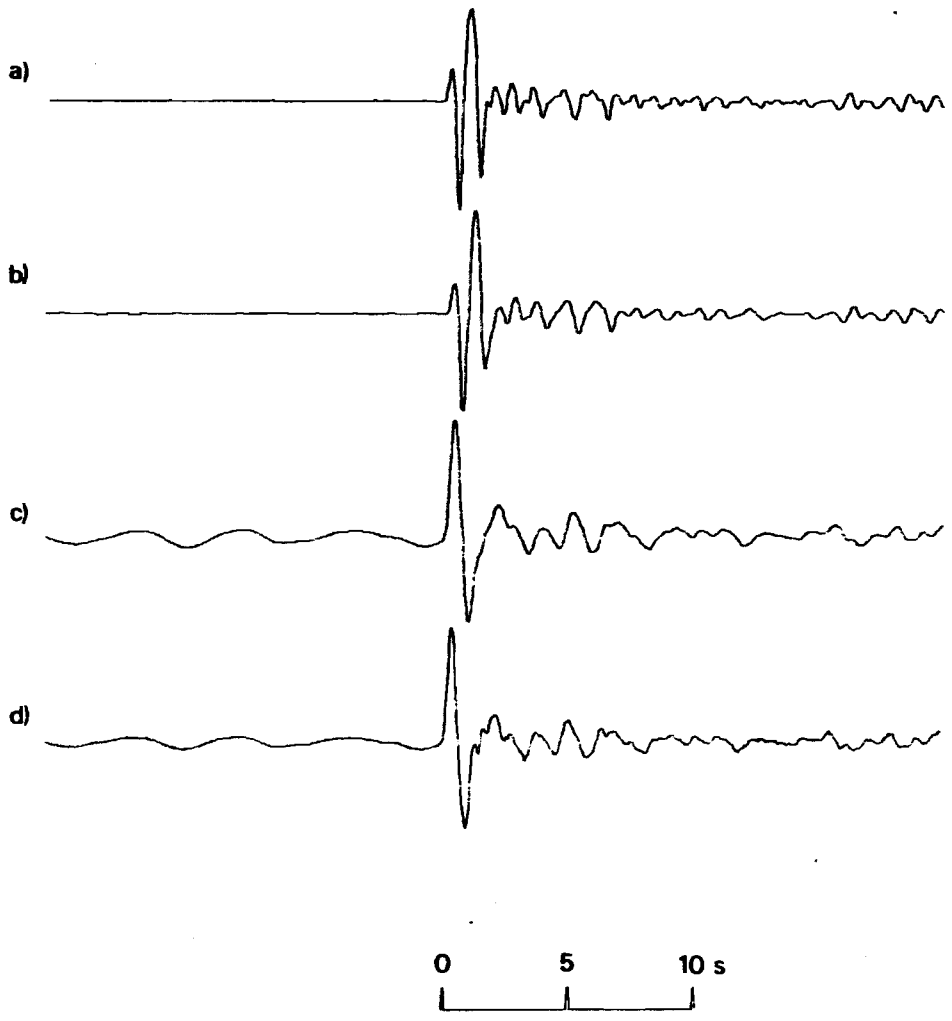

Figure A161 (a) Short-period array-sum seismogram recorded at GBA from the 27 December 1981 Shagan River explosion.
(b) Seismogram (a) filtered to simulate the effects of an additional t* of 0.2s.
(c) Seismogram (a) after Wiener filtering converted to a phaseless-broad-band instrument response.
(d) Same as seismogram (c) except that the effects of path attenuation of t* = 0.15s have been corrected for.

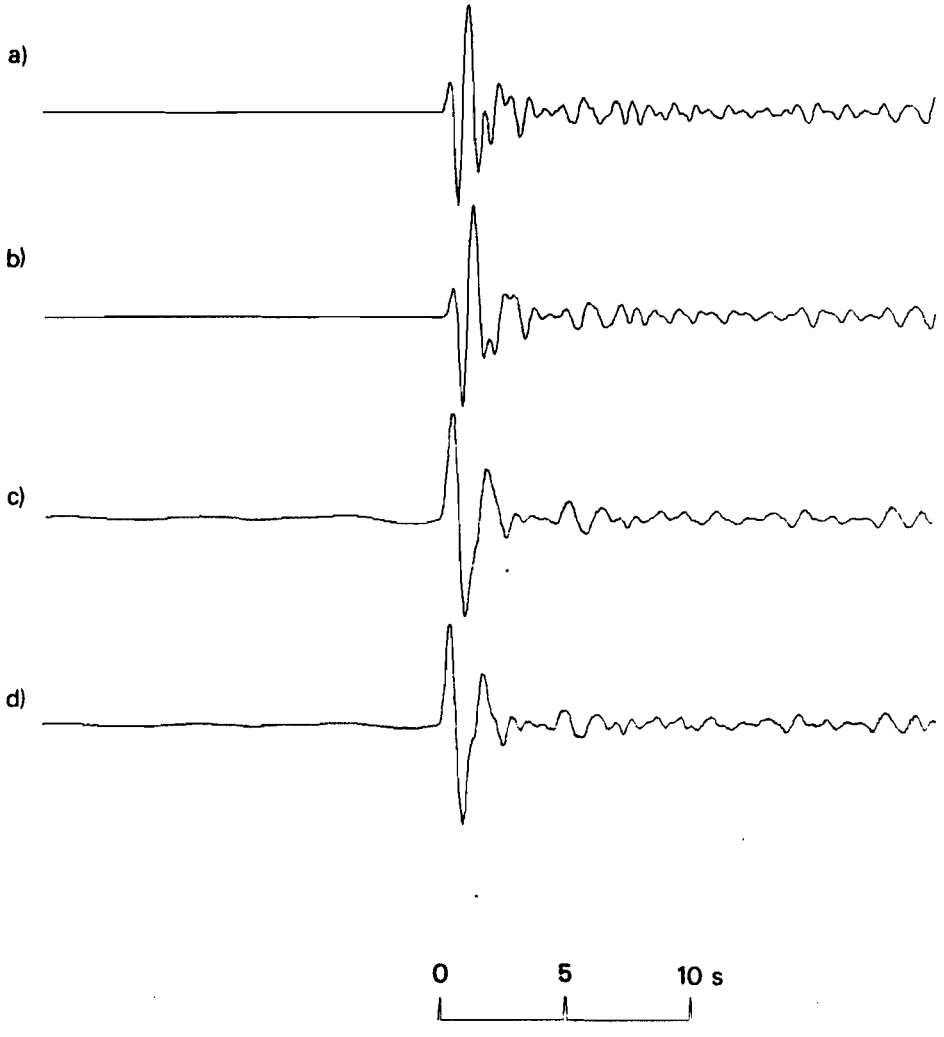

Figure A162 (a) Short-period array-sum seismogram recorded at GBA from the 25 April 1982 Shagan River explosion.
(b) Seismogram (a) filtered to simulate the effects of an additional t* of 0.2s.
(c) Seismogram (a) after Wiener filtering converted to a phaseless-broad-band instrument response.
(d) Same as seismogram (c) except that the effects of path attenuation of t* = 0.15s have been corrected for.

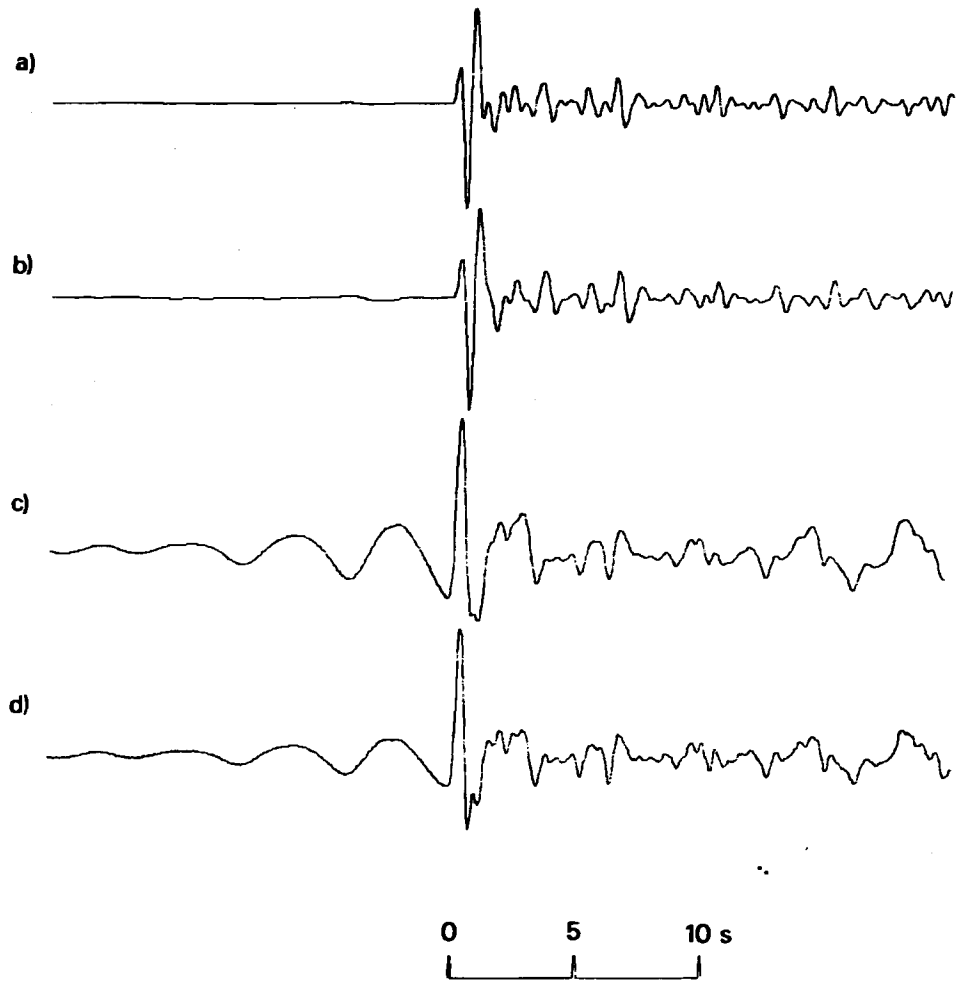

Figure A163 (a) Short-period array-sum seismogram recorded at WRA from the 25 April 1982 Shagan River explosion.
(b) Seismogram (a) filtered to simulate the effects of an additional t* of 0.2s.
(c) Seismogram (a) after Wiener filtering converted to a phaseless-broad-band instrument response.
(d) Same as seismogram (c) except that the effects of path attenuation of t* = 0.15s have been corrected for.
Note that PcP should arrive within a few seconds of P.

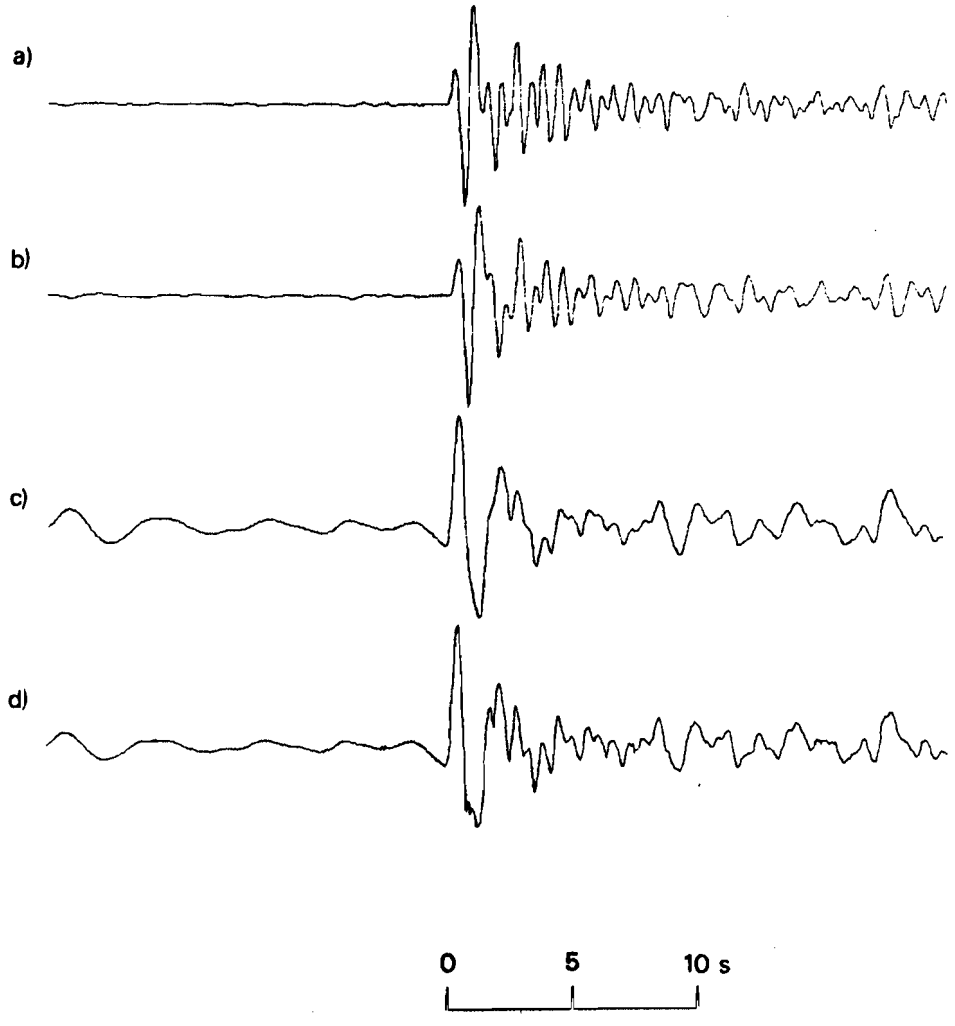

Figure A164 (a) Short-period array-sum seismogram recorded at EKA from the 4 July 1982 Shagan River explosion.
(b) Seismogram (a) filtered to simulate the effects of an additional t* of 0.2s.
(c) Seismogram (a) after Wiener filtering converted to a phaseless-broad-band instrument response.
(d) Same as seismogram (c) except that the effects of path attenuation of t* = 0.15s have been corrected for.

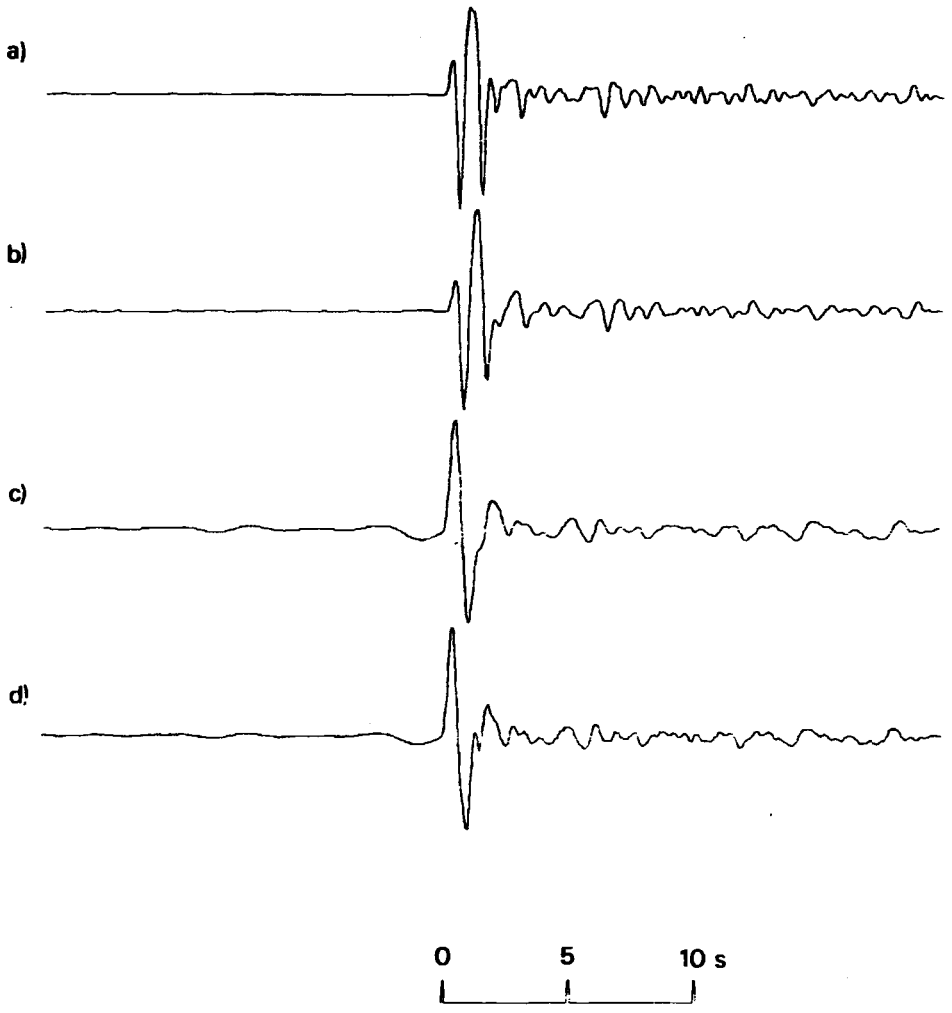

Figure A165 (a) Short-period array-sum seismogram recorded at GBA from the 4 July 1982 Shagan River explosion.
(b) Seismogram (a) filtered to simulate the effects of an additional t* of 0.2s.
(c) Seismogram (a) after Wiener filtering converted to a phaseless-broad-band instrument response.
(d) Same as seismogram (c) except that the effects of path attenuation of t* = 0.15s have been corrected for.

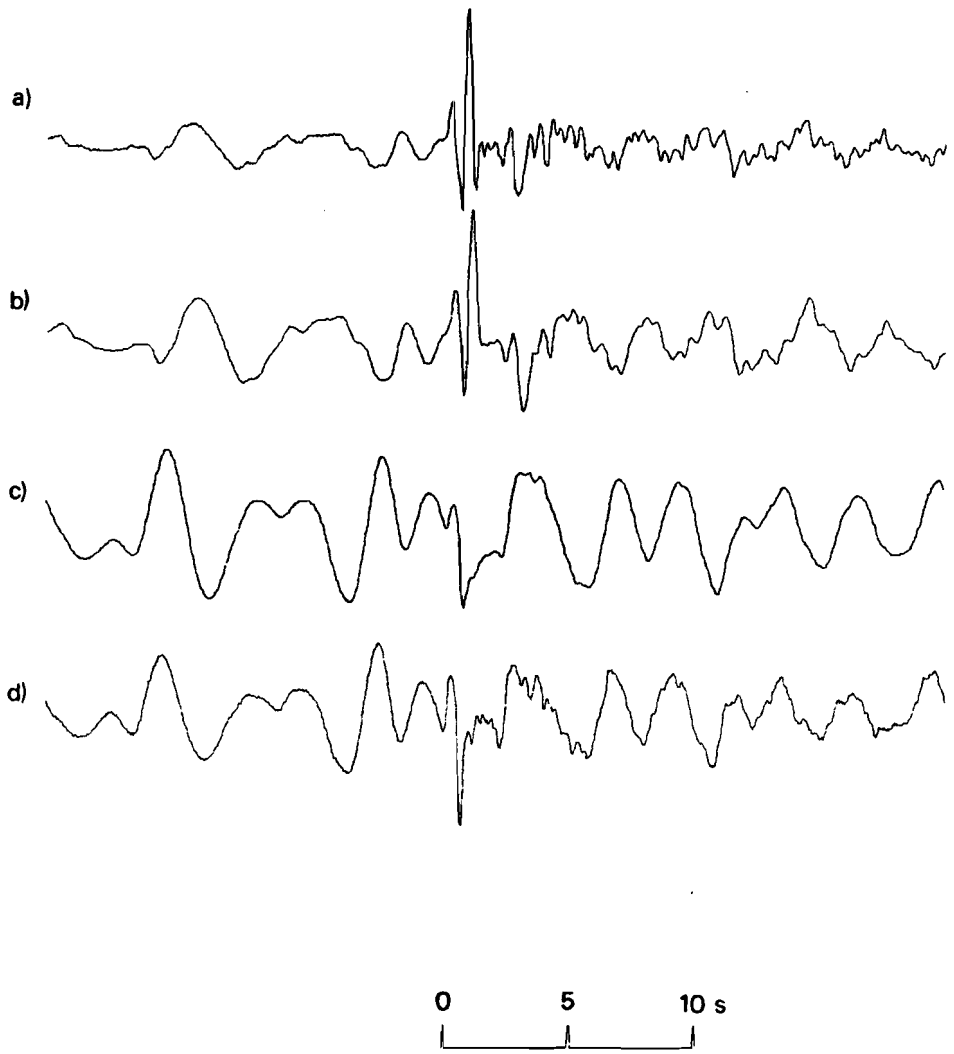

Figure A166 (a) Short-period array-sum seismogram recorded at EKA from the 31 August 1982 Shagan River explosion.
(b) Seismogram (a) filtered to simulate the effects of an additional t* of 0.2s.
(c) Seismogram (a) after Wiener filtering converted to a phaseless-broad-band instrument response.
(d) Same as seismogram (c) except that the effects of path attenuation of t* = 0.15s have been corrected for.

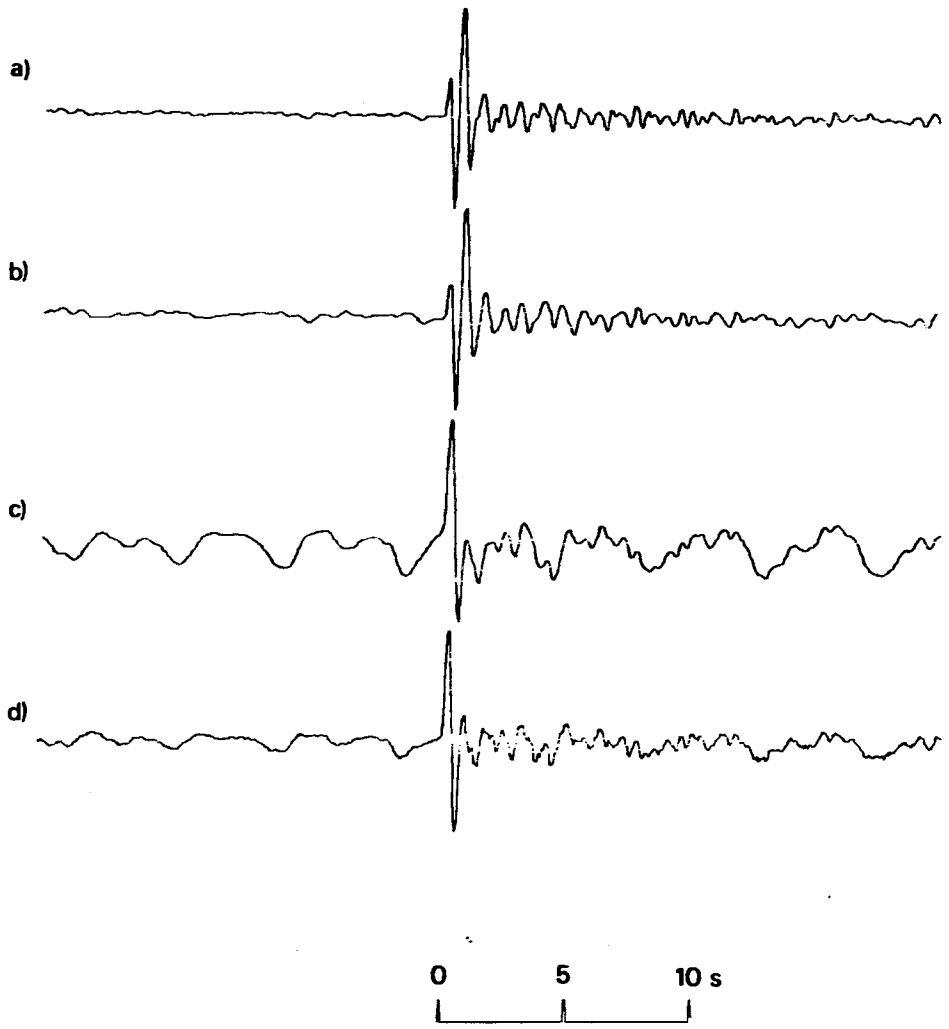

Figure A167 (a) Short-period array-sum seismogram recorded at YKA from the 31 August 1982 Shagan River explosion.
(b) Seismogram (a) filtered to simulate the effects of an additional t* of 0.2s.
(c) Seismogram (a) after Wiener filtering converted to a phaseless-broad-band instrument response.
(d) Same as seismogram (c) except that the effects of path attenuation of t* = 0.15s have been corrected for.

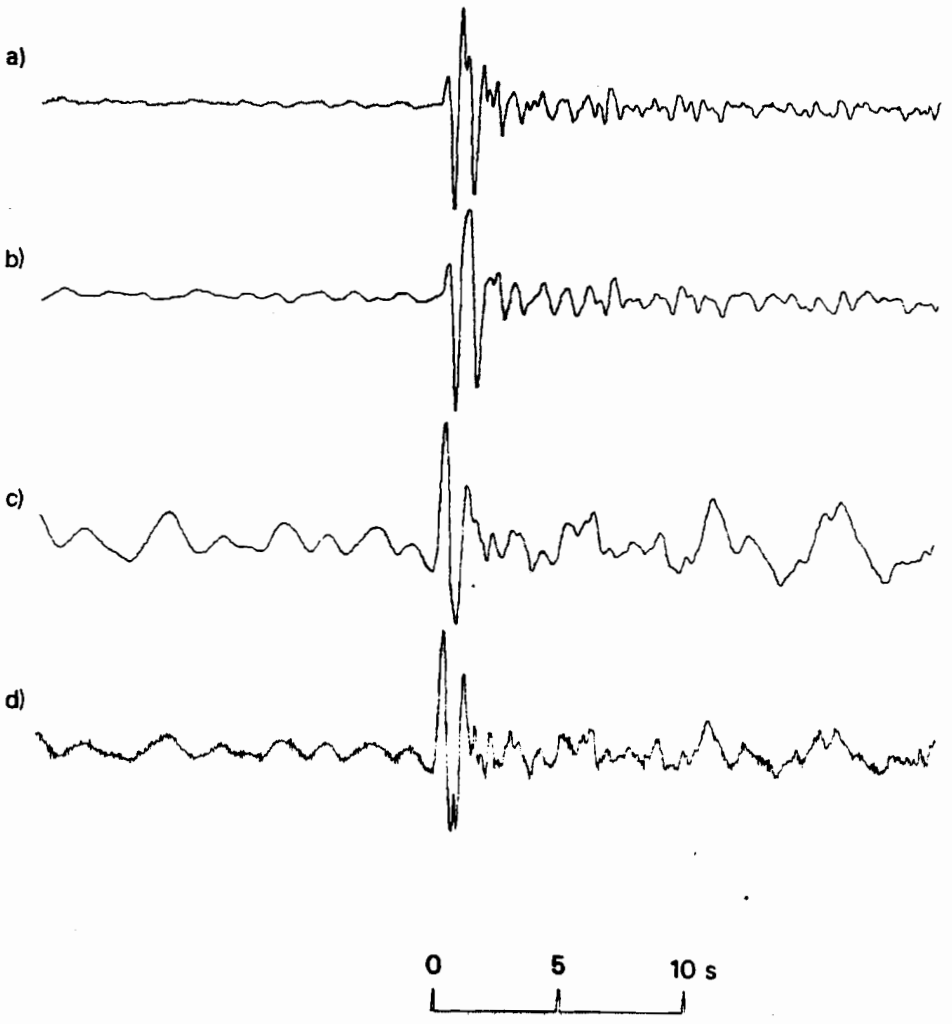

Figure A168 (a) Short-period array-sum seismogram recorded at GBA from the 31 August 1982 Shagan River explosion.
(b) Seismogram (a) filtered to simulate the effects of an additional t* of 0.2s.
(c) Seismogram (a) after Wiener filtering converted to a phaseless-broad-band instrument response.
(d) Same as seismogram (c) except that the effects of path attenuation of t* = 0.15s have been corrected for.

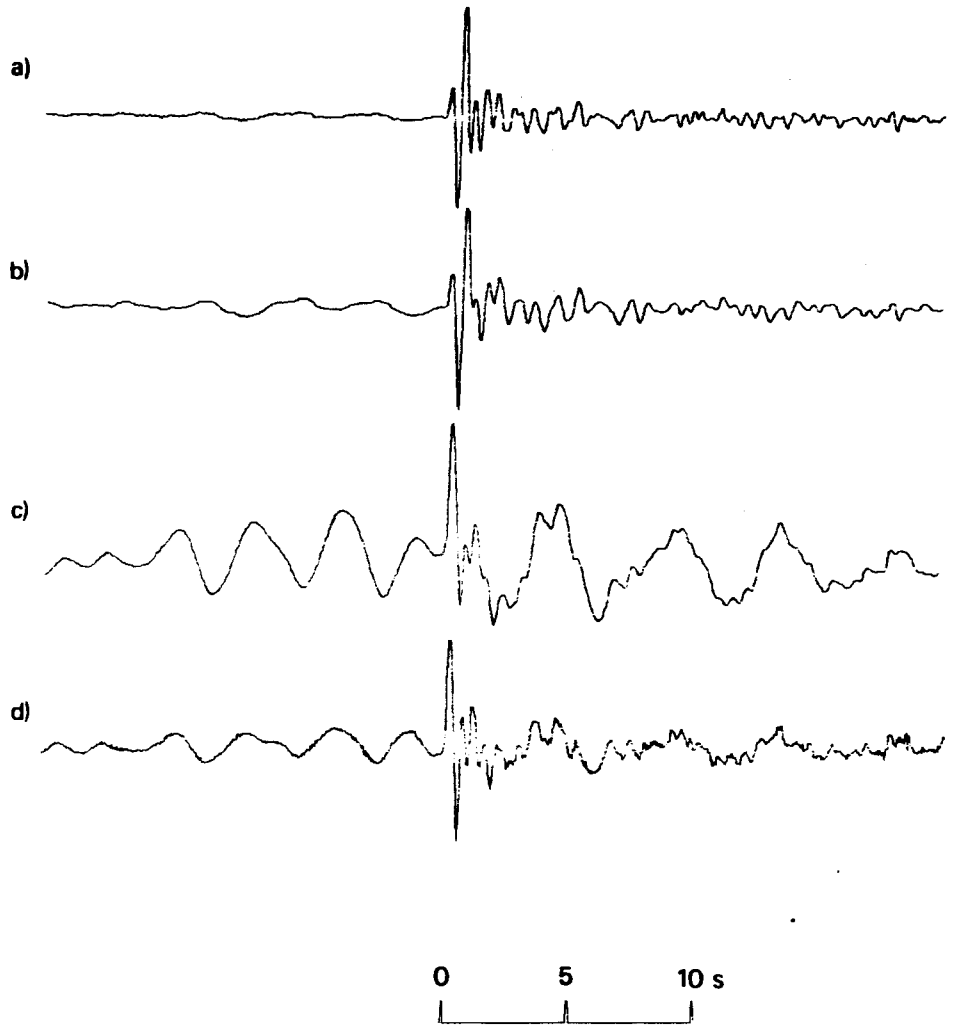

Figure A169 (a) Short-period array-sum seismogram recorded at WRA from the 31 August 1982 Shagan River explosion.
(b) Seismogram (a) filtered to simulate the effects of an additional t* of 0.2s.
(c) Seismogram (a) after Wiener filtering converted to a phaseless-broad-band instrument response.
(d) Same as seismogram (c) except that the effects of path attenuation of t* = 0.15s have been corrected for.
Note that PcP should arrive within a few seconds of P.

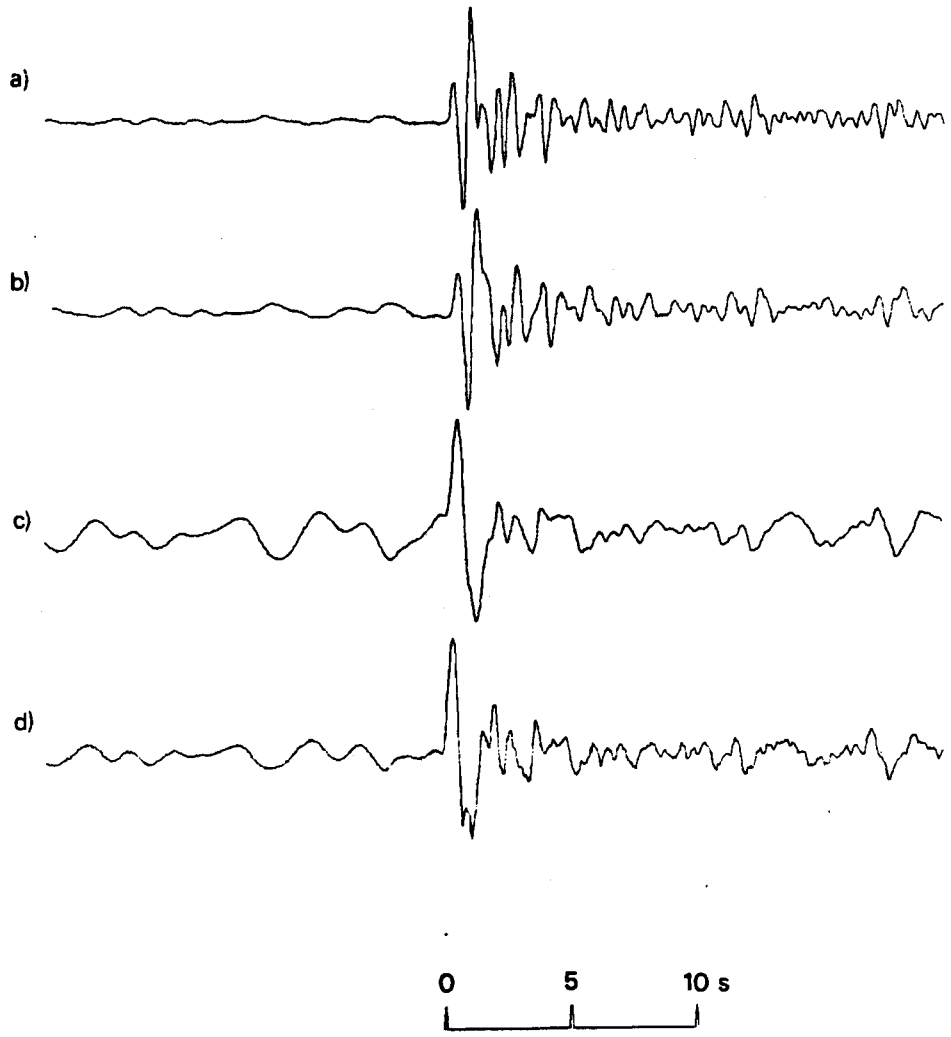

Figure A170 (a) Short-period array-sum seismogram recorded at EKA from the 5 December 1982 Shagan River explosion.
(b) Seismogram (a) filtered to simulate the effects of an additional t* of 0.2s.
(c) Seismogram (a) after Wiener filtering converted to a phaseless-broad-band instrument response.
(d) Same as seismogram (c) except that the effects of path attenuation of t* = 0.15s have been corrected for.

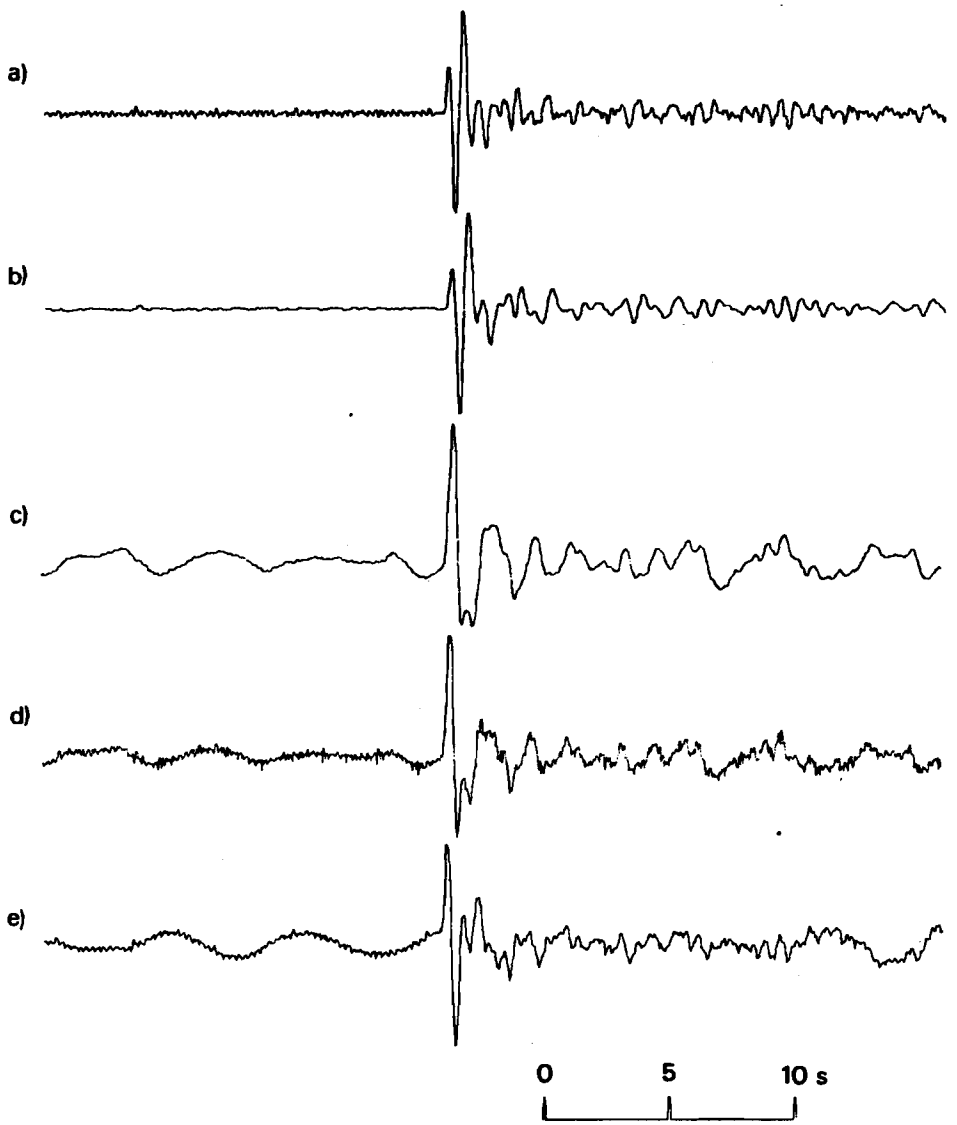

Figure A171 (a) Short-period seismogram that would be recorded at YKA from the 5 December 1982 Shagan River explosion: derived from the velocity-broad-band seismogram (e).
(b) Seismogram (a) filtered to simulate the effects of an additional t* of 0.2s.
(c) Seismogram (a) after Wiener filtering converted to a phaseless-broad-band instrument response.
(d) Same as seismogram (c) except that the effects of path attenuation of t* = 0.15s have been corrected for.
(e) Velocity-broad-band seismogram recorded at YKA.

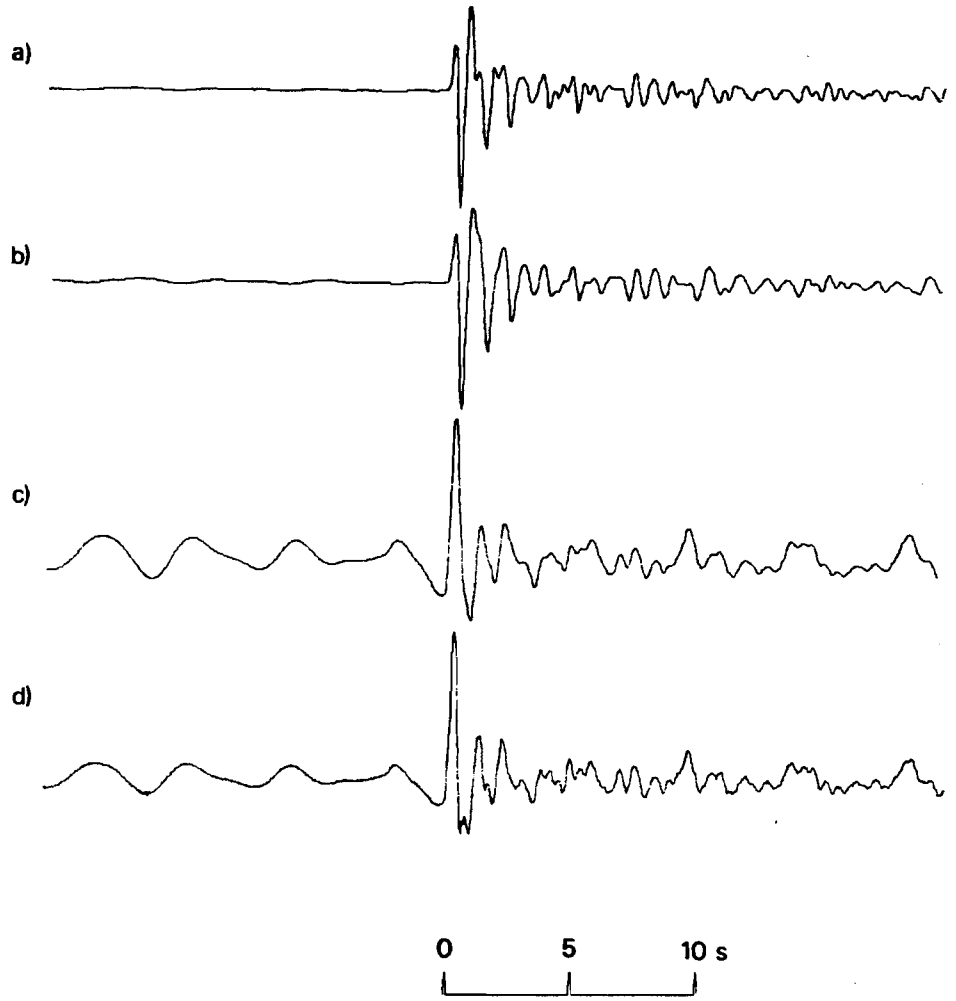

Figure A172 (a) Short-period array-sum seismogram recorded at WRA from the 5 December 1982 Shagan River explosion.
(b) Seismogram (a) filtered to simulate the effects of an additional t* of 0.2s.
(c) Seismogram (a) after Wiener filtering converted to a phaseless-broad-band instrument response.
(d) Same as seismogram (c) except that the effects of path attenuation of t* = 0.15s have been corrected for.
Note that PcP should arrive within a few seconds of P.

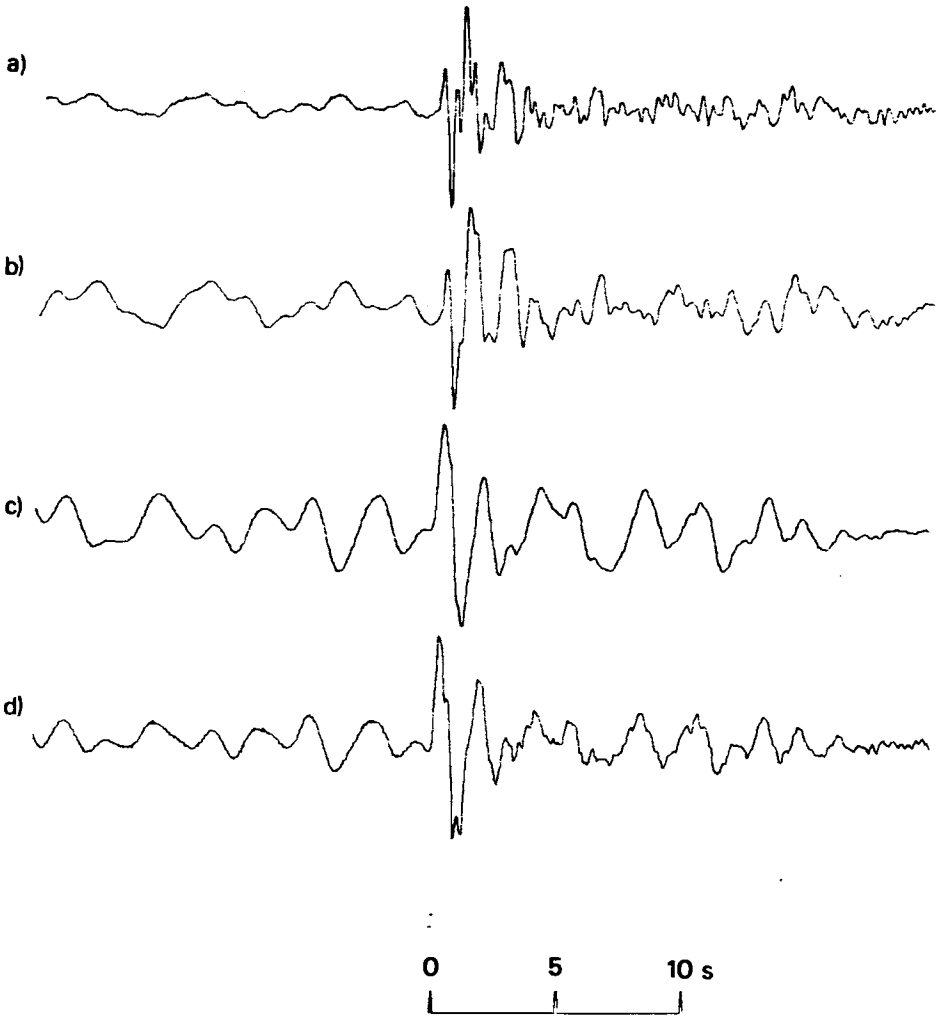

Figure A173 (a) Short-period array-sum seismogram recorded at EKA from the 26 December 1982 Shagan River explosion.
(b) Seismogram (a) filtered to simulate the effects of an additional t* of 0.2s.
(c) Seismogram (a) after Wiener filtering converted to a phaseless-broad-band instrument response.
(d) Same as seismogram (c) except that the effects of path attenuation of t* = 0.15s have been corrected for.

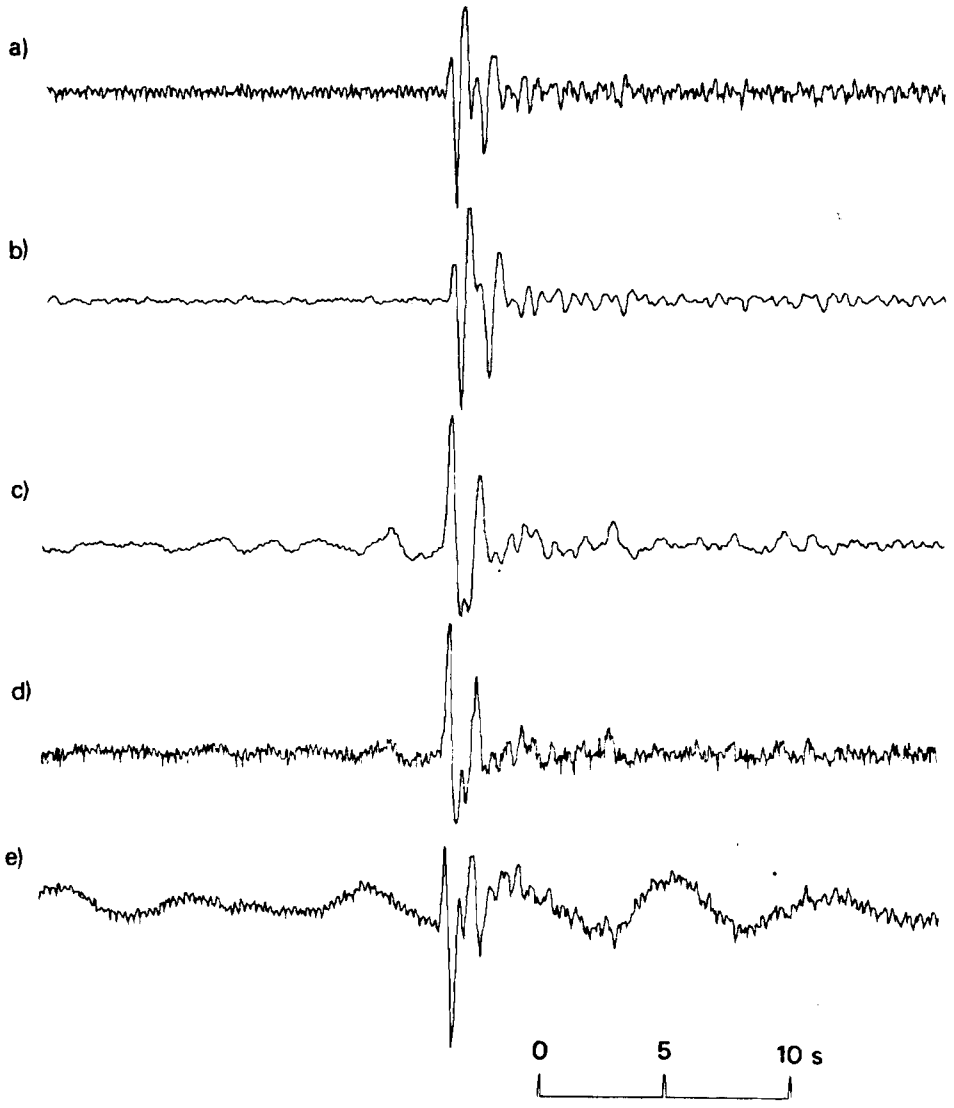

Figure A174 (a) Short-period seismogram that would be recorded at YKA from the 26 December 1982 Shagan River explosion: derived from the velocity-broad-band seismogram (e).
(b) Seismogram (a) filtered to simulate the effects of an additional t* of 0.2s.
(c) Seismogram (a) after Wiener filtering converted to a phaseless-broad-band instrument response.
(d) Same as seismogram (c) except that the effects of path attenuation of t* = 0.15s have been corrected for.
(e) Velocity-broad-band seismogram recorded at YKA.

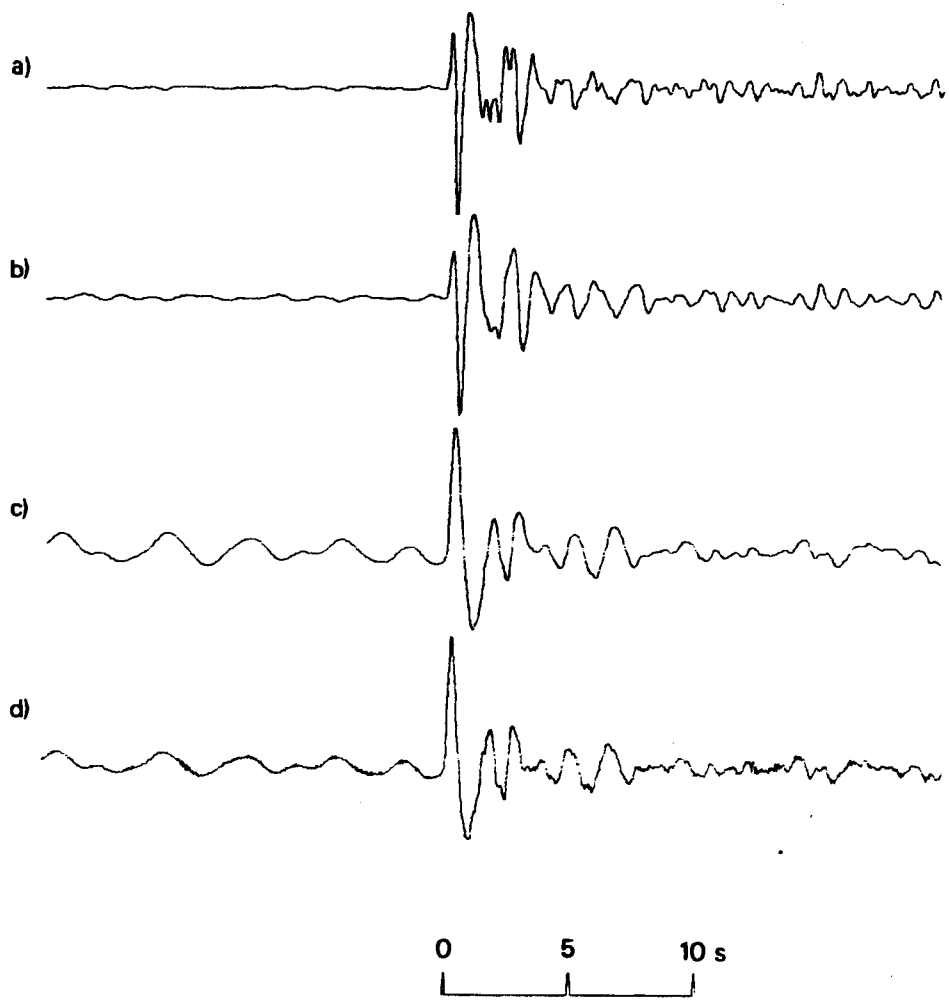

Figure A175 (a) Short-period array-sum seismogram recorded at GBA from the 26 December 1982 Shagan River explosion.
(b) Seismogram (a) filtered to simulate the effects of an additional t* of 0.2s.
(c) Seismogram (a) after Wiener filtering converted to a phaseless-broad-band instrument response.
(d) Same as seismogram (c) except that the effects of path attenuation of t* = 0.15s have been corrected for.

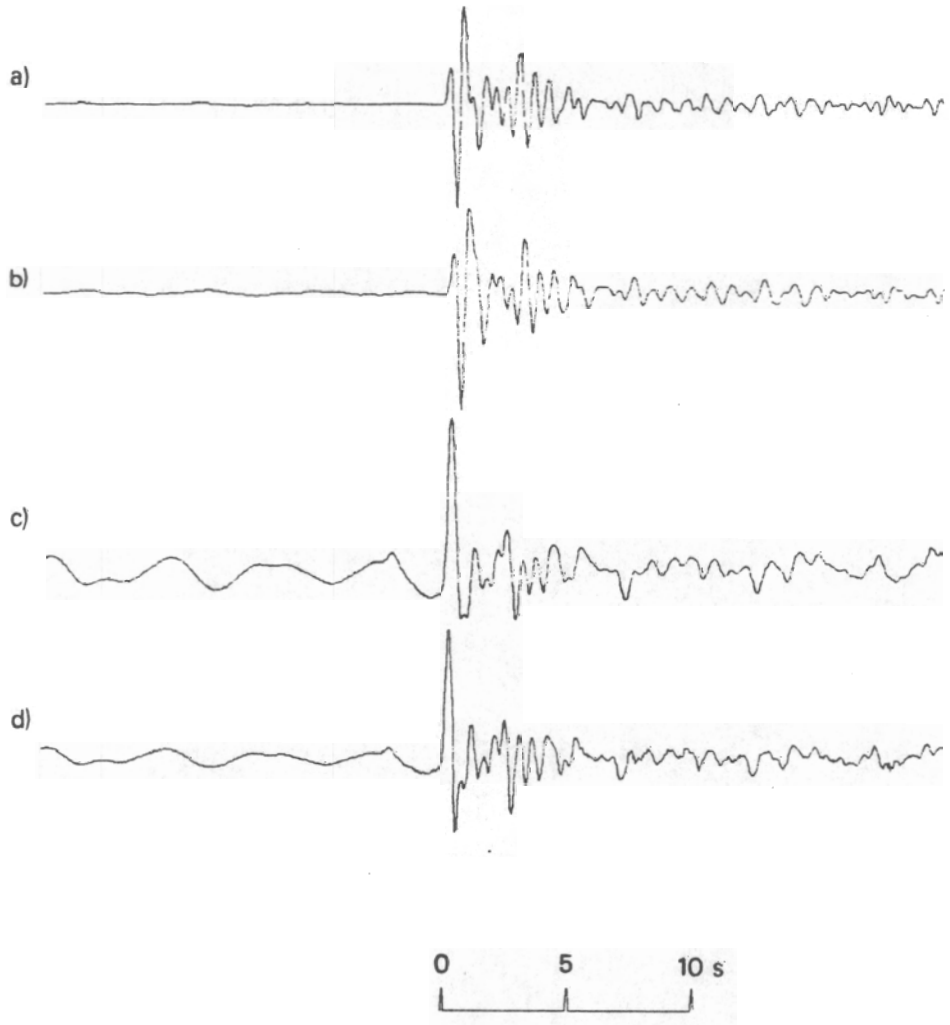

Figure A176 (a) Short-period array-sum seismogram recorded at WRA from the 26 December 1982 Shagan River explosion.
(b) Seismogram (a) filtered to simulate the effects of an additional t* of 0.2s.
(c) Seismogram (a) after Wiener filtering converted to a phaseless-broad-band instrument response.
(d) Same as seismogram (c) except that the effects of path attenuation of t* = 0.15s have been corrected for.
Note that PcP should arrive within a few seconds of P.

APPENDIX B

MEASURED DATA

This appendix contains tables of data used in the preparation of this report, although not directly discussed in it. The tables are as follows:-

Table B1 — Amplitudes, periods, log(A/T)s measured from all the short-period seismograms, both original and attenuated. Estimates of $\frac{1}{2}T_{bc}$ that were biased by an inflection are flagged (*).

Table B2 — Initial estimates of pulse duration, network values and station effects. Estimates that were later revised are flagged (*).

Table B3 — Initial estimates of log ψ_∞, network values and station effects. Estimates that were later revised are flagged (*).

Table B4 — Reduced displacement potentials (m^3) measured at each station and network values (equivalent to table 7).

Table B5 — Station magnitudes, network magnitudes and station effects using oa amplitude data.

Table B6 — Station magnitudes, network magnitudes and station effects using ab amplitude data.

Table B7 — Station magnitudes, network magnitudes and station effects using attenuated (t* = 0.2 s) peak-to-peak amplitude data.

Table B8 — Station magnitudes, network magnitudes and station effects using attenuated (t* = 0.2 s) oa amplitude data.

Table B9 — Station magnitudes, network magnitudes and station effects using attenuated (t* = 0.2 s) ab amplitude data.

TABLE B1

Amplitudes, Periods, Log (A/T)s Measured from all the Short-Period Seismograms both Original and Attenuated

Estimates of 1/2 Tbc that were biased are flagged (*)

			ORIGINAL SEISMOGRAM								ATTENUATED SEISMOGRAM (t*=0.2)							
			uncorrected amplitude(nm)			period (seconds)		log(A/T)			uncorrected amplitude(nm)			period (seconds)		log(A/T)		
no	date	array	Aoa	Aab	Abc	Tox	1/2Tbc	oa	ab	pp	Aoa	Aab	Abc	Tox	1/2Tbc	oa	ab	pp
01	15/ 1/65	EKA	77.7	238.	296.	0.74	0.23	1.81	2.00	2.08	32.8	106.	116.	0.82	0.70*	1.45	1.66	1.70
02	19/ 6/68	EKA	28.3	108.	156.	0.65	0.65*	1.36	1.64	1.80	12.6	55.3	71.6	0.82	0.67*	1.04	1.38	1.49
	19/ 6/68	YKA	51.2	150.	182.	0.63	0.25	1.61	1.78	1.86	20.7	57.1	73.8	0.78	0.36	1.24	1.38	1.48
	19/ 6/68	GBA	9.65	31.3	38.7	0.69	0.42*	1.20	1.41	1.50	3.58	14.0	18.4	0.80	0.46*	0.79	1.08	1.20
	19/ 6/68	WBA	19.0	59.9	79.5	0.59	0.32	1.48	1.68	1.80	6.65	23.8	30.9	0.72	0.38	1.04	1.29	1.41
03	30/11/69	EKA	113.	463.	614.	0.63	0.23	1.96	2.27	2.40	46.2	207.	255.	0.80	0.68*	1.60	1.95	2.04
	30/11/69	WBA	41.5	110.	132.	0.74	0.40	1.84	1.96	2.05	17.0	48.1	61.0	0.87	0.44	1.48	1.64	1.75
04	30/ 6/71	EKA	10.8	44.7	68.4	0.61	0.69*	0.94	1.26	1.44	4.92	18.7	26.8	0.67	0.71*	0.60	0.88	1.04
	30/ 6/71	YKA	33.4	113.	126.	0.65	0.25	1.43	1.66	1.70	12.9	41.9	49.6	0.76	0.29	1.03	1.24	1.30
	30/ 6/71	GBA	10.0	38.2	45.5	0.61	0.29	1.20	1.48	1.56	4.51	15.5	22.0	0.68	0.46*	0.86	1.10	1.25
	30/ 6/71	WBA	4.09	13.7	13.7	0.59	0.42*	0.81	1.04	1.04	1.83	4.46	4.69	0.63	0.40	0.47	0.55	0.61
05	10/ 2/72	EKA	22.1	64.4	112.	0.80	0.61*	1.28	1.44	1.68	8.89	29.5	49.8	0.84	0.44	0.89	1.11	1.35
	10/ 2/72	WBA	8.76	32.2	55.5	0.67	0.34	1.15	1.42	1.65	3.20	14.3	23.5	0.80	0.36	0.74	1.09	1.29
06	2/11/72	EKA	158.	556.	782.	0.82	0.36	2.14	2.38	2.51	73.5	290.	389.	0.89	0.44	1.82	2.12	2.25
07	10/12/72	EKA	93.7	271.	343.	0.84	0.67*	1.91	2.08	2.18	42.9	134.	180.	0.89	0.67*	1.59	1.78	1.91
09	14/12/73	EKA	72.1	212.	239.	0.80	0.63*	1.79	1.96	2.01	36.2	91.9	91.9	0.94	0.36	1.54	1.64	1.58
10	16/ 4/74	YKA	4.07	16.9	24.6	0.49	0.27	0.51	0.83	0.99	1.38	6.41	8.79	0.63	0.32	0.04	0.41	0.55
11	31/ 5/74	EKA	77.1	285.	474.	0.84	0.38	1.83	2.10	2.30	35.5	140.	246.	0.89	0.44	1.51	1.80	2.05
12	16/10/74	EKA	15.4	55.9	84.8	0.65	0.61*	1.10	1.36	1.54	5.89	22.1	33.5	0.74	0.59*	0.69	0.96	1.14
	16/10/74	YKA	15.2	63.3	100.	0.63	0.38	1.09	1.40	1.62	7.71	30.9	47.4	0.86	0.40	0.83	1.14	1.30
	16/10/74	GBA	8.27	33.4	44.9	0.61	0.27	1.12	1.42	1.55	3.31	13.4	16.2	0.67	0.36	0.73	1.03	1.12
13	27/12/74	EKA	15.5	45.5	53.5	0.65	0.78*	1.10	1.27	1.34	5.61	19.4	23.0	0.80	0.74*	0.68	0.92	0.99
	27/12/74	YKA	32.6	89.0	113.	0.59	0.36	1.41	1.55	1.67	13.2	38.2	46.3	0.76	0.36	1.04	1.20	1.28
	27/12/74	GBA	7.62	28.5	36.7	0.65	0.25	1.09	1.36	1.46	3.53	12.4	15.3	0.74	0.36	0.77	1.01	1.10
14	27/ 4/75	EKA	31.2	161.	197.	0.63	0.65*	1.40	1.82	1.90	13.8	68.4	97.4	0.78	0.59*	1.07	1.46	1.62
	27/ 4/75	YKA	38.1	136.	194.	0.82	0.32	1.52	1.77	1.89	17.6	63.6	90.7	0.82	0.34	1.18	1.44	1.56
	27/ 4/75	GBA	18.7	84.1	123.	0.67	0.31	1.48	1.83	1.99	8.22	34.3	46.6	0.74	0.38	1.13	1.45	1.59
15	30/ 6/75	EKA	2.65	11.9	17.7	0.59	0.52*	0.33	0.68	0.85	0.75	4.38	6.65	0.63	0.59*	-.22	0.25	0.43
	30/ 6/75	YKA	4.44	12.2	18.6	0.74	0.44	0.56	0.70	0.92	2.07	5.43	8.65	0.84	0.44	0.26	0.37	0.59
	30/ 6/75	GBA	0.86	7.33	8.91	0.59	0.27	0.14	0.77	0.85	0.20	2.99	3.20	0.67	0.31	-.49	0.38	0.41
16	29/10/75	EKA	44.3	145.	228.	0.76	0.42	1.57	1.78	2.00	20.4	71.1	122.	0.82	0.44	1.25	1.49	1.74
	29/10/75	YKA	44.3	151.	211.	0.65	0.44	1.55	1.78	1.98	21.0	69.6	105.	0.82	0.44	1.26	1.48	1.68
	29/10/75	GBA	15.3	75.6	114.	0.68	0.25	1.39	1.79	1.96	7.08	32.6	46.6	0.70	0.27	1.06	1.43	1.57
	29/10/75	WBA	3.73	13.5	19.7	0.65	0.34	0.78	1.04	1.20	1.55	6.17	9.08	0.84	0.40	0.44	0.74	0.89

TABLE B1 (Cont'd)

no	date	array	ORIGINAL SEISMOGRAM uncorrected amplitude(nm) Aoa	Aab	Abc	period (seconds) Tox	1/2Tbc	log(A/T) oa	ab	pp	ATTENUATED SEISMOGRAM (t*=0.2) uncorrected amplitude(nm) Aoa	Aab	Abc	period (seconds) Tox	1/2Tbc	log(A/T) oa	ab	pp
17	25/12/75	EKA	60.2	200.	323.	0.80	0.31	1.71	1.93	2.12	30.3	104.	146.	0.84	0.34	1.42	1.66	1.78
	25/12/75	YKA	34.4	141.	215.	0.80	0.42	1.47	1.78	1.97	14.9	70.7	114.	0.87	0.46	1.12	1.50	1.73
	25/12/75	GBA	34.2	128.	167.	0.68	0.23	1.74	2.02	2.12	14.4	52.7	65.4	0.74	0.53*	1.38	1.64	1.74
	25/12/75	WRA	9.70	37.1	56.0	0.68	0.25	1.20	1.48	1.65	3.85	15.9	23.7	0.72	0.34	0.80	1.12	1.28
18	21/ 4/76	EKA	14.4	48.0	68.5	0.68	0.34	1.07	1.29	1.45	5.43	21.9	30.0	0.80	0.40	0.67	0.97	1.11
	21/ 4/76	YKA	29.3	105.	128.	0.59	0.32	1.37	1.62	1.71	9.89	38.2	51.6	0.84	0.38*	0.94	1.22	1.35
	21/ 4/76	GBA	4.53	21.6	37.5	0.68	0.38	0.87	1.24	1.50	1.93	9.58	17.5	0.74	0.40	0.51	0.90	1.18
19	9/ 6/76	EKA	9.92	26.3	31.5	0.67	0.42	0.91	1.03	1.14	4.21	12.4	15.8	0.84	0.52*	0.57	0.74	0.84
	9/ 6/76	YKA	19.3	83.9	125.	0.61	0.34	1.19	1.52	1.70	8.68	37.9	57.0	0.80	0.42	0.87	1.21	1.40
	9/ 6/76	GBA	9.01	30.4	43.9	0.61	0.27	1.16	1.39	1.54	3.25	13.4	20.3	0.67	0.40	0.72	1.04	1.24
20	4/ 7/76	EKA	70.6	264.	414.	0.80	0.44	1.78	2.05	2.27	34.0	127.	193.	0.82	0.46	1.47	1.74	1.95
21	28/ 8/76	EKA	58.9	204.	303.	0.67	0.61*	1.68	1.92	2.09	27.0	85.4	129.	0.84	0.61*	1.37	1.57	1.75
	28/ 8/76	YKA	40.4	152.	203.	0.80	0.34	1.54	1.81	1.91	20.7	74.4	98.8	0.91	0.46	1.28	1.53	1.66
	28/ 8/76	GBA	27.5	105.	129.	0.65	0.23	1.65	1.93	2.01	12.6	43.1	49.6	0.76	0.63*	1.33	1.56	1.62
22	23/11/76	EKA	53.5	211.	286.	0.78	0.65*	1.66	1.95	2.08	27.5	97.2	144.	0.86	0.67*	1.39	1.64	1.80
	23/11/76	GBA	25.5	93.7	118.	0.74	0.27	1.63	1.89	1.97	11.8	42.8	51.0	0.82	0.80*	1.31	1.57	1.65
23	7/12/76	EKA	74.9	271.	402.	0.80	0.31	1.81	2.06	2.21	33.6	134.	197.	0.84	0.36	1.47	1.77	1.91
	7/12/76	GBA	6.24	17.6	140.	0.51	0.27	0.99	1.14	2.04	3.47	5.68	69.6	0.59	0.38	0.74	0.65	1.77
24	29/ 5/77	EKA	67.5	285.	436.	0.71	0.23	1.75	2.07	2.25	26.4	122.	165.	0.80	0.31	1.35	1.72	1.83
25	29/ 6/77	EKA	17.3	52.1	95.5	0.69	0.50*	1.15	1.33	1.59	7.02	19.2	38.2	0.76	0.55*	0.77	0.91	1.20
	29/ 6/77	YKA	13.2	63.2	123.	0.65	0.36	1.03	1.40	1.70	6.12	29.9	56.9	0.80	0.42	0.72	1.10	1.40
	29/ 6/77	GBA	9.01	36.5	53.6	0.61	0.23	1.16	1.46	1.63	3.49	14.7	19.0	0.65	0.31	0.75	1.07	1.18
	29/ 6/77	WRA	7.67	22.5	29.5	0.65	0.44	0.79	0.96	1.12	3.32	9.45	14.7	0.80	0.48	0.45	0.60	0.85
26	5/ 9/77	EKA	40.1	138.	278.	0.88	0.55	1.56	1.79	2.19	17.5	79.0	155.	0.90	0.52	1.21	1.56	1.91
	5/ 9/77	GBA	24.1	115.	177.	0.76	0.32	1.61	1.99	2.15	11.8	54.4	72.5	0.80	0.38	1.31	1.67	1.78
	5/ 9/77	WRA	56.7	190.	235.	0.65	0.36	1.66	1.88	1.98	24.7	86.7	118.	0.82	0.48*	1.33	1.57	1.70
27	29/10/77	EKA	69.6	160.	226.	0.70	0.61*	1.76	1.82	1.97	15.5	69.6	86.7	0.80	0.63*	1.12	1.47	1.57
	29/10/77	GBA	32.5	87.9	87.9	0.59	0.27	1.71	1.84	1.84	13.4	36.2	42.8	0.80	0.59	1.36	1.49	1.72
	29/10/77	WRA	61.7	200.	261.	0.53	0.29	1.69	1.90	2.02	22.4	80.8	101.	0.68	0.29	1.26	1.51	1.60
28	30/11/77	EKA	82.3	293.	448.	0.76	0.48	1.84	2.09	2.34	36.7	146.	234.	0.84	0.44	1.51	1.81	2.02
	30/11/77	WRA	39.3	142.	187.	0.65	0.36	1.50	1.76	1.89	16.9	63.6	77.7	0.82	0.42	1.16	1.44	1.53
29	11/ 6/78	EKA	85.1	292.	470.	0.80	0.29	1.86	2.10	2.28	38.9	139.	209.	0.82	0.38	1.53	1.78	1.94
	11/ 6/78	YKA	140.	495.	693.	0.59	0.29	2.05	2.29	2.44	48.5	188.	268.	0.68	0.32	1.59	1.88	2.03
	11/ 6/78	GBA	32.2	126.	164.	0.76	0.38	1.73	2.02	2.14	15.1	58.2	84.7	0.82	0.51	1.42	1.71	1.94

TABLE B1 (Cont'd)

no	date	array	ORIGINAL SEISMOGRAM uncorrected amplitude(nm)			period (seconds)		log(A/T)			ATTENUATED SEISMOGRAM (t*=0.2) uncorrected amplitude(nm)			period (seconds)		log(A/T)		
			Aoa	Aab	Abc	Tox	1/2Tbc	oa	ab	pp	Aoa	Aab	Abc	Tox	1/2Tbc	oa	ab	pp
29	11/ 6/78	WRA	88.8	340.	457.	0.59	0.23	1.85	2.13	2.26	36.6	130.	145.	0.65	0.25	1.47	1.72	1.76
30	5/ 7/78	EKA	69.3	245.	372.	0.78	0.44	1.77	2.02	2.22	27.9	114.	174.	0.86	0.46	1.39	1.70	1.91
	5/ 7/78	YKA	105.	312.	381.	0.61	0.38	1.92	2.10	2.20	34.0	115.	153.	0.68	0.38	1.44	1.67	1.80
	5/ 7/78	GBA	28.3	125.	177.	0.68	0.53	1.66	2.01	2.28	13.9	57.3	86.6	0.87	0.53	1.40	1.71	1.97
	5/ 7/78	WRA	66.3	258.	351.	0.65	0.25	1.73	2.02	2.14	29.4	105.	127.	0.78	0.32	1.39	1.65	1.71
31	29/ 8/78	EKA	78.8	262.	380.	0.80	0.67*	1.83	2.05	2.21	39.8	122.	190.	0.92	0.65*	1.57	1.76	1.95
	29/ 8/78	YKA	142.	512.	668.	0.65	0.27	2.06	2.31	2.42	59.4	214.	269.	0.80	0.40	1.70	1.96	2.06
	29/ 8/78	GBA	40.7	139.	169.	0.80	0.27	1.85	2.08	2.13	18.9	64.5	75.1	0.93	0.36	1.55	1.78	1.79
	29/ 8/78	WRA	99.3	333.	467.	0.68	0.27	1.90	2.13	2.27	40.3	146.	197.	0.72	0.34	1.52	1.78	1.90
32	15/ 9/78	EKA	88.3	299.	474.	0.80	0.40	1.88	2.11	2.31	40.1	155.	228.	0.82	0.42	1.54	1.83	2.00
	15/ 9/78	YKA	137.	433.	515.	0.63	0.34	2.04	2.24	2.32	51.6	166.	193.	0.65	0.40	1.62	1.83	1.91
	15/ 9/78	WRA	74.9	283.	402.	0.63	0.25	1.78	2.05	2.20	33.5	120.	156.	0.74	0.32	1.44	1.69	1.80
33	4/11/78	EKA	33.0	111.	177.	0.80	0.65*	1.45	1.68	1.88	15.7	50.8	90.9	0.97	0.65*	1.18	1.39	1.64
	4/11/78	YKA	71.6	252.	341.	0.63	0.27	1.76	2.00	2.13	27.6	103.	144.	0.70	0.40	1.35	1.62	1.79
	4/11/78	GBA	20.0	66.8	88.0	0.71	0.34	1.52	1.74	1.85	8.61	31.0	40.2	0.80	0.38	1.17	1.43	1.53
	4/11/78	WRA	42.5	142.	186.	0.65	0.27	1.53	1.76	1.87	17.0	62.2	81.2	0.74	0.40	1.15	1.41	1.54
34	29/11/78	EKA	107.	443.	692.	0.78	0.40	1.96	2.27	2.47	41.7	208.	318.	0.84	0.40	1.56	1.96	2.13
	29/11/78	YKA	163.	532.	795.	0.63	0.40	2.12	2.33	2.53	61.6	212.	297.	0.76	0.40	1.71	1.95	2.10
	29/11/78	WRA	103.	349.	423.	0.63	0.32	1.92	2.15	2.23	41.5	150.	168.	0.80	0.36	1.55	1.81	1.84
35	1/ 2/79	EKA	19.0	54.1	118.	0.78	0.52*	1.21	1.36	1.70	6.71	26.9	60.9	0.86	0.48	0.78	1.08	1.47
	1/ 2/79	YKA	34.9	131.	208.	0.61	0.23	1.44	1.72	1.92	13.7	54.0	81.7	0.70	0.34	1.05	1.34	1.52
	1/ 2/79	GBA	14.3	67.2	105.	0.58	0.27	1.36	1.73	1.92	6.34	26.6	37.8	0.67	0.31	1.01	1.33	1.48
36	23/ 6/79	EKA	57.8	207.	304.	0.82	0.38	1.70	1.95	2.11	27.1	104.	154.	0.84	0.44	1.38	1.66	1.84
	23/ 6/79	YKA	194.	616.	820.	0.61	0.40	2.19	2.39	2.54	77.2	248.	338.	0.76	0.40	1.81	2.02	2.16
	23/ 6/79	WRA	169.	567.	657.	0.65	0.29	2.13	2.36	2.42	71.3	239.	261.	0.68	0.34	1.76	1.98	2.02
37	7/ 7/79	EKA	22.8	71.4	98.6	0.67	0.63*	1.27	1.46	1.60	10.1	32.0	46.4	0.84	0.65*	0.95	1.15	1.31
	7/ 7/79	YKA	137.	471.	614.	0.59	0.25	2.04	2.27	2.39	53.9	191.	239.	0.74	0.29	1.65	1.90	1.98
38	4/ 8/79	EKA	52.7	203.	319.	0.84	0.44	1.66	1.95	2.16	25.3	99.3	151.	0.88	0.48	1.36	1.65	1.86
	4/ 8/79	YKA	147.	466.	614.	0.65	0.36	2.07	2.27	2.40	53.4	201.	248.	0.68	0.40	1.64	1.91	2.02
	4/ 8/79	GBA	127.	551.	916.	0.70	0.32	2.02	2.36	2.57	63.6	266.	457.	0.84	0.42	1.75	2.07	2.30
	4/ 8/79	WRA	148.	476.	554.	0.63	0.34	2.08	2.28	2.35	59.2	203.	248.	0.80	0.40	1.70	1.94	2.02
39	18/ 8/79	EKA	68.8	253.	319.	0.74	0.61*	1.76	2.02	2.12	32.4	112.	156.	0.84	0.63*	1.45	1.69	1.83
	18/ 8/79	YKA	117.	361.	544.	0.68	0.34	1.98	2.16	2.34	49.4	183.	251.	0.82	0.40	1.63	1.90	2.03
	18/ 8/79	GBA	157.	645.	949.	0.74	0.40	2.12	2.43	2.61	70.0	290.	430.	0.80	0.46	1.78	2.10	2.30

TABLE B1 (Cont'd)

no	date	array	ORIGINAL SEISMOGRAM uncorrected amplitude(nm) Aoa	Aab	Abc	period (seconds) Tox	1/2Tbc	log(A/T) oa	ab	pp	ATTENUATED SEISMOGRAM (t*=0.2) uncorrected amplitude(nm) Aoa	Aab	Abc	period (seconds) Tox	1/2Tbc	log(A/T) oa	ab	pp
39	18/ 8/79	WRA	87.3	255.	326.	0.78	0.47	1.87	2.03	2.18	37.4	119.	168.	0.87	0.49	1.52	1.73	1.91
40	28/10/79	EKA	26.6	94.1	133.	0.82	0.63*	1.36	1.61	1.76	11.9	45.4	65.7	0.84	0.69*	1.02	1.30	1.46
	28/10/79	YKA	171.	608.	747.	0.59	0.27	2.13	2.38	2.46	62.8	233.	307.	0.68	0.30	1.70	1.97	2.09
	28/10/79	WRA	129.	395.	540.	0.70	0.27	2.02	2.21	2.33	49.5	173.	242.	0.74	0.32	1.61	1.86	1.99
41	2/12/79	EKA	38.7	147.	246.	0.76	0.31	1.51	1.79	2.00	17.7	70.0	109.	0.86	0.36	1.20	1.49	1.65
	2/12/79	WRA	108.	373.	506.	0.61	0.23	1.93	2.17	2.31	40.0	159.	198.	0.68	0.29	1.51	1.81	1.90
42	23/12/79	EKA	64.8	324.	504.	0.74	0.25	1.73	2.13	2.31	27.3	147.	208.	0.82	0.31	1.37	1.80	1.93
43	25/ 4/80	YKA	39.8	141.	194.	0.68	0.28	1.51	1.76	1.89	16.6	60.8	86.4	0.81	0.38	1.15	1.41	1.56
	25/ 4/80	GBA	23.2	116.	150.	0.63	0.42*	1.28	1.67	1.79	11.9	49.2	75.8	0.76	0.46*	1.00	1.32	1.50
	25/ 4/80	WRA	35.4	139.	199.	0.59	0.23	1.45	1.74	1.90	14.3	51.1	67.9	0.70	0.27	1.07	1.32	1.43
44	12/ 6/80	YKA	64.2	209.	247.	0.61	0.42*	1.71	1.92	1.99	19.1	75.2	97.0	0.65	0.40	1.19	1.48	1.62
	12/ 6/80	GBA	28.0	116.	175.	0.74	0.29	1.37	1.68	1.85	14.3	54.7	77.8	0.78	0.40	1.08	1.37	1.52
	12/ 6/80	WRA	41.6	140.	214.	0.63	0.34	1.52	1.75	1.94	15.2	60.7	93.2	0.71	0.36	1.10	1.40	1.58
45	29/ 6/80	EKA	51.9	197.	324.	0.78	0.25	1.64	1.92	2.12	22.3	92.9	133.	0.82	0.36	1.29	1.60	1.74
	29/ 6/80	YKA	88.8	350.	418.	0.46	0.29	1.85	2.14	2.22	28.8	121.	152.	0.63	0.34	1.36	1.69	1.79
	29/ 6/80	GBA	24.2	109.	165.	0.68	0.61*	1.59	1.95	2.13	11.9	49.1	81.3	0.72	0.57	1.29	1.61	1.98
	29/ 6/80	WRA	58.3	223.	313.	0.55	0.23	1.67	1.95	2.10	23.6	85.1	106.	0.76	0.26	1.29	1.55	1.62
46	14/ 9/80	GBA	152.	690.	936.	0.76	0.23	2.11	2.46	2.59	73.4	316.	482.	0.82	0.44	1.80	2.14	2.34
47	12/10/80	EKA	70.8	230.	245.	0.78	0.67*	1.78	1.99	2.01	32.0	105.	122.	0.86	0.67*	1.45	1.67	1.73
	12/10/80	YKA	100.	321.	374.	0.61	0.49*	1.90	2.11	2.17	35.1	122.	161.	0.72	0.46	1.46	1.70	1.88
	12/10/80	GBA	71.8	279.	391.	0.72	0.31	1.77	2.06	2.20	34.3	131.	184.	0.80	0.44	1.47	1.75	1.92
	12/10/80	WRA	86.7	259.	363.	0.65	0.34	1.84	2.02	2.17	35.3	120.	175.	0.80	0.38	1.48	1.71	1.86
48	14/12/80	EKA	82.0	358.	428.	0.82	0.55*	1.85	2.19	2.27	35.0	168.	222.	0.86	0.61*	1.49	1.87	1.99
	14/12/80	YKA	71.8	208.	228.	0.65	0.40	1.76	1.92	1.99	25.9	87.0	101.	0.74	0.74*	1.33	1.56	1.62
	14/12/80	GBA	85.7	361.	616.	0.76	0.38	1.86	2.18	2.41	42.6	176.	306.	0.84	0.42	1.57	1.89	2.13
	14/12/80	WRA	55.2	200.	276.	0.80	0.29	1.67	1.93	2.04	22.9	91.5	119.	0.82	0.36	1.30	1.60	1.69
49	27/12/80	EKA	77.8	221.	322.	0.63	0.50*	1.80	1.95	2.12	33.2	94.2	129.	0.78	0.55*	1.45	1.60	1.74
	27/12/80	GBA	65.3	196.	196.	0.74	0.34	1.74	1.91	1.90	26.4	84.2	99.6	0.84	0.61*	1.36	1.57	1.64
	27/12/80	WRA	81.0	302.	423.	0.61	0.29	1.81	2.08	2.23	32.4	122.	152.	0.76	0.31	1.43	1.71	1.79
50	29/ 3/81	EKA	36.0	72.3	116.	0.76	0.61*	1.48	1.48	1.69	17.6	29.6	63.4	0.76	0.67*	1.17	1.09	1.42
	29/ 3/81	YKA	39.7	167.	252.	0.57	0.36	1.50	1.82	2.01	17.5	67.7	96.9	0.68	0.32	1.15	1.44	1.59
	29/ 3/81	GBA	29.6	113.	138.	0.65	0.29	1.38	1.66	1.75	11.9	44.9	55.4	0.67	0.40	0.99	1.26	1.38
51	22/ 4/81	EKA	94.1	342.	527.	0.80	0.38	1.91	2.16	2.34	43.8	168.	242.	0.86	0.40	1.59	1.87	2.01
	22/ 4/81	GBA	73.9	312.	503.	0.78	0.40	1.80	2.12	2.33	36.2	152.	265.	0.89	0.46	1.52	1.84	2.09

TABLE B1 (Cont'd)

no	date	array	ORIGINAL SEISMOGRAM uncorrected amplitude(nm) Aoa	Aab	Abc	period (seconds) Tox	1/2Tbc	log(A/T) oa	ab	pp	ATTENUATED SEISMOGRAM (t*=0.2) uncorrected amplitude(nm) Aoa	Aab	Abc	period (seconds) Tox	1/2Tbc	log(A/T) oa	ab	pp
51	22/ 4/81	WRA	109.	395.	456.	0.59	0.25	1.94	2.20	2.26	44.8	155.	172.	0.74	0.74*	1.57	1.81	1.85
52	27/ 5/81	EKA	17.7	72.1	125.	0.65	0.68*	1.16	1.47	1.71	7.56	30.5	55.4	0.84	0.68*	0.82	1.13	1.39
	27/ 5/81	YKA	43.7	139.	141.	0.55	0.40*	1.54	1.74	1.75	15.8	45.7	50.2	0.74	0.40	1.12	1.28	1.33
	27/ 5/81	GBA	15.7	59.8	87.9	0.65	0.25	1.11	1.39	1.56	6.78	27.8	36.9	0.80	0.32	0.76	1.08	1.18
	27/ 5/81	WRA	24.6	84.6	109.	0.61	0.27	1.29	1.53	1.64	9.62	32.7	41.2	0.68	0.27	0.89	1.12	1.21
53	13/ 9/81	EKA	127.	496.	692.	0.78	0.46	2.03	2.32	2.51	61.4	248.	339.	0.88	0.48	1.74	2.05	2.21
	13/ 9/81	YKA	159.	480.	604.	0.68	0.40	2.11	2.29	2.41	62.0	203.	241.	0.80	0.40	1.72	1.94	2.01
	13/ 9/81	GBA	128.	503.	855.	0.76	0.42	2.03	2.33	2.58	58.4	246.	428.	0.87	0.44	1.72	2.04	2.29
	13/ 9/81	WRA	103.	365.	504.	0.68	0.32	1.92	2.17	2.31	43.9	159.	215.	0.82	0.38	1.58	1.84	1.95
54	18/10/81	EKA	99.8	356.	562.	0.80	0.40	1.93	2.18	2.38	43.9	183.	283.	0.86	0.44	1.59	1.91	2.11
	18/10/81	YKA	137.	402.	516.	0.57	0.36	2.04	2.20	2.33	45.1	153.	200.	0.65	0.36	1.56	1.79	1.91
	18/10/81	GBA	90.6	383.	566.	0.70	0.49*	1.87	2.20	2.37	43.7	178.	297.	0.87	0.53*	1.59	1.90	2.12
	18/10/81	WRA	98.5	373.	499.	0.65	0.23	1.90	2.18	2.30	41.5	157.	197.	0.68	0.27	1.53	1.80	1.89
55	29/11/81	EKA	37.8	152.	218.	0.67	0.34	1.49	1.79	1.95	14.1	67.8	107.	0.76	0.46	1.07	1.45	1.70
	29/11/81	YKA	59.3	174.	213.	0.49	0.34	1.67	1.84	1.94	16.4	58.6	85.8	0.65	0.38	1.12	1.37	1.55
	29/11/81	GBA	30.1	142.	225.	0.68	0.32	1.39	1.76	1.96	14.2	64.7	113.	0.84	0.40	1.10	1.45	1.68
	29/11/81	WRA	25.9	96.8	143.	0.59	0.27	1.31	1.59	1.75	18.0	66.7	87.9	0.68	0.32	1.16	1.43	1.55
56	27/12/81	YKA	188.	647.	920.	0.61	0.32	2.18	2.41	2.57	73.0	277.	381.	0.65	0.36	1.77	2.05	2.19
	27/12/81	GBA	139.	593.	840.	0.74	0.40	2.06	2.39	2.56	62.3	267.	424.	0.82	0.44	1.73	2.06	2.28
57	25/ 4/82	GBA	111.	455.	741.	0.78	0.34	1.97	2.29	2.48	50.6	221.	371.	0.84	0.44	1.65	1.99	2.23
	25/ 4/82	WRA	82.5	329.	469.	0.68	0.29	1.82	2.12	2.27	35.9	146.	196.	0.80	0.38	1.49	1.79	1.91
58	4/ 7/82	EKA	127.	496.	732.	0.80	0.32	2.04	2.33	2.47	60.1	250.	342.	0.84	0.38	1.72	2.04	2.16
	4/ 7/82	GBA	110.	507.	685.	0.76	0.32	1.97	2.33	2.45	56.5	235.	359.	0.87	0.46	1.70	2.02	2.23
59	31/ 8/82	EKA	20.5	60.2	111.	0.67	0.25	1.22	1.39	1.65	9.04	25.8	45.8	0.78	0.34	0.88	1.04	1.27
	31/ 8/82	YKA	28.6	98.2	151.	0.52	0.27	1.36	1.59	1.78	9.32	36.1	58.2	0.61	0.38	0.87	1.16	1.38
	31/ 8/82	GBA	10.9	52.5	79.7	0.65	0.23	0.95	1.33	1.52	4.77	22.5	30.8	0.70	0.44*	0.59	0.97	1.10
	31/ 8/82	WRA	15.4	63.7	107.	0.55	0.23	1.09	1.40	1.63	5.88	24.3	36.7	0.63	0.25	0.67	0.99	1.16
60	5/12/82	EKA	121.	381.	583.	0.82	0.25	2.02	2.22	2.37	55.6	183.	249.	0.84	0.36	1.69	1.90	2.01
	5/12/82	YKA	158.	492.	686.	0.63	0.32	2.10	2.29	2.44	55.6	195.	272.	0.68	0.32	1.65	1.90	2.04
	5/12/82	WRA	104.	378.	466.	0.61	0.25	1.92	2.18	2.27	44.2	159.	183.	0.74	0.32	1.56	1.82	1.86
61	26/12/82	EKA	43.9	145.	209.	0.65	0.52*	1.55	1.77	1.93	16.9	58.3	84.8	0.76	0.61*	1.15	1.39	1.55
	26/12/82	YKA	63.0	256.	343.	0.59	0.34	1.70	2.01	2.14	23.2	90.8	127.	0.68	0.32	1.27	1.56	1.71
	26/12/82	GBA	39.1	127.	141.	0.65	0.31*	1.50	1.71	1.76	15.4	52.8	64.3	0.74	0.47?	1.11	1.34	1.43
	26/12/82	WRA	47.6	182.	263.	0.65	0.23	1.58	1.87	2.02	19.7	75.9	97.7	0.70	0.27	1.21	1.49	1.59

TABLE B2

Initial Estimates of Pulse Duration, Network Values and Station Effects
Estimates that were later revised are flagged (*)

no.	date	EKA	YKA	GBA	WRA	network mean	95% c.l.
01	15/ 1/65	0.92*				0.81	
02	19/ 6/68	0.59	0.41	0.68	0.43	0.53	0.09
03	30/11/69	0.66			0.61	0.60	0.12
04	30/ 6/71	0.52	0.46	0.44	0.34	0.44	0.09
05	10/ 2/72	0.81*			0.60*	0.67	0.12
06	2/11/72	0.80	0.54			0.65	0.12
07	10/12/72	1.05	0.52			0.77	0.12
08	23/ 7/73		0.65			0.72	
09	14/12/73	0.88*	0.47			0.66	0.12
10	16/ 4/74		0.36			0.43	
11	31/ 5/74	0.58	0.57			0.56	0.12
12	16/10/74	0.73*	0.67	0.59		0.65	0.10
13	27/12/74	0.60	0.51*	0.64		0.57	0.10
14	27/ 4/75	0.62	0.65	0.58		0.60	0.10
15	30/ 6/75	0.68*	0.52	0.55		0.57	0.10
16	29/10/75	0.60	0.62	0.54	0.71	0.62	0.09
17	25/12/75	0.67	0.71	0.45	0.52	0.59	0.09
18	21/ 4/76	0.48	0.48	0.52		0.48	0.10
19	9/ 6/76	0.58	0.60	0.50		0.55	0.10
20	4/ 7/76	0.68				0.57	
21	28/ 8/76	0.75	0.65*	0.64		0.67	0.10
22	23/11/76	0.91*		0.54		0.67	0.12
23	7/12/76	0.62		0.78		0.65	0.12
24	29/ 5/77	0.56				0.45	
25	29/ 6/77	0.64*	0.58	0.41	0.61	0.56	0.09
26	5/ 9/77	0.92		0.61	0.69	0.72	0.10
27	29/10/77	0.88		0.59	0.58	0.66	0.10
28	30/11/77	0.65		0.44	0.70	0.57	0.10
29	11/ 6/78	0.64	0.45	0.56	0.48	0.53	0.09
30	5/ 7/78	0.68	0.43	0.61	0.44	0.54	0.09
31	29/ 8/78	0.83	0.53	0.58	0.60	0.64	0.09
32	15/ 9/78	0.63	0.60		0.61	0.61	0.10
33	4/11/78	0.84	0.47	0.66	0.62	0.65	0.09
34	29/11/78	0.66	0.47	0.60	0.60	0.58	0.09
35	1/ 2/79	0.60	0.51	0.49		0.52	0.10
36	23/ 6/79	0.70	0.50		0.65	0.62	0.10
37	7/ 7/79	0.92	0.45			0.67	0.12
38	4/ 8/79	0.68	0.60	0.72	0.66	0.66	0.09
39	18/ 8/79	0.74	0.62	0.72	0.74	0.70	0.09
40	28/10/79	0.88	0.48x		0.57	0.69	0.12
41	2/12/79	0.65			0.55	0.56	0.12
42	23/12/79	0.61				0.50	
43	25/ 4/80		0.54	0.56	0.51	0.57	0.10
44	12/ 6/80		0.48	0.61	0.55	0.58	0.10
45	29/ 6/80	0.60	0.37	0.56	0.48	0.50	0.09
46	14/ 9/80			0.67		0.67	
47	12/10/80	0.87	0.54	0.69	0.59	0.67	0.09
48	14/12/80	0.79	0.57	0.65	0.68	0.67	0.09
49	27/12/80	0.80*		0.68	0.51	0.64	0.10
50	29/ 3/81	0.67	0.48	0.50		0.54	0.10
51	22/ 4/81	0.72		0.70	0.54	0.63	0.10
52	27/ 5/81	0.85	0.50	0.60	0.45	0.60	0.09
53	13/ 9/81	0.73	0.62	0.65	0.53	0.63	0.09
54	18/10/81	0.71	0.46	0.65	0.56	0.60	0.09
55	29/11/81	0.62	0.38	0.61	0.43	0.51	0.09
56	27/12/81		0.54	0.63		0.62	0.12
57	25/ 4/82			0.68	0.65	0.68	0.12
58	4/ 7/82	0.68		0.68		0.63	0.12
59	31/ 8/82	0.48	0.44	0.42	0.43	0.44	0.09
60	5/12/82	0.61	0.43		0.63	0.56	0.10
61	26/12/82	0.82*	0.43	0.64	0.51	0.60	0.09
station effect		0.11	-0.07	0.00	0.04		
95% c.l.		0.02	0.02	0.02	0.03		

TABLE B3

Initial Estimates of Log ψ_∞, Network Values and Station Effects
Estimates that were later revised are flagged (*)

no.	date	EKA	YKA	GBA	WRA	network mean	95% c.l.
01	15/ 1/65	3.98*				3.92	
02	19/ 6/68	3.40	3.28	3.20	3.35	3.31	0.14
03	30/11/69	4.13			3.92	4.00	0.20
04	30/ 6/71	3.00	3.28	3.02	2.59	2.98	0.14
05	10/ 2/72	3.62*			3.31*	3.45	0.20
06	2/11/72	4.43				4.37	
07	10/12/72	4.43				4.37	
08	23/ 7/73						
09	14/12/73	4.08*				4.02	
10	16/ 4/74		2.30			2.25	
11	31/ 5/74	3.93				3.87	
12	16/10/74	3.26*	3.37	2.98		3.20	0.16
13	27/12/74	3.03	3.25*	3.03		3.10	0.16
14	27/ 4/75	3.64	3.65	3.36		3.55	0.16
15	30/ 6/75	2.43*	2.45	2.40		2.42	0.16
16	29/10/75	3.61	3.64	3.38	3.02	3.42	0.14
17	25/12/75	3.87	3.80	3.43	3.24	3.59	0.14
18	21/ 4/76	2.98	3.18	2.90		3.02	0.16
19	9/ 6/76	2.90	3.37	2.98		3.08	0.16
20	4/ 7/76	3.94				3.88	
21	28/ 8/76	3.74	3.81*	3.58		3.71	0.16
22	23/11/76	4.06*		3.57		3.83	0.20
23	7/12/76	3.95		3.62		3.80	0.20
24	29/ 5/77	3.85				3.79	
25	29/ 6/77	3.14*	3.19	2.96	2.93	3.06	0.14
26	5/ 9/77	4.11		3.70	3.92	3.93	0.16
27	29/10/77	3.83		3.59	3.78	3.75	0.16
28	30/11/77	4.05			3.83	3.92	0.20
29	11/ 6/78	3.97	3.91	3.71	3.89	3.87	0.14
30	5/ 7/78	3.97	3.72	3.76	3.83	3.82	0.14
31	29/ 8/78	4.08	4.06	3.77	4.00	3.98	0.14
32	15/ 9/78	4.01	4.00		3.96	3.96	0.16
33	4/11/78	3.75	3.68	3.54	3.68	3.66	0.14
34	29/11/78	4.21	4.03		4.09	4.08	0.16
35	1/ 2/79	3.37	3.38	3.15		3.30	0.16
36	23/ 6/79	3.92	4.13		4.30	4.08	0.16
37	7/ 7/79	3.62	3.93			3.72	0.20
38	4/ 8/79	3.92	4.12	4.22	4.25	4.13	0.14
39	18/ 8/79	3.94	4.16	4.23	4.20	4.13	0.14
40	28/10/79	3.76	4.04x		4.13	3.92	0.20
41	2/12/79	3.64			4.08	3.84	0.20
42	23/12/79	3.97				3.91	
43	25/ 4/80		3.52	3.39	3.43	3.46	0.16
44	12/ 6/80		3.56	3.46	3.58	3.55	0.16
45	29/ 6/80	3.77	3.67	3.69	3.71	3.71	0.14
46	14/ 9/80			4.28		4.37	
47	12/10/80	4.01	3.86	3.93	3.99	3.95	0.14
48	14/12/80	4.15	3.78	4.00	3.99	3.98	0.14
49	27/12/80	3.97*		3.78	3.92	3.91	0.16
50	29/ 3/81	3.37	3.49	3.28		3.37	0.16
51	22/ 4/81	4.14		4.00	4.03	4.07	0.16
52	27/ 5/81	3.50	3.33	3.21	3.26	3.33	0.14
53	13/ 9/81	4.31	4.14	4.17	4.11	4.18	0.14
54	18/10/81	4.21	3.91	4.02	4.06	4.05	0.14
55	29/11/81	3.69	3.37	3.53	3.52	3.53	0.14
56	27/12/81		4.15	4.19		4.19	0.20
57	25/ 4/82			4.10	4.13	4.17	0.20
58	4/ 7/82	4.29		4.15		4.24	0.20
59	31/ 8/82	2.96	3.14	2.93	3.10	3.03	0.14
60	5/12/82	4.05	3.95		4.10	4.00	0.16
61	26/12/82	3.72*	3.59	3.49	3.68	3.62	0.14
station effect		0.06	0.05	-0.09	-0.01		
95% c.l.		0.04	0.04	0.04	0.04		

TABLE B4

Reduced Displacement Potentials (m^3) Measured at Each Station and Network Values (Equivalent to Table 7)

no.	date	EKA	YKA	GBA	WRA	network mean
01	15/ 1/65	8280				7413
02	19/ 6/68	2537	1900	1572	2246	2042
03	30/11/69	13465			8238	10000
04	30/ 6/71	1002	1899	1054	390	955
05	10/ 2/72	2486			1211	1660
06	2/11/72	26976				23988
07	10/12/72	27202				23988
08	23/ 7/73					
09	14/12/73	7811				6918
10	16/ 4/74		201			178
11	31/ 5/74	8554				7586
12	16/10/74	1477	2322	950		1479
13	27/12/74	1060	1494	1079		1175
14	27/ 4/75	4392	4489	2279		3548
15	30/ 6/75	230	283	254		251
16	29/10/75	4065	4370	2401	1055	2630
17	25/12/75	7452	6300	2666	1748	3890
18	21/ 4/76	957	1513	787		1047
19	9/ 6/76	790	2320	950		1202
20	4/ 7/76	8681				7762
21	28/ 8/76	5534	5173	3798		4786
22	23/11/76	10379		3714		6457
23	7/12/76	8866		4160		6310
24	29/ 5/77	7078				6310
25	29/ 6/77	1185	1559	915	852	1096
26	5/ 9/77	12806		5060	8408	8511
27	29/10/77	6823		3930	6037	5623
28	30/11/77	11227			6787	8318
29	11/ 6/78	9353	8084	5109	7751	7413
30	5/ 7/78	9365	5200	5693	6721	6607
31	29/ 8/78	11947	11437	5888	10018	9550
32	15/ 9/78	10181	9904		9040	9120
33	4/11/78	5618	4741	3461	4813	4571
34	29/11/78	16339	10623		12353	12023
35	1/ 2/79	2351	2387	1422		1995
36	23/ 6/79	8229	13429		19768	12023
37	7/ 7/79	4134	8548			5370
38	4/ 8/79	8269	13074	16640	17928	13490
39	18/ 8/79	8751	14361	16857	15673	13490
40	28/10/79	5702	10945x		13388	8318
41	2/12/79	4352			12155	6918
42	23/12/79	9250				8318
43	25/ 4/80		3303	2456	2675	2884
44	12/ 6/80		3641	2916	3782	3548
45	29/ 6/80	5825	4721	4879	5077	5129
46	14/ 9/80			19062		22909
47	12/10/80	10332	7165	8571	9704	8913
48	14/12/80	14146	5997	10027	9688	9550
49	27/12/80	8295		6034	8344	7762
50	29/ 3/81	2331	3085	1896		2399
51	22/ 4/81	13655		9890	10667	11749
52	27/ 5/81	3153	2151	1614	1827	2089
53	13/ 9/81	20322	13774	14744	12849	15136
54	18/10/81	16237	8160	10509	11525	11220
55	29/11/81	4925	2361	3394	3286	3388
56	27/12/81		14215	15649		15488
57	25/ 4/82			12650	13501	14454
58	4/ 7/82	19416		14059		17378
59	31/ 8/82	905	1392	846	1255	1072
60	5/12/82	11248	8888		12668	10233
61	26/12/82	4311	3898	3099	4821	3981

TABLE B5

Station Magnitudes, Network Magnitudes and Station Effects Using oa Amplitude Data

no.	date	EKA	YKA	GBA	WRA	network mean	95% c.l.
01	15/ 1/65	6.11				6.10	
02	19/ 6/68	5.66	6.01	5.16	5.8	5.67	0.15
03	30/11/69	6.26			6.2	6.20	0.21
04	30/ 6/71	5.24	5.83	5.16	5.1	5.35	0.15
05	10/ 2/72	5.58			5.5	5.52	0.21
06	2/11/72	6.44				6.43	
07	10/12/72	6.21				6.20	
08	23/07/73						
09	14/12/73	6.09				6.08	
10	16/ 4/74		4.91			4.63	
11	31/ 5/74	6.13				6.12	
12	16/10/74	5.40	5.49	5.08		5.34	0.18
13	27/12/74	5.40	5.81	5.05		5.44	0.18
14	27/ 4/75	5.70	5.92	5.44		5.71	0.18
15	30/ 6/75	4.63	4.96	4.10		4.58	0.18
16	29/10/75	5.87	5.95	5.35	5.15	5.63	0.16
17	25/12/75	6.01	5.87	5.70	5.57	5.79	0.15
18	21/ 4/76	5.37	5.77	4.83		5.34	0.18
19	9/ 6/76	5.21	5.59	5.12		5.33	0.18
20	4/ 7/76	6.08				6.07	
21	28/ 8/76	5.98	5.94	5.61		5.86	0.17
22	23/11/76	5.96		5.59		5.95	0.21
23	7/12/76	6.11		4.95		5.70	0.22
24	29/ 5/77	6.05				6.04	
25	29/ 6/77	5.45	5.43	5.12	5.16	5.29	0.15
26	5/ 9/77	5.86		5.57	6.03	5.91	0.18
27	29/10/77	6.06		5.67	6.06	6.02	0.18
28	30/11/77	6.14			5.87	5.97	0.21
29	11/ 6/78	6.16	6.45	5.69	6.22	6.13	0.15
30	5/ 7/78	6.07	6.32	5.62	6.10	6.03	0.15
31	29/ 8/78	6.13	6.46	5.81	6.27	6.17	0.15
32	15/ 9/78	6.18	6.44		6.15	6.14	0.18
33	4/11/78	5.75	6.16	5.48	5.90	5.82	0.15
34	29/11/78	6.26	6.52		6.29	6.24	0.18
35	1/ 2/79	5.51	5.85	5.32		5.58	0.18
36	23/ 6/79	6.00	6.59		6.50	6.25	0.18
37	7/ 7/79	5.57	6.44			5.86	0.21
38	4/ 8/79	5.96	6.47	5.98	6.45	6.22	0.15
39	18/ 8/79	6.06	6.38	6.08	6.24	6.19	0.15
40	28/10/79	5.66	6.54x		6.39	5.99	0.22
41	2/12/79	5.81			6.30	6.02	0.21
42	23/12/79	6.03				6.29	
43	25/ 4/80		5.91	5.24	5.82	5.66	0.18
44	12/ 6/80		6.11	5.33	5.89	5.78	0.18
45	29/ 6/80	5.94	6.25	5.55	6.04	5.94	0.15
46	14/ 9/80			6.07		6.42	
47	12/10/80	6.08	6.30	5.73	6.21	6.08	0.15
48	14/12/80	6.15	6.16	5.82	6.04	6.04	0.15
49	27/12/80	6.10		5.70	6.18	6.09	0.18
50	29/ 3/81	5.78	5.90	5.34		5.69	0.18
51	22/ 4/81	6.21		5.76	6.31	6.19	0.18
52	27/ 5/81	5.46	5.94	5.07	5.66	5.53	0.15
53	13/ 9/81	6.33	6.51	5.99	6.29	6.28	0.15
54	18/10/81	6.23	6.44	5.83	6.27	6.19	0.15
55	29/11/81	5.79	6.07	5.35	5.69	5.72	0.15
56	27/12/81		6.58	6.02		6.33	0.21
57	25/ 4/82			5.93	6.19	6.20	0.21
58	4/ 7/82	6.34		5.93		6.31	0.21
59	31/ 8/82	5.52	5.76	4.91	5.46	5.41	0.15
60	5/12/82	6.32	6.50		6.29	6.25	0.18
61	26/12/82	5.85	6.10	5.46	5.95	5.84	0.15
station effect		0.01	0.28	-0.35	0.06		
95% c.l.		0.04	0.04	0.04	0.05		

TABLE B6

Station Magnitudes, Network Magnitudes and Station Effects Using ab Amplitude Data

no.	date	EKA	YKA	GBA	WRA	network mean	95% c.l.
01	15/ 1/65	6.04				6.06	
02	19/ 6/68	5.68	5.92	5.11	5.79	5.63	0.14
03	30/11/69	6.31			6.07	6.17	0.19
04	30/ 6/71	5.30	5.80	5.18	5.15	5.36	0.14
05	10/ 2/72	5.48			5.53	5.48	0.19
06	2/11/72	6.42				6.44	
07	10/12/72	6.12				6.14	
08	23/07/73						
09	14/12/73	6.00				6.02	
10	16/ 4/74		4.97			4.72	
11	31/ 5/74	6.14				6.16	
12	16/10/74	5.40	5.54	5.12		5.37	0.16
13	27/12/74	5.31	5.69	5.06		5.37	0.16
14	27/ 4/75	5.86	5.91	5.53		5.79	0.16
15	30/ 6/75	4.72	4.84	4.46		4.69	0.16
16	29/10/75	5.82	5.92	5.49	5.15	5.76	0.16
17	25/12/75	5.97	5.92	5.72	5.59	5.80	0.14
18	21/ 4/76	5.33	5.76	4.94		5.36	0.16
19	9/ 6/76	5.07	5.66	5.08		5.29	0.16
20	4/ 7/76	6.09				6.11	
21	28/ 8/76	5.96	5.95	5.63		5.87	0.16
22	23/11/76	5.99		5.59		5.94	0.19
23	7/12/76	6.10		4.84		6.12	0.27
24	29/ 5/77	6.11				6.13	
25	29/ 6/77	5.37	5.54	5.16	5.07	5.29	0.14
26	5/ 9/77	5.83		5.69	5.99	5.92	0.16
27	29/10/77	5.86		5.54	6.01	5.89	0.16
28	30/11/77	6.13			5.87	5.98	0.19
29	11/ 6/78	6.14	6.43	5.72	6.24	6.13	0.14
30	5/ 7/78	6.06	6.24	5.71	6.13	6.04	0.14
31	29/ 8/78	6.09	6.45	5.78	6.24	6.14	0.14
32	15/ 9/78	6.15	6.38		6.16	6.13	0.16
33	4/11/78	5.72	6.14	5.44	5.87	5.79	0.14
34	29/11/78	6.31	6.47		6.25	6.25	0.16
35	1/ 2/79	5.40	5.86	5.43		5.58	0.16
36	23/ 6/79	5.99	6.53		6.47	6.23	0.16
37	7/ 7/79	5.51	6.41			5.85	0.19
38	4/ 8/79	5.99	6.41	6.06	6.39	6.21	0.14
39	18/ 8/79	6.06	6.30	6.13	6.14	6.16	0.14
40	28/10/79	5.65	6.53x		6.32	5.97	0.19
41	2/12/79	5.83			6.28	6.04	0.19
42	23/12/79	6.17				6.19	
43	25/ 4/80		5.90	5.37	5.85	5.70	0.16
44	12/ 6/80		6.06	5.38	5.86	5.76	0.16
45	29/ 6/80	5.96	6.28	5.65	6.06	5.99	0.14
46	14/ 9/80			6.16		6.45	
47	12/10/80	6.03	6.25	5.76	6.13	6.04	0.14
48	14/12/80	6.23	6.06	5.88	6.04	6.05	0.14
49	27/12/80	5.99		5.61	6.19	6.01	0.16
50	29/ 3/81	5.52	5.96	5.36		5.63	0.16
51	22/ 4/81	6.20		5.82	6.31	6.19	0.16
52	27/ 5/81	5.51	5.88	5.09	5.64	5.53	0.14
53	13/ 9/81	6.36	6.43	6.03	6.28	6.28	0.14
54	18/10/81	6.22	6.34	5.90	6.29	6.19	0.14
55	29/11/81	5.83	5.98	5.46	5.70	5.74	0.14
56	27/12/81		6.55	6.09		6.34	0.19
57	25/ 4/82			5.99	6.23	6.22	0.19
58	4/ 7/82	6.37		6.03		6.36	0.19
59	31/ 8/82	5.43	5.73	5.03	5.51	5.42	0.14
60	5/12/82	6.26	6.43		6.29	6.23	0.16
61	26/12/82	5.81	6.15	5.41	5.98	5.84	0.14
station effect		-0.02	0.25	-0.29	0.06		
95% c.l.		0.04	0.04	0.04	0.04		

TABLE B7

Station Magnitudes, Network Magnitudes and Station Effects Using Attenuated (t* = 0.2 s) Peak-to-Peak Amplitude Data

no.	date	EKA	YKA	GBA	WRA	network mean	95% c.l.
01	15/ 1/65	5.60				5.56	
02	19/ 6/68	5.39	5.48	4.76	5.38	5.25	0.15
03	30/11/69	5.94			5.72	5.81	0.21
04	30/ 6/71	4.94	5.30	4.81	4.58	4.91	0.15
05	10/ 2/72	5.25			5.26	5.24	0.21
06	2/11/72	6.15				6.10	
07	10/12/72	5.61				5.77	
08	23/07/73						
09	14/12/73	5.48				5.44	
10	16/ 4/74		4.55			4.32	
11	31/ 5/74	5.95				5.90	
12	16/10/74	5.04	5.30	4.68		5.01	0.17
13	27/12/74	4.89	5.28	4.66		4.94	0.17
14	27/ 4/75	5.52	5.56	5.15		5.41	0.17
15	30/ 6/75	4.33	4.59	3.97		4.30	0.17
16	29/10/75	5.64	5.68	5.13	4.86	5.35	0.16
17	25/12/75	5.68	5.72	5.30	5.25	5.49	0.15
18	21/ 4/76	5.01	5.35	4.74		5.03	0.17
19	9/ 6/76	4.74	5.40	4.80		4.98	0.17
20	4/ 7/76	5.85				5.81	
21	28/ 8/76	5.65	5.66	5.18		5.50	0.17
22	23/11/76	5.70		5.21		5.57	0.21
23	7/12/76	5.81		5.33		5.68	0.21
24	29/ 5/77	5.73				5.68	
25	29/ 6/77	5.10	5.40	4.74	4.82	5.02	0.15
26	5/ 9/77	5.81		5.34	5.68	5.69	0.17
27	29/10/77	5.47		5.28	5.57	5.52	0.17
28	30/11/77	5.92			5.50	5.69	0.21
29	11/ 6/78	5.84	6.03	5.50	5.73	5.78	0.15
30	5/ 7/78	5.81	5.80	5.53	5.68	5.70	0.15
31	29/ 8/78	5.85	6.06	5.35	5.87	5.78	0.15
32	15/ 9/78	5.90	5.92		5.76	5.77	0.18
33	4/11/78	5.54	5.79	5.09	5.51	5.48	0.15
34	29/11/78	6.03	6.10		5.81	5.89	0.18
35	1/ 2/79	5.37	5.52	5.04		5.31	0.17
36	23/ 6/79	5.74	6.16		5.99	5.88	0.18
37	7/ 7/79	5.21	5.98			5.46	0.21
38	4/ 8/79	5.76	6.02	5.86	6.00	5.91	0.15
39	18/ 8/79	5.74	6.03	5.86	5.88	5.88	0.15
40	28/10/79	5.36	6.09x		5.96	5.64	0.21
41	2/12/79	5.55			5.87	5.69	0.21
42	23/12/79	5.83				5.78	
43	25/ 4/80		5.56	5.06	5.40	5.36	0.18
44	12/ 6/80		5.62	5.08	5.55	5.43	0.18
45	29/ 6/80	5.64	5.79	5.54	5.59	5.64	0.15
46	14/ 9/80			5.90		6.16	
47	12/10/80	5.63	5.88	5.48	5.83	5.71	0.15
48	14/12/80	5.89	5.62	5.69	5.66	5.72	0.15
49	27/12/80	5.64		5.20	5.76	5.60	0.17
50	29/ 3/81	5.32	5.59	4.94		5.28	0.17
51	22/ 4/81	5.92		5.65	5.82	5.87	0.18
52	27/ 5/81	5.29	5.33	4.74	5.18	5.14	0.15
53	13/ 9/81	6.12	6.01	5.85	5.92	5.97	0.15
54	18/10/81	6.01	5.91	5.68	5.86	5.87	0.15
55	29/11/81	5.60	5.55	5.24	5.52	5.48	0.15
56	27/12/81		6.19	5.84		6.04	0.21
57	25/ 4/82			5.78	5.88	5.97	0.21
58	4/ 7/82	6.06		5.78		6.03	0.21
59	31/ 8/82	5.17	5.38	4.66	5.13	5.09	0.15
60	5/12/82	5.91	6.04		5.84	5.84	0.18
61	26/12/82	5.45	5.70	4.99	5.56	5.43	0.15
station effect		0.04	0.22	-0.26	0.00		
95% c.l.		0.04	0.04	0.04	0.05		

TABLE B8

Station Magnitudes, Network Magnitudes and Station Effects Using Attenuated (t* = 0.2 s) oa Amplitude Data

no.	date	EKA	YKA	GBA	WRA	network mean	95% c.l.
01	15/ 1/65	5.75				5.73	
02	19/ 6/68	5.34	5.64	4.75	5.41	5.28	0.15
03	30/11/69	5.90			5.85	5.84	0.21
04	30/ 6/71	4.90	5.43	4.82	4.84	5.00	0.15
05	10/ 2/72	5.19			5.11	5.11	0.21
06	2/11/72	6.12				6.10	
07	10/12/72	5.89				5.87	
08	23/07/73						
09	14/12/73	5.84				5.82	
10	16/ 4/74		4.44			4.19	
11	31/ 5/74	5.81				5.79	
12	16/10/74	4.99	5.23	4.69		4.99	0.17
13	27/12/74	4.98	5.44	4.73		5.07	0.17
14	27/ 4/75	5.37	5.58	5.09		5.37	0.17
15	30/ 6/75	4.08	4.66	3.47		4.09	0.17
16	29/10/75	5.55	5.66	5.02	4.81	5.38	0.17
17	25/12/75	5.72	5.52	5.34	5.17	5.44	0.15
18	21/ 4/76	4.97	5.34	4.47		4.95	0.17
19	9/ 6/76	4.87	5.27	4.68		4.96	0.17
20	4/ 7/76	5.77				5.75	
21	28/ 8/76	5.67	5.68	5.29		5.57	0.17
22	23/11/76	5.69		5.27		5.63	0.21
23	7/12/76	5.77		4.70		5.39	0.21
24	29/ 5/77	5.65				5.63	
25	29/ 6/77	5.07	5.12	4.71	4.82	4.93	0.15
26	5/ 9/77	5.51		5.27	5.70	5.58	0.17
27	29/10/77	5.42		5.32	5.63	5.54	0.17
28	30/11/77	5.81			5.53	5.63	0.21
29	11/ 6/78	5.83	5.99	5.38	5.84	5.76	0.15
30	5/ 7/78	5.69	5.84	5.36	5.76	5.66	0.15
31	29/ 8/78	5.87	6.11	5.51	5.89	5.84	0.15
32	15/ 9/78	5.84	6.02		5.81	5.78	0.17
33	4/11/78	5.48	5.75	5.13	5.52	5.47	0.15
34	29/11/78	5.86	6.11		5.92	5.86	0.17
35	1/ 2/79	5.08	5.45	4.97		5.19	0.17
36	23/ 6/79	5.68	6.21		6.13	5.90	0.17
37	7/ 7/79	5.25	6.05			5.52	0.21
38	4/ 8/79	5.66	6.03	5.71	6.07	5.87	0.15
39	18/ 8/79	5.75	6.03	5.74	5.89	5.85	0.15
40	28/10/79	5.32	6.11x		5.98	5.61	0.21
41	2/12/79	5.50			5.88	5.65	0.21
42	23/12/79	5.67				5.65	
43	25/ 4/80		5.55	4.96	5.44	5.32	0.17
44	12/ 6/80		5.59	5.04	5.47	5.37	0.17
45	29/ 6/80	5.59	5.76	5.25	5.66	5.56	0.15
46	14/ 9/80			5.76		6.08	
47	12/10/80	5.75	5.86	5.43	5.85	5.72	0.15
48	14/12/80	5.79	5.73	5.53	5.67	5.68	0.15
49	27/12/80	5.75		5.33	5.80	5.71	0.17
50	29/ 3/81	5.47	5.55	4.95		5.34	0.17
51	22/ 4/81	5.89		5.48	5.94	5.85	0.17
52	27/ 5/81	5.12	5.52	4.72	5.26	5.16	0.15
53	13/ 9/81	6.04	6.12	5.68	5.95	5.95	0.15
54	18/10/81	5.89	5.96	5.55	5.90	5.82	0.15
55	29/11/81	5.37	5.52	5.06	5.53	5.37	0.15
56	27/12/81		6.17	5.69		5.97	0.21
57	25/ 4/82			5.61	5.86	5.87	0.21
58	4/ 7/82	6.02		5.66		5.99	0.21
59	31/ 8/82	5.18	5.27	4.55	5.04	5.01	0.15
60	5/12/82	5.99	6.05		5.93	5.88	0.17
61	26/12/82	5.45	5.67	5.07	5.58	5.44	0.15
station effect		0.02	0.25	-0.32	0.06		
95% c.l.		0.04	0.04	0.04	0.04		

TABLE B9

Station Magnitudes, Network Magnitudes and Station Effects Using Attenuated (t* = 0.2 s) ab Amplitude Data

no.	date	EKA	YKA	GBA	WRA	network mean	95% c.l.
01	15/ 1/65	5.70				5.70	
02	19/ 6/68	5.42	5.52	4.78	5.40	5.28	0.13
03	30/11/69	5.99			5.74	5.84	0.18
04	30/ 6/71	4.92	5.38	4.80	4.66	4.94	0.13
05	10/ 2/72	5.15			5.20	5.15	0.18
06	2/11/72	6.16				6.16	
07	10/12/72	5.82				5.82	
08	23/07/73						
09	14/12/73	5.68				5.68	
10	16/ 4/74		4.55			4.32	
11	31/ 5/74	5.84				5.84	
12	16/10/74	5.00	5.28	4.73		5.02	0.15
13	27/12/74	4.96	5.34	4.71		5.02	0.15
14	27/ 4/75	5.50	5.58	5.15		5.43	0.15
15	30/ 6/75	4.29	4.52	4.08		4.31	0.15
16	29/10/75	5.53	5.62	5.13	4.85	5.44	0.15
17	25/12/75	5.70	5.64	5.34	5.23	5.48	0.13
18	21/ 4/76	5.01	5.36	4.60		5.01	0.15
19	9/ 6/76	4.78	5.35	4.74		4.97	0.15
20	4/ 7/76	5.78				5.78	
21	28/ 8/76	5.61	5.67	5.26		5.53	0.15
22	23/11/76	5.67		5.27		5.61	0.18
23	7/12/76	5.81		4.35		5.81	0.26
24	29/ 5/77	5.76				5.76	
25	29/ 6/77	4.95	5.25	4.77	4.72	4.92	0.13
26	5/ 9/77	5.60		5.37	5.68	5.63	0.15
27	29/10/77	5.52		5.19	5.62	5.52	0.15
28	30/11/77	5.85			5.55	5.68	0.18
29	11/ 6/78	5.82	6.02	5.41	5.83	5.77	0.13
30	5/ 7/78	5.74	5.81	5.41	5.75	5.68	0.13
31	29/ 8/78	5.80	6.10	5.48	5.89	5.82	0.13
32	15/ 9/78	5.87	5.97		5.81	5.79	0.15
33	4/11/78	5.43	5.76	5.12	5.52	5.46	0.13
34	29/11/78	6.00	6.09		5.92	5.91	0.15
35	1/ 2/79	5.12	5.48	5.03		5.23	0.15
36	23/ 6/79	5.70	6.16		6.09	5.89	0.15
37	7/ 7/79	5.19	6.04			5.50	0.19
38	4/ 8/79	5.69	6.05	5.77	6.05	5.89	0.13
39	18/ 8/79	5.73	6.04	5.80	5.84	5.85	0.13
40	28/10/79	5.34	6.12x		5.97	5.63	0.19
41	2/12/79	5.53			5.92	5.70	0.18
42	23/12/79	5.84				5.84	
43	25/ 4/80		5.55	5.02	5.43	5.33	0.15
44	12/ 6/80		5.62	5.07	5.51	5.40	0.15
45	29/ 6/80	5.64	5.83	5.31	5.66	5.61	0.13
46	14/ 9/80			5.84		6.12	
47	12/10/80	5.71	5.84	5.45	5.82	5.70	0.13
48	14/12/80	5.91	5.70	5.59	5.71	5.73	0.13
49	27/12/80	5.64		5.27	5.82	5.65	0.15
50	29/ 3/81	5.13	5.58	4.96		5.24	0.15
51	22/ 4/81	5.91		5.54	5.92	5.87	0.15
52	27/ 5/81	5.17	5.42	4.78	5.23	5.15	0.13
53	13/ 9/81	6.09	6.08	5.74	5.95	5.96	0.13
54	18/10/81	5.95	5.93	5.60	5.91	5.85	0.13
55	29/11/81	5.49	5.51	5.15	5.54	5.42	0.13
56	27/12/81		6.19	5.76		6.00	0.18
57	25/ 4/82			5.69	5.90	5.91	0.18
58	4/ 7/82	6.08		5.72		6.04	0.18
59	31/ 8/82	5.08	5.30	4.67	5.10	5.04	0.13
60	5/12/82	5.94	6.04		5.93	5.88	0.15
61	26/12/82	5.43	5.71	5.04	5.60	5.44	0.13
station effect		0.00	0.23	-0.28	0.05		
95% c.l.		0.04	0.04	0.04	0.04		

APPENDIX C

The Earthquake of 20 March 1976

On 20 March 1976, a seismic disturbance occurred near the Semipalatinsk test sites. On the m_b:M_s criterion, this disturbance is identified as an earthquake. Pooley et al (26) show that the polarities and relative amplitudes of the main arrivals seen on a collection of short-period P-wave seismograms can be accounted for by assuming the source was an earthquake at a depth of about 20 km with a fault-plane solution that has one nodal plane nearly coincident with the strike of the nearby Chingiz fault. There is no evidence that the disturbance was anything other than an earthquake. Since it occurred close to the test sites the seismograms recorded at the four arrays from the 20 March 1976 earthquake are included here, processed in the same way as the explosions discussed in this report.

Table C1 gives the epicentral details of the earthquake given by Pooley et al (26). The SP array-sum seismograms recorded at EKA, YKA, GBA and WRA are shown in figure C1. Figure C2 shows these seismograms converted to a phaseless-broad-band instrument response and Wiener filtered. The deconvolved seismograms are shown in figure C3, ie, processed as for those in figure C2, but also filtered to correct for a path attenuation of $t^* = 0.15$ s.

TABLE C1

Epicentral Details for the Seismic Disturbance of 20 March 1976, East Kazakhstan (NEIC PDE Data, M_S from Sandvin and Tjstheim (27))

Location:	50.05°N, 77.34°E
Origin time:	04:03:39.3 UTC
Depth:	0.0 km (restrained)
Body-wave magnitude, m_b:	5.1
Surface-wave magnitude, M_S:	4.0

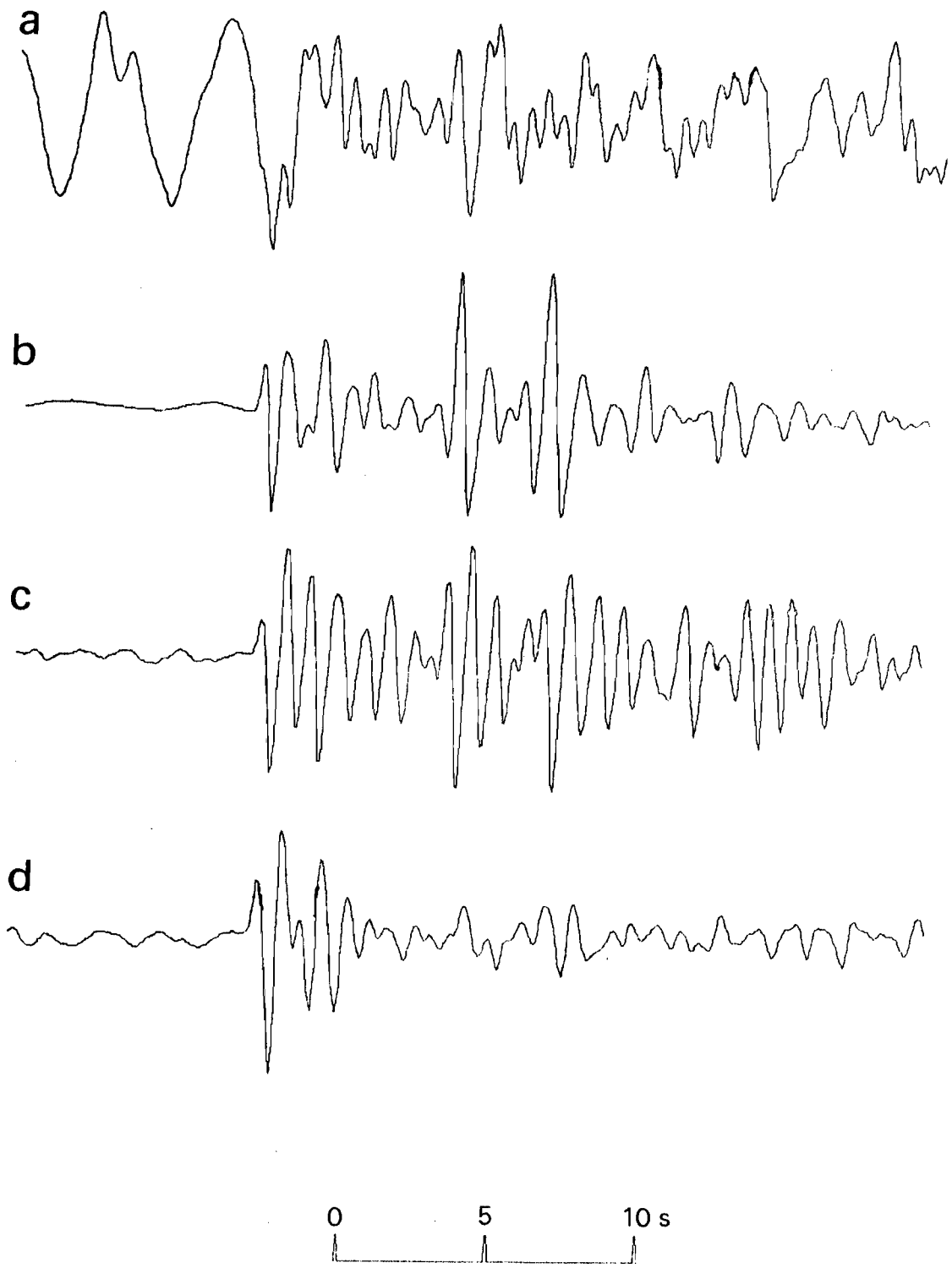

FIGURE C1. SHORT-PERIOD ARRAY-SUM SEISMOGRAMS FROM THE 20 MARCH 1976 E KAZAKH SEISMIC DISTURBANCE RECORDED AT (a) EKA, (b) YKA, (c) GBA AND (d) WRA

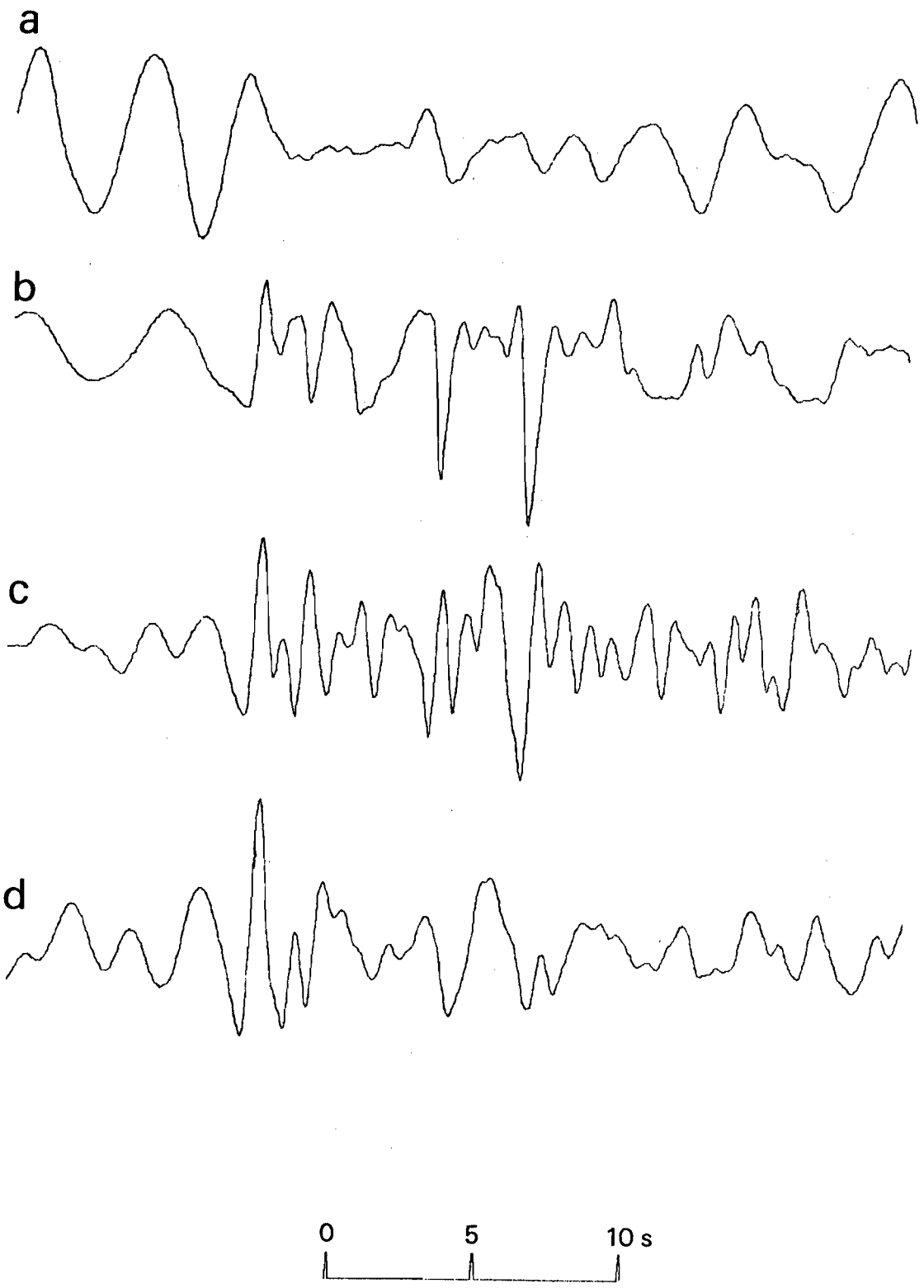

FIGURE C2. THE SEISMOGRAMS OF FIGURE C1 CONVERTED TO A PHASELESS-BROAD-BAND INSTRUMENT RESPONSE AND FILTERED USING A WIENER FILTER

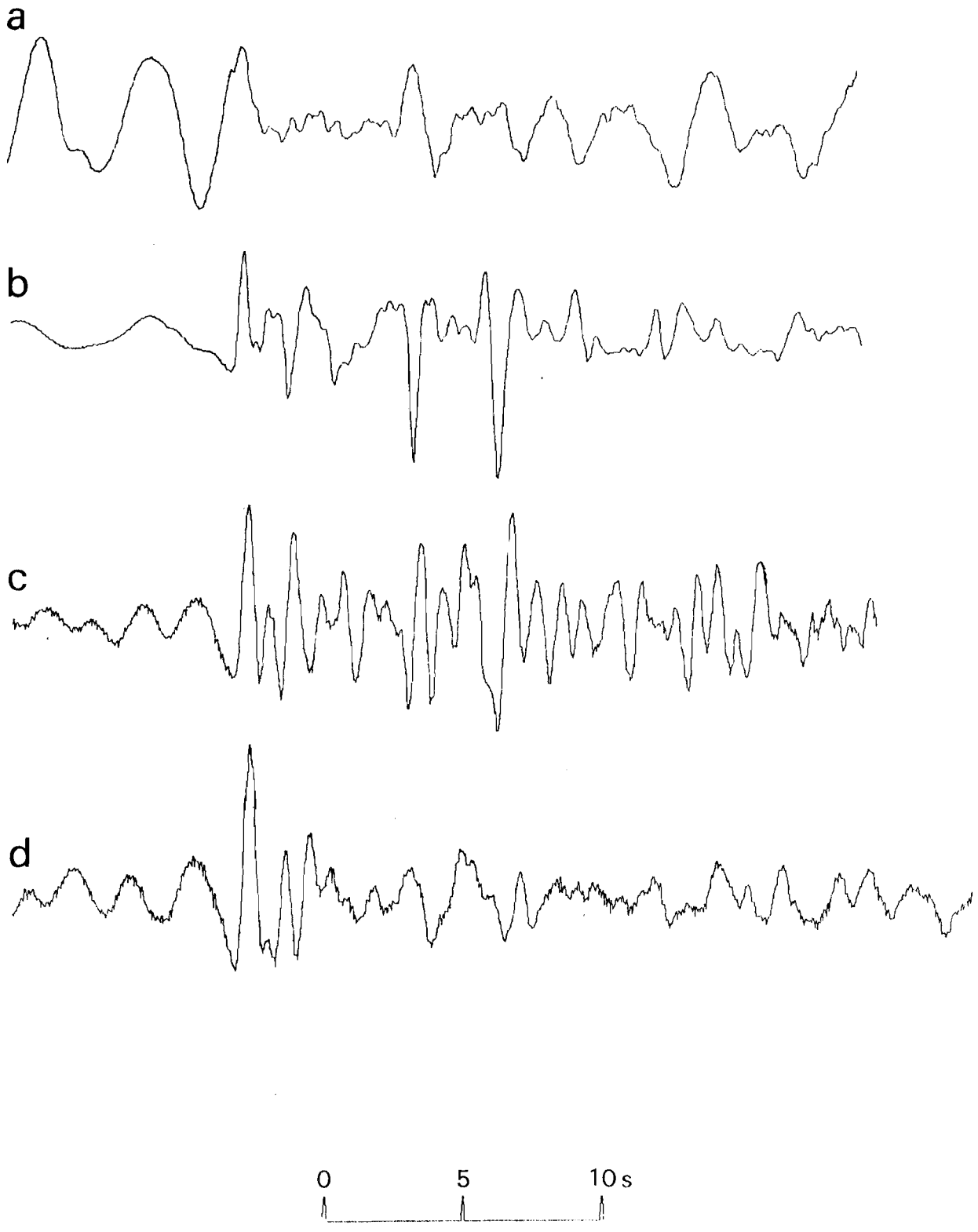

FIGURE C3. AS IN FIGURE C2, EXCEPT THAT A FILTER HAS BEEN APPLIED THAT CORRECTS FOR A PATH ATTENUATION OF $t^* = 0.15s$

DOCUMENT CONTROL SHEET

Overall security classification of sheet ..... UK Unclassified .....

(As far as possible this sheet should contain only unclassified information. If it is necessary to enter classified information, the box concerned must be marked to indicate the classification eg (R), (C) or (S)).

1. DRIC Reference (if known)	2. Originator's Reference	3. Agency Reference	4. Report Security Classification
-	AWE O 4/88	-	UK Unlimited

5. Originator's Code (if known)	6. Originator (Corporate Author) Name and Location
-	Atomic Weapons Establishment, Aldermaston

5a. Sponsoring Agency's Code (if known)	6a. Sponsoring Agency (Contract Authority) Name and Location
-	-

7. Title

P-Wave Seismograms from Underground Explosions at the Shagan River Test Site Recorded at Four Arrays

7a. Title in Foreign Language (in the case of Translation)

-

7b. Presented at (for Conference Papers). Title, Place and Date of Conference

-

8. Author 1.Surname, Initials	9a. Author 2	9b. Authors 3, 4	10. Date	pp	ref
Stewart, R C	-	-	February 1988	249	27

11. Contract Number	12. Period	13. Project	14. Other References
-	-	-	-

15. Distribution Statement

See front cover

16. Descriptors (or Keywords) (TEST)

Primary Waves — Underground Explosions
Seismic Arrays — Seismology

continue on separate piece of paper if necessary

Abstract

This report presents the P-wave seismograms recorded at four medium aperture arrays from 62 underground explosions fired at the test site at Shagan River, USSR. Four types of seismograms are illustrated for each explosion the short-period (SP), the SP seismogram with additional attenuation equivalent to a t* (ratio of travel time to specific quality factor, Q) of 0.2 s, a broad-band (BB) seismogram and a BB seismogram corrected for anelastic attenuation using a t* of 0.15 s. The attenuation-corrected seismogram is used to investigate the nature of the P-pulse radiated from the source.

CONTINUED ON SEPARATE SHEET

From each recording of an explosion, measurements are made of the body-wave magnitude, the P-pulse rise time, the P-pulse duration and the P-pulse area. From the pulse area an estimate is made of the long-term level of the reduced displacement potential, ψ_∞, which should be directly related to the yield of the explosion. The measurements made are used to obtain the least-squares estimates of network values and station effects. Estimates are given of the time between the direct P arrival and the free-surface reflection pP, although identification of the latter is not always straightforward.

Rise times measured on the BB seismograms corrected for attenuation are estimates of the rise time of the source function. Using the estimates of ψ_∞ as a measure of yield, the rise times of Shagan River explosions are roughly proportional to the fourteenth root of the yield. The pulse durations show a similar scaling with yield, but also depend on in which of the two regions of the test site the explosion was fired (the test site being readily divided into two parts on variations in the observed waveforms). The measured pP-P times also seem to depend on the region of firing, suggesting a possible difference in depth or overburden wave-speed between explosions in the two parts of the test site.

The seismograms from one of the disturbances are unusual and can be explained as resulting from two explosions separated by about 5½ km and detonated simultaneously.

There is one earthquake recorded at teleseismic distances known to have occurred close to the test site. The array recordings of this, processed in the same manner as the explosions, are presented to provide a comparison with the explosion recordings.

Available from
HER MAJESTY'S STATIONERY OFFICE
49 High Holborn, London W.C.1
13a Castle Street, Edinburgh 2
41 The Hayes, Cardiff CF1 1JW
Brazennose Street, Manchester 2
Southey House, Wine Street, Bristol BS1 2BQ
258-259 Broad St., Birmingham 1
80 Chichester Street, Belfast BT1 4JY
or through any bookseller.

Printed in England

ISBN 0 85518186

UK UNLIMITED